MULTIDISCIPLINARY STUDIES OF AU-VEIN FORMATION

APPLICATION TO THE WESTERN PART OF THE HESPERIAN MASSIF (SPAIN-PORTUGAL)

PROJECT N° MA2M-CT90-0033

Multiannual R&D Programme (1990-1992) on

"Primary raw materials and recycling of non-ferrous metals"-C.E.C.

FINAL REPORT

1993

M. CATHELINEAU, M.C. BOIRON,

CREGU, BP 23, 54501, Vandoeuvre-les-Nancy Cedex, France

F. GARCIA PALOMERO

Rio Tinto Minera S.A., 76, Zurbano, Madrid, Spain

R. URBANO, P. FLORIDO

I.T.G.E., 23, Rios Rosas, 28003, Madrid, Spain

E. S. PEREIRA

DCGM, 7, A. Enes, Lisboa, 1097 Cedex, Portugal

F. NORONHA

Porto University, 877, Campo Alegre, Porto, 4100, Portugal

F. BARRIGA, A. MATEUS

Lisboa University, Lisboa, 1700, Portugal

B. YARDLEY, D. BANKS

Leeds University, Woodhouse Lane, Leeds, LS2 9JT, U.K.

Abstract

This study carried out through the contract MA2M-0033 presents the results of detailed multiscale and multidisciplinary approaches of Au-bearing vein formation in north-western Iberian peninsula. This area (Galicia, Asturias, Leon, Minho and Trás-os-Montes) is well known for its gold, silver and tin mineralizations since proto-historic times, and underwent new exploration efforts of national mining bureaus and geological surveys (ITGE-Madrid, and DGGM-Porto), and exploration companies (Rio Tinto Minera s.a.), sometimes with involvement of universities (Porto and Lisboa Univ.). In order to get a better understanding of the processes at the origin of Au-enrichments in areas characterized by fairly good mining potentialities, integrated studies of both regional studies, industrial research and laboratory approaches, have been carried out and included :

-the careful characterization of geological environments of Au-veins (nature of host rocks (type of granite, chemistry and physical characteristics of metasediments and volcanics), degree and style of deformation, thanks to geological and geochemical mapping, short and deep drilling (around 750m at Corcoesto). The role of pre-concentrations, the effects of contrasted rheological properties of rocks units on the propagation of deformation, and the fluid-rocks interactions controlling redox processes have been especially investigated.

- the definition of the main factors controlling the ore forming processes : studies are focused on the geochemical and structural traps, the role of microfissural permeability on the control of ore fluid migration, the effects of changes in the physical chemical conditions on the gold deposition.

A multidisciplinary approach yielding to a complete characterization of the paleofluid pathways, the reconstruction of physical-chemical conditions, and the identification of the gold-bearing assemblages has been used and includes i) the P-T-X-V reconstruction of the properties of migrating fluids combining results from microthermometry, Raman spectroscopy and H-P ion chromatography on fluid inclusions leachates, ii) the characterization of the geometric traps for gold, and of the relationships between gold and sulphides, especially arsenopyrite.

Studied districts are : i) the Western Galicia with the major regional shear zones, Malpica-Tui and mineralizations included in granitic intrusions located in the East side of M.T. Unit., at Corcoesto and Tomino, ii) the northern Portugal with intrametamorphic concentrations : the Vila Pouca de Aguiar region (Trás-os-Montes) including the Três-Minas roman open-pits and other outcrops, the França deposit along the Villariça fault, iii) the intragranitic deposits of Penedono (Portugal) and Pino (Spain), iii) the intrametamorphic Montemor area.

A metallogenic model has been established, as well as the reconstruction of the successive stages necessary to get economic ores. Three successive stages are recorded in the formation of the studied Late Hercynian gold-bearing quartz veins, each characterized by its own set of P-T conditions, mineral assemblages, fluid compositions and deformational state (closely related to the fluid flow regime). The order of succession knows no exception.

Early stage: formation of milky quartz veins.

Milky quartz veins and veinlets formed mostly after the emplacement of late peraluminous granites (probably Westphalian); they also post-date the ductile deformation of the granite as well as the early subsolidus alterations affecting these granites (albitization and quartz dissolution at Pino, greisenization at Tomino, albitization at Corcoesto, muscovitization at Penedono). Diffuse alteration, and sulphide crystallization (mostly arsenopyrite) in the surrounding rocks preceed the deposition of massive milky quartz in open space (tension cracks at Corcoesto, and Tomino). Locally, a discrete ductile shearing of the early quartz crystals may occur (Tomino, Corcoesto) . But no true mylonites were developed in the surroundings of the quartz veins. These features are at variance with those of typical late Variscan shear-zones. These shear zones may be in some instances at the origin of the early fault formation prior to the quartz matrix formation .

Early C-H-O-(N) fluids of metamorphic derivation are found in the surroundings of the early milky quartz veins, and as rare relics within the quartz itself. These are dense fluids trapped under pressures above 1Kb (frequently in the 1.5-3 Kb range) and temperatures of 350° to 450°C. These conditions are roughly the same as those which prevailed during the late metamorphic stage in the Variscan terranes during or just after the hyper-collision event. Pyrite and barren

arsenopyrite are found in the milky quartz. There is no clear evidence of gold deposition at that stage, even at low concentrations in sulphides.

Intermediate stage

Due to repeated tectonic reactivation, early milky quartz veins were strongly reworked. A first event resulted in brecciation and development of the so-called "microcrystalline quartz" as a cement to the breccias, leading to the present shape of the massive quartz lenses which are the host for later ore deposition. Earlier pyrite and arsenopyrite were brecciated as well. Sulphide deposition (arsenopyrite) locally took place in the microcrystalline quartz, but was never massive.

Later on, these lenses were repeatedly subjected to intense fracturation; there was several alternances of micro-crack formation and healing or sealing by hyaline quartz. Fluids involved in the formation of hyaline quartz belong to the C-H-O-N system and are essentially similar to those of the early stage. But at that stage, temperatures range from 250° to 350°C and pressures from 0.5 to 2.0 Kb depending on the localities reflecting strong pressure variations linked to changes in the fluid pressure regime from lithostatic to hydrostatic.

Late stage: main gold deposition/enrichment

A renewal of tectonic reactivation (frequently a compressive regime characterized by new specific directions of major stresses) under quite different P-T conditions resulted in the main stage of gold ore deposits formation. Reactivation of early quartz veins (stages 1-2), results in microcracks which were healed. Native gold deposition took place, together with sulphides and sulphosalts (Pb-Ag dominated), along these cracks, especially when they crosscut earlier sulphides. In that case, it is difficult to determine wether the native gold deposited results entirely from a new gold input in the structure, or from a partial reworking of early concentrations into new mineral assemblages, although new inputs are in any case obvious.

The integrated studies carried out in this work make possible to set up new concepts about the metallogeny of the north-western iberic peninsula :

- the Au concentrations appears to be extremely specific, especially **not genetically linked to granites**, at variance of the Sn metallogeny.
- there is a **lack of direct link between shearing (especially ductile) and Au enrichment,** at variance of any "shear" model ; the role of mechanical heteogeneities and microfissuration is the most important for the formation of the trap, although the early shearings may be at the origin of fault or discontinuities which may be reactivated later on .
- the early stages (quartz matrix formation, sulphide precipitation) are necessary (but not sufficient) to get economic concentrations. Therefore , all the factors contributing to the formation of the quartz-arsenopyrite vein are important (early opened zones linked to nearby shear zones, fluid production, and As concentration, ...).
- the enrichments are related to the best structural trap which is characterized by **a long lived deformational system,** and by the existence of **late microfissuring stages necessary to the ore fluid migration.** The most competent units located nearby a major deformation zone are the best candidates to host mineralizations.
- the permanence of localized heat flows (late granites or magma injection , abnormal heat flows along shear zones or major lineaments) which allowed fluids to leach the specialized crustal series (source of Au, As, S) observed in the studied areas.

The evolution recorded by Au quartz veins is extremely complete and describes most of the **transition from late metamorphic conditions (retrograde metamorphism) to hydrothermal stages,** which occurred generally during the basement uplift. The importance of long lived history of microfissuring and fluid percolation seems absolutely necessary to get ores.

Finally, **supergene stages have contributed to the dispersion, or enrichments** of the surficial levels, and must be taken into consideration during the interpretation of the geochemical anomalies in soils, in relation with paleorelief studies. (Bio-)oxidation of sulphides may have liberated some gold in some instances, and locally contributed to surficial enrichments, may be a part of those exploited during Roman times.

Abstract-Foreword

This is the final report for the contract n° MA2M-CT90-0033 entitled :

Multidisciplinary of Au-vein formation: application to the western part of the Hesperian massif (Spain-Portugal)

from the Multiannual R&D Programme (1990-1992) on "Primary raw materials and recycling of non-ferrous metals" of the C.E.C. (D.G. XII, Unit 5).

This report contains the summaries of the works which have been carried out during the two years period of the contract, as well as detailed presentation of selected results.

I take the opportunity of this foreword to thank all the partners of this contract for an excellent and motivated contribution to this project, which has run from the beginning to the end, comformly to the initial investigation programme. The two field trips gave the opportunity to all groups to meet and work to gether in the field thanks to a warm welcome and perfect organization by each industrial, or universitary team in charge of the different studied areas.

In addition, several students and senior investigators from DGGM, Porto and Lisboa universities spent periods from 2 weeks to several months in CREGU working to this project, allowing mutual benefit and collaboration between the laboratories, and technology transfer.

The results of this project have already been presented at EC seminars and conferences, and 7 communications dealing with general or partial aspects of the work have been already accepted in international conferences.

M. Cathelineau
April 30, 1993

PROJECT STAFF

Project Co-ordinator : **Dr. M. Cathelineau (CREGU)**

CREGU

Project leader : Dr. M. Cathelineau

Dr. M.C. Boiron

Dr. S. Essarraj, A. Barakat, Dr. M. Cuney, Dr. J. Dubessy, Dr. M. Lespinasse

with the collaboration of C. Marignac (School of Mines, Nancy), and R. Castroviejo (School of Mines, Madrid)

RIO TINTO MINERA s.a.

Project leader : **Dr. F. Garcia Palomero**

J.Ayala Leal, V. Capio Cuellar

DIRRECAO GERAL DE GEOLOGIA DE MINAS

Project leader : **Dr. E. Pereira**

P. Castro, N. Fereira, C. Mereiles

INSTITUTO GEOLOGICA Y MINERO DE ESPANA

Project leader : **Ing. R. Urbano**

P. Florido, J.M. Toyos

PORTO UNIVERSITY

Project leader : **Prof. F. Noronha**

A. Doria, P. Nogueira, M.A. Ribeira

LEEDS UNIVERSITY

Project leader : **Prof. B. Yardley**

D. Banks

LISBOA UNIVERSITY

Project leader : **Prof. F. Barriga**

A. Matteus

CONTENTS

INTRODUCTION

A-MAIN OBJECTIVES

Au-vein type deposits from Western Europe display rather similar features :

- a multistage metallogenesis ;
- a multistage and complex deformation of the vein structures which bear the ores. Such a deformation includes ductile to brittle stages, and produces superimposed effects on the ore gangue minerals, especially quartz. Each deformational stage is characterized by specific metal deposition and wall rock alteration.
- a clear spatial, but not necessarily genetic, relationships between gold and arsenopyrite, a mineral which may contain gold either as native metallic particles or as a combined element within the sulphide lattice (Cathelineau et al, 1989).

In spite of numerous data, detailed metallogenic models based on rigourous and systematic quantification of processes, especially the parameters controlling the economic ores formation are still lacking. Especially, most available studies do not provide the time-space relationships between deformational events, the percolating fluid types and the specific resulting fluid-rock interactions and metal deposition. Some processes of critical importance remain unknown ; for instance, it is not determined wether gold ores result from a multistage introduction within the veins, or if they result from successive reworkings of an early concentration.

Therefore, it is necessary to know if significant displacements occurred from source rocks (or Au-precursors and Au-preconcentration) towards the ore zones.

This project presents an attempt to get a modelling of Au-bearing vein formation, and to define the processes at the origin of Au-enrichments in areas characterized by fairly good mining potentialities. Proposed studies are based on detailed multiscale and multidisciplinary approaches. They include the characterization of :

- ore features, especially how gold distribute within the minerals, at what content, and under which state (combined or metallic)
- geochemical printing of ore processes (typical mineral assemblages and associated elements)
- ore forming processes : studies are focused on the geochemical and structural traps, the role of microfissural permeability on the control of ore fluid migration, the effects of changes in the physical chemical conditions on the gold deposition.

Such studies need to compare ores formed during similar geological events, and located within a same metallogenic province. The area chosen is the hisperic province (Fig. 1), which is one of the most actively prospected area for gold, in Europe, at the moment. Althrough general features, e.g. geological, structural and geodynamic characteristics of this region, are relatively well-known, relatively few coordinated works have been still carried out from the point of view of gold metallogeny.

B- MAIN FEATURES OF THE STUDIED AREA

The careful characterization of geological environments of Au-veins is essential for a correct understanding of the role played by surrounding rocks, and is of prime importance in exploration. Thus, the nature of host rocks (type of granite, chemistry and physical characteristics of metasediments and volcanics), and the degree and style of deformation, are key factors for the understanding of ore forming processes. The role of pre-concentrations, the effects of contrasted rheological properties of rocks units on the propagation of deformation, and the fluid-rocks interactions controlling redox processes have to be especially investigated.

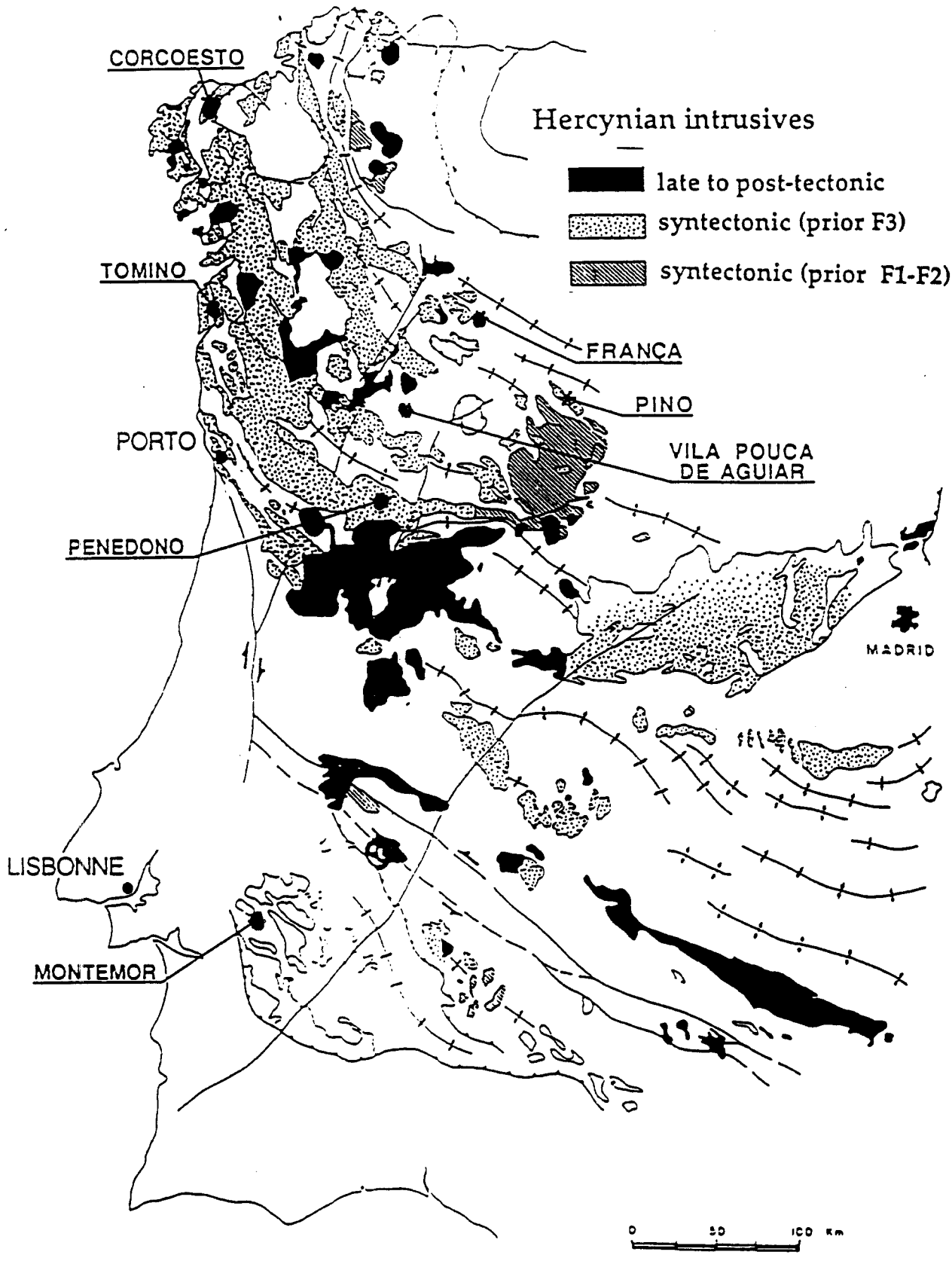

Fig. 1 : Location of the main Au-districts studied in the project.

Surrounding rocks of the studied area display a significant variety of geochemical units :

a) syntectonic granites at Pino, Tomino, Penedono with ores located within the granites, or in some cases within both the granite and the surrounding rocks (gneisses at Corcoesto) ;

b) anchi- to epizonal metamorphic series displaying enrichments in organic matter presenting rather low maturation index, quartzites, metavolcanites metasediments ;

c) greenschist/lower amphibolite facies metasedimentary sequences (França) ;

d) high grade (amphibolite - granulite) metasediments and volcanics (micaschists and leptinites) - Montemor.

The main geologiacl and structural features of the studied area are summarized below.

1 - Iberian Massif vs Iberian Terrane

The Iberian Massif is a wide and continuous outcrop of Ante-Permian Units in the Iberian Peninsula, affected by Hercynian tectonothermal events. Lithological, structural and metamorphic criteria allow us to consider the Iberian Massif as composed of different zones (Julivert et al., 1972), (Fig.2). The so-called Central-Iberian Zone (C.I.Z) comprises the "Galaico-Castelhana" and "Luso-Alcudiense" Zones of Lotze (1945) as well as the "Galiza Tras-os-Montes" Zone, as claimed by Farias et al (1987) and Arenas et al (1988).

According to the geodynamic models based on plate movements, the Iberian Massif encloses the southern part of the Armorican Plate, separated from Gondwana by: i) active rifting in the early Paleozoic; ii) oceanization in the Silurian-Devonian; iii) continental collision during Carboniferous. Several hypothesis have been proposed to understand the evolution of the different crustal elements comprising the Iberian Massif (Jonhson, 1973, 1978; Bard et al., 1973; Lefort and Ribeiro, 1980;, Matte and Burg, 1981; Ribeiro et al, 1983; Matte, 1983, 1986; Behr et al., 1984; Ziegler, 1984; Ribeiro et al., 1990; etc.).

Those hypotheses, based on paleomagnetic, biostratigrafic and, rarely, paleobiogeographic correlations, emphasise the limits of the "palinspastic" models, as they correlate the lithosphere plate concept with complex crustal parts, disconnected from their original position. To avoid such inconvenience, and with the reconnaissance that orogenic belts are formed by structural units limited by major thrusts, it was recently introduced the concept of tectono-stratigraphic unit, the so-called "Terrane" (Coney et al, 1980, Howell and Jones, 1984, Howell et al, 1985). This terrane detailed analysis, tested in the Ceno-Mesozoic circum-pacific orogenes, was successfully applied in the Circum-Atlantic most ancient orogenies (Dallmeyer, 1989).

These concepts allow us to define the following terranes in the Iberian massif (Ribeiro et al, 1987, 1990): i) Iberian terrane, including the Cantabrian (C.Z.), West Asturian-Leonese (W.A.L.C.), Central Iberian (C.I.Z) and Ossa-Morena (O.M.Z.) Zones; ii) Oceanic terran, enclosing C.I.Z allochtonous ophiolitic nappes (Cabo Ortegal, Ordenes, Bragança and Morais complexes), as well as Pulo do Lobo Zone (P.L.Z), comprising the Beja-Acebuches ophiolite, (Munha, 1986), in the southern boundary of the O.M.Z; iii) continental exotic terrane, represented by the upper allochthonous nappes of Cabo Ortegal, Ordenes, Bragança and Morais complexes; iv) South Portuguese terrane, separated from the Iberian terrane by the P.L.Z., with oceanic affinity.

These tectono-stratigraphic terrane divisions might be consistent with the most recent geodynamic models of the Iberian massif (Matte, 1986, Ribeiro and Pereira, 1986, Ribeiro et al., 1990). Although the sedimentary and the faunistic data (i- Gondwana affinity for the south Iberian domain; ii- Armorican affinity for the Central Iberian domain, separated by the Badajoz-Cordoba major shear zone) presented by Robardet and Gutierrez Marco, (1990), questioned that division.

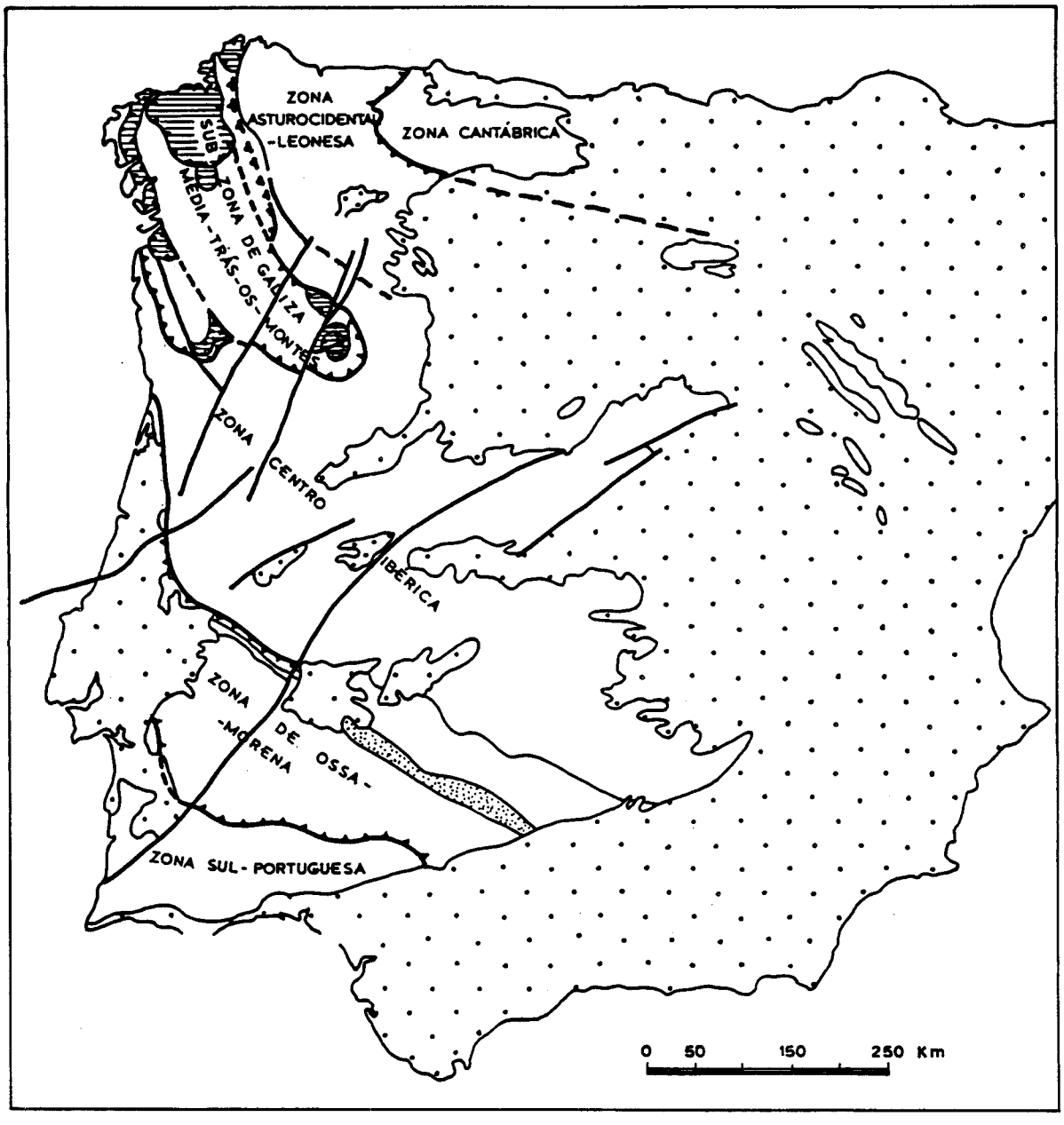

Fig. 2 : Paleogeographic and tectonic zones of the Iberian Massif (Tectonic map of the Iberia, modified), (Pereira, 1987).

In this project, however as the investigation of gold-occurrences was done in the C.I.Z, as defined by Julivert et al., (1972) the regional tectonic setting will just be referred to the Iberian terrane.

2. - Geological, paleogeographic and tectonic evolution of the Iberian Terranne.

Following the widest tectonic-stratigraphic terraine concept, the evolution of the Cental-Iberian basin must be correlated with the enclosing Cantabrian and Ossa-Morena Plateforms till the generation of the newly-formed Hercynian crust (Fig. 3), as a result of the accretion of lower and upper Proterozoic crustal segments. Besides the occurrence of oldest crust in the O.M.Z. (Pasqual, 1981; Herranz, 1983), they were found in this zone evidences of the Cadomian cycle or even Pan-African (Quesada et al., 1987; 1990). Rifting in the upper Proterozoic leads to the genesis of a passive margin and to the formation of oceanic crust, where the "Serie Negra" metasediments, bimodal volcanism and serpentinites interlayered within the Blastomylonitic Badajoz-Cordoba band are evidences. A Volcano-Sedimentary Formation of active margin characterized by wide volcanism, of either Andean or island-arc types, and syn-orogenic flysch-type sedimentary sequence (Quesada et al, 1990), show the beginning of a tectonic activity propagating to the foreland, i.e., the northen part of the Iberian Terrane. The tangential tectonic style and the high-pressure metamorphic regime, points out the collisional nature of the deformation.

During Cambrian age, a new continental rifting produces an extensive bimodal volcanic activity in the O.M.Z and an-orogenic magmatism in the C.I.Z. western margin. Meanwhile, in its eastern margin the "Ollo de Sapo" volcanism and magmatism takes place (Martinez Garcia, 1973, Diaz Balda, 1990). The Central Iberian bassin, initially a Cadomian marginal bassin, in the sequence of the north continent subduction, suffers strong subsidence, providing the deposition of a large volume of turbidites (Douro and Beiras Groups, Slate-Greywacke Complex, Sousa, 1982). This sedimentray megacycle, which started during the upper Proterozoic is interrupted by the Sardic tectonic phase, responsible for the unconformity between the lower Ordivician and the subjacent units.

The Ordovician is transgressive. It starts with conglomeratic, terrigeneous and volcanic facies, which are followed by the Armorican Quartzite, formed within a sedimentary bassin of high energy. The middle Ordovician is composed of carbon-argillaceous fine sediments (Pizarras de Luarca). These facies have a bentonic fauna from shallow waters. The upper Ordovician shows scattered basic volcanism and alcaline volcanism in the blastomylonitic zone, suggesting both crustal confinated traction and development of intracontinental rifting. The maximum subsidence axis prograde to the south, towards to the Ossa-Morena boundary. The transition to the Silurian is characterized by a clear regressive regime with associated glacigenic deposits observed in several places of the Iberian Peninsula, Armorican massif and North Africa (Babin et al., 1976; Robardet, 1980; Robardet and Dore, 1988). These features show polar latitudes which agree with the high latitude atributed to Gondwana in this period. It is admited that the Iberian terrane belonged to that supercontinent in that period.

The Silurian shows sediments of a low energy euxinic bassin, with scattered volcanism in the north, while in the OMZ bord the ocean rifting develops. The oceanic expansion occurs in the Silurian-Devonian transition. The Armorican plate moves to equatorial latitudes, disconnecting from Gondwana. This is testified by the Beja-Acebuches ophiolite and Pulo do Lobo Zone.

The Hercynian tectonogenesis begins in the Devonian. It consists of three ductile phases and a latter brittle phase, the associated deformation migrating from the inner to the outer zones.

In the inner zones, (O.M.Z and C.I.Z.), anorogenic sedimentation occurs in the Sieginian-Emsian. This is supported by: i) uniform facies representing open marine basin, shallower in the Gedinian, deeper in the Emsian; ii) marked subsidence in the south, moderate

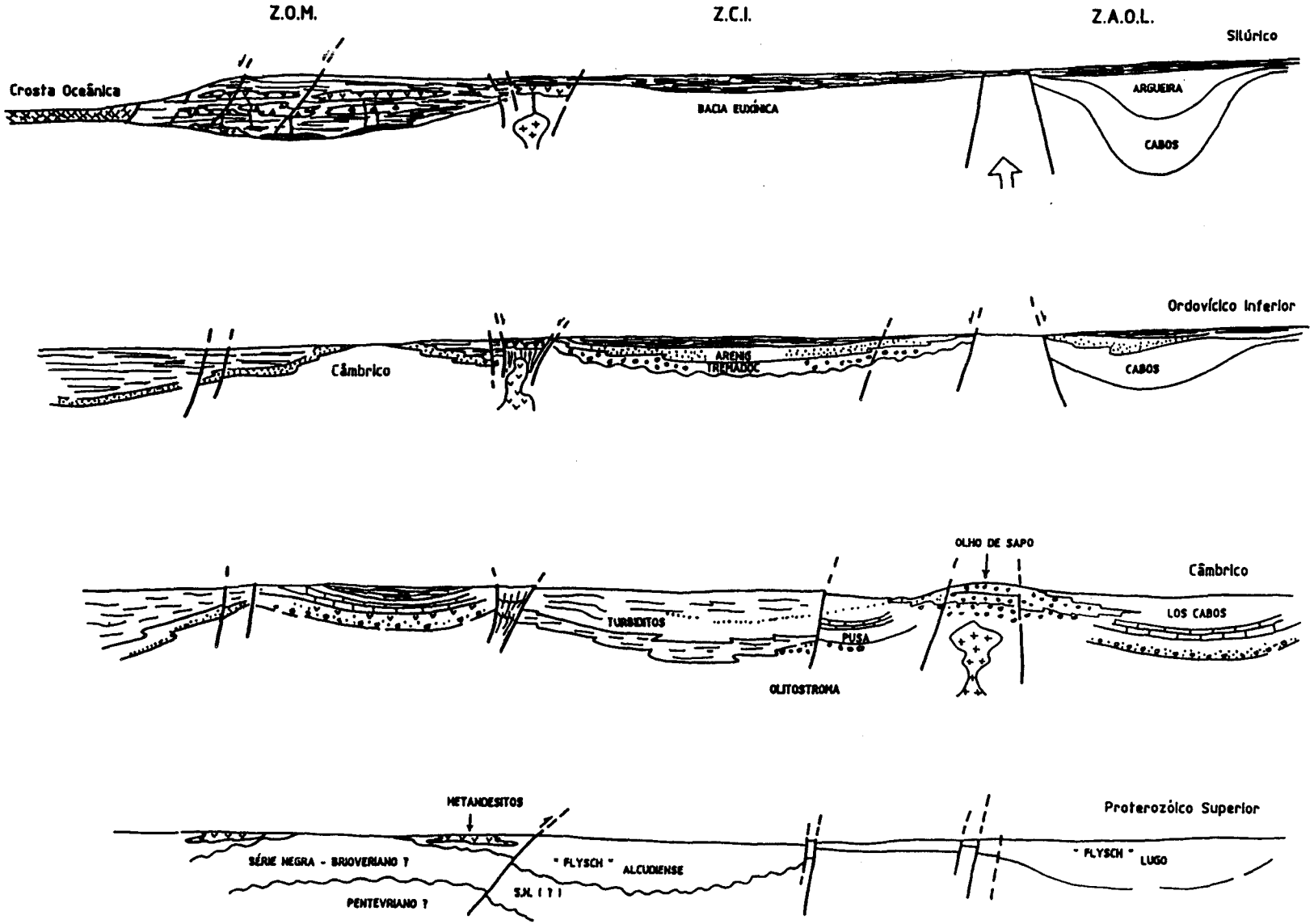

Fig. 3 : Iberian terranes: geological and paleogeographic sketch cross-sections

in the north; iii) general lack of of middle Devonian. First (D1) and second (D2) progressive deformation phases are post lower Devonian. The deposition of flyschoid facies, the Sobrado and Santos formations (Pereira, 1987), occours simultaneously, testifying the begining of the orogeny.

The early phases in the inner zones develop along thrust planes, with crustal shortening and stacking of Allothonous Units. The spatial location of the thrusted nappes corresponds to the Galiza-Tras-os-Montes Zone (Farias et al., 1987). At the edge of the prograding nappes, the extremely condensed lower Devonian plateform facies (Quiroga, 1980) are followed by the Bragança-Zamora flysch of upper Devonian/lower Carboniferous age (Teixeira and Pais, 1973; Ribeiro, 1974; Perez Estaun, 1974). This flysh includes clastic material deformed by the early phases, thus post dating them.

After the nappes emplacement the 3rd phase of deformation, D3, is developed by transcurrent shear, sub-paralel to the colisional suture admitting conjugated systems. The deformation in this phase is controled by these events; during the regional metamorphism the regime is ductile becoming brittle as metamorphism breaks down.

The D4 phase develops (Permian ?) controls the emplacement of late-to-post orogenic granitoids and is mainly brittle, cutting the main granitoids (aluminous granites). The brittle fracture systems in D4 strikes NE-SW to N.NE-S.SW with senextral horizontal movement. This movement develops a significant conjugated system striking NW-SE retaking previous structures now with brittle dextral wrench regime. With the breakdown of the orogenic tensions, this phase creates graben systems, distensible systems when the movement along the brittle faults is combined with traction and riedel systems and finally compressive systems in specific instances (see Chap III).

C- EXPLORATION IN THE IBERIAN TERRAIN

Since proto-historic times the Iberian Peninsula is well known for its gold, silver and tin mineralizations. An important gold-silver district is situated in NW of Iberian Peninsula namely in Galicia, Asturias, Leon, Minho and Trás-os-Montes.

Some were known (and mined) in Roman and pre-Roman times, others were found in more or less times, mostly as a result of the efforts of national mining bureaus and geological surveys, and exploration companies, sometimes with involvement of universities.

Galicia

Gold ores in West Galicia are closely related to shear zones, following a deformation band of several km wide, which extends from Malpica, in the North, with direction NNE-SSW, to La Guardia - Tui in the South, with direction NNW - SSE (Fig.4). Most gold mines are located in the northern part of this band, between Malpica and Noya, comprising a ore-belt trending NNE-SSW along the eastern margin of the allochthonous Malpica-Tui Unit and the metasediments and granitic intrusions of the "Dominio Esquistoso de Galicia Central", in the East side of M.T. Unit.

Most of the gold ores have been mined since pre-Roman times. Among the main mining areas are Corcoesto and Vilarcovo, showing numerous roman open-pits and underground workings. Gold ores are hosted by metasediments, silicified gneisses and leucogranites. Last mining activity have been carried out at the begining of this century. The maximum depth of mining workings in these two areas is 90-100 m. In the last two decades a research activity was carried out over the whole area and several prospects were drilled.

The southern extent of Malpica-Vigo shear band is not so well studied and defined. The intragranitic gold vein-systems of Tomino area have been worked in the past by possibly Roman open-pits, with a maximun depth of at least 5 m. San Antonio mine, in the southern end of the area, associated with shear zones in the metasediments, was mined by Roman open-

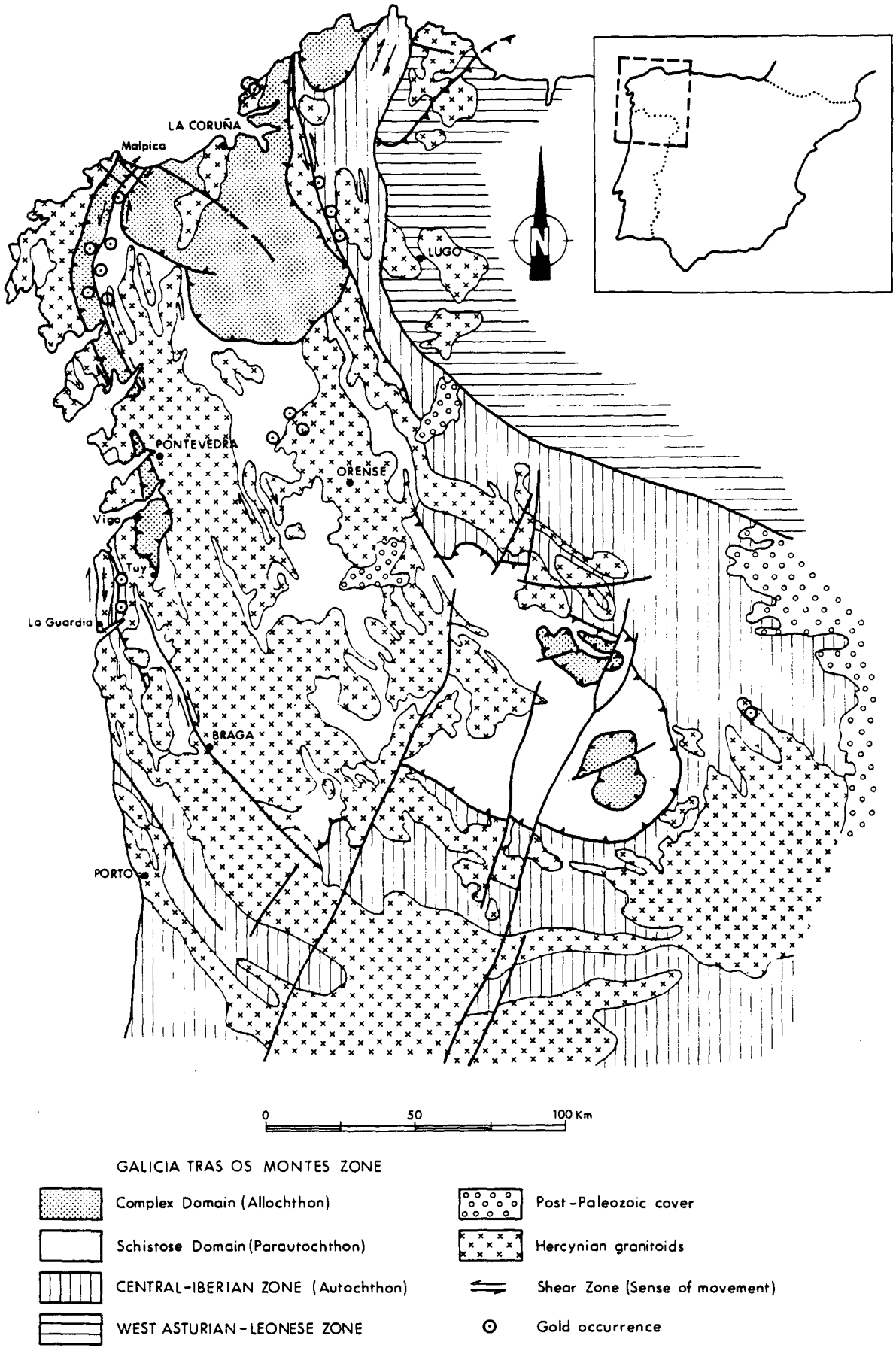

Fig. 4 : Major belts in the NW of Iberian peninsula with indication of the main structures and location of hydrothermal gold occurences.

pit, and in recent time, was made a shaft of 35 m depth and galeries from it, of a few tens of meters.

There is not much available information about ore reserves and grades. In relation with quartz-veins of Corcoesto area, Revista Minera (1900) refers a average gold content of 24 g/t, and Macia (1983) refers a possible ore reserves of 227 000 t with 16.7 g Au/t.

About the genetic and structural control of gold mineralization, several studies and hypothesis have been realized in the last years : Iglesias (1980) studied some of the Hercynian ductile shear zones of North Western Iberian Peninsula, defining, between them, the dextral Malpica-Vigo shear zone. Gouanvic (1981) relate the gold ocurrences of the Northwest with shear zones. Castroviejo (1990) explains the origin of gold ores of Fervenza area (South of Corcoesto) in terms hydrothermal discharge, associated with mainly brittle deformation and possibly related to granitic magmas. Pages (1992) describes the structural control of gold mineralization in the mylonitic shear zone Busto-Limideiro (Santa Comba, La Coruna).

Several old historians, since Possidonius and Plinius, had emphasized the mineral wealth of Hispânia and refer roman works, subsequent to the "pacification". Today the situation is rather different, since no active mines exist in Portugal and Spain although auriferous veins and placers had been exploited in the past.

Northern Portugal (Fig. 5)

The Jales mine, on Vila Pouca de Aguiar region (Trás-os-Montes), was exploited since roman times until the end of 1992, the only Au-Ag active mine in the Iberian Peninsula, exploiting hydrothermal quartz veins N20-40E, 65NW-90-80SE (Campo and Desvio veins). From 1933 to 1989 this mine produced about 25 tons of gold and 100 tons of silver. In 1990, the production of gold-silver as sulphide concentrates amounted to 1327 t. Drill cores up to 120 m below level 16 (the deeper level at 620m) show that the mineralization and the veins present the same characteristics. Between levels 3 and 15 the "tout-venant" of 1m width averages 12,9 g/t and there is a Ag/Au ratio of 3,6. (Neiva and Neiva 1990).

Somewhat more northwards of Jales, the Três-Minas roman open-pits are located, where impressive explorations judged by the size can be observed. There exist three open-pits (cortas) Covas, Ribeirinha and Lago Pequeno; Ribeirinha is the bigest one with 350m x 110m x 100m (height) corresponding to 9,45 Mt of "tout-venant", and Covas with 480m x 60m x 80m corresponding to 6,20Mt.

In spite of the importance of gold mineralizations, illustrated by the two referred examples, not many studies have been realized on gold metallogeny. Among the first studies, reference is made to Neiva (1945) describing gold mineralizations from Minho and Cerveira (1947,1952) describing mineralizations of Beira (Escádia Grande) and Trás-os-Montes (Freixeda). Both authors relate the Au mineralizations with magmatic differentiation by fractional crystallisation of a granitic magma of calc-alkaline chemistry during the Permian. Cerveira (1952) proposed a relationship between gold and tungsten mineralizations.

Brink (1960), studying the Jales area, proposes two metallogenic periods: the earlier gold-silver related with two mica granites ("older granites" 308 Ma.) and the tungsten one related with later biotitic granites ("younger granites" 290 Ma.).

Schermerhorn (1981) considers an Autunian age to the gold mineralizations and concretely considers the Jales deposit to be genetically linked to the "younger granites".

Thadeu (1989) says that the gold mineralizations are accepted as being Hercynian (in age) and related to Hercynian granites. However, their age and what type of granites are linked, are matter of discussion.

More recently, Neiva and Neiva (1990) and Neiva (1992) also suggests a genetic relationship of Jales Au-mineralization with hydrothermal fluids of late stages of fractional crystallization of two-mica granites. Also, the Au (Sb) mineralizations of Valongo (Porto) area have been ascribed to the late-tectonic biotitic granites, to later hydrothermal activity and remobilisation of Sb-Au in older metassediments (Ferreira 1971, Couto et al. 1990).

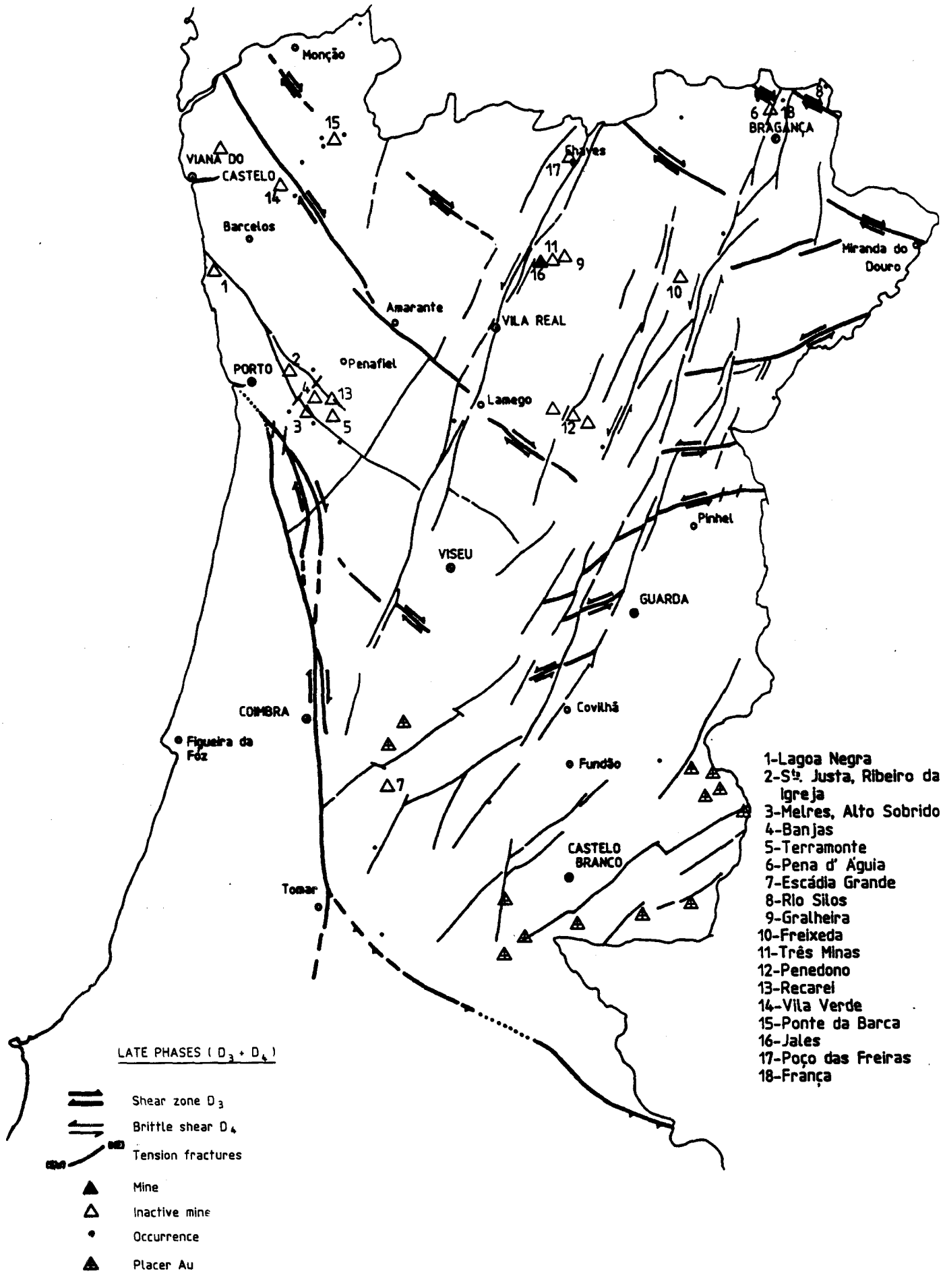

Fig. 5 : Au occurrences and mines in the C.I.Z. (Portugal)

However Oliveira and Farinha (1987) and Oliveira(1990), relatively to Três-Minas, considered that the gold mineralizations are associated with hydrothermal systems of siliceous character and does not reject the possibility of gold occurrences being "related to ancient sedimentary processes (paleoplacers?)".

The gold mineralizations are generally regarded as Hercynian but their origin and age are still not clear.

We must envisage a different role for the Hercynian granites relatively to gold mineralizations. Not excluding the possibility of pre-concentrations in Paleozoic metasediments, its stock-metal can be remobilized during deformation and metamorphism and, consequently, the main role of the granites, in case of being decisive, consisting on the mobilisation of the pre-concentrations and the fluids, was more of activating rather than mineralizing.

D- Methodological approach

Conditions of ore formation may be estimated through multidisciplinary characterization of wall-rocks, paleofluids, paleopathways, traps, deformation and ores. The project includes the following steps :

1- Regional, field and mine studies of the enclosing formations.

Main study cases are presented in Figure 6. Detailed geological, petrological, geochemical, and structural characterization of each study area chosen will be carried out :

- analysis of the ore zone geometry, by mapping, geochemical studies, short (ITGE) and deep (RTM) drillings, and structural studies of main fault systems.

- characterization of the surrounding rocks by mineralogy, major and trace element geochemistry, studies of geochemical halos around ores.

2 - Laboratory studies

Most of the gold is borne by quartz veins or veinlets containing sulphides (dominant arsenopyrite, locally accompanied by pyrite, stibnite, or galena (Vila Pouca, França). Ore veins develop sometimes rock alteration, such as greisens (mineralized) in the Pino granites, silicification and muscovitization in Montemor, and quartz - carbonate - (Fe) chlorite ± sericite ± pyrite in França.

These Au bearing quartz veins are characterized by fairly complex succession of quartz crystallization, deformation, and healing. The chronology of ore deposition, fluid migration and trapping in relation with the deformational events is in general difficult to establish using standard techniques (e.g. optical microscopy for instance). Therefore, it is necessary to develop a multidisciplinary approach yielding to a complete characterization of the paleofluid pathways, the reconstruction of physical-chemical conditions, and the identification of the gold-bearing assemblages :

- paleofluid pathways : in selected areas, a characterization of the geometry (dip, orientation, density) of cracks, fluid inclusion trails, and veinlets will be carried out on oriented samples.

- P-T-X-V reconstruction of the properties of migrating fluids could be derived from data obtained by combining results from microthermometry, Raman spectroscopy (Dubessy et al, 1989) and H-P ion chromatography on fluid inclusions (Bottrell et al, 1988, Grant et al, 1990).

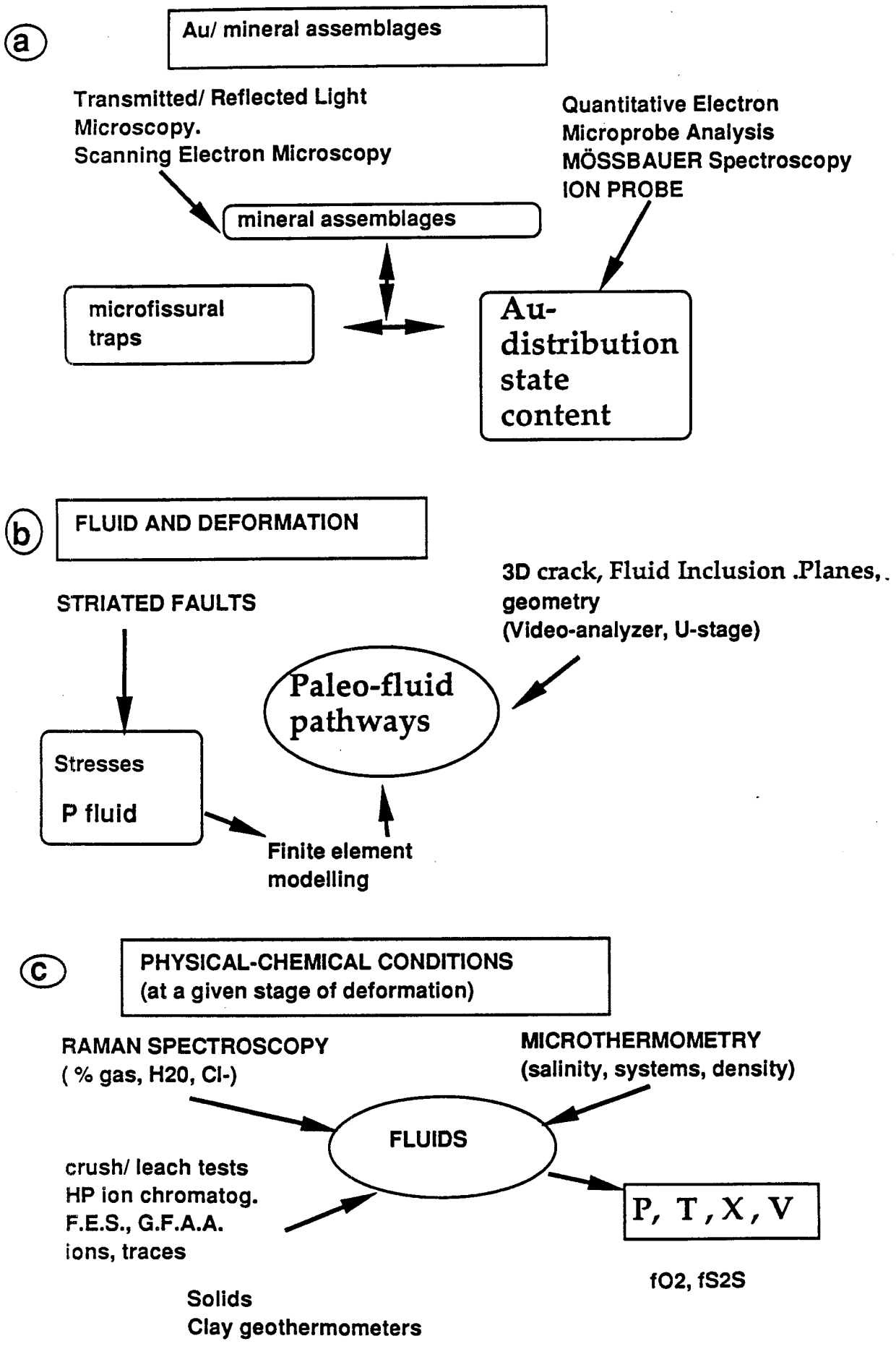

Fig 6 : Schematic representation of the methodological approach followed at the laboratory. a : mineral assemblage characterization, b : relationships between host minerals deformation and gold deposition, c) determination of the physical - chemical conditions.

- characterization of the geometric traps for gold, and the relationships between gold and sulphides, especially arsenopyrite. As arsenopyrite (and pyrite) represents one the most common host mineral for gold, research will be focused on the improvements of the characterization (distribution, state, content) of combined and metallic gold in such minerals.

Such data will help the setting up of metallogenic models, and the reconstruction of the successive stages necessary to get economic ores (Boiron et al, 1989). This project tried to stimulate interactions between regional studies, industrial research and laboratory approaches. This has been helped by the experience of both teams in most aspects of this works.

I- INDIVIDUAL DESCRIPTIONS

AU MINERALIZATION IN GRANITES

The major district studied is the Malpica-Tuy shear zone with two zones :

Corcoesto (North Westren Galicia, Spain: Rio Tinto Minera), characterized by an intense subparallel faulting and microfracturing of sandwiches of granite bands and metamorphic series. This is one of the major scientific and technological objectives of the contract which includes a deep drilling.

Tomino (South Galicia, Spain, ITGE), where the granite is affected by an intense microfracturing accompanied by strong water-rock interactions of relatively high temperature (greisens)

Two other granites have been studied for some complementary features :

Penedono (Central Portugal, DGGM), where quartz-arsenopyrite veins and alteration envelopes display in some places relatively high Au contents

Pino (Zamora province, Spain, ITGE), characterized by a complex superimposition of ductile to brittle deformation of the granite, and Au-As concentrations associated with early subsolidus alteration (albite episyenite).

A- CORCOESTO (RIO TINTO MINERA PROSPECT)

1-GEOLOGICAL SETTING AND ENVIRONMENT

a-The early exploration

The north-western part of Spain has been considered as a gold rich area since Roman times. Roman exploitations have been active without interuption since the first century before J.C to the third century after J.C in this region. The second stage of exploitation begun in the XIXth century by english and french companies. The third stage of activity is linked to the new gold exploration which started in the seventies (ERT, Consolidated Gold fields, followed by ADARO, BRGM, and Rio Tinto Minera S.A.).

The Rio Tinto Minera s.a company has developped series of exploration campain in the Malpica region. In the Corcoesto zone, after a first geological and structural mapping, a series of four drillings have been made in order to evaluate in depth the potentialities of a thin mineralized band of granite. The increase of the average value of Au content in this band with depth has encouraged the company to carry out a deep drilling crosscutting the mineralized granite at a probable depth of around 300 to 400 hundred meters.

b-Regional geology

The Corcoesto area belongs to the northern part of the major deformation zone , so-called Malpica-Tuy shear band in Galicia (Spain) (Fig I-1). This major shear zone is underlineated by series of syntectonic granite intrusions formed during the D3 deformational stage. This area belongs to the axial zone of the Hercynian belt. The general curved feature of the major structures, already mentionned in the introduction, are the result of two main superimposed tectonic stages : i) the early (370-335Ma) is responsible of the wide flat folds in the autochtonous units; folds are kilometric and dip to the east or the south-east in direction of the inner part of the arc (Bayer and Matte, 1979, Iglesias et al., 1983) ii) the second phase (D3) is homoaxial of the first phase, and develops vertical and restricted folds, with axial planes dipping towards the west (Marquinez, 1982). Syntectonic granites are associated to the second deformational stage, and calc-alkaline granites postdate the stage D3 (Capdevilla and Floor, 1970, Capdevila et al., 1973, Carneciro Gomez, 1982). The Corcoesto pluton, south to the

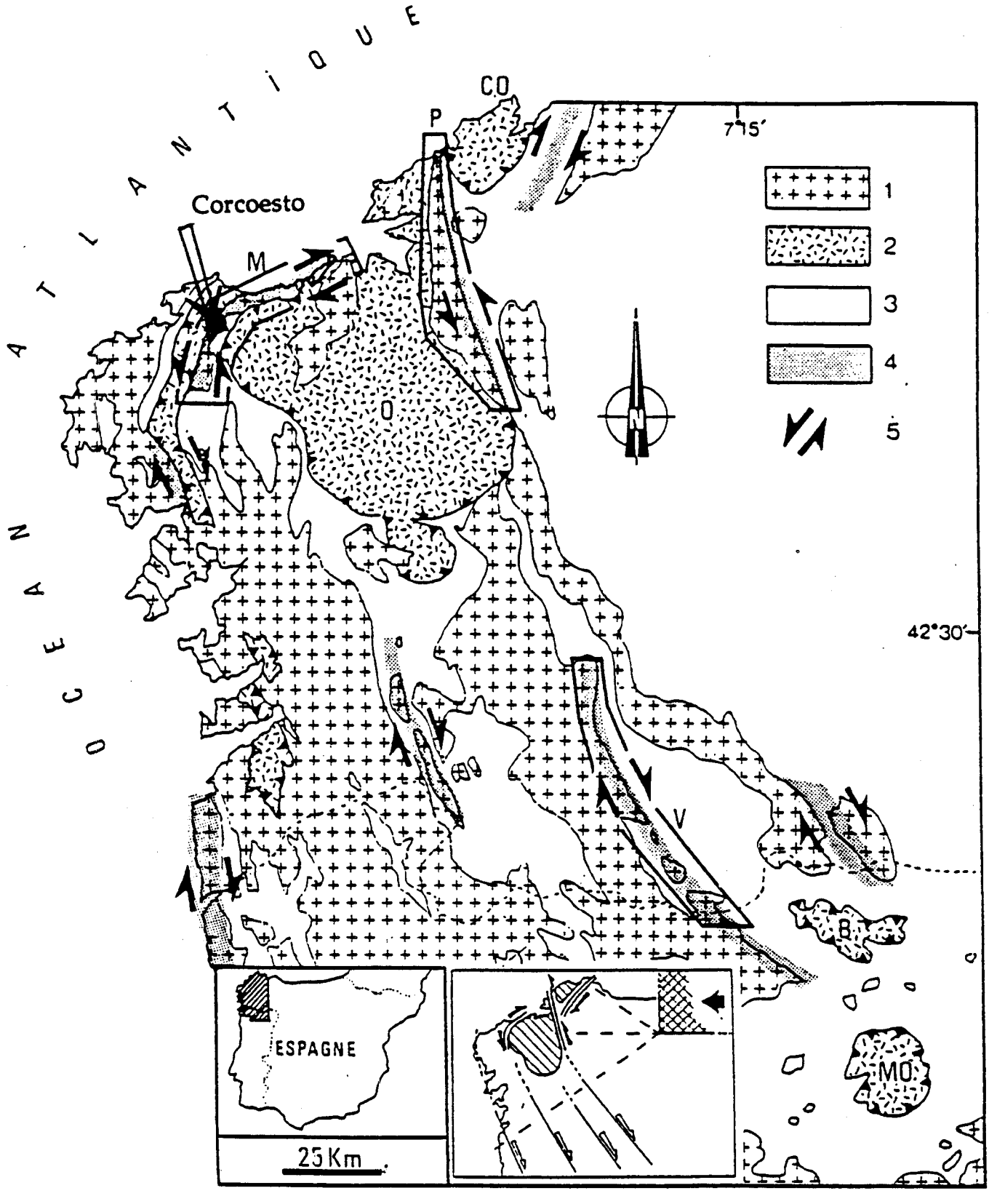

Fig. I- 1 : Location of the Corcoesto area with indication of the different granites and ductile shear zones in Galicia (Courrioux et al, 1986).
1 - Hercynian granites; 2 : Basic complex (CO : Cabo Ortegal, O : Ordenes; B : Bragança, Mo Morais); 3 : Precambrian and Paleozoic metasediments; 4 : Ductile shear zones ; 5 : Shearing.

studied area, belongs to the late granites and is affected by ductile deformation due to a major transcurrent shear zone (Iglesias and Choukroune, 1980). The latter is a dextral shear orientated NNE-SSW, and results from an E-W compression of regional extent.

Most rocks of the Malpica-Tuy bands underwent a final episode of recrystallization under medium-pressure greenschist facies conditions. This episode has affected gneisses and orthogneisses without changing significantly the primitive mineralogies. Gil Ibarguchi and Ortega Girones (1985) and Diaz Garcia (1986) have described retrograde greenschist-facies parageneses with quartz-albite-chlorite-sphene and epidote in some orthogneisses from the Malpica Tuy shear band.

Main deformational stages

The studied granites are located north to the Corcoesto pluton along bands of variable width (1m to 1km). From the inner part of the Corcoesto pluton which is preserved from the deformation, towards the enclosing formation, the foliation (subvertical) tends to become parallel to the granite margin (Burg and Iglesias, 1985). Locally, conjugated shear zones may be observed.

The deformation of the Corcoesto granite is similar to the one observed in the granites associated to the south armorican shera zone (Berthe et al., 1979). The subvertical foliation (S) is defined by the mean flatening plane and by the orientation of micas. C planes are orientated at 5 to 35° from the S plane. Shearing is dextral (Berthe et al., 1979, White et al., 1980). Nearby the margin of the granitic batholith, the movements along the C planes are compatible with the general direction of shearing indicated by the "global" foliation planes oriented NE-SW (associations of C/S planes).

Veins and veinlets observed by Burg and Iglesias (1985) at the regional scale are considered as representative of the main shortening direction. They are perpendicular to the elongation direction, and form a relatively high angle with the foliation plane. These veins are interpreted as tension gashes normal to the extension direction and parallell to the main stress direction. These tension gashes could form in depth under high fluid pressure conditions (Paterson, 1978, Nicolas and Jackson, 1982). However, numerous quartz veinlets crosscut the foliation and some shear planes without any deformation. Their formation is thus later than the initiation of the propagation of the C/S planes; the formation of some quartz veins along the C plane has been explained as the latest sliding along the planes induced by the compression (Burg and Iglesias, 1984).

2-THE DEEP DRILLING

a- Realization (Rio Tinto)

Location

The map shown in Figure I-2 gives the emplacement of the drilling which crosscut vertically the series of two granite sills intruded within the N30° band of metamorphic series of Corcoesto.

Characteristics of the drilling

Field works at Corcoesto carried out by Rio Tinto Minera have consisted in the complete drilling of the deep drill hole using a Longyear-44 drill. The work begun the 9th of August and ended on the 23rd of October 1991, at a depth of 746.5 m.

The operating conditions were the followings :

- a motor Diesel (6 cylinders) 90 CV, a drill installed on a REO-KAISER 6X6 all purpose truck equiped with a Beam-Royal 535 (and then 820) pump ; the hydraulic system was impulsed by a PV-20 pump (210Kg/cm2 pressure; flow of 60 liters/minute). These equipments allowed operators to reach the following performances :
- 8.377kg; RPM : 1350, extraction : 11.179 kg, 15.570 kg.

and with a motor Diesel 20 CV :

- 130 liters/mn, maximal pressure : 60 kg/cm2.

- the drill core diameter was 116 B type B (101.7 mm diameter) for the 9 first meters.

These first meters were equiped by a tube of 104x113 mm, and the drilling continued with a "wire-line" system (diameter H), from 9 to 53.60m meters depth (63.5 mm diameter cores). Then the diameter of the drilling was reduced to a N size (47.6 mm) down to the final depth, by covering the initial tubes by HQ.

The drilling begun in August 1991 with the conventional system (116-B diameter, four operations of 0.8 m length to 3.2 meters depth, single lifting). The fresh granite has been reached then at 9 meters. After changing the drilling system to a wire line system, the depth of 14.2 m is reached after 3 operations, and continued down to 19.55 m depth where all the water was loss.

A tube (104x113) was thus emplaced by rotation down to this depth. The drilling could then continued down to 25.05 meters depth, and was covered again by the same tubing than above mentionned. Water loss at 26.0, 27.6, and 32 m depth obliged a tubing under the same conditions at these depths. Drilling continued with HQ down to 44 meters (new water loss), and then to 53.6 m with continued water loss where the rock was sufficiently fresh. The tube HQ was then emplaced down to this depth .

Each lifting was then around each 24.0 meters, down to 172.85 m where new water loss was noted. The second lifting was used at 364.95 meters depth. Most of the drilling continued under these conditions. A decrease in the drill speed was noted below 575.00m, where hard fresh rocks where encountered. The drilling crown was thus changed every 60 to 80 meters, down to the end of the drilling.

The drilling deviation was measured using a TRO-PARI equipment :

depth	slope
0 m	0°
150 m	0.5°
300 m	1.5°
500 m	2°
740 m	3.5°

Sampling

Oriented blocks have been sampled for a comparative study of microcrack networks at Corcoesto in surface and depth, and for a a comparative study of deformation styles in granites.

Sampling of the deep drilling (host rocks: granites, schists, and quartz vein types (barren or mineralized) have been carried out by CREGU (M. Cathelineau) and Leeds (D. Banks) at Rio Tinto in the end of November 1991.

b- General description of the well cores

logging, petrography (Plate I-1)

From the surface towards depth, the main lithological units are the followings (Fig II-3) :

- two sills of aluminous granites including porphyroid biotite-granite, and a series of peraluminous granites including leucogranites, garnet aplites and felsites.
- the enclosing rocks of the granite sills are metamorphic series mostly constituted of biotite-muscovite micaschists, displaying a foliation orientated N30°E diping around 50 to 70° W-NW
- at greater depth, biotite rich orthogneisses are found, intercalated with biotite granites.

Most granites display rather strong foliation, orientated parallel to the enclosing rock foliation plane. The granites show locally stronger ductile deformation indicating the permanence of shearings after their emplacement.

In most mineralized zones (the two granite sills), the dominant structures are thin quartz-arsenopyrite veinlets, displaying raher similar orientations . The geometry of the veinlet network has been carried out on the drilling cores, by measuring the angle bewteen the foliation

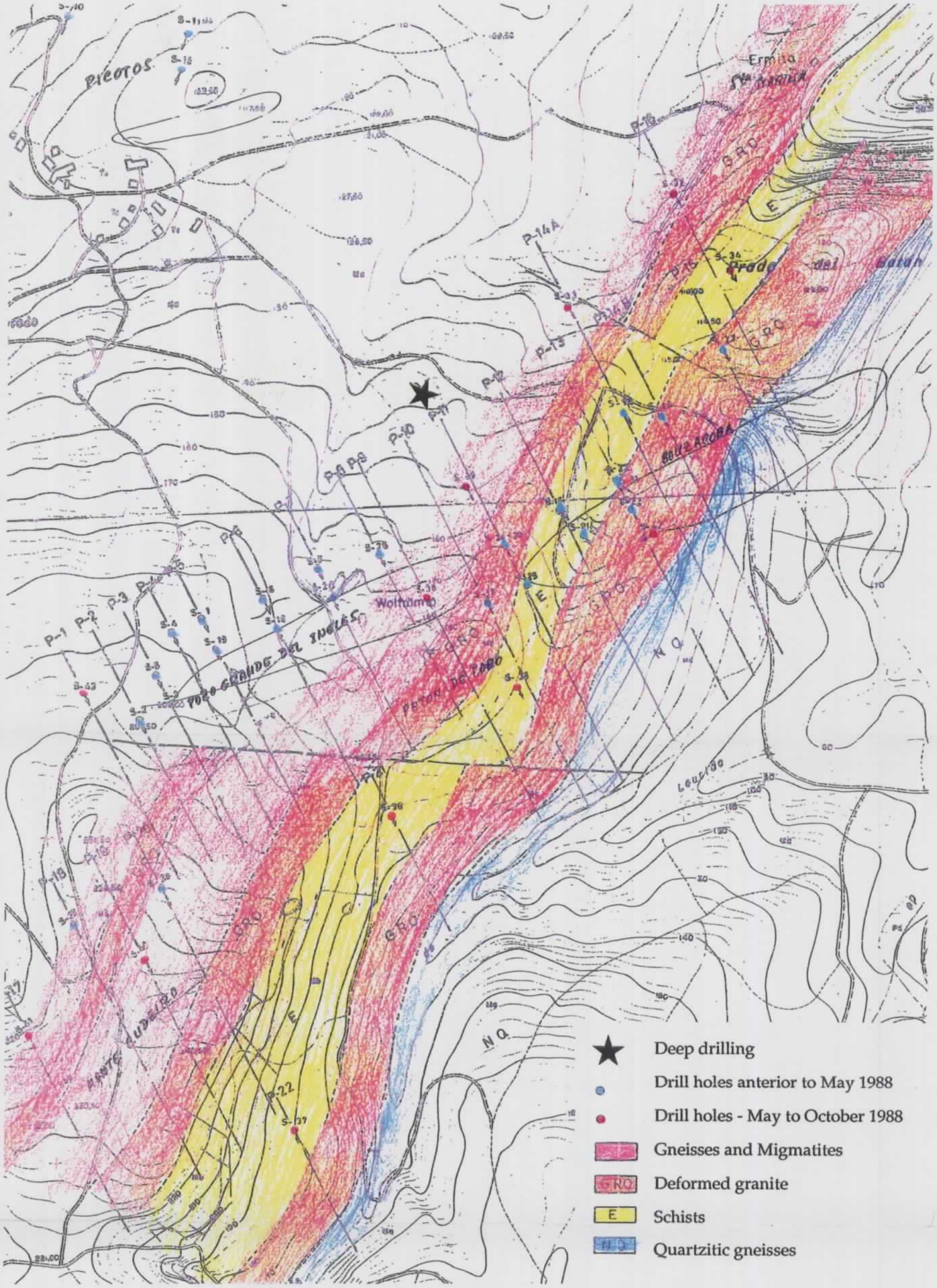

Fig. I- 2 : Geological map of the Corcoesto area with indication of the deep drilling and previous drill holes (1/5 000)

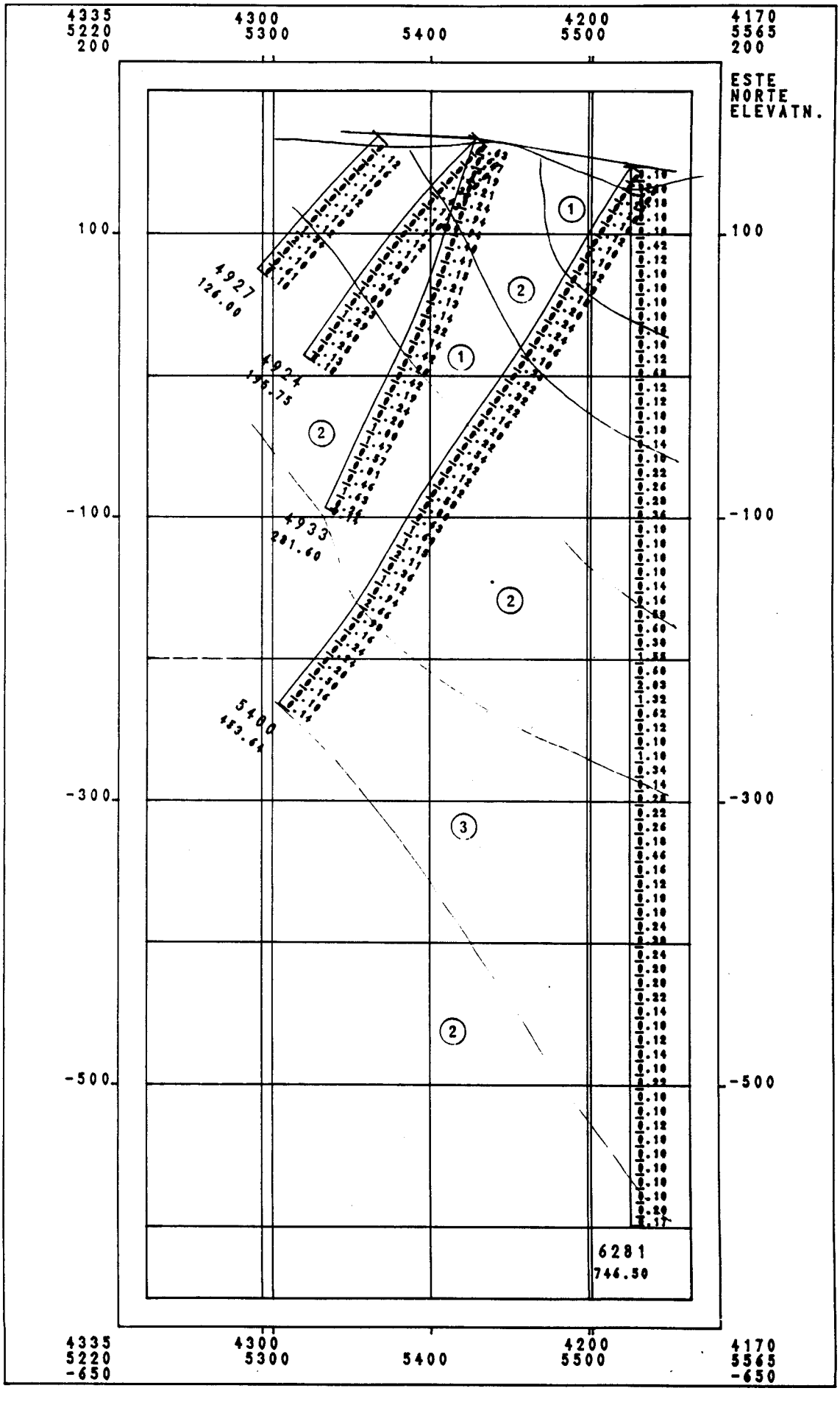

Fig. I- 3: Geological cross section of the Corcoesto drill holes with indication of the Au content (Au is given in ppm/ 10 meters). 1 : schist, 2 : oriented granite, 3 : gneiss.

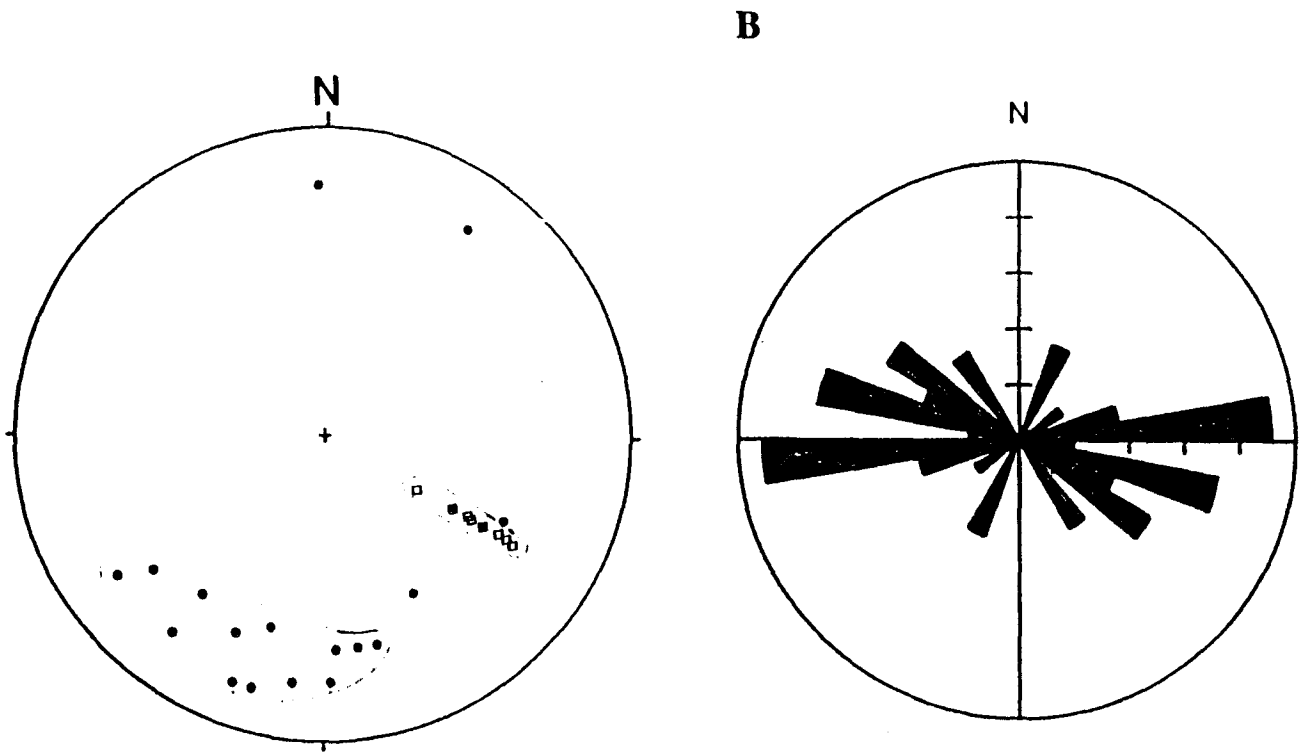

Fig I - 4 : A : Stereoplot of the orientation of the granite foliation (points) and the quartz veins (diamonds). B : Rose diagram showing the direction of the quartz veins from Corcoesto area.

plane (considered as constant around ≈ N30°E) and the quartz veinlets in horizontal sections. The main orientation are the followings (Fig.I -4):

- N30° E, nearly parallel to the foliation plane (dip : 50±10°W)
- N90° to N110°E, the E-W direction being dominant
- N150°, less frequent,

Most vein quartz dip to the NE. No change in the direction of the veins has been found with depth.

Trace element (Au, ...) geochemistry

On the deep drilling carried out for the EC program, representative samples of 2 meters long drilling cores have been systematically analysed for Au, Ag, S Cu, Pb, Zn, As (Rio Tinto Minera). Figure II-3 presents the distribution of Au values in the four early drillings carried out at Corcoesto, and the deep drilling as a function of the interpreted lithology. It turns out that most significative Au values are closely associated with the presence oriented granites, as shown by the figure I-5 showing the distribution of Au, As and S contents with depth. Au values reach a few ppm (up to 5 ppm) on 2 meters samples mostly in the second band of mineralized granite crosscut by the drilling. These values may be also correlated with the density of quartz arsenopyrite tension gashes. Therefore, the mineralization seems to be significantly controlled by the rock rheology especially the competency heterogeneities between granites and other metamorphic series. The distribution of As values shows clearly three enriched zones with constant values around 1500-2500 ppm although enclosing rocks display values around a few hundreds of ppm : the surficial levels (0-200m depth), and the two granites (Fig. I-5).

Values in other trace elements (Zn, Cu, Ag) are generally extremely low confirming that most of the mineralized structures are characterized by the presence of arsenopyrite-pyrite and gold without significant contributions of other sulphides.

Local enrichments in these elements correspond mostly to other or subordinate processes:

- Pb enrichments in the gneisses in the 488-538 m depth interval;
- sulphide enrichments (mostly pyrite) at 630-656 m depth;
- only 3, 25, and 3 samples over 373 display significant values in Zn, Pb, and Cu respectively. Contrary to many other deposits, there is very little amount of elements accompanying Au, at the exception of As.

The Au-S, Au-As, and S-As binary diagrams have been used the type of relationships between gold and sulphides. Examination of figures I 6 to 8 yield the following remarks :

- As-S diagram (Fig. I-6) : two types of trends are found : i) an S increase at low As values, which corresponds to samples dominated by pyrite (samples from 640 m depth) containing a small As content (around 0.5%). ii) the As-S correslation typical of the stoechiometry of the analyzed arsenopyites from Corcoesto : in these samples, arsenopyrite is dominant,. iii) several samples display S contents which are a litlle higher, indicating the presence of small quantities of pyrite (1% wt. pyrite) in addition of arsenopyrite.
- the Au-As diagram (Fig. I-7) shows clearly that the high Au content are not correlated to As and correspond to native Au particles; however, the highest Au values are found in samples rich in As. Considering the highest Au contents found by ion probe in arsenopyrite (combined Au), it turns out that Au is present at the metallic state at more than 90-95%.
- the Au-S diagram (Fig I-8) shows that the highest Au values are found in samples containing less than 1% pyrite, and arsenopyrite in the same amount than pyrite (around 0.5 to 0.7 wt% of both minerals).

c- Mineralogical features

Selected samples, every 10 to 50 m, with an increased number of samples in the mineralized areas display the following assemblages :

fresh granite mineralogy

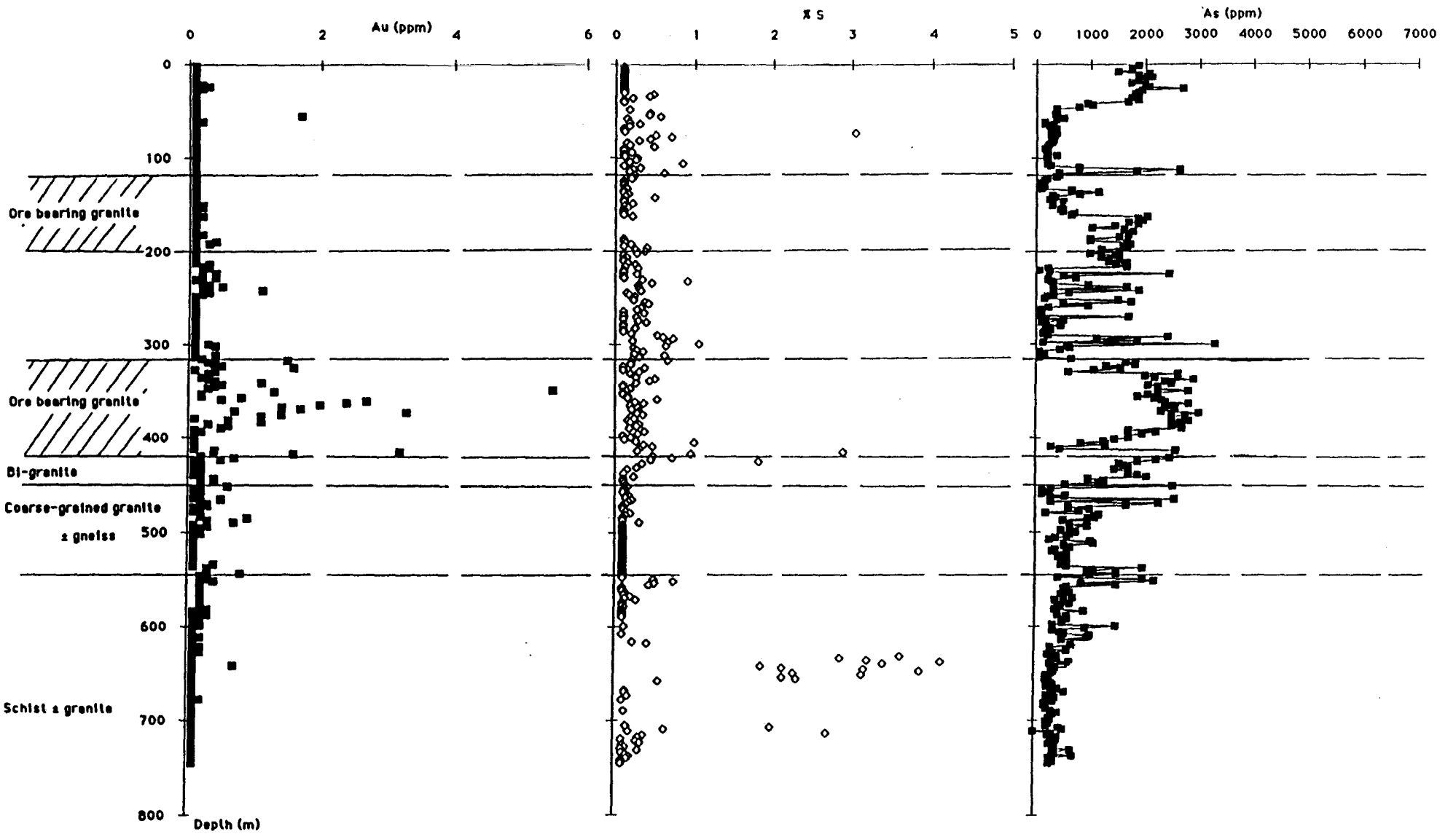

Fig. I- 5: Distribution of Au, S and As contents with depth on the deep drilling with indication of the petrographic characteristics of the rocks.

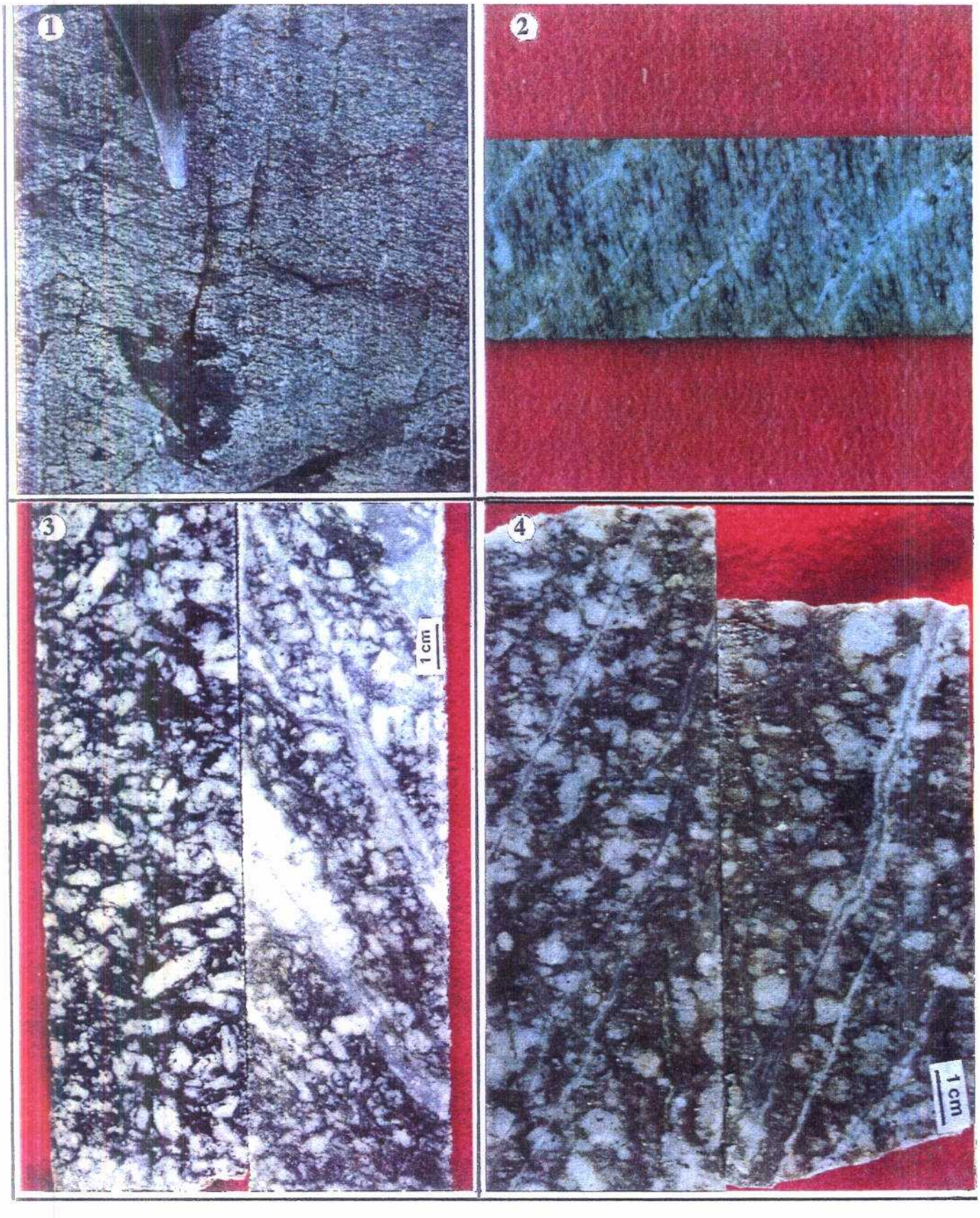

Plate I-1 : Macroscopic aspects of the quartz veins from Corcoesto area.
1 - Network of quartz veinlets in the granite (outcrop). 2- Series of tension gashes filled by quartz and arsenopyrite. 3- Fresh biotite rich granite with K-feldspar porphyroclasts croscut by quartz veinlets. 4 - Quartz veinlets in the granite showing the milky quartz Q1 followed by clearer quartz Q2.

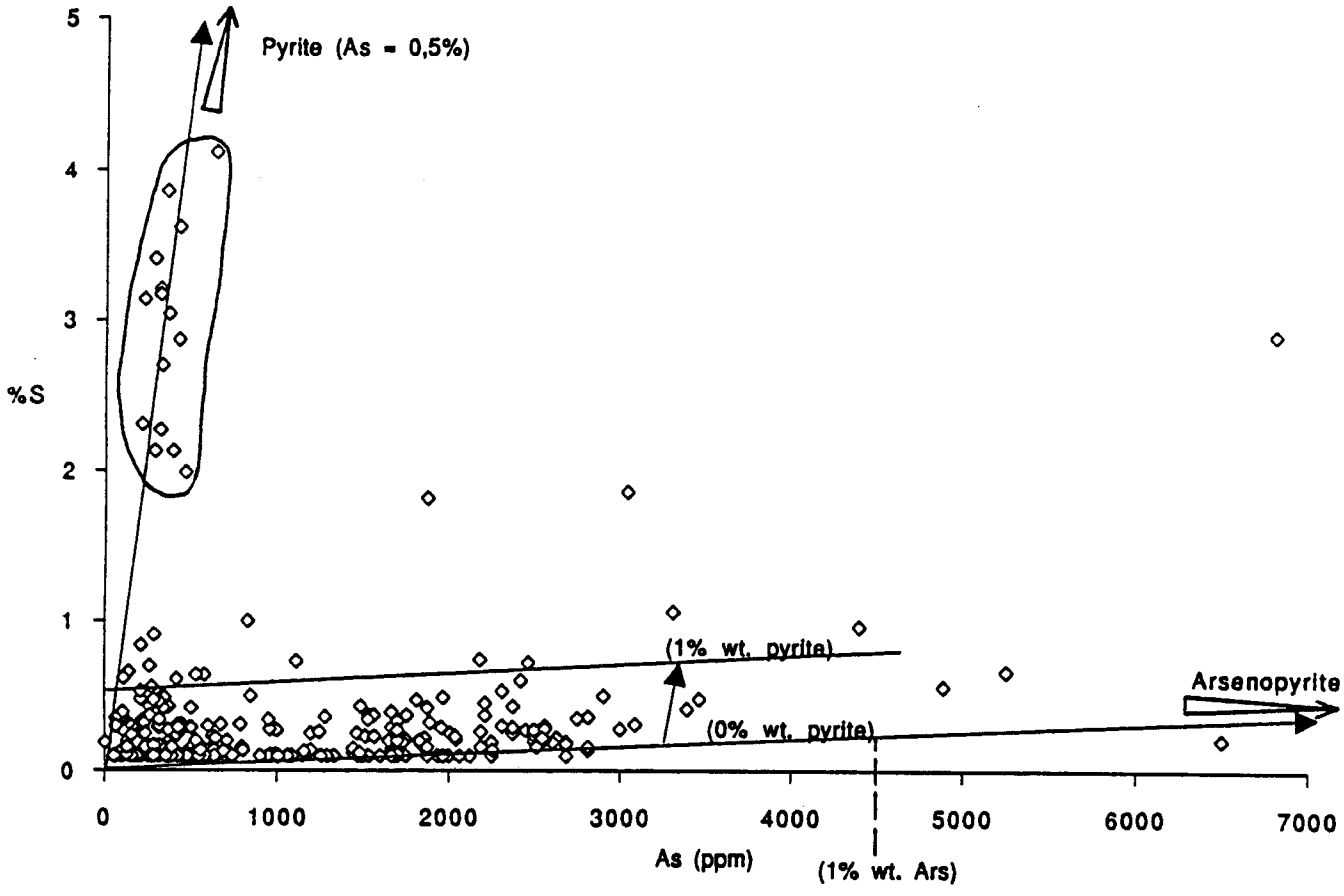

Fig. I- 6: S- As binary diagram applied to chemical analysis of samples from the deep drilling rocks.

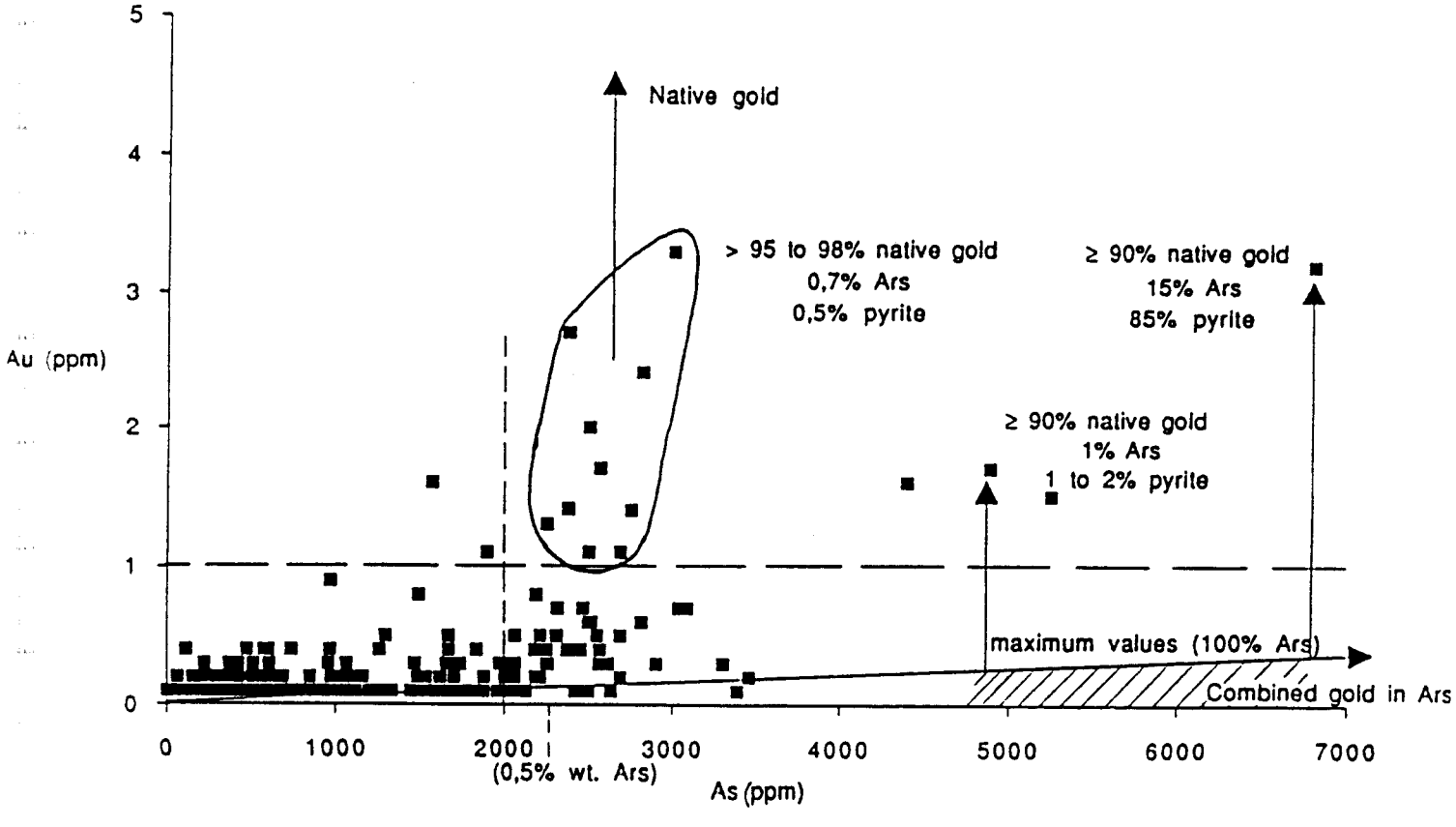

Fig. I- 7 : Au-As binary diagram applied to chemical analysis of samples from the deep drilling rocks. (Ars : arsenopyrite).

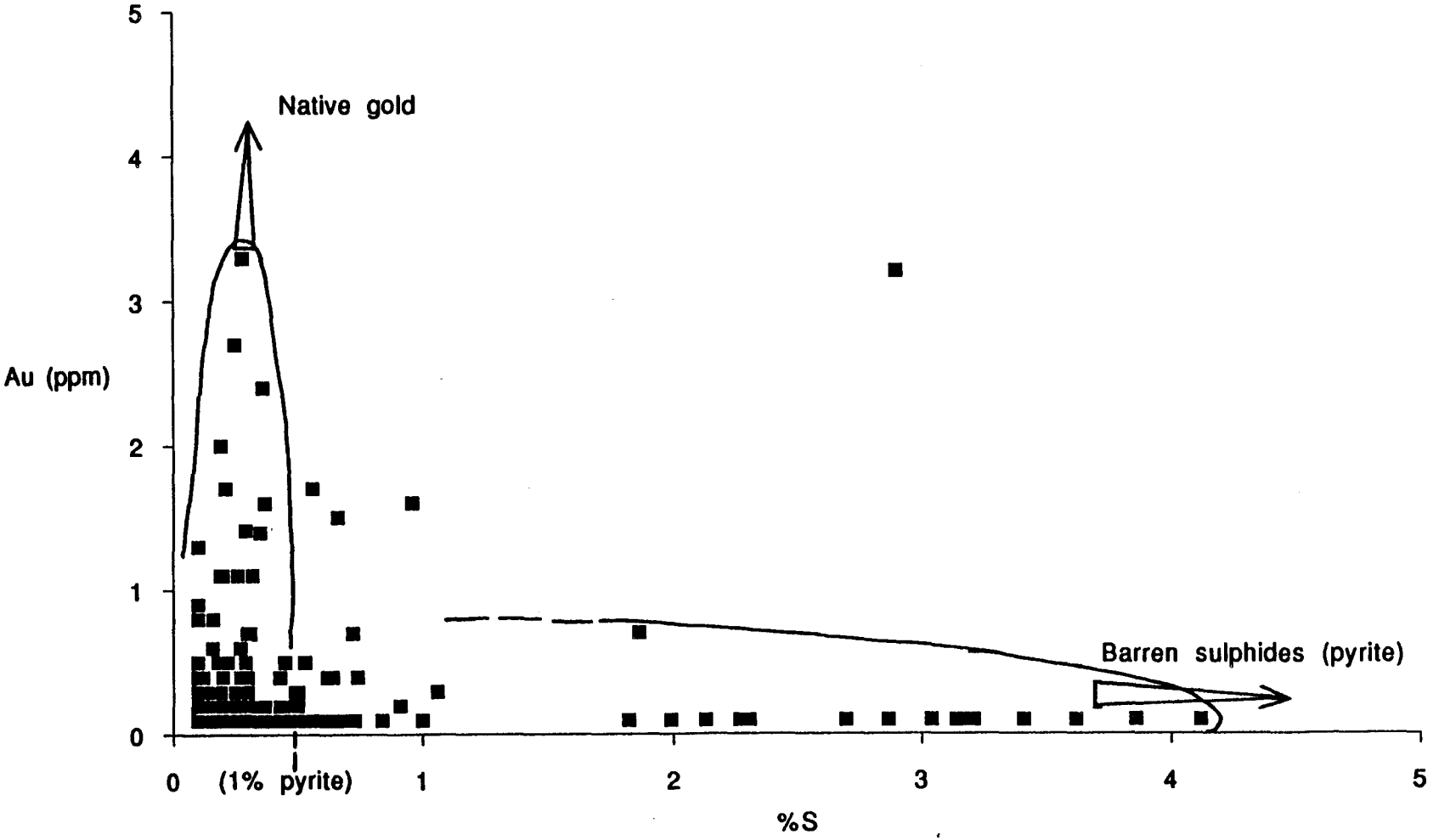

Fig. I- 8 : Au - S binary diagram applied to chemical analysis of samples from the deep drilling rocks.

Most leucogranites are extremely poor in biotites and display a deformed assemblage with segregation of quartz layers, and feldspar - muscovite layers, accompanied by garnets in some instances.

Biotite granites are rich in biotites, contains K-felspars porphyroclasts, and display distinct degrees of deformation.

ore assemblages

The ore assemblages are extremely constant at the scale of the whole drilling. Most mineralized areas are characterized by the presence of :

- i) early quartz veinlets with no sulphides, of relatively large thickness (a few centimeters) compared to the dominant veinlet;
- ii) disseminated arsenopyrite crystals within the host rocks which are difficult to relate to a specific stage;
- iii) the major quartz veinlet network is made of quartz-arsenopyrite resulting from multistage quartz deposition :

Q1 is composed of xenomorph agregates of milky quartz, containing frequently great quantities of tiny fluid inclusions;

Q2 is clearer that Q1 and ends with clear growth zones, sometimes developed in cavities with euhedral shapes;

Q3 is a very clear quartz wich cements the arsenopyrite crystals, or develops as euhedral quartz prisms.

- iv) later stage assemblage are composed of thin (100 μm) veinlets where the following succession is recorded : illlite/ calcite-quartz-chlorite.

alteration minerals

In mineralized areas, two cases are distinguished :

i) quartz-arsenopyrite rich zones : they are characterized by the nearly lack of alteration, no changes being observed in the wall-rock of the veinlets. The quartz-2feldspars-biotite association is especially stable, indicating rather high temperature conditions for the vein formation.

ii) bleached zones

In the richest zones in quartz-arsenopyrite veinlets, a bleaching of the rock is frequently observed. It is linked to the disappearance of the biotite and its replacement by chlorite accompanied in some instances by phengites. The bleaching is also accompanied by the alteration of plagioclases to K-micas.

Locally, some brecciae display more complex association (414 m depth for instance) :

- strong early alteration (albitization)
- phengite crystallization in association with arsenopyrite,
- strong K-mica developments (small K-micas platelets)

In conclusion, the sequence of hydrothermal events at Corcoesto has a rather simple expression compared to other deposits, even if some complexity appears locally. The homogeneity of the As mineralization (quartz-arsenopyrite veinlets with no wall-rock alteration) followed by a discrete overprint by a later hydrothermal probably responsible of the Au enrichments (chlorite-phengite/ carbonate stage) is remarkably distinct from most known deposits in the Variscan range.

This deposit therefore displays unusual features characterized by : i)the huge volume of rocks affected by the process, ii) the amount of As, Au deposited, even at relatively low contents (average Au values around 1-2 ppm), iii) the homogeneity of the processes at the scale of the observations

This concentration seems to have suffered of the lack of tectonic reworkings to get abnormal concentrations necessary for a today economic exploitation. However, it can be considered as one of the biggest Au-As targets at the scale of the Variscan range, such as the Villeranges-Chatelet zone (Boiron et al., 1989), the Salsigne district (Tollon, 1969), or the Mokresko-Celina (Moravek, et al., 1989) in Tchecoslovaquia.

B - TOMINO AREA

1 - GEOLOGICAL SETTING

Tomino area is located in the NW part of the Iberian Peninsula, southwestern end of Pontevedra province, limited southwards by the portuguese border.

Geologically, the area is situated in the NW of the Hesperian Massif, within the Central Iberian Zone following the classical division of Julivert et al, (1972) (Fig.I-9). According to the new division proposed by Farias et al., (1987), it belongs to the Schistose Domain of Galicia-Tras-Os-Montes Zone. Two major transcurrent ductile shear zones are flanking the Tomino area : the Vilanova de Cerveira - Cernancelhe shear zone in the eastern side, and another one that extends parallel to the western coast.

Gold bearing occurrences are located within a generally North-South trending belt of lower Paleozoic metasediments, intruded by hercynian granitic bodies and bounded eastern and western by extensive granitic massifs.

2 - LITHOSTRATIGRAPHY

The metasedimentary series has been divided into several lithostratigraphic units, which are, from the bottom to the top :

- Slate and greywacke Complex - Douro Group

The oldest rocks occurring in this area belong to the upper part of the pre-Ordovician slate and greywacke complex (Teixeira,1955), also known as Douro Group (Sousa,1982), for which an upper Precambrian to Cambrian age is estimated.

It consists of grey micaschist showing reddish weathering colour, with metasandstone, quartzite and quartzose metaconglomerate intercalations.

The outcrops of this unit along the schistose band are relatively small. It appears in a narrow zone along the western side of the band, and in the core of Tabagón Antiform.

The Douro Group is usually unconformably overlain by the Lower Ordovician formations in Portugal. In this area, the existence of this unconformity, although not evident, can be assumed.

--Santa Justa Formation

The Santa Justa Formation, mostly of Arenig age, was defined by Romano and Diggens (1973-74) in the Valongo Anticlyne region, in Portugal. This unit is made up of white-yellowish and reddish metasandstones, with some quartzite and schist intercalations, and several centimetric garnetiferous beds. Cross lamination and graded bedding are occasionally observed in metasandstones and quartzites.

It exhibits a thickness of 170-180 m in the Tabagon Antiform, whereas along the western side of the schistose band, it is represented by a discontinuous quartzite bed no more than 40 cm thick.

--Valongo Formation

This formation was also defined by Romano and Diggens (1973-1974) in the same area as the former, where it has been dated as Llanvirn- Llandeilo

In the Tomiño Area, the characteristic lithologies of this unit are dark-grey micaschist and schist bearing abundant greyish andalusite porphyroblasts.

The maximun thickness is about 100 m, in the southern part of the band, decreasing gradually to the north. In the northern edge (Monteferro Peninsula) this unit is 20 m thick.

- Monteferro Schist

This unit takes its name from Monteferro Peninsula, where a representative section can be observed. It is composed of alternating grey and brown schist, metasandstones and micaschist. Some graphitic phyllite and schist, and quartzite intercalations also occur.

It appears in graduate contact over Valongo Formation, and shows significant variations of thickness, specially in the Tabagón Antiform sector. The maximun thickness is about 300 m.

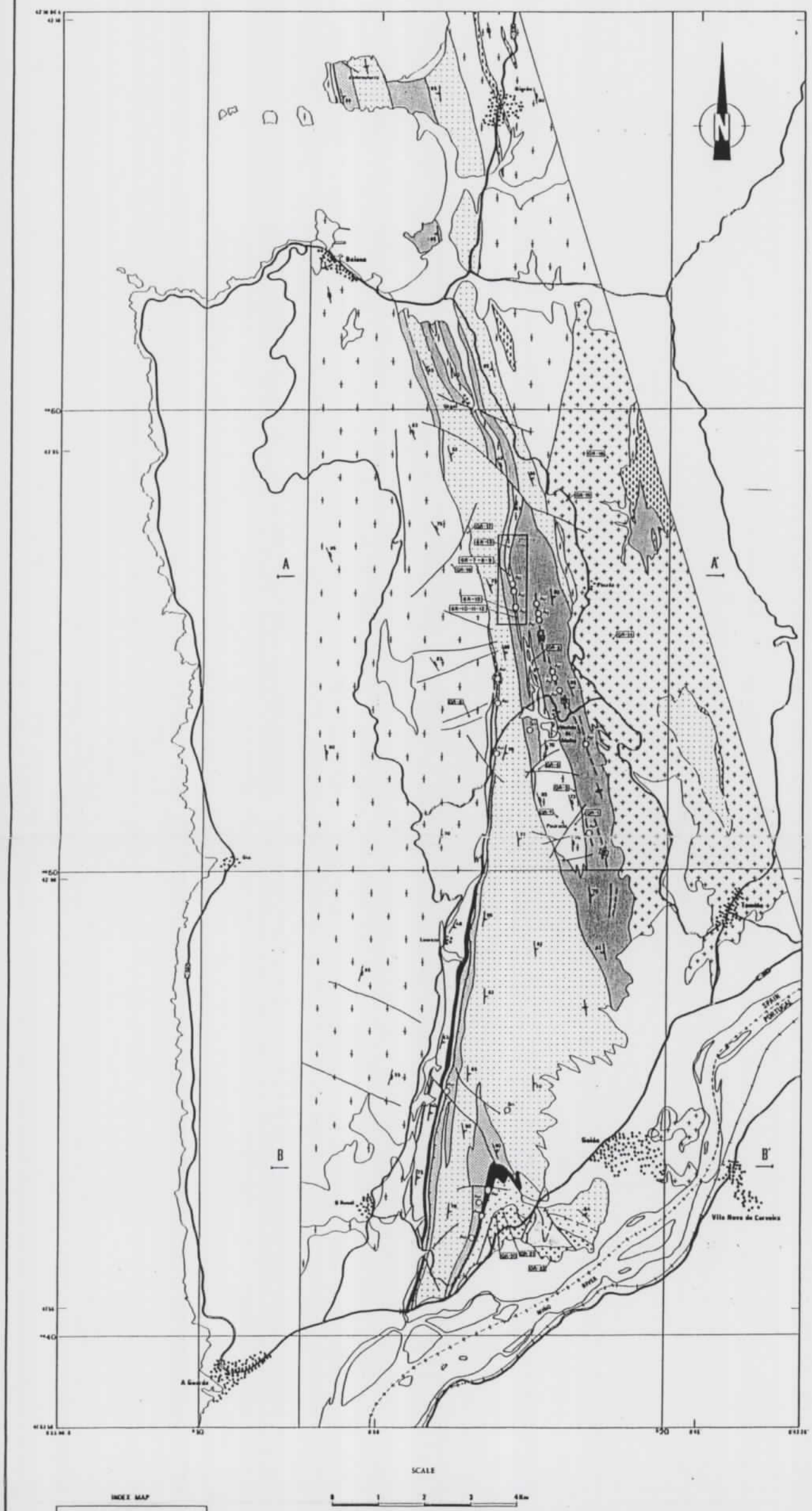

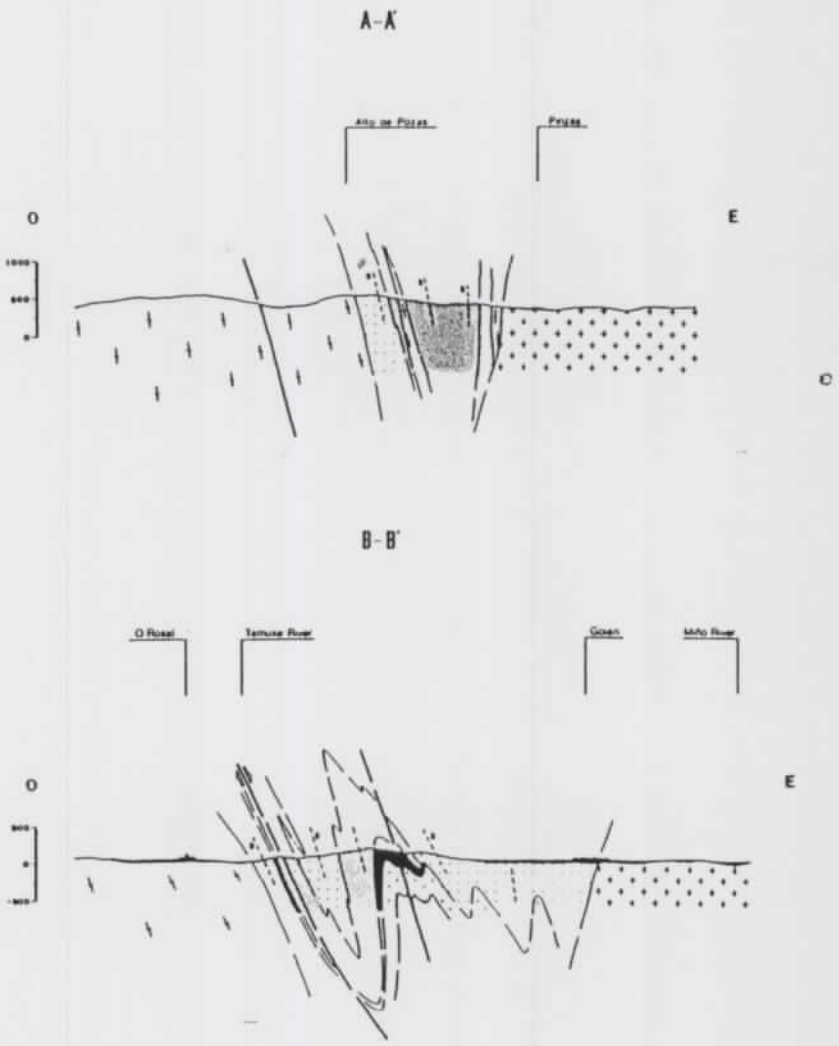

LEGEND

QUATERNARY

7 Recent deposits

PALEOZOIC

ORDOVICIAN – SILURIAN

6 VILACHAN SCHIST
Grey schist and micaschist with graphitic filite and schist intercalations

5 ARGALLO MICASCHIST
Grey, frecuently andalusitic, micaschist

4 MONTEFERRO SCHIST
Alternating schist and micaschist, with some quartzite and graphitic schist intercalations

3 VALDOXO FM.
Dark-grey andalusitic micaschist and schist

2 SANTA JUSTA FM.
White, grey and reddish metasandstones and schist with some quartzite intercalations

CAMBRIAN

1 SLATE AND GREYWACKE COMPLEX (DOURO GROUP)
Grey micaschist with schist, metasandstone and metaconglomerate (cg) intercalations

IGNEOUS ROCKS

LATE TO POSTECTONIC GRANITOIDS
- Biotite granite ± muscovite
- Two-mica granite

SYNTECTONIC GRANITOIDS
- Two-mica granite
- Early granodiorite

SYMBOLS

- Lithological contact
- Fault
- Normal fault
- Brittle-ductile shear zone
- Foliation
- Vertical foliation
- Foliation in granitic rocks
- Vertical foliation in granitic rocks
- Gold (Au) and tin (Sn) mineral occurrences (old workings)
- Location of sample
- Alto de Pozas sector

Fig. I - 9 : Geological map of the Tomino area, (1/10 000)

- *Argallo Micaschist*

This unit is essentially made up of homogeneous grey micaschist with brown-yellowish weathering colours, sometimes with sandy laminations. The lower part usually bears abundant andalusite poikiloblasts.

It outcrops extensively along the Argallo Range, with a estimated thickness of 200 to 300 m.

In the eastern limb of Tabagon Antiform, the lower contact of Argallo Micaschist cuts gradually from the N to the S the underlying formations of Monteferro Schist and Valongo Fm., up to be located just in contact with Santa Justa Fm.; this fact suggests the possible presence of a cartographic unconformity below this unit.

-*Vilachan Schist*

In the upper part of the metasedimentary sucession, there is a unit composed of grey schist and micaschist with frequent graphitic phyllite and schist intercalations of decimetric to metric thickness. Some scarce calc-silicate beds have also been observed.

The most representative outcroppings of this unit are located between Vilachan and Vilachan do Monte, and the maximum thickness that can be observed is around 500 m.

The corresponding lithology in Portugal have been dated as Silurian (Llandovery-Wenlock), according to the graptolite associations contained in graphitic beds (Romariz, 1969).

3 - GRANITIC INTRUSIONS

Two main types of peraluminous granitic rocks occurs in this area: two mica granites, syntectonic in relation with the third phase of Hercynian deformation (D3)(La Guardia, Pedrada and Urgal granites), and late-tectonic granitoids in relation with D3 (Tabagón and Pinzas granites). Pegmatitic and aplitic dykes are abundant. A third intrusive body was intercepted in a deep drill hole (DDH).13, althouth is not exposed in outcropping (Alto de Pozas granodiorite) (Fig I-10).

La Guardia granite is emplaced in the western side of metasediments band, while the main part of the eastern border is occupied by the Pinzas granite.

The metasediments band is intruded by the Pedrada, Urgal and Tabagon granitic bodies:

- the Pedrada massif, intruded in the central part of the metasediments, as a granitic stock of elongated shape of about 4 km2.
- the Urgal granite is emplaced in the northern extension of Pedrada massif, as a dyke of about 10 km length, parallel to the regional structures, with width ranging from about 20 m in the southern end to more than 150 m in the northern end. The central part of this dyke (Alto de Pozas) hosts the most important mineralized quart vein systems, which have been studied in detail .
- the Tabagón granite occupes the core of a anticline in the south end of the metasediments.
- the Alto de Pozas granodiorite was found in DDH.13 at 270 m depth, appearing to be intruded by the Urgal granite dyke.

In Table I-1 are summarized the main characteristics of this group of granites.

4 - TECTONIC AND METAMORPHISM

The rocks in this schistose band show a strong deformation produced during Hercynian orogeny. Two main tectonic phases can be distiguished, corresponding to the first and third regional phases (D1 and D3).

The most significant structures on all the scales are attributed to D3. They are tight to isoclinal folds, with subvertical axial plane or with a slight vergence to the W, and hinges usually dipping northwards. There is also an axial plane foliation (schistosity type) associated to these folds, widely developed in the schistose band; locally, it can be seen as a crenulation cleavage.

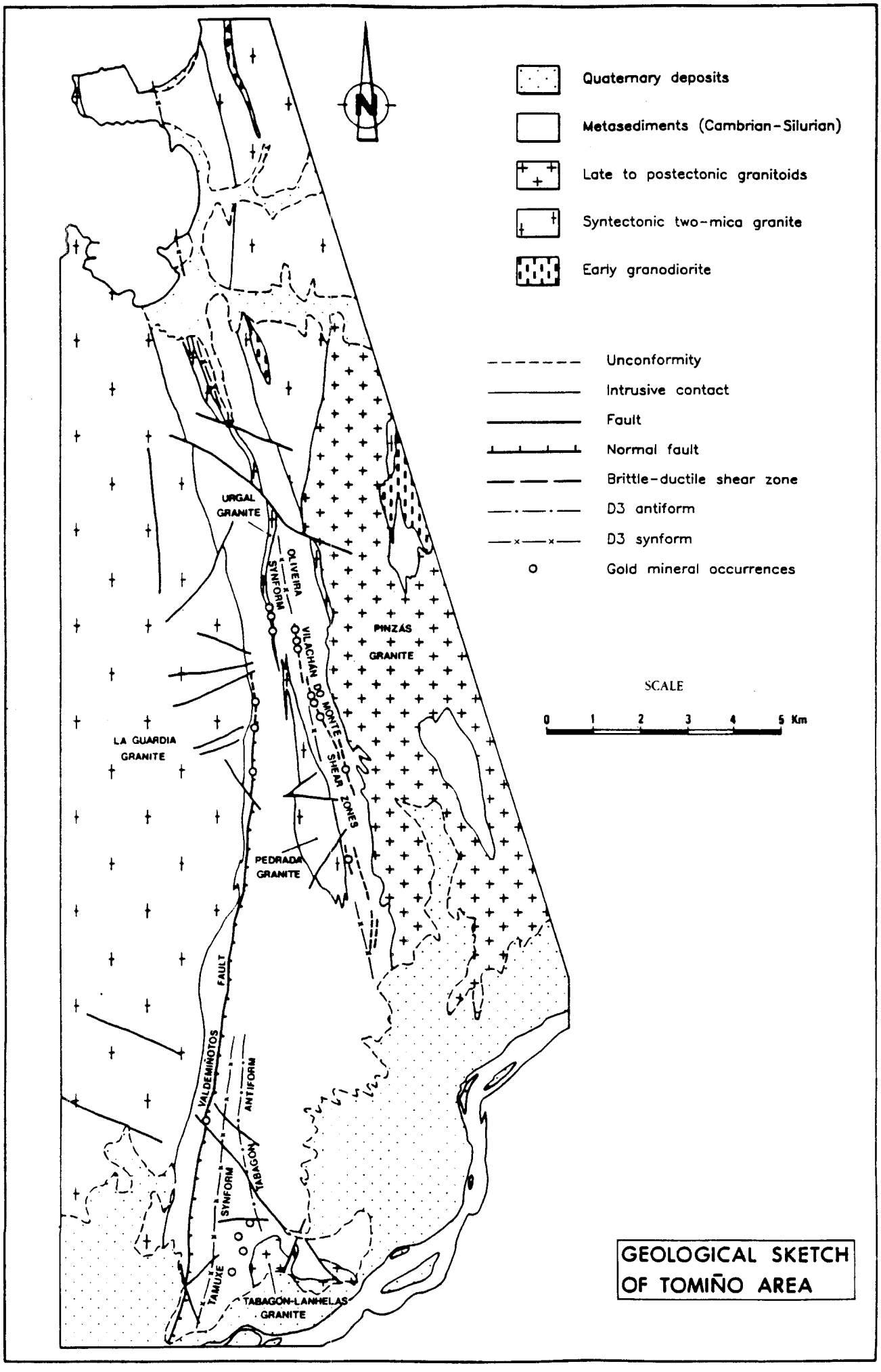

Fig. I - 10 : Geological sketch of the Tomino area with indication of the major structures and granite bodies.

SUMMARY OF CHARACTERISTICS OF TOMIÑO GRANITES						
	LA GUARDIA	*PEDRADA*	*URGAL*	*TABAGON*	*PINZAS*	*DDH.13*
Relation with host rock	*Concordant Clear intrusive contact*	*Concordant Clear intrusive contact*	*Concordant Clear intrusive contact*	*Concordant Clear intrusive contact*	*Concordant Clear intrusive contact*	
Mesoscopic structures	*Foliation*	*Foliation*	*Foliation*	*Mineral orientation*	*Mineral orientation*	*Foliation*
Endogranite veins	*Wide occurrence (pegmat/aplite)*	*Wide occurrence (pegmatites)*	*Relative freq. (pegmat/aplite)*	*Low occurrence (pegmatites)*	*Scarce (pegamatites)*	
Texture	*Medium-fine gr. Equigranular*	*Fine-medium gr. Equigranular*	*Fine-medium gr. Equigranular*	*Fine-medium gr. Equigranular*	*Medium-fine gr. Equigr./porphyr*	*Fine-medium gr. microphenocryst*
Petrological classification	*Leucogranite muscovit./biot.*	*Leucogranite muscovit./biot.*	*Leucogranite muscovit./biot.*	*Leucogranite muscovit./biot.*	*Granite biotitic/musc.*	*Tonalite biotitic*
Essential minerals	*Q,Fk,Ab,Ms±Bi*	*Q,Fk,Ab,Ms±Bi*	*Q,Fk,Ab,Ms±Bi*	*Q,Fk,Ab,Ms±Bi*	*Q,Fk,Pg,Bi,Ms*	*Q,Pg,Bi*
Accessory minerals	*Ap,Zr±Turm*	*Ap,Zr±Turm*	*Ap,Turm,(Zr)*	*Ap,Turm,Zr (occas.Garnet)*	*Ap,Zr (sec.Epid+Ilm)*	*Ap,Zr,Allan. (sec.Sphene)*
Ba (ppm)	*<300*	*<300*	*<300*	*<350*	*>700*	*>900*
Sr (ppm)	*<50*	*<60*	*<60*	*<60*	*>600*	*>1000*
Rb (ppm)	*>450*	*>350*	*>350*	*>300*	*<150*	*<150*

Table I -1 : Summary of the petrological and geochemical characteristics of the Tomino granites

Some scarce structures can be attributed to D1: refolded isoclinal folds, and foliations crenulated by D3 or included in porphyroblasts.

There are also other structures related with several tectonic episodes developed after D3, which have special interest because they act as structural control of gold mineralizations.
Some brittle-ductile shear zones and faults appear, usually with a N-S strike, parallel to main foliation. Two shear episodes, sometimes overprinted in the same structure, can be distinguished:
i) shear zones with a normal slip component are developed, followed by ii) dextral strike-slip shear zones.

Brittle deformation, taking place almost exclusively restricted to granitic rocks, has produced several joints and veins sets.

Later, different fractures affecting all rocks and previous structures are developed.

The metasediments are affected by a medium grade metamorphism, previous to D3 (paragenesis with staurolite + garnet + andalusite) which is superimposed by a thermal metamorphism syn- to post-D3, produced by the granitic intrusions.

5 - MINERALIZATION

Two types of gold-bearing mineralization can be distinguished:

-Individualized quartz-veins filling C-planes of brittle-ductile shear zones developped within the metasediments band. The main mineralization consists of locally diseminated to massif-narrow bands of sulphides (arsenopyrite - pyrite) with occasionaly native gold. The emplacement of quartz-veins are accompanied of alteration of wall-rock (silicification, sericitization, chloritization).

-Intragranitic quartz-vein systems filling shear-fractures or tension-gashes, accompanied of greisenization and hydrothermal alteration of wall-rock. Sulphides mineralization with associated gold occurs in quartz-filling and greisenized zones.

a - Mineralized quartz veins of Pedrada massif

The quartz vein systems are located in the south-ending of this massif, within a band of 150 m wide by 300 m northwards. The mineralized quartz veins are oriented about N25°E, dipping 80°E. The thickness ranges from simple fissures to 30 cm maximum. The quartz veins are accompanied of a, generally weak, greisenization of wall-rock. Sulphides mineralization, mainly composed of arsenopyrite and pyrite, occurs as locally massive within the quartz vein to disseminated in the greisen, with gold contents of no economic interest.

b - Mineralized quartz veins of Urgal granite dyke

The highest density of mineralized quartz veins occurs in the central part of the granite dyke, within a sector of 2 km long (Alto de Pozas). Old open-pits are localized in the central-southern part of this sector, along 800 m, in coincidence with the zones of deepest weathering. This circunstance added to the scarcity of outcropping and the dump material of old-workings, makes difficult to localize all sets of quartz veins. On the other hand, the significant results obtained from the preliminar sampling, advised to carry out a drilling programme to intercept the quartz veins and to know their development at depth as well as their gold contents.

c - Drilling programme

A series of drill holes was designed within the main part of the granite dyke and along 1700 m (Fig. I-11), at depths comprised between 80 m and 330 m, with directions N159°E and N163°E and inclination 55°S, approaching as possible to the perpendicular of quartz vein plan. Each drill hole starts close to the hanging-wall of the granite dyke and ends crosscuting the foot-wall and its contact with the metasediments. 3300 m of drill core have been logged, 810 of core samples have been analyzed for gold, part of them have been analyzed also for Sn, W/Cu, Pb, Zn, As, Hg by ICP. 43/30 polished / thin sections have been prepared for microscopic studies. The core sampling are restricted to the quartz vein and greisenized zones.

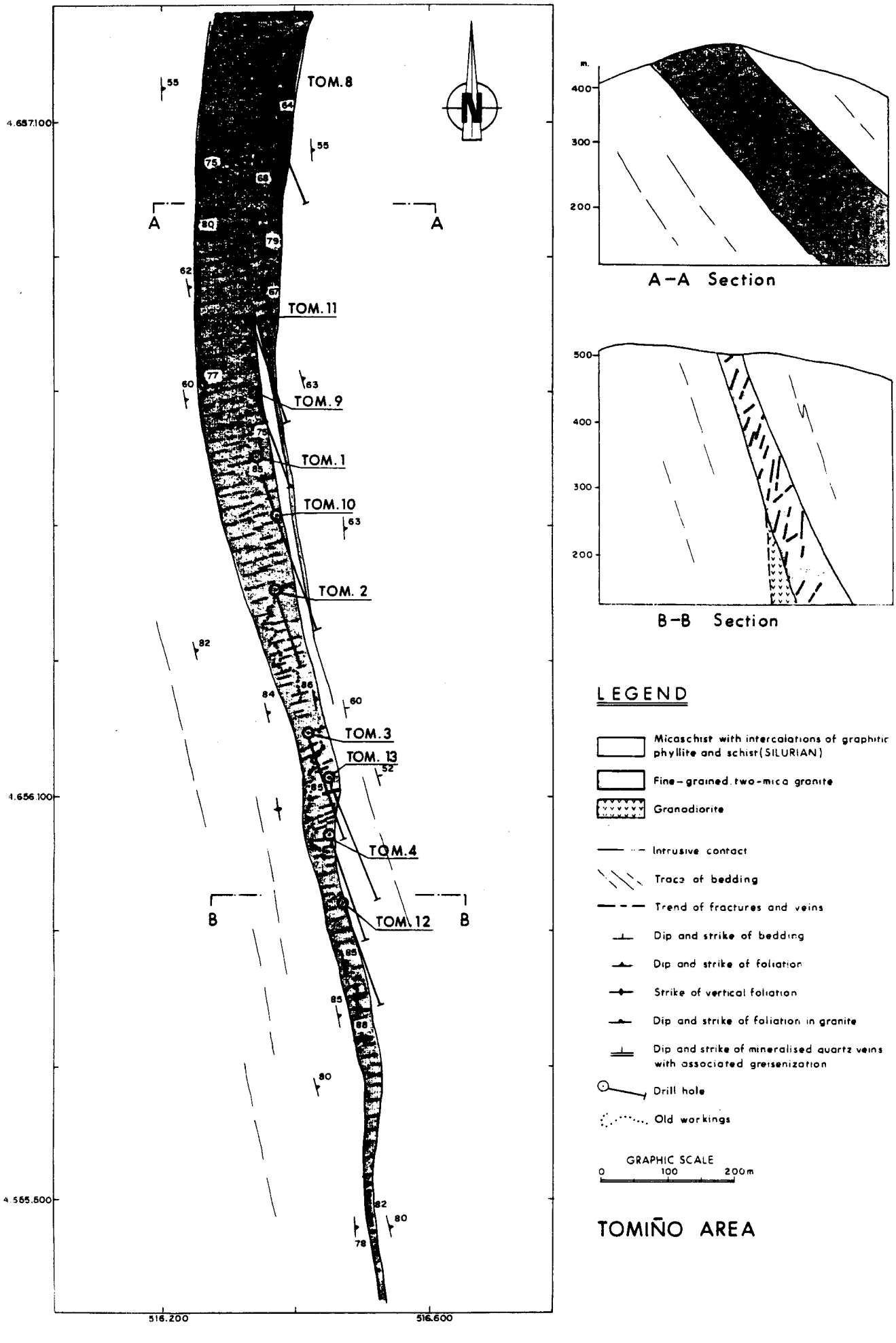

Fig. I - 11 : Geological sketch of the granite dyke hosting the mineralized quartz veins.

As result of the information obtained, it can be summarized the features of the quartz vein systems, host rock, mineralization, etc, as follows :

- *Granite dyke*

Drilling has shown that the granite dyke plungs eastwards, steeply dipping 80°E in the southern end and ranging to about 50°E in the northern end. The width of the dyke ranges from 40 m in the southern part increasing gradually northwards to 120 m. From the observations in outcropping, all together with the drilling information it can be assumed a disposal of the dyke parallel or subparallel to the structure of the metasediments.

Some centimetric to decimetric pegmatitic vein-dykes occur within the granite dyke, oriented in the direction of the main foliation, the same as tourmalinic bands and tourmaline bearing leucocratic facies of a few meters width.

In the deepest point of contact of the granite dyke, reached in DDH.13 at 270 m depth, was intercepted a granodioritic body, biotitic,with microporphyritic texture, appearing to be intruded by the granite dyke.

d - Ore petrography

Within the quartz veins, sulphides mineralization occurs generally as shattered massive, disseminated and filling cavities and fissures. Occasionally, it can occur as centimetric veins of massive sulphides without free quartz. In the greisenization zones, sulphides mineralization occurs generally as disseminated, with size crystals less than 1 cm.

The core sampling for analysis was carried out taking for each sample, the whole of quartz vein and associated greisened zone. Occasionally, quartz vein and greisen was sampled separately.

The gold content within the quartz veins is very irregular, with maximum of 60 g/t in analysed core samples. The amount of gold in greisen is lower, at most 5 g/t. In Table I-2, are summarized some of the more significative averages of gold contents in core drilling.

According to the microscopic study, it can be distinguished five type of mineral assemblages, depending on the location from the altered granite to the quartz vein have been distinguished (Fig.I-12):

- Early postmagmatic paragenesis : albite + tourmaline + apatite
- Greisen assemblages: quartz + muscovite + (apatite + albite + tourmaline + scheelite) eosphorite-childrenite + ilmenite + rutile / arsenopyrite + pyrite + pyrrotite + chalcopyrite + galena + sphalerite + bismuthinite + native bismuth + gold.
- Early vein paragenesis: quartz + muscovite + albite / arsenopyrite + pyrite / chalcopyrite + sphalerite + bismuthinite + native bismuth + gold.
- Late vein paragenesis: chlorite + kaolinite + muscovite / opal-calcedony + marcasite + chalcopyrite + tetrahedrite + sphalerite + native bismuth + native gold.
- Supergenic minerals: chalcocite-covelline, escorodite- mansfieldite, goethite-lepidocroite, marcasite, opal-calcedony. In the endogreisen paragenesis native gold is very scarcely and only has been observed as very tiny inclusions (<8 μm) within others minerals (pyrite, chalcopyrite).

These assemblages show clearly that each zones are characterized by superimposed mineral assemblages.

In the quartz vein, gold is observed as inclusions in chalcopyrite, occasionally in pyrite and very rare occurrences in arsenopyrite. Later, native gold occurs as coarser grains (25-175 μm) in fractures, crosscutting the sulphides (hydrofracturing process) and also related with late chalcopyrite.

In the crystallization sequence of alteration paragenesis, it may be observed a relationship between the progressive hydrothermal process and the enrichment in some minerals: chalcopyrite. sphalerite (rare), bismuthinite, native bismuth and gold. In this evolution may be enphasized the affinity of gold with chalcopyrite, in contrast with the general association of gold with arsenopyrite and pyrite observed in other areas of the NW.

DDH	From	To	Length in cm	Au g/T
TOM 1	38.65	39.35	70	3.50
	52.20	52.60	40	13.20
	60.45	60.85	40	5.20
TOM 2	99.75	100.45	70	7.50
TOM 3	68.95	69.65	70	9.50
	220.10	220.45	35	6.85
TOM 4	98.10	98.90	80	4.95
	117.80	118.40	60	5.32
	249.60	250.30	70	6.25
	275.10	275.80	70	6.45
TOM 8	14.90	15.30	40	11.35
	25.60	26.00	40	5.50
	116.85	117.05	20	30.00
TOM 9	16.20	17.25	105	9.05
	73.60	74.10	50	4.50
	75.40	75.80	40	6.60
	90.35	90.65	30	17.80
	121.00	121.50	50	10.80
	135.60	136.55	95	6.50
TOM 10	11.70	12.00	30	4.72
	56.20	56.45	25	17.00
	179.45	179.70	25	22.00
	197.65	197.80	15	43.00
TOM 12	87.65	88.65	100	3.80
	155.05	155.75	70	10.62
	158.30	158.70	40	13.45

Table I -2 Gold content of drilling core samples from Tomino area.

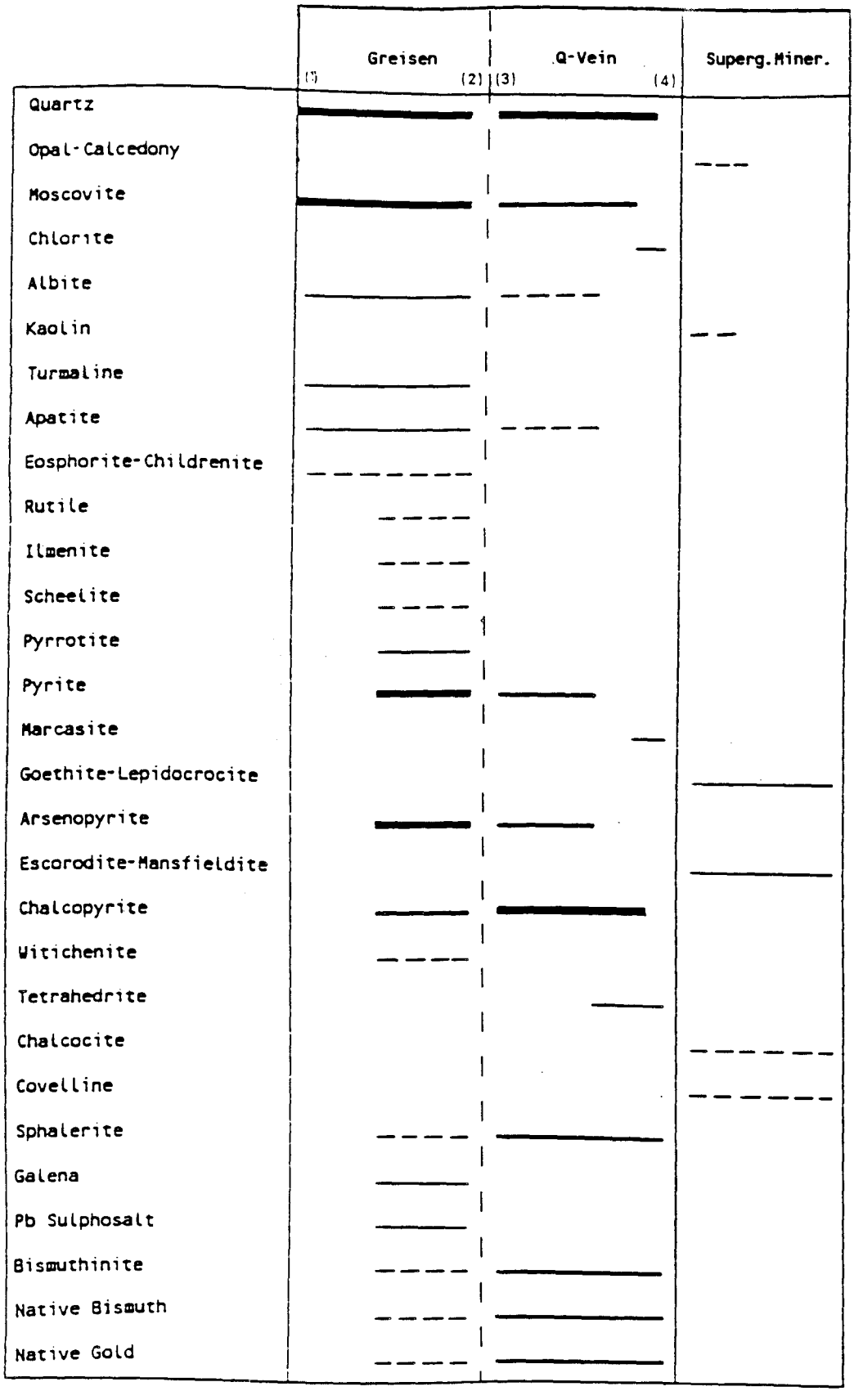

Fig. I - 12 : Mineral association in altered wall-rocks and veins in the Tomino area. The thickness represent schematically the relative quantities of the deposited mineral. 1 : early post magmatic paragenesis; 2 : greisen assemblage; 3 : early vein paragenesis; 4 : late vein paragenesis.

At microscopic scale, a ductile deformation affecting the endogreisen can be observed (strong ondulose extinction of quartz, kinks in muscovite, anisotropism of pyrite and tectonic twining in arsenopyrite) followed by a brittle deformation : microfracturing of quartz and sulphides, and later hydraulic brec..ation accompanied by fracture- filling and crystallization of chlorite + kaolinite and chalcopyrite, sphalerite, bismuthinite, native bismuth and native gold.

C- PENEDONO

I - GOLD MINERALIZATION IN PENEDONO

The gold mineralization at Penedono has been demonstated by several mines and occurrences; three areas have been selected for their mining importance, and appropriate exposures in outcrops (Plate I-2). Some of these areas have been object of mining concessions such as Dacotim and St Antonio-Vieiros. The other area studied is just a claim where some mining works for evaluation have been done in the past, named Ferronha.

The Penedono area is located in the C.I.Z., Central Portugal, on the south margin of the Douro River in the Viseu District. The three groups of mines are disposed along an axis oriented NW-SE, spaced one each other about 5 Km.(Fig. I- 13). The mines of St Antonio-Vieiros and Ferronha are emplaced in a large flat platform of the Miocenic erosion level at 950-1000 meters. The mine of Dacotim at the level of 650 meters is in the slope of this platform.

The area have been mapped on the 1/25.000 scale in order to establish the geological settings. The main geological features common to this group of mines can be listed as follows:

- the mineralization is intragranitic and occurs in two mica granites with an emplacement syn to late D3 Hercynian phase; the mineralization is mainly associated to arsenopyrite bearing quartz veins, associated to shear zones, developed in the granites. The quartz veins have an "en echelon" distribution and exhibit deformation and it is possible to identify several kinds of arsenopyrite associated to this deformation. A strong hydrothermal alteration is developed in the contact of the veins with the granite, and in the neighbourhood of the mineralized areas.
- the mines and mineral occurrences are lined up on an axis striking N60W, agreeing with the elongation of the granitic massifs where they are installed;
- country metasediments are of Cambrian age, belonging to the so-called Complexo Xisto-Grauvaquico, Douro Group, affected by three phases of Hercynian deformation. In this region just the first, D1, and the third, D3, phases are identifiable. D1 is responsible by the regional structure of the metasediments, developing mesoscopic folds of sub-horizontal axis and axial planes striking N60W. The associated S1 foliation is expressed by an axial plane cleavage and the orientation of micaceous minerals is well defined in the pelitic layers. The D3 phase is also expressed by mesoscopic folds homoaxials with D1 folds. A crenulation cleavage S3 is well developed, also with recrystallization and orientation of biotite (Sousa, 1982). The granitic massif related to the mineralization intrudes a major D3 anticline defined by the Cambrian metasediments, of the Complexo Xisto-Grauvaquico. The internal structures defined in these granites such as both orientation of the different facies mapped, and foliation on those who exhibit deformation, are parallel to the D3 structures defined in the metasediments.

Some K-Ar radiometric ages have been obtained for the different facies of this massif, giving ages ranging from 320 to 300 Ma (Ferreira et al.,1987), clearly in the limits of the age inferred for the syn to late D3 hercynian phase (Noronha et al., 1979).

2 -MINING INFORMATION (see Table I-3)

The area has been exploited for gold since the Roman times. Roman mining works are still observable and consists in the exploitation of the mineralized quartz veins on the surface and normally are not deeper than 30 meters. The method of extraction the quartz vein is possible to be reconstituted by the marks made by the pick cutting the soft granite in the contact with the vein.

In the forties a mining company "Companhia das minas de ouro de Penedono" started the exploitation with underground mining works, till 1957, when the mine was closed. The main exploitation was done in the mine of St Antonio-Vieiros, where we found a group of thirteen major veins oriented N40-50°W are concentrated on a band of 800m wide (Fig. I-14). In vein n° 2, a well with 80 meters of depth gives access to the underground works in this vein and in vein n° 3. In this mine, it was also located the plant for ore treatment of all the gold mines of the area. In the mines of Dacotim and Ferronha the mining works had smaller importance. Available data from that time, taken from official departments, indicate that the main production was obtained from 1954 to 1957 in the concession of St Antonio- Vieiros, with 100 800 tons,

PENEDONO AREA

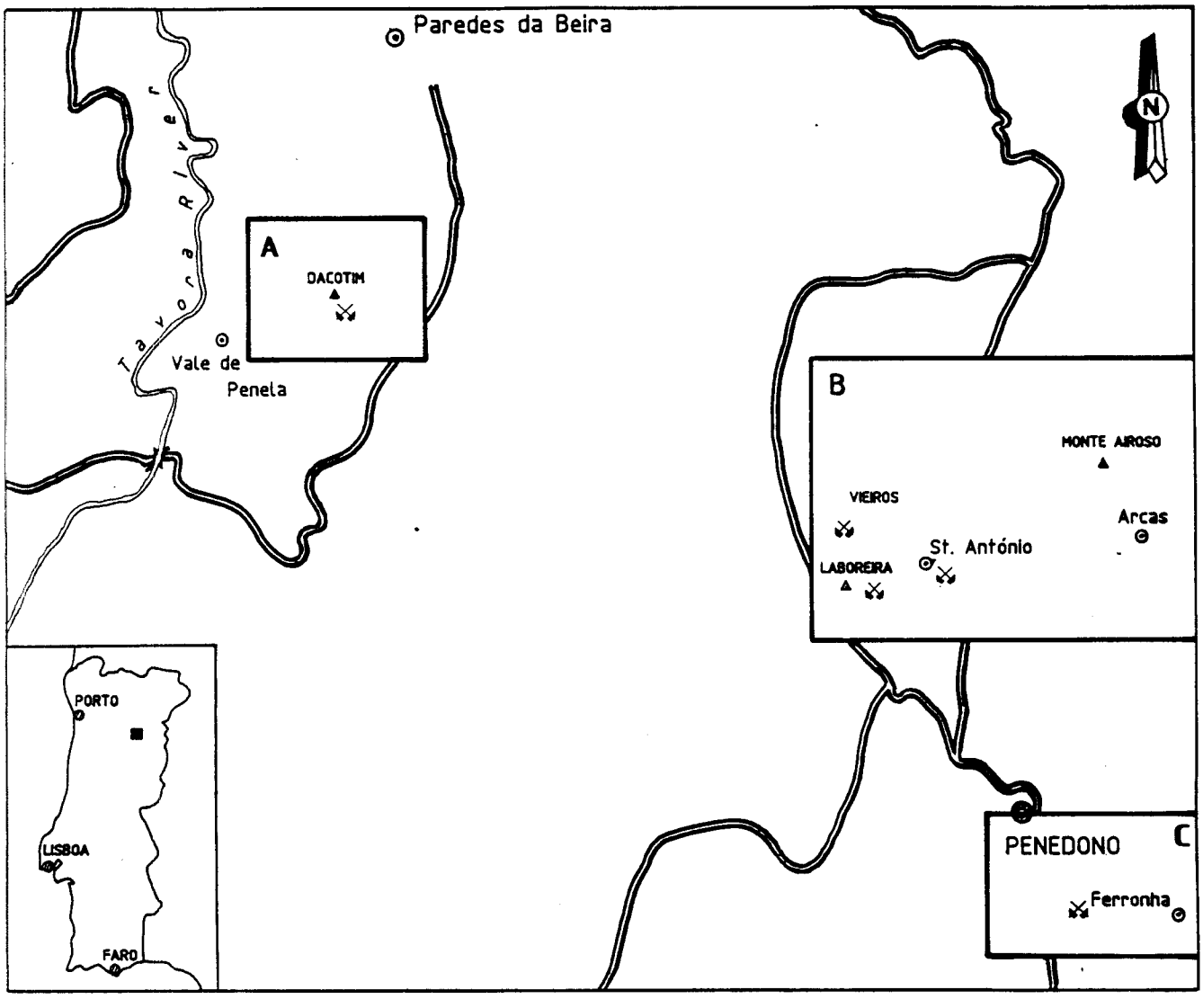

A - Docotim mine

B - St. Antonio mine

C - Ferronha mine

Mining works

Fig. I - 13 : Location of the studied areas in the Penedono distict.

	Dacotim		St° António - Vieiros		Ferronha	
values in ppm	Au	Ag	Au	Ag	Au	Ag
n. analyses	69		544		50	
max	44,7	64	19,3	74	73	63
min	3,7	26	1,8	5	6,6	19
average	15,7	42,9	8,9	24,9	27,1	40,4
st deviation	8,2	10,8	3,4	10,1	14,3	8,6
correlation	0,432		0,388		0,471	

Table I- 3 : Au and Ag contents of veins and trenches from the three groups of mines (Penedono).

	1953	1954	1955	1956	1957
Sto Antonio - Vieiros	16	16.000, 7,0 g/ton	49.766, 7,0 g/ton	1.838, 6,0 g/ton and 15.886, 7,0 g/ton	17.156, 6,0 g/ton

Table I -4: Production, in tons and Au contents at St Antonio Vieiros.

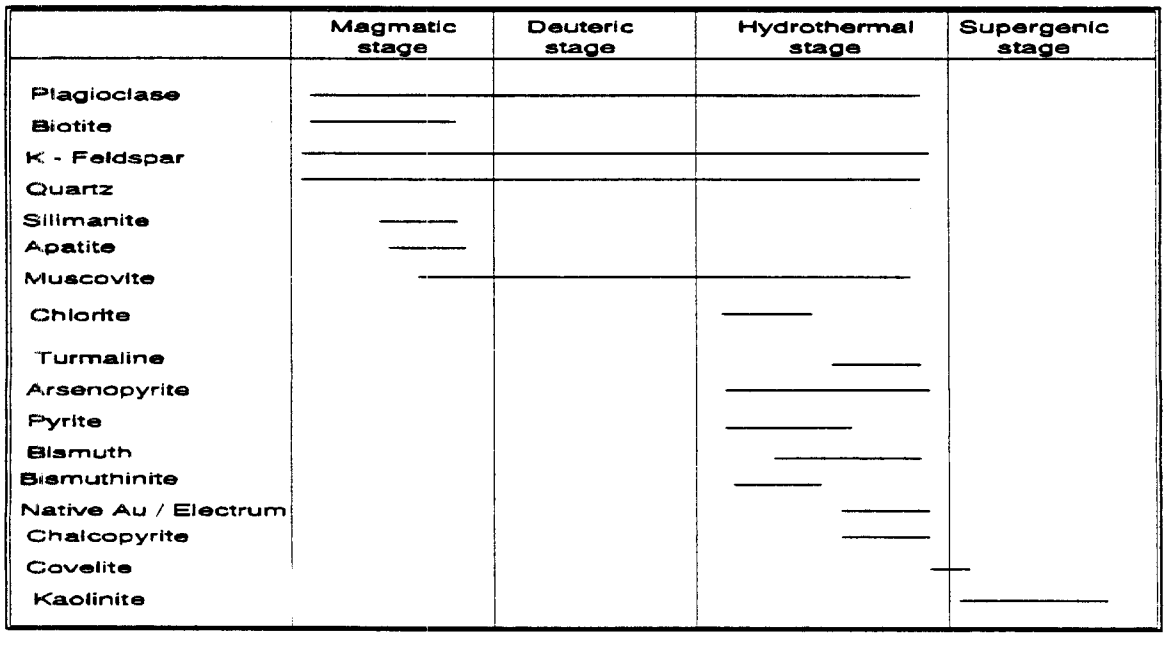

Fig. I - 18 : Paragenetic sequence for the Penedono mineralized granites

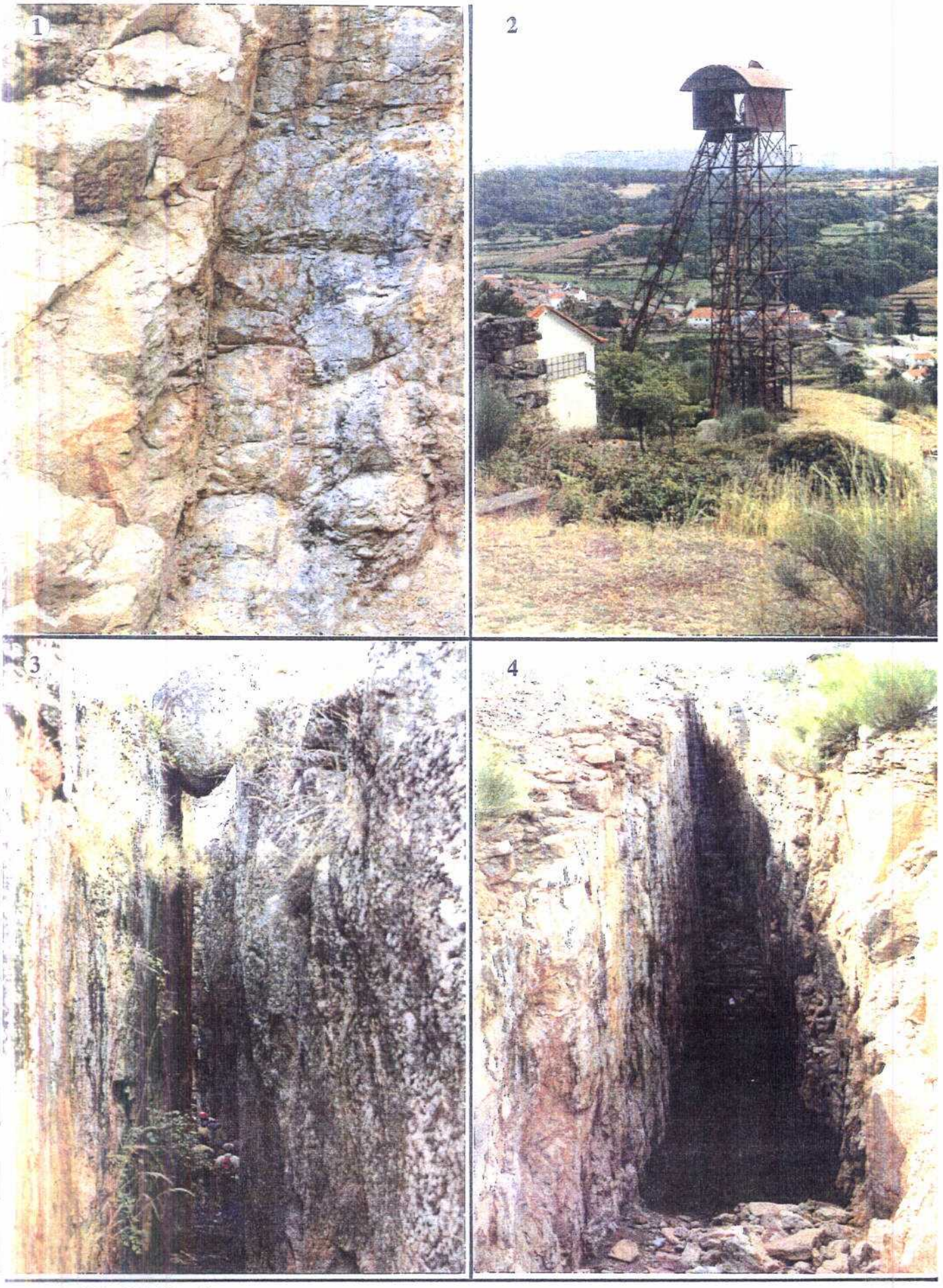

Plate I-2 : Penedono area
1 - Dacotim Mine, mineralized arsenopyrite quartz vein (50 cm to 1 m) within the granite. 2- View of the St Antonio mine shaft. 3 and 4 - Old exploitation works of quartz veins .

Fig. I -14

GEOLOGICAL SKETCH MAP

LABOREIRA - MONTE AIROSO - ARCAS

(P E N E D O N O)

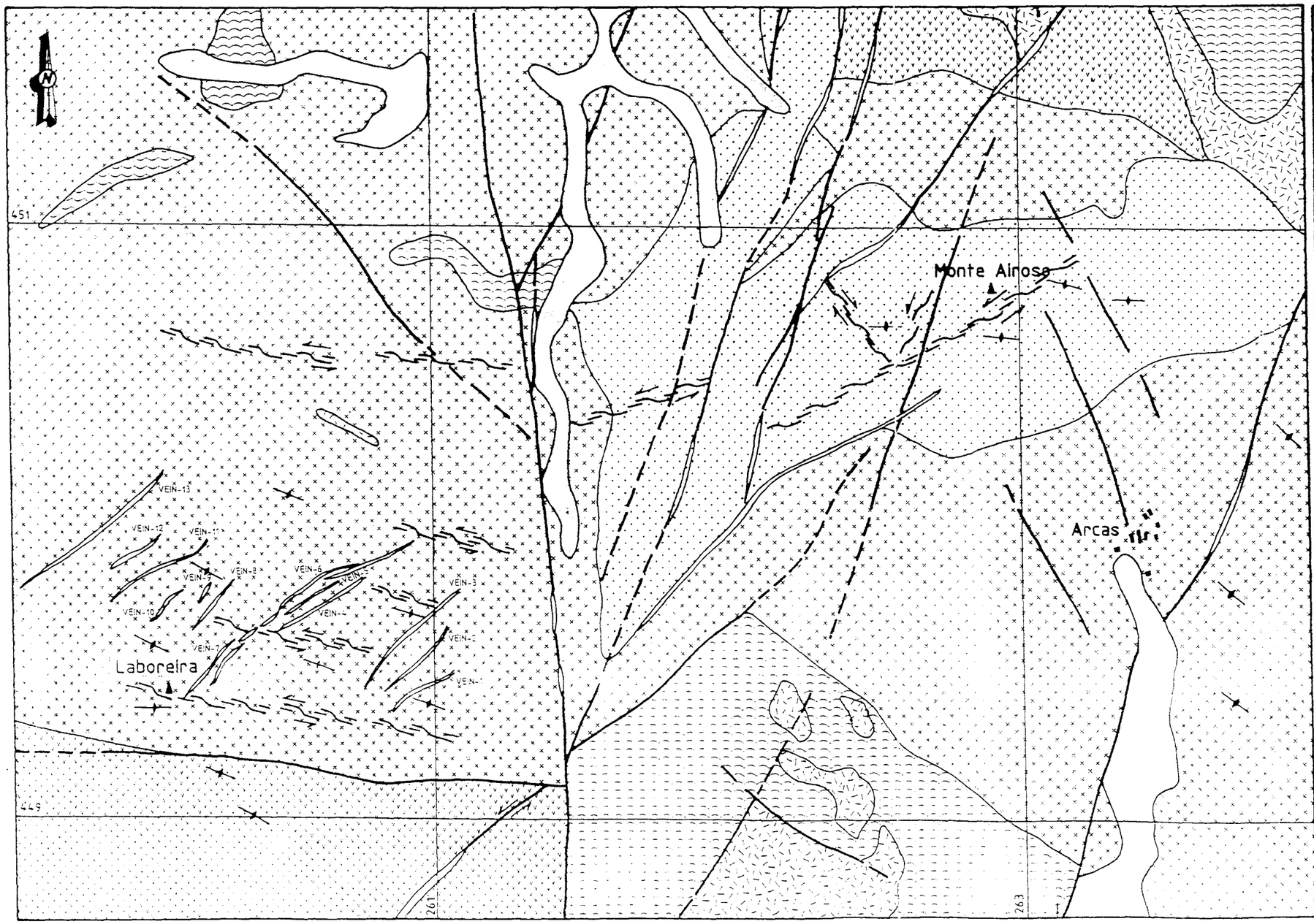

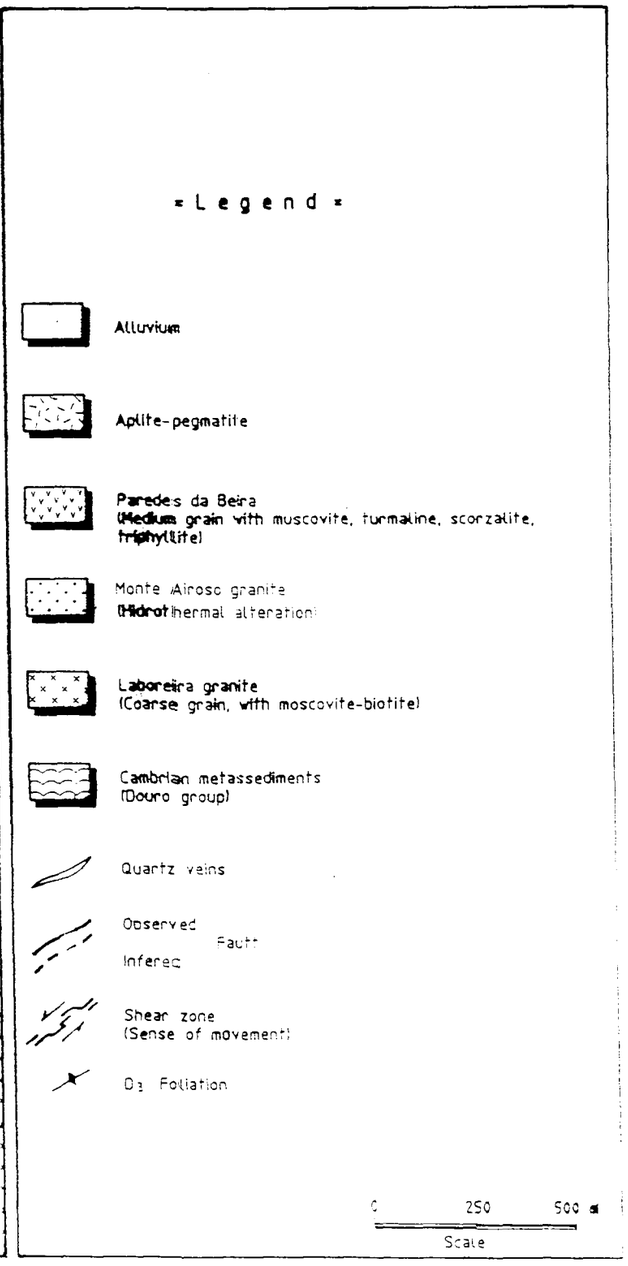

41° 45'

with a medium content for Au of 7,0 g/ton (see table I-4). The mine have been closed because of the low price for gold at that time and also due to the occurrence of a big accident in the treatment plant.

In the early eighties another company "Caulinorte" retook the mining works with sampling in the veins of the three mines, opening of trenches and taken of big samples to treat on a pilot plant. In 1986 a consulting company (Partex, Companhia Portuguesa de Servicios) produced a preliminary feasibility study of the gold mines of Penedono. To make this report the company has consulted all the documents available and checked the contents with some channel sampling. The estimated reserves for the area are summarized in Table I-5. The sampling of the veins was mainly made at surface or in upper levels, when taken in the mine. This is the reason why the calculations of the estimate reserves have been done to a depth of 80 meters. This value was taken by precaution because no data is available for width and contents below this depth. Although, it is suggested that the veins can keep the content and width for more than 200 meters depth. The calculations did not consider the reserves in the area of Ferronha, because of the kibble-chain structure of the veins and the scarce analyses of both contents and widths, could not allow a reasonable calculation. However, in this mine the available analyses indicates the highest content for gold of all the studied areas with an average of 27 g/ton and four quartz veins with hectometric extension and 0,4 meters width in measured outcrop (not representative). The reserves estimates for St Antonio-Vieiros and Dacotim reach 1.200.000 tons c.a. of mineralized vein with 11.500 Kg c.a. for Au.

Problems with the recovering of the gold during the activities of the company who as exploited the area in the forties and fifties is responsible by a waste dump with 105.000 ton with a medium content of 3.8 g/ton of Au.

No drill holes have been made to evaluate the behaviour of the veins with depth and their contents.

The sampling of veins and trenches give an idea about the content in gold and silver in the three groups of mines (Table I-3). The plotting of the Au/Ag contents for the three mines define tendencies for each mine (Fig I-15a and 15b). Projections represent maximum vs. minimum Au/Ag values (Fig I-15a) and average plus standard deviation vs. average less standard deviation (Fig I-15b). Also histograms (Fig I-16a, 16b and 16c), representing the content of Au show clearly different distributions for each area. These diagrams for that available data, representing a total of 772 analyses, pretend to demonstrate a clear enrichment in Au (and Ag) content from the mine of St Antonio-Vieiros to the mines of Dacotim and Ferronha. Structural, mineralogical and fluid inclusion studies will be oriented in order to obtain data to clarify these facts.

3 - GEOLOGICAL SETTING

The area with gold mineralization of Penedono is located in a wide band of Hercynian two mica granites. They present characteristics of the "S type" (Chappel and White, 1974), and occur as alochthonous and parauthoctonous massifs, generated by the melting of big portion of crust, induced by the intrusion of basic magmas, along big shear zones related with Hercinian D3 (Ferreira et al., 1987). These granites intrude metasedimentes with Cambrian age of the Schist-Greywake Complex (SGC) of the Douro Group. It is possible to identify two different massifs, Tabuaço and Penedono. They have typical internal structures and they are physically separated by panels of schists (Fig I-17). The Tabuaço Massif has an elliptic shape with the elongation N 60 W intruding a big anticline of SGC. The deformation expressed by the orientation of the micas, is not too strong, being only identifiable in some facies, and it is parallel to the elongation of the massif. All the facies are affected by ductile to brittle shear. The granites of Penedono Massif are strongly deformed with a very regular foliation, also N60W, parallel to the internal structures, defined by the contacts between the different facies, containing several restites and schlieren aligned along the same direction. These facts make us consider the Massif of Penedono relatively more in situ than the Tabuaço massif. This massif is considered to represent a greater displacement from their roots, as to be intruded at a higher crustal level. This difference between the two massifs can also correspond to a slight difference in the age of intrusion. In fact, some K-Ar datation confirms an age for the Penedono Massif of

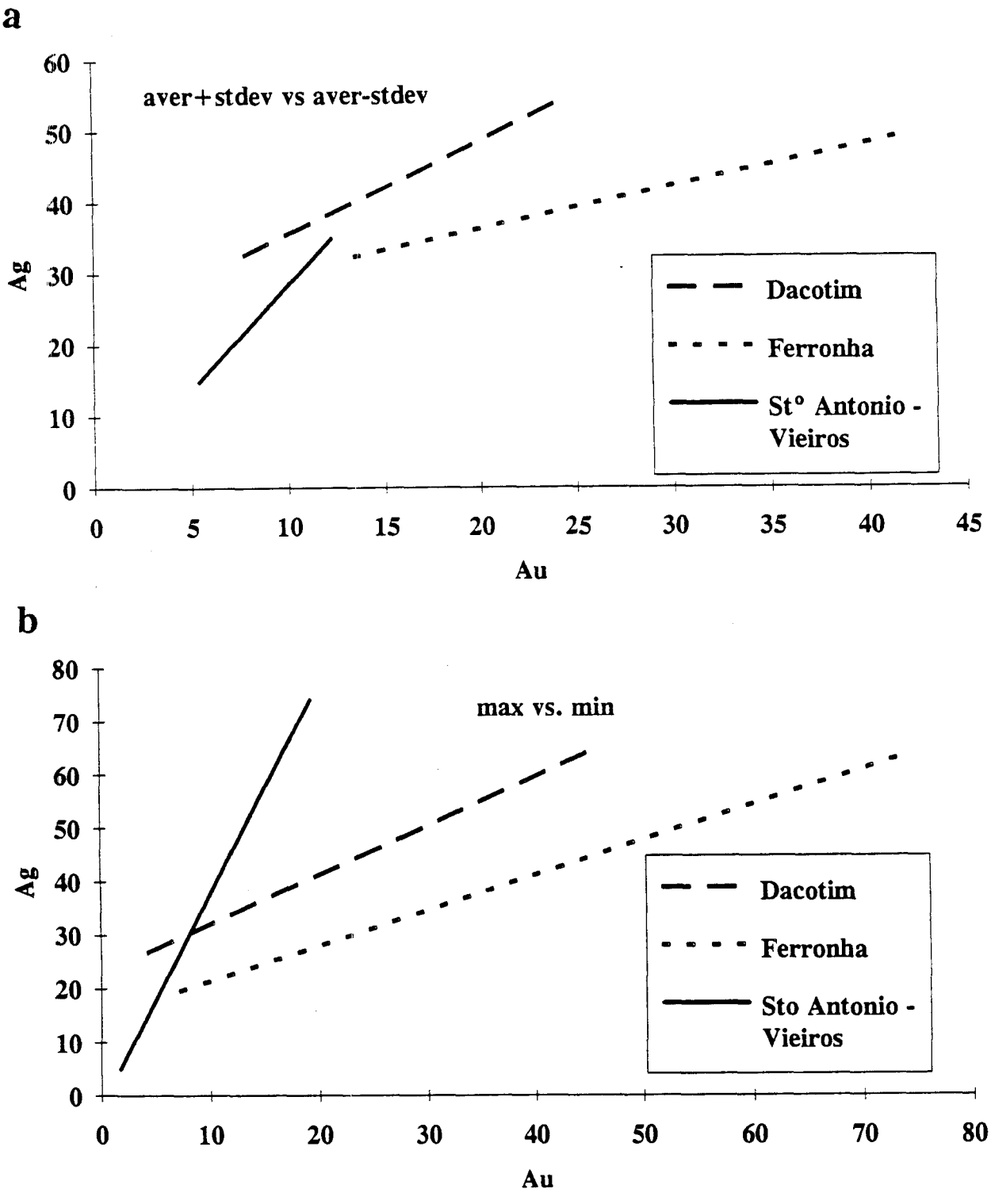

Fig. I - 15 : Au-Ag binary diagram applied to chemical analysis of the veins from the three mines in the Penedono area.
a : average + standard deviation versus average - standard deviation
b : maximum versus minimum

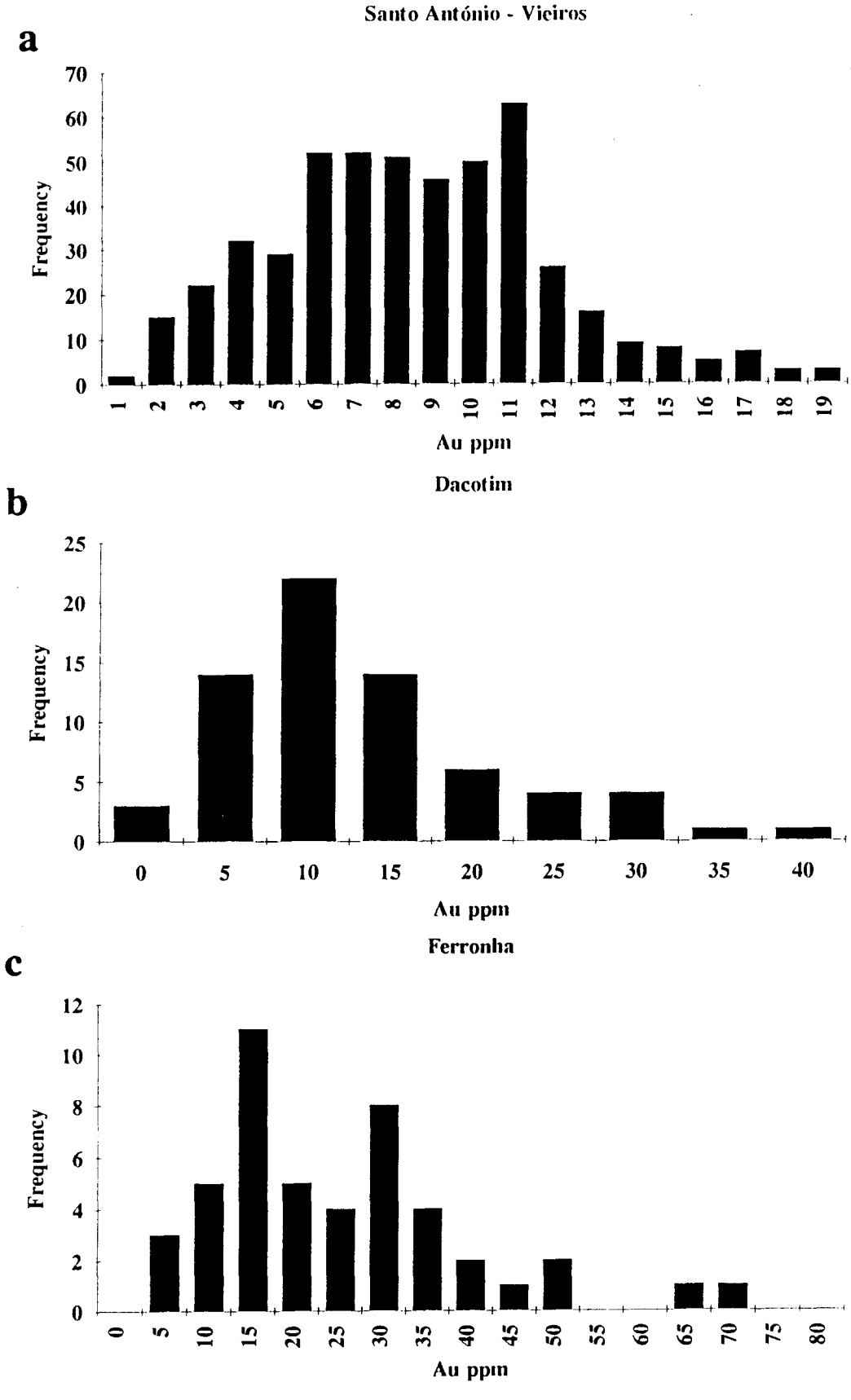

Fig. I - 16 : Histogram for Au contents (veins and trenches) from the three mines in the Penedono area. a : St Antonio Vieros; b : Dacotim; c : Ferronha.

Table I -5 : Estimated reserves for the Penedono mines

	Sto Antonio - Vieiros											Dacotim		
	Vein 1	Vein 2	Vein 3	Vein 4	Vein 5 **	Vein 6	Vein 7	Vein 8	Vein 11	Vein 12	Vein 13	Vein 1	Vein 2	Total
Average Width (meters)	2,5	0,96	1,45	0,7		0,8	0,84	0,7	0,83	0,825	0,8	0,86	1,06	
Au Average Content (gr/ton)	5	9,5	9,8	8,1	6,8	8,5	9,1	8,4	9,8	9,9	7,9	16,1	15,4	
N° of vein samples	41	60	59	31	22	10	32	35	15	8	61	22	48	444
Known lenght (meters)	260	500	570	270	200	680	310	330	460	160	400	450	340	
Estimated reserves (ton)	156.000	161.280	198.360	45.360		130.560	62.496	55.440	91.632	31.680	76.800	92.880	86.496	1.188.984
Total Au (Kg, estimated)	780	1.532	1.943	367		1.109	568	465	897	313	606	1.495	1.332	11407

* Estimated reserves calculated to a depth of 80 meters

** Not enought data available to estimate reserves for vein 5, 9 and 10 of Sto Antonio - Vieiros, and veins of Ferronha.

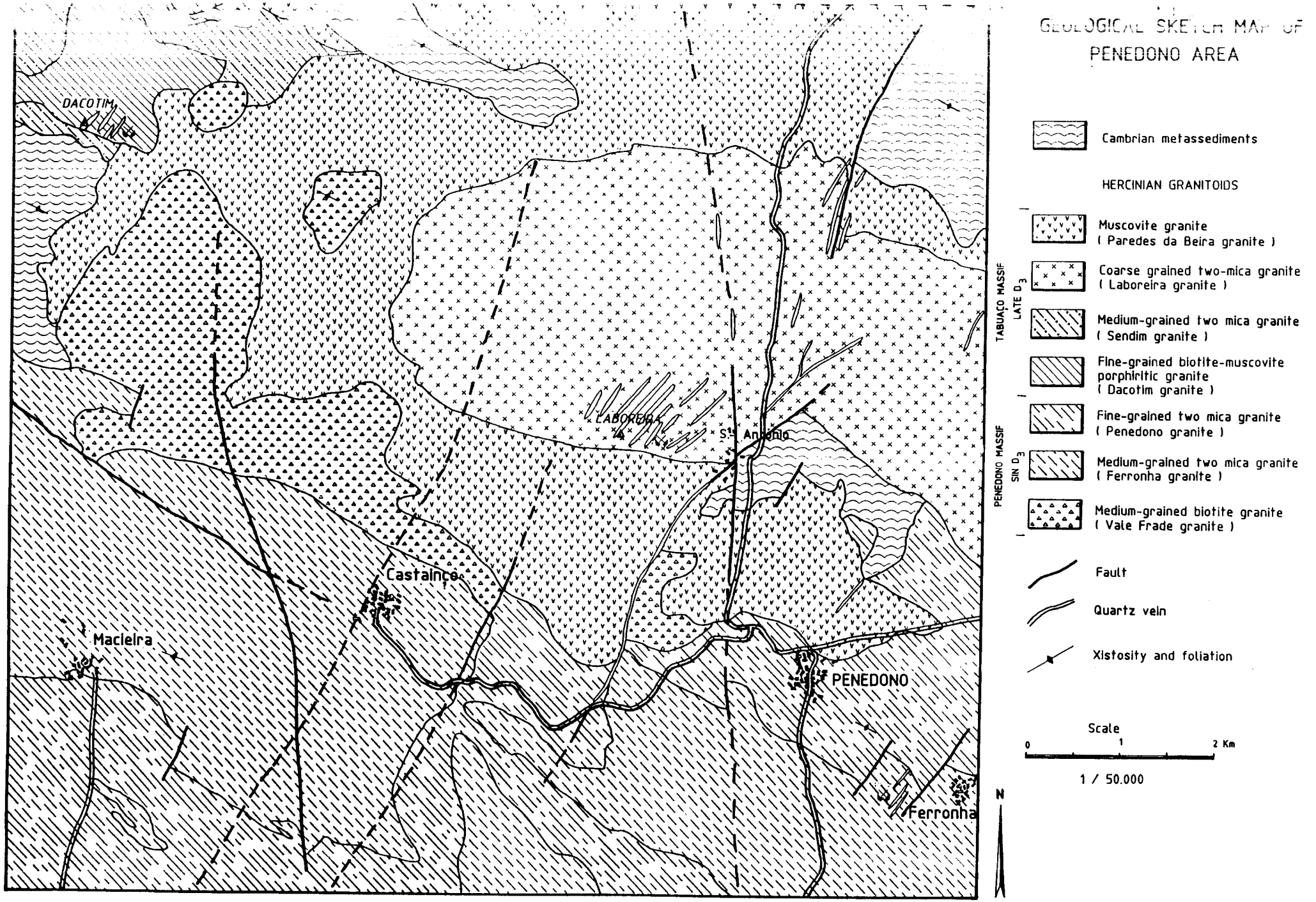

Fig. I - 17 : General geological map of the Penedono area.

320-315 Ma, clearly syntectonic to D3 and an age of 315-300 Ma. to the Tabuaço Massif, corresponding to a late- D3 installation (Ferreira et al., 1987). All the granites of both massifs are alkaline, and two micas which can dominate one against the other.

Several facies were identified in the two massifs with typical petrographic and field relations.

- the dominant granite in the Tabuaço massif is a two mica medium grained granite (f= 2-3 mm) with a very weak foliation oriented N60W, the Sendim granite, and in the area of the mine of St Antonio-Vieiros the grain size increases to 4-5 mm, the Laboreira granite. A sub facies of this granite, the Monte Airoso granite, results of a very intense shear that affects this granite. This shear is accompanied with the total alteration of biotite to muscovite, and the presence of tourmaline. Associated to the Sendim Granite, and with a very gradual limit, we pass to a muscovitic granite with rare biotite, locally silicified, and with phosphates (groups of triphilite-scorzalite), tourmaline and dispersed sulphides, the Tabuaço-Paredes da Beira granite. This granite makes the contact between the Tabuaço massif and the Cambrian metasediments of SGC. In the Penedono area the contact of this granite with the regional two mica granites is sharp and the granite is associated to a big amount of stocks and veins of aplites and pegmatites, frequently mineralized with Sn-W. Intruding the centre of the massif occurs a porphyritic granite with fine grain, biotite dominant, the Dacotim granite. The foliation in this granite is very weak and becomes stronger when affected by shear.
- the structure of the Penedono massif is similar to the Tabuaço massif. The contact between the two massifs is made by an alignment of panels of schists and by a granitic facies with a strong foliation also N60W. This facies, the Vale Frade granite, is biotites with medium grain, has an heterogeneous looking of composition with variations in the grain size and local concentrations of biotite. The main granite of this massif is very similar to the facies of Sendim granite in the Tabuaço massif, with the difference of the intensity of the foliation N60W much more developed in that of Penedono, and also the frequent association with schlieren, and restites. Two facies have been identified, separated only by the grain size. A fine grained with two micas in the external border of the massif and as cupfuls, the Penedono granite, and a medium grained two mica granite in the center of the massif, the Ferronha granite. Ductile to brittle shear oriented around EW, senestral, affect all the facies of both massifs. We consider these shear associated to the major shear Vigo-Braga-Moimenta da Beira.

4 - MICROSCOPIC FEATURES

The granites associated to the Au mineralization at Penedono are two mica granites, with an hipautomorphic ("granitic s.l.") porphyritic texture, ranging from fine to coarse grained. The mineralogy that represents the main evolution conducting to, and related, Au-mineralization, is summarized in figure I-18. Earlier studies (Silva and Neiva, 1990, Sousa and Ramos, 1991) also present, more detailed, mineralogic studies.

After the magmatic stage, deuteric processes produced an initial sodic alteration, shown by the albitization of plagioclase accompanied by the growth of white mica over the same plagioclase. Later, potassic alteration is represented by the growth of microcline, both intergranular and as replacing albitized plagioclase. Deuteric alterations do not change completely earlier mineralogy.

The hydrothermal stage is identified associated to and in mineralized veins. Greisenisation occurs in the contact vein/granite, and is responsible by lost of feldspars and an increasing in white mica.

Due to the strong deformation that affects the granites, quartz shows systematic ondulating extinction, sometimes with mortar texture. Silimanite occur as needle-like crystals, associated to the deformation. Plagioclase, originally with a composition about An15-10. grades to albite, An5. Biotite alters to white mica in the igneous stage, concomitant to the beginning of crystallization of muscovite, and to chlorite in the hydrothermal stage. It includes zircons and monazite, developing pleochroïc halos. Microcline, when igneous, is perthitic; when associated to deuteric potassic alteration, it replaces albite. This replacement does not affect plagioclase that was not completely affected by albitisation. White micas occurs during

the different stages, exhibiting different textures. Originally as subhedral slabs or replacing biotite, the muscovite crystallizes then, needle-like, along shear planes during the late magmatic stage, associated to local subgranulation. In the deuteric stages, it replaces albitised plagioclase along structural planes of it, along fractures of feldspars and as disseminated minute crystals bordering plagioclase. In the hydrothermal stage, white micas crystallize as minute crystals enclosing earlier muscovite in greisen type aggregates, associated or not to sulphides.

The presence of sulphides and other minor metallic minerals that accompanies Au-mineralization, characterize the mineralisation. Arsenopyrite (Apy) is the most common sulphide, with subordinated pyrite (Py). Bismuth and bismuthinite, this one with a small Ag amount, occurs included in arsenopyrite. Chalcopyrite occurs lately to the Apy / Py ensemble. A first breccification of Apy is concomitant to a release of native bismuth. Native gold and/or electrum are introduced with an increment of Apy breccifiation. These breccifiation is accompanied by a generalized corrosion of the arsenopyrite. Nevertheless, in the mine of St Antonio - Vieiros, electrum is observed in contact with automorphic, non corroded Apy, which contains bismuth included in the border of the grain. Arsenopyrite is unzoned or slight zoned under the scanning microscope, a fact that is confirmed by electron microprobe analyses (see chap IV a).

Supergene alteration induced the occurrence of argilaceous minerals of the kaolinite group. These kaolinites are intergranular, coating matrix minerals. Covellite which occurs bordering quartz in interstitial sulphides in not clearly related to chalcopyrite, a fact that lead us to consider the possibility of its occurrence in the mineralization stage (even not associated to gold/electrum, these two minerals have the same textural position) and not only in the supergenic alteration stage.

D - PINO AREA

1.- INTRODUCTION.

The Pino area is located in the western part of Zamora province (Spain), close to portuguese border. It is comprised in the Central-Iberian Zone of the Hesperian Massif (Julivert et al., 1973), within the domain of Recument Folds defined by Diez Balda et al., 1990) (Fig.I-19).

The Mining Service of Castilla-Leon Community in 1985-1986 prospected the area and defined the arsenopyrite-gold mineralization from Pino as structurally controlled by sinistral shear bands.

After, within metallogenetic map works, on 1:200.000 scale, of the "Alcañices" sheet, , in which Pino is included, carried out by the Geomining Technological Institute of Spain (I.T.G.E.) a regional shear band, named "Villalcampo", was defined and studied in detail. A pattern was propossed, in order to define the location of gold mineralisations, relating this regional structure to Pino shear bands, (Fig.I-20), (Gonzalez Clavijo, 1990, Gonzalez Clavijo et al. in press.).

Thus, from the metallogenetic point of view, this area is remarked by occurrences of gold veins related to minor shear bands of N60º-70ºE trend developed over an extensional fan which is considered to be the NW ending of the "Villalcampo shear band", a regional structure of N135°E in direction , more than 40 km long and, in some places, 2 km. width.

In 1991-1992, I.T.G.E., within the present C.E.C. contract mapped Pino area on 1:5.000 scale (roughly 24 km^2) and carried out soil and rock geochemical surveys (I.T.G.E., 1992). In the follows the geological and metallogenetic setting and main geochemical results are described.

2.- GEOLOGICAL SETTING

Ricobayo granite (Fernandez Turiel, 1987) is the main body cropping-out in the area, intruded in ordovician and preordovician sequences and hosts most of Pino gold mineralisations.

a- Stratigraphy.

Two main lithostratigraphic units are distinguished in the mapped area, cropping-out into two regional structures: the Villadepera Antiform, constituted by preordovician sequences, and the Alcañices Synform which includes lower ordovician to devonian-lower carboniferous series.

a) Biotite-muscovite gneiss and schists of precambrian-cambrian age (Neises de Villadepera Formation, from Villar, 1990). This unit is located at the south border of the Ricobayo granite, and constitutes the upper unit of the preordovician sequence outcropping in the Villadepera Antiform.
These materials show a medium to high grade metamorphism, but non metamorphic aureole is developed in relation with the granitic intrusion.
This unit appear to be of volcanosedimentary origin and most of geologist working in this area correlate this unit to microglandular facies of "Ollo de Sapo" formation.

b) Schists, sandstones and quartzites that appear like roof pendants over the granitic area in the northern area of the mapped zone. They have been related to "Capas de Cerezal" formation (Quiroga, 1981) of Tremadoc- Arenig age, defined in the south limb of Alcañices

synform, although this relation is problematic to settle. Some works relate part of this unity to preordovician sequences of the Villadepera antiform.

Mainly they are sandy schists and thin quarzite beds, that show contact metamorphism. Petrographic studies define them like mica-quartz hornfelses with andalusite.

b - Structure

In the Central-Iberian Zone, two main tectonic domains have been defined on the basis of the style of the megascopic structures of the first Hecynian phase of deformation: a) the domain of recumbent folds and b) the domain of vertical folds (Diez Balda et al., 1990). Pino area belongs to the former.

Most of geologists working in the area agree in the tectonic pattern, defining three deformation phases, D1, D2, D3, and other later one of fracturing. The Alcañices synform and Villadepera antiform are megastructures of D3 phase. The former is developed on the north of the Ricobayo granite. The roof pendant outcropping in the upper part of the mapped area can be considered like a relict of the materials located in its core. Villadepera antiform is the result of the superimposition of D1 and D3 folds.

D1 is associated with a S1 cleavage that is the more penetrative cleveage showed on both structures. In our area, only D1 minor folds have been seen in the "Villadepera gneiss" formation.
The D2 structures are developed outside Pino area, within the "Alcañices" synform, in narrow bands associated with thrust faults, with a translation sense of the thrusting block towards the east (Diaz Balda et. al., 1990).

Villacampo shear band.

In addition to preceding structures, vertical brittle-ductile shear bands have been identified in the "El Sayago" massif (Lopez Plaza, 1982),located at south of Pino area. They constitute conjugate sets NW-SE (dextral) and ENE-WSW (sinistral). These shear bands affect to post-D2 granitic bodies, and they should be compatible with stress system related to the 3 rd phase of deformation (Gonzalez Clavijo, 1990). One of those dextral shear bands is the "Villalcampo" one, that affect both Ricobayo granit and Villadepera antiform, and it is the regional structure which controls the location of the gold-bearing shear bands of Pino.

The "Villalcampo" shear band has been studied in detail by Gonzalez Clavijo (1990) and a summary of its main characteristics are set out:

- Direction: N135ºE.
- Dip : subvertical.
- Mylonite lineation: direction N145ºE.
  plunge 0º to 10ºNW.
- Movement sense: dextral.
- Amount of displacement: 3.500 m. approximately.
- Type: Brittle-ductile shear.
- Main structures: S-C mylonites.

c -Intrusions

Three facies of granite can be distinguished in Ricobayo massif, which predates D3 phase of deformation.

Two micas granite. : it constitutes the main facies of Ricobayo massif. It is a medium-coarse grained granite made up of quartz, potassium feldspar, sodium plagiocase, biotite and muscovite, with sillimanite, garnet and zircon as accessory minerals. It occurs in the central zone of the mapped area, between Villadepera antiform and Ordovician outcrops.

Biotite granite. : this facies crops out, pathshaped, within two mica granite, mainly at north of the mapped area , although dykes or subhorizontal sheets of similar composition have been seen in the trench made in the two mica granite. Principal minerals are quartz, potassium feldspar, plagioclase and biotite.

Leucocratic granite. : it is a fine-medium grained granite that appears mostly in the south boundary of Ricobayo massif, or as dykse into the two mica granites. It is composed of quartz, potassium feldspar, plagioclase and muscovite. These granites are interpreted as the most differentiated magmas and in regional scale they represent the facies that controls the Sn mineralisation.

In addition to these types of granitic rocks, later intrusives are aplite and pegmatite, diabase. Barren quartz dykes crosscut most former facies.

3.- ORE-BEARING STRUCTURES.

Mineralized zones at Pino area are born by sinistral and vertical shear bands, whose strike is N68ºE. These structures are called in this study "mineralized bodies" or "mineralized structures". Most of gold occurrences are spatially associated within those shear bands, although some of they are located in the less deformed zones between individual shears bands.

Rocks display in the Pino shears bands characteristics of both brittle and brittle-ductile shear deformation : gouge, fault breccia, S-C mylonites, laminated grey quartz veinlets (mylonitic quartz), white quartz veinlets (both could be barren or mineralized).

The shear bands shape can be considered tabular to lenticular, depending of the scale. Mineralized structures range from some meters to 1km in length and between 1m and 200 m in width. By far, most of shear bands are not wider than 5 to 10 meters. In fact, internal structure is defined by a anastomosing array of deformed and no deformed zones.

Up to 16 major mineralized structures are mapped, although other smaller have been identified and sampled.

4.- MINERALIZATION-ALTERATION.

The phenomena of alteration and mineralization cannot be meaningfully separated, since gold ore may be emplaced both as open-space fillings and as host rocks replacements.

Within mineralizated body, the common textural types of gold mineralization are mainly representated by disseminated (in altered host rocks), veinlet (oriented veinlet set), breccia (both in matrix and fragments) and individual quartz veins (in the less deformed zones between shear bands).

The altered zone can arise up to 2 or 3 meters enveloping the individual vein or veinlet set. Three types of alteration are developed in relation to hydrothermal processes sourcing gold mineralization: Silicification, potassification (episyenitization, sericitization). In addition, chloritization develops only locally in some ore ocurrences at the south of the Ricobayo granite near the boundary with Villadepera Neises formation.

By far, silicification is the most important alteration and it affects pervasively the host rock, being some times very difficult to distinguish between hydrothermal quartz and recrystallized quartz issued from ductile deformation.

Feldspatization is always linked with silicification and this association is the most characteristic phenomena related to ored process. Some samples studied by microscopy have been defined as episyenites.

Fig. I -19 **REGIONAL GEOLOGICAL SETTING**

(After Gonzalez Clavijo - 1990)

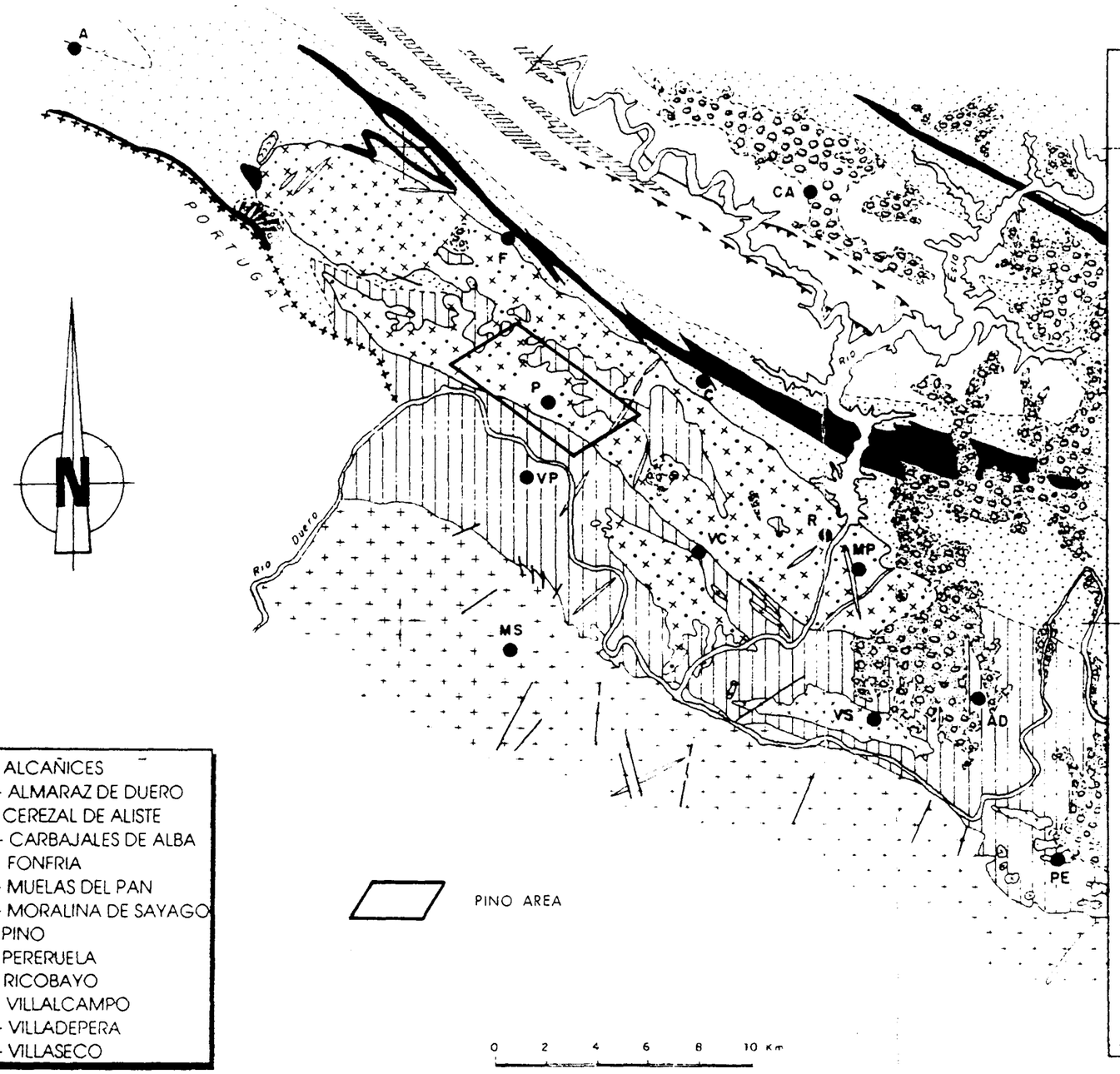

A - ALCAÑICES
AD - ALMARAZ DE DUERO
C - CEREZAL DE ALISTE
CA - CARBAJALES DE ALBA
F - FONFRIA
MP - MUELAS DEL PAN
MS - MORALINA DE SAYAGO
P - PINO
PE - PERERUELA
R - RICOBAYO
VC - VILLALCAMPO
VP - VILLADEPERA
VS - VILLASECO

LEGEND

- Quaternary-tertiary
- Carboniferous flysch (San Vitero Fm.)
- Silurian-devonian. Black shales, limestones lenses, greywackes, quartzites and volcanic rocks (Almendra Fm. and Manzanal Fm.)
- (a) Ordovician. Blue shales and shales and quartzites interbedded a) massive quartzites (Sierra de la Culebra Fm.)
- Precambrian-cambrian. Schists and Biotite-moscovite gneiss.
- Sayago two micas granites and granodiorites
- Ricobayo two micas granites
- Villaseco-Pereruela leucogranites
- Moveros diorites
- Quartz dykes

Fig. I - 20

GEOLOGY AND MINERALIZED ZONES OF PINO AREA

(After Gonzalez-Clavijo, E.; Ortega, C.; Florido, P.; Locutura, J.; 1991)

LEGEND

- Quaternary
- Precambrian-ordovician metamorphic units
- Ricobayo granite
  a) Garnet-sillimanite facies
- Ore-bearing ductile-brittle shear bands
  a) Brittle structures
  b
- Quartz veins
- 97 Gold-occurrences
- 1:5.000 scale detailed mapped zone

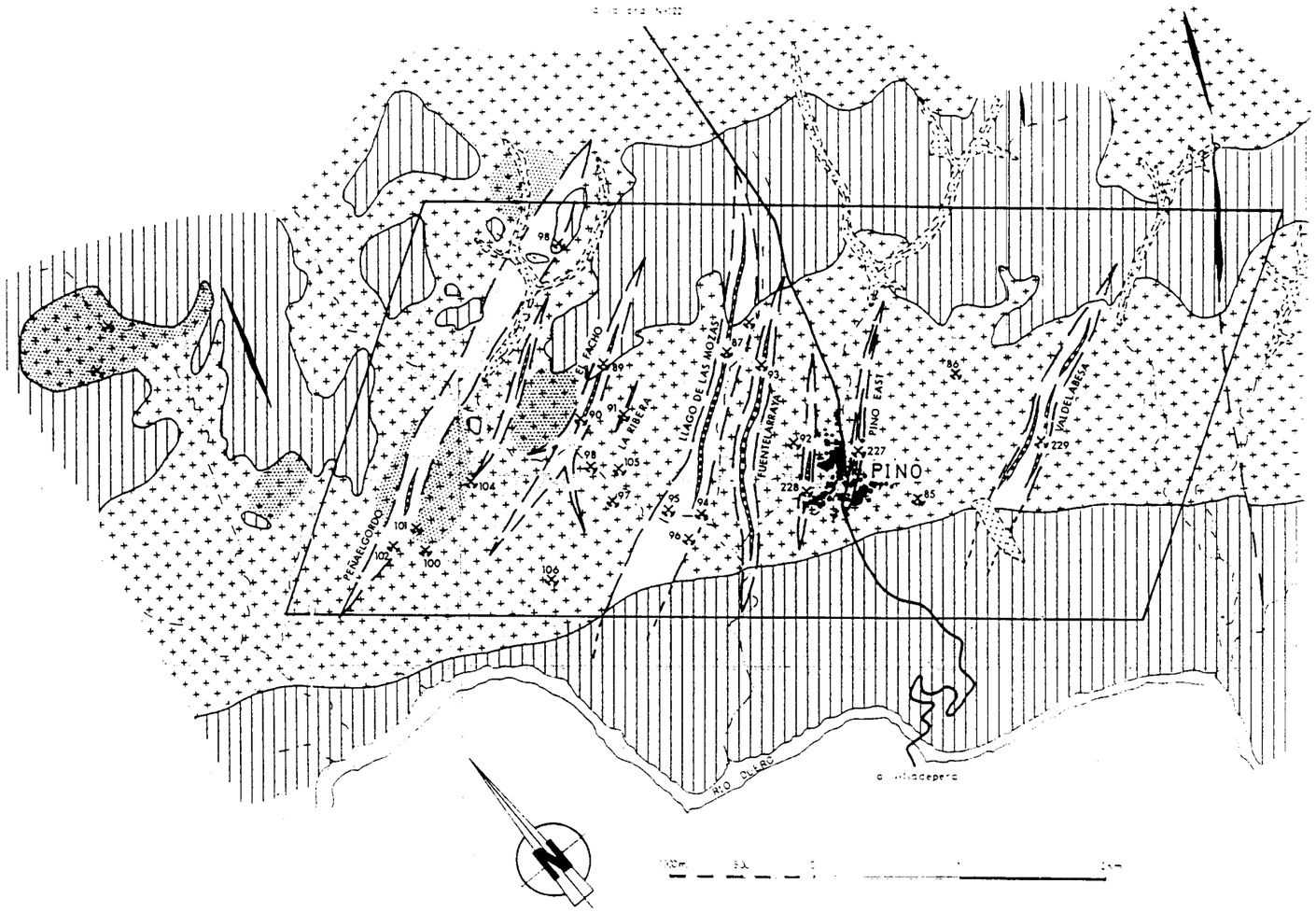

LEGEND

- Aluvial deposits
- Schists, sandstones and quartzites
- Two micas granite. a) Outcrops
- Mylonites
- Breccias
- Quartz veins
- Diabase dykes
- Aplite and/or pegmatite dykes

CONVENTIONAL SYMBOLS

- Unconformity
- Igneous boundary
- Fault
- Foliation within igneous rock
- Cleavage
- Vertical cleavage
- Bedding
- Shear with or without sense of movement
- Slickensides
- Joints
- (12) Drill - Holes (1986)
- Old mining works: Small open pits and shafts
- 93 Gold - Showings
- PP-3 Sample for petrography studies
- Garnets
- Pyrite – arsenopyrite
- Kaolinisation - sericitizacion
- K Potassification
- Si Silicification

0 100 200 300 400 500 m

Fig. I - 21

Instituto Tecnológico GeoMinero de España

PROYECTO					CLAVE
DETAILED EXPLORATION OF PINO AREA (ZAMORA)					
GEOLOGICAL MAPPING OF FACHO - LLAGO DE LAS MOZAS ZONE					PLANO N.º
DIBUJADO ITGE	FECHA Sept. 1992	COMPROBADO	AUTOR ITGE	ESCALA 1: 5.000	CONSULTOR

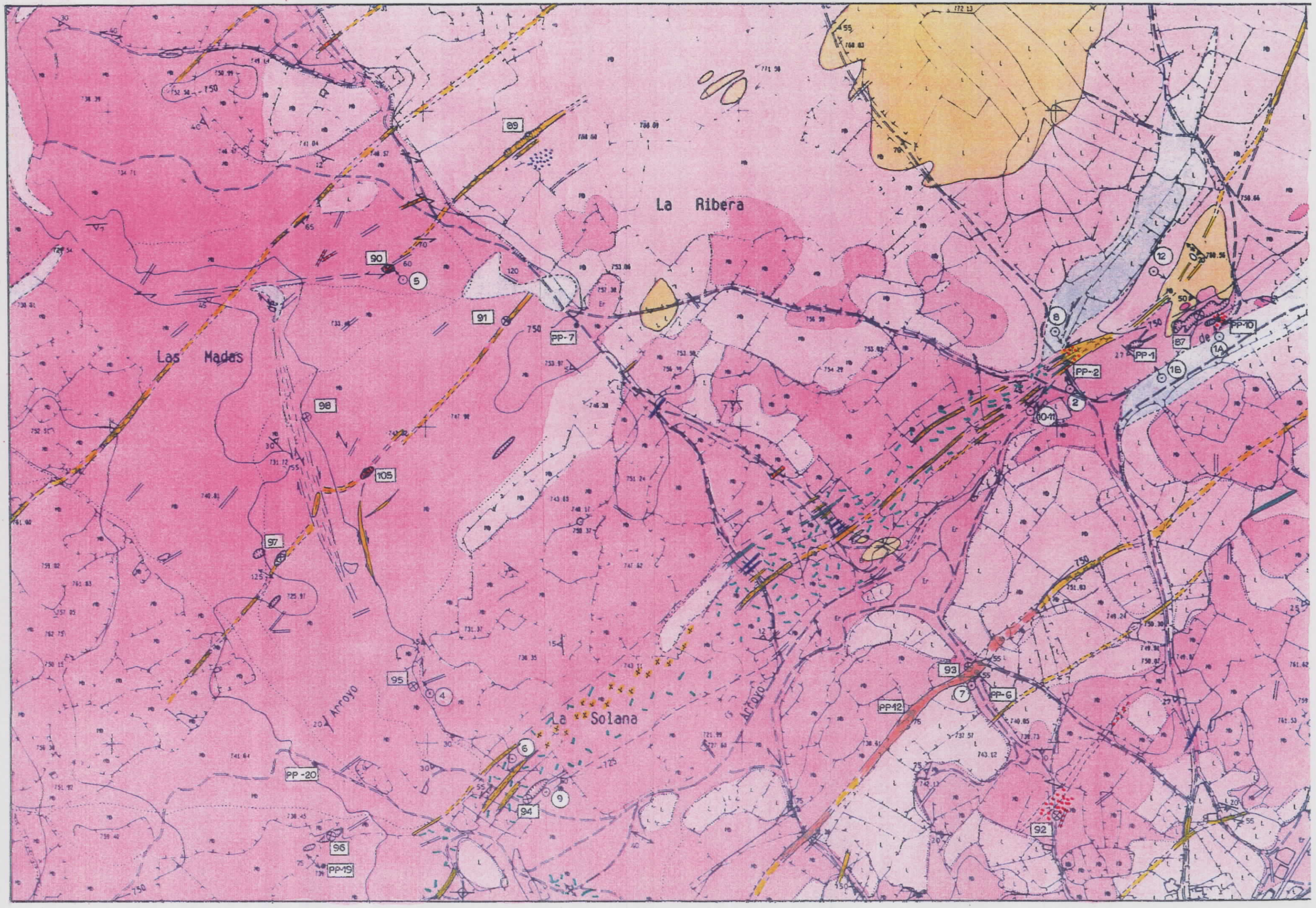
La Ribera
Las Madas
La Solana
Arroyo
Arroyo
de
89
90
91
98
105
97
95
96
94
93
92
PP-7
PP-20
PP19
PP42
PP-6
PP-2
PP-1
PP-10
10-11
12
8
5
4
6
9
7
2
1A
1B
87

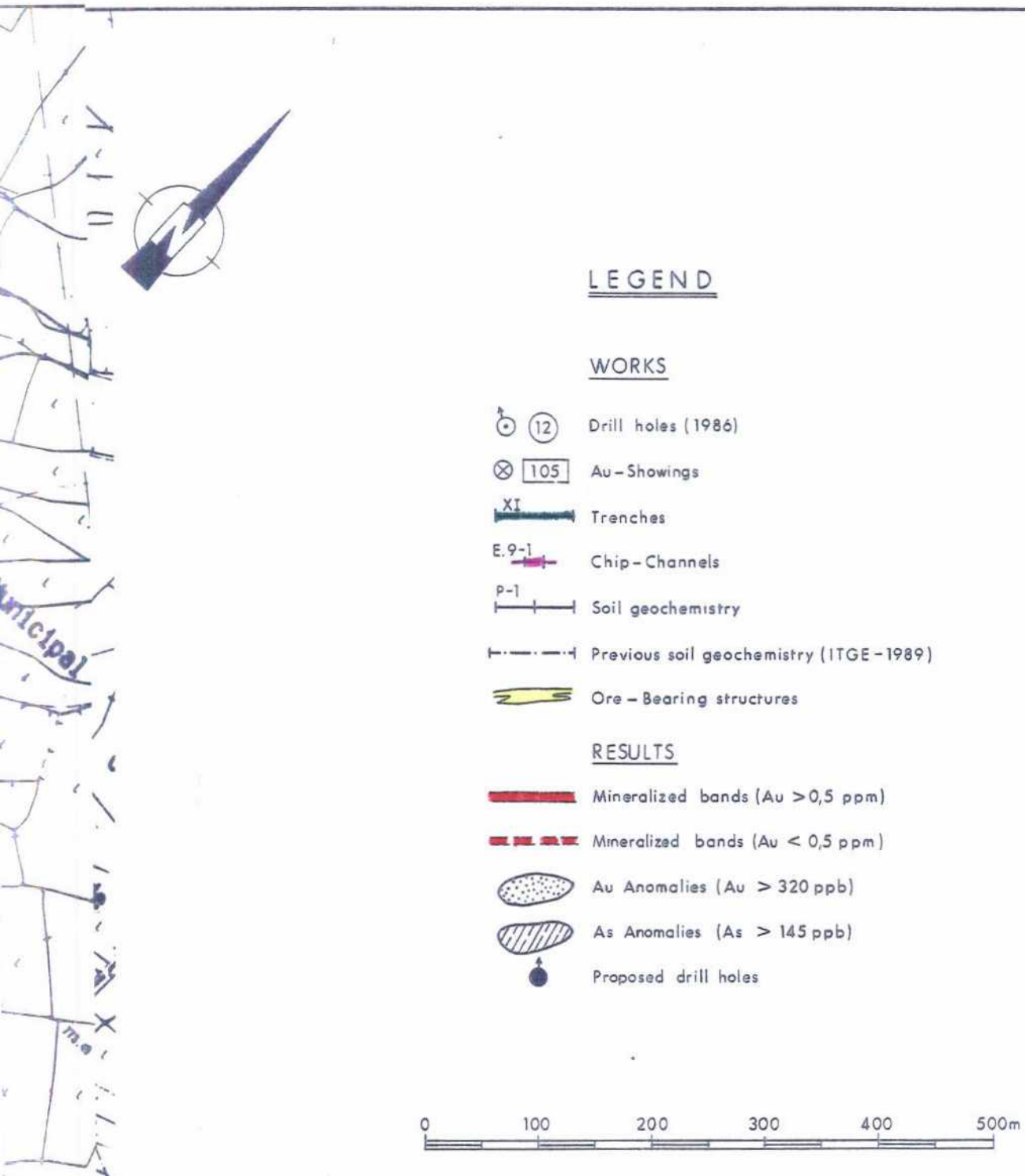

Fig. I - 22

Instituto Tecnológico GeoMinero de España

PROYECTO					CLAVE
DETAILED EXPLORATION OF PINO AREA (ZAMORA)					
FACHO ZONE : SUMMARY OF WORKSAND RESULTS					PLANO N.º
DIBUJADO ITGE	FECHA Sept. 1992	COMPROBADO	AUTOR ITGE	ESCALA 1:5.000	CONSULTOR

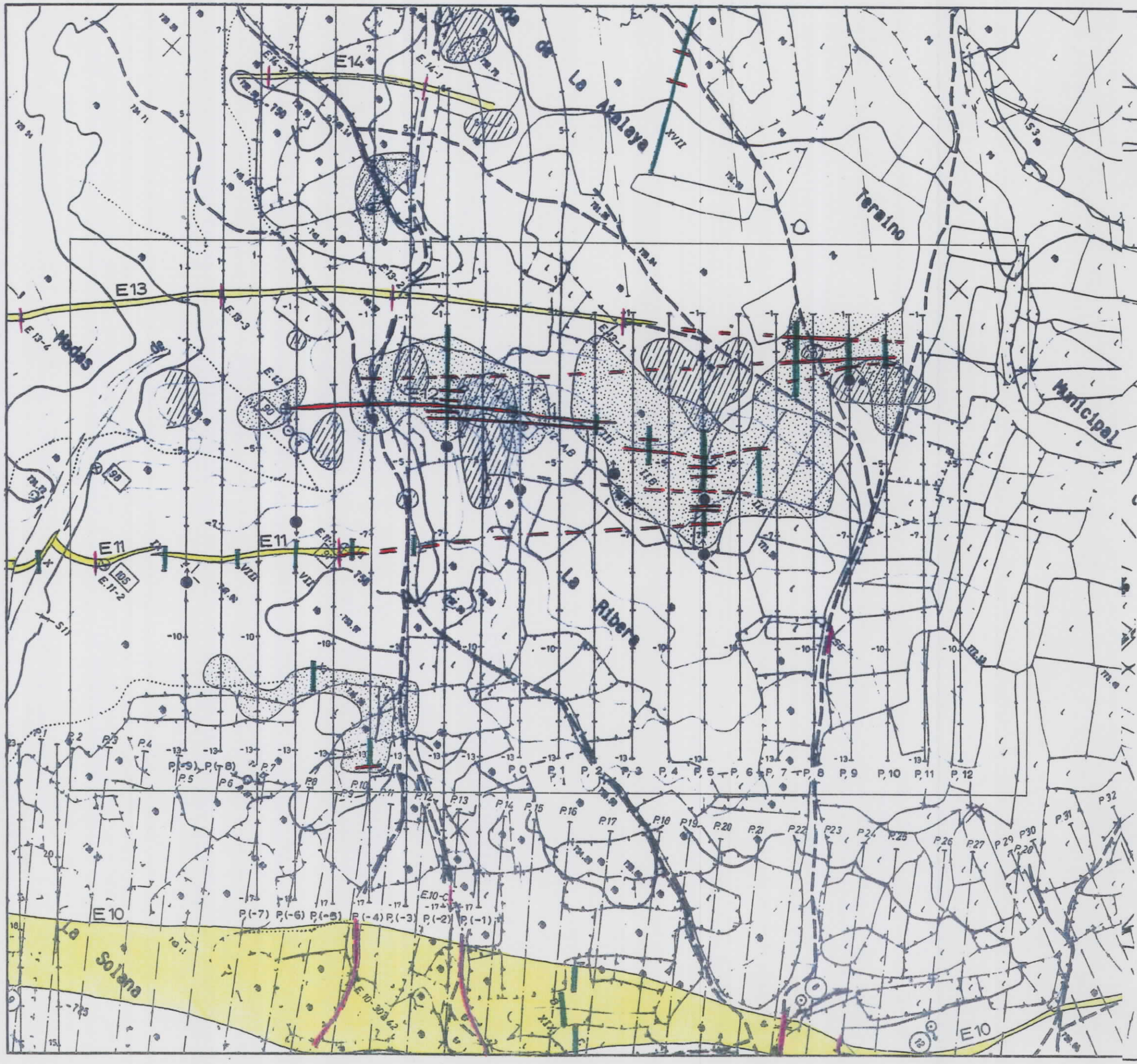

LEGEN

WORKS

- Drill holes
- Au – Showir
- Trenches
- Chip – Cha
- Soil geoch
- Previous s
- Ore – Bear

RESULTS

- Mineralize
- Mineralized
- Au Anoma
- As Anomal
- Proposed

0 100 200

Fig. II - 22

Instituto Tecnológico GeoMinero de España

PROYECTO
DETAILED EXPLORATION

FACHO ZONE : SUMMARY

DIBUJADO	FECHA	COMPRO
ITGE	Sept. 1992	

Sericitization is always related to silicification, but sericization and potassification have never been found together. It develops in open spaces around quartz veins, oriented in C-shear surfaces and cutting the latter in transversal planes.

The distribution of the altered zones show an arrangement in the same way that the internal shape of the mineralized structures, and no zoning can be defined.

Ore assemblage is very simple and similar in almost all ocurrences. Arsenopyrite is the most abundant mineral and can be found as idiomorphic crystals by metasomatic replacement of former minerals, as idiomorphic crystals in the cement of breccias or as broken crystals into fragments of mylonites inside the breccias. Very often, arsenopyrite is altered to scorodite.

Microscopic studies define zoned idiomorphic crystals of pyrite filling open space pyrite wich cut arsenopyrite crystals. In hand sample, pyrite occurs in path-shape filling cavities along of quartz veinlets.

On microscopic studies, gold has been found free within quartz vein and cataclasite. No gold appears in arsenopyrite from the studied samples. Chalcopyrite and magnetite appear like subordinate mineral in same samples. Sphalerite appear only in a small ore ocurrence, located in the south part of Ricobayo granite, which is the only one where cloritic alteration has been defined.

5- SOIL GEOCHEMISTRY.

Previous surveys carried out by Mining Service of Castilla-Leon Community (1986) reveal that As is the only element wich has,in some way, a geochemical signature similar to Au. These two elements have been therefore analyzed systematically.

On basis of geological mapping and metallogenetic studies five zones have been selected to carry out soil geochemical surveys. These zones are named A, B ,C ,D, E and F, and correspond to a set of mineralized structures mostly NW-SE :

- the soil samples have been collected in a square grid of 50x50 meters.
- the threshold values have been calculated for each area and then for the whole area.

The following thresholds of anomalies of first order have been considered:

Area	A	B	C	D+E	F	WHOLE
Samples collected	144	256	471	1124	644	2.639
Au (ppb)	40	265	615	100	90	320
As (ppm)	70	245	190	75	50	145

Analyses show a Au-As correlation coefficient on normal values of 0.63 and on logarithm values of 0.61, wich can be considered medium-high.

Two main, closely situated, anomaly areas have been found. They are defined both by Au and As values, within C area enclosing Facho structure and alineated on its direction (Fig. I- 21, 22 and 23). Other two anomalies locate at north and south of the former. Trenches and chip channels made to search these anomalies have cut several mineralized bands with gold values ranged between 1 and 32.95 ppm. Smaller Au anomalies are located in B and D areas, but in these ones As and Au anomalies areas do not overlap.

6 - ROCK GEOCHEMISTRY.

Rock geochemistry survey has been made to test exploration targets defined after the mapping of structures and the determination of the soil geochemical anomalies.

Ore-bearing structures, which are numbered from nº1 to nº16 (in SE to NW way), have been tested by chip channels and soil geochemistry anomalies were tested by trenchs (Total: 608 samples).

Sampling in chip channels was made along several transversal sections along each structure. In a general way one sample was collected for each section, so each analysis shows the media of whole width of the structure in that section. Only on Llago de Las Mozas-La Solona structure (n° 10) several samples have been collected along each section due its anomalous thickness (near 200 m. in some places). Also some individual samples have been collected to test particular bands with veinlets or altered zones.

Samples from trenchs are usually 1 meter in width. Petrography, structural features of the crosscut structures have been studied and confronted to the Au content distribution. Examples of typical mineralized structures are shown in figure I-24 The latter shows the clear spatial assocaition of mineralized structures with subsolidus alteration such as feldspathization (episyenites).

Table I-6 shows that Au contents in rock samples from mineralized areas vary from 0.5 to 8 ppm, the highest value got beeing 32.9 ppm Au.in a sample from a trench from El Facho zone. Comparing chip channel samples to those from trenchs, the later ones show higher values than the former due the different thickness of the samples.

The Au and As contents show contrasted behaviour along the trenches (Fig I-25) : i) the high values or the two element contents may be found in the same samples, indicating a control of Au by the arsenopyrite, ii) the high As contents may be found in places where no gold concentrations are detected, and vice versa, indicating a spatial association at the meter scale, but the lack of correlation at the sample scale. It is rather difficult to interpret the distribution of the Au values in these surficial trenches. It is especially difficult to know if the present day location of the gold accumulation is controlled only by the initial distribution or by weathering effects which could have produce local redistribution.

Histograms and cumulated frequencies of Au and As contents are presented in Figure I-26. Values in the trenches are mostly in the 10-1100 ppm with a mode 100 ppm, and Au in the 0.01-9 ppm with a mode around 0.1 ppm. The rock analysis show a Au-As correlation coefficient very similar to the one got in soil geochemistry: 0.61 for the whole area and 0.618 considering only the Facho area data (Fig. I-27).

The best results from chip channels ad trenchs, both on gold content and ore bearing structure cut in trenchs, yield there where Au and As geochemistry anomalies clearly overlap.

Data from drill hole done by Junta Castilla-Leon (1986) in Pino area show the heterogeneity of the ore shear bands in vertical sense, both of internal shape, thickness, and gold content.

The study has helped to define the best objective where I.T.G.E. will carry out a geophysical survey (I.P.) over all ore-bearing structures and a drill hole programme, which will let to know the vertical extent of the surface data obtained in this study.

7.- CONCLUSIONS.

- Gold and arsenopyrite are controlled by the same structures, then As can be used in strategical exploration tool for gold.
- In detail, rock geochemistry shows some samples with high gold content and very low As content. On the other hand, gold in polish section has only been seen like free gold.

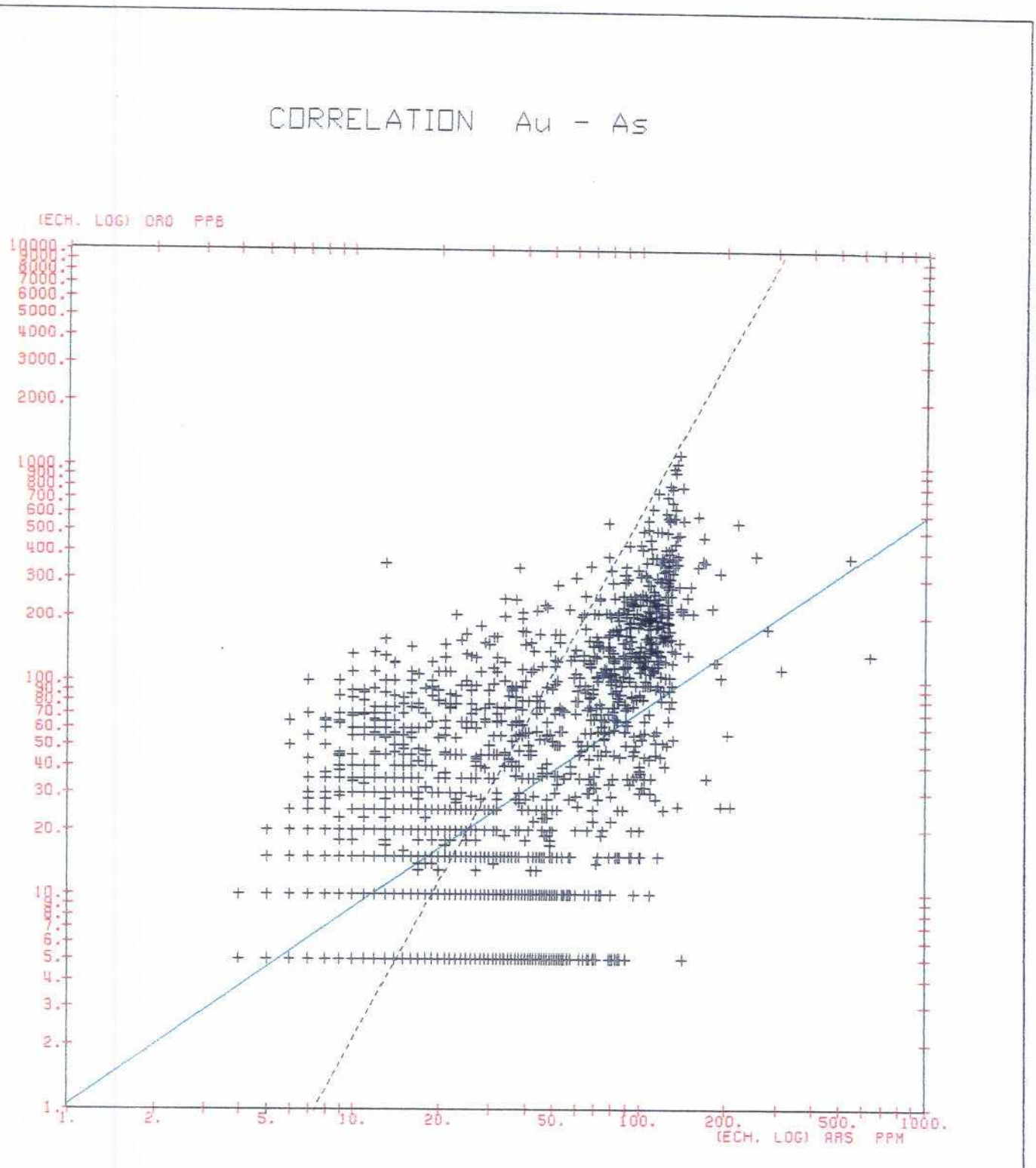

2639 SAMPLES
GEOM. MEANS: 20.4 (Au) 25 (As)
VARIANCES : 2.0 1.38
CORRELATION COEFFICIENT: 0.613
REGRESSION LINES:

——— LOG(Au)=0.919*LOG(As)+0.0
------ LOG(As)=0.409*LOG(Au)+1.0

Fig. I - 23 : Au-As binary diagram applied to soil chemical analysis.

C - I

p.p.m Au	0.07		0.03	0,112	3,433	0,215	0,204	0,150	0.08	0.113	0.01	0.07	0.065	0.065	1,625	0,812	0,587	0,475	0.412	0,415	0.2	0,05	0.2	0.25	0.187	0.03	0.075	0,02	0,125
p.p.m As			29	75	491	188	289	35	87	93	66	77	63	85	331	397	1407	245	287	196	321	336	706	948	293	328	261	119	194
Nº muestra	1		2	3	4	5	6	7	8	9	10	11	12	13	14	15	16	17	18	19	20	21	22	23	24	25	26	27	28

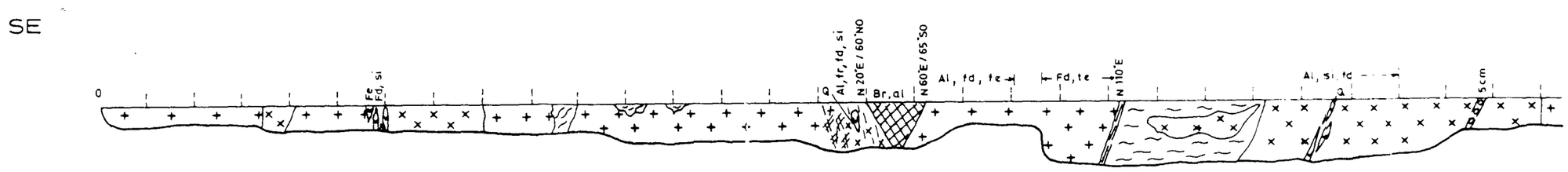

C - III

p.p.m Au	0,04	0,02	0,02	0,184	<0.005	< 0.005	< 0.005	0,185	0,326	7,525	0,119	1,520	0,087	0,641	0,42	0,27	0,18	0,25	0,24	0,195	0,293	0,26	0,16	0,174	0,17			
p.p.m As	61	48	112	109	120	83	85	145	284	279	327	1224	112	1764	932	746	265	305	307	310	810	280	176	173	99			
Nº muestra	1	2	3	4	5	6	7	8	9	10	11	12	13	14	15	16	17	18	19	20	21	22	23	24	25			

1
2
3
4
5

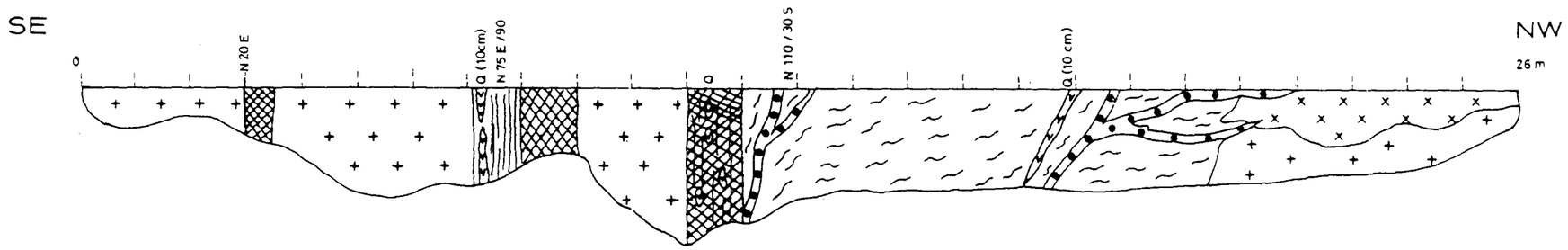

Fig. I - 24 : Examples of typical profiles along mineralized structures with indication of the petrographic and structural features.
1 - Schists; 2 - Two micas coarse grain granite, 3 - Fine grain biotitic granite, 4 - aplite, 5 - Breccia. Q: Quartz, Al : alteration , Fr : fractures, Br : brecciation., Fd : feldspars, Fe : Fe oxydes, Si : silicification.

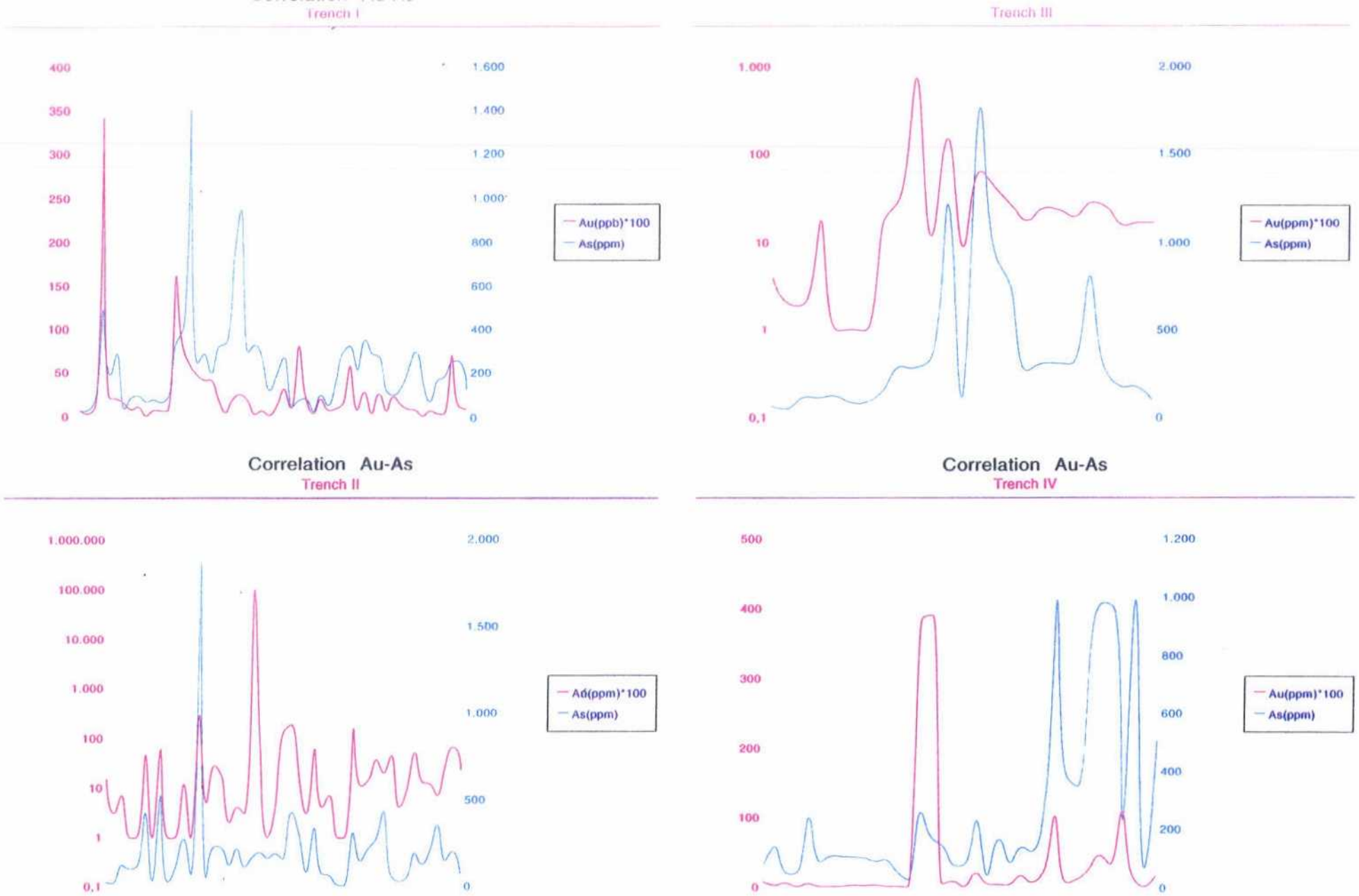

Fig. I - 25 : Au-As profiles along the trenches carried out in the Facho zone.

Fig. I - 26 : Histograms and cumulated frequencies of Au and As content for the trench samples from the Facho zone.

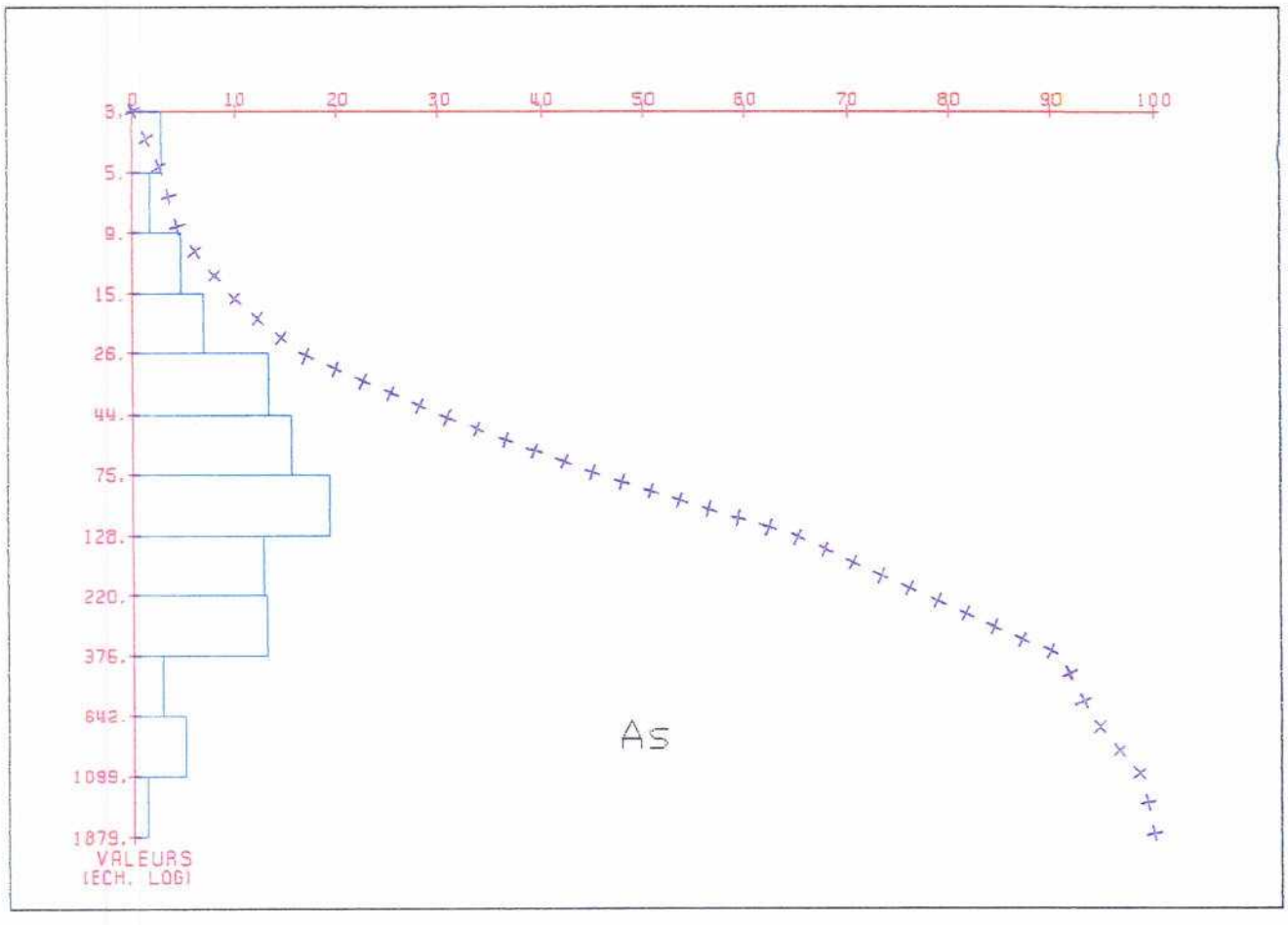

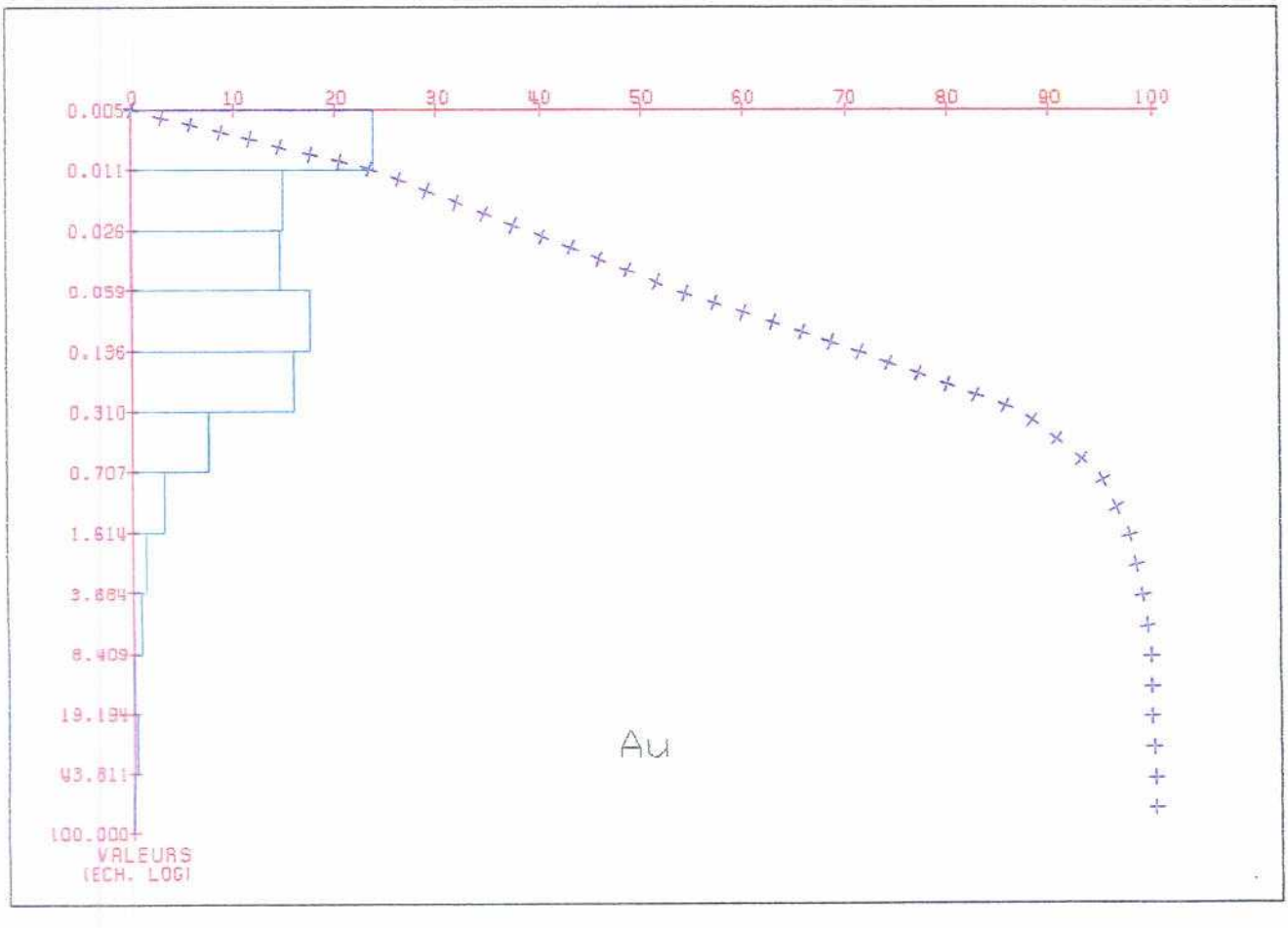

Structure	Prospect nº	Main textures	Au(ppm) (*)
Peñaelgordo	100-101-102	Quartz vein Breccia Altered granite	1.20 (1m.-tr) 0.68 (g.s.)
El Facho	89-90	Altered granite Quartz veinlets myloniytes Breccia	3.88 (2m.-tr) 1.02 (1m.-tr) 1.08 (1m.-tr) 2.07 (1m.-tr) 32.9 (1m.-tr) 36.0 (g.s.)
La Ribera	91-97-105	Quartz vein	8.17 (3.5m-chip) 1.66(4.8m.-chip) 2.66 (g.s) 15.00 (g.s.) 3.75(1m.-tr) 1.30 (1m-tr)
Llago de las Mozas	87-94	Quartz veinlets Altered granite	1.50 (g.s.) 7.70 (g.s.) 5.44(from.m 57 to m.65 of d.h)
Fuentelarraya	97	Quartz veinlets Altered granite	3.80 (g.s)
Pino East	227	altered granite	0.33 (g.s.) 0.29 (4m.-tr)
Valdelabesa	229	Breccia Quartz vein	 1,22 (g.s.)

(*) tr: sample from trenches
ch: sample from chip channels
d.h.: sample from drill hole

1m.: thickness of the sample

g.s.: geological sample

Table I - 6 : Main gold analysis of Pino mineralized zones

These datas agree with those from fluid inclussions about the distinct stages of concentrations of gold and arsenic.

- Gold ocurrences are located both in ore-bearing sinistral shear bands and in the less deformed zones between those structures.

- Geological sections and Au-As analysis, both got from trenches made in zones without outcrops, indicate that soil geochemistry is a good tool for exploration of this type of mineralization.

- The higher gold values are shown in the structures with a ductile-britle behaviour while the lower gold content are shown in those where brittle deformation prevails.

AU CONCENTRATIONS IN METAMORPHIC SERIES

Two zones have been chosen :
- a major district in North-Eastern Portugal, which includes the Vilarica fault zone (Franca deposit, and other gold showings from the Vila Pouca de Aguiar zone) and the Moraïs domain ;
- the Montemor area, in the Ossa-Morena Zone.

A- FRANCA

The França mine is located in Tras-os-Montes province, northeast of Portugal,15 Km north of Bragança town, near the Spanish border. The Au-Ag mining area is composed by four mining concessions: Pingao dos Quintais, Fonte Cova, Vale do Cancelo and Covas Altas. The "Sociedade Mineira da Serra do Cercal" is the actual owner of the concession (Fig. I-28).

The mining activity in this area moves backwards to the Antiquity, most probably to pre-roman period. Some ancient open pits like the "Boca da Caborca" pit remain from that time. The modern mining activity started in 1910-11. The mining owner was Burnay Bank. Old reports from this period reefer to Roman underground mining activity in the "Pingao dos Quintais" concession, where a quartz vein was exploited till 16 m dip (Burnay Bank, 1910).

The explorations and mining works in this period have been concentrated in the concessions near the village, namely in the "Pingao dos Quintais" mining concession. A report from 1911 about "Vale do Cancelo" concession refers to the small and little important old mining works. Soon the concession was relinquished by the mining company.

In the "Covas Altas", several N70-75°W/80°N or vertical quartz veins are reported with an average thickness of 0.8 m. The Au ore grades range from 5 to 30 g/ton. In the 1946-51 exploitation period the ore grade was 5-10 g/ton. Au (Burnay Bank, 1910, 1948).

In the "Pingao dos Quintais" concession, a set of ten N75°E/60°N quartz veins had been recognized. At least four of these mineralized structures were mined. Each one were mapped at the surface for more than 300 m along strike and they are distant 100 m from each other (Burnay Bank, 1913). Their maximum thickness were 1m. Chemical analyses reveal a Ag/Au ratio around 5:1 (Burnay Bank, 1948). The ore grade was less than 10 g/ton Au and 50 g/ton Ag (Carvalho, 1979).

Till 1951 more than 600 m of galleries up to 70 m depth were done. These works were concentrated in one of them, called the "Pingao dos Quintais" lode. It was recognized by galleries in 350 m along strike till the depth of 45 m (three levels). The vein has 1 m of average thickness. It is mineralized in pyrite, chalcopyrite, galena, arsenopyrite and siderite; gold and silver are associated to the arsenopyrite (Carvalho, 1979).

The exploration mining works stopped about 1951. By 1960 the mining legal rights were transferred to the actual owner company. It was not found any information about the production of this mine. It is possible that officialy it was considered allways in the exploration stage by the owner of the concessions.

More recently (1988-89) with the rising of gold prices some exploration work were carried out by a joint venture C.M.P.-Cercal-Prominas. Surface and underground geological mapping was done, as well as an extensive lithogeochemical program sampling.

Only two galleries, with a total length of 200 m, were re-opened in the "Pingao dos Quintais" lode,which exhibits a gently dip to S (30°-60°) and strikes E-W. This lode was sampled for gold analysis, and the average grade is 15 g/t for 1m average width (vein thickness + 0,5 m of host rock). This grade goes down to 5 g/t with the dillution of the 2,5 m width gallery (Prominas, 1988) (Fig I - 29).

Some comments can be draw about the extensive sampling program carried out by the joint venture in the mine area (Prominas, 1988). A wide range of lithologies were collected and analysed for gold (455 samples): fault breccia, (14); graphite shales, (26); magnetite level, (14);

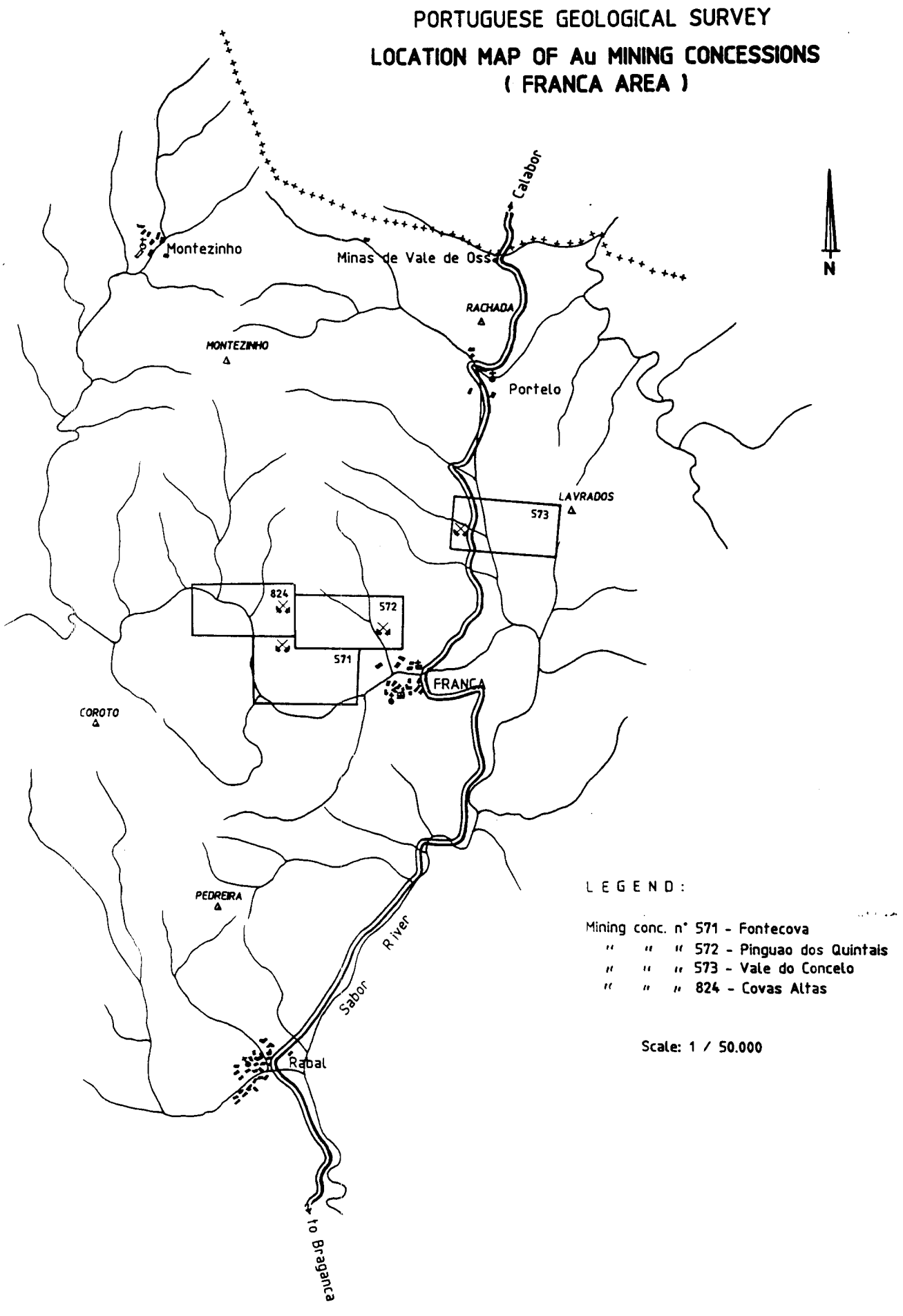

Fig. I - 28 : Location map of the mining concessions in the França - Rabal area (1:50.000 scale)

quartz veins, (137); quartzites, (69); slates, (195) (Fig I-29). Excepted the fault rocks and veins, all the lithologies belongs to the Ordovician metasediments. The analyses were obtained at the OMAC Laboratories, Ireland.

Concerning the fault breccias and quartz veins, it should be noted that the majority of the samples were taken in E/W or N80°E and N60°W structures. The average grade of quartz veins is 1.7 ppm, although localy it may reaches 43 ppm (Fig. I- 29 and 30).

In general, the host rocks of the mineralized veins show Au contens less than 20 ppb, but in the vicinity of the Au rich quartz veins the gold average is around 0.7 ppm.

Only a small part of the underground minig works was studied by this joint venture. It is obvious that the re-evaluation of this mine is still not done. It will be necessary: 1) a large drilling program that was never done before; 2) the reopened of all the underground works; 3) an accurate geology of all these galleries and much more analysis. The gold prices in 1988 were favourable for a more strong investment in the exploration as the grades seams to be quite good. Today, with the lower prices of gold, it is not economicaly workable.

For the França area, three main questions were open at the beginning of the present study: (a) the real potential of the quartz veins exploited in the 20th century works in the França mine was not properly assessed, and the causes of the mine failure were unknown; (b) the mineral paragenesis of the veins had not been described, nor were there any characterization thereof; (c) a comparative study of the modern and the Roman mining works was still lacking. The present study yielded a complete characterization of the gold–silver ores at the França mine and there is now complete answer to questions (a) and (b) above:

1 – the richest ore consists of quartz breccias located along the main trace of the Vilariça fault, and was apparently completely exploited by the Romans; there is evidence for Roman exploroitation (oxidized fault breccias) in regional shear zones N80°E far from the mine site.

2 – tension fractures related to a releasing bend of the Vilariça fault, first mentioned in Mateus (1989), contain the best prospects for gold exploration nowadays in the mine sector;

3 – the modern mining work exploited quartz veins associated to the reactivation of a regional shear zone almost normal to the Vilariça fault trend.

4 – the 20th century mine run out of ore because an incorrect structural control was followed: the regional shear zone towards the W. Nevertherless, the presence of Roman works, along the regional shears far from the França mine suggests that these structures may control some Au-lodes, probably of a different age.

5 – the quartz breccias referred to in (1) grade vertically upwards to barren (extremely) oxidized equivalents, due to supergene processes dating from the Pliocene–Early Quaternary. In the present study, we show that barren breccias at the surface may be a good indicator of ore at depth.

2 - LOCAL GEOLOGY AND STRUCTURAL FEATURES (Fig. I-31)

The França lode gold–silver deposit is located in the Autochthon Domain of the Central–Iberian Zone (Ribeiro, 1974, 1981), where it comprises a succession of quartzites interbedded with black schists (Arenigian – Llanvirnian ?) and slates with carbonaceous horizons (Llandeilian) (Fig. I-32). These lithologic units outcrop along the axial domains of first order D1 folds (anticline and syncline, respectively) with vergence to the NE and axes oriented 10°, 125°–130°; in general, the S1 foliation strikes WNW to NNW with a steep SW dip. The Vilariça strike–slip fault zone, one of the main Late Variscan left–lateral strike–slip fault in the Iberian Peninsula, brings to contact the above Upper Ordovician units with graphitic slates and lidites of Silurian age (Llandoverian).

The metasedimentary sequences experienced regional metamorphism of generally low pressure and temperature (chlorite facies). However, near the syntectonic granites (intruded during D1 and D2 Variscan deformation phases), they exhibit (regional) mineral parageneses characteristic of higher grade facies (biotite and andalusite zones).

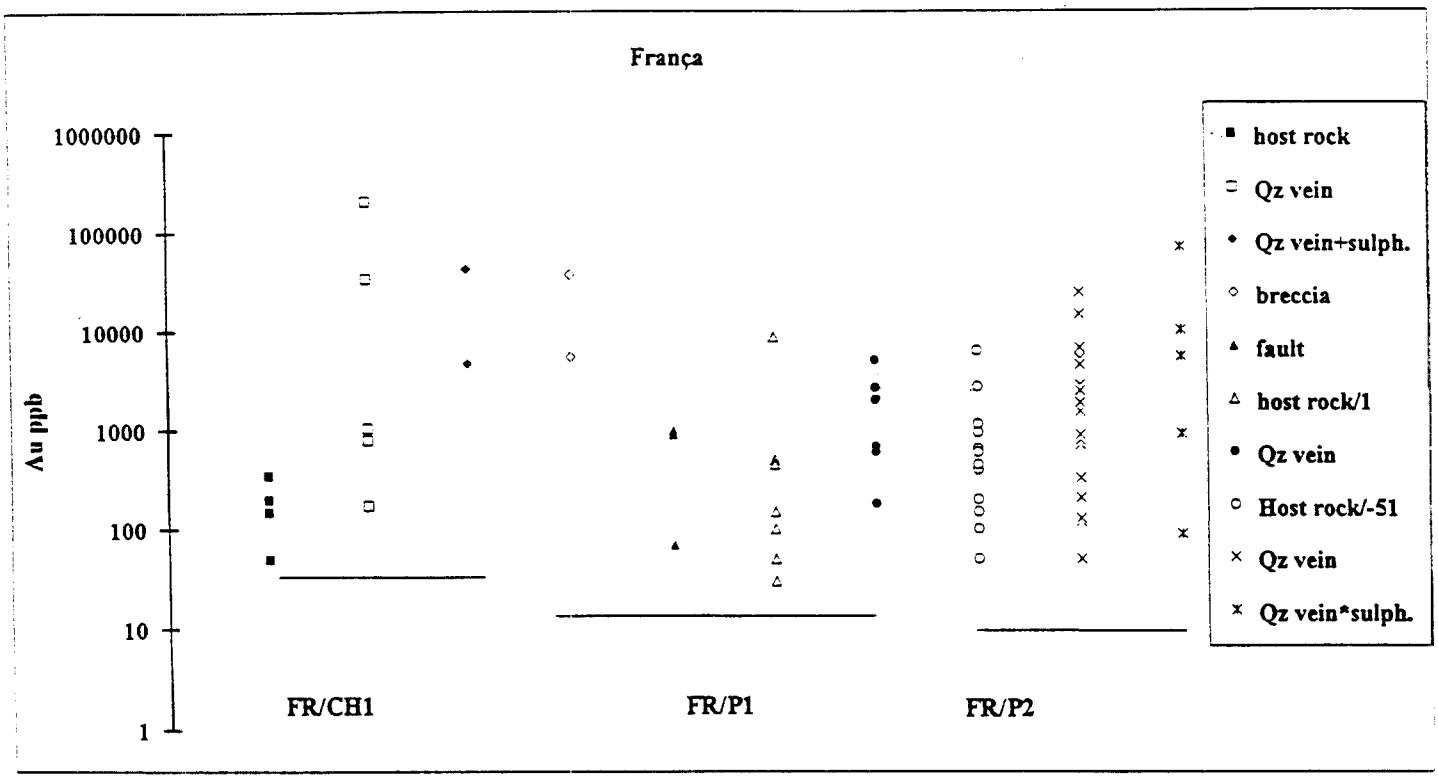

Fig. I -29 : França mine : Au content in Pingao dos Quintas lode (Prominas, 1988); FR/CH1 : mining shaft 1, FR/P1 : mining level 1, FR/P2 : mining level 2.

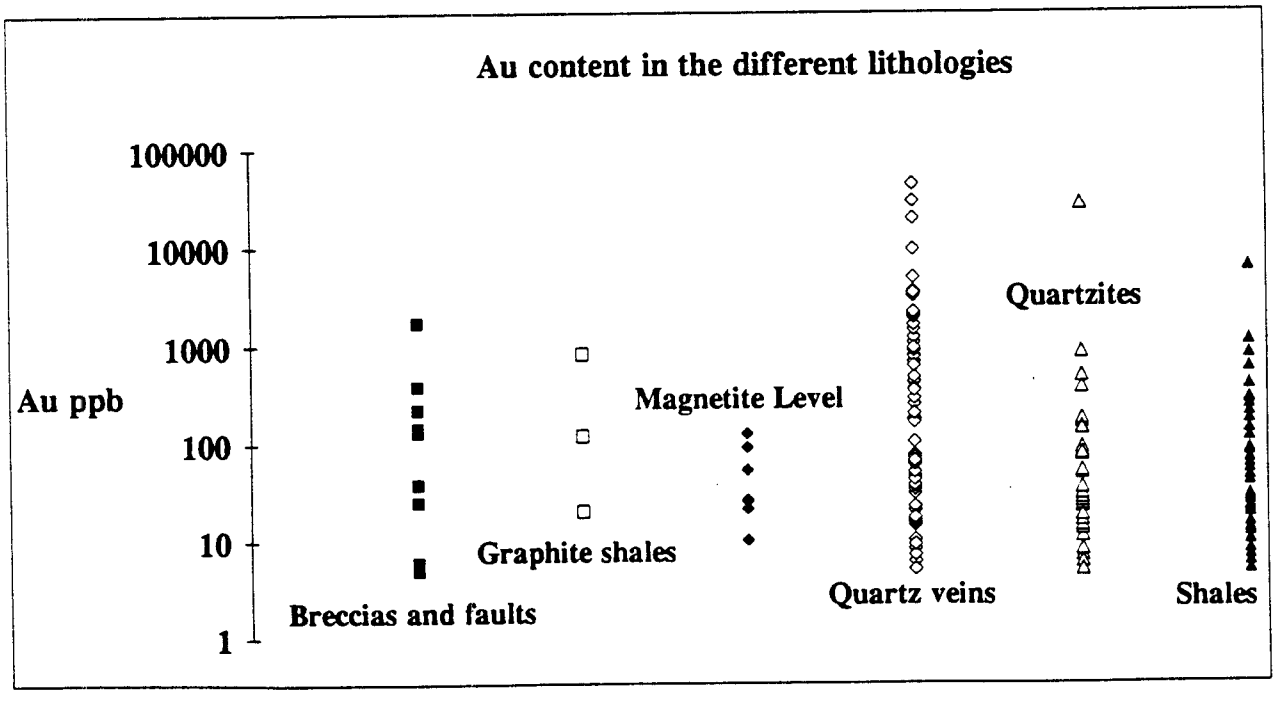

Fig. I - 30 : França mine : Au content in different Ordovician lithologies (Prominas,1988)

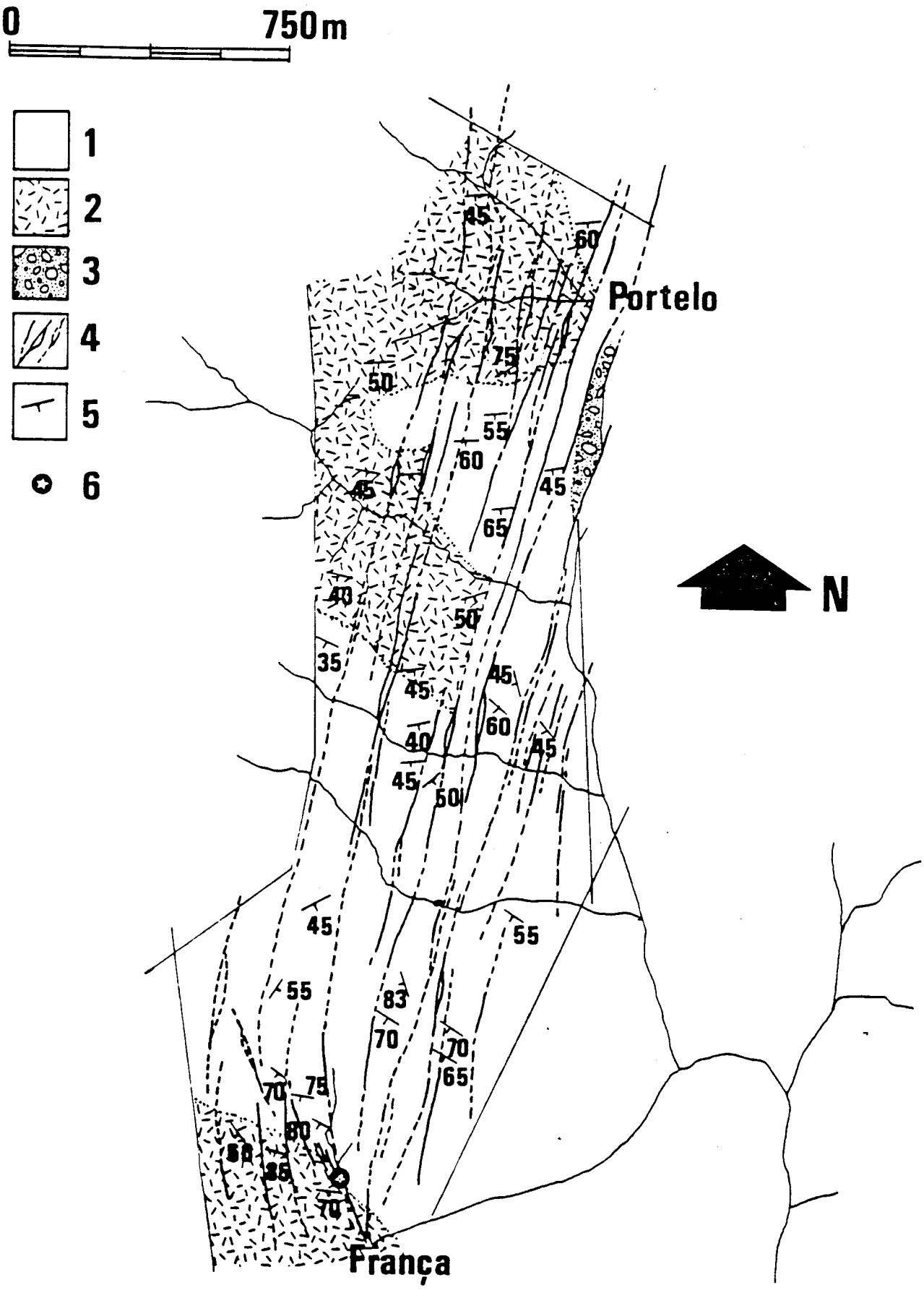

Fig. I - 32 : Geological map of the França /Portello sector. 1 - slates with thin iron lenses and carbonaceous horizons (Llandeilian); 2- quartzites interbedded with (black) schists (Arangenian- Llanvirnian?); 3 - Rana cover deposits; 4- fault zone underlined by brecciated, iron-enriched quartz fillings; 5- regional foliation S1; 6 - mining works.

The studied area comprises 40 Km2 of the army 1:25,000 scale maps, n° 12 and 25. Its limits are the 312,000 meridian at the West; the Spanish border at the North; the Vilariça fault system at the East and the allocthonous Bragança massif at the South (Fig. I - 33).

ORDOVICIAN.

Upper quartzites - Arenigian.

It is composed by quartzites with dark-grey shales and psammites intercalations. The quartzites are grey in colour with iron oxides due to recent supergene alteration. Some are light yellow and more mica rich. The mineral composition of this rock is: quartz, some muscovite, abundant Fe and Ti oxides and a few tourmaline crystals. Only one cleavage (S0/S1) is evident. In some fractures parallel to this structure, abundant prehnite and epidote occurs suggesting a lower metamorphic grade associated to later hydrothermal activity.

Some sulphide rich dissemination levels (3-5 cm) occur within the quartzites, namely in "Boca da Caborca" open pit. They are composed essencialy by pyrite and limonite. It is possible that a volcanogenic origin be the responsable by this mineralization.

Some iron rich levels are common. The most important of them has an extension of 1,5 Km between the ancient open pit "Boca da Caborca" and the actual mining workings. Its thickness hardly exceeds 5m.

It is composed by coarse euhedral crystals of magnetite replaced by hematite along cleavage planes. The limonite is abundant and is associated either with the light minerals or surrounding the magnetite. Martite is probably related to an earlier hydrothermal event (fluids along shearing ?).

Grey phyllites with psamitic intercalations were mapped in the core of the quartzite antiform (Prominas, 1988). It could correspond to the intermediate shales subdivision proposed by Ribeiro (1974).

Slate Formation - Landeilian.

The armorican high deposition energy is followed by a monothonous sequence of pelagic carbonaceous muds characterized by the presence of purple-grey to blue-grey slates. Two deformation phases are evident and expressed by two cleavages: S1 slaty cleavage almost transposed and folded by S2 strain-slip cleavage. Quartz, moscovite and green biotite are the main minerals; chlorite and few tourmaline also occur; the iron oxides are abundant. Some low temperature veins, mainly silica and chlorite rich, may occur.

SILURIAN

In the Silurian formations there is a predominance of schists with strong lateral facies changes. It is accepted two distinct series, based in graptholite faunas, with Midle Llandoverian and Upper Llandoverian ages respectively. Regionaly a quartzite sandstone level makes the distinction of both series (Ribeiro, 1974).

In the contact with the Ordovician two situations can occur: 1- in the West block of the Vilariça fault, there is probably a transition from the Llandeilian to the Llandoverian; in the Silurian, the metasediments becomes more carbon-rich and occurs graphitic black shales. 2- the Vilariça fault put in contact the Ordovician metasediments with the lowest Silurian units; this can be seen within the mega kink Vilariça structure, near França village.(a and b units). From bottom to the top, it is possible to establish the following sequence for the Llandoverian:

Middle Llandoverian.

a) Basal conglomerate (tillite) and dark green shales.

This glacial conglomerate has regionaly a wide occurrence and it is considered to be the beginning of less stable Silurian sedimentary regime (Ribeiro, 1974). It is formed mainly by different clasts of quartzites, black cherts, and greywackes in a mud-flow pelitic matrix. The tillite seams to be interbeded with dark green carbonaceous shales, with psamitic and quartzitic centimetric intercalations. A few small lydites occurs (black chert lenses).

b) Greywackes unit.

It is composed by decimetric dark green greywackes with centimetric dark shales intercalations.

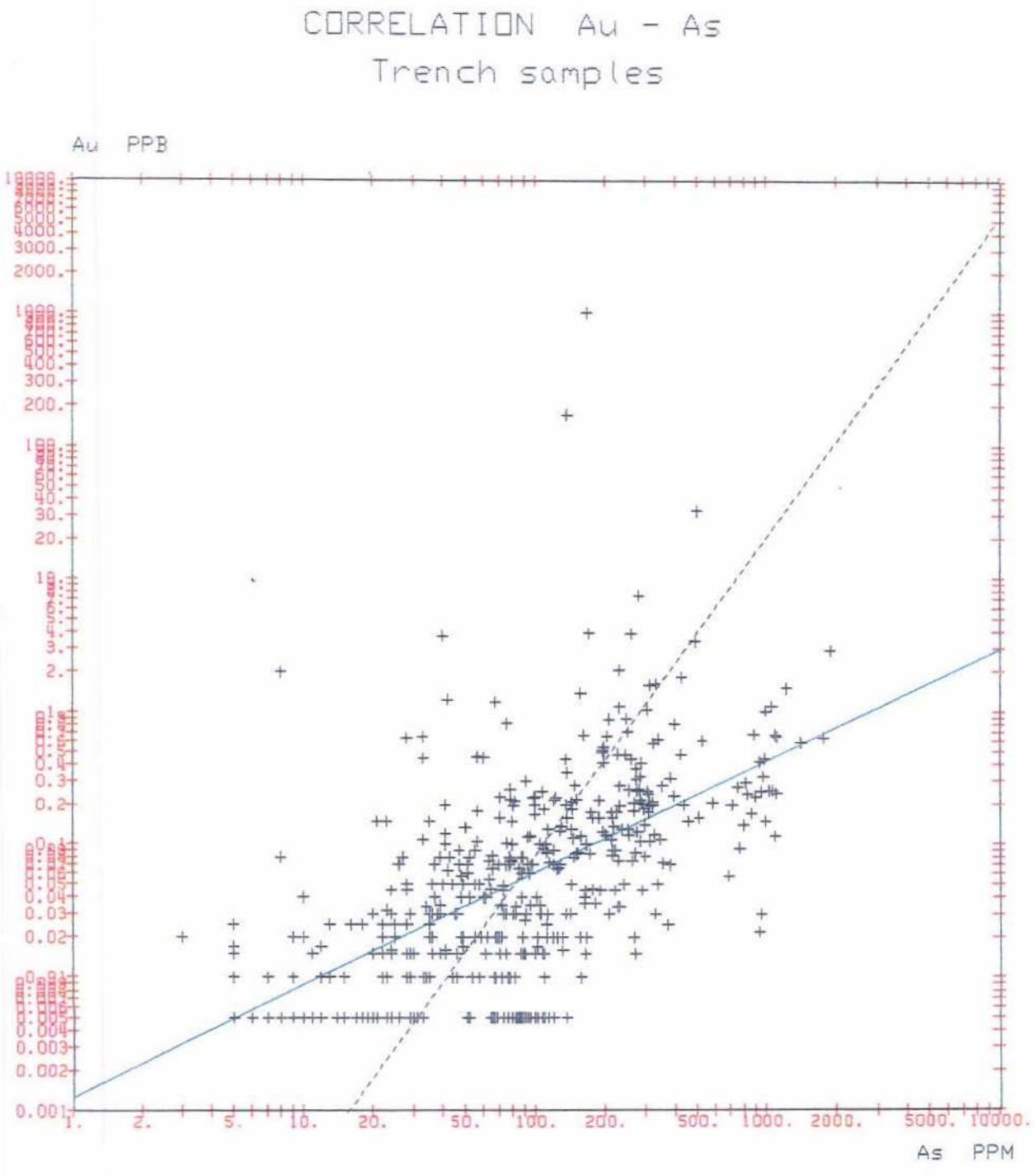

456 SAMPLES
GEOM. MEANS: 0.052 (Au) 82 (As)
VARIANCES: 3.866 1.951
CORRELATION COEFFICIENT: 0.592
REGRESSION LINES:
——— LOG(Au)= 0.843*LOG(As)-2.898
------ LOG(As)= 0.417*LOG(As)+2.0

Fig. I - 27 : Au-As binary diagram applied to chemical analyses of trench samples from the Facho zone.

Fig. I - 31 GEOLOGICAL MAP OF FRANÇA/RABAL AREA

GEOLOGICAL SURVEY OF PORTUGAL

SCALE: 1/25.000
DATE: FEV/93
AUTHOR: C. MEIRELES
DRAWN: J. OLIVEIRA

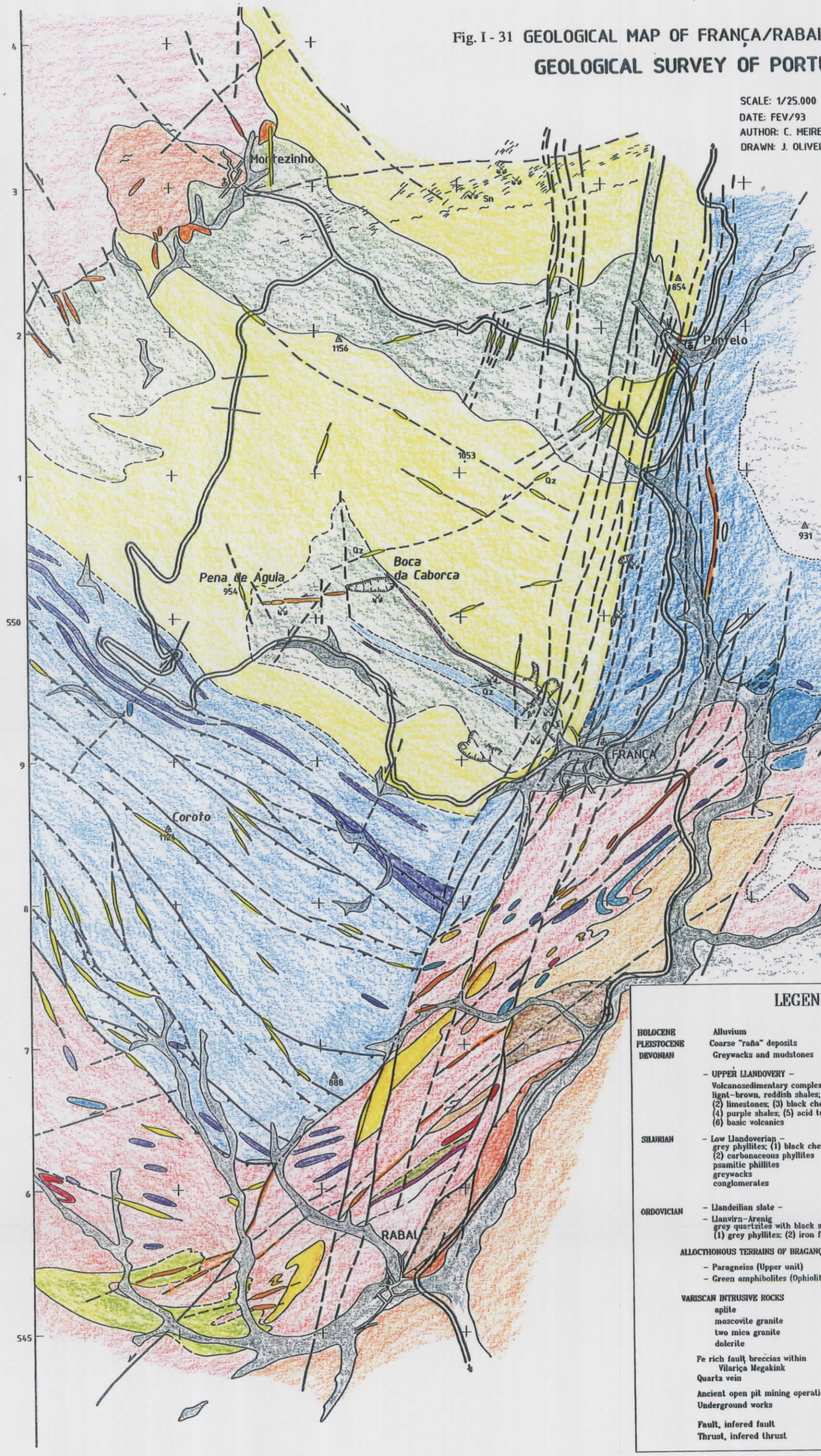

LEGEND

HOLOCENE — Alluvium
PLEISTOCENE — Coarse "raña" deposits
DEVONIAN — Greywacks and mudstones

– UPPER LLANDOVERY –
Volcanosedimentary complex
light-brown, reddish shales; (1)quartzites;
(2) limestones; (3) black cherts;
(4) purple shales; (5) acid tuffs;
(6) basic volcanics

SILURIAN — – Low Llandoverian –
grey phyllites; (1) black cherts;
(2) carbonaceous phyllites
psamitic phillites
greywacks
conglomerates

ORDOVICIAN — – Llandeilian slate –
– Llanvirn-Arenig
grey quartzites with black shales intercalations;
(1) grey phyllites; (2) iron formation

ALLOCTHONOUS TERRAINS OF BRAGANÇA MASSIF
– Paragneiss (Upper unit)
– Green amphibolites (Ophiolitic unit)

VARISCAN INTRUSIVE ROCKS
aplite
moscovite granite
two mica granite
dolerite

Fe rich fault breccias within Vilariça Megakink
Quartz vein
Ancient open pit mining operation
Underground works
Fault, infered fault
Thrust, infered thrust

STRUCTURAL DATA MAP FRANÇA/RABAL AREA

GEOLOGICAL SURVEY OF PORTUGAL

SCALE: 1/25.000
DATE: FEV/93
AUTHOR: C. MEIRELES
DRAWN: J. OLIVEIRA

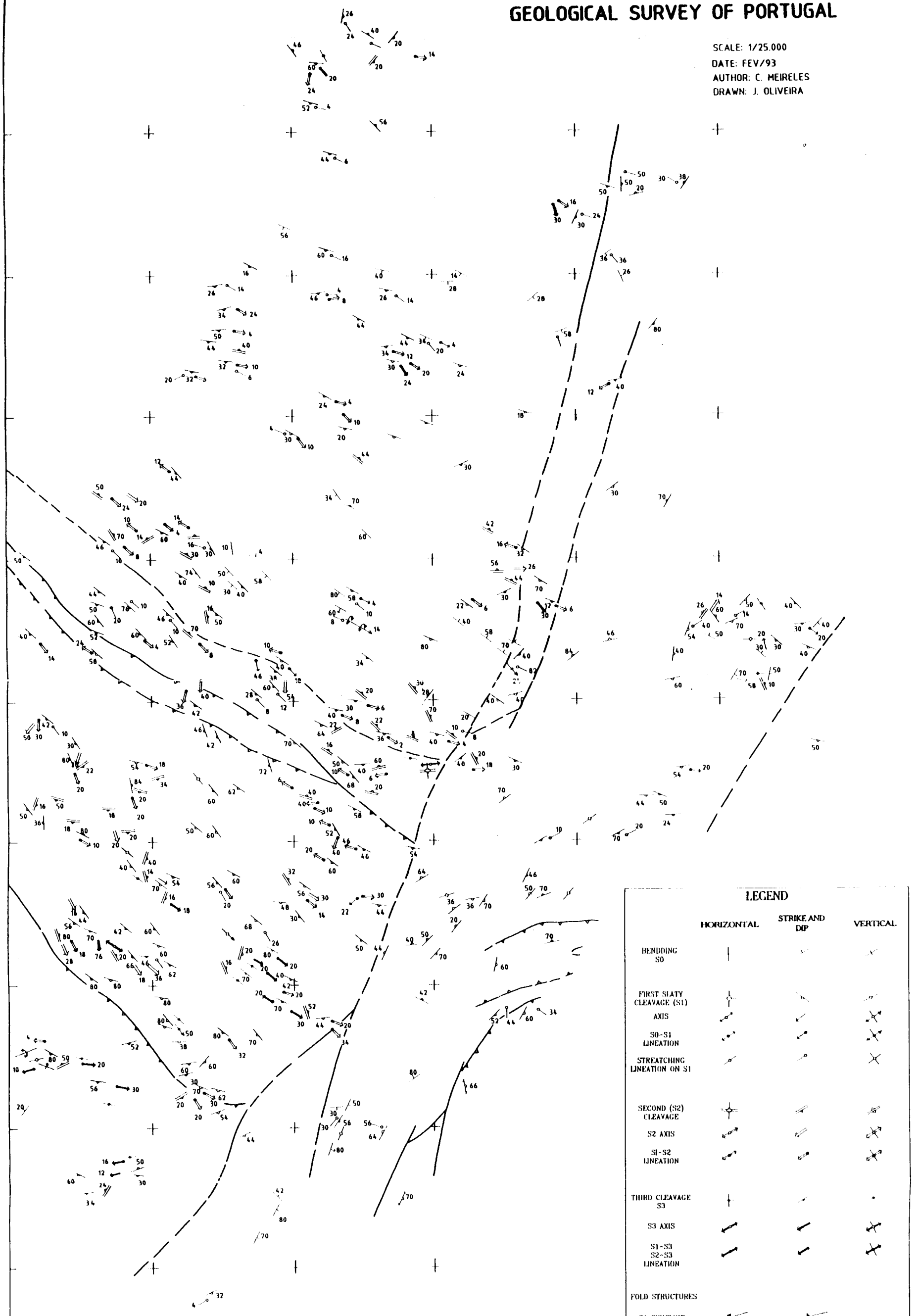

LEGEND

	HORIZONTAL	STRIKE AND DIP	VERTICAL
BENDDING S0			
FIRST SLATY CLEAVAGE (S1)			
AXIS			
S0-S1 LINEATION			
STREATCHING LINEATION ON S1			
SECOND (S2) CLEAVAGE			
S2 AXIS			
S1-S2 LINEATION			
THIRD CLEAVAGE S3			
S3 AXIS			
S1-S3 S2-S3 LINEATION			

FOLD STRUCTURES

S1 SYNCLINE
S1 ANTICLINE

S3 SYNCLINE
S3 ANTICLINE

Fig. I - 33 : Interpreted structural map of the França - Rabal area (1:25.000 scale)

c) Graphitic shales

Graphitic shale lenses occurs in the transition from the Ordovician slates to the Silurian grey phyllites. This black phyllites has abundant sulphide dissemination. They contain quartz, muscovite, and organic matter; few grains of plagioclase and tourmaline occurs as well; limonite is abundant. A decimetric dark limestone occurs in this graphitic level, 1km west of França village.

d) Grey phyllites with lydites lenses (black cherts)

This unit is composed by a monothonous sequence of grey carbonaceous phyllites with lenses of lydites (black cherts). Clay minerals constitute the prevailing mineral in phyllites. The grain size is more fine than the one observed in Ordovician slates. There are also present two cleavages. Some chloritoid postdated the S2 crenulation.

The lydites are mainly composed by quartz and organic mater. Two quartz generations occurs: (1) microfolded coarse quartz in a (2) very fine quartz matrix, probably resulting from recrystallized silica; pyrite is the main sulphide mineral.

Upper Llandoverian.

d) volcano-sedimentary complex: various shales with basic volcanics, purple shales, porphyritic acid tuffs, black cherts and quartzites intercalations.

It is a volcanosedimentary sequence mostly composed by light rose to light brown shales. Some green shales (tuffites), siltstones and dark grey shales intercalations also occur.

From top to the bottom of the sequence there are diverse lenses of : massive white quartzitic sandstone; grey limestone; lydites (black chert) with syngenetic pyrite and variscite (secondary phosphate mineral); purple shales (lie-de-vin); minor lenses of acid-intermedium piroclastics tuffs; porphyritic acid tuffs and basic volcanic extrusive rocks.

DEVONIAN.

There is a change in the pelitic and silicious Silurian sedimentation to a greywacke-flysch type sedimentation. These metasediments are preserved in regional D1 sinforms within the megakink Vilariça structure. They were mapped only between França and Rabal villages.
The greywackes shows chlorite matrix with quartz, feldspar and litic clasts. They are decimetric levels with centimetric mudstone intercalations. Some conglomerates also occur. It was found plant remains. They are similar to other flysch sediments of Upper Devonian age (Ribeiro, 1974).

D1 semi–ductile shear zones (particularly the left–lateral system, striking E–W 15°) are well represented in this França sector. Field evidence supports their reactivation during the subsequent variscan deformation phases, particularly during the third regional phase of variscan deformation (D3) and during the late tectonic event (D4), of probable Early Permian age, responsible for the development of the Late Variscan fracture network.

In the França area the Vilariça fault is divided into various branches striking from N–S to N20°E; these accidents are usually underlined by abundant fault gouge and, in some fault segments, by brecciated quartz fillings.

3 – MINERALIZED STRUCTURES AND HYDROTHERMAL ALTERATION OF THE FRANÇA LODE GOLD–SILVER DEPOSIT

Three main types of mineralized structures can be recognized in the França lode gold–silver deposit: (1) irregular N15–30W quartz–siderite veins related to a major releasing bend of the Vilariça strike–slip fault; (2) discontinuous, N80–100E,40–50S, en echelon quartz veins within a regional N70–80W shear intersected by the Vilariça fault and reactivated during the D4 phase of variscan deformation; and (3) quartz breccias associated to the above mentioned releasing bend of the Vilariça accident, which were probably object of Roman exploitation (see

section III of the present report).However, it shoud be notice that the N70-80°W shear mentioned in (2) corresponds in fact to a local variation in strike of a regional N80°E shear, probably due to the proximity of its dextral conjugate which underlines the northern contact between the quartzites and slates Ordovician age.

a – Wall -rock hydrothermal alteration

Hydrothermal alteration, usually giving rise to rocks characterized by pervasive silicification and different degrees of sericitization and carbonatization with local dissemination of pyrite and sparse arsenopyrite, preceded and accompanied brecciation and opening of multi–stage veinlets in the host rocks. These phenomena can be observed as far as 0.5 to 1 m from mineralized structures associated to the Vilariça strike–slip fault system. In some highly fractured domains, slates of Llandeilian age show a characteristic orange–reddish color due to strong, and probably selective, bleaching. Argilized bands are quite common adjoining major (reactivated) fault branches. Near the mineralized structures, the Ordovician quartzites exhibit always a profuse network of late–quartz veinlets which sometimes contain disseminated pyrite.

In general, the observed hydrothermal alteration comprises the deposition of several generations of quartz, fine–grained white–micas and chlorites, locally associated with sulphides (mainly pyrite) and carbonates (mostly Mg–siderites). Previous petrography (Mateus, 1989; Mateus and Barriga, 1991) enabled the distinction of three main mineral parageneses of hydrothermal alteration. The earliest paragenesis, best preserved in domains adjoining mineralized quartz– siderite veins, consists of quartz + carbonate + high Fe–chlorite sericite pyrite. This assemblage is commonly replaced by late quartz + vermicular chlorite + hematite high Fe– sericite which, in domains of high permeability, gives rise to illite–smectite aggregates + goethite quartz. Recent evaluation of the available petrographic data, coupled with new observations, confirmed the proposed hydrothermal alteration mineral assemblages and gave important details about the textural relationships of the minerals just referred to and the ore minerals. This study, complemented by the comprehensive examination of the ore samples, enabled also the characterization of the paragenetic sequence for the França Au–Ag deposit (Fig. I-34).

It is now well established that the earlier alteration paragenesis comprises the association of slightly deformed quartz (Qtz I), aggregates of high Fe–chlorite (Chl E–I), and minor amounts of nearly pure albite (although slightly Na deficient). Coarser and sometimes fractured isolated crystals of sericite (Ser E–I), as well as micrometric subeuhedral grains of carbonate I (with modes of FeCO3 and MgCO3 of the order of 63.32 and 30.89 mole %, respectively, Fig. I-35) can occur in some domains. The intense deposition of quartz (which in general do not displays optical features of intracrystalline slip – Qtz II), and fine–grained sericite (Ser E–II), locally associated with euhedral grains of disseminated pyrite and arsenopyrite and more rarely with subeuhedral–anhedral carbonate II crystals (with modes of FeCO3 and MgCO3 of the order of 82.20 and 8.32 mole %, respectively), characterize the second event of hydrothermal alteration.

The deposition of sericite (E–IIIa, b) and fine–grained chlorite (E–II) along late veinlets and fractures, as well as the development of aggregates of vermicular chlorite (E–III) filling voids and replacing altered sulphides and carbonates, are characteristic of the late hydrothermal assemblages. Hematite (sometimes poorly crystallized), goethite, and illite–smectite aggregates are locally present, particularly in highly fractured domains. The late quartz generations (specially the IVth and Vth generations) may seal more or less complex fracture networks. Veinlets filled with euhedral crystals of Qtz V usually display abundant cavities.

b – Synthesis of ore petrography

Arsenopyrite, pyrite, and galena are the main sulphide minerals in the França ore deposit. In addition, minor or trace amounts of sphalerite, chalcopyrite and electrum have been

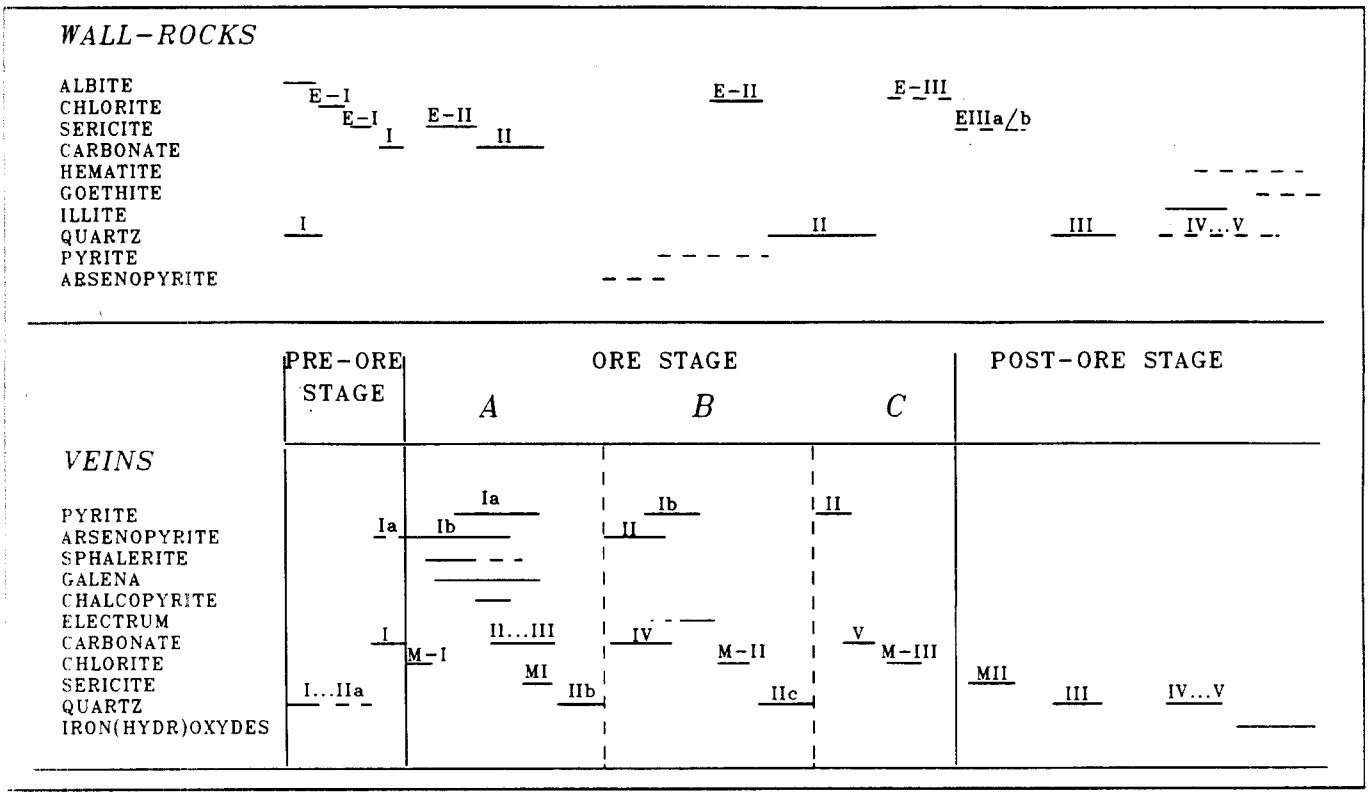

Fig. I - 34 : Paragenetic sequence for hydrothermally altered wall rocks and mineralized veins of the França ore deposit.

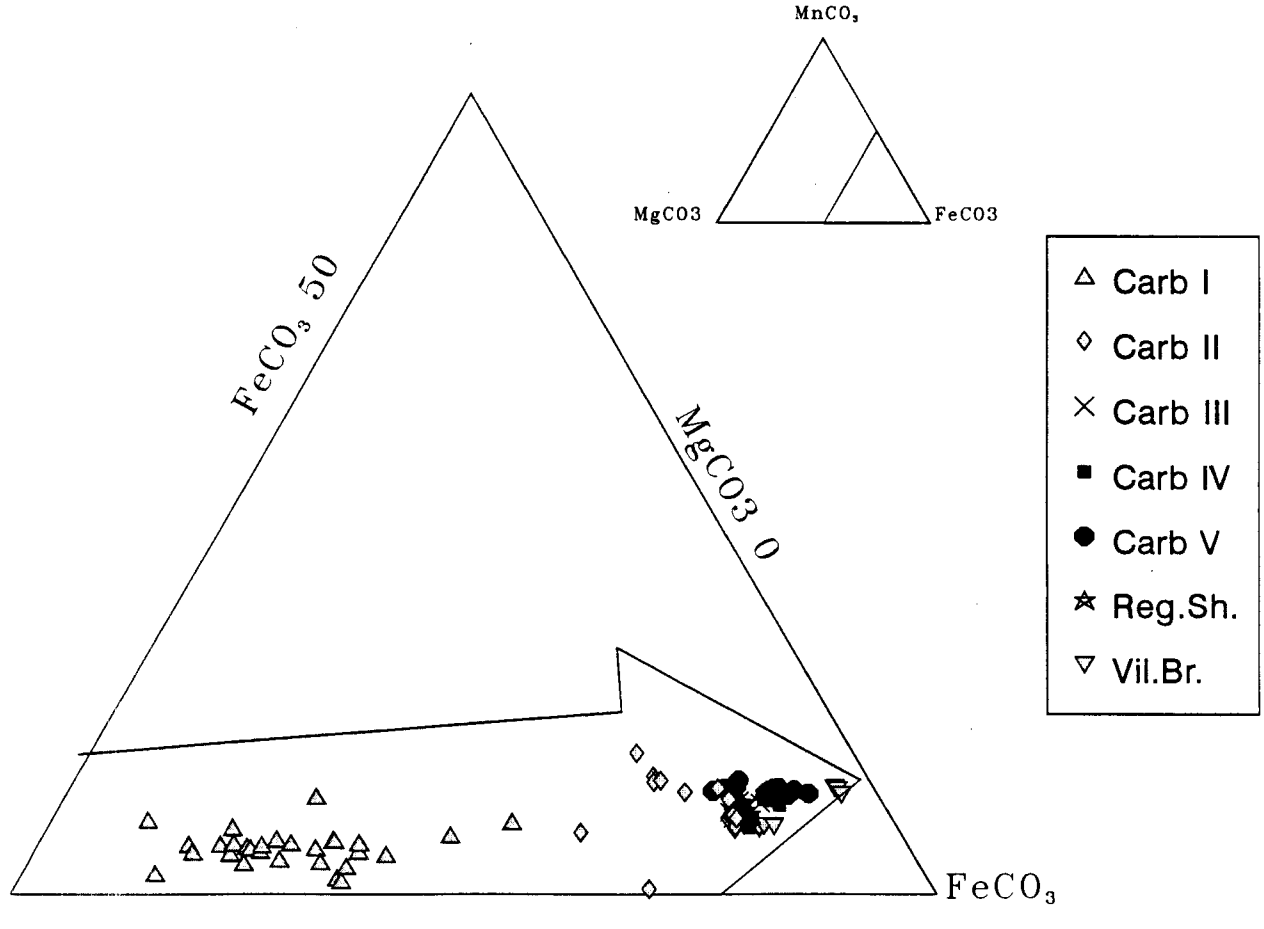

Fig. I - 35 : Examined carbonates in a MnCO3-MgCO3-FeCO3 diagram.

observed. The mineralogy of the gangue is largely dominated by quartz and carbonates, although sericite and chlorite may be locally important.

The ore–samples examined show that the early, highly deformed quartz generations (Qtz Ia and IIa) do not accompany the mineralization. Quartz of generation I exhibit notorious wavy extinction, sparse deformation bands, and intense subgranulation along grain boundaries. Quartz of generation IIa displays optical features of only slight work–hardening, and is intimately associated to domains where recovery microstructures of quartz I are negligible. The distinction between these quartz types (I and IIa) is not always clear; in some domains, quartz IIa may be interpreted as the result of incipient dynamic recovery of quartz I, or simply as a different feature of the heterogeneous deformation of quartz I. Nevertheless, it should be noted that quartz IIa is, at least partially, coeval with carbonate I deposition. Quartz of generations IIb, IIc and III, locally affected by brittle deformation, coexist with late carbonate, sericite, chlorite and sulphide generations; the IIc and III quartz types are characteristic of mineralized veins along the N70–80W shear. Late quartz veinlets (representing the V^{th} and VI^{th} generations) are common in the ore zones.

Arsenopyrite is ubiquitous in the mineralized samples studied, and two main generations can be recognized. The first generation (Aspy Ia, Ib) consists of medium–grained (usually greater than 1 mm) subeuhedral–euhedral fractured crystals coexisting with Carb I and Qtz IIa, or with Carb II and III (with modes of FeCO3 and MgCO3 of the order of 85.40 and 7.48 mole %, respectively), as well as chlorite M–I, and, at least partially, with earlier sulphides (pyrite Ia, sphalerite, galena and chalcopyrite). The second generation (Aspy II) comprises fine–grained (< 0.5 mm) euhedral undeformed crystals in textural equilibrium with electrum (70–80 wt%, on average, of Ag), pyrite Ib and late carbonates (type IV – with modes of FeCO3 and MgCO3 of about 86.74 and 7.44 mole %, respectively). Arsenopyrite II coexists locally with chlorite (Chl M–II and M–III). Chemically, both generations of arsenopyrite are similar, and the relative proportion of their main components follows roughly the classical substitution $Fe(As,Sb)_{1-x}S_{1+x}$.

Later, isolated electrum particles of small size (< 50 μm), characterized by gold concentrations ranging from 30 to 80 wt%, are also common in N15–30W quartz veins.

Pyrite Ia (modes of 47.00 and 52.20 wt % of Fe and S, respectively) may be surrounded by, or intimately intergrown with carbonates characteristic of the II and III generations, but convincing replacement textures are absent. Nevertheless, in some samples pyrite Ia is partially replaced by Carb III, and there are few examples where micrometric pyrite relics occur within Carb III crystals. Pyrite Ib (modes of 46.06 and 52.82 wt % of Fe and S, respectively) is optically similar to the Ia specimens, although it occurs predominantly associated with Aspy II as scattered subeuhedral grains (< 1 mm, on average). Micrometric, euhedral crystals of pyrite II (modes of 46.67 and 52.510 wt % of Fe and S, respectively), also occur, in general along discrete cracks. These are usually cut by late fractures filled with chlorite and sericite of M–III and M–II types.

Galena (compositionally quite close to ideal PbS, with modal values of 86.12 and 13.62 wt % of Pb and S, respectively) is much less widely distributed than pyrite or arsenopyrite. It usually occurs as irregular grain aggregates that are spatially associated with arsenopyrite Ib and/or pyrite Ia. Isolated (< 0.5 mm) and anhedral chalcopyrite crystals (chemically close to the ideal composition, showing modes of 34.06, 30.09 and 34.73 wt % of Cu, Fe and S, respectively) are in textural equilibrium with arsenopyrite Ib, and may be found near galena aggregates. On the contrary, sparse anhedral (1–2 mm) sphalerite grains (modes of 60.89, 5.03 and 33.42 wt % of Zn, Fe and S, respectively), sometimes with chalcopyrite exsolutions, are mainly concentrated within bands rich in pyrite Ia.

Late sulphide oxidation, coupled with extensive carbonate breakdown, produced areas of conspicuous (iron oxide) alteration, especially important in some fault domains where late

brecciation, related to the last seismogenic cycles undergone by the Vilariça fault, apparently facilitated the circulation of low temperature, oxidizing fluids.

c. Quartz breccias associated to dilatant jogs of the Vilariça strike-slip fault

The fault rocks examined include mainly quartz breccias and fault gouges. The former underline either the major tectonic branches of the Vilariça strike–slip fault (particularly in the França/Portelo sector) or the reactivated D3 shear zones (ESE França/Rabal area). In general, quartz breccias are related to highly fractured domains of the tectonic structures, where multiple overprinting of different quartz–vein arrays can occur.

Major quartz breccias associated to the Vilariça fault (type I) can be grouped into three major subtypes, as follows:

(1) Breccias IA – earthy and highly porous, iron–manganese enriched matrices, which may also contain sparse pyrite - arsenopyrite relics. In these quartz fillings (usually outcropping above 750 m of altitude in the França/Portelo sector), the variation of matrix color, from dark brown – yellow to dark brown – red, is consistent with the degree of dispersion and relative abundance of the main hydrated and anhydrous iron – manganese oxides/hydroxides. Minor amounts of hydrous–phyllosilicates (hydrosericites - illites - smectites) complete the observed mineralogical paragenesis. On the basis of geochemical data, complex, poorly crystallized, hydrated arsenates and phosphates are probably present as well (see section IIc of the present report). Gold and silver contents of these breccias are usually quite low (20 to 110 ppb and 0.1 to 0.5 ppm, respectively).

(2) Breccias IB – massive, sometimes earthy, matrices with abundant relics of primary minerals (mostly siderite, pyrite and arsenopyrite) which are surrounded and corroded by complex mixtures of metal oxides/hydroxides and arsenates. Hydrosericites, and quite altered chlorites, are also present, and constitute the main accessory phases. The occurrence of this breccia subtype, like the further one (IC), is circumscribed to the ancient mine works in the França mine area, and the elevation of the present outcrops ranges from 735 to 745 m. Gold and silver contents of these breccias are usually scattered in the ranges 0.5–22 ppm and 7–100 ppm, respectively.

(3) Breccias IC – massive matrices which comprise sulphides showing brittle deformation (particularly pyrite, arsenopyrite and galena), primary phyllosilicates (sericite ? chlorite), and, sometimes carbonates (fragmented). These fault rocks, outcropping near 700 m of altitude and occurring within one major tectonic branch of the Vilariça system that in higher topographic levels exhibits IB and IA breccia subtype fillings, are solely present in the França mine area and were probably object of Roman exploitation. The available chemical data show that gold and silver contents of these breccias are usually scattered in the ranges 2–7 ppm and 70–80 ppm, respectively.

Fault gouges and/or friable late–quartz breccias are present along some fault domains of the Vilariça structure, particularly in those where compact quartz fillings are missing; their Au and Ag contents are quite variable, ranging from 0.002 to 0.5 ppm and from 0.1 to 3 ppm, respectively. These fault rocks (type II), comprise always abundant fragments of variable dimension of the surrounding metamorphic rocks and exhibit local enrichments in iron and manganese oxides/hydroxides. The matrix of the late breccias typically consists of quartz, hydrous–phyllosilicates, and minor amounts of pyrite, goethite, pirolusite, and hydrated arseniates.

B - VILA POUCA DE AGUIAR REGION (PORTO UNIVERSITY)

1 - INTRODUCTION

Vila Pouca de Aguiar municipality is situated in northern Portugal, in the Vila Real district , Tras-os Montes province, 130 km from Oporto.

Vila Pouca de Aguiar gold district is a vast area characterized by several occurrences of gold mineralizations: Jales the only portuguese gold mine (explotation suspended after october 1992); Gralheira an ancient roman gold mine, recently (1990/1991) prospected by BP-BRGM; three roman open pits (Três-Minas) and the northeasternmost area (Curros) with several occurrences of gold indices and mineralizations, namely Vale de Campo, Velhaquinhas ,Vale d'Égua and Penabeice (Fig. 1). Both the latter area and the Três-Minas area have been the subject of our investigation and are considered to give the best image of the relationships between metasedimentary host rocks with mineralized stuctures (VPA metasedimentary area).

The VPA metasedimentary area (**VPA area**) is framed by syn- to late- tectonic two mica granites near the northern and southern limits, and by post-tectonic biotite granites near the western limit, being traversed by abundant fault systems namely the NNE-SSW well represented by the important Régua-Vila Pouca-Chaves-Verin regional fault (Fig I-36).

We must also refer some tin mineralizations namely at Revel, Jogadouro and Argeriz, respectively near the southern and northern limits on the proximity of the contact with the two mica granites.

Au-concentrations occur in different structural settings: an association either with quartz veins, predominantly subvertical and striking N 30 to N 50 (Vale de Campo, Vale d' Égua and Velhaquinhas); or with metasediments showing deformation followed by silicification which are related to shear zones having NW-SE direction (N120). Três Minas mineralization seems to have been controlled by such a structure and represents an exemple of a mineralized silicified schists.

The metasedimentary host rocks belong to a sequence of attributed Lower Silurian age, enclosed in a parautochthonous domain ("Peritransmontano Domain") (Ribeiro 1974). The contact of this unit with the autochthonous domain ("Douro Inferior Domain") is adjacent to the south limit of the studied area (Fig.I-36).

The VPA metasedimentary area is framed by syn- to late-tectonic two mica granites (near the northern and southern limits) and by post-tectonic biotite granites (near the western limit).

In the same geological environment, barren synmetamorphic segregation quartz and subvertical postectonic quartz veins (Cabeço do Seixo) striking from NNW-SSE to NNE-SSW also occur (Moura, 1988). Both mineralized and barren structures, are hosted in metasediments mainly composed of quartzites, chlorite phyllites, phyllites with dispersed organic matter (*"black shales"*), interbedded metavolcanic and calc-silicate rocks. These metasediments show at least the effects of three tectonic phases.

Mining activity

The mining activity in the area has begun during proto-historic times and had an important increasing in roman times. Três-Minas open-pits are an impressive example of these times; there are three open-pits ("cortas") - Covas, Ribeirinha and Lago Pequeno - in which Ribeirinha is the biggest one with 350 m x 110 m x 100 m (height) corresponding to 9,45 Mt of "tout-venant", and Covas with 480 m x 60 m x 80 m corresponding to 6,20Mt. The modern mining activity started in the begining of this century (1901-1910) with some prospecting works in Três Minas with the cleaning and opening of galleries and at Vale do Campo were there is a vertical shaft 20 m long and about 140 m of galleries on a quartz vein for lead explotation.

Confirming the potential interest of the area on gold mineralizations, different projects of prospection were carried out after 1983: by "Sociedade Portuguesa de Empreendimentos" SPE) associated with Newmont Co. (1983/1989) in Tres-Minas area; by BP associated with BRGM (1989/1991) in Sevivas-Velhaquinhas area and actually SEREM(BRGM) - EDM -

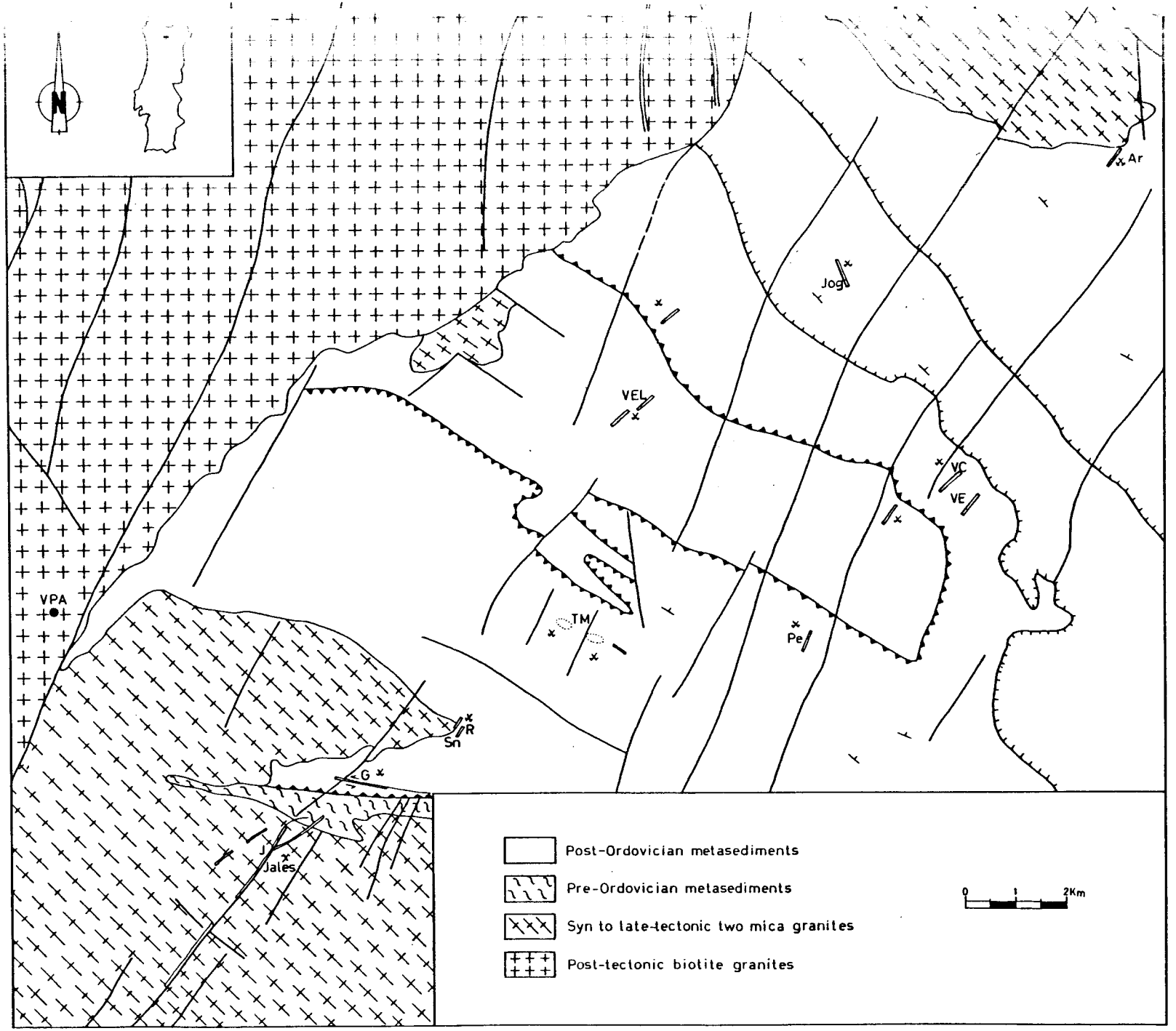

Fig. I - 36 : Simplified geological setting of VPA area (Based on Brink,1960; Neiva and Neiva, 1990 and present work).

(1992/) which also prospects a large area namely comprising Três-Minas, Vale de Campo and Penabeice.

2- GEOLOGY

The studied area involves host rocks of metasedimentary origin. Cartography and lithostratigraphic studies of the metasediments allowed the individualization of four units, predominantly constituted by quartzites, chlorite phyllites, black shales interbedded with acid metavolcanic and calc-silicate rocks.

For a precise characterization of the relationships between the different lithostratigraphic units from VPA metasedimentary area we have carried out field work for mapping (1/25000) and sampling. Figure I-37 represents the geological sketch map of the studied sector where mineralized structures occur.

a - Lithostratigraphy

The geological mapping of VPA area (of about 180 Km^2), allowed the definition and caracterization of four lithostratitgraphic units. A sketch of the geological map can be seen in figure 2 including the lithostratigraphic units, which from the base to the top are (Fig. I-38): the Curros unit (A unit), the Vale de Égua unit (B unit), the Cubo unit (C unit), the Sta Maria de Émeres (D unit).

The lithological and sedimentological aspects that have supported the individualization of the lithostratigraphic units were confirmed and precised by the petrographic and lithogeochemical analysis.

Curros unit (A unit) is a flyschoid sequence, with rhythmic alternance of thin arenaceous and pelitic layers ("gresophyllites"), with phyllites and green schists. This unit, defined in the central part of VPA area, shows a good lithological homogeneity essentially of pelitic composition, still with well marked stratification planes (S_0) . Usually this unit shows a predominantly greenish colour, becoming reddish near the contact with Vale de Égua unit.

Vale de Égua unit (B unit) is caracterized essentially by lithologies with abundant organic matter (lydites and black shales), but also by a large lithologial variation. The lydites and black shales are more abundant at the top of the unit, while, at the base, volcano-sedimentary terms (acid metavolcanite and calc-silicated rocks) are more frequent.

The differences described above justify the definition of two subunits, from the base to the top:

B1 subunit presenting intercalations of acid metavolcanites and calc-silicated rocks with banded quartzphyllites and phyllites with some organic matter (grey phyllites).

B2 subunit having abundant terms very rich in organic matter (black shales and lydites), which occur intercalated with gray phyllites and some volcano-sedimentary rocks.

Cubo unit (C unit) has essentially a detritic nature with intercalations of quartzites and microconglomeratic quartzites, with siliceous schists and quartzphyllites, sometimes with reddish colour.

Sta Maria de Émeres unit (D unit) has a lithology very similar to the subunit B1. There are frequent layers of acid volcanites and calcsilicate rocks intercalated with banded quartzphyllites, phyllites and some gray to black shales. Lithologies with abundant organic matter are rare.

The lithostratigraphic similarity between Vale de Égua, Cubo and Sta Maria de Émeres units suggests that they were conditioned by an identical paleogeography during the three separate periods of sedimentation. However, Cubo unit shows a greater terrigenous supply in more oxidizing conditions, accompanied by a decrease of the volcano-sedimentary contribution.

The characteristics of Curros unit suggest that its sedimentation was controlled by a different paleogeography. Its rhythmic alternance with flyschoid aspects allows to point out its lithostratigraphic correlation with autochthonous units, namely "Santos unit" from Celorico de

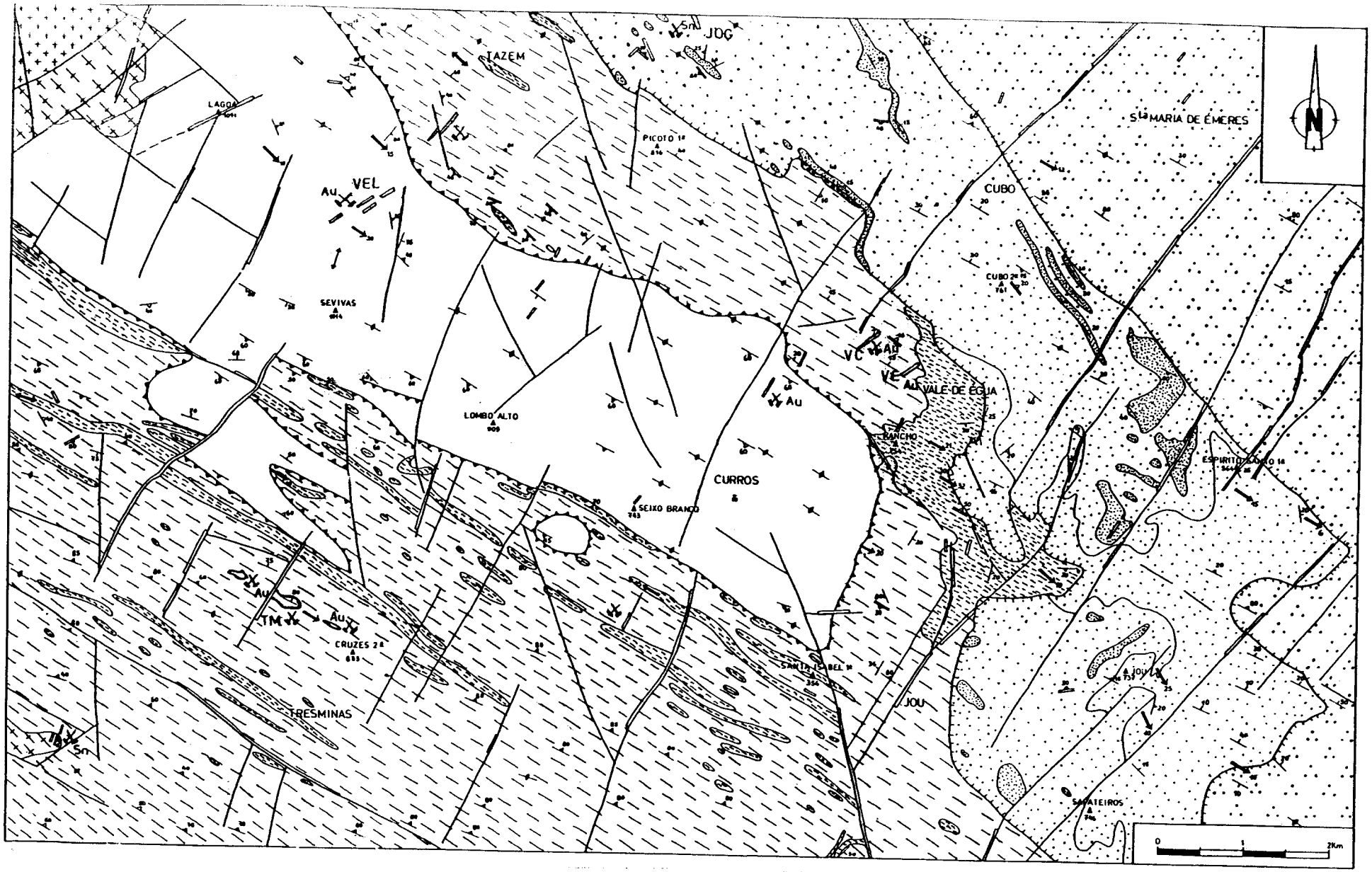

Fig. I - 37 : Geological map of Vila Pouca de Aguiar area (legend on the next page).

=Legend=

METASEDIMENTS

Autochthonous Unit:

CURROS UNIT (A UNIT): flyschoide sequence with alternance of thin arenaceous and pelitic layers ("greso-phyllites") with chlorite-phyllites.

Parautochthonous Units:

VALE DE ÉGUA UNIT (B UNIT): black shales and lydites(*) intercalated with volcano-sedimentary terms (acid and calc-silicate rocks), quartz-phyllites and phyllites.

CUBO UNIT (C UNIT): quartzites (*) intercalated with quartz-phyllites and some phyllites.

STA MARIA DE ÉMERES (D UNIT): volcano-sedimentary rocks (acid and calc-silicate rocks) intercalated with quartz-phyllites, phyllites and some gray to black shales.

GRANITES

Post-tectonic biotite granites

Syn- to late-tectonic two-mica granites

VEINS

Quartz

MINERALIZED STRUCTURES:

Quartz veins

TM silicified metasediments

VEL - Velhaquinhas; JOG - Jogadouro; VC - Vale de Campo; VE - Vale de Égua; TM - Três Minas

Faults

Thrusts (D2)

Thrusts (D3)

Bedding (S0)

Schistosity (S1)

Shear cleavage (S2)

Crenulation cleavage (S3)

Crenulation (L3)

Fig. I - 37 : Geological map of Vila Pouca de Aguiar area

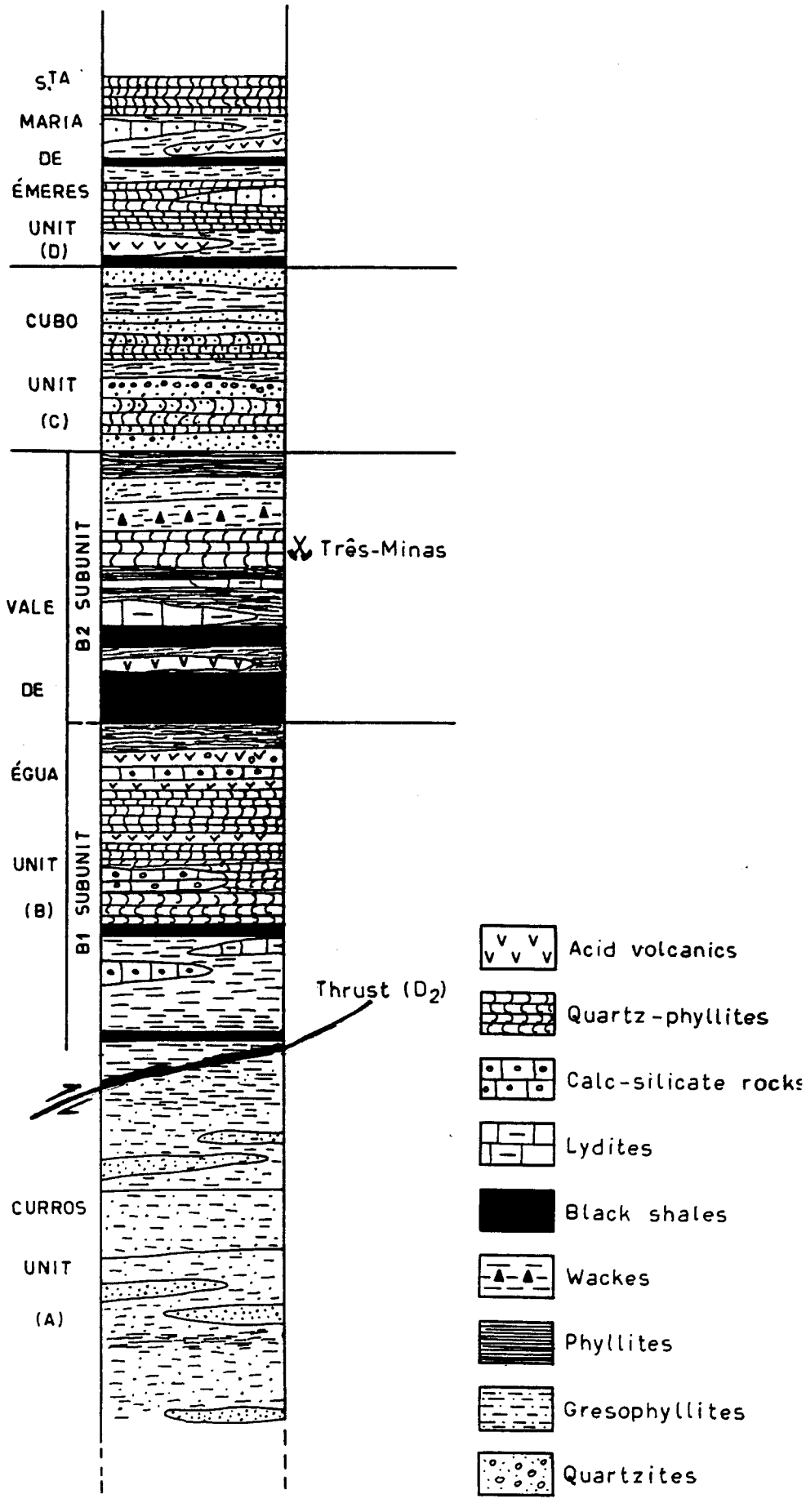

Fig. I - 38: Lithostratigraphic log of the VPA serie.

Basto area (Pereira,1987) of Ludlovian to lower Devonian age. Moreover this correlation is suggested by the major thrust D2 at the contact between Curros and the other parautochthonous units. Its flyschoid character suggests a preorogenic sedimentation already associated with the beginning of diastrophic phases.

b - Tectonic

Regional structure

VPA area shows the effects of four tectonic phases (D1, D2, D3 and D4) of Hercynian age. These phases marked the Curros unit with structures that are different from those occurring in the other three units.

Besides the lithostratigraphic differences between Curros and the other units, there are structural differences mainly concerning the ductile deformation.

The Curros unit occurs in the core of a large antiform D3, with subhorizontal axis 5 to 10 -> N120E, having a NE-subhorizontal limb and a SW-subvertical limb (Fig.I-39).

D1 develops a well marked schistosity (S1) in all units .

D2 is related with the thrust responsible for the parautochthon character of the Peritransmontano Group. This phase is not well marked in Curros unit, in which the S1 foliation predominates, while in the other units (Vale de Égua, Cubo, Stª Maria de Émeres) D2 developed a S2 "shear cleavage" type foliation that transposes the S1 cleavage, mainly in the most pelitic lithologies.

D3 deformation affects all the units with a subvertical crenulation cleavage, striking N120E, but this S3 cleavage is more penetrative in Curros unit and corresponds to the formation of the main antiform structure.

All the sequence shows a late- to post-D3 (late D3 to D4) brittle-ductile and brittle deformation, but there are different strains in SW-subvertical and NE-subhorizontal limbs of the large antiform.

The late D3 brittle-ductile deformation is expressed mainly by a tensional fracture system N40° to N50°E. The rotation of the greastest main stress ($\sigma 1$) from NE to NNE induces a sinistral shear sense in these tensional fractures and, in the SW limb, the earlier subvertical foliation N120E (So//S1//S2) is reactivated with dextral shear sense. In some places this shear deformation is accompanied by intense hydrothermal alteration with silicification and chloritization (Três-Minas).

D4 is a brittle phase with two conjugated fracture systems striking N10°W and N20°E, conditioned by a strain field that is consistent with a dextral shearing prevailing in the previous shear planes N120°E in SW limb. The regional Régua-Verin fault (N10°E), situated to the west of studied area and controling the emplacement of post-tectonic biotite granites of Vila Pouca de Aguiar, is a D4 structure (Fig. I-36).

In the NE subhorizontal limb the same fracture systems are associated with D3 and D4, but here the early subhorizontal foliation is reactivated by late to post-D3 thrusts.

Mineralized structures

Au-mineralizations occur in different structural settings: an association either with quartz veins, predominantly subvertical and striking N30° to N50°E (Vale de Campo, Vale d' Égua and Velhaquinhas) corresponding to traction fractures related to D3 and without any specific lithologic control for this structures; or in siliciceous metasediments showing deformation folowed by silification which are related to dextral D3 shear zones having N120°E direction. Três Minas mineralization seems to have been controlled by such a structure and represents an exemple of a mineralized silicified schists (Fig.I-39). In Três-Minas, contrary to the quartz veins, there is a specific lithologic control; the localisation of the mineralized structure is on the B2 subunit, so the local environment of the mineralizations is essentially characterized by abundant terms very rich in organic matter intercalated with quartz-phyllites, gray phyllites and volcanosedimentary rocks (Fig.I-38). In the open-pits, strongly silicified rocks occur. Gold mineralization is preferentially concentrated in these zones. They are related to the dextral D3

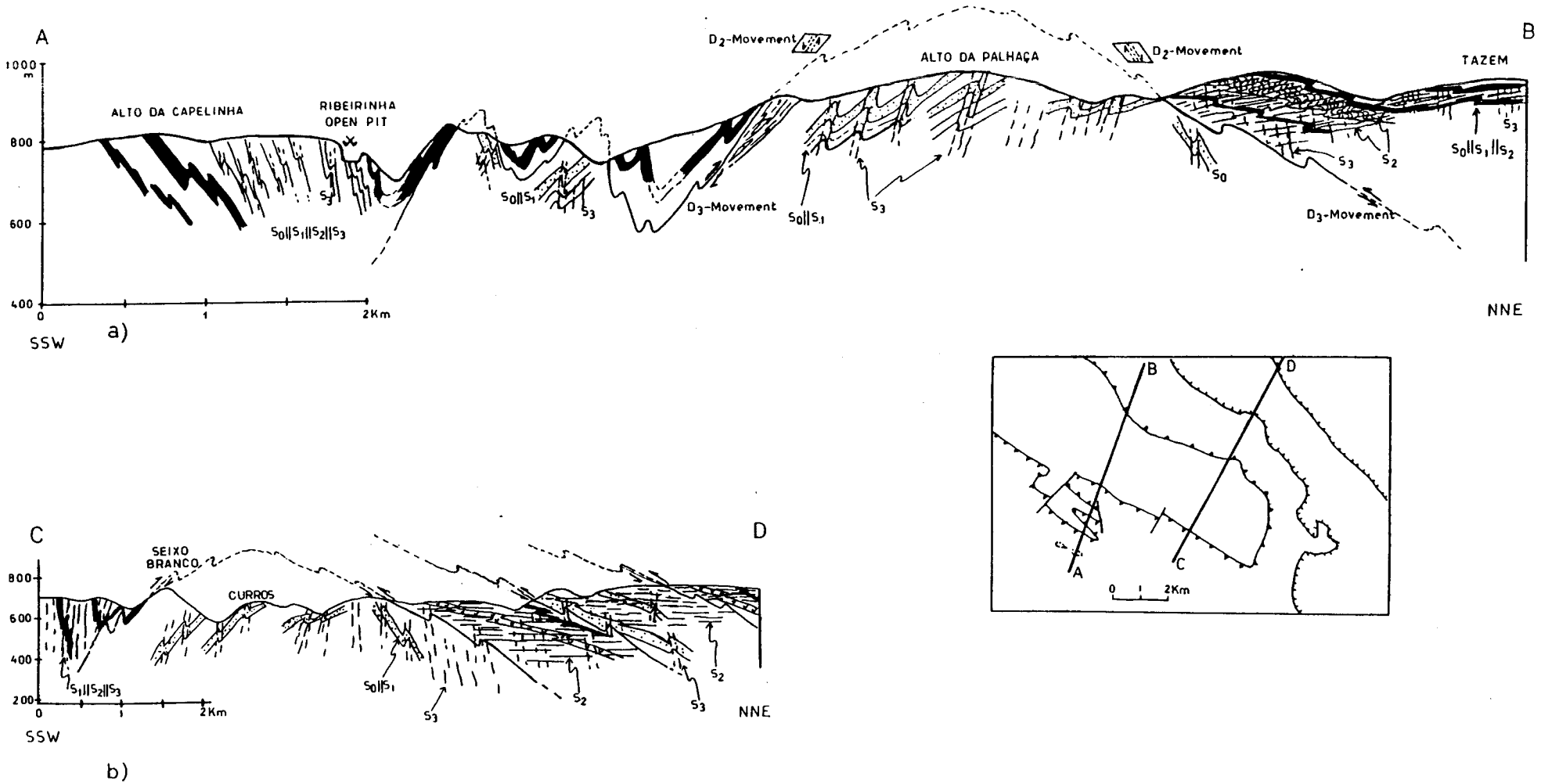

Fig. I - 39 : NNE-SSW cross-sections :
a) From Três Minas (SSW) to Tazem (NNE).
b) From SSW of Seixo Branco to NNE of Cubo

shear zones N120E and the silicification is more evident ; so, there is a structural control at Três- Minas and the lithologies richer in quartz, namely the quartz-phyllites, are more competent and consequently display subsequently a better aptitude for circulation and trapping of fluids. Oliveira and Farinha (1987) and Oliveira (1990) describing the lithostratigraphic sequence of Três-Minas, refer that gold mineralization is preferentially concentrated within compact lenses of quartzite and schistoid quartzite and suggest the possible existence of a paleoplacer.

Barren postectonic strctures

In the same geological environment, barren subvertical postectonic (Post-D4) quartz veins with a striking from NNW-SSE to NNE-SSW also occur and present thicknesses varying from 0,02 to 3m, locally concordant with the orientation of gold quartz veins.

3 - PETROGRAPHY

Petrography of metasedimentary rocks

The petrographic description of the different lithologies of the units defined allowed to show, not only the different compositions of the original sedimentary and volcano-sedimentary rocks, but also the different metamorphic evolution.

The **phyllites** and **green schists** are similar rocks, though green schists are much richer in chlorite. The green schists are particularly frequent in the Curros unit. The mineralogical composition of these pelitic lithologies is:

- sericite + quartz ± chlorite ± biotite in phyllites and
- chlorite + sericite + quartz ± biotite in green schists

Both lithologies have in some places post-D2 biotite blastesis .

The **gresophyllites** and **banded quartzphyllites** have names which may have the same meaning because their lithological and textural characteristics are somewhat similar. However, the mineralogical composition and metamorphic evolution of both rock types are not the same, and they result from different sedimentary rocks, belonging to different sequences.

The **banded quartzphyllites** have a grano-lepidoblastic texture with quartz-feldspathic and pelitic (biotite+sericite) bands. These bands materialize the metamorphic foliation S1, transposed by "shear cleavage" S2. However, in thin microlithons untransposed S1 foliation can still be observed. The mineralogical composition of this rocks is: quartz + K-feldspar + plagioclase + muscovite + biotite ± chlorite.

K-feldspar has a porphyroblastic texture with poikiloblastic aspects due to an inside S1 foliation. This blastesis is post-S1 and ante-S2.

Quartzphyllites are present only in Vale de Égua and S^{ta} Maria de Émeres units.

The **gresophyllites** have pelitic bands with lepidoblastic texture alterning with psammite-pelitic bands having grano-lepidoblastic texture. The pelitic bands have a sericitic composition and the psammitic-pelitic bands are quartz-sericitic. In the gresophyllites these bands materialize the bedding planes S0, locally transposed by the S1 schistosity. The mineralogical composition of this lithology is: quartz + muscovite ± plagioclase ± biotite ± chlorite.

The gresophyllites are abundant in Curros unit. In Cubo unit the so-called gresophyllite lithologies have similar mineralogical composition.

Associated with banded quartzphyllites in Vale de Égua and in S^{ta} Maria de Émeres units there are **acid metavolcanites** and **calc-silicate rocks.** This lithologies have the following mineralogical compositions:

- quartz + plagioclase + muscovite ± K-felspar + chlorite ± biotite in the acid metavolcanites, and
- quartz + epidote + tremolite-actinolite ± chlorite ± garnet in the calc-silicate rocks.

The mineralogical composition and its relationships with the structures in different lithologies indicate a regional metamorphism in the chlorite isograde with a peak pre- to syn-D2. However we must refer to a local and later occurrence of biotite in more phyllitic terms;

this biotite is post-S3 foliation and consequently we cannot exclude the possibility of a thermal event post-D3 probably related with the emplacement of post-tectonic biotite granites.

Petrography of organic matter

The 10 samples with organic matter were subjected to several methods for organic matter separation.

The identification and analyses of organic matter was attempted since it is known to provide paleothermal information. Several samples of different lithologies (phyllites, lydites and black shales) from unit B were prepared for organic petrologic analyses in the following way:

The "Whole Rock" (WR) of each sample was either directly or after light crushing, embedded and mounted in Epofix resin and then polished. Such a preparation allowed the study of the relationships between organic and mineral matter.

In addition, the samples were crushed below 200 m then dispersed (by ultrasonic) in a mixture of bromoform and alcohol. A "ligth fraction" (LF) at a density 2.45 was separated by centrifugation at 3000 rpm. This density was chosen since it approximates that of graphite. Each LF was concentrated on a Millipore screen, mounted and polished on a plexiglass slide.

According to the concentration richness reported for the LF, four of the samples (AD 8, AD 12, AD 16 and AD 62) were selected for preliminary petrographic studies. From corresponding WR samples, the rather frequent presence of very thin intercrystalline "filaments" associated to the quartz grains was noted. These filaments are considered to be organic and have been identified as a form of Migrabitumen (kata-impsonite to bitumen coke). Such considerations have been established from sample AD 62 where the optical properties are more clearly observed. Such properties include very fine mosaic-like anisotropic texture in crossed nicols and, in some cases, even "devolatilization" pores or vesicles. Reflectance values were rather difficult to obtain but they ranged from about 2.5 to 4% (random reflectance). Nevertheless, such migrabitumen have been reported to originate, inter alia, from the Asphaltite family when the latter is subjected to temperatures below 300 C.

Besides the intercrystalline migrabitumen, very rare figured and thin bodies were observed. Their origin/identification is difficult to ascertain, but in some cases they resembled graphitoid-like needles.

The LF observations confirmed the nature of the organic constituents but did not improve on the possibility of quantitatively obtaining reflectance values. Such difficulties were also due to the "pocked" surface textures exhibited by the larger particles, in which case, the reflectance values are thought to be underestimated.

Due to the difficulties responsible for the lack of reflectance measurements, complementary Laser Raman microprobe analyses (LRM) should be performed.

Several recent publications demonstrate the usefulness of LRM as a reliable analytical tool in the study of organic carbon present either in a rock matrix or in individual fluid inclusions.

LRM was carried out on fluid inclusions containing organic matter, and the resulting spectrum clearly shows a peak at 1578.8 cm-1 (Fig. I-40) corresponding almost to the well crystallized pure carbon graphite single band peak reported by some authors at -1582 cm-1.

Mineralogy

Quartz textures

Petrographic studies carried out in barren and mineralized structures enable us to distinguish several generations of quartz.

A-Barren quartz

Three main types of metamorphic quartz, assumed to be contemporaneous with regional metamorphism, have been recognized: (i) a deformed milky quartz in segregation veins (QI); (ii) a clear subeuhedral quartz in segregation veins (QI A); (iii) a recrystallized polygonal quartz in veinlets from the black-shales (QII).

A postectonic non-deformed milky quartz represented in later veins was also defined (QV).

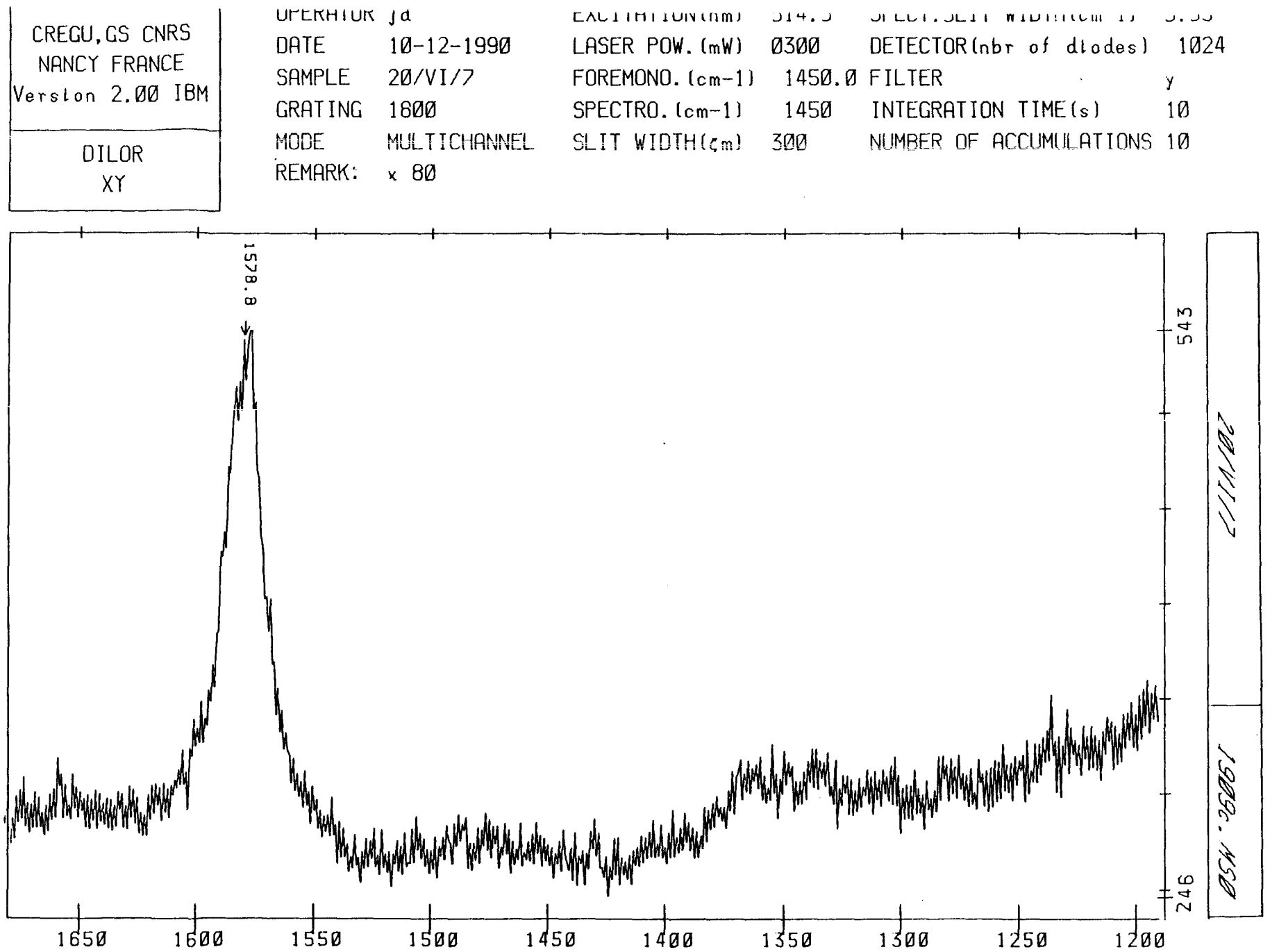

Fig. I - 40 : Raman spectrum of graphite from a VPA lydite.

B-Quartz from mineralized veins

In the veins - Vale de Campo, Vale de Égua and Velhaquinhas, three main generations of quartz have been identified: i) an early milky quartz (QIII) showing deformation materialized by undulose extinction and deformation bands; ii) a microcrystalline quartz resulting from deformation of the former milky quartz, often associated with shear zones (Vale de Campo) (QIIIr); iii) a late non-deformed hyaline quartz filling tension gashes and healing microcracks crosscuting the sulphides (QIV). The presence of an overgrowth of quartz surrounding the arsenopyrite and pyrite is distinctly observed in Vale de Égua replacing the earlier quartzes.

The early milky quartz, which is the most representative and earlier to the main mineralizing episode, is considered to be syn-to late D3.

C-Quartz from silicified schists

At Três Minas silicified metasediments four types of quartz have been recognized: i) a milky quartz, exhibiting undulose extinction and deformation bands with sub-granulation (QI TM) which, with increasing deformation, can be optically individualized with the formation of "neo-grains", considered as ii) recrystallized quartz (QII TM); iii) a non-deformed microcrystalline quartz in S-planes (QIII TM); iv) a non-deformed hyaline quartz, filling tension gashes and geodes associated with vermicular chlorite (QIV TM).

Ore Mineralogy

Metallographic and microprobe studies of mineralized veins from Vale de Campo, Vale de Égua and Velhaquinhas, and silicified structures from Três- Minas were carried out in order to characterize the mineralogical assemblages and compositions of the different phases. An attempt to establish a correlation with the different types of quartz has been done.

Three main stages of ore deposition from mineralized veins and Três-Minas can be identified (Tables I-7 and 8).

Arsenopyrite, pyrite and galena are the most abundant sulphides in the veins, being pyrite and pyrrhotite the most abundant in Três-Minas.

Arsenopyrite I, pyrite I and pyrrhotite correspond in both cases (mineralized veins and Três-Minas) to the **early stage** of deposition. This stage is synchronous to posterior to the deposition of the milky quartz (QIII).

The **intermediate stage** is mainly characterized by arsenopyrite II in Três-Minas and by arsenopyrite II, pyrite II and galena filled with inclusions and/or exsolutions of Ag-Sb-Te sulphides in the mineralized veins. This is accompanied by microcrystalline (QIIIr) and recrystallized quartz (QII TM) .

The Au-paragenesis occurs in both cases in the **late stage,** being generally formed by gold and/or electrum (Três-Minas - Au~70%, Ag~30%; Vale de Egua - Au~86.5%, Ag~13.5%; Vale de Campo - Au~46%, Ag~54%), Ag-Au sulphides and Pb-Sb-Ag sulphosalts. The sulphosalts identified are mainly of Pb, Ag, Sb, Cd (As=0,69 S=18,90 Pb=26,8 Ag=25,4 Sb=26,8 Cu=0,4 Cd=0,5) and Ag, Au, Cd (S=8,7 Fe=0,7 Au 27,8 Cd=0,6 Ag=61,8). Gold occurs preferentially in intergranular spaces between pyrite and arsenopyrite (Três-Minas, Vale de Campo, Velhaquinhas) or associated with galena II in veinlets cutting these two minerals (Vale de Égua and Vale de Campo) .

The non-deformed hyaline quartz (QIV and QIV TM) filling microcracks and tension gashes is related to the late stage. The occurrence of chlorite, spharelite together with the hyaline quartz is the outstanding feature of this stage in Três-Minas. However we must emphasize the fact that at Três-Minas it is very difficult to see macroscopic sulphides and when present, they are very scattered suggesting an impregnation process.

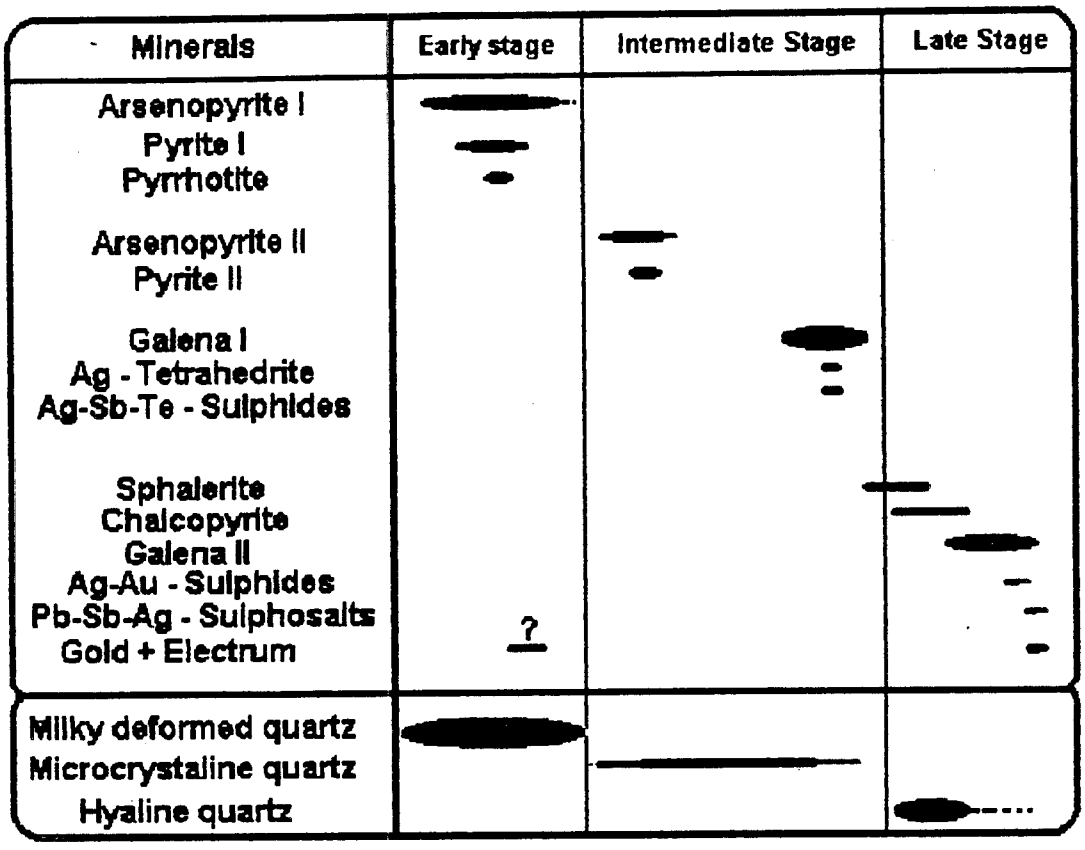

Table I - 7: Schematic order of deposition in mineralized veins

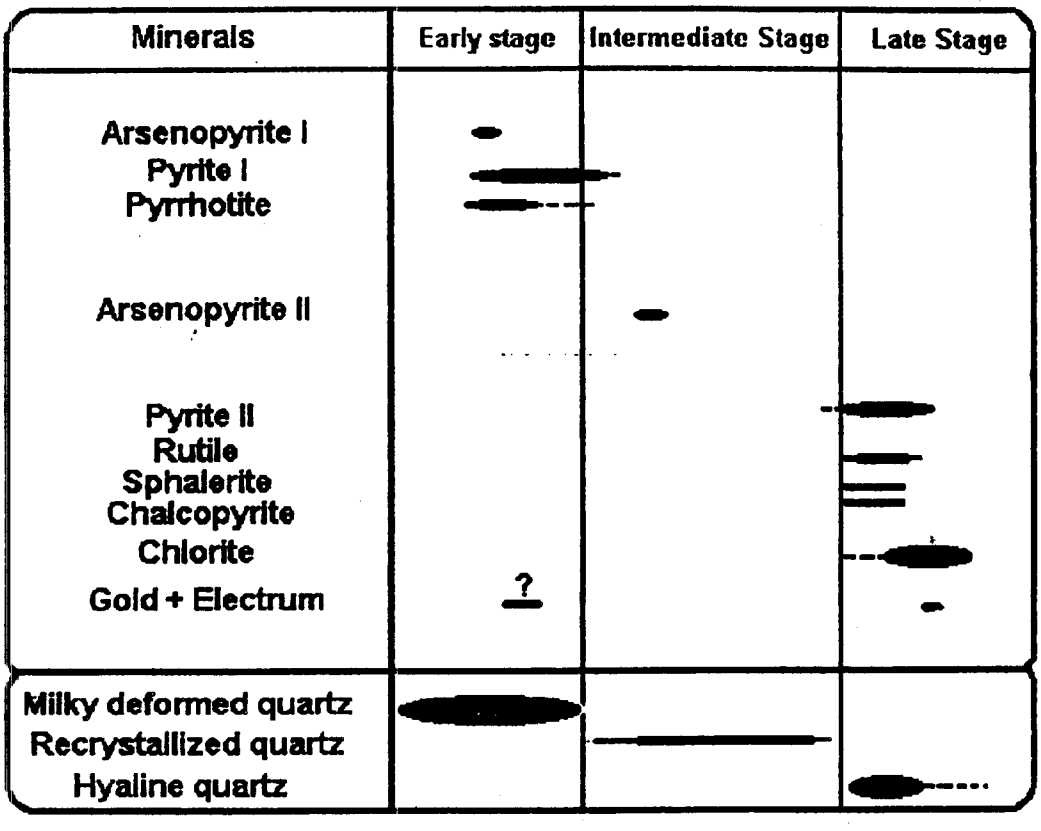

Table I -8 : Schematic order of deposition in Três-Minas

C- MONTEMOR AREA (ESCOURAL,W OF EVORA, PORTUGAL)

1 - INTRODUCTION

The gold mineralizations of Escoural are located near Montemor–o–Novo, 30 km NW Evora, where evidence of Roman exploitation are present. In this region, Au–As soil anomalies were firstly put in evidence by DGGM (Direcção Geral de Geologia e Minas) during the fifties, in a regional prospecting campaign. This geochemical campaign evidenced Au–As major anomalies along a regional NW–SE trend, standing over the high Au–As regional background which seems to be, at least, spatially related with metamorphic rocks of acid nature. At that time, the unfavourable global economics did not support further detailed studies.

During the eighties, RIOFINEX obtained a prospecting concession in the Escoural region, particularly the Tabuleiros–Azinhaga sector, an re–evaluated the economic potential of the previously outlined Au–As anomalies. Comprehensive soil and rock sampling put in evidence the presence of two subparallel running Au and As anomalies in non–economic segments of the regional trend, and the presence of superimposed Au–As anomalies in two potentially interesting targets: Chaminés and Casas Novas. Trench opening and extensive drilling disclosed the discontinuous ore bodies responsible for the soil anomalies (currently under economic evaluation). RIOFINEX performed and commissioned representative sampling of key–outcrops and selected portions of the drill–cores was done in order to establish the main petrographic and geochemical characteristics of the (hydrothermally altered?) metamorphic rocks in the vicinity of the mineralisation and the intersected ore bodies (Houston, 1989; Charley, 1989; Mateus and Barriga, 1987); metallurgic studies were also performed to achieve the mineralogical and granulometric constraints to the economic exploration of the ore bodies. In spite of these multidisciplinary data, two major questions remained unsolved: (1) is the geometry of the ore bodies controlled by a regional shear zone or is it mainly a singenetic characteristic transposed by the variscan deformation? (2) are the mineralogical variations in host lithologies inherited features reinforced during the regional metamorphism, or are they due to the circulation of late hydrothermal fluids along one major tectonic accident ? The integration of the available results led the geologists of RIOFINEX to envisage a model for the mineralisation genesis and distribution, which could be employed as a basis for further mining in Chaminés – Casas Novas and prospecting projects in similar areas of the Ossa Morena Zone. In 1991 the concession was sold to EDM (Empresa de Desenvolvimento Mineiro). Previous data are presently being re–evaluated in order to determine whether the future exploration of Chaminés and Casas Novas ore bodies is economic or not.

The interpretation of field, petrographic and geochemical data obtained in the course of the present research contract gave some clues to the answer of the above questions, suggesting a different genetic model for the mineralisation, with consequent implications in prospecting and in the eventual exploration of the known ore–bodies.

2- GEOLOGICAL SETTING

a - Stratigraphy

The study area (Fig.I-41) is the Tabuleiros–Azinhaga sector of the Escoural (Montemor) prospect. It comprises different geotectonic units within the Ossa–Morena Zone (OMZ), some of them of Upper Proterozoic age. Quesada et al. (1990) suggest a model for the Upper Proterozoic stratigraphy of the OMZ, based on tectonic cycles, dividing the formations in a pre–orogenic series, installed untill the Upper Riphean, and a syn–orogenic series formed between the Upper Riphean and the top Vendian. The pre–orogenic sequence, the so called Valencia de las Torres–Cerro Muriano Supergroup, comprises, from bottom to top, the Blastomylonitic Formation and the Série Negra. The former formation is mainly composed of volcano–derived gneisses, with some sporadic black cherts and marbles. The rocks display features of medium to high grade metamorphism and are highly deformed. The Blastomylonitic Formation grades upwards to the Série Negra, which is subdivided in two sequences: at the base, a thick unit of graphite–rich pelites, quartzowackes and amphibolites towards the top,

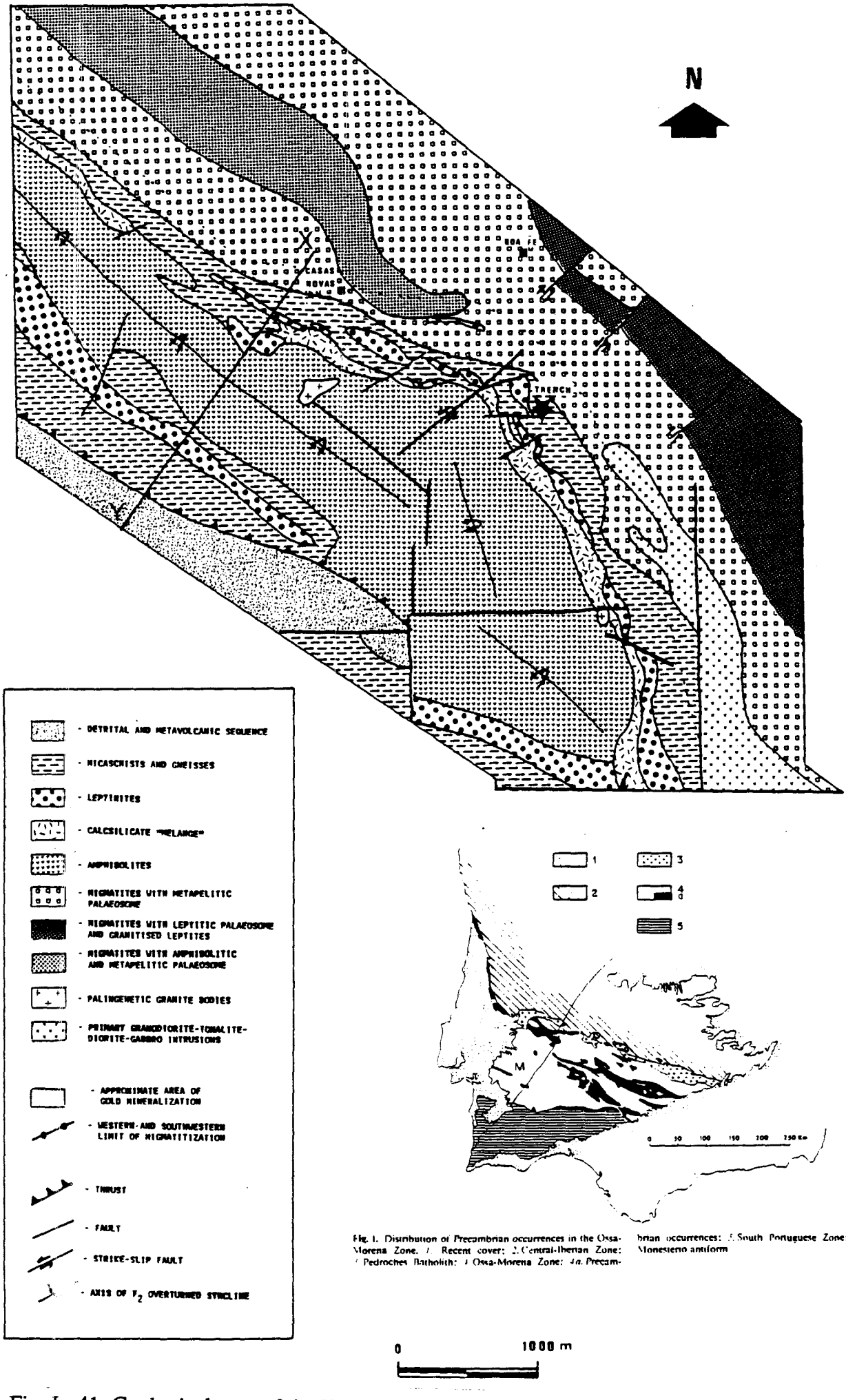

Fig. 1. Distribution of Precambrian occurrences in the Ossa-Morena Zone. 1 Recent cover; 2 Central-Iberian Zone; 3 Pedroches Batholith; 4 Ossa-Morena Zone; 4a. Precambrian occurrences; 5 South Portuguese Zone; M Olivenza-Monesterio antiform

Fig. I - 41: Geological map of the Tabuleiros–Azinhaga sector (modified after Faria 1988).

with lenticular bodies of black cherts and marbles; at the top a volcanic derived sequence characterised by the rarity of amphibolites.

The Syn–orogenic series rests unconformably over the Série Negra. Its genesis was strongly controled by a compressive tectonic phase from the Upper Riphean, probably related to a subduction zone. This series consists of a Volcano–sedimentary complex and a Flyschoid complex deposited between the Upper Riphean and the Upper Vendian. The Volcano–sedimentary complex corresponds to intercalations of calc–alkaline volcanic (mainly pyroclastic) rocks with turbiditic beds, with some levels of pelites, carbonates and scarce conglomerats. The sedimentation was predominantly marine. The deposition of the complex was coeval with intrusions of calc–alkaline plutons in shallow levels of the crust. The Flyschoid complex consists of turbiditic sucessions with local occurences of carbonates and reworked volcanic intercalations.

b - Deformation

In the Ossa Morena Zone (ZOM) the Hercynian orogeny is expressed by two main deformation phases. During the Middle/Upper Devonian the sequences were folded by recumbent folds with axis trending NW–SE to NS, verging SW to S (D1a); the persecution of the movement induced the rupture of the reverse flanks with the formation of thrusts, also verging SW to S (D1b). During Carboniferous the second deformation impulse affected the ZOM formations, with the development of folds with axial planes striking NW–SE, steeply dipping, as a response to the NE–SW main compressive stress. This impulse was also responsible for the development of a conjugate set of ductile shears, the right–handed running N–S to NNW–SSE and the left– handed running N60W to E–W. The late stages of the Hercynian orogeny are mostly expressed by strike–slip fracturing. Under a regional stress field with horizontal maximum compression ranging N–S to NNE–SSW and minimum compression also horizontal between E–W and WNW–ESE, subvertical strike–slip faults developed in two conjugate sets, one right–handed with directions between NNW–SSE and NW–SE, and the other, left–handed with directions close to NE–SW.

In the Tabuleiros–Azinhaga sector the Proterozoic (Proterozoic–Phanerozoic) formations are deformed by the two variscan deformation phases. The whole sequence is folded in a NW–SE trending sinform (D2) which deforms a D1a SW to W verging recumbent anticline and a D1b SW to W verging thrust; the polarity is reversed (the normal flanks of the major structure have already been eroded) (fig. I-42). In the eastern portion of this sector a prominent D2 right–handed shear, affects the structures D1, forcing a rotation of the S1 schistosity to near NNW–SSE. This shear (some times called the Mega–shear–see below) exhibits a complex history, with late fragile movements, of left–handed, strike–slip character.

c- Metamorphism

The research on metamorphism of OMZ points to, at least, two tectonothermal events responsible for the present regional metamorphic pattern, of late Precambrian, and Hercynian ages, respectively. Although extensive research is still to be done, the present knowledge suggests the presence of alterning low and medium/high grade belts.

The lithologies of the Tabuleiros–Azinhaga sector experienced medium to high–grade regional metamorphism (sillimanite + muscovite zone). Its development predates the D2 deformation phase. Locally, evidence of eclogitic facies were found (Charley, 1989). The metamorphic event in this area shows some features of very high–grade metamorphism, with development of migmatites which gradually evolve to anatetic granodiorites and granites.

In the course of the present research contract, a 4 km^2 area, comprising the Chaminés and Casas Novas gold occurrences, was mapped at a 1:5000 scale in order to bring some light into several lithological and structural problems that arise when one attempts to extrapolate core data to the mesoscopic scale (Fig. I-43). Concerning the stratigraphic ordering, there was no new data, and one could summarise the general characteristics of the observed sequence, from bottom to top, as follows:

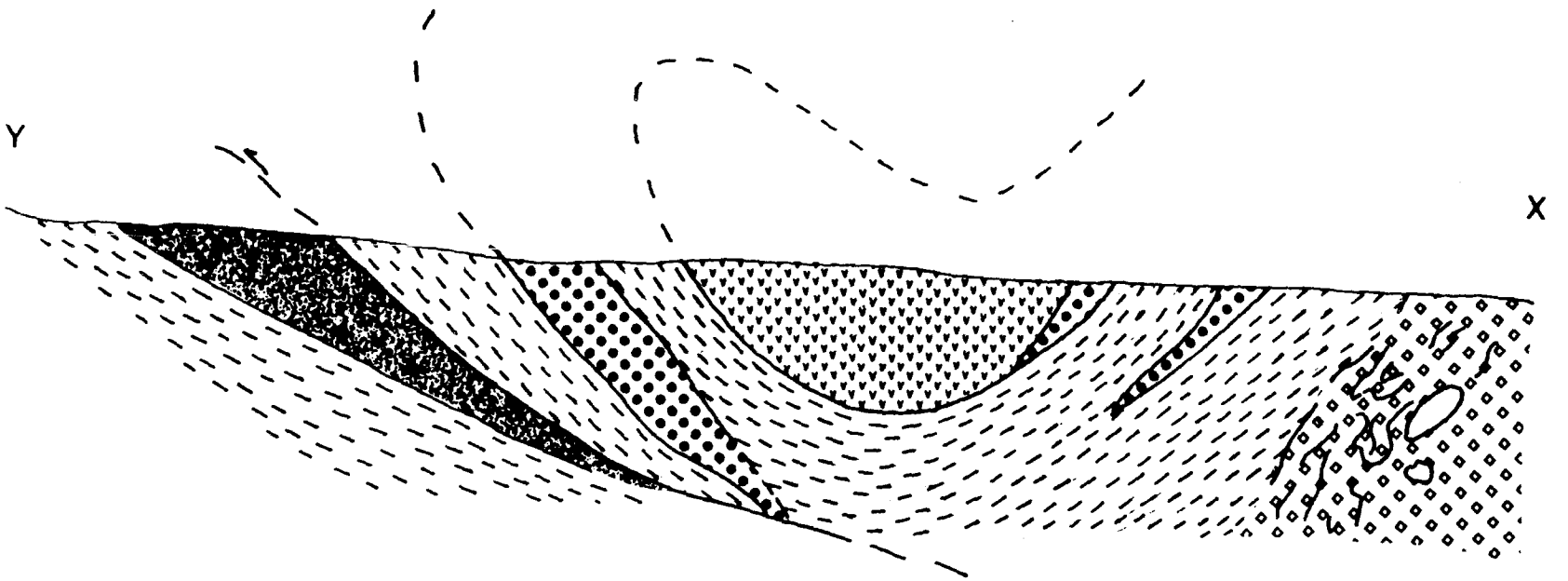

Fig. I -42: Geological cross–section of the Escoural–Boa Fé (Tabuleiros–Azinhaga) sector.

(1) – amphibolites (located at the core of the D2 sinform) with a well developed S2 clevage, with a general trending NW–SE direction, varying between N20W and N60W, subvertical, which sometimes exhibits a pronounced stretching lineation.

(2) – biotite and chlorite schists, often mapped together under the general designation of "micaschists". The chlorite schists are an retrogression product of biotite schists, with intermediate terms ("slightly chloritised biotite schist") present at the outcrop level. The scarcity of outcrops prevents an accurate outline of the chloritisation bands and the genetic relations are not obvious at the mesoscopic scale. Near shear zones the biotite–chlorite schists are frequently silicified. Along the major, right–handed, shear zone, besides the silicification one may find occurrences of arsenopyrite and pyrite, sporadically associated with gold (plus minor amounts of chalcopyrite, maldonite, loellingite, bismuthinite, and bismuth). The association mineralisation–silicified biotite (/chlorite) schists testifies the circulation of hydrothermal fluids along the mega–shear.

(3) – within the biotite/chlorite schists unit, lenticular bodies of leptinites are found. The persistence of this lithology in the SW flank of the sinform (Fig. I-41), strongly supports the idea of an individual unit of leptinites. Still, at the northern flank of the structure, the outcrops of leptinites are characteristically small, suggesting the existence of tectonic contacts.

(4) – Migmatites with strong foliation parallel to D2 structures, comprising restites of amphibolites and biotite schists. The contacts between these lithologies and the surrounding schists are either gradual or sharp, but in the latter situation quartz veins with arsenopyrite and pyrite are always present. An unsolved question is whether or not there is any relation between mineralisation emplacement and migmatization, since there seems to be a close spatial relation of gold occurrence to the vicinity of the migmatization front.

3 - WALL–ROCK HYDROTHERMAL ALTERATION

The fundamental aspects of alteration of wall–rocks by the hydrothermal fluids are extensive silicification, with associated sericitization. Arsenopyrite and more rarely pyrite are also found in the altered rocks. Feldspatisation is also evident, although in a subsidiary scale. Carbonates are sporadically present. In biotite rich lithologies a variable degree of chloritisation is present, ranging between slightly chloritized terms and others where the biotite is absent by a complete alteration to chlorite and rutile.

In chlorite rich samples the development of sericite is strongly limited, probably due to the absence of a K–rich phase (biotite), suggesting an antecedence of chloritization relatively to the main alteration phase.

4- MINERALIZATION

Gold mineralization occurs along a NW–SE band which inflects to N–S in its central segment (Fig. I-44). The main host lithologies are micaschists, and minor gneisses invariably strongly silicified. Leptinites and amphibolites are often found nearby.

a - Structural control of mineralizations

The higher mineralisation concentration and ore grades are found associated with the NNW– SSE to N–S right–handed mega–shear, close to Chaminés (Fig I -43). The ore is, at that location, a subvertical, close to N–S striking, silicified zone. Away from the mega–shear, the ore grades shows a tendency to decrease.

The history of movement of the mega–shear is complex with several phases of movements in ductile and fragile regimes. The genesis of this shear–zone was contemporaneous of the folding associated to the deformation phase D2; with a maximum compressive stress sub–horizontal close to NE–SW, a NNW–SSE to N–S, sub–vertical family of right–handed shears developed in association with its conjugate, a set of N60W to E–W, subvertical left–handed shears. Some tardi–Hercynian reactivation is also probable, although field evidence is not clear. During tardi– Hercynian deformation, the orientation of the shear zone was suitable for a reactivation as a right–handed strike–slip fault. However there is also some evidence of late brittle reactivation as left–handed strike–slip fault, expressed at several points along the mega–shear and at the trench. This reactivation could be explained as the

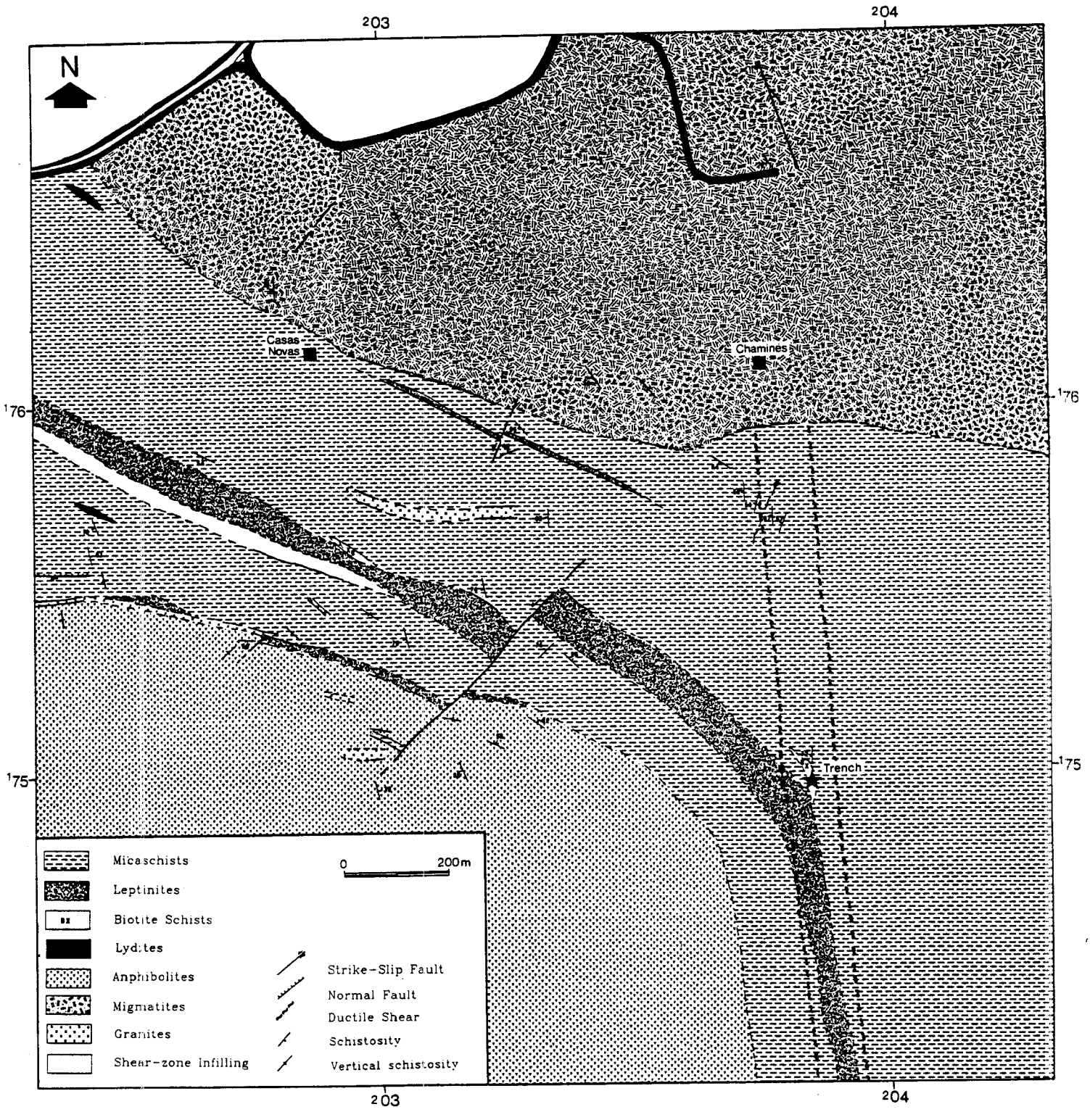

Fig. I - 43: Geological map of the Chaminés–Casas Novas Area.

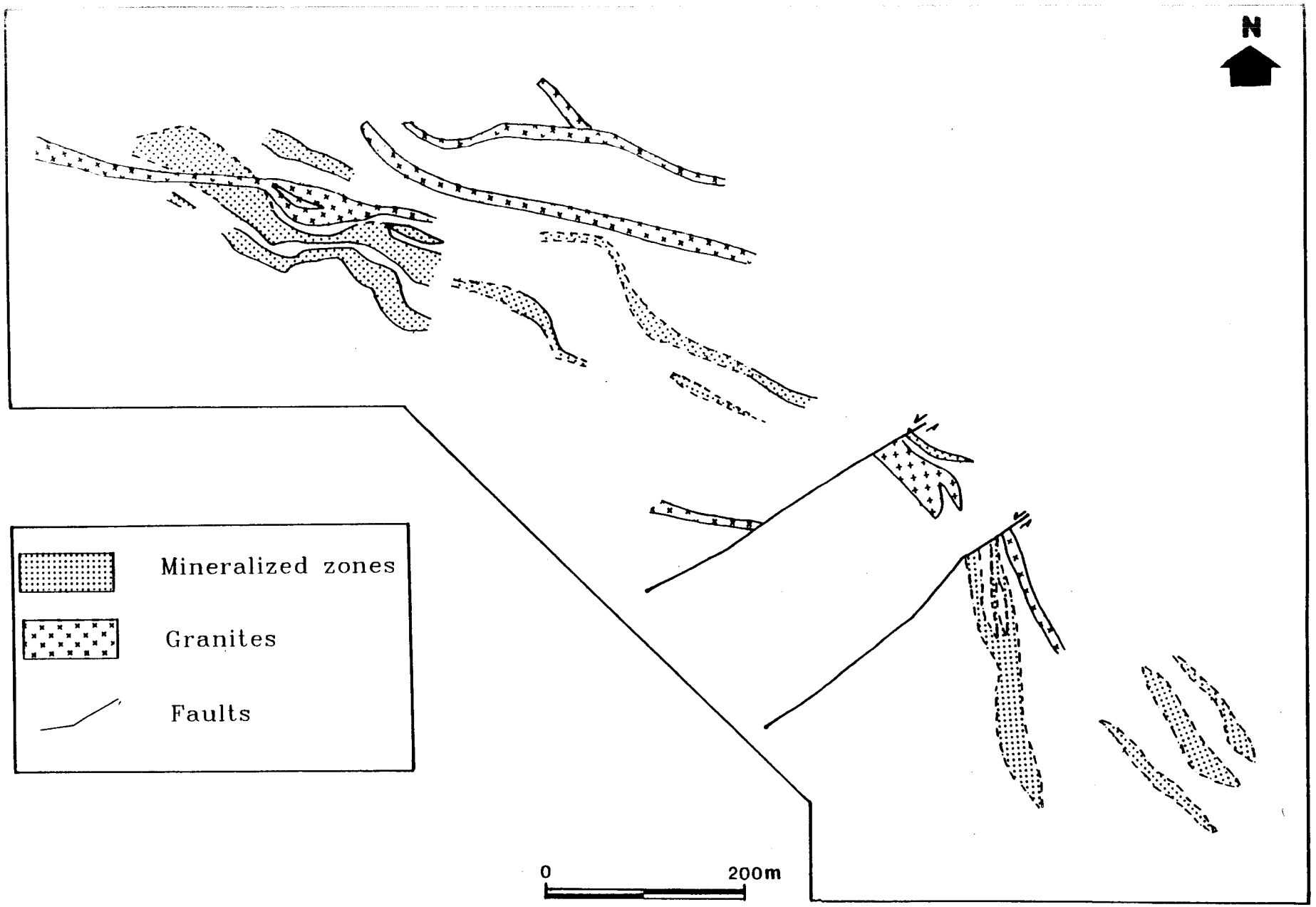

Fig. I - 44 : Mineralized zones according to RIOFINEX interpretation.

expression of Alpine deformation or as a singularity of the tadi–Hercynian deformation, a restricted phenomenon due to a local variation in the stress field.

The ore bodies display very slight deformation, expressed petrographically as some sporadic ondulose extinction of the hydrothermal quartz, while the pre–existing quartz in the wall–rocks, shows extensive sub–grain development. This data suggests that the ore bodies were formed late in the tectonic history of the shear–zone.

The available Au and As concentrations for the Chaminés sector (on metric samples along drill cores) are presented in figures I - 45, 46, and 47 in plan views, drawn using the morphological, field evidence concerning the geometry of the orebodies (lenticular, subvertical bodies).

The figures show the existence of approximately NW–SE enriched bands both for Au and As. This disposition is compatible with a model for structural control in tension–gashes along a left– handed NNW–SSE shear (Fig. I-48). The geometry of the Au–As bands constrains the age of mineralization as being late in the structural history of the mega–shear, which is consistent with the petrographic observations, already mentionned.

b - Vein geometry

Several vein generations are present, spatially or genetic related to the mineralising event, clustered in two different groups: 1) non–mineralised veins; 2) mineralised veins.

The non–mineralised veins group is composed of:
a) Folded quartz+feldspar+sericite veins devoid of gold or any sulphide. The folds characteristically display steeply plunging axes, in agreement with a genesis related to a strike–slip movement along a sub–vertical shear–zone;
b) Late (barren) milky–quartz veins, of centimetric thickness, without any aspects of deformation.

The mineralised veins are grouped in two tipological and chronological distinct groups:
c) Centimetric, quartz+arsenopyrite veins, folded by D1a (displaying axial plane S1 schistosity). Their content in gold is still unknown.
d) The main ore structures, centimetric to metric in thickness. These display frequent interdigitations with the surrounding host–rocks, mineralogically composed of quartz+arsenopyrite+pyrite+gold, grading to the surrounding schists by a gradual silicification. The only kind of deformation is some ondulose extinction in quartz.

The undeformed character of d)–type veins constraints its age as being post–D2, placing a hiatus of mineralization between D1a (c) veins) and post–D2.

c - Ore mineralogy

Gold occurs mainly in its native form, in small crystals (usually less than 5 μm), in close association with the ubiquitous arsenopyrite. Small amounts of native bismuth, bismuthinite and loellingite are spacially associated with gold. Arsenopyrite is the commonest ore mineral, occuring either in anhedral massive aggregates (2–3 cm) or in euhedral individual crystals. Frequently, arsenopyrite is found intergrown with loellingite. Anhedral crystals of pyrite, sometimes present, crystallised during two events. One of the events of pyrite crystallisation occurred clearly prior to the main arsenopyrite–gold deposition and in some samples both events of pyrite crystallization seem to predate the main ore development. Chalcopyrite is also present, although with subordinate importance, generally as veinlets in arsenopyrite or in small, anhedral crystals. Sporadic occurences of maldonite, pyrrothite, sphalerite, and marcassite are found. Covellite, chalcocite and digenite are also reported as supergene alteration products of arsenopyrite and chalcopyrite.
The prevailing gangue mineralogy comprises quartz + sericite + chlorite + alkaline feldspar + carbonates + tourmaline.The paragenetic sequence of mineralization is represented in Fig. I-49.

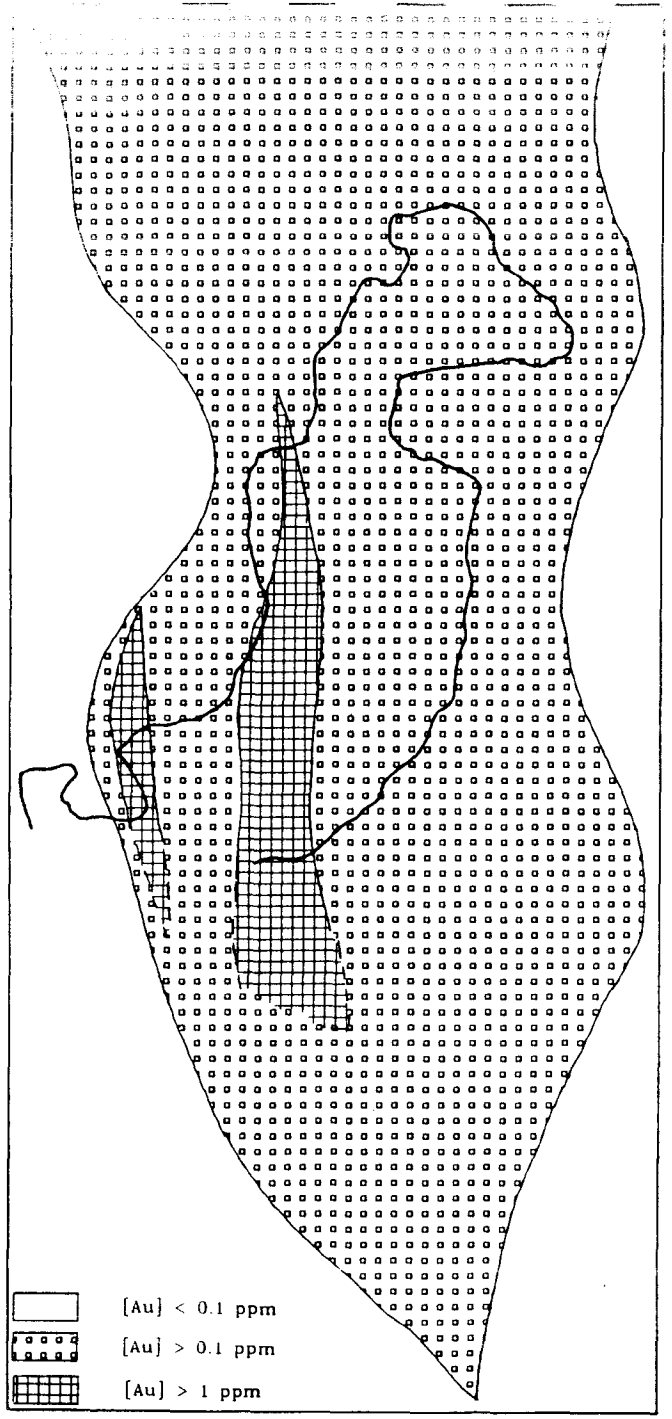

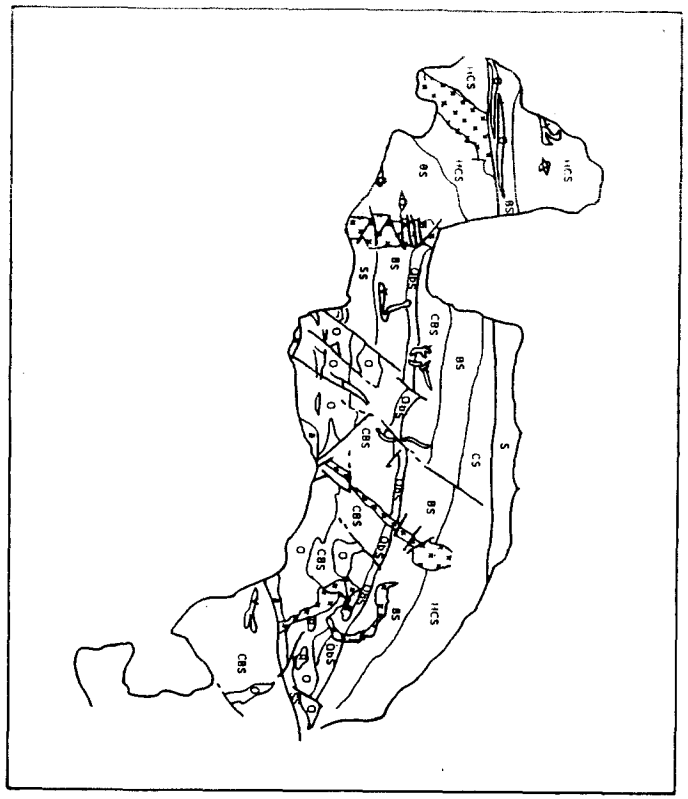

Granite

O Ore
BS Biotite schists
CBS Chloritised Biotite schists
CS Chlorite schists
HCS Highly Chloritised schists
SS Silicified schists
QbS Quartz-Banded schists
S Schists
V Vein
q Quartz
a Recent alluvium
Fault

Fig. I - 45 : Au enrichment at Chaminés (surface) and relation with the trench.

0 20 m

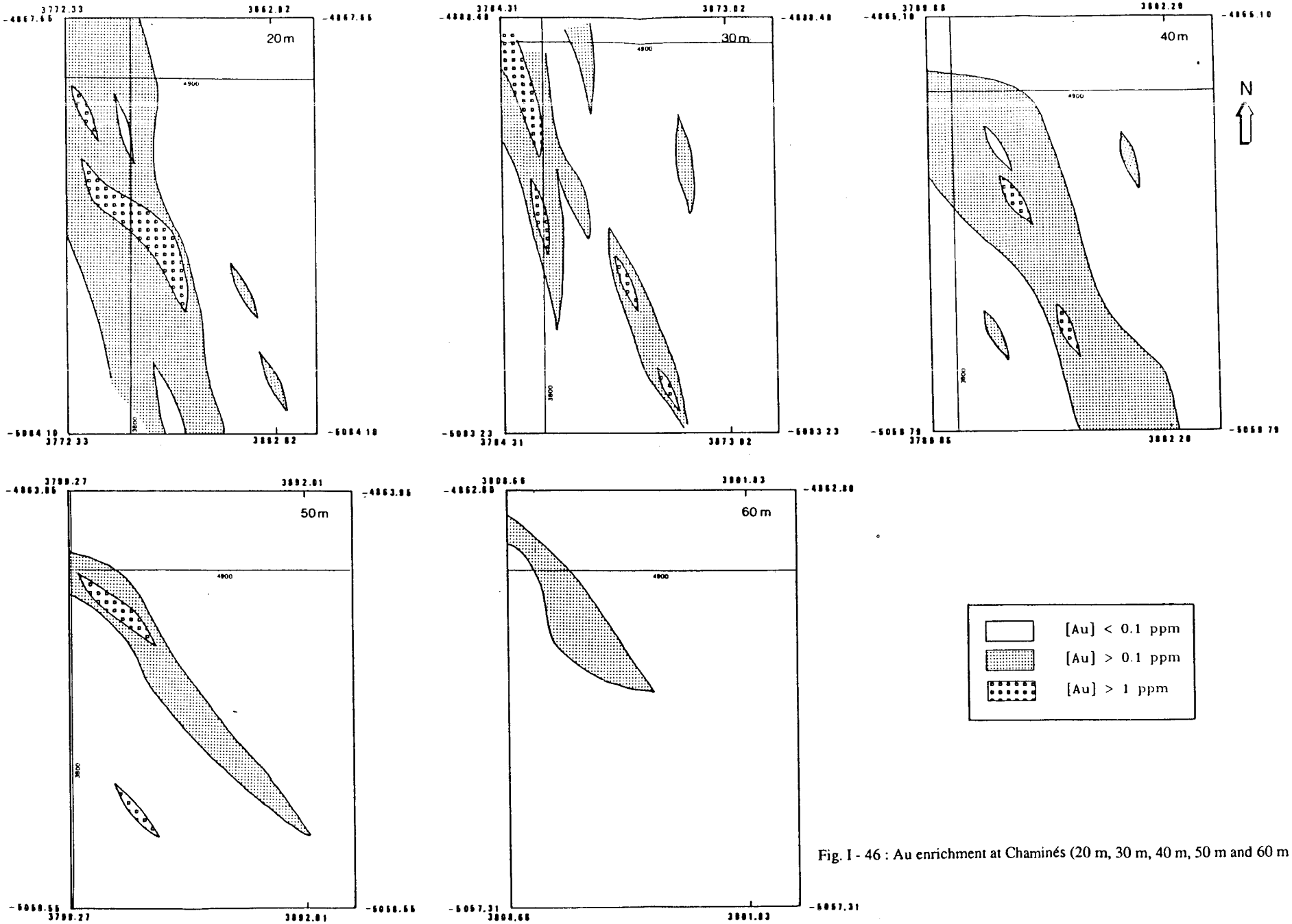

Fig. I - 46 : Au enrichment at Chaminés (20 m, 30 m, 40 m, 50 m and 60 m below surface).

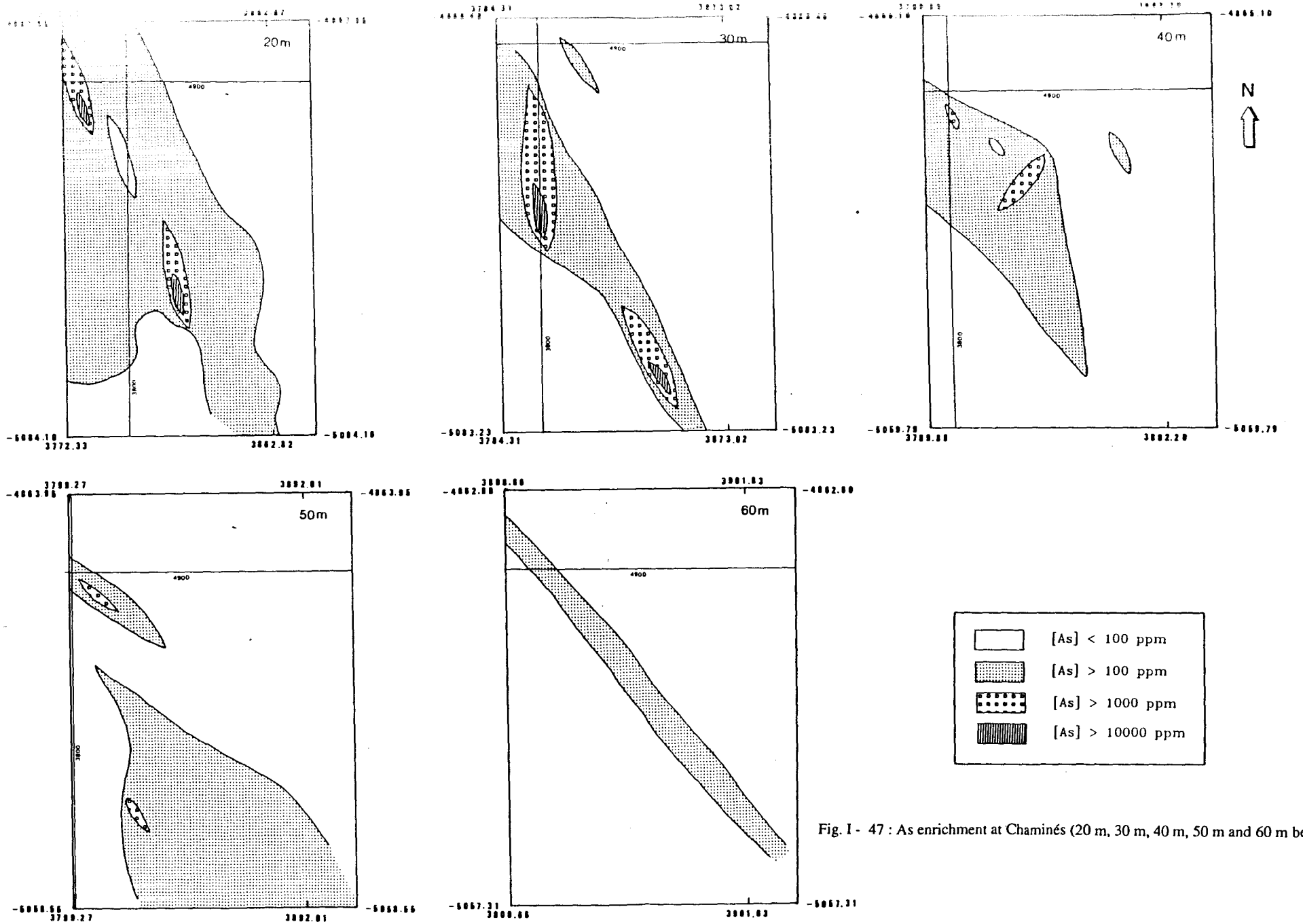

Fig. I - 47 : As enrichment at Chaminés (20 m, 30 m, 40 m, 50 m and 60 m below surface).

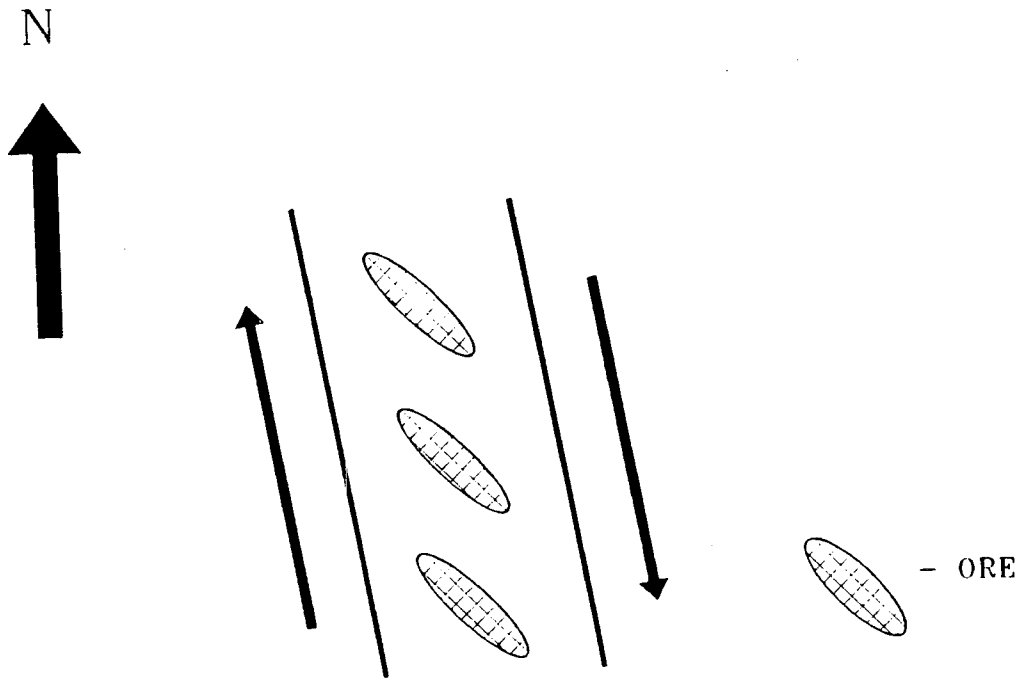

Fig. I - 48 : Possible scenario for Au/As enrichments associated with a left–handed strike–slip movement along the "Mega–shear" zone.

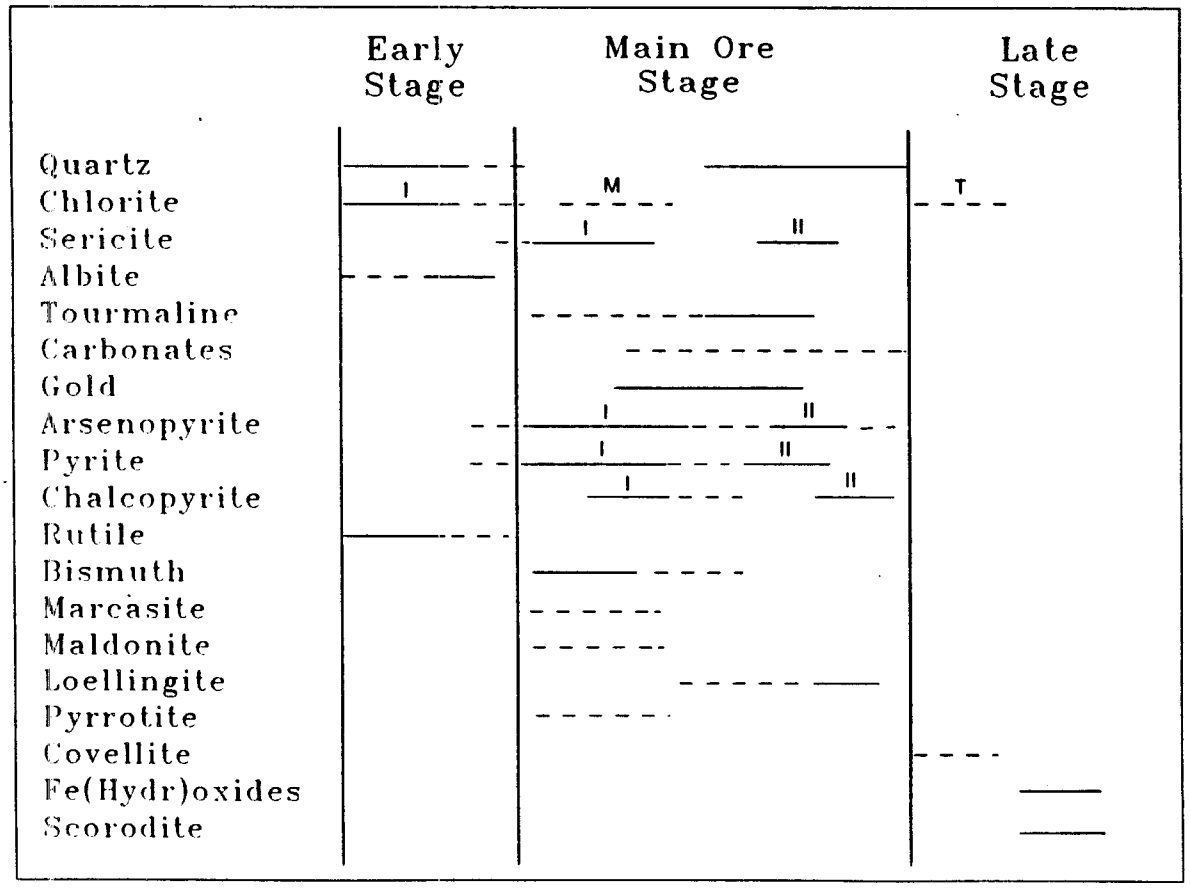

Fig. I - 49 : Paragenetic sequence of Montemor mineralization.

II - LITHOSTRATIGRAPHIC CONTROLS

The existence of pre-concentration of Au with sedimentary or volcanic-exalative origin, remobilized by metamorphic and tectonic fluids, is accepted by different authors (Boiron, 1987; Boiron et al., 1990, Bonnemaison and Marcoux,1989; Cathelineau et al. 1990; Braux et al., 1991).

The mineral deposits and occurrence of precious metallic elements in the C.I.Z. correlates to important structural and lithological controls (Pereira and Meireles, in prep).Truly, Au/Ag deposits in the NW Iberia of Hercynian age are controlled by ductile and brittle shear, mostly emplaced in Armorican Quartzite, Ordovician and Silurian black shales and, sparsely, within granites or in the Schist-Greywacke Complex. The lithological control acts as a first concentration stage of the ore and, mainly, as a chemical control for ore deposition.

A- GRANITES

The granites are not believed to represent any gold source because of the low Au background concentrations measured in the fresh rocks (below a few ppb). They do not also present any clear genetic relationships with the mineralization contrary to most Sn and W mineralizations. However, granites of the D3 phase host a large part of the deposits. Therefore, it has been examined how their chemical characteristics vary from one district to another, and if the water-rock interactions in the vicinity of the veins yield specific mass transfer which eventually could be used as geochemical tracers, at the prospection stage.

1-MAIN GEOCHEMICAL FEATURES OF THE HOST GRANITES

Most granites are peraluminous granites (alumino-potassic according to the classification of La Roche et al., 1980) including the biotite granites of Corcoesto to two mica leucogranites which are by far the most abundant in most areas. Series of representative fresh and altered granites have been sampled in the Corcoesto drill cores (CREGU analyses), at Tomino (analyses of regional facies by ITGE, fresh and altered enclosing the mineralization by CREGU), and regional facies of Penedono (analyses by DGGM).

The major geochemical features of the granites are presented in a series of chemical-mineralogical diagrams from La Roche et al (1979, 1980) and Debon and Lefort (1985) :

- the A-B diagram (Fig. II-1), where the parameter A= Al/3 -(K+Na+2Ca) allows to discriminate the peraluminous granites (with muscovite, garnet, andalousite or other peraluminous mineral present) and the parameter B = Fe+Mg+Ti is proportional to the amount of femic minerals (biotite mainly) and is used as a differentiation index. For example, the B parameter is well correlated with Th in the the Corcoesto granite (see Th-B diagram, Fig. II-2). Most analysed granites have a B parameter lower than 45 at Corcoesto, lower than 30 at Tomino and lower than 20 at Penedono (II-1b). Therefore, most of these granites are leucogranites, since the definition of this kind of granite implies a maximum of 7 vol. % biotite, corresponding to B=37,5.
- the Q-F diagram , where the quantity of Si not bound to feldspars (Q=Si/3-(K+Na+2Ca/3) is indicative of the quartz content, and is opposed to the relative abundance of the two feldspars with the F parameter (F=K-[Na+Ca]).

Some trace element have been analysed and binary diagrams have been used to describe the variations of the main incompatible elements : Rb, Sr, Li, F.

*At **Penedono***, average chemical analyses for major elements in wt % and for some minor elements in ppm are listed in Table II-1 (annexe). Average composition and standard deviation are given for each granite group. Detailed studies by Silva & Neiva (1990), stress out their peraluminous characteristics with a molecular ratio Al2O3/(CaO+Na2O+K2O) ranging from 1.19 to 1.58, and normative corundum lower than 3.14. In the same study, two trends were defined in La Roche (1964) diagrams, evidentiating fractionation and metasomatism. Trace elements indicate their origin by crustal melting during a collision episode.

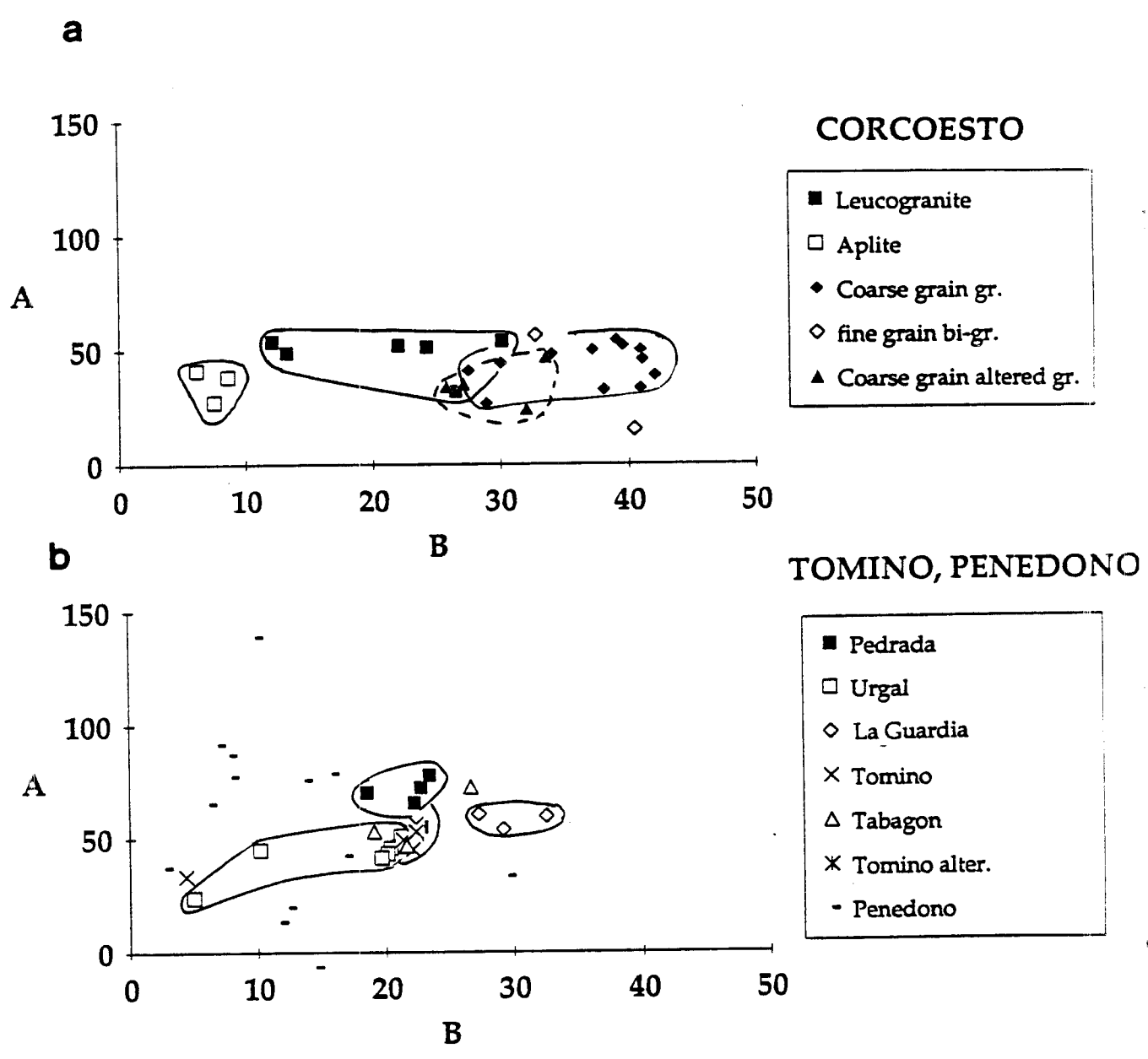

Fig II - 1 : A versus B diagram (A= Al/3 -(K+Na+2Ca) and B = Fe+ Mg+Ti)
a : Corcoesto granites; b : Tomino and Penedono granites.

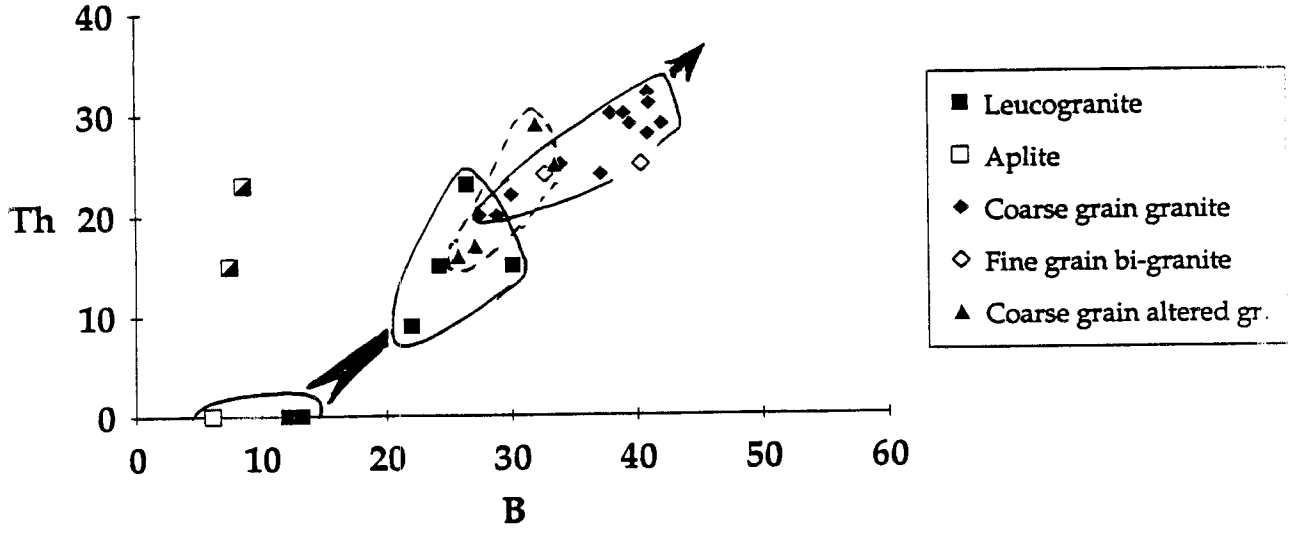

Fig II - 2 : Th versus B (Fe+ Mg+Ti) diagram for Corcoesto granites.

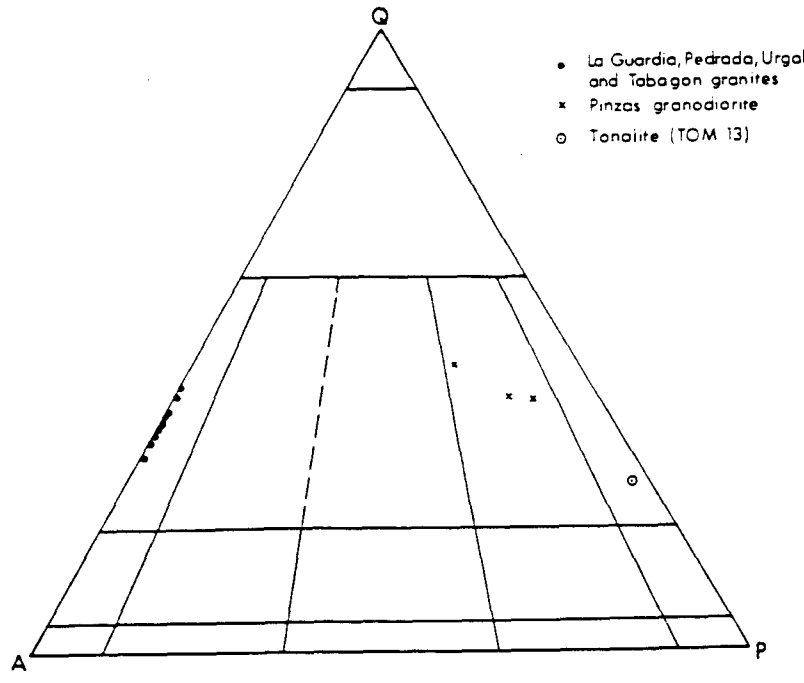

Fig II - 3 : Petrological classification based on ICPW mormative composition for the Tomino granites.

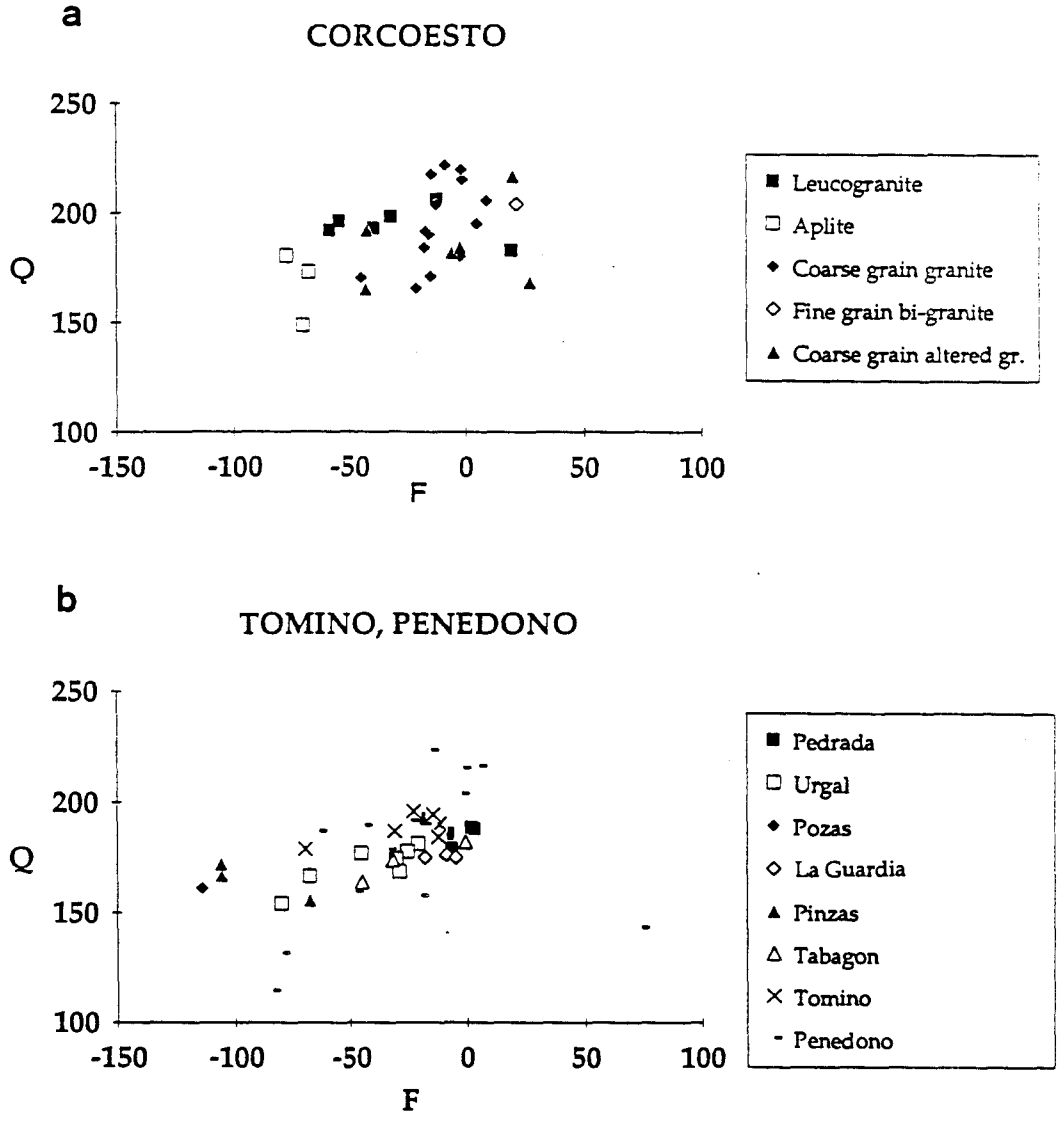

Fig II - 4 : Q-F diagram, (Q= Si - (K+ Na+ 2Ca/3 and F= K-(Na+Ca))
a : Corcoesto granites; b : Tomino and Penedono granites.

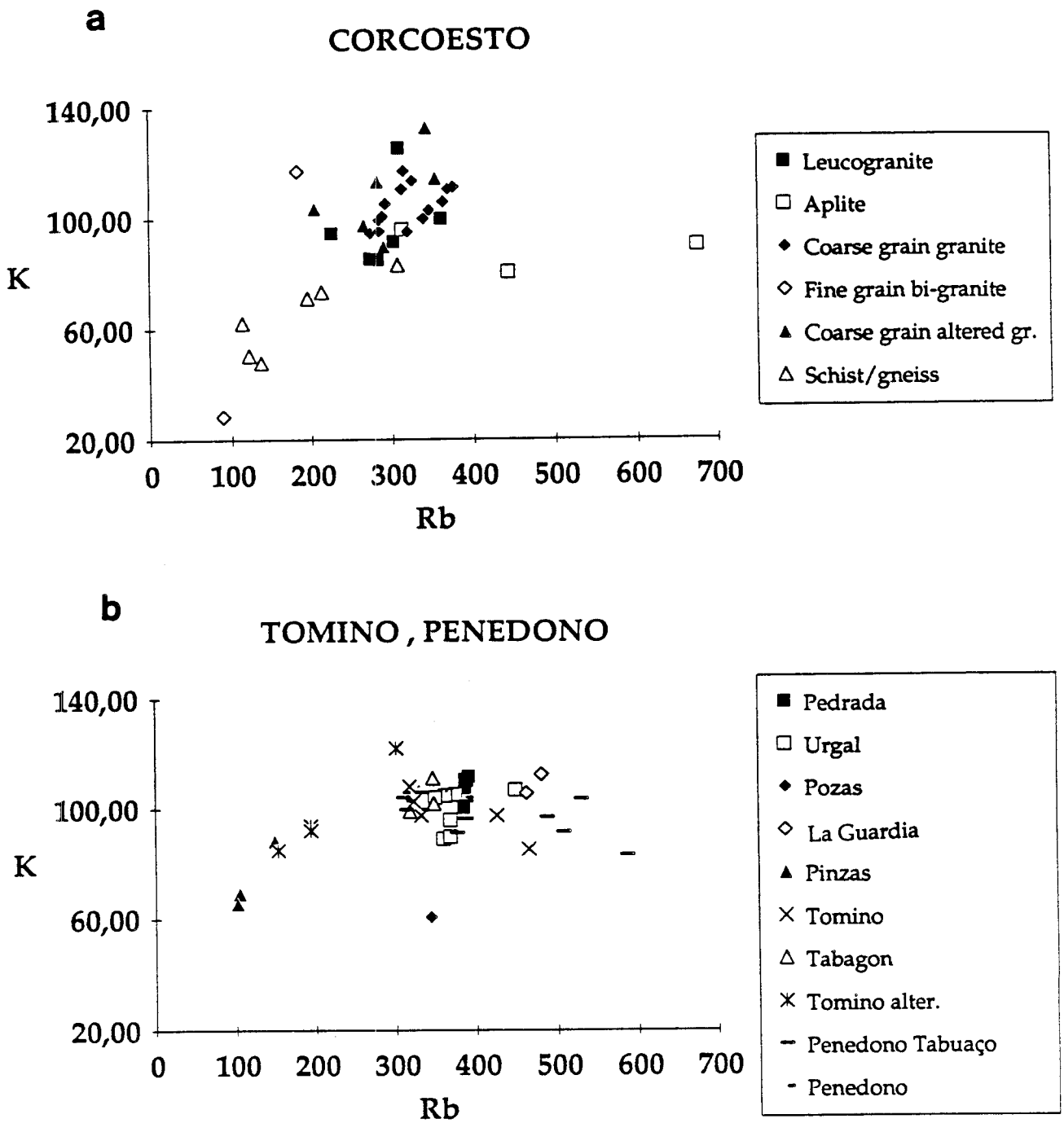

Fig II -5 : K - Rb diagram
a : Corcoesto granites; b : Tomino and Penedono granites.

In the Penedono granites, when the altered samples are discarted (plagioclase of sample 149A16 is strongly altered to K-micas : I.L.=4,04wt%, Na_2O=1,26%, K_2O=7,13%, Al_2O_3=20,16% ; samples 149A6 (5,25 % Na_2O), 149A9 (5,04 % Na_2O), 149A10 (4,25 % Na_2O) and 139R24 (4,18 % Na_2O) seems to be albitized, the remaining samples define a negative correlation between the B and A parameters classical of Variscan peraluminous leucogranites (Cuney et al., 1990).

For the other granites, the peraluminous index A does not show any significative changes with increasing magmatic differentiation (decreasing B parameter) in most cases, although the A parameter values displays a relatively inportant scattering (25<A<70 or more for altered samples) (Fig. II-.1 and 2)

At Tomino, most granites are peraluminous leucogranites, at the exception of the Pinzas facies, which is a biotite granite distinct from the main granite body, and the tonalite of Pozas (GR15, B=118) which has been found in one of the drilling carried out in the prospected granites. It can be noted that the La Guardia granite is less differentiated than the Urgal and Pedrada granite (Fig. II-3) and see Chap I-1 in chap I.

Samples GR14, 18 and 19 correspond to biotite rich granites (B=56 to 62, i.e. 12to 15 vol.% biotite). These samples are also rich in Ba (700-1000 ppm), Sr (700-1150 ppm) and Rb-poor (100 ppm).

The Q-F digram shows a significant change in the F value indicating a decrease in Ca and an increase in Si and K with increasing differentiation, from the Pinzas granite to the Pedrada granite at Tomino. A similar evolution characterizes the Penedono series (Fig. II-4).

The Penedono and the Tomino leucogranites are also characterized by high phosphorus content (0.40 to 0,80 wt%) and Rb (300 to 400 ppm) as generally observed in highly fractionated peraluminous leucogranites.

At Corcoesto, there is a clear evolution in composition from the biotite and Kf-porphyroclast rich facies to a leucocratic end member represented by the garnet bearing aplites. Other granites (leucogranites, fine grained biotite granites and coarse grained biotite granites) display intermediate compositions between two end members :

- *leucogranites* , enriched in Si, and poor in most compatible elements (Fe, Mg, Ca, Ti, Ba, Sr, Th, Zr...) ; the "felsite", especially rich in Na_2O (4,58 wt%), Y (184 to 195 ppm) and Rb (443 to 675 ppm) have compositions very close from the garnet aplite (4,91 wt% Na_2O), excepted for few trace elements (Th).
- *biotite granites* are enriched compatible elements ; there is practically no difference between the fine grained bitotite granites and the coarse grained facies, excepted for some trace elements (Rb for instance which is low around 100 ppm).

Major trends in trace elements are the following :

- **Rb** : an Rb content increase with a simultaneous decrease of K content is typical of subsolidus muscovitization, and concerns mostly the Penedono-Tabuaco granite unit which is the most differentiated (Fig. II-5). In other sites, Rb remains relatively constant at the exception of the Tomino greisens. Rb is remarkably constant in the Corcoesto granite, whilst Sr decreases slightly from the less to the more differentiated granites (Fig. II-6).

- **Li-F**: Li content is variable compared to F which remains nearly constant at the exception of the greisens (up to 2200 ppm) and in the Penedono granite (up to 2400 ppm). Li values vary from 1 to 400 ppm in the Urgal-Pedrada granites (Fig II-7-c), for a a nearly constant biotite content, from 100 to 300 ppm in the Penedono granite series. In the Penedono granite, F-content is higher than in the other granites.

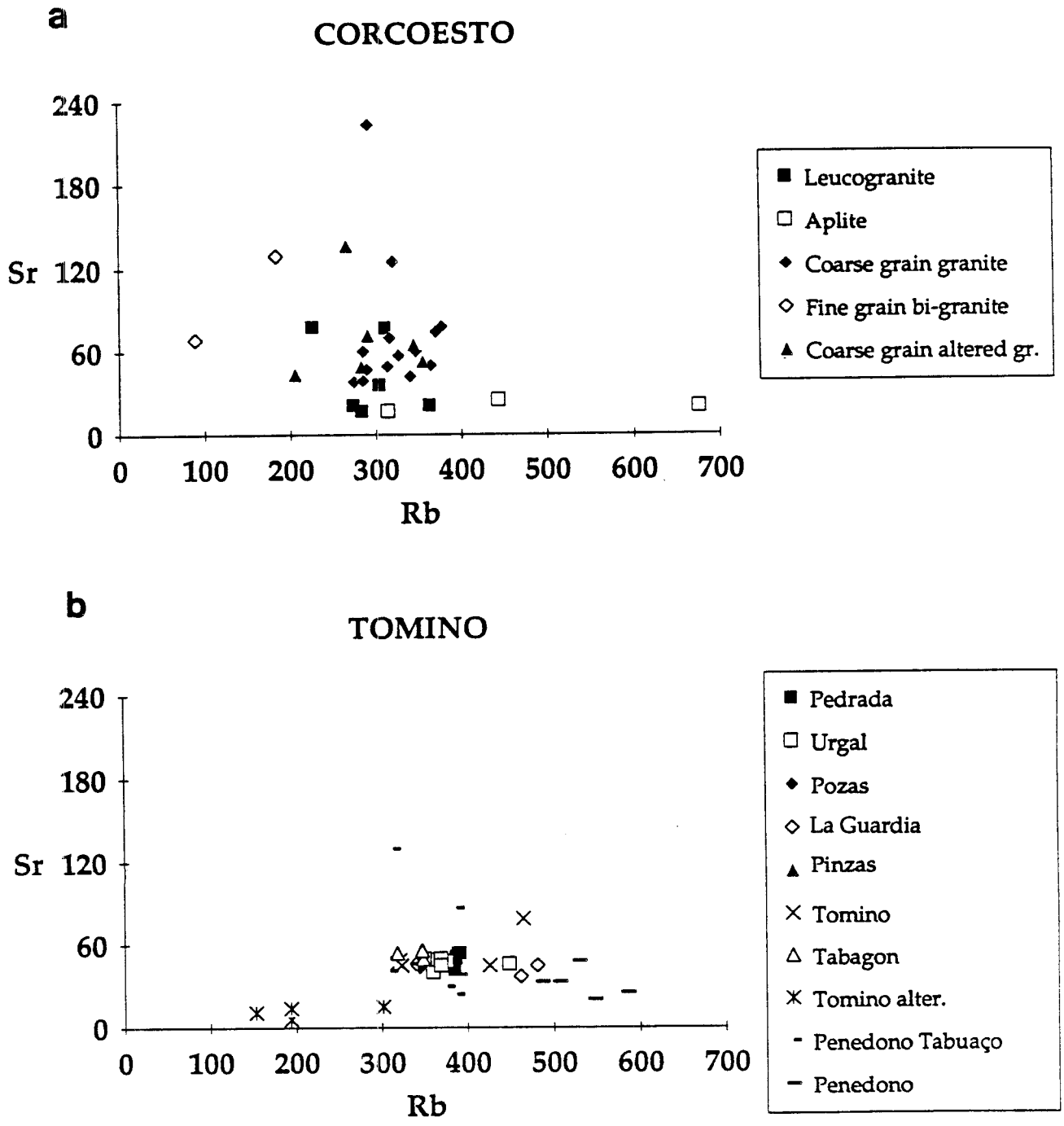

Fig II - 6 : Sr - Rb diagram
a : Corcoesto granites; b : Tomino and Penedono granites.

2- INFLUENCE OF ALTERATION ON ROCK GEOCHEMISTRY

- the case of greisenization at Tomino

Greisen display typical compositions of quartz muscovite rocks as defined by Charoy (1979) in Cornwall, especially :

-high Si and K contents

-nearly complete loss in Na, linked to the albite alteration to muscovite.

- strong decrease in Rb and Sr due to the feldspar alteration, and a strong increase in F linked to muscovite crystallization.(Fig. II-6)

The "greisenized" granite from Peneodono displays similar geochemical features apart from their relatively lower SiO_2 content, which is indicative of dominant muscovite new formation rather than a feldspar --> muscovite + quartz alteration. Such a muscovite new formation is typical of W veins as for intance in the southern French Massif Central (Ramboz, 1980).

- the bleached zone at Corcoesto

They correspond to zones affected by the alteration of biotite to chlorite and phengite, and by slight deposition of carbonates. These alterations are spectacular at the macrosocopic scale but are nearly isochemical. There is only a slight decrease in Fe and Mg related to the biotite alteration, and a slight increase in the F parameter related to Na-loss and K-increase (Fig. II-6).

CONCLUSION

As a conclusion, most granites hosting Au-mineralizations are peraluminous, and most of them are leucogranites. The spatial association between granites and Au-mineralizations may be the consequence of two factors :

1 - the syntectonic granites are emplaced in active structural zones which remain preferentially mobile during the later tectonic reactivations generating the structures which can be mineralized.

2 - as shown in Chap. III, the amount of quartz is one of the major parameter favouring rock deformation ; therefore, the granites richer in quartz are generallly the most leucocratic and thus the most able to react positively to britlle deformation in giving series of tension gashes networks (this is the case of the Tomino and Corcoesto leucogranites, rarely in biotite richer granites).

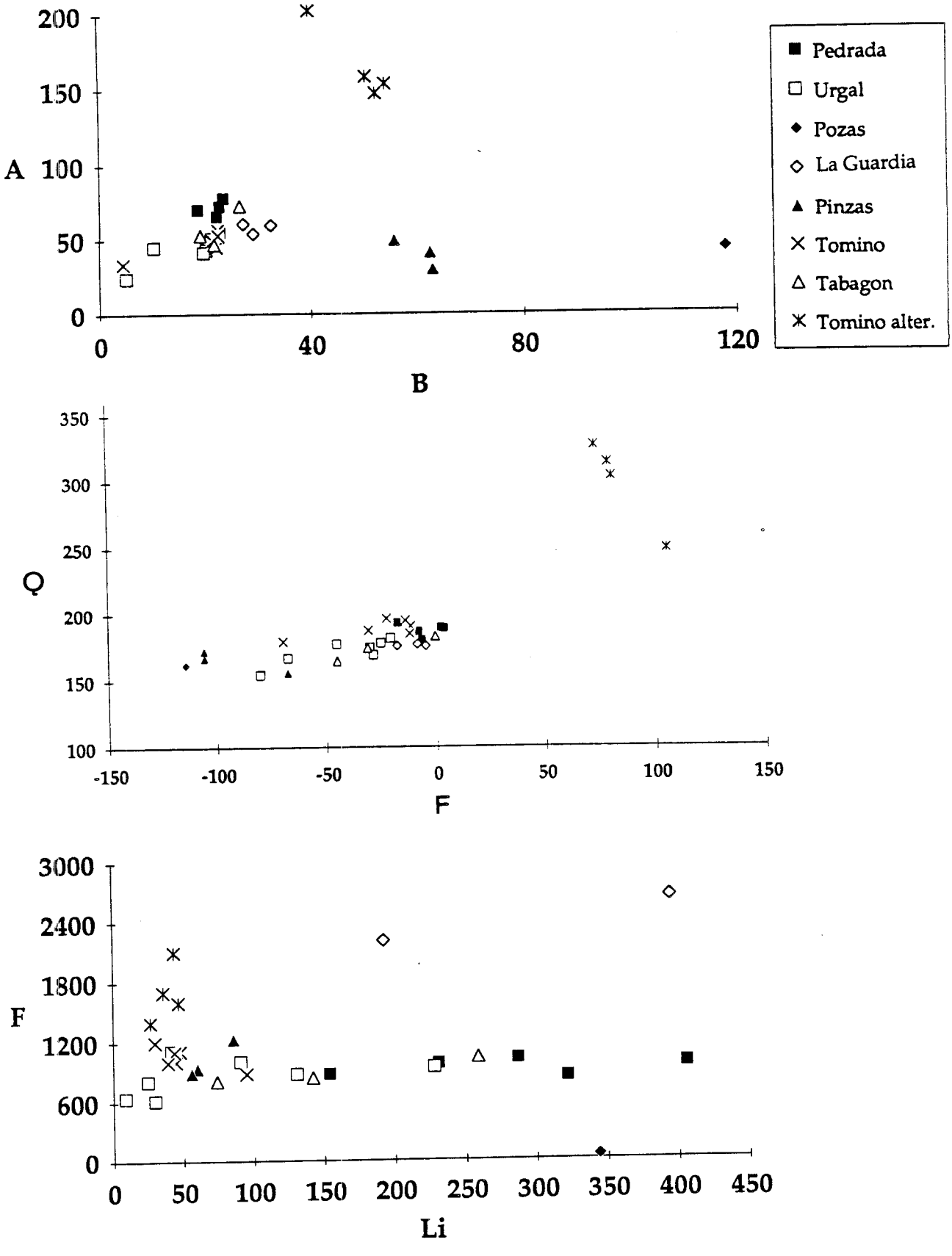

Fig II - 7 :Tomino fresh and altered rocks granites
a : A-B diagram; b : Q-F diagram , c: Li-F diagram

B - METAMORPHIC SERIES

1-WHOLE ROCK GEOCHEMISTRY OF THE VILA POUCA DE AGUIAR (VPA) GOLD DISTRICT - PORTUGAL.

a- Introduction

In the Vila Pouca de Aguiar gold district (Portugal), 67 samples have been analyzed by ICP-ES and wet chemical analysis. These samples belong to the four cartographic units (A, B, C et D) and to 11 petrographic types (Annex I). There is two main rock groups :

- (i) argillaceous rocks [phyllites, green schists, gresophyllites, banded quartz-phyllites and black shales] ;
- (ii) more or less siliceous rocks [banded quartz-phyllites, siliceous schists, silicified schists, quartzites and wackes].

Minor rock types [vulcanites, calc-silicates and other particular facies] will be not considered for the ACP treatment.

The analytical results has been treated in three ways :

- (i) spidergrams has been realized for the average composition of each main facies normalized to the upper crust ;
- (ii) multi-variable statistical analysis (A.C.P.) ;
- (iii) from the A.C.P. results, several discriminating binary diagrams have been drawn.

b - Lithogeochemistry

Major elements

The geochemistry of major elements confirms the same heterogeneity of Vale de Égua, Cubo and S^{ta} Maria de Émeres units, and the homogeneity of the Curros unit. Two chemical-mineralogical diagrams concernig major elements are presented (Fig. II -8 and 9): Al/3-K=f(Al/3-Na) (La Roche, 1968) and Si/3-(Na+K)=f(Al-(Na+K)) (Moine, 1975). The first diagram allows to show the sedimentary or volcanic nature of the different lithologies, as well as the geochemical degree of maturity of the sedimentary rocks which is a function of the differential behaviour of alkalis and alumina during the entire sedimentary process. In the second diagram it is possible to vizualize the proportion of quartz, feldspars and phyllites. This diagram shows also the geochemical degree of maturity or the sedimentary evolution.

The interpretation of Al/3-K=f (Al/3-Na) diagram allows the individualization of four groups (FigII-8):

Group I - corresponds to the more siliceous lithologies: the banded quartzphyllites (Ia) and the lydites (Ib) of Vale de Égua unit and the siliceous schists of Cubo unit (Ic). In this diagram the banded quartzphyllites are placed in the transition to the igneous domain.

Group II - This group includes acid volcanites and banded quartzphyllite of Vale de Égua and S^{ta} Maria de Émeres. These lithologies fall out of the sedimentary field of the diagram and have the most important volcanic contribution.

Group III - Represents the pelitic group and includes samples of the four units. Curros unit belongs mainly to IIIa subgroup- gresophyllites- and to IIIb subgroup - phyllites and green schists. The pelitic terms of the other units are less homogeneous and are partially superimposed over both IIIa and IIIb subgroups.

Group IV - Represents the calc-silicate rocks of Vale de Égua and S^{ta} Maria de Émeres units.

The sample MA 117 (Curros unit) is an exception because it is very rich in plagioclase.

The diagram Si/3-(Na+K)=f (Al-(Na+K)) shows two main groups (Fig.II-9):

Group I - Greso-pelitic group between the quartz-chlorite and the quartz-illite lines. This group includes the Ia subgroup - lydites and silicified schists of Vale de Égua unit- and the Ib subgroup - all the samples of Curros units with the exception of sample MA 117. All the units show pelitic terms having compositions between those of chlorite and illite, but Curros unit has the most aluminous character.

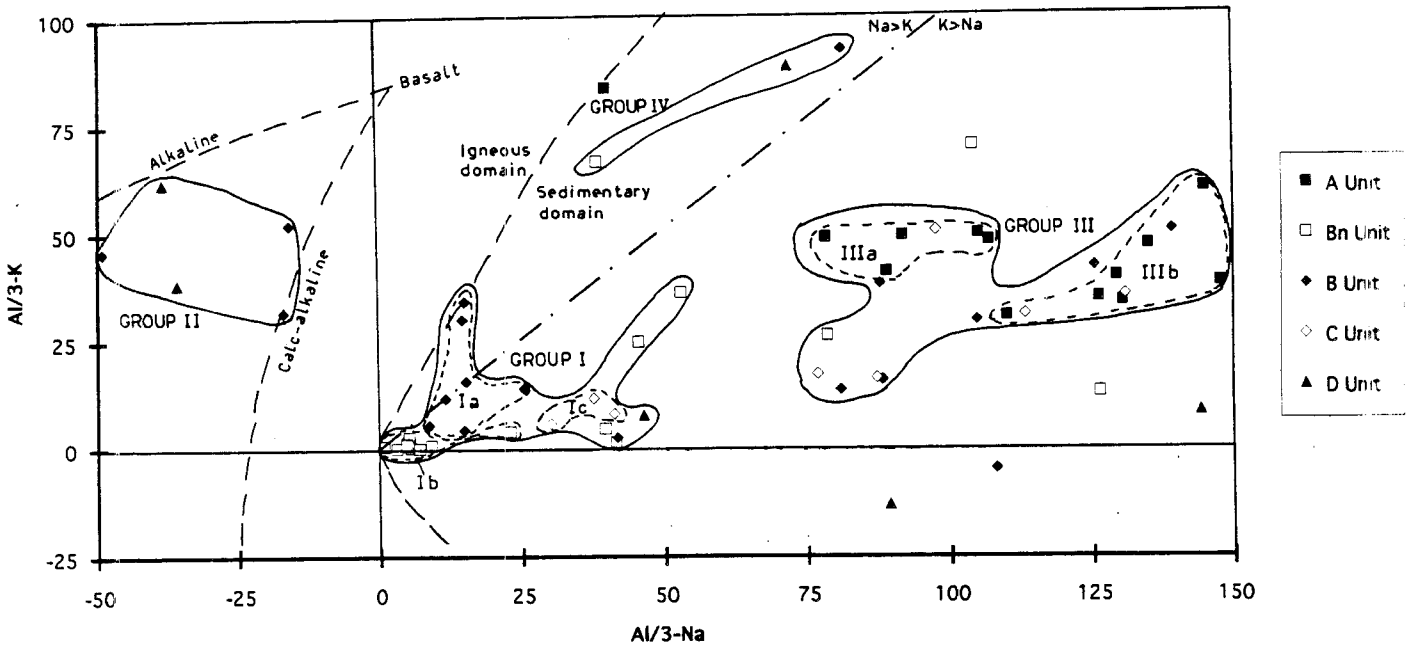

Fig II - 8 : Al/3-K = f (Al/3-Na) diagram of VPA metasediments.

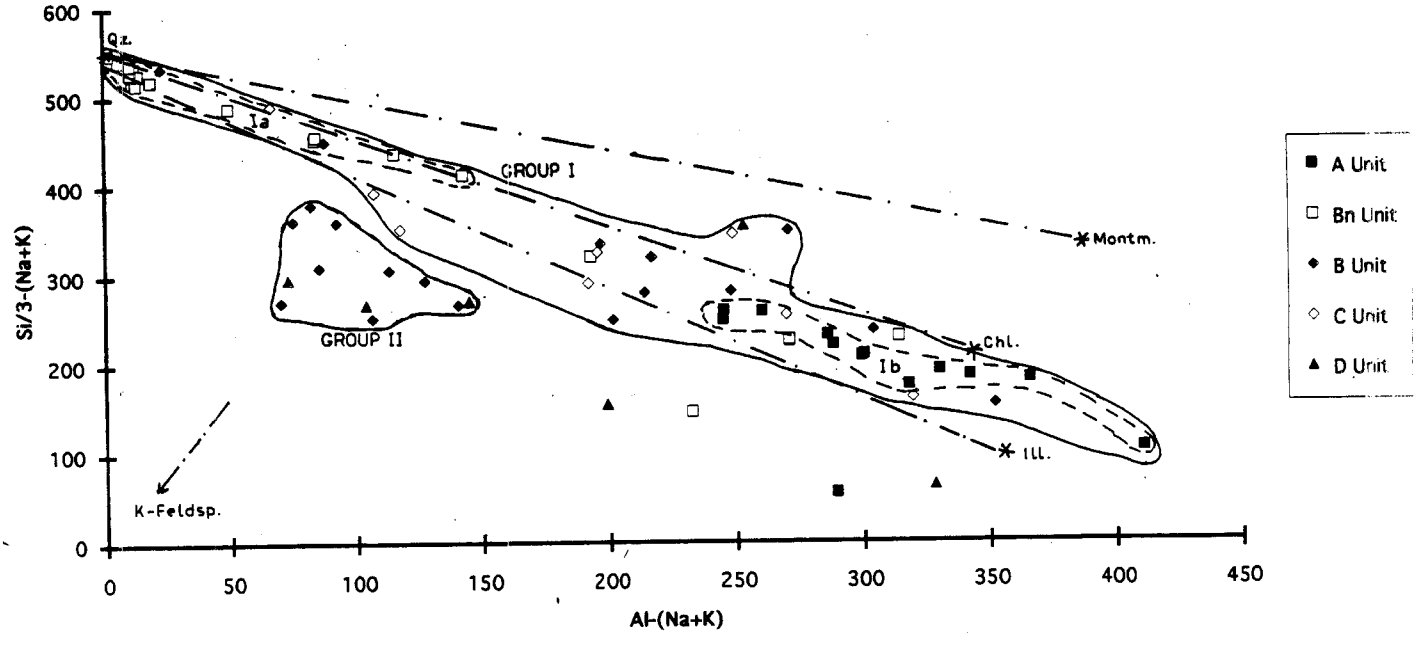

Fig II - 9 : Si/3-(Na+K) = f (Al-(Na+K)) diagram of VPA metasediments.

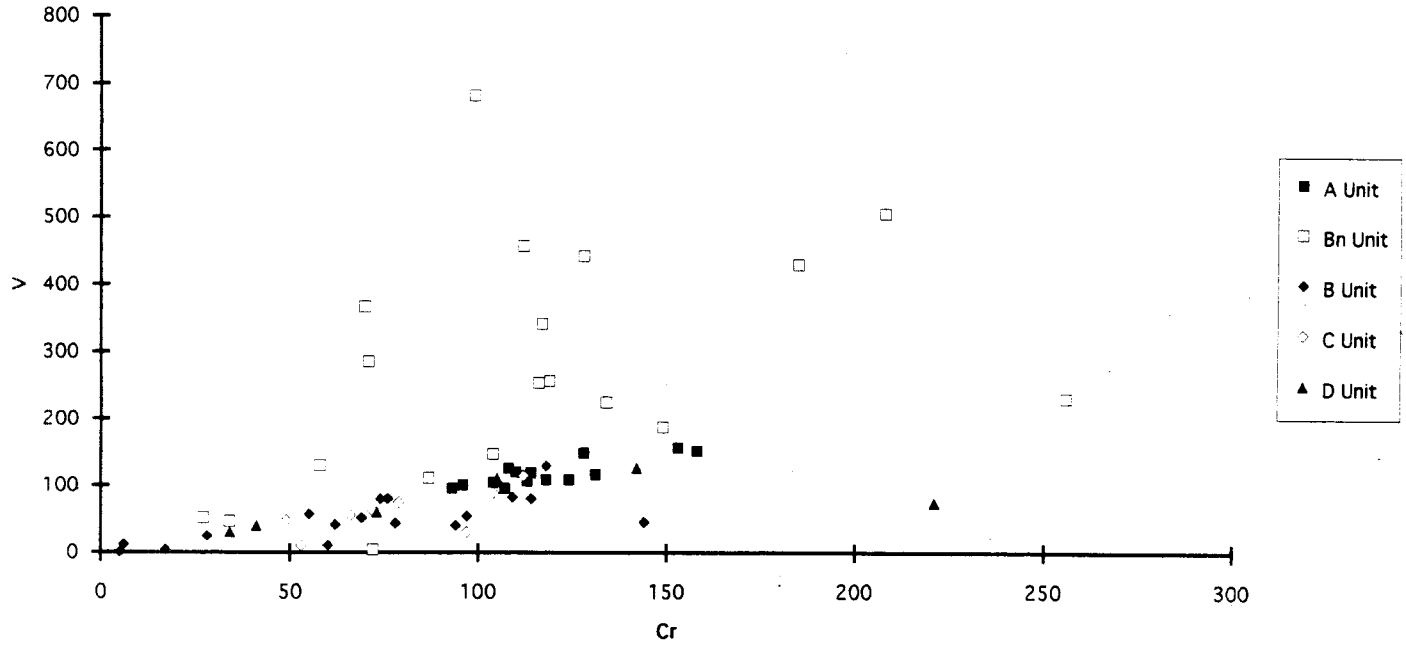

Fig II - 10 : V = f (Cr) diagram of VPA metasediments (Bn - lydites and black shales).

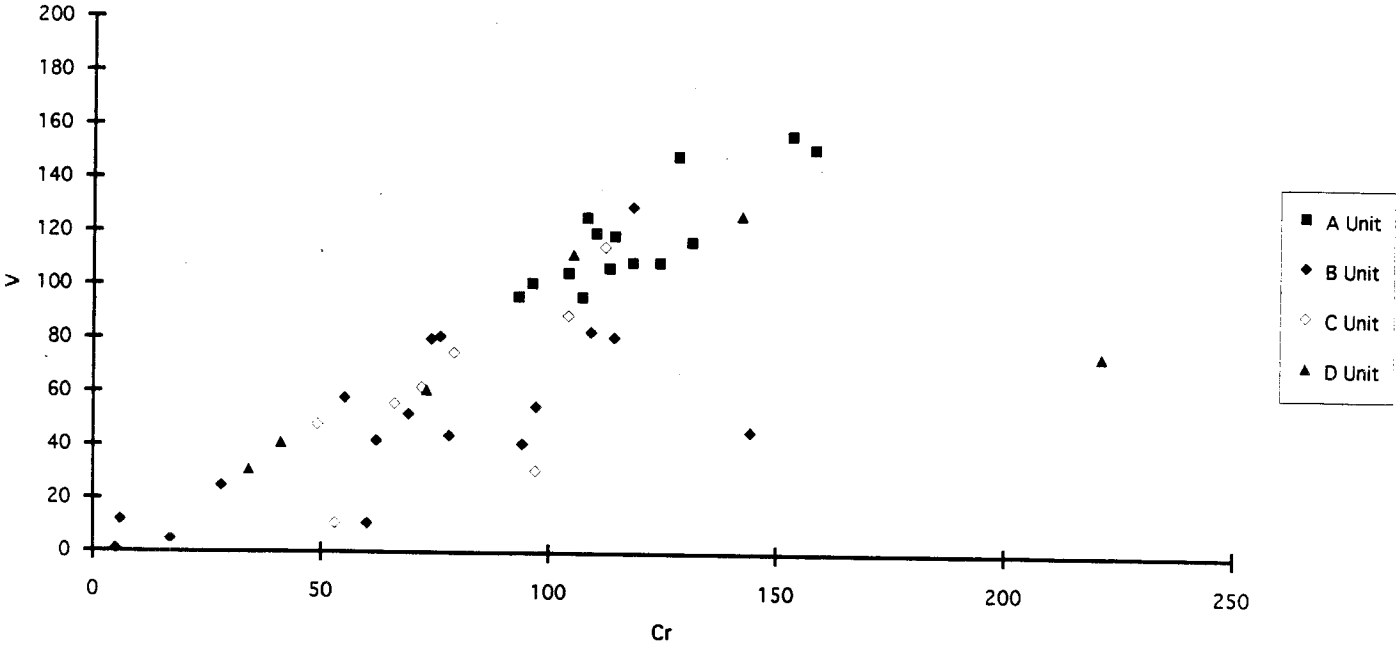

Fig II - 11 : V = f(Cr) diagram of VPA metasediments (without lydites and black shales).

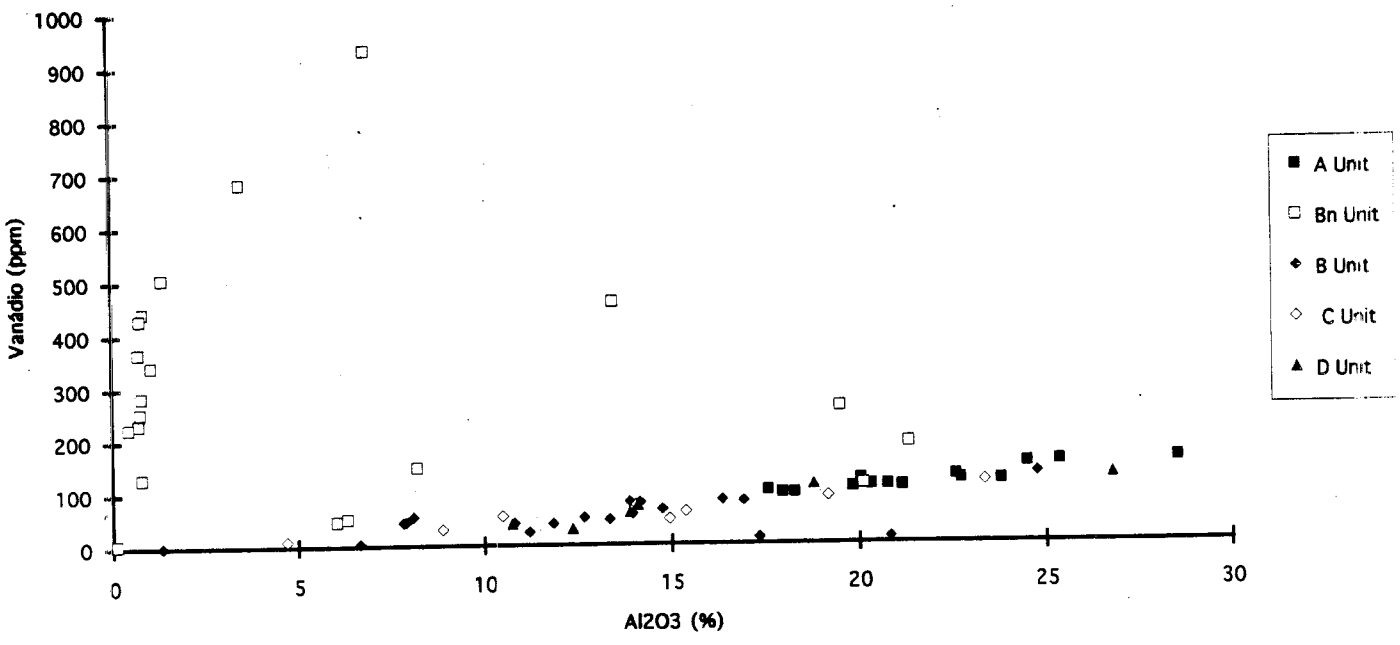

Fig II - 12 : V = f(Al_2O_3) diagram of VPA metasediments (Bn - lydites and black shales).

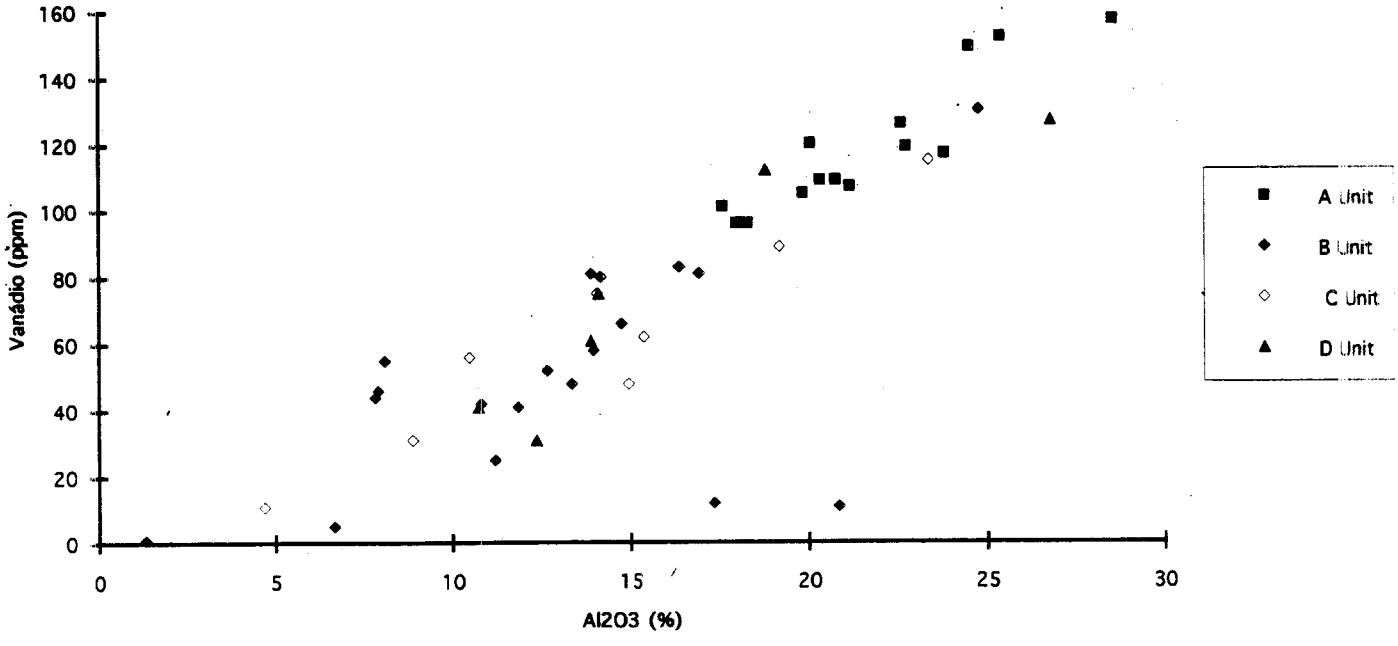

Fig II -13 : V = f(Al_2O_3) diagram of VPA metasediments (without lydites and black shales).

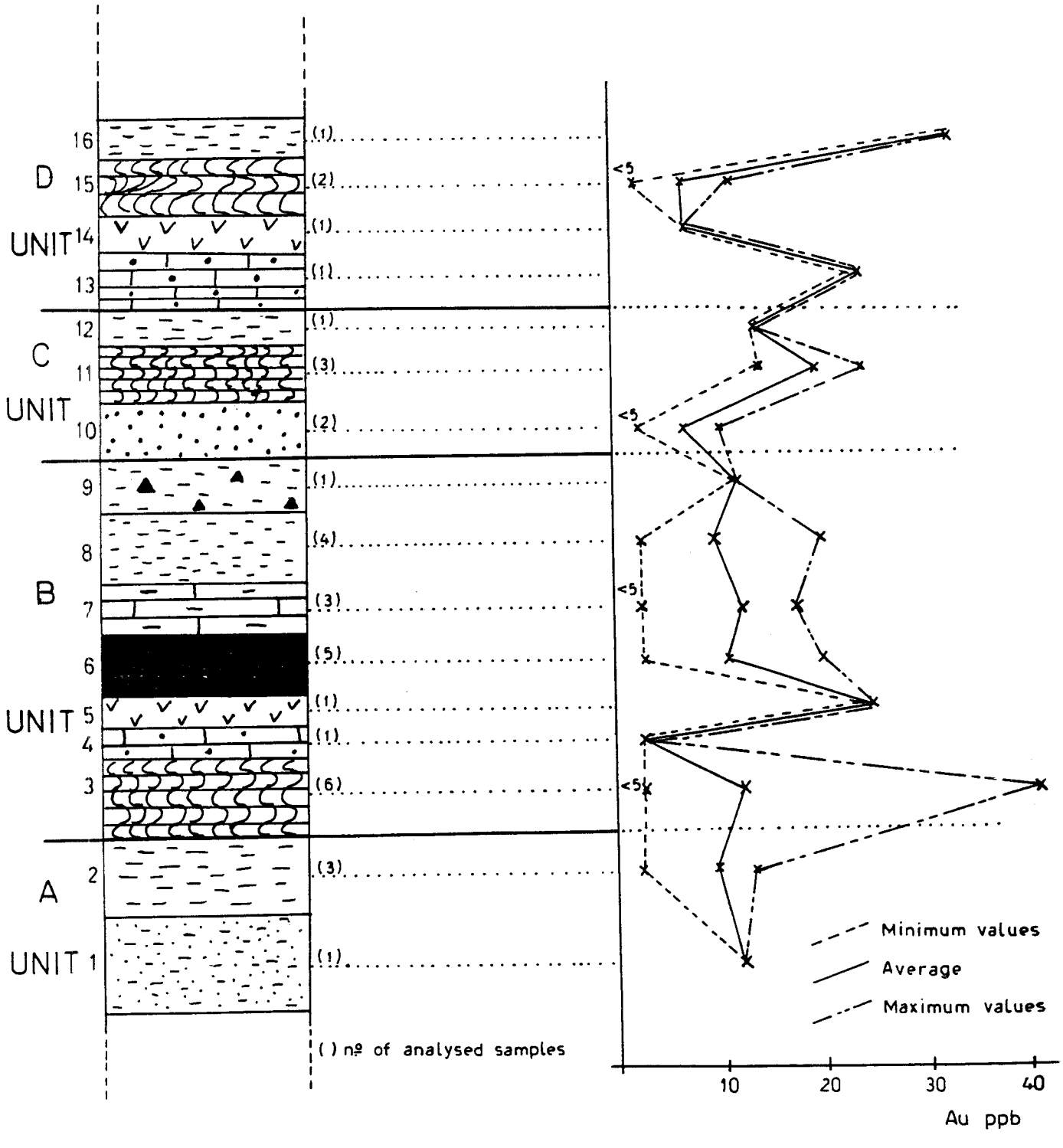

Fig II -14 : Distribution of Au (ppb) contents in a schematic lithological log. (1,2,3,..... - see table II -1)

LITHOLOGY	Position along the lithological log	Au ppb
PHYLLITE		
MA 117 (A)		13
MA 118 (A)	2	13
MA 160 (A)		<5
MA 17 (B)		<5
MA 19 (B)	8	14
MA 26 (B)		<5
MA 128 (B)		20
MA 129 (C)	12	13
MA 22B (D)	16	33
GRESOPHYLLITE		
MA 59 (A)	1	11
QUARTZ-PHYLLITE		
MA 121 (B)		<5
MA 122 (B)		<5
MA 123 (B)	3	<5
MA 130 (B)		19
MA 145 (B)		<5
MA 146 (B)		41
MA 120 (C)		14
MA 125 (C)	11	24
MA 133 (C)		21
MA 20 (D)	15	11
MA 110 (D)		<5
QUARTZITE		
MA 132 (C)	10	<5
MA 136 (C)		10
SILICIFIED SCHIST		
MA 127(B-TM)	not	15000
MA 147 (B-TM)	present	22800
BLACK SHALE		
AD 8 (B)		13
AD 7 (B)		9
AD 59 (B)	6	10
AD 60 (B)		20
AD 63 (B)		<5
LYDITE		
AD 11 (B)		<5
AD 18 (B)	7	17
AD 26 (B)		17
CALC-SILICATE		
AD 9 (B)	4	<5
MA 22A (D)	13	24
VULCANITE		
MA 36 (B)	5	25
MA 22 (D)	14	7
WACKE		
MA 126 (B)	9	12

Table II - 1 : Data on gold contents in VPA metasediments

	SiO2 %	Al2O3 %	Fe2O3 %	MnO %	MgO %	CaO %	Na2O %	K2O %	TiO2 %	P2O5 %	P.F. %	Total
RIBEIRINHA												
Black-shale	82,00	6,94	4,08	0,02	0,24	0	0	0,96	0,20	0,15	5,22	99,81
Black-shale	88,93	6,33	0,27	0	0,06	0	0	1,87	0,20	0,08	2,01	99,75
Wacke	67,34	13,88	10,19	0,05	1,2	0	0,1	2,45	0,93	0,08	3,47	99,69
Green schist	61,45	20,82	6,44	0,03	1,72	1	0,34	4,39	1,02	0,12	4	100,33
Silicified schist	96,4	1,31	1,04	0	0,22	0	0	0,14	0	0	0,92	99,93
LAGO PEQUENO												
Quartz-phyllite	74,65	14,16	2,79	0	0,56	0	0,14	3,59	0,64	0,08	3,2	99,81
Silicified schist	88,43	6,66	1,16	0	0,28	0	0,06	1,92	0	0,04	1,3	99,85

	Au ppb	Ag	As ppm	Ba ppm	Cr ppm	Cu ppm	Ni ppm	Rb ppm	Sb ppm	Sr ppm	W ppm	V ppm
RIBEIRINHA												
Black-shale	10	<5	26	243	139	280	84	38	1	12	7	930
Black-shale				601	27	0	7	38		0	nd	52
Wacke	12	<5	16	437	76	31	51	114	0,5	42	<4	81
Green schist	20	<5	19	739	60	26	8	221	1,1	93	<4	11
Silicified schist	15000	<5	11	1	5	123	1	10	0,4	1	<4	1
LAGO PEQUENO												
Quartz-phyllite	41	<5	62	490	74	24	10	172	3,8	24	5	80
Silicified schist	22800	<5	12	277	17	8	1	79	1	9	<4	5

Table II - 2 : Lithogeochemistry of the Três-Minas samples.

Group II - Represents the volcanites and the banded quartzphyllites of Vale de Égua and Sta Maria de Émeres units. The geochemical differences between banded quartzphyllites and gresophyllites (Ib subgroup) are very clear in this diagram.

The lithogeochemistry of major elements allows to point out the following:

- A great pelitic homogeneity of Curros unit, with the highest values of Al2O3 and of Fe+Mg+Ti.
- The volcanic contribution in Vale de Égua and Sta Maria de Émeres units with a bimodal character represented by acid volcanites (between the calc-alkaline and alkaline domains) and calc-silicate rocks associated with quartzphyllite depleted in Al2O3 relatively to the other pelitic lithologies.

Au- (V, Cr, Ni) geochemistry

V, Cr and Ni. These elements have a positive correlation, with the exception of the lithologies containg organic matter (lydites and black shales) that are anomalous in V and not in Cr. Al2O3 has also a positive correlation with V, Cr and Ni with the exception of black lithologies (Figs. 10 to 13). Curros unit is homogeneous and is the richer both in V, Cr and Ni, and in Al2O3. These facts suggest the influence of ultrabasic rocks and a sedimentary evolution with geochemical maturity.

Au : considering the results of Au contents on the 38 analysed samples (Table II-2, annexe), we can conclude that all units reveal some Au values higher than 1,8 p.p.b. (Fig.II-14 and Table II-1), the normal value for upper continental crust (Taylor and Mc.Lennon, 1986). Relatively to lithologies, if we exclude the specific case of silicified schists from Três-Minas, we cannot affirm that there are some more specialized terms, because all lithologies have examples of anomalous values (Table II-1); consequently, there are no preferencial concentrators namely the black shales. However we must emphasize the important volcanic contribution well marked namely by vulcanites and certain quartz-phyllites from D and B units, precisely the units that exhibit more Au "anomalous" values, suggesting an eventual role of volcanism in the gold metallogeny in VPA area.

The example of Três-Minas is very particular and the geochemical data, presented on table II-2, suggest that **Au has a very specific behaviour irrespective of the other metalic elements.** The silicified schists from Ribeirinha and Lago Pequeno have a hight content in gold and a relative low content on other elements, namely As and W. This means a specific Au concentration process, independent from other elements; the concentration is associated to a silicification and this process corresponds to a specific structural situation of shear zone.

b - Spidergrams

In order to compare globally the geochemical characteristic of the VPA metamorphic formations to the average composition of similar formations in the world, spidergrams have been realized following the element order given by Thompson et al. (1984) : Ba, Rb, Th, K, Nb, Ta, La, Ce, Sr, Nd, P, Sm, Zr, Hf, Ti, Tb, Y, Tm and Yb. Ta and Tm, with low values or no determinations have not been considered for the spidergrams. The analytical results below the detection limit (<5 ppm) have been assumed to correspond to 1 ppm (excepted for Ba, Sr and Nb for which a value of 2 ppm has been choosen). For detection limits below 1, 2 and 0.5 a value of 0.2 has been choosen. "Trace" concentrations have been considered as "0".

According to the rock type, the composition has been normalized to average chemical compositions of Paleozoic graywackes [for siliceous rocks], average chemical compositions of Proterozoic cratonic shales [for argillaceous rocks] and average chemical compositions of Paleozoic felsic volcanic rocks [for volcanic rocks] (after Kent C. Condie, 1993).

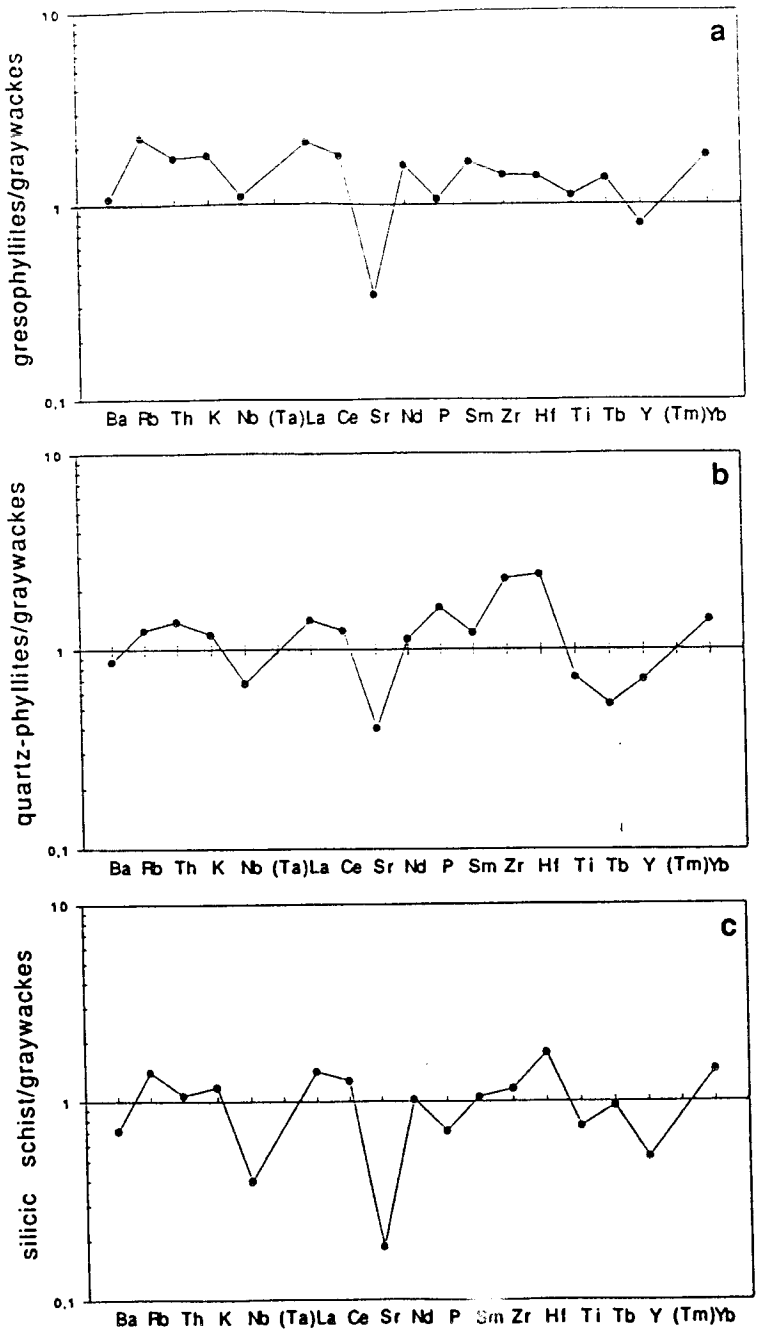

Fig II -16 : Gresophyllites, banded quartz-phyllites and silicic schists normalized to average chemical compositions of Paleozoic graywackes.

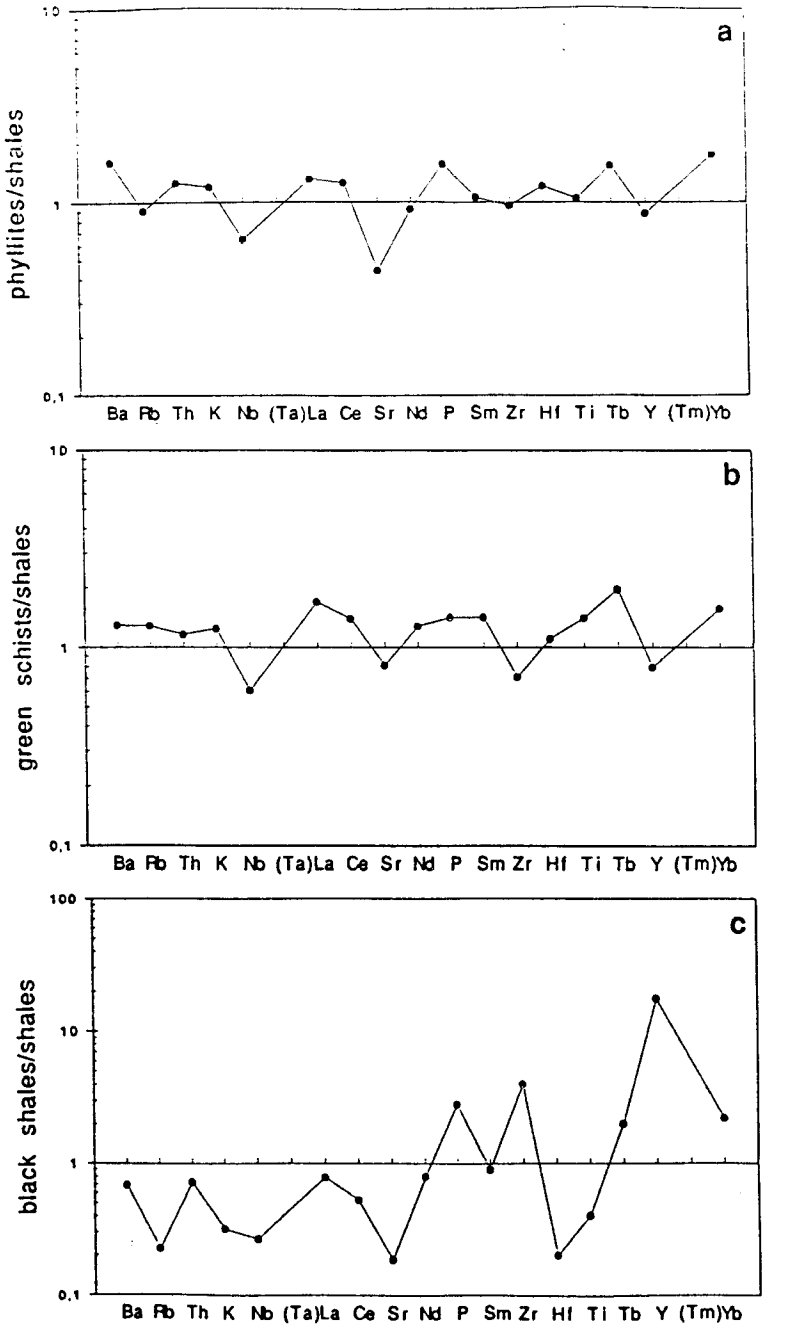

Fig II -15 : Phyllites, green schists and black shales normalized to average chemical compositions of Proterozoic cratonic shales.

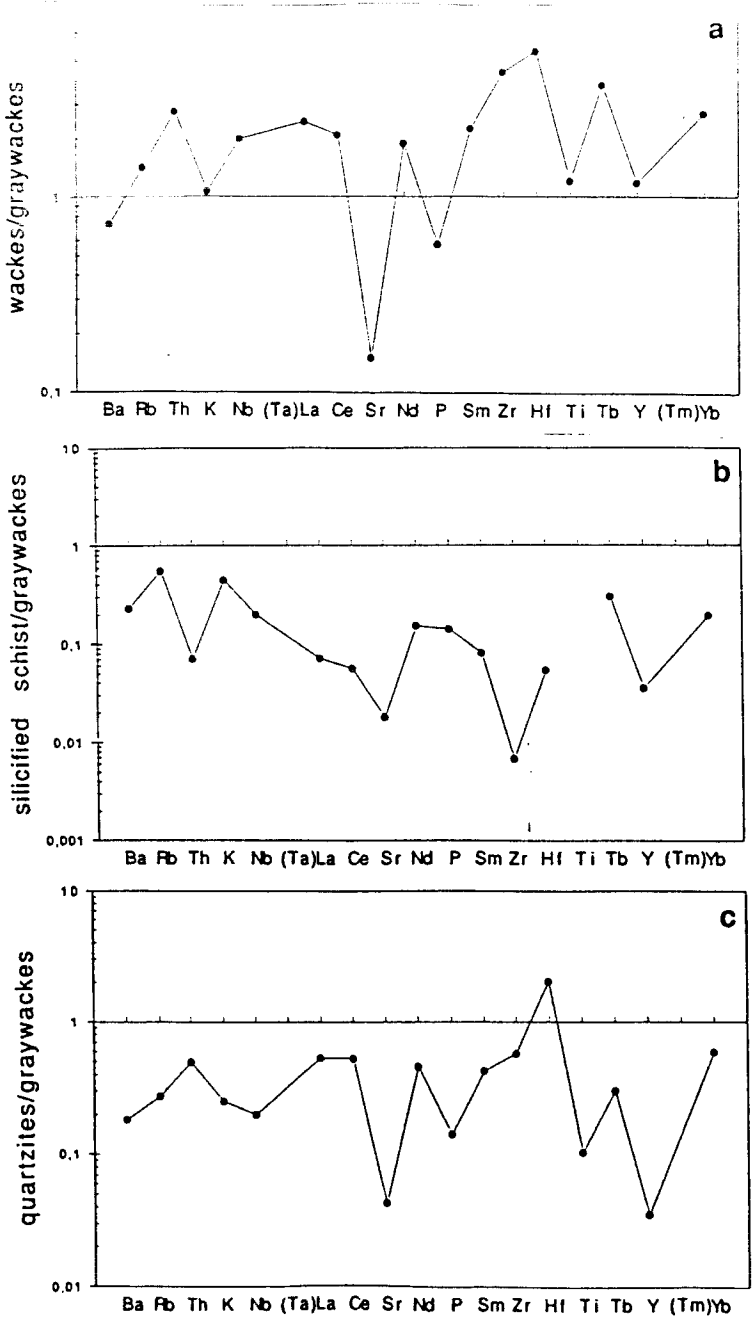

Fig II -17 : Wakes, silicified schists and quartzites normalized to average chemical compositions of Paleozoic graywackes.

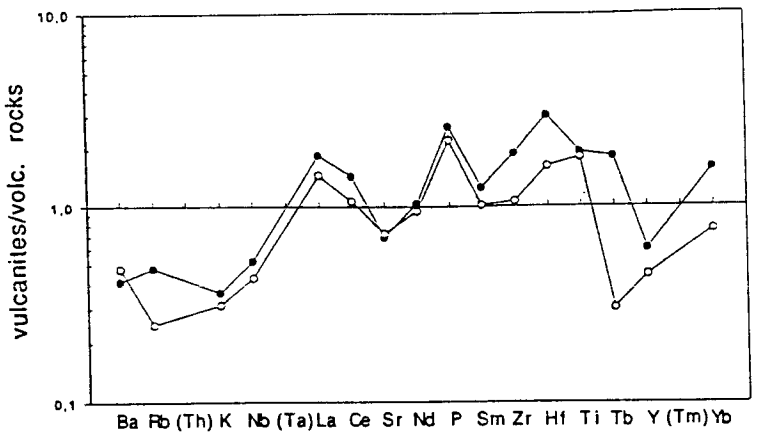

Fig II -18 : Vulcanites normalized to average chemical compositions of Paleozoic volcanic rocks.

- *Argillaceous rocks*

Phyllites and green schists of the VPA district present composition close to the average chemical composition of Proterozoic cratonic shales (Fig. II-15a and b). Slight negative anomalies are observed for Nb and Sr for phyllites and for Nb (±Sr, Zr and Y) for the green schists. For both facies types, slight positive anomalies are observed for LREE, P, Tb and Yb.

For black shales (Fig. 15c), large variations in the distribution of all elements is observed. The strongest positive anomalies are observed for P, Zr and Y, and negative anomalies are observed for Rb, K, Nb, Sr, Hf and Ti.

- *Siliceous rocks*

Gresophyllites, banded quartz-phyllites and silicic schists present average chemical composition close (but slightly enriched for most of the elements) to that of Paleozoic graywackes (Fig. II-16a, b and c), excepted for Sr which shows a strong negative anomaly.

Other negative anomalies are :

(i) for Nb and Tb in banded quartz-phyllites ;

(ii) for Nb and Y in silicic schists.

The higher positive anomalies are :

(i) Zr and Hf which represent zircon enrichment in the banded quartz-phyllites ;

(ii) Only Hf for silicic schists.

The numerous anomalies observed for the wackes most probably correspond to the fact that only one sample has been analyzed (Fig. II-17a). Most of the elements are enriched compared to average Paleozoic graywackes, with strong positive anomalies for Zr, Hf, Th, Tb and Yb, expressing enrichment of the wackes in accessory minerals. The stronger negative anomaly is for Sr.

Quartzites and silicified schists are strongly depleted for most elements compared to average Paleozoic graywackes (Fig. II-17b and c) because of the large quartz content of these rocks. The strongest negative anomalies are for Sr and Y for both facies and for Th, LREE, Sm and Hf for silicified schists and for Ti, P, K, Ba and Nb for quartzites because of the smaller argillaceous componant compared to graywackes.

.- *Vulcanites*

Only two vulcanite samples have been analyzed. This explain the large variations observed in the spidergrams, but the two samples present a similar pattern (Fig. II-18). Ba, Rb, K, Nb and Y present much lower concentration than Paleozoic felsic volcanic rocks. These characteristics indicate a much less potassic character of the VPA volcanism compared to average Paleozoic volcanism, whereas La, P, Hf and Ti present higher concentrations.

- *Conclusions*

Most of the argillaceous facies, excepted black shales present average compositions close to that of average Proterozoic shales and most silicic facies present average compositions close to that of average Paleozoic graywackes, excepted for extreme terms like silicified schists and quartzites.

However, the metasediments of the Vila Pouca de Aguiar gold district show some specific characteristics :

- the most striking one is the occurence of a **systematic large negative anomaly in Sr** all the faciès excepted for the volcanites ;
- negative Nb anomalies are observed mainly in the argillaceous facies,
- and enrichment in accessory heavy minerals occurs for the greywacke sample and quartz phyllites.

c.- Multi-variable (A.C.P.) statistical analysis

The aim of A.C.P. is to systematically define all the correlations existing between major and trace elements for all samples which can be reported on selected binary diagrams or maps.

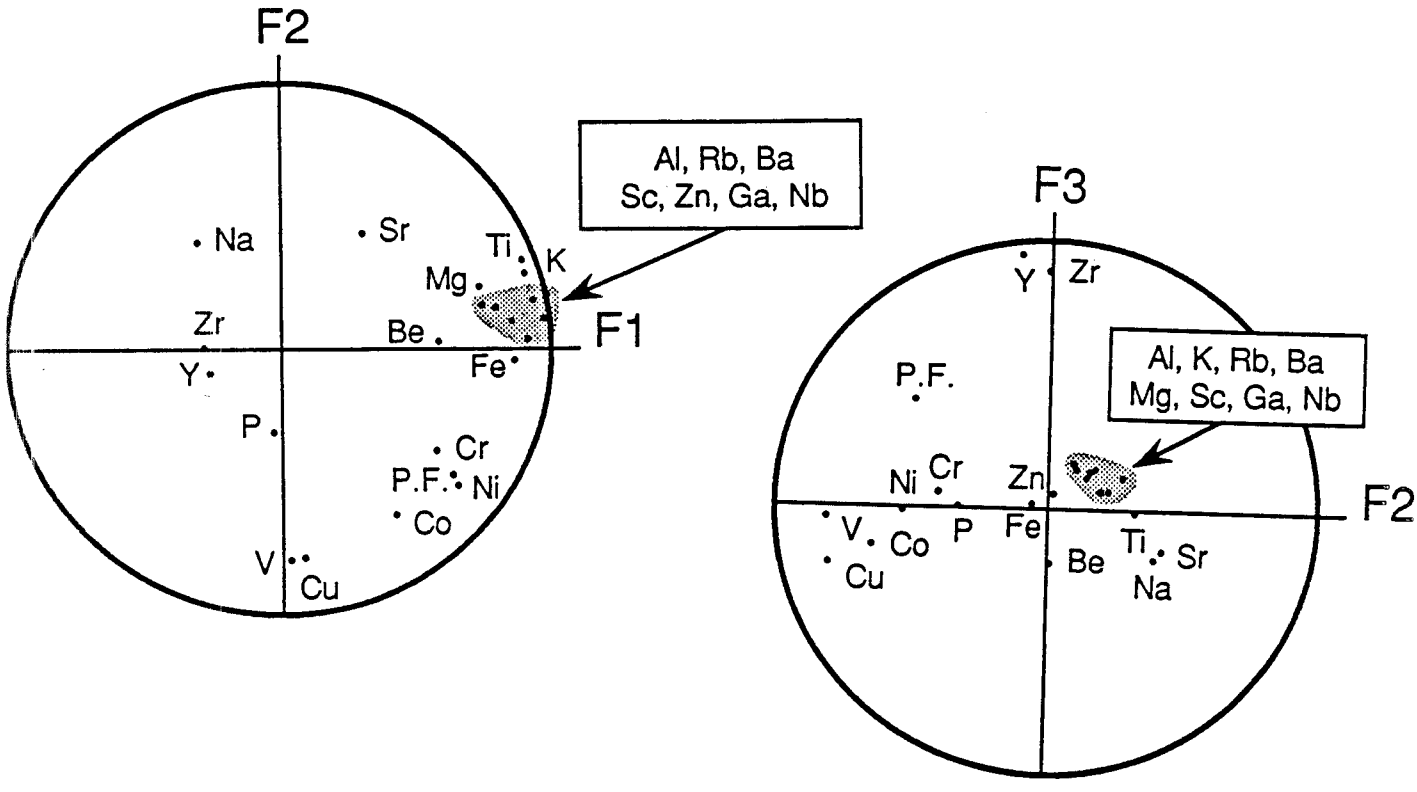

Fig II -19 : Circles of correlations F1-F2 and F2-F3 for 23 elements and 50 samples considered in the A.C.P. treatment.

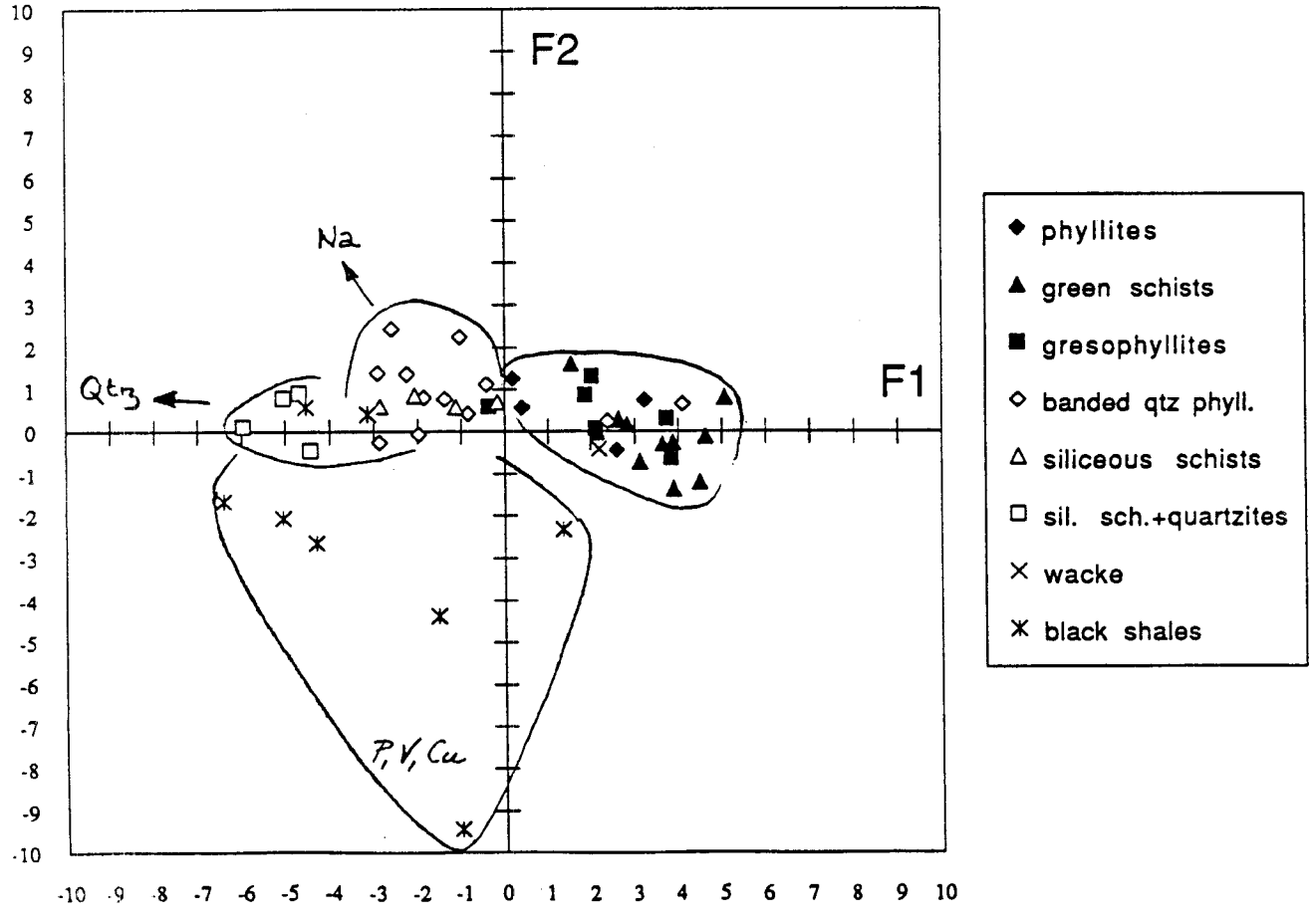

Fig II -20 : Samples plotted by facies in a F1-F2 diagram after the score factorsdata.

- ***Data choice***

Some elements have not been analyzed for all samples and some elements are frequently under the detection limit. So, for all the ACP treatment Au, As, Br, Cs, Hg, Ir, Mo, Sb, Se, Ta, W, Dy and Er have not been considered.

Three data selections have been treated in A.C.P. One with all samples (except vulcanites, calc-silicates and unspecified rocks) but only with selected elements ; another with most elements but with selected samples ; and a third with all samples and a selection of elements.

.- ***Results***

- All samples sort ed by facies and a selection of elements

All facies have been considered in this first ACP treatment, except vulcanites, calcsilicates and four peculiar samples. Elements are selected when they have significant values for most of the samples. Element choosen are Al, Fe, Mg, Na, K, Ti, P, Ba, Be, Co, Cr, Cu, Ga, Ni, Rb, Sc, Sr, Nb, V, Y, Zn and Zr. "Si" was not considered because it is a too dominant element traducing silicic facies.

Three factors give 66% of the information in the loading factors (Table II-3 annex). In the matrix (table II-4 annex) and circles of correlations (Fig. II-19), there is a strong positive correlation between Al, Fe, Mg, K, Ti, Rb, Ba, Sc, Zn, Ga and Nb. This group represent the argillaceous pole. V, Cu, Co, Cr, Ni and P.F. (ignition loss) indicate sulfide componants. V is mainly bounded to Cu (r=0.60), (see F1-F2 correlation circle), but also to Co (r=0,48), Cr (r=0,43) and Ni (r=0,36). There is a very strong correlation between Zr and Y (r=0.97), componants of detrital accessory minerals. Na is slightly bounded to Sr (r=0.51) in feldspars.

"Score" factors show the distribution of the different facies in a F1-F2 diagram (table II-5 annex and Fig. II-20). The F1 factor control the spreading of most samples with a good discrimination between :

- the siliciceous rocks (banded quartz phyllites, siliceous schists and quartzites) and
- the argillaceous rocks (phyllites, green schists and gresophyllites).

The very heterogeneous characteristics of the organic matter rich samples is well expressed by the large scattering of the samples of this group.

- Most of elements and a selection of samples sort ed by facies

Element considered for this second study are Al, Fe, Mn, Mg, Ca, Na, K, Ti, P, Ba, Be, Co, Cr, Cu, Ga, Hf, Ni, Rb, Sc, Sr, Nb, V, Y, Zn, Zr, LREE, Eu, Yb, Lu, U and Th. But numerous values at "0" or under the detection limit conduct to consider a selection of only 34 samples (table II-8 annex). Three factors give 64% of the information in the loading factors . In the matrix (table II-7 annex) and correlations circles (Fig. II-21), there is several informations :

- Al, K, Rb, Ti, Sc, Zn still represent the argillaceous pole ;
- LREE, Th, Eu, Yb and Lu represent the accessory minerals ;
- the Fe, Mg, Y, Co, Cr, Ni group which may represent a sedimentary contribution from basic rocks and sulfides becomes more closely correlated with the Al group ;
- Na, Ca and Sr represent the plagioclase contribution ;
- a number of other good correlations are observed :
  - Zr-Hf (0.917) for zircon,
  - Ga-Nb (0.735),
  - Cu-Be (0.793),
  - U-Ba (0.649), U-P (0.574) and U-V (0.721), the two last correlations represent classical geochemical associations for uranium enrichments in sedimentary rocks,
  - Th-Ti (0.736), Th-Y (0.792) and Th-REE corresponding to detrictic accessories.

But most of these positive correlations in binary diagrams appear in fact to be directed by few samples with extreme values.

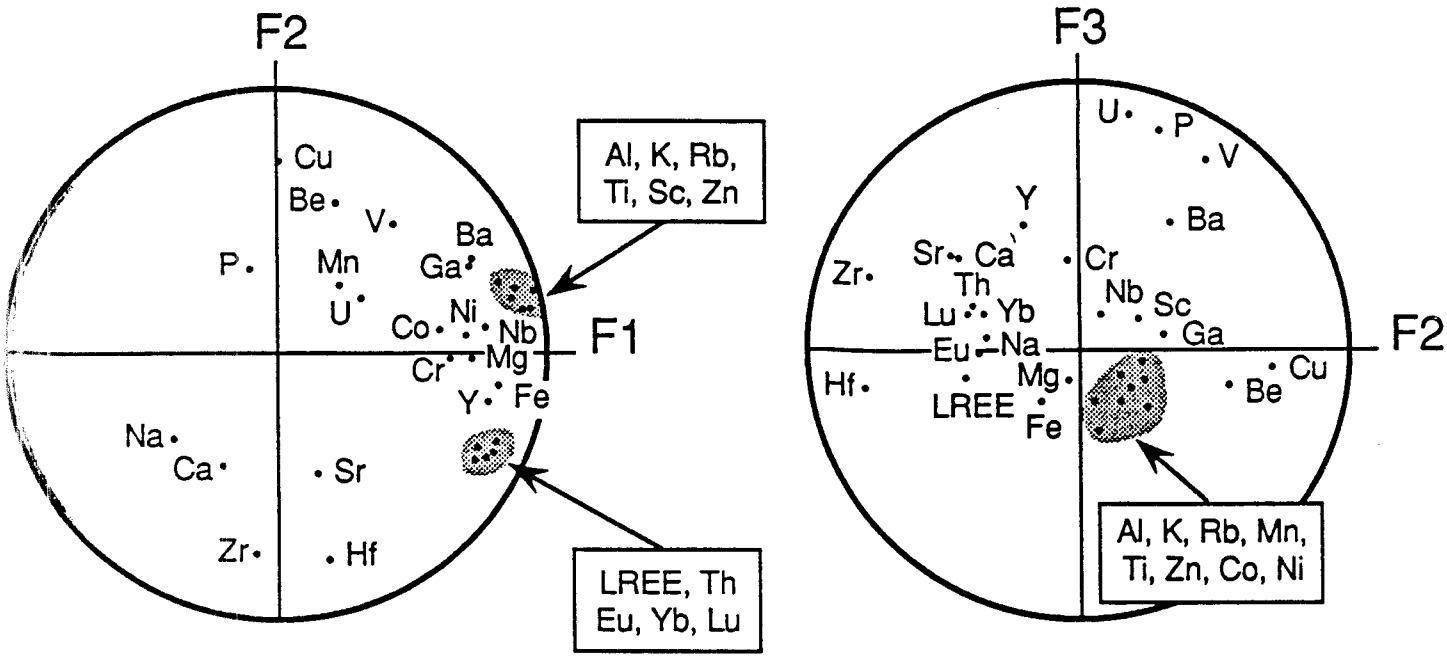

Fig II -21 : Circles of correlations F1-F2 and F2-F3 for 32 elements and 34 samples considered in the A.C.P. treatment.

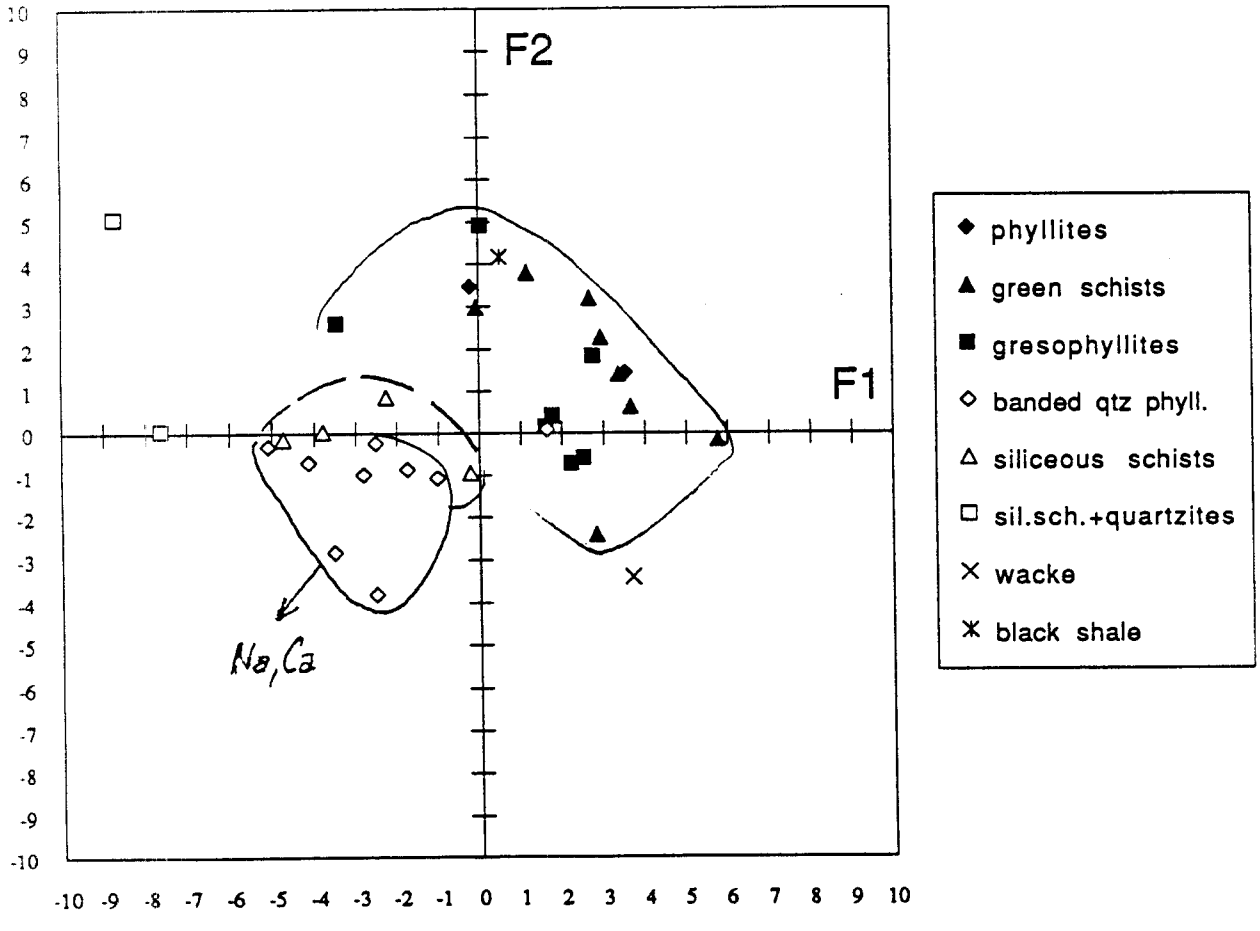

Fig II -22 : Samples plotted by facies in a F1-F2 diagram after the score factor data.

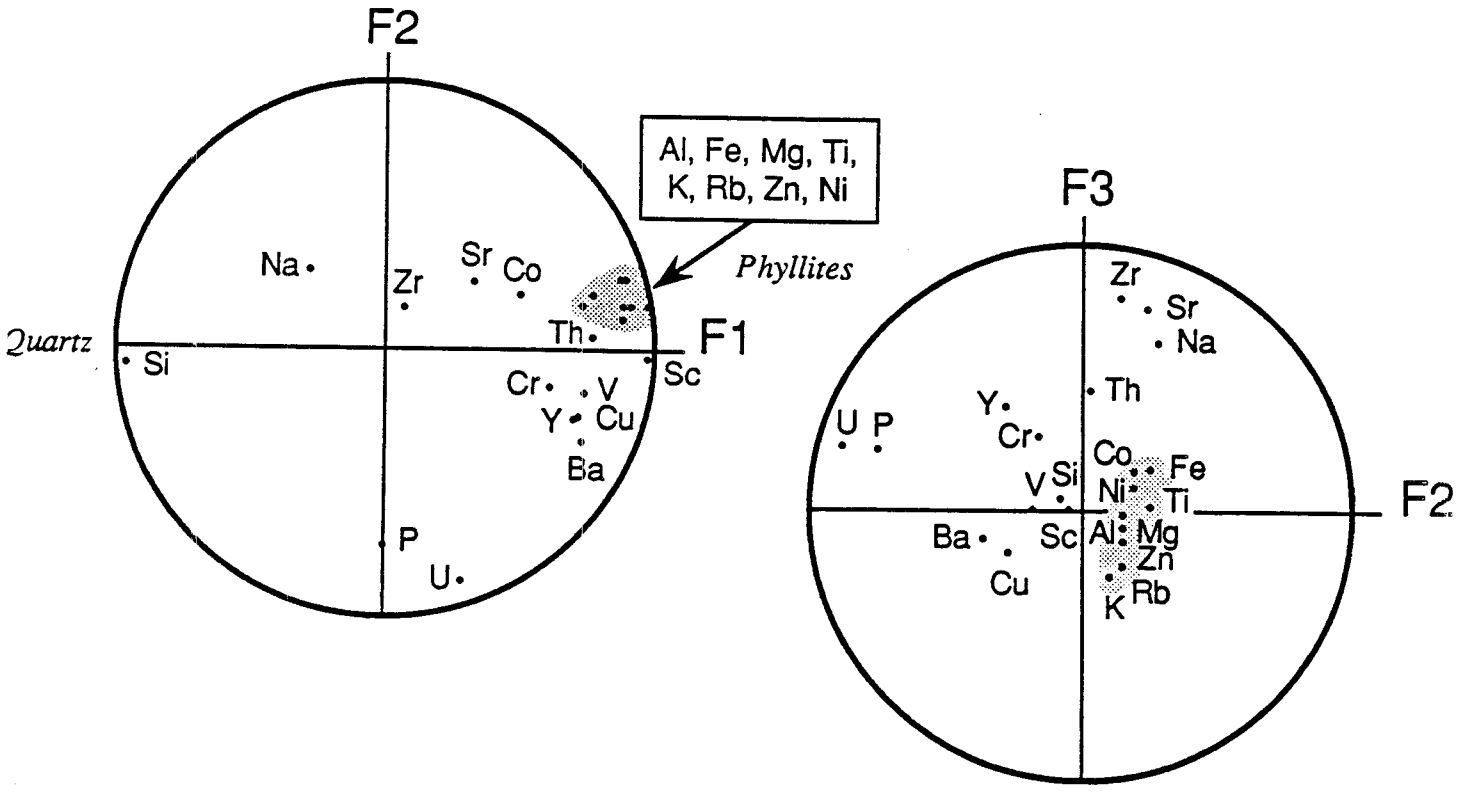

Fig II -23 : Circles of correlations F1-F2 and F2-F3 for 19 elements and 49 samples considered in the A.C.P. treatment.

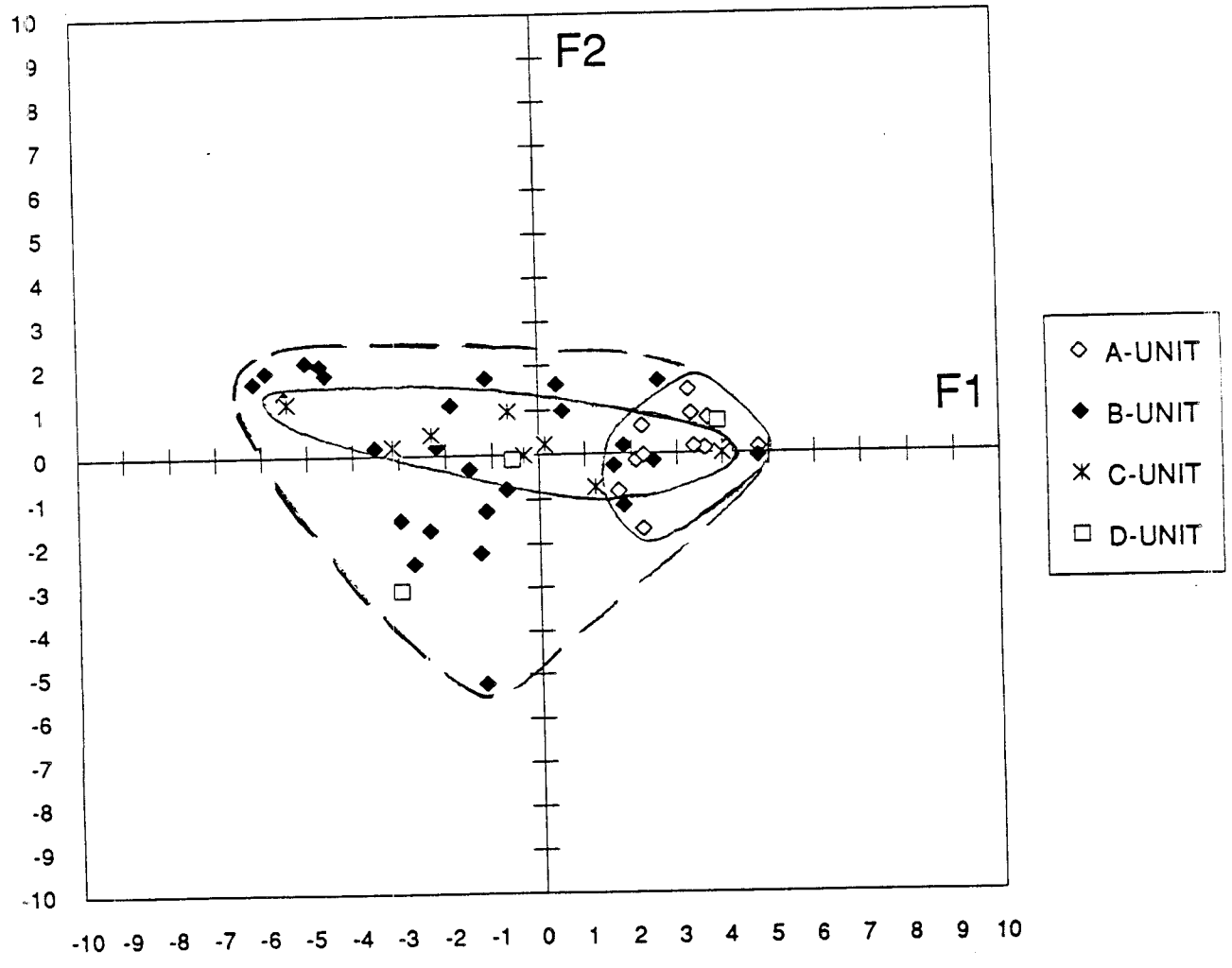

Fig II -24 : Samples plotted by units in a F1-F2 diagram after the score factor data.

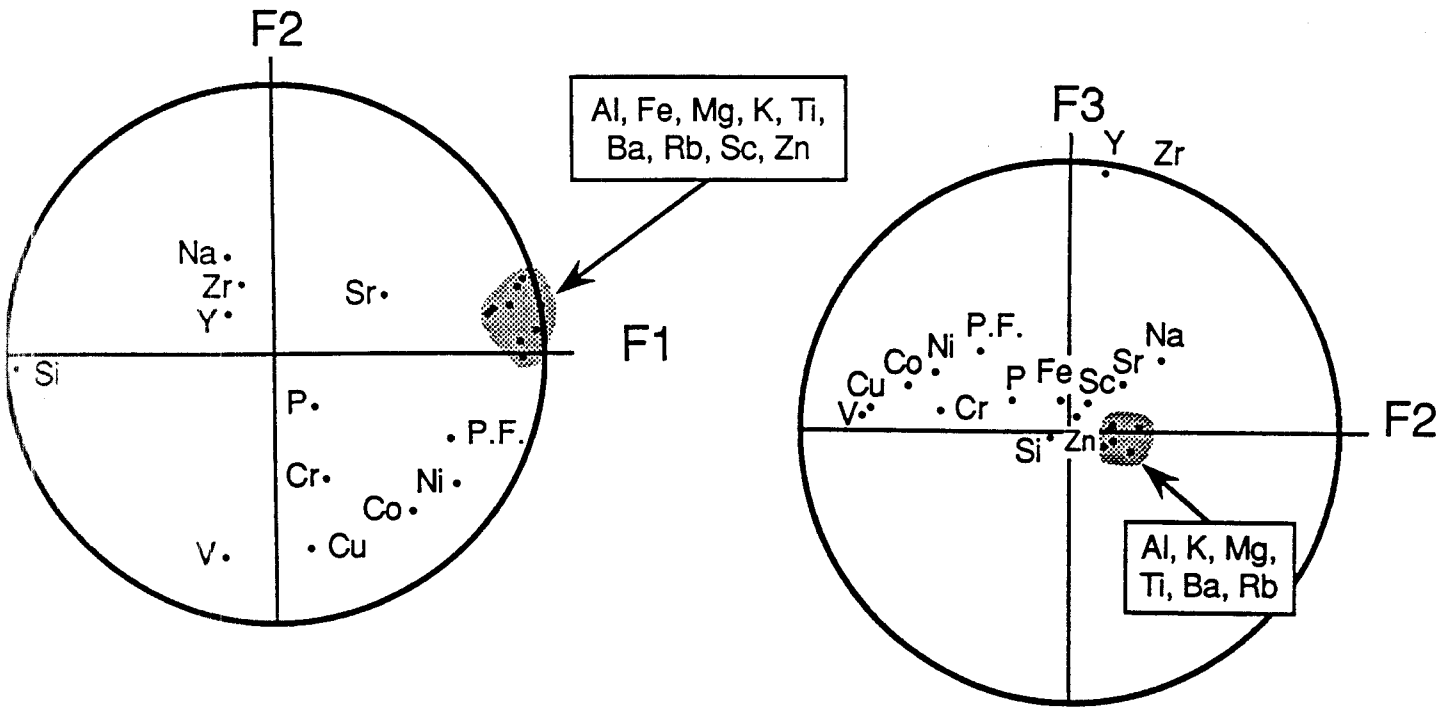

Fig II -25 : F1-F2 and F2-F3 correlation circles for 21 elements and 67 samples in ACP treatment.

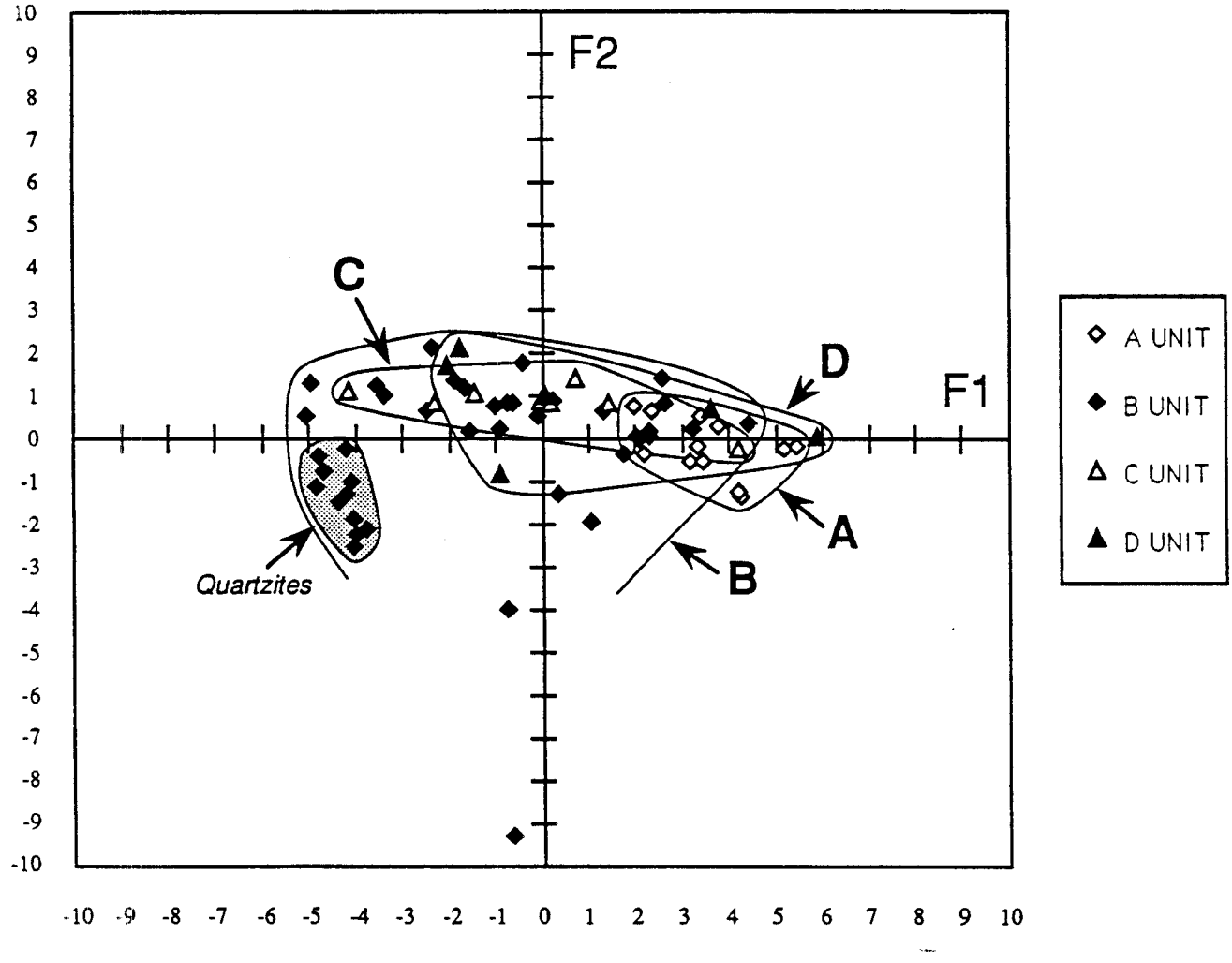

Fig II -26 : F1-F2 diagram, after the score factor data, where all the samples are plotted by units

The F1-F2 binary diagram drawing with the score factors data still shows a good discrimination between argillaceous facies and silicic facies (table II-8 annex and Fig. II-22).

- All samples sorted by units and a selection of elements

Elements selected for this third treatment are : Si, Al, Fe, Mg, Na, K, Ti, P, Ba, Co, Cr, Cu, Ni, Rb, Sc, Sr, V, Y, Zn, Zr, U, and Th. Results are very similar to the preceding ones (tables II-9 annex and II-10 annex ; Fig. II-23) with a distribution of the different elements between the argillaceous and siliciceous poles. But the distribution by units permits in the F1-F2 diagram drawn with the score factors data to visualize the distribution of the different facies in each unit (table II-11and Fig. II-24) :

- the B-unit always appears to be the most heterogeneous. The large spreading of the data covers most other units ;
- contrarily, the A-unit is well grouped and the dispersion of the samples is nearly only controlled by the F1 factor (clay/quartz proportion) ;
- the C-unit is much more heterogeneous with a large dispersion of the clay/quartz proportion (F1 factor) ;
- in the D-unit, the three samples are largely dispersed mainly along the F1 axis.

All samples sorted by units and a selection of elements

An other treatment (Fig. II-25, and tables II-11 and 12, annex) with all samples and a selection of elements expressed by units allows to compare the four units in the F1-F2 diagram, after the score factors (Fig. II-26 and table II-13, annexe). There is always the well grouped A-unit which is represented by phyllitic samples. The B-unit is very dispersed (black shales). However, the B-unit shows few samples better grouped, representing a quartzite pole. The C-unit is controled by the F1 factor with a large dispersion according this axis corresponding to the occurence of quartzites and detritic facies on the left of the diagram and more argillaceous facies at the right. Samples of the D-unit are distributed between the A and C-units expressing volcanic and phyllitic contributions.

Conclusions from ACP analysis : the statistical analysis confirms the characteristics of each lithologic unit defined from the field work and the major element data and allow to define the main correlations between the elements, the most significant of them being examined in the next paragraph.

d- *Binary diagrams*

The aleatory sampling and the low number of analysed samples advise some caution in data interpretation.

- K/Ba and K/Rb geochemistry (Fig. II-27 a, b) : these two elements are mainly bound to K-micas and feldspar. The two main group of lithologies are also clearly discriminated in these diagrams :

- the argillaceaous one compared favorably to undepleted Proterozoic cratonic shales average with a K/Rb ratio of 200 (corresponding to that of micas) and a K/Ba ratio of 40 ;
- the quartz-rich one compared favorably to undepleted Paleozoic cratonic greywackes average with a K/Rb ratio of 200, but presents higher K/Ba ratios (≥40) ;
- two graphite-rich quarzites present abnormaly high K/Rb (≥400) ratios suggesting Rb depletion and all graphite rich samples present normal K/Ba (close to 20) ratio compared to Paleozoic cratonic greywackes average.

- Cu/Be geochemistry : In the circles and matrix of correlations from § 3.3.2, Cu and Be are positively correlated (r=0.79). This good correlation (if the graphite-rich samples are discarted) can be observed in a Cu/Be diagram (Fig.II-28), the Cu and Be richer samples of the correlation corresponding to the clay-rich sediments.

However, in this diagram, several samples are richer in Be and so depart from the linear correlation. These deviations, noted by arrows on the drawing, may to samples close to

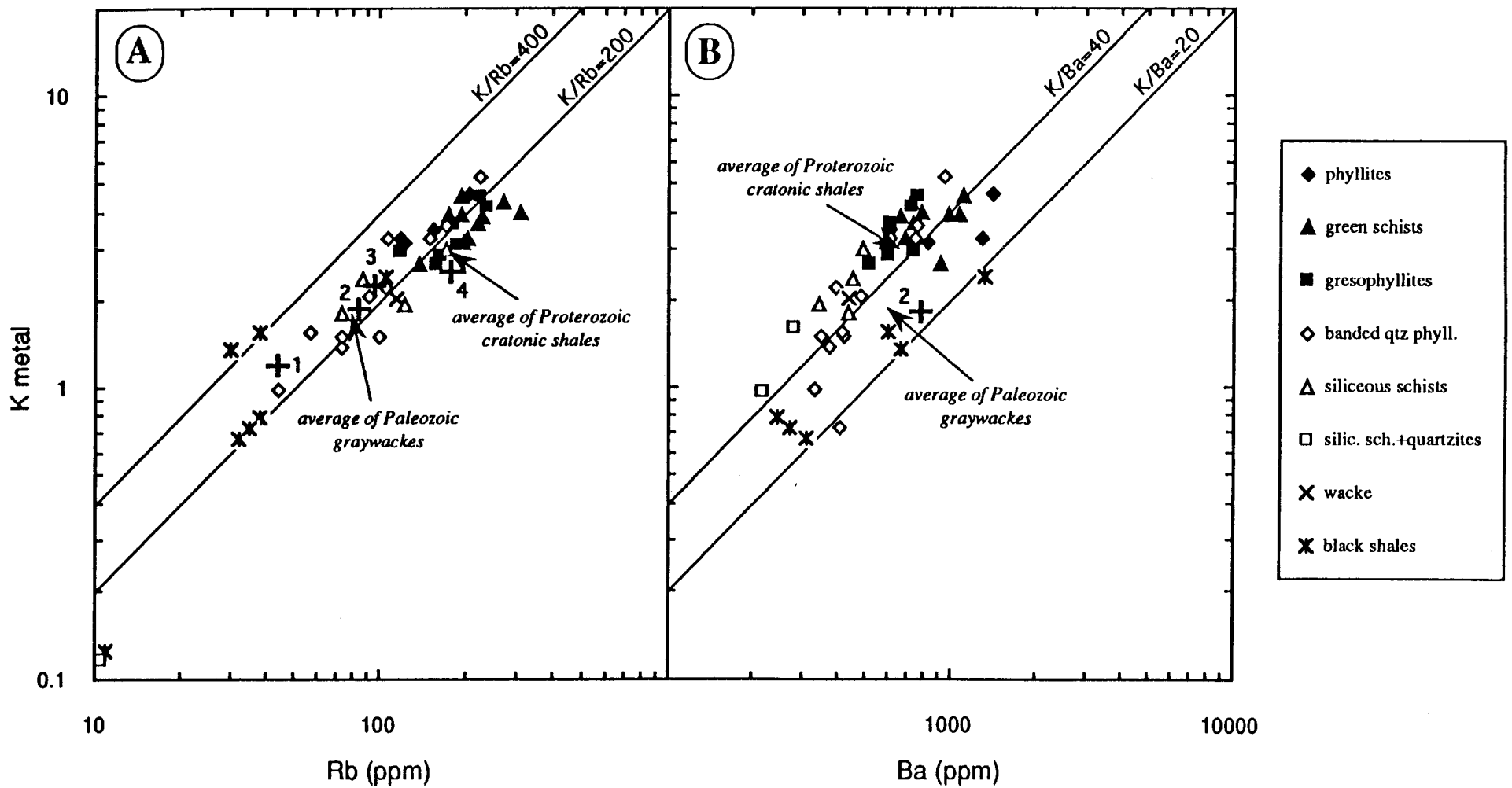

Fig II -27: K - Rb (A) and K - Ba (B) plots for the Pouca de Aguiar samples. Cross symbols represent averages of : [1] sands and sandstones (Heier and Billings, 1970), [2] metagraywackes (Senior and Leake, 1978), [3] continental crust (Taylor, 1964) and [4] shales (Heier and Billings, 1970). Arrows point to averages of Proterozoic and Paleozoic shales and graywackes (Condie, 1993).

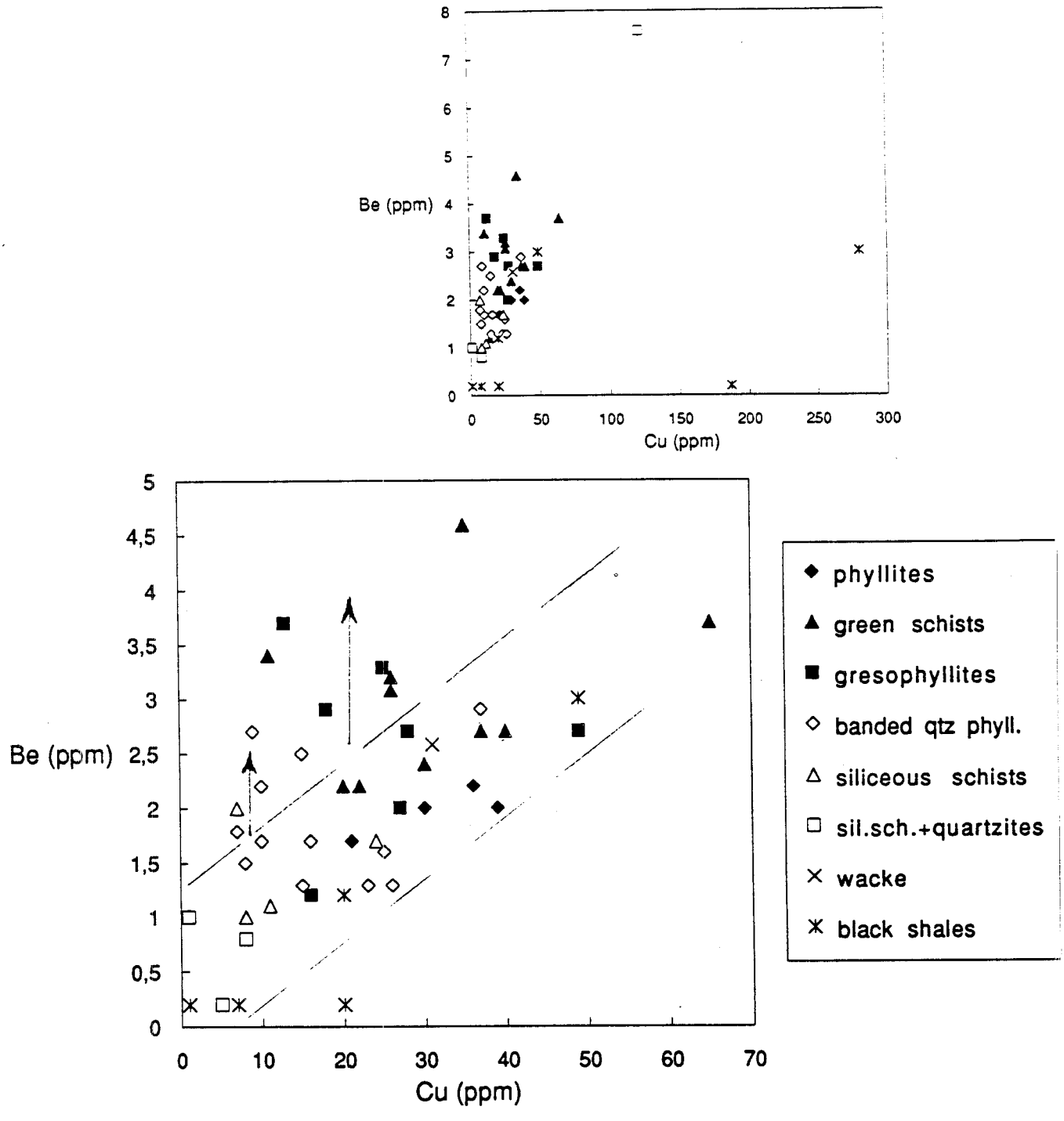

Fig II -28 : Cu/Be diagram for Vila Pouca de Aguiar sampling.

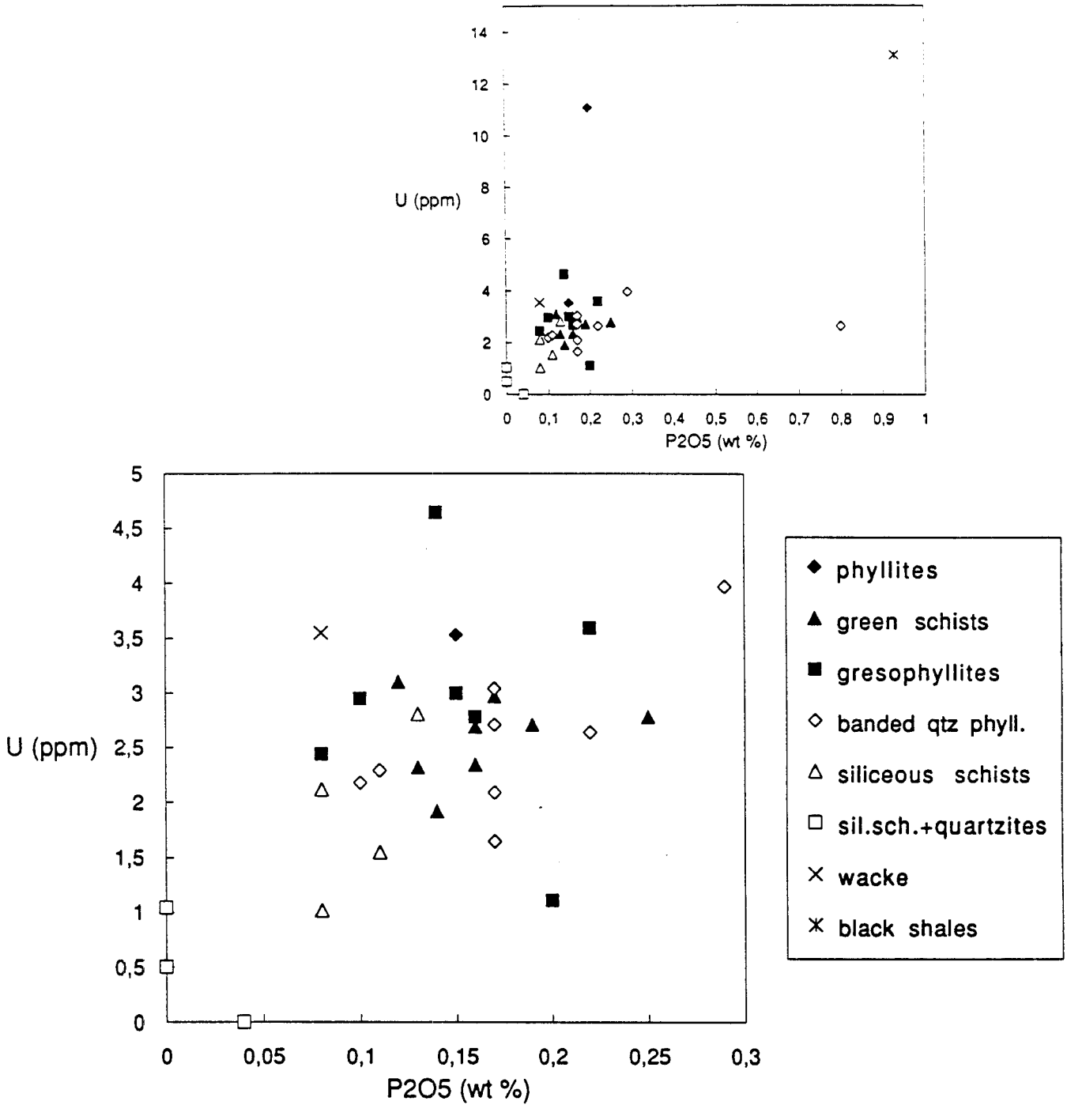

Fig II -29 : P/U diagram for Vila Pouca de Aguiar sampling.

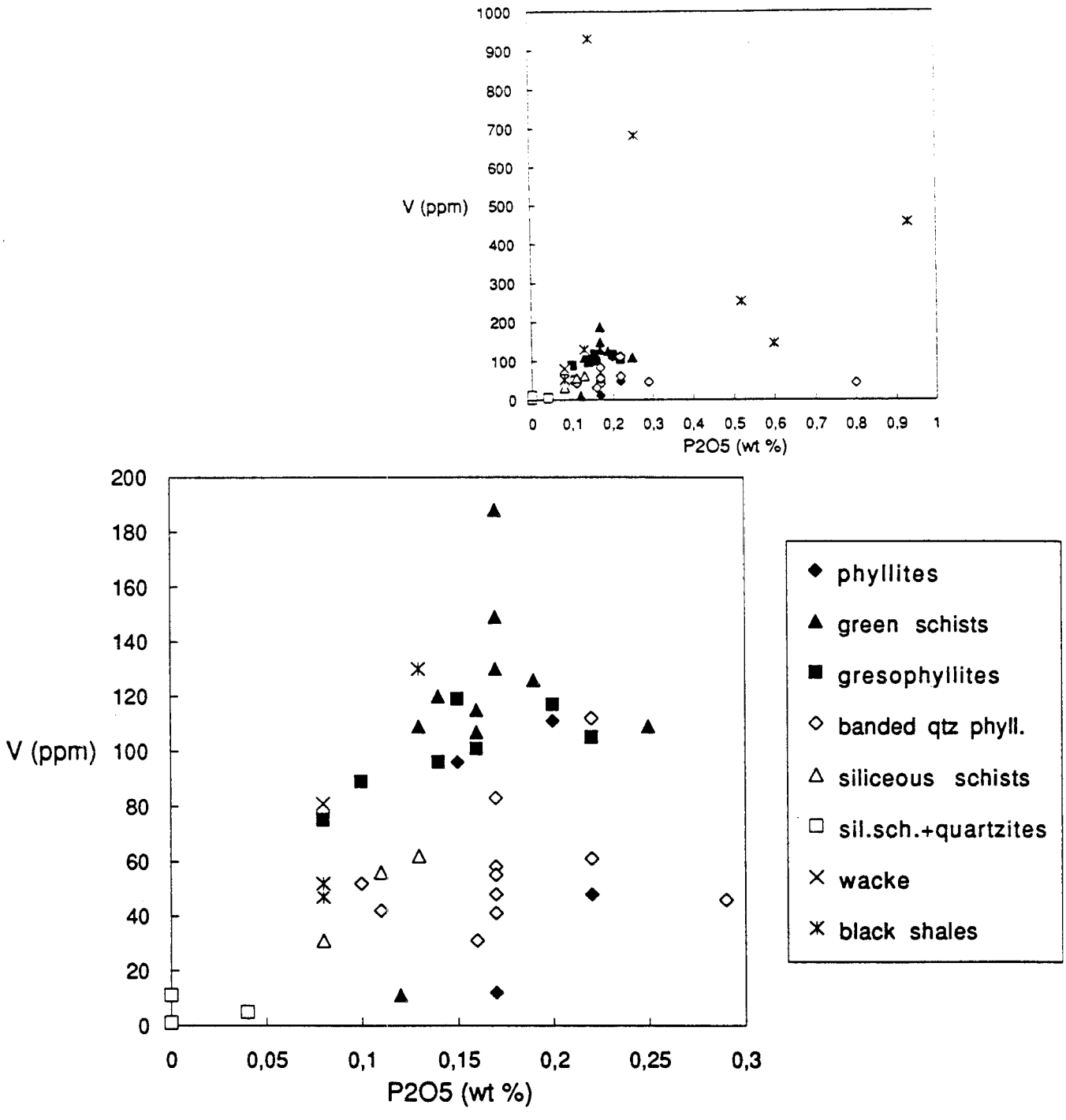

Fig II -30 : P/V diagram for Vila Pouca de Aguiar sampling.

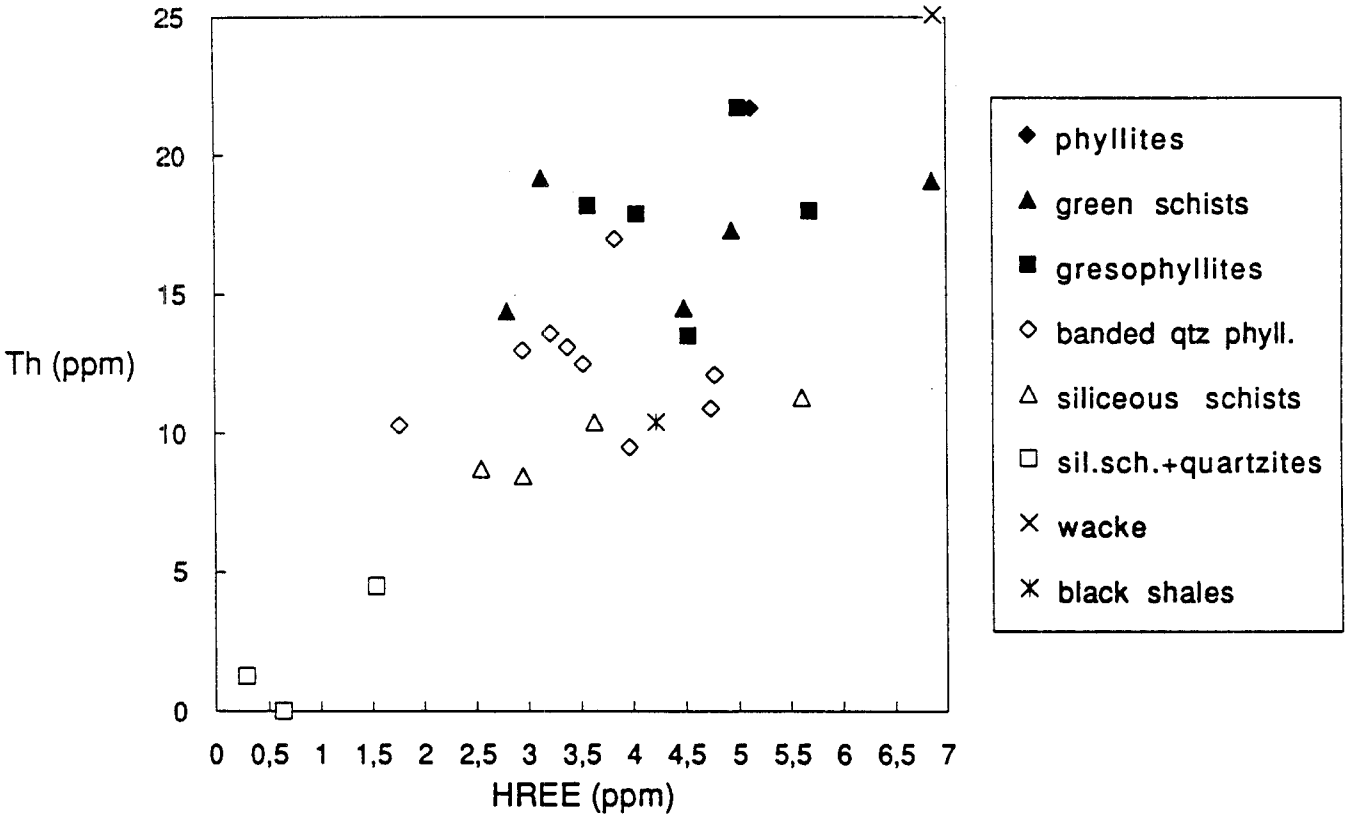

Fig II -31 : HREE/Th diagram for Vila Pouca de Aguiar sampling.

granitic intrusions leading to a Be enrichment of enclosing rocks during diffusion of the magmatic fluid after melt oversaturation.

- *U/P geochemistry* (Fig.II-29) *:* if two uranium anomalously rich samples and one P-rich quartz phyllite are discarted a slight positive correlation do exist between uranium and phosphorus. Such a correlation is a common association for syn-sedimentary uranium.

- *V/P geochemistry* (Fig.II-30)*:* the clay-rich lithologies appears logically to be the richest in vanadium and present the best correlation between V and P.

- *HREE/Th geochemistry* (Fig.II-31)*:* The clay-rich sediments appears to be distincly richer in Th suggesting its transport mainly adsorbed on clay minerals surfaces. HREE appear to be relatively well correlated with thorium in the quartz-rich metasediments.

f - Discussion and conclusions

The geochemical study of whole rock from Vila Pouca de Aguiar made possible the distinction of two main groups among all defined facies types :

- siliceous series, including siliceous schists, silicified schists, quartzites and wackes ;
- argillaceous series, including phyllites, green schists, gresophyllites and black shales.

Normalized to average Paleozoic metasedimentary rocks and continental crust, the different lithologic formations show limited variations excepted for Sr which shows a systematic negative anomaly, and REE, Hf, P enrichments linked to the presence of accessory minerals in the quartz phyllites. There is a great homogeneity of pelites (Curros unit), contrary to black shales which display geochemical variability due to distinct detrital contributions. The volcanic contribution in Vale de Égua and S^{ta} Maria de Émeres units with a bimodal character is represented by acid volcanites (between the calc-alkaline and alkaline domains) and calc-silicate rocks.

Considering the Au geochemistry, all units reveal some Au values higher than the normal value for upper continental crust . Because all lithologies have examples of anomalous values, there is no apparent preconcentrations in specific units. However, the important volcanic contribution may suggest an eventual role of volcanism in the gold source of the VPA area.

2 – MONTEMOR AREA

A suite of 12 samples was analysed (whole rock, 52 elements) to have a preliminary geochemical characterization of the ore bodies and the host metasediments, as well as to evaluate the potential of some chemical elements for use as pathfinders for Au–mineralization. The host–rocks of mineralization (mostly biotite schists with variable degrees of hydrothermal alteration) are represented by:

a) Migmatites (Mig – analysis 12); b) Biotite schists devoid of disseminated sulphides (with variable sericitazation and chloritization, S–I, analyses 8–9–10, and S–II, analysis 11);c) sericitized biotite schists with disseminated arsenopyrite (D–II; analyses 6 and 7);d) chloritized biotite schists with disseminated arsenopyrite (D–I; analysis 5);

The selected ore samples comprise: e) main mineralized bodies (veins mainly composed of quartz, arsenopyrite, pyrite, and gold, with minor amounts of chalcopyrite, loellingite, marcassite and bismuth, grading laterally to silicified biotite schists – M–I; samples 1 and 2); f) minor mineralized veins (late, cross–cutting veins exhibiting breccia textures, mainly composed of quartz and pyrite – M–II; samples 3 and 4).

All the samples are from the Chaminés area; samples 1 and 12 are from outcrops, while the remaining samples were collected in drill–cores. After petrographic charaterization, the samples were mechanically crushed and subsequently splitted. Chemical analyses were performed at the Activation Laboratories, Ltd. (Ancaster, Ontario–Canada), with a routine precision better than 1 percent (relative) for most of the major elements, and better than 5 percent for most of the minor elements. The analytical methods employed, as well as the corresponding detection limit for each analysed element, are given in Table II- 15, (annexe). Geochemical data for the analysed samples are reported in Table II-16, (annexe), following the above mentioned classification.and the preliminary interpretation are the followings :

a) Migmatites : The composition of the analysed migmatite (sample 12), is consistent with the data presented by Mehnert (1986) for diatexites evolved from a biotite–plagioclase gneiss. Chemically, such a parent–rock should chemically resemble closely the biotite schists, which probably constitute the parent–rock of the migmatites in the Chaminés area. This sample does not display any anomalous metal contents, and its gold content is below the detection limit of the analytical method used (2 ppb).

b) Biotite schists devoid of dissiminated sulphides. The analysed schists belonging to the S–I group represent the less hydrothermally altered terms (weakly chloritized), and their compositions probably resemble those of the original schists (Table II- 16, annexe). Although low, the CO_2 values (0.06–0.19 wt%) and the Zn content (41–100 ppm) represent the highest ranges reported for all the analysed samples. Gold remains below 8 ppb.

In sample 11 (S–II) petrography indicates stronger hydrothermal alteration. However, it not possible to draw simple correlations with the samples above, probably because of original heterogeneities. It perhaps noteworthy that Au is slightly anomalous, at 24 ppb.

c) Sericitized biotite schists with disseminated arsenopyrite (D–II). The main hydrothermal alteration exhibited by the biotite schists of D–II type (sericitization) is illustrated both by the slight increase of the K2O abundances (ranging from 2.12 to 2.60 wt%), and by the relative decrease of the remaining alkaline and alkali–earth elements contents (CaO – 0.62–1.08 wt%; Na_2O – 2.82–3.70 wt%). Rubidium contents of these rocks are scattered in the range 86–92 ppm, and the comparison with the other analyzed bitotite schists, suggests that Rb follows closely the K_2O behavior. The Au content of these samples is still relatively low (24–38 ppb), but slightly higher than in b) above.

d) Chloritized biotite schists with dissimated arsenopyrite (D–I). The concentrations of the alkaline and alkaly–earth elements are compatible with the relatively low abundances of albite and sericite reported on the petrographic synthesis of this report. The contents of Ni (56

ppm), Co (43 ppm), and As (1400 ppm), as well as the Au content (71 ppb), however, are higher than those in S–I–type biotite schists, reflecting the presence of sulphides.

e) Main mineralized bodies. The mineralized samples of M–I type exhibit the higher Au values reported (6110–11700 ppb). Since rocks of M–I type grade to the host (more or less hydrothermally altered) schists, some gradual enrichment (or depletion) of chemical elements would be expected, following gold enrichment. Nevertheless, it should be noted that the available analyses may be insufficient to induce generalized chemical paths, and the following conclusions should be taken as preliminary clues. Thus, the bulk comparison between the mineralized samples M–I and the different types of biotite schists show that:

1 – the Fe_2O_3 content has a non–linear positive correlation with Au content; for non–mineralized samples the Fe_2O_3 values are relatively constant (3.08–6.40 wt%) while in the mineralized samples the values are clearly higher (7.48–23.12 wt%). This is obviously related to the iron allocated to arsenopyrite and pyrite which accompanied gold deposition;

2 – the S content increases (as expected) with the proximity mineralization; from 0.1–1% in the weakly chloritized biotite schists to 5–10% in the mineralized samples;

3 – the Sb abundances (<0.1–1.2 ppm in barren samples to 6.2–37 ppm in M–I samples) are positively correlated with the Au content;

4 – the arsenic and copper contents (scattered in the ranges 20–1300 ppm and 10–15 ppm and 43000–54000 ppm and 78–229 ppm for barren schists and M–I samples, respectively) are covariant with gold abundances.

5 – the distribution of the zinc content (9–20 ppm), although laking a linear correlation, seems to decrease with the increase of gold content.

6 – the abundances of Ni (50–107 ppm) and Co (44–91 ppm) have good positive linear correlations with gold content.

f) Minor mineralized veins (Late). Mineralized samples of M–II type are, to a first approximation, similar to M–I. However, some significant differences can be seen between the two mineralization types. M–II samples depict lower values of Sb (<0.1 ppm), As (1250–2400 ppm), Pb (<5–5 ppm), SiO_2 (42.20–48.00 wt%), and Bi (<5–6 ppm). On the contrary, the TiO_2 (1.42–1.9 wt%), Fe_2O_3 (16.38– 23.12 wt%), MgO (4.26–4.92 wt%), CO_2 (0.13– 2.20 wt%), Co (66–150 ppm), Zn (66–74 ppm), and Sc (27–37 ppm) contents in M–II samples are significantly higher than those of M–I. Th is strongly depleted in M–II samples (0.7–0.9 ppm). The gold content in M–II samples is also lower (246–3500 ppb) than that of the M–I samples.

C- WEATHERING PROCESS AND AU ENRICHMENTS : THE EXAMPLE OF FAULT ROCKS ASSOCIATED WITH THE VILARIÇA STRUCTURE AND REACTIVATED D3 SHEAR ZONES

1 - PURPOSE AND LOCATION OF THE STUDIED FAULT ROCKS

Relative abundances of some metals in fault gouges, as well as detailed examination of some geochemical relations, were carried out in order to evaluate which chemical elements may be suitable pathfinders for Au–Ag halos associated to the above mentioned tectonic accidents. The metallogenetic implications of some geochemical distributions related to Au–Ag mobilization/reprecipitation along the reconstructed weathering profile of the Vilariça fault system will be also discuss.

2 - MACROSCOPIC FEATURES, PETROGRAPHY AND X-RAY DIFFRACTROMETRY OF THE EXAMINED FAULT ROCKS

The fault rocks sampled include mainly quartz breccias and fault gouges. The exact location of the examined samples is illustrated in figure II-32.

The former lithologies underline either the major tectonic branches of the Vilariça strike–slip fault (particularly in the França/Portelo sector) or the reactivated D3 shear zones (ESE França/Rabal area). In general, quartz breccias are related to highly fractured domains of the tectonic structures, where multiple overprinting of different quartz–vein arrays can occur. The main vein family included in the characteristic siliceous fillings of the Vilariça fault comprises subvertical structures, ranging usually from N15W to N25W, which show variable millimetric thickness and, locally, irregular geometry; their development clearly postdates the establishment of late–fracture networks where the main brittle system, N–S – N5E, is subvertical and shows left–lateral movement. Similar quartz veins are associated with NW–SE D3 shear zones; these structures, commonly ranging from N25W to N35W, cut earlier N55–60E veinlets and, locally, are affected either by N15W,60E – N10W,75E right–lateral anisotropies, or by N60–70E reactivated fractures (subparallel to S1).

In França/Portelo sector, the outcrops of the major fault breccias IA (samples nº 1 to 4) located along the different branches of the Vilariça system are usually above 750 m of altitude. As already mentioned, the matrices of these rocks comprise mainly quartz, iron (and sometimes manganese) oxides and hydroxides, variable amounts of hydro–phyllosilicates, and sparse relics of pyrite - arsenopyrite. This mineralogical association is quite different from the one that characterize similar fault rocks along the same tectonic structures, outcropping in the França Mine area, between 700 and 745 m of altitude. Between 745 and 730 m of altitude, the fault plane contains breccias rich in iron oxides and abundant relics of primary sulphides and carbonates (type IB breccias – samples nº 5 to 8). At the 700 m level the equivalent breccias are extremely rich in sulphides and carbonates, without iron oxides (type IC – samples nº 9 to 10). These key sites are presently inaccessible; sampling was possible during the evaluation of the ancient mine performed by PROMINAS SARL in 1987/88. Since the development of oxides in these rocks is clearly the result of the destruction of primary minerals, it is obvious that the former fault rocks represent an altered product of the latter lithologies. Furthermore, our data show that fault breccias IA (preserved at higher topographic levels) can be interpreted as the final product of the intense chemical weathering in the near surface environment, and that the horizontal chemical gradients along the fault zone are negligible. The establishment of this probable weathering profile that is based on the spatial distribution and geochemical analyses of the 10 samples of type I (outcropping between França and Portelo, fig II-33) is also consistent with the mineralogical variation and geochemical signature of the fault gouges that fill some fault segments South of França (NNW–NW of Rabal village).

Fault gouges and/or friable late–quartz breccias are present along some fault domains of the Vilariça structure, particularly in those where compact quartz fillings are missing. These fault rocks (type II), represented by samples n° 11 to 19, comprise always abundant fragments of variable dimension of the surrounding metamorphic rocks and exhibit local enrichments in

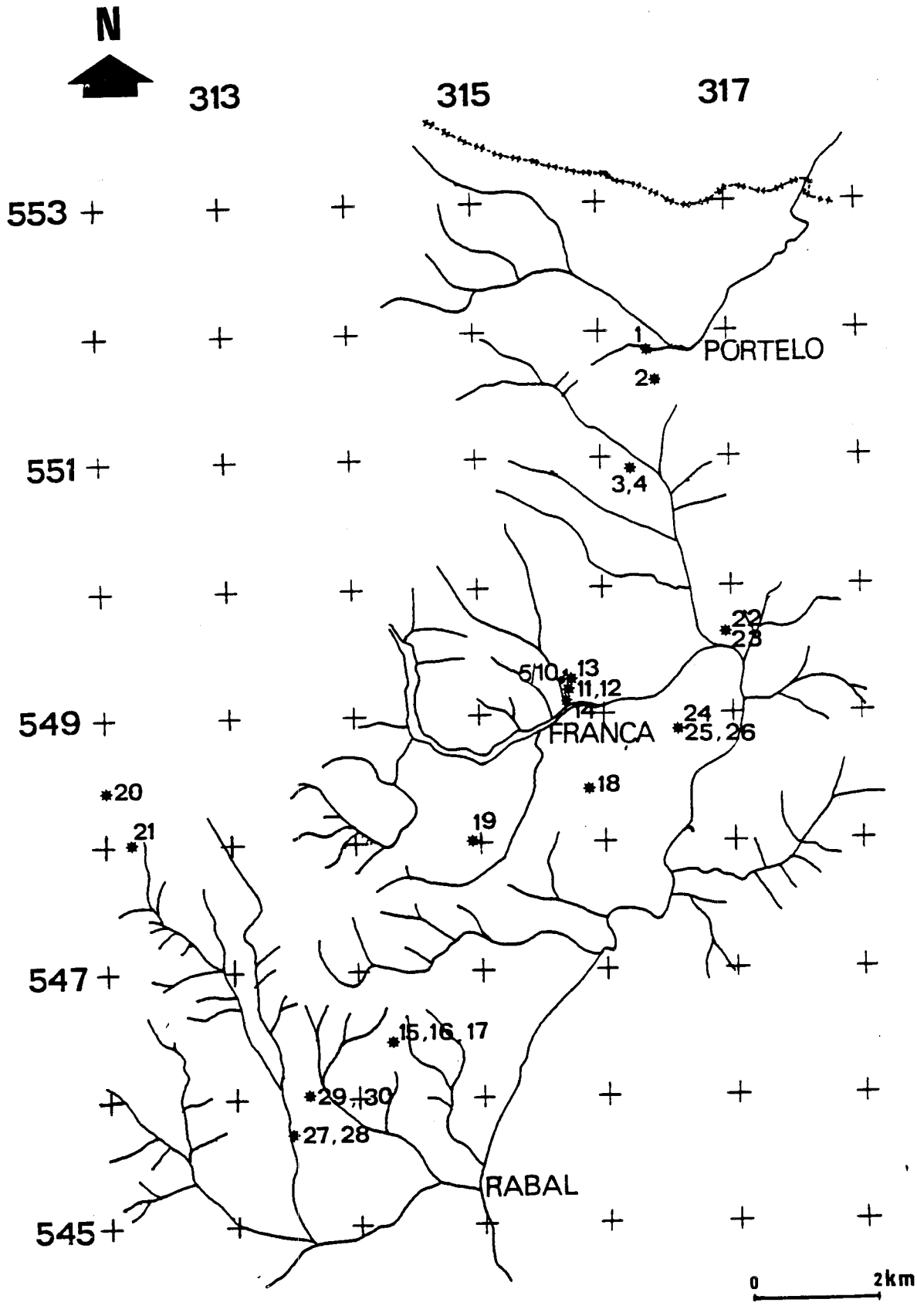

Fig II-32 : Location of the examined fault rock samples in the three sectors of França area.

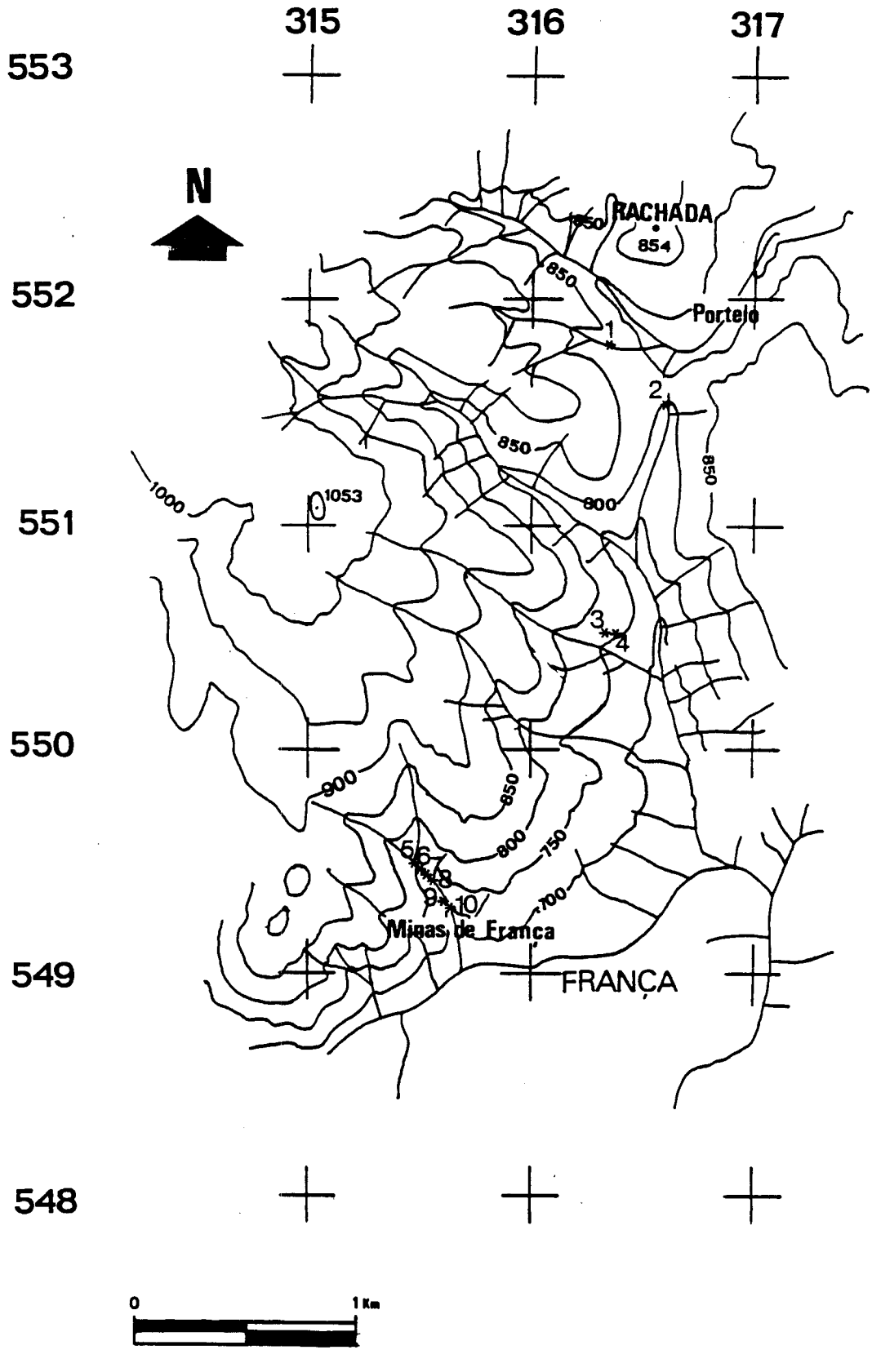

Fig II-33 : Location of the mineralized quartz breccias of the Vilariça fault in the França - Portelo.

iron and manganese oxides/hydroxides. The cement of the late breccias typically consists of quartz, hydrous–phyllosilicates, and minor amounts of pyrite, goethite, pyrolusite, and hydrated arsenates.

Quartz breccias associated to the reactivated D3 NW–SE and NNE–SSW – NE–SW shear zones (type III, sample n° 20, and type IV, samples n° 23 and 25 to 29, respectively) are, in general, infill breccias since resorption and recrystallization of hydrothermal quartz fragments are missing and the major matrix component (> 60%) is a late siliceous phase more or less iron enriched. Matrices of these fault rocks are thus mainly composed of quartz, hydrous–phyllosilicates, variable amounts of iron oxides/hydroxides (locally with manganese oxides), and sparse pyrite crystals, besides the frequent incorporation of fragments of metamorphic nature (which can be the prevailing clastic element of some breccias, like the one represented by sample n° 21). Highly brecciated domains, where thick fault gouges occur (samples n° 22, 24 and 30), are usually related with late brittle deformation events.

3– GEOCHEMICAL DATA

A suite of forty–six samples of quartz breccias and fault gouges were analysed at the Activation Laboratories, Ltd. (Ancaster, Ontario– Canada), with a routine precision better than 1 percent (relative) for most of the major elements, and better than 5 percent for most of the minor elements. The analytical methods employed, as well as the corresponding detection limit for each analysed element, are given in Table II-15 (annexe). Geochemical data for 30 samples of different fault rocks from the França sector are reported in Tables II-17 to 21, (annexe), following the above mentioned classification.

As expected, the entire suite of quartz breccias and fault gouges is typically rich in SiO2 and/or Fe2O3 with a strong inverse correlation SiO2–Fe2O3. This geochemical trend is usually accompanied by notorious LOI values, which are quite variable for fault rocks of type I and II (ranging from near 1 to 14% and 1 to 10%, respectively), and display a characteristic range of 4–7 % and 1–4% for breccia types III and IV.

The analysed rocks are almost devoid of Na2O (excluding some of the fault rocks type IV), and show consistently low values of MgO, CaO and K2O. The distributions of Al2O3, alkali and earth–alkali metals, Fe2O3, and LOI values suggest that, at least for some quartz breccias, the LOI content does not reflect solely the presence of iron hydroxides and/or hydrous–phyllosilicates. As a matter of fact, Al2O3 seems to be independent of LOI values, and for breccia types IB and IC one can put in evidence the coexistence of extremely low contents of alumina with anomalously high (>10%) LOI values.

Relatively high P2O5 concentration in fault rocks type II, III and IV could be related to host–metamorphic rock fragments incorporated into these rocks.

One of the most striking features of the trace–element distribution in fault rocks type IA, II and IV is the anomalously high values of Rb, Cs, Sr and Ba, which can be easily correlated with clay forming at the expense of primary phyllosilicates. Clay minerals (especially vermiculite, as reported by Duddy, 1980) may also accommodate significant amounts of LREE, as suggested by the relative LREE enrichment with the gradual increase of the hydrous mineral content in series of samples of tectonic–modified or altered (weathered) rocks. This interpretation is also consistent with the progression of the calculated Ce/Y, La/Yb and La/Lu ratios with decreasing weathering, (fig. II-34) (Table II-20, annexe).

The high field–strength elements analysed (Y, Nb, Th, U, Zr, Ta and Hf) display relatively irregular distributions in the entire suite of quartz breccias and fault gouges examined.

Another point of interest is the distribution of some first transition series metals (like Sc, V, Cr, Co and Ni) which are anomalously abundant in some fault gouges and related late–breccias of type II, III and IV. In general, the V and Co content of these rocks are covariant

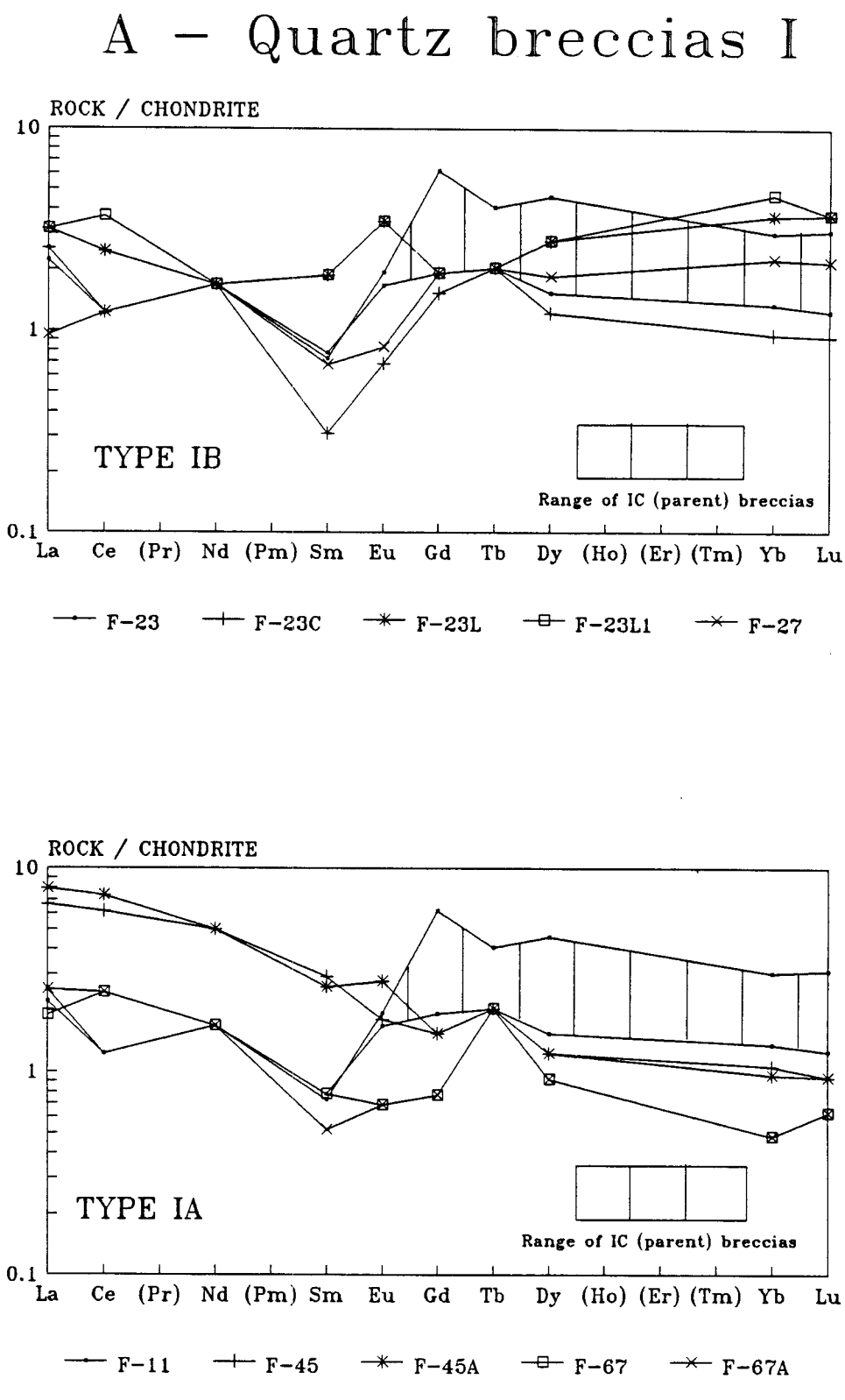

Fig II-34 : REE patterns for the fault rocks associated to the Variça structures (A and B) and reactivated D3 shear zones (C and D) in França sector. REE concentrations are plotted normalized to the Leedey L/6 chondrite (in ppm), on a logathmic scale versus REE atomic number. Elements not determined are in parentheses. Solid lines are linear extrapolations.

B – Fault gouges and associated late-breccias type II

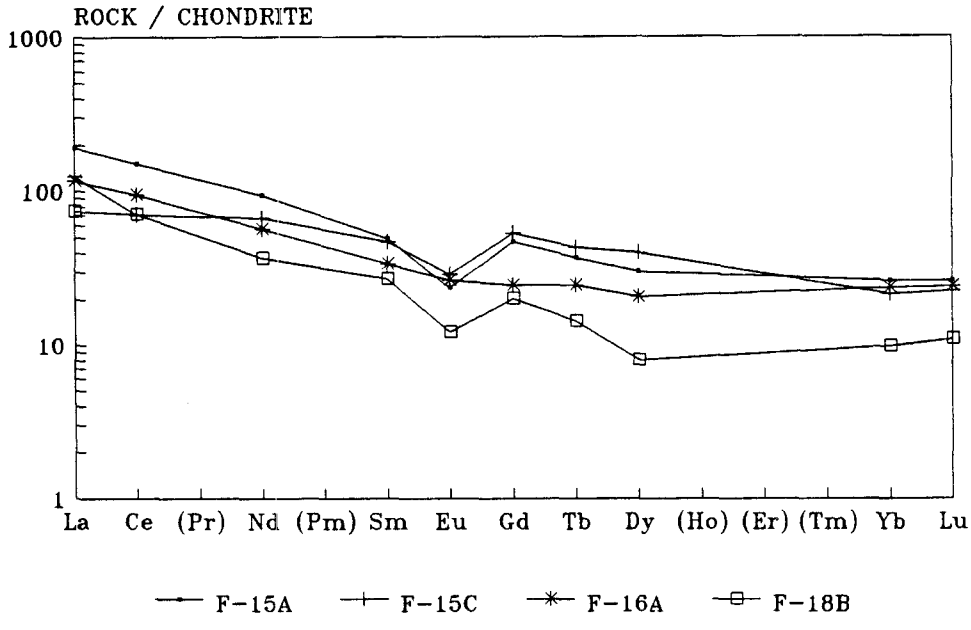

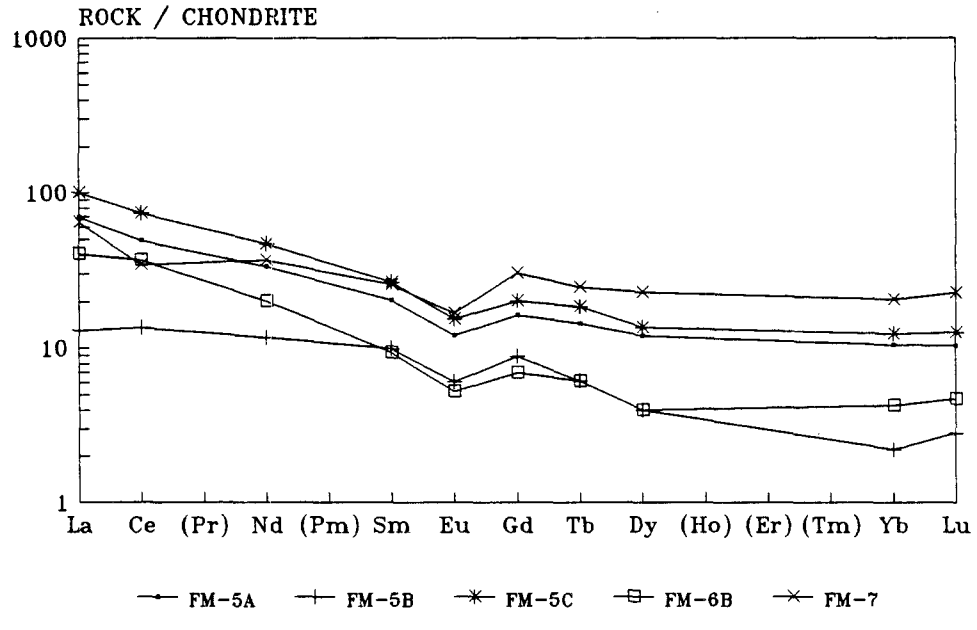

C – Late-breccias of type III related with the reactivation of the NW-SE regional shears

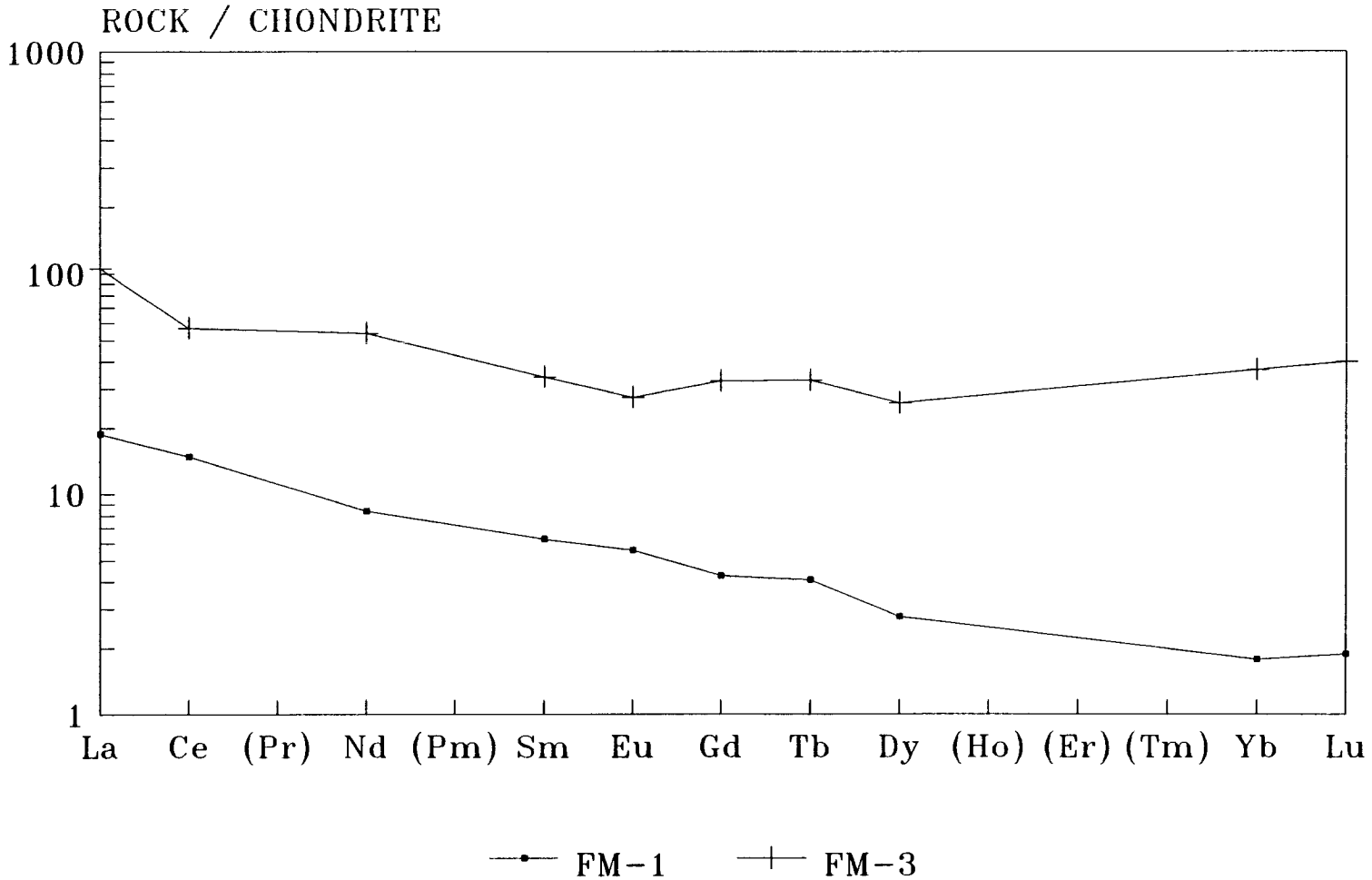

D – Fault rocks related with the reactivation of the NNE–SSW – NE–SW regional shears

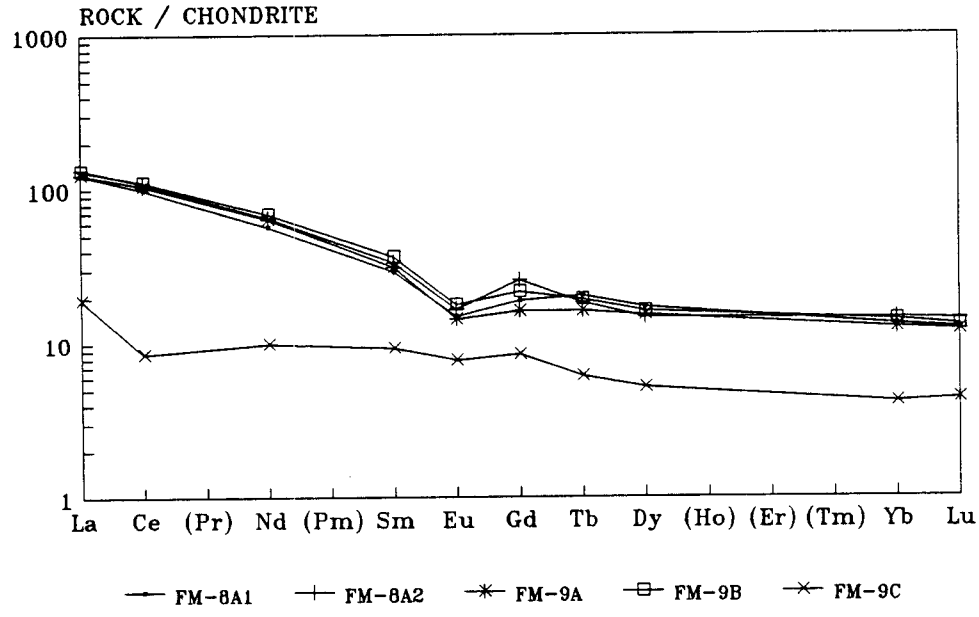

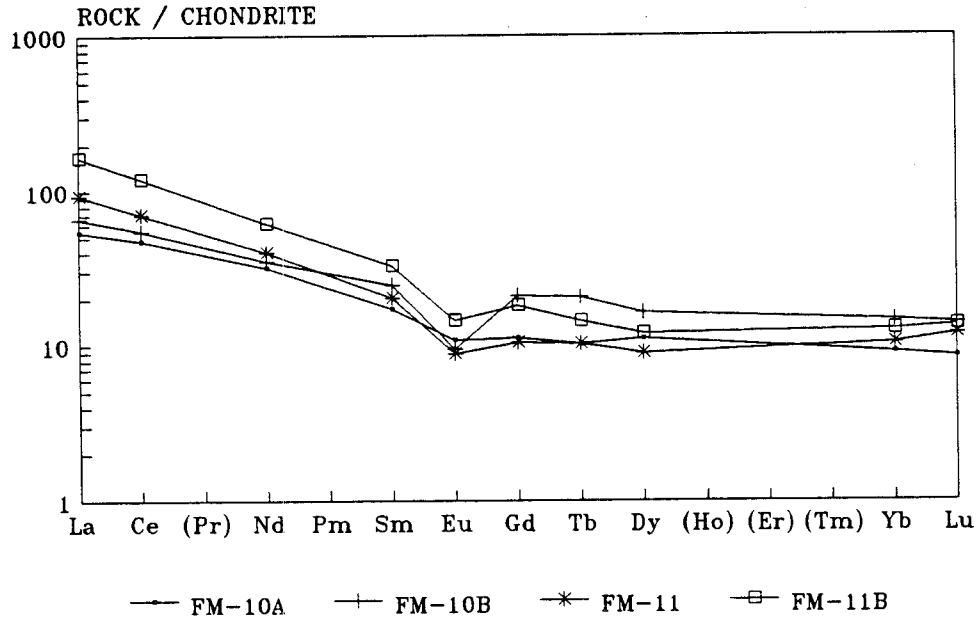

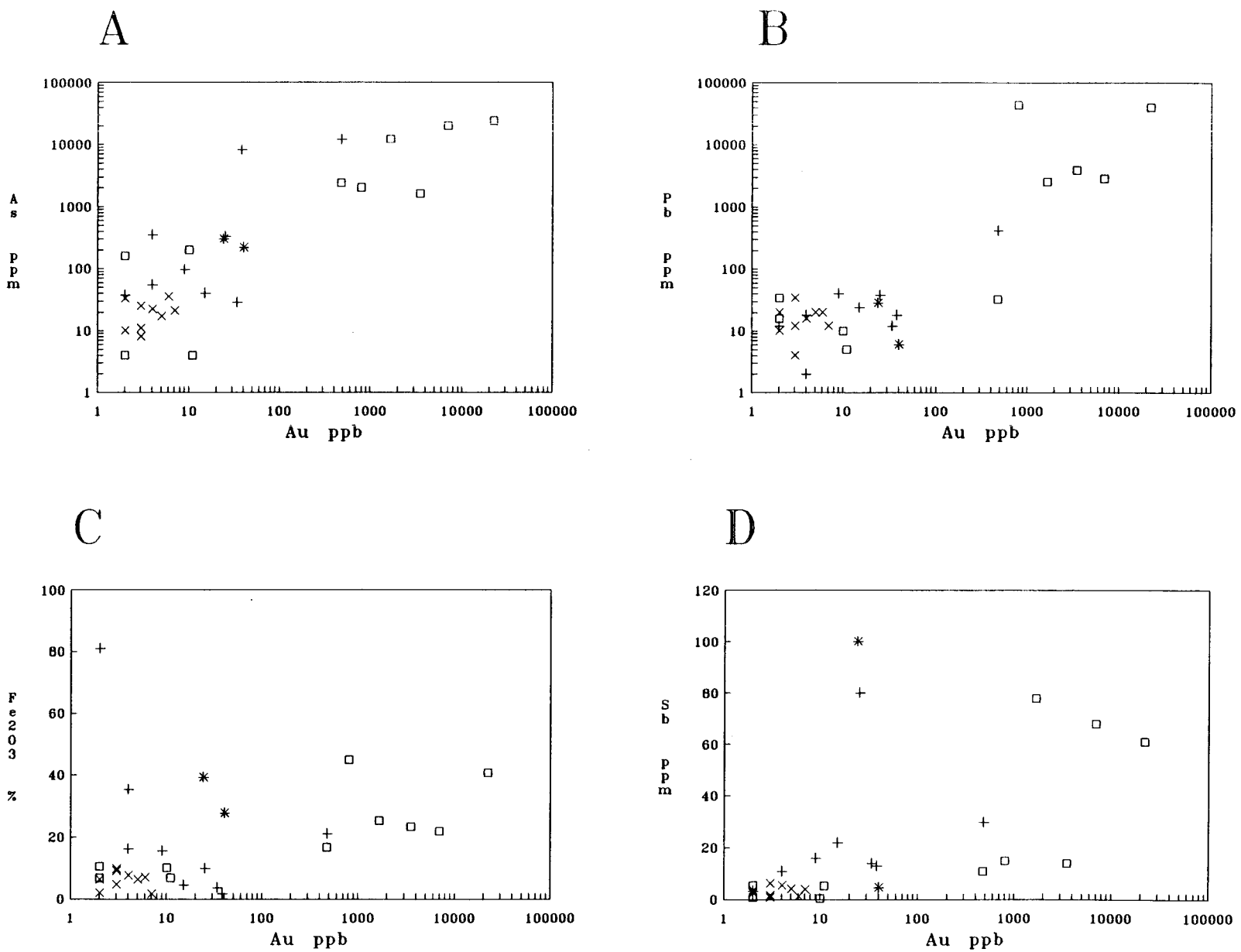

Fig II-35 : Au-As (A), Au-Pb (B), Au-Fe2O3 (C) and Au-Sb diagrams for the fault rocks associated to the Variça structure and reactivated D3 shear zones : Symbols as in figure II-34.

with Sc, Al and, to a lesser extent, with Zr values, suggesting that their concentrations can be interpreted as a result of incorporation of host–metamorphic lithologies into fault rocks.

The distribution of Mn is quite variable and apparently does not exhibit any particular correlation with the remaining metals; high Mn concentrations (> 100 ppm) are however characteristic of fault rocks IV, quartz breccias IB and IC, as well as of some samples of fault gouges II. With similar distributions, Cu and Zn concentrations are especially notorious in representative samples of fault rocks associated with the Vilariça structure. On the other hand, Pb high values can be found in quartz breccias IB and IC only. Nevertheless, for the entire suite of fault rocks, these metals are positively correlated with sulphur and arsenic.

Gold and silver contents of the fault rocks analysed are quite variable. Ag contents are often below the detection limit of the analytical method used (0.1 ppm) in representative samples of fault rocks IV, and exhibit anomalous values, although lower than 15 ppm, in breccias of type III. However, in quartz breccias IB and IC, Ag values are commonly greater than 50 ppm. Fault gouges II carry usually low Ag content (< 3 ppm). Gold values are only anomalous in quartz breccias IB and IC, ranging from 0.475 to 22 ppm; for the remaining fault rocks, the Au content is, in general, between 0.002 and 0.010 ppm. The distribution of this precious metal shows high positive affinity with As and Pb, and coarser covariant relationships with Fe and Sb (fig. II-35), which is consistent with the mineralogical nature of these rocks.

5 – METALLOGENETIC IMPLICATIONS OF THE GEOCHEMISTRY OF THE VILARIÇA FAULT BRECCIAS

a - Chemical profiles

A very important characteristic of the geochemical processes involved in weathering is provided by elemental solution and leaching or redeposition, phenomena that depend on many factors, but mainly on the nature and properties either of the aqueous solutions or the primary minerals, besides the bulk rock permeability which controls fluid/rock interaction. All these features may be evaluated by establishing the elemental chemical profiles which are its extant expression.

The geochemical profiles of the analysed elements (abundances versus altitudes) almost always show striking discontinuous variations between 730 and 750 m of altitude, corresponding in general to the fault zone horizon where breccias IB are preserved.

The pattern followed by the chemical profiles of Fe, Pb, Au, and Ga (fig. II-36) illustrate clearly both the strong and efficient leach experienced by these elements in the upper levels of the weathering profile, and the development of a pronounced positive peak circumscribed to the intermediate horizon of the fault zone profile, suggesting that conditions for their solubilization and subsequent mobility were achieved. Although less obvious, similar paths can also be found for Zn, Cu, Mn, and Ag distributions. It should be noted however that the unexpected relatively high contents of Zn and Cu in the upper levels of the weathering profile (where protolith concentrations are approached) can be interpreted as a result of their fixation in autigenic minerals, which is compatible with the gradual increase of Th and U concentrations towards the higher levels of the fault zone (Fig. II-37), suggesting enrichment from external sources, perhaps meteoric waters.

Other prominent characteristic of the geochemical profiles obtained is illustrated by the behavior of elements, such as Sb, S, As (and CO_2), which have been removed at all levels, although less so at the 730–750 m horizon (Fig. II-38). Therefore, one may conclude that they behave as perfectly mobile elements during development of the weathering profile over primary mineralized fault breccias IC.

The remaining analysed elements show more variable behavior, and the complex patterns of variation with respect to protolith concentrations are, in general, of difficult interpretation. Nevertheless, for Rb, Sr, Na, and probably K, the pattern followed by the

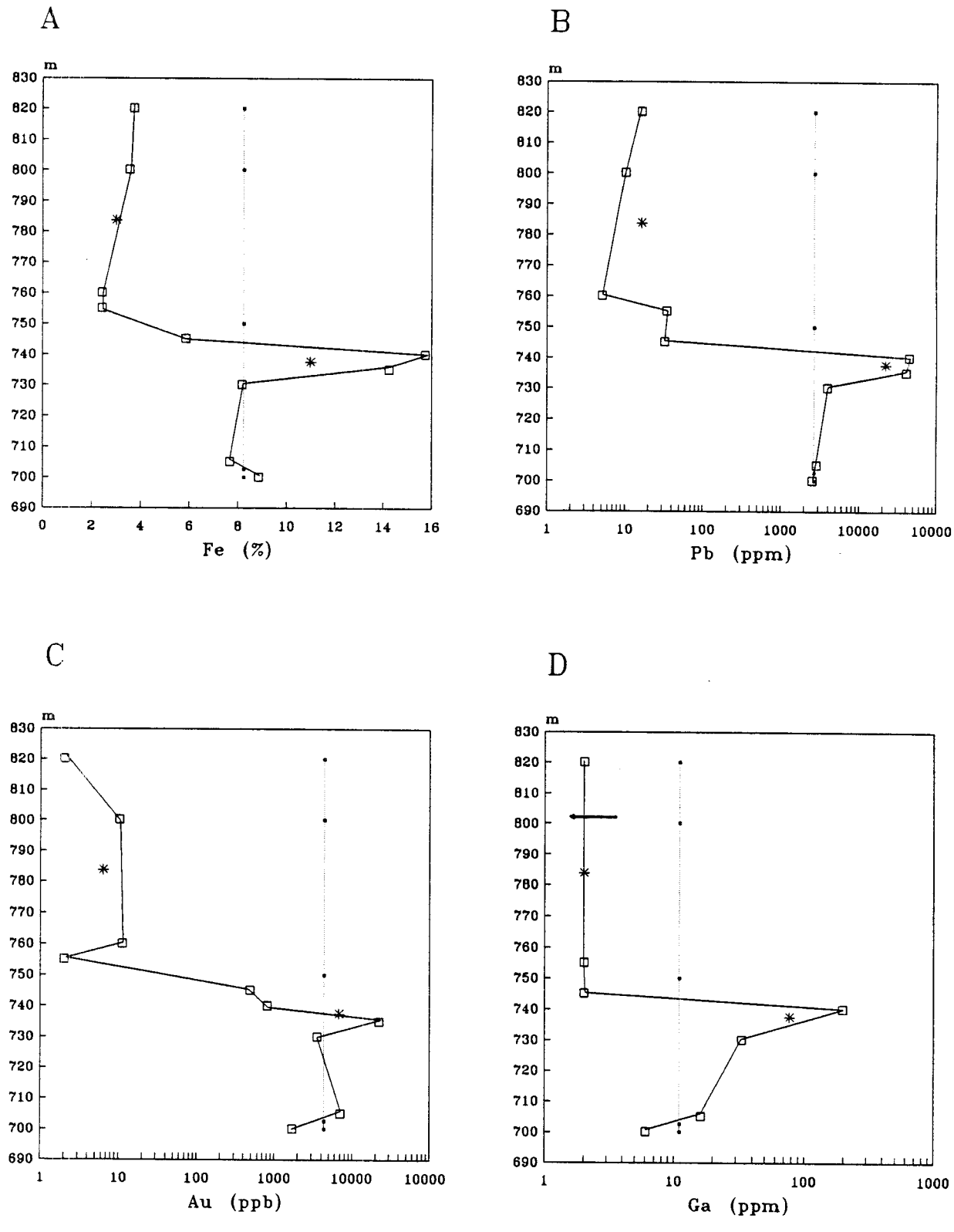

Fig II-36 : Chemical profiles of Fe, Pb, Au and Ga for Vilariça fault breccias in the França - Portelo sector. Dotted lines represent the average concentration of two protolith samples (IC : F-23, F-11), and the asterisks illustrate the average concentration of the remaining two breccias groups (IA : F-67, F-67A, F-45A and IB : F-27, F-23L, F-23L1, F-23).

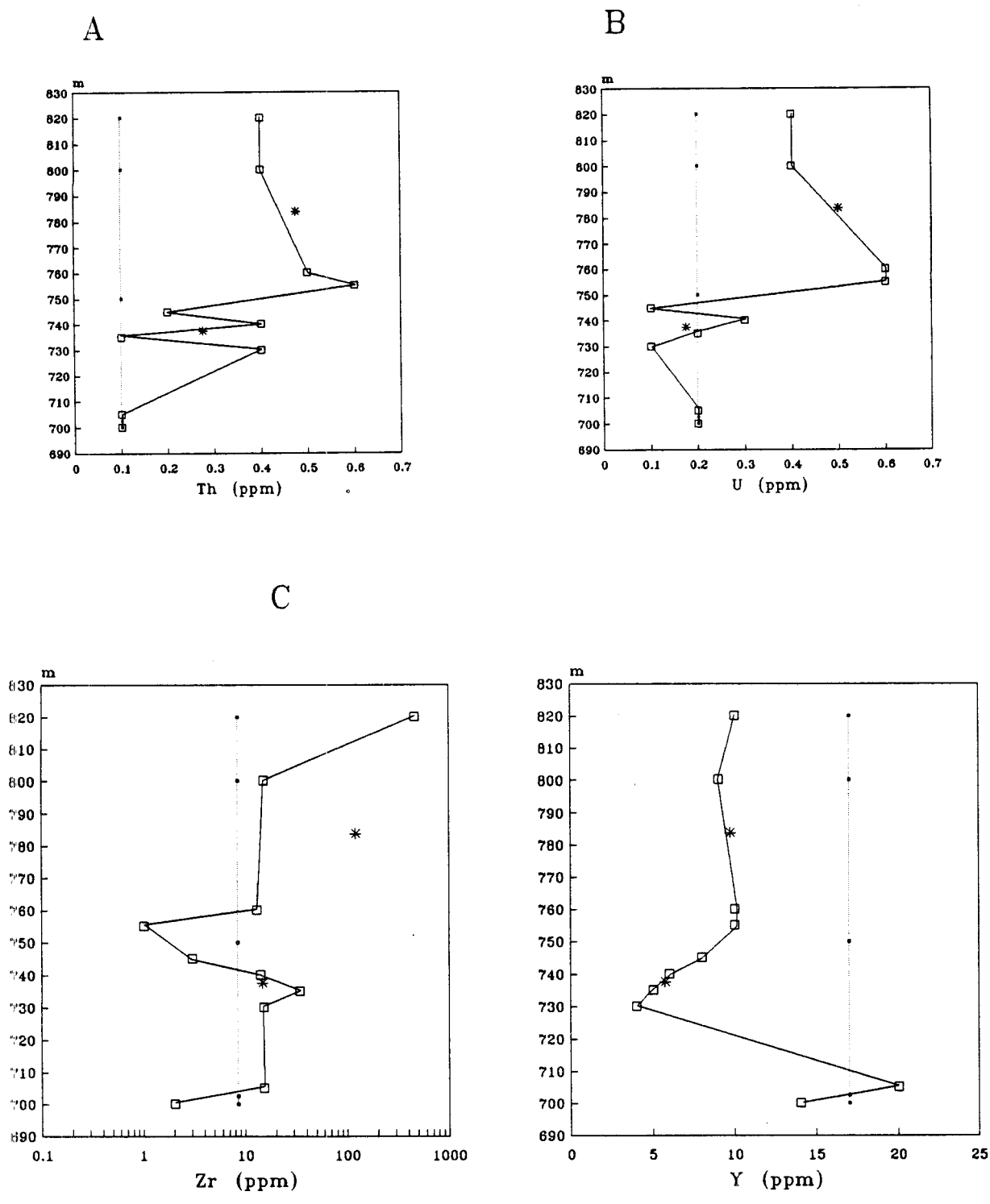

Fig II-37 : Chemical profiles of Th, U Y and Zr for Vilariça fault breccias in the França - Portelo sector. Dotted lines represent the average concentration of two protolith samples (IC : F-23, F-11), and the asterisks illustrate the average concentration of the remaining two breccias groups (IA : F-67, F-67A, F-45A and IB : F-27, F-23L, F-23L1, F-23).

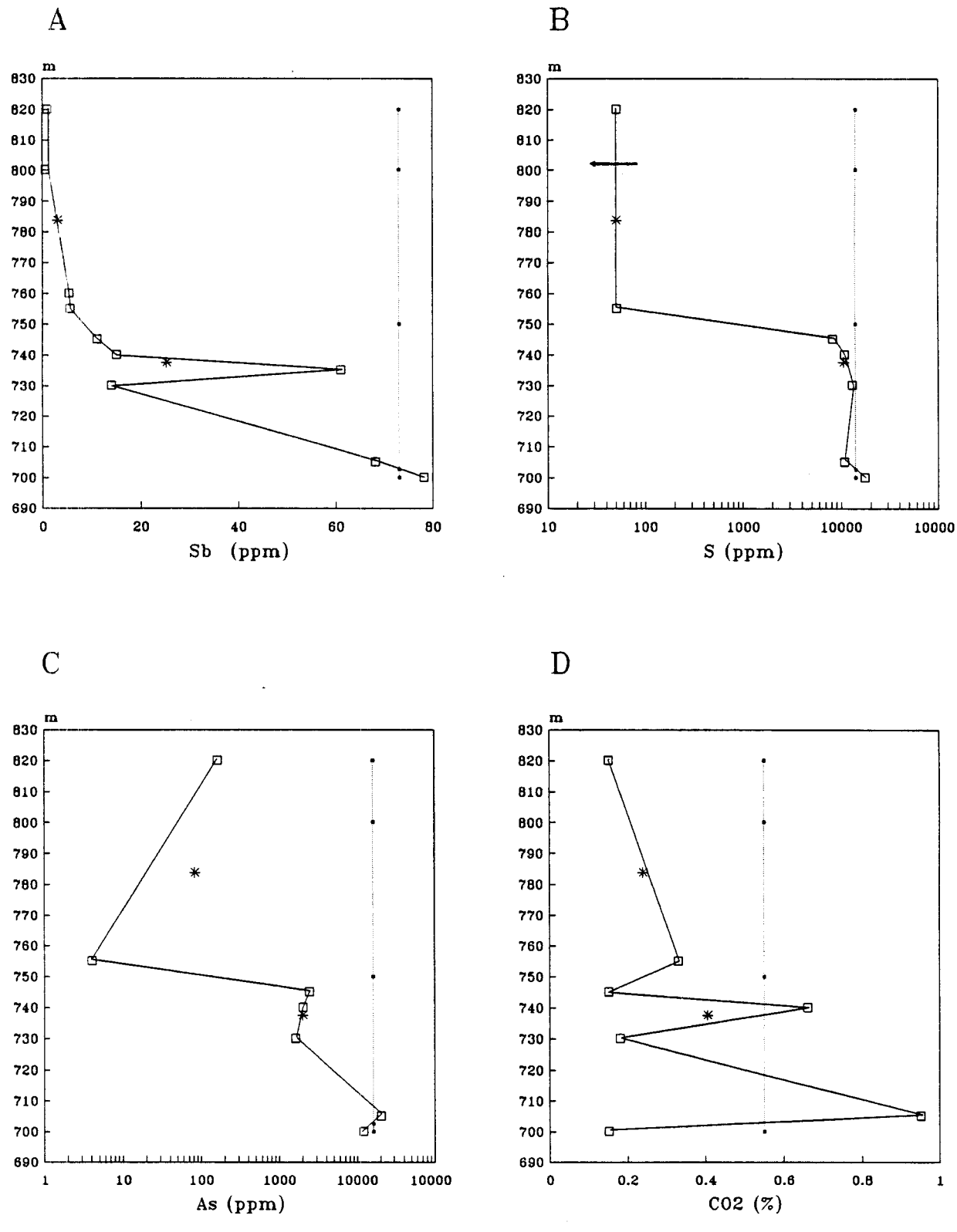

Fig II-38 : Chemical profiles of Sb, S, As and CO2 for Variça fault breccias in the França - Portelo sector. Dotted lines represent the average concentration of two protolith samples (IC : F-23, F-11), and the asterisks illustrate the average concentration of the remaining two breccias groups (IA : F-67, F-67A, F-45A and IB : F-27, F-23L, F-23L1, F-23).

chemical profiles suggests that these elements were leached from a narrow part of the weathered profile (today at 730–745 m of altitude) and differentially concentrated along the upper levels of the fault zone. Similar paths are characteristic of Mg, Ca and Ba, although with local deflections between 740– 760 m; note however that the average values for Ba show no systematic variation with respect to those obtained for protolith samples.

Very few elements (with the possible exception of Zr, and perhaps Y, Fig. II-37) seem to have been immobile in the course of the weathering profile development.

b – Supergene enrichment

According to the previous interpretation, some metals (like Fe, Cu, Pb, Zn, Au, Ag, and Ga), were locally moved from a depleted source zone (leached zone) to a complementary enriched horizon, where reprecipitation took place. In these circumstances, mass conservation constraints imposed by the two related and sequential chemical sub–systems (see, e.g. Brimhall et al., 1985; Brimhall & Crerar, 1987; Brimhall & Dietrich, 1987), enable some inferences about the chemical weathering and geomorphical evolution experienced by the Vilariça fault zone (Fig. II-39).

In order to solve the mass balance equations (Brimhall et. al., 1985), bulk density measurements were made for the fault rocks analysed. The results obtained are reported on Table II-3, and plotted as function of elevation (Z) in figure. II-40. This density profile shows that specimens of leached zone have densities well below sulphide breccias (protore), and fault breccias IB of the enriched level have intermediate values of density. Only the average density of the protolith, leached and enriched zones are considered in the calculation.

Supergene mass balance calculations

For the considered fault zone profile, the total leached zone thickness was estimated so that the amount of a supergene metal j in the enriched zone (TE,j °25 m) in excess of the average protore metal grade for that chemical profile (assuming no lateral fluxes) is balanced by its deficiency in the remaining leached zone. Amplitudes of T°L,j were calculated using the equation proposed by Brimhall et al. (1985) and Brimhall & Dietrich (1987), and constant average values for concentrations in j (Cj,l, Cj,e), and bulk densities (dl, de, and dp). An estimation of T°L,j(MAX) was also achieved, considering the highest deviation in Cj between leached and enrichment horizons, and constant average values for the variables Cj,p and dp. These leached– zone column heights when added to the present elevation of the top of the enrichment level (Z2 around 750 m), provides the basic requirements to Z1,j determination. In addition, leaching efficiency (EL,j) for each supergene element was evaluated as the percent of original metal j removed, expressing the chemical mobility of j. A summary of the results obtained is shown in Tables VIII and IX.

As pointed out by Brimhall et al. (1985), paleo–topographies calculated on the basis of T°L,j values lead, in general, to three possible situations: (1) the elevation of the original oxidation surface is consistent with other geological data, and, so, all the assumptions (closed and non– deformational system, and vertically homogeneous protore metal grade, in the present case) are acceptable; (2) the elevation Z1,j calculated is geologically unrealistic because during the establishment of the weathering profile there were lateral metal fluxes into or out of the fault zone; (3) Z1,j values are geologically impossible since the assumed protore metal grades are incorrect, and/or we must take into account the probable rapid lateral variation of elemental concentrations along the fault zone. In the present case, the altitude of the paleo–oxidation surface, estimated from the average T°L,Pb, T°L,Zn and T°L,Ga values, is compatible with the present elevation (around 900 m) of the remnants of a regional pediplain of Late–Pliocene age which is usually covered by alluvial fan sediments, locally known as "ran–as". Anomalously high Z1,j elevations are obtained when we take the maximum T°L,j values for some supergene metals, namely for Pb and Ga. Nevertheless, the estimated topographic difference from the average altitude of 900 m suggests that , at least, 40–100 m of

Vertical control volume in a non-deformational system for supergene enrichment

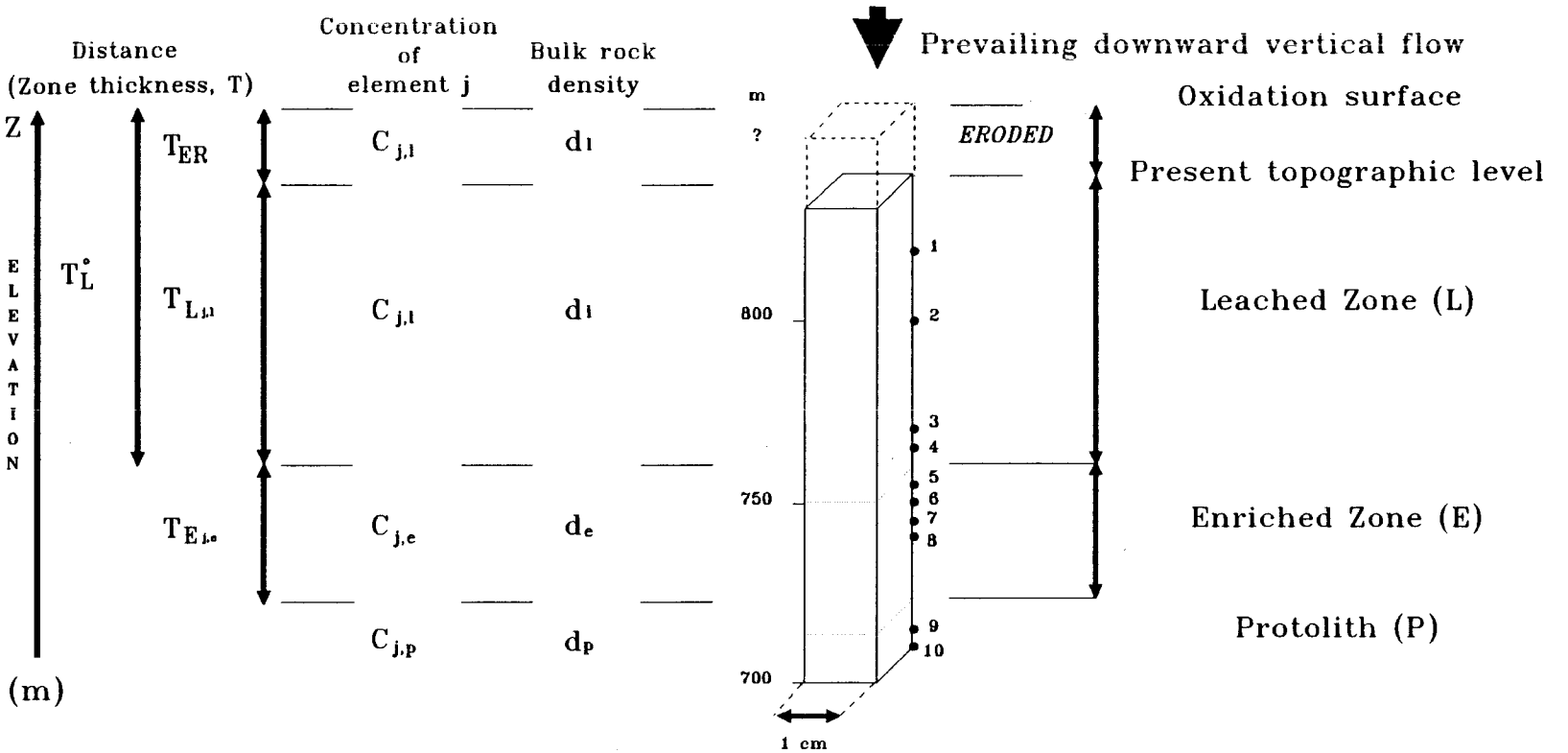

Probable weathering profile

Mass of j in protolith = Excess of j in enrichment horizon + Mass of j remaining in leached zone + lateral fluxes (assumed negligible)

$$V_{T_{j,p}}\ d_p\ C_{j,p} = [\ V_{E_{j,e}}(\ d_e\ C_{j,e} - d_p\ C_{j,p}\ )] + V_{L_{j,l}} d_l\ C_{j,l}$$

Fig II-39 : Schematic representation of mass balance equation for vertical supergene chemical transport and secondary enrichment of an element j in a non-deformational system. It is also stated the different variables that were used to describe the vertical control volume, including distances, concentrations and rock density terms. Samples of fault breccias I (from 1 to 10) are located along the constructed weathered profile. Adapted from Brimhall et al (1985), Brimhall and Crerar (1987) and Brimhall and Dietrich (1987).

erosion must have taken place, if the assumptions of vertically constant protore grade and no lateral fluxes are valid. Thus, if we accept an average age of pediplanation development of 2.5–2 Ma (Cabral, 1985), the erosion rates estimated range from 0.016–0.04 mm to 0.02–0.05 mm per year, respectively, which demonstrates the geological consistency of the Z1,j elevations calculated.

Calculated Z1,j average and maximum elevations for the remaing supergene metals (Au, Ag and Fe) are clearly below 900 m of altitude, suggesting that at least one or both of the two major assumptions of our modelation are not valid for these elements. In order to evaluate which of the basic assumptions is more likely to be incorrect, it was taken into account the possible influences of both parameters (lateral flux and vertical protore metal grade variation) on Z1,j values.

In general, the net lateral flux balance for Au, Ag and Cu is given by a relatively small negative number (Table IX), suggesting that the fault zone might have acted as a source region for these metals. Moreover, considering an average period of time of 500,000 years for the development of the regional pediplanation (Cabral, 1985), one can obtain suitable lateral metal fluxes per year for each metal: 1–3 ppb/year for Au, 0.05–0.06 ppm/year for Ag, and 0.007 ppm/year for Cu. The geological acceptability of these values contrasts with the estimated lateral flux of iron, where the large negative number obtained indicates that we postulate, at least, too much leached material for the grades observed, as stated above. Another point of interest is the contrasting behaviors of gold and silver during the development of the weathering fault zone profile. In fact, the apparently higher fluxes of Ag suggest that this metal was easily mobilized from the fault zone; this is an indirect evidence for a greater stability of silver complexes in this weathering environment. Although the directions of lateral fluxes cannot, at present, be determined, we may speculate that they were from NW–SE to W–E, probably controlled by the Montesinho ridge which stood out in relief during the regional episode of erosion (there is no tectonic evidence for the elevation of Montesinho block in Quaternary times), determining the geometry of the paleoground–water table.

An alternative to the above lateral flux interpretation for anomalous Z1,j values, is to consider errors related to the average protore metal grade due to: (1) gradual variation of metal grades with depth ascribable to primary sulphide–zoning features, and/or (2) abrupt grade changes associated to specific lithological–structural contacts which affect the control volume of interest.

The results of the leaching efficiency (EL,j), shown in Table II-5, illustrate the almost complete leaching of Pb, Au and Ag (with EL,j > 99%), coupled by extensive depletion of Ga. Surprinsigly, EL,j values for Cu and Zn did not take the high magnitude we expected due to the absence of relics of Zn and Cu sulphides in the upper horizons of the weathered fault profile. This incomplete leaching may however be interpreted as a result of Zn and Cu incorporation in some authigenic minerals.

5 – CONCLUDING STATEMENT

Fault rocks related to the Vilariça strike–slip fault and to reactivated oblique D3 shear zones, although macroscopically similar, exhibit a different chemical signature. Concentrations of As, S, Pb, Cu, Sb, Au, and Ag are especially notorious in representative samples of quartz breccias along the Vilariça structure, particularly those of types IB and IC.

The establishment of the fault zone weathering profile, based on the spatial distribution and geochemical analyses of 10 samples of type I, enable the conclusion that there are almost always discontinuous chemical variations between 730 and 750 m of altitude, corresponding in general to the fault zone horizon where breccias IB are preserved. These geochemical variations, consistent with the mineralogic nature of the quartz breccias that underline the main branches of the Vilariça fault in the França/Portelo sector, strongly suggests that some metals (like Cu, Pb, Zn, Au, Ag, and Ga), were locally moved from a leached zone (represented by

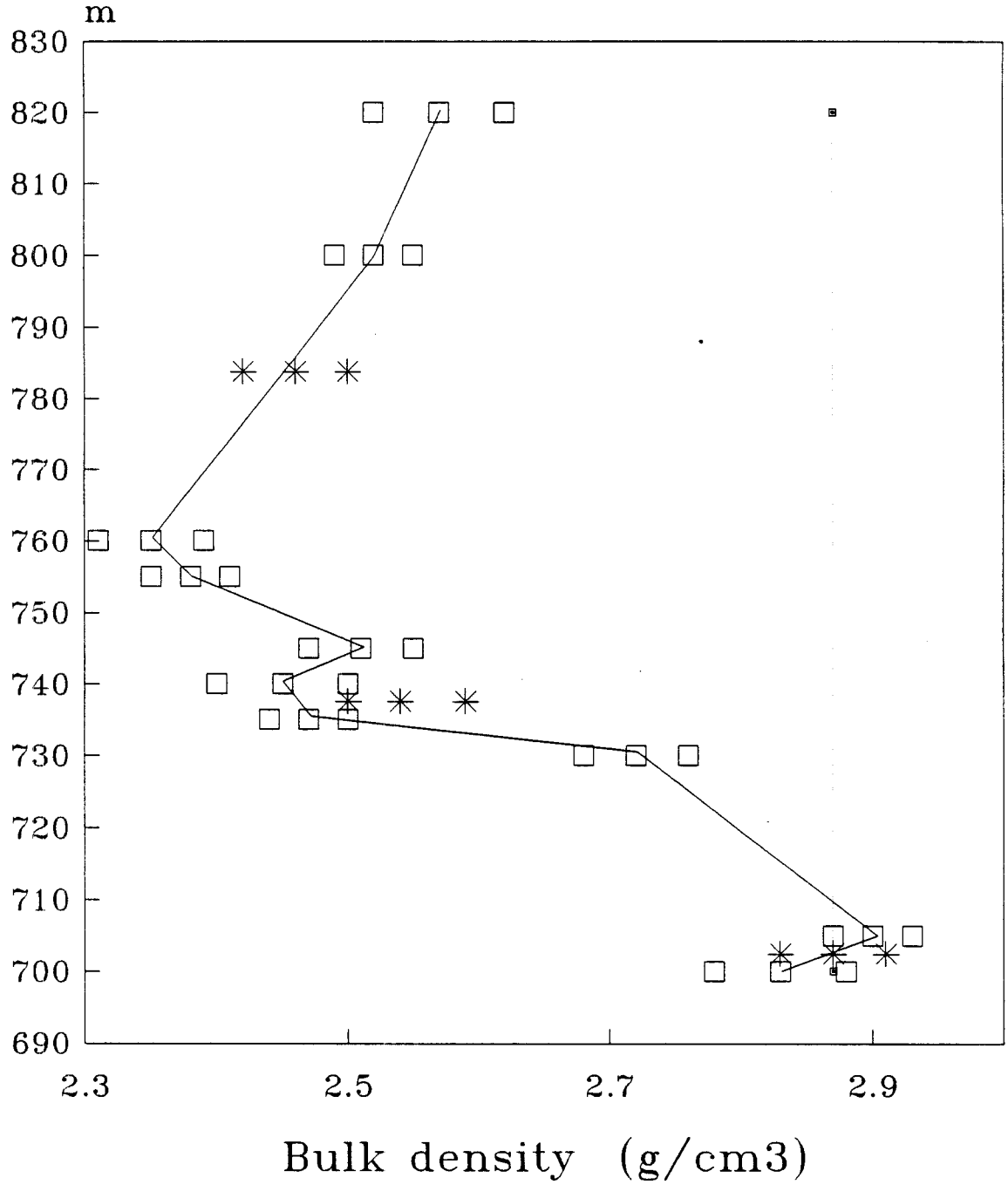

Fig II-40 : Variation of bulk density of the analysed fault breccias. For each sample, the three squares represent the ranges of the obtained density values based on four determinations; the continuous line connect the average density of different samples. The range of average density values for the three groups of breccias are illustrated by asterisks. The average of protolith material is shown with a dotted line.

	Sample N°	Density * (g/cm³)	Average Density
Group IA	(F-67) 1	2.57±0.05	2.46±0.04
	(F-67A) 2	2.52±0.03	
	(F-45A) 3	2.35±0.04	
	(F-45) 4	2.38±0.03	
Group IB	(F-27) 5	2.51±0.04	2.54±0.04
	(F-23L) 6	2.45±0.05	
	(F-23L1) 7	2.47±0.03	
	(F-23C) 8	2.72±0.04	
Group IC	(F-23) 9	2.90±0.03	2.87±0.04
	(F-11) 10	2.83±0.05	

Table II - 3 - Bulk density values for the three groups of fault breccias settled along the Variça fault in the França sector

		Cu	Pb	Zn	Au	Ag	Ga	Fe
(m) $T°_{L,j}$	Ave.	95	159	156	10	2.5	154	6.5
	Max	198	356	189	85	8	263	25
(m) $Z_{1,j}$	Ave.	845	909	906	760	753	904	757
	Max.	948	1106	939	835	758	1013	775

Table II-4 : Maximum and average valus for T°LJ and Z1j relative to supergene elements.

		Cu	Pb	Zn	Au	Ag	Ga	Fe
(g/cm²) F^{l}_{j}	Ave.	-0.35	—	—	-0.17	-2.9	—	-2330
	Max.	—	—	—	-0.08	-2.7	—	-2070
(%) $E_{L,j}$	Ave.	37.9	99.4	33.9(*)	99.8	99.7	84.4	68.6
	Max.	73.9	99.6	51.6	99.9	99.8	89.9	77.5
		(ppm)	(ppm)	(ppm)	(ppb)	(ppm)	(ppm)	(%)
$C'_{j,p}$	Ave.	51	2791	75	864	11	3	3.6
$T°_{L,j}$	Ave.	3.8	6.3	6.2	0.4	0.1	6.2	0.3
$T_{E,j}$	Max.	7.9	14.2	7.6	3.4	0.3	10.5	1.0

Table II-5 : Total flux (F1j), leaching efficiency (ELj), estimated protore grade (C'j,p) and the thickness ratio between the enriched and leached horizons of the weathered profile.

breccias IA) to a complementary enriched horizon, where reprecipitation took place (fault zone level represented by breccias IB).

The present analysis evaluates also the use of mass balance equations for supergene elements (Cu, Pb, Zn, Au, Ga and Fe) in a non–deformational system, assuming a vertically homogeneous protore (fault breccias IC). The altitude of the paleo–oxidation surface, estimated from the average leached column height of Pb, Zn and Ga, with an enrichment blanket thickness of the order of 25 m which top is now at 750 m of altitude, is consistent with the present elevation (around 900 m) of the ancient, well preserved, regional pediplanation of Late Pliocene age. Anomalously high elevations for the paleo–oxidation surface are obtained when we include in the calculations the estimated maximum leached column heights of Pb, Zn, Ga and Cu. The values obtained are however geologically realistic, suggesting that, at least, 40–100 m of erosion must have taken place after pediplanation development. Accepting an average age of pediplanation development being 2.5–2 Ma, the estimated erosion rates range from 0.016–0.04 mm to 0.02– 0.05 mm per year, respectively. It is also important to point out that the vertical component of movement associated to the reactivation of the Vilariça system in França sector during Quaternary times is unanimously considered to be very small and therefore should not be a significant source of error in these estimations.

For the remaing supergene metals (Au, Ag and Fe), the calculated elevation of the paleo– oxidation surface is negatively anomalous. For gold and silver, the corresponding low topography anomalies, can be explain by the existence of significant lateral fluxes, probably controlled by the Montesinho ridge which stood out in relief during the regional episode of erosion of Late Pliocene age, determining the geometry of the paleoground–water table. Our modeling suggests also that lateral fluxes for Ag are far greater than the ones obtained for Au, which is interpreted as an evidence for a greater stability of silver complexes during the development of the weathering fault zone profile.

The obtained large negative lateral flux of iron and/or the abrupt decrease in its concentration in protolith specimens required by the estimated low topography anomaly, are not consistent with the mineralogic signature shown by the examined fault breccias. Thus, a very large part of the iron contained in the original section remained unaccounted for in our calculations, producing an underestimation of the altitude of the paleo–oxidation surface.

The implications of our work are obvious and far–reaching: in the Iberian Peninsula, apparently barren quartz veins are frequently seen standing out in the landscape, at altitudes where, according to our data, no geochemical anomalies are to be expected. These may sometimes correspond to blind deposits.

III - STRUCTURAL CONTROL OF THE MINERALIZATION

The characterization of the structural controls of the ore formation has been carried out thanks to a multiscale study of tectonic markers from the field to the microcrack scale. Thus, the main succession of deformation events and their effects on the formation of tectonic traps is summarized for some remarkable test cases. As most Au bearing quartz veins are characterized by fairly complex succession of quartz crystallization, deformation, and healing, the chronology of ore deposition, fluid migration and trapping in relation with the deformational events , new integrated approaches have been developped on specific areas, in order to get more detailed investigations on the paleofluid pathways.

A- TECTONICS IN THE NW IBERIAN HERCYNIAN SEGMENT AND DEVELOPMENT OF REGIONAL SHEAR

All the areas studied in this project (at the exception of Montemor) are in the NW Iberian segment. For this reason, the tectonic events of this part of the Iberian Terrane will be approached in detail emphasizing the development of the regional shear and related secondary structures. Both shears and secondary structures determine in general the structural control of the mineralization.

One of the most significant features of the NW Iberian segment is its strong curved structures. Regional ductile shears acting symmetrically in the basement induce thrust systems on the surface, depicting the Ibero-Armorican Arc (Jegouzo,1980), (Fig. III-1). Several models have been suggested to represent the genesis of this Arc: - an orocline type model, with an increasing southward displacement ratio (Ries and Shackleton, 1976); megashear (Badham, 1982); plastic indentation associated to collision (Matte and Ribeiro, 1975); or oblique collision (Silva et al., 1990). The geometric and kinematic features associated to the structures in the NW Portugal, lead to a flake tectonic interpretation as a result of the subduction and associated odduction to the East of a RHEIC oceanic crust (Ribeiro and Pereira, 1986, Ribeiro et al., 1990). Relics of this crust are found in several places of central and northern Europe as well as in Galiza and Tras os-Montes allochtonous massifs.

In spite of the type of collision, the plastic indentation around the Cantabrian block is the ideal interpretation for the conjugated shear in the Iberian and Armorican branches.

a - Age, geometry and kinematics of the early deformation phases (D1 and D2)

The first phase of deformation (D1) was dated by the granitic intrusion at 379±12 Ma from the Oliveira de Azemeis area (Pinto et al., 1987). Those granites, affected by D1, record the begining of the orogenic internal collision. A similar age was achieved by Dallmeyer et al. (1990).

The geometry of the structures in D1 have a general WNW-ESE orientation in the central and SE part of the C.I.Z., and rotates to the North when approaching the virgation axis of the Iberian-Armorican Arc. In this sector, NW Iberia, there are a concentration of transcurrent ductile shears with a sinistral sub-horizontal displacement. The tangential shearing in the basement induces an E.SE and E direction of the allochthonous nappe movement. The geometry and kinematics of the structures in D1 display different patterns in the following sectors of C.I.Z.:

- North of the Carboniferous trough and Juzbado-Penalva do Castelo shear;
- South of these shears; and East of Porto-Tomar-Portalegre shear (FigIII-2).

i - sector North of the Carboniferous trough and Juzbado-Penalva do Castelo shear:

The displacement of the nappes to SE and East induces the deformation within the nappes, developing sheath folds and axial-planar schistosity S1 distinct from the same schistosity S1 in the autochthonous. A stretching lineation X1 is divergent to the sense of the

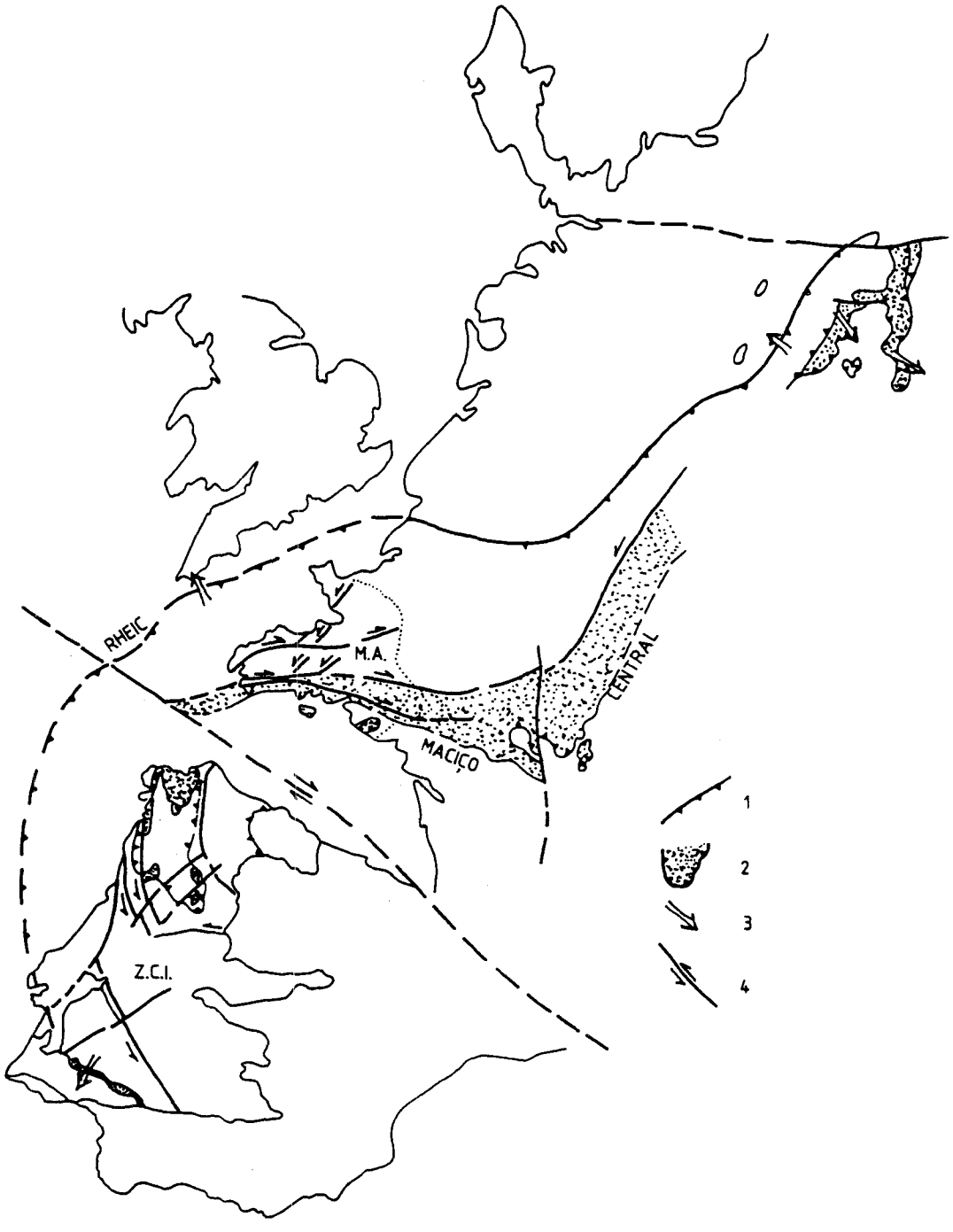

Fig III-1 : Ibero-Armorican Arc (Variscan Fold Belt).1- thrust, 2- nappe zone, sometimes, with ophiolite terrane; 3- vergence; 4- transcurrent shear

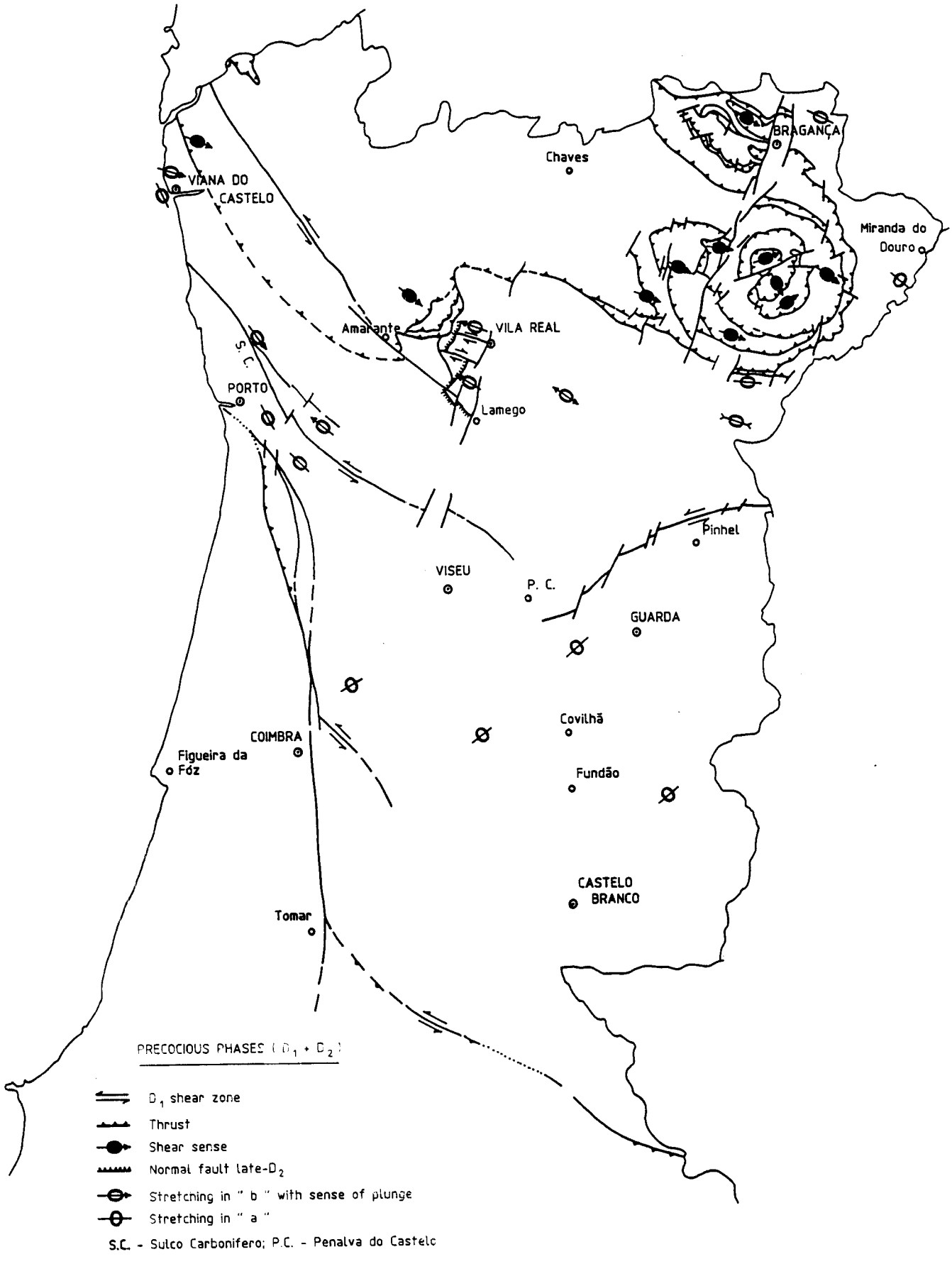

Fig.III - 2 : Shear and stretching lineations of the Hercynian early stages, D1+D2, after Ribeiro, Pereira & Dias (1990), modified.

movement, being progressively reoriented in the vicinity of the thrust planes (Quinquis et al., 1978; Cobbold and Quinquis, 1981). The second phase of deformation D2 occurs associated to the thruts planes of D1, being either compressive or extensive (Diaz Balda, 1990). It represents the continuity of the movement along those planes, and is characterized by folds of curved axis, axial-planar schistosity S2 and X2 stretching, all in continuity with D1 structures.

The structure in the autochthonous between Salamanca and Porto shows a distinct divergent vergence, on both sides of the Amarante shear (flower structure). In the zones of more intense regional deformation an inhomogeneous simple shearing, that changes gradually to a transpression regime, develops folds with sub-horizontal axis, gently inclined S1 axial-planar schistosity. The angles between this schistosity and the thrust planes are reduced to NW, i. e., in the sense of the intensity of the deformation and the virgation of the arc. In the upper structural levels, near the shears, the slaty cleavage transcepts the folds. The foliation shows b stretching lineation X1 paralell to the fold axis. Although the inhomogeneous deformation and the differential stretching implies the plunge of the fold axis and of the stretching in the sense of increasing deformation. Far from the transcurrent shears, the structures have a similar pattern, as in the south sector, described below.

The confined occurrence of the allochtonous to this sector, as well as the occurrence of D1 recombent structures, with opposite vergences in both south and north of the terminal areas of the Juzbado-Penalva do Castelo shear zone, verging to NE in the south and to SW in the north, respectively, lead Iglesias and Ribeiro (1981) to consider this shear active during D1, associated to the reactivation of a pre-hercynian lineament. This interpretation contradicts the observations of Alonso et al (1992).

ii) Sector South of the Carboniferous trough and Penalva do Castelo-Juzbado shear zones.

In the Portuguese domain of this sector, shears are not known or show gentle expression. D1 structures display NW-SE folds with very steep axis, influenced by the Sardic folds, running NE-SW. The strain slip cleavage (S1) with sub-vertical axial plane, admits a subvertical stretching lineation (X1), in the plane of schistosity which stresses the sardic folding, and, consequentely, the bent of the D1 fold axis. This kind of stretching points out the changing from simple shear regime, with a stretching on b kinematic axis, as seen East of Porto, to stretching on a kinematic axis, in this sector (Ribeiro et al., 1990), (Fig III-3).

iii) Marginal sector to the Porto-Tomar-Portalegre suture.

The pattern of D1 structures East of this suture, i.e., in the C.I.Z., due to the local boundary between C.I.Z. and O.M.Z., illustrates the instabilities and the movement ratios during the hercynian orogeny. So, during D1, the accident SE of Tomar is a senextral shear; its continuity to the North is unknown, and probably it shows the NW of Porto. Between Porto and Tomar, the accident has a complex record (Ribeiro et al., 1980):- senestral transcurrent fault in D1, passing to dextral transcurrent fault in D3, with both ductile and brittle component and a displacement amounting to 100 Km; in upper Stephanian, it acts as a brittle senextral transcurrent fault; after Stefanian, and before Triassic, becomes a thrust fault, moving eastward; lately, in the Post Mesozoic and recent ages it becomes a normal fault, plunging to West.

Between Albergaria and Porto, the accident divides in three branches. In the internal part of the ramification, the D1 structures are oriented N-S, generating recumbent folds, with 1 Km of reverse limb, vergent to the west; they admit axial-planar schistosity S1 coplanar with the foliation of the granites with an age of 379±12 Ma. The West branch is a thrust boundary between schists and greywackes in the C.I.Z. or between phyllites of the "Serie Negra" and micaschists and gneisses from the Proterozoic Polimetamorphic Complex of O.M.Z. The internal branch is to the so-called Beiras Metalliferous dike. At last, the East arm is a dextral transcurrent fault, as refered earlier.

From Albergaria to the Lousπ fault, D1 structures are gradually steeper, always with a vergence to West. SE of the Lousa fault, the structures turn NW-SE, parallel to the accident, and SE of Tomar the thrusting component induces a NE vergence.

iv) Secondary structures associated to the shear zones (D1 and D2)

In the presence of both transcurrent shear or thrust systems, the ductile-brittle deformation always produces secondary structures. Similar results were obtained in classic

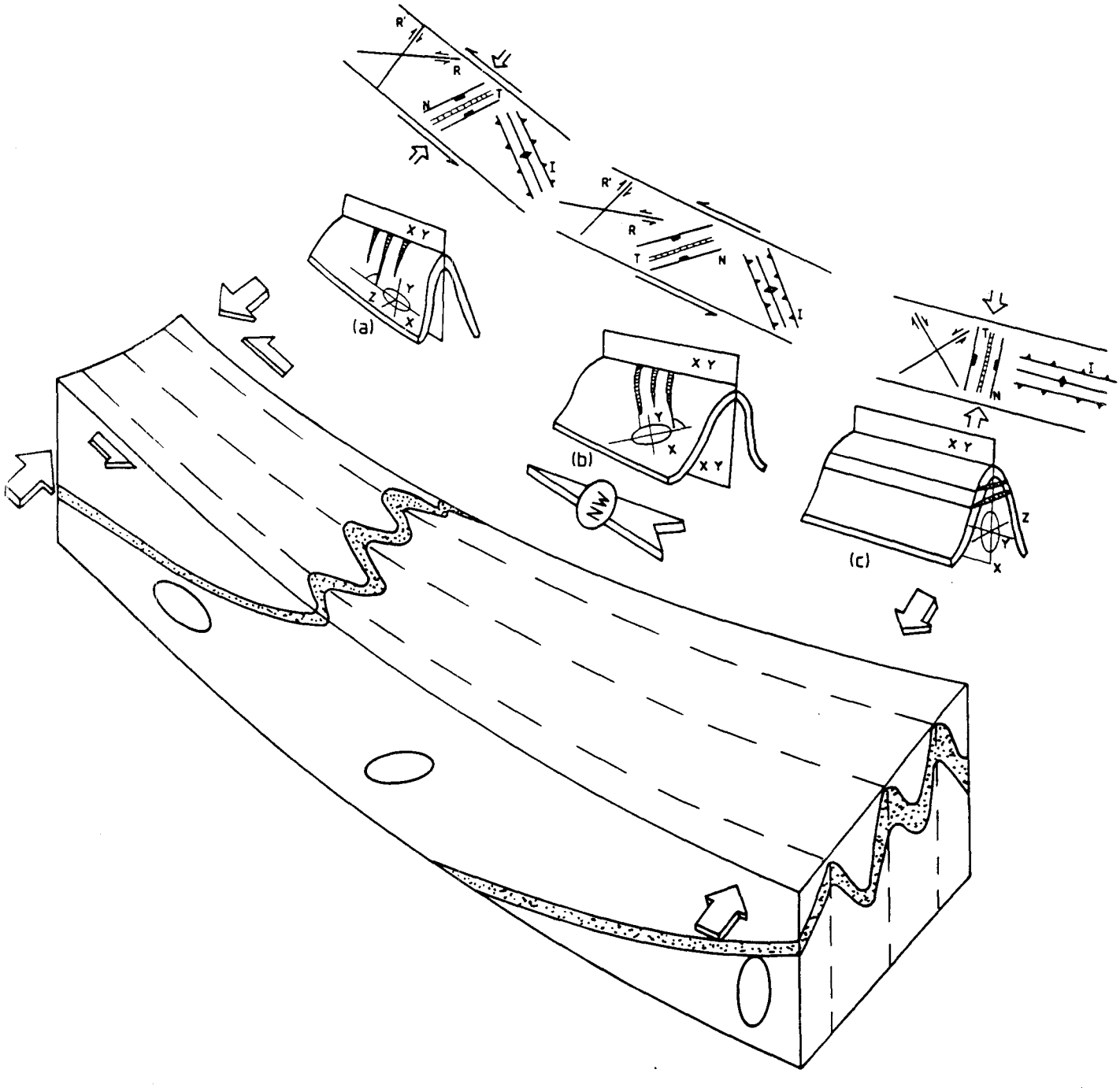

Fig.III -3 : NW-SE variation from a transpression regime to pure compression in the C.I.Z. (Portugal), showing the stretching lineation (X1) evolution and the secundary structure patterns T- tension gashe; N- normal fault; R, R'- Riedel and conjugated Riedel fracture

experimental works (Tchalenko, 1970), in factual observations (Gamond and Giraud, 1982), in theoretical experiments of rock mecanics (Sanderson and Marchini, 1983; Harris and Cobbold, 1984) or even in more recent concepts (Gamond, 1987; Petit, 1987). Figure III-4 is a synthesis of the main secondary structures and their spatial distribution in different extreme regimes: transpression (a), simple shear (b) and pure shear (c).

b - Age, geometry and kinematics of late deformation phases (D3+D4)

Different metamorphic and deformation regimes are the leading features for each one of these late orogenic phases; as a consequence they have a different age.

D3 - This phase develops after the emplacement of the C.I.Z. nappes, in an advanced collisional stage. Thrusting stoped due to maximum crustal shortening. Then the deformation develops as ductile intracontinental shear, parallel the collision suture that is now blocked by earlier magmatic intrusions and metamorphic recrystallization. Theses D3 extended shears command metamorphic evolution and control the granite emplacement, They reactivate D1 shears with dextral displacement and develop conjugated senextral shearing (Fig.II-4). Strain slip movement along the principal shear planes is unimportant, (in the order of 1-10 Km, as along the conjugated shear), a fact that points out to a regional control of the deformation rather than to an orogenic global control. As the Cantabrian nappes are installed during this tectonic phase, D3 emphasizes the bending of the Iberian-Armorican Arc.

The age of this phase about 320 Ma., is well defined by the installation of syn- to late-tectonic granitoids, affected by D3. The occurrence of deformed clasts coming from this granitoids in the Westphalian B conglomerate at Bougado, Trofa, agrees with that age.
D3 folds, with subvertical axial plane and subhorizontal axis, have a sigmoidal geometry and an "en echelon" pattern, relatively to the shear planes. The deformation is heterogeneous, associating simple heterogeneous shear to a volume decrease near C planes. In the blocks among these discontinuity planes, and far from their control, is possible to reach pure shear regimes. Planes.C and S3 have variable angles which point up the non coaxial caracter of the deformation; the horizontal stretching X3 parallel to the B geometric fold axis and therefore in agreement with the transcurrent regime.

In the simple shear, the secondary structures have the same patterns as mentionned above, (Fig III-5), while in pure shear, only traction gashes occur, parallel to the maximum stress or making 45° with it.

D4 - This phase develops during the Permian because it controls the emplacement of late-to-post orogenic granitoids with the same age. It is mainly brittle; it affects the granitoids and develops at the favour of some of weakness zones that correspond to previous traction gashes. This is especially shown by the brecciation of the filling material and its cementation by a new hydrothermal phases put this fact in evidence.

The brittle fracture systems in D4 strikes NE-SW to N.NE-S.SW with senestral horizontal movement. This movement develops a significant conjugated system striking NW-SE retaking previous structures now with britle dextral wrench regime. By the geometry and movement along the conjugated systems, we infer that the tension field rotates substantially, getting close to N or N.NW of maximum stress.

Because of the brittle nature of the main system, the secondary fractures T , R/R' and P, make smaller angles with the movement plane than in the ductile shears. With the break down of the orogenic tensions, it creates : - graben systems , distensive systems when the movement along the brittle faults is combined with traction and riedel systems and finally compressive systems when the movement along the brittle faults is transmitted to the P fractures (Fig. III-6).

In the particular case of the Hercynian in NW Iberia, most Au/Ag ore deposits are concentrations associated to shear zones, at the exception of placer deposits (see especially for Portugal, the typology proposed by Meireles and Carvalho, in prep.). So the ore deposits studied during this project, can be linked by the relative age of the tectonic phases that produced the different shear zones and by the overall structures that control the mineralization.

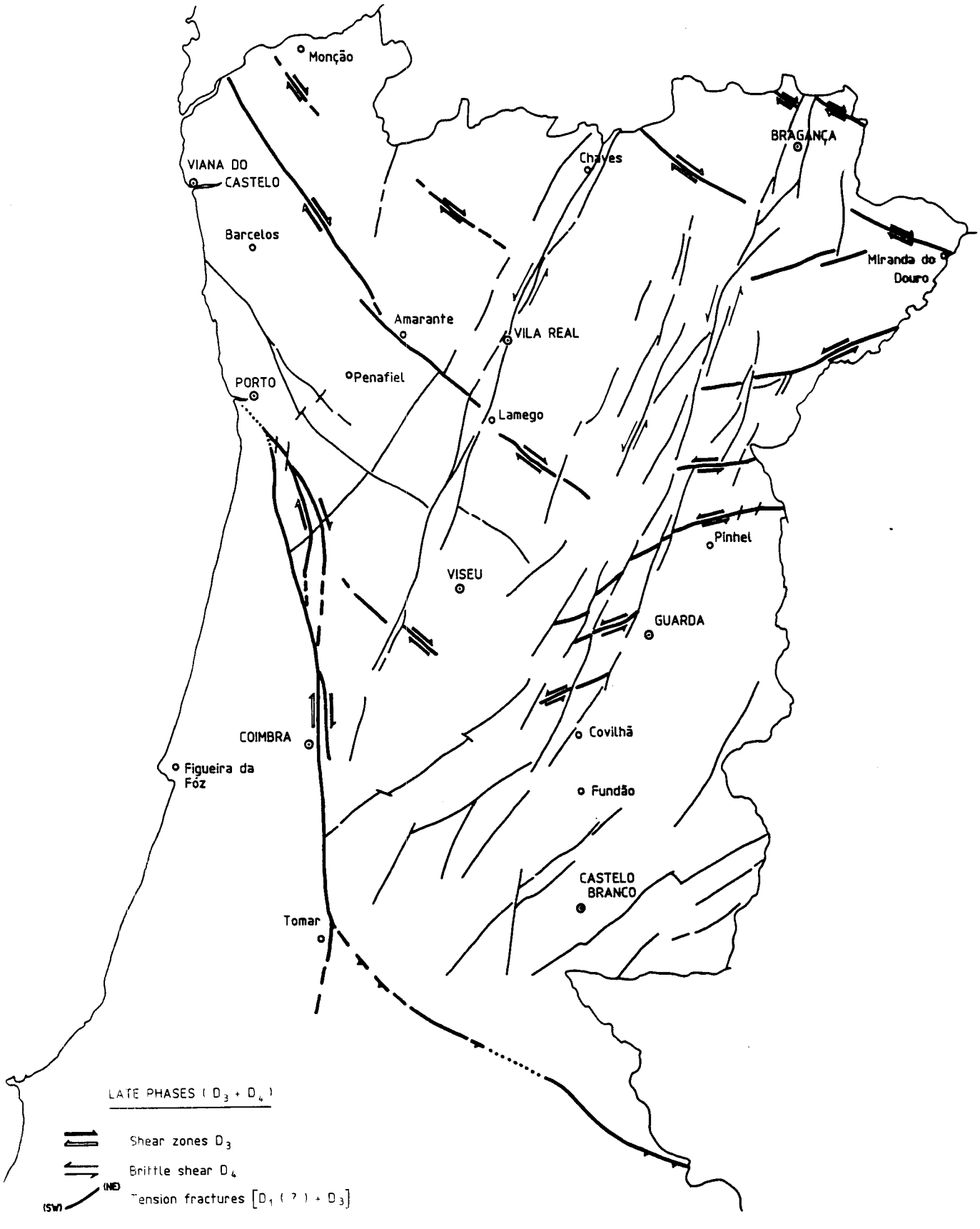

Fig.III - 4 : Ductile and brittle shears of the late Hercynian phases

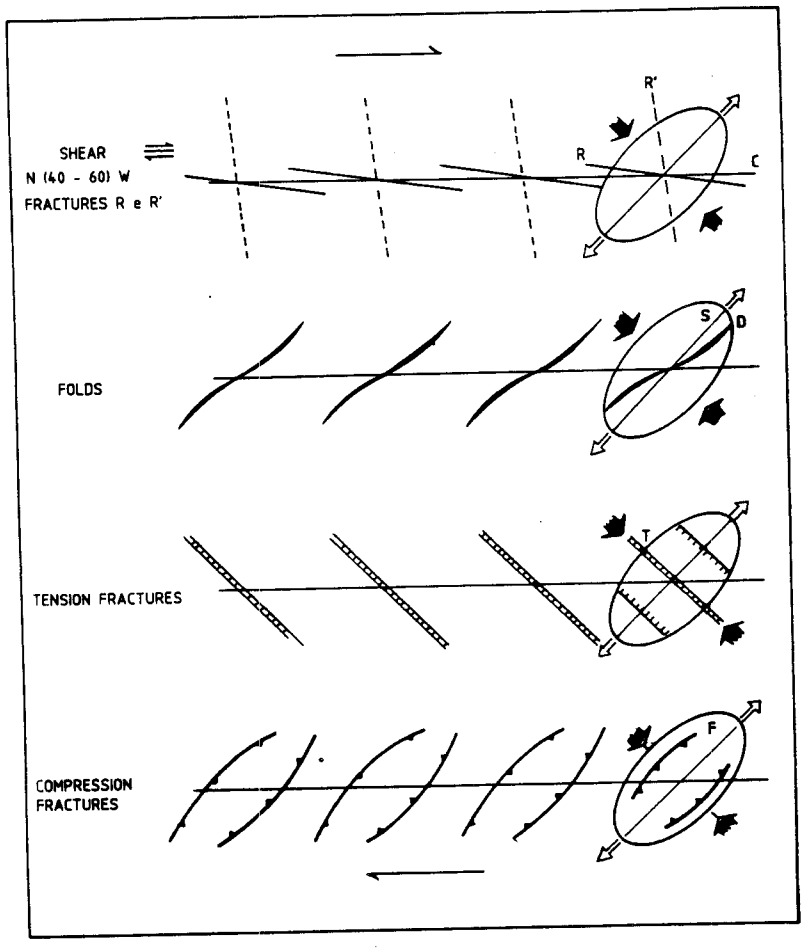

Fig.III - 5: General structures originated by simple shear in D3 hercynian phase: C- shear; R,R'- Riedel and Riedel conjugated fractures; S- schistosity (S3); T- tension gashes; F- compression fractures

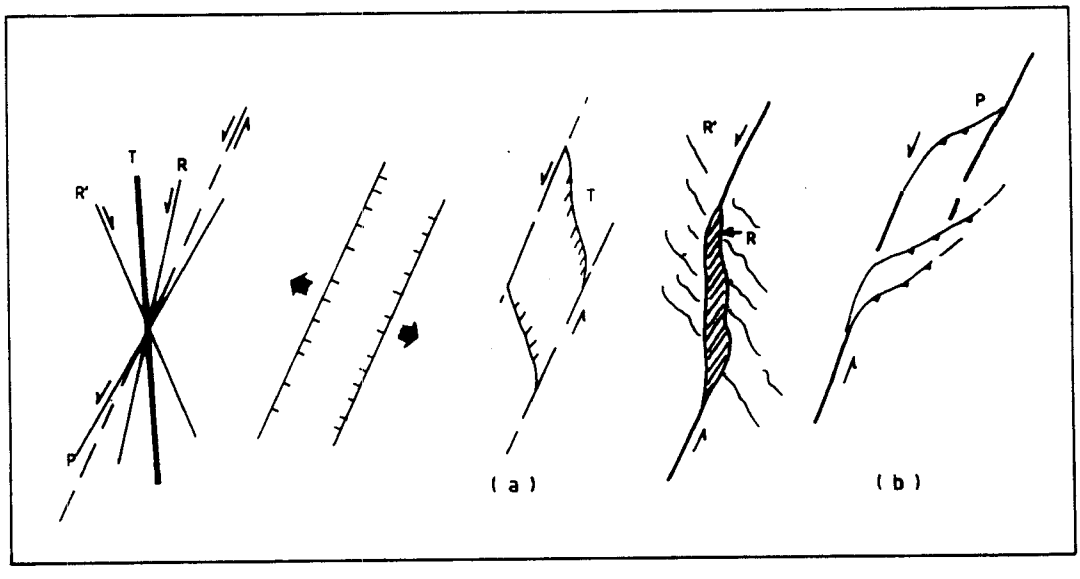

Fig.III - 6 : Brittle fracture systems in D4 hercynian phase; progressive movement can generate tractive (a) or compressible (b) tensions.

B-DETAILED STUDY OF STRUCTURAL CONTROLS

1-Fluid migration and microfracturing : methodological approach (CREGU)

Most Au bearing quartz veins are characterized by fairly complex succession of quartz crystallization, deformation, and healing. The chronology of ore deposition, and the different stages of fluid migration and trapping in relation with the deformational events is especially difficult to establish using standard techniques (e.g. optical microscopy for instance). In many studies, tectonics, ore mineralogy and fluid inclusions have been studied separately, at distinct scales, and do not give sufficient data for a reliable reconstruction of the ore fluid migration. To decipher the time - space relationships between deformational events, mineral healing or recrystallization, fluid trapping and ore deposition, a multidisciplinary approach yielding to a complete characterization of the paleofluid pathways has been developped and is presented in the following sections.

a - Sampling

Oriented blocks of quartz are sampled along profiles from mineralized zones to the barren surrounding rocks. On each sample, horizontal and vertical sections are sawn for macroscopic observation of textures, and oriented blocks are then prepared for oriented thin sections and oriented wafers.

b - Microstructure characterization and geometry of fluid migration

Since gold bearing quartz veins display in most cases relatively complex superimposition of microstructures making difficult the identification of primary and secondary inclusions as well as the discrimination between the different networks of microstructural markers, the geometry and chronology of fluid migration are investigated by combined techniques :

- macroscopic observations of oriented horizontal planes ;
- transmitted light microscopy on oriented thin section ;
- systematic and stastistic analysis of the microstructural markers.

The quantification of the abundance and geometric characteristics of each marker are carried out using a statistical analysis of the microstructural markers in horizontal and oriented planes. In most veins, the microstructural markers are distinguished according to the mineral filling of the microstructures and the relationships between microstructures and their host minerals. Three different kinds of structures are commonly distinguished : (i) fractures and microfractures with fillings which could be either quartz, or alteration and ore minerals. (ii) closed microfractures with or without recrystallization of the host minerals (iii) fluid inclusion planes which correspond to healed microcracks which have trapped the percolating fluids.

Systematic measurements of microfissures are carried out in each section by manual counting and by using an interactive videographic analyser adapted to such studies (Lapique et al., 1988). Analysis of the microfissures takes into account different parameters such as the nature of the crack, the type of crosscutted mineral and the density of each crack family. Results are given in density of cracks for length and number.

2-INTRAGRANITIC DEPOSITS

a- TOMINO : An example of multistage tension gash formation at all scales

The most interesting intragranitic auriferous quartz vein system from the Tomino area is located in the Pedrada massif. This massif is intruded in the central part by metasediments as a granitic stock of elongated shape, extended Northwards as a dyke of 10 km lengh parallel to the regional structures with width ranging 40-150m.

The highest density of quartz veins occurs in the central part of the granite dyke (Alto de Pozas), within a segment of 2 km length (Fig.III-7). The sets of quartz veins are limited to granitic dyke and oriented N70°-80°W, steeply dipping Northwards. The quartz veins are often spaced about 1 m, with thickness ranging from simple fissures, with occasional filling sulfides

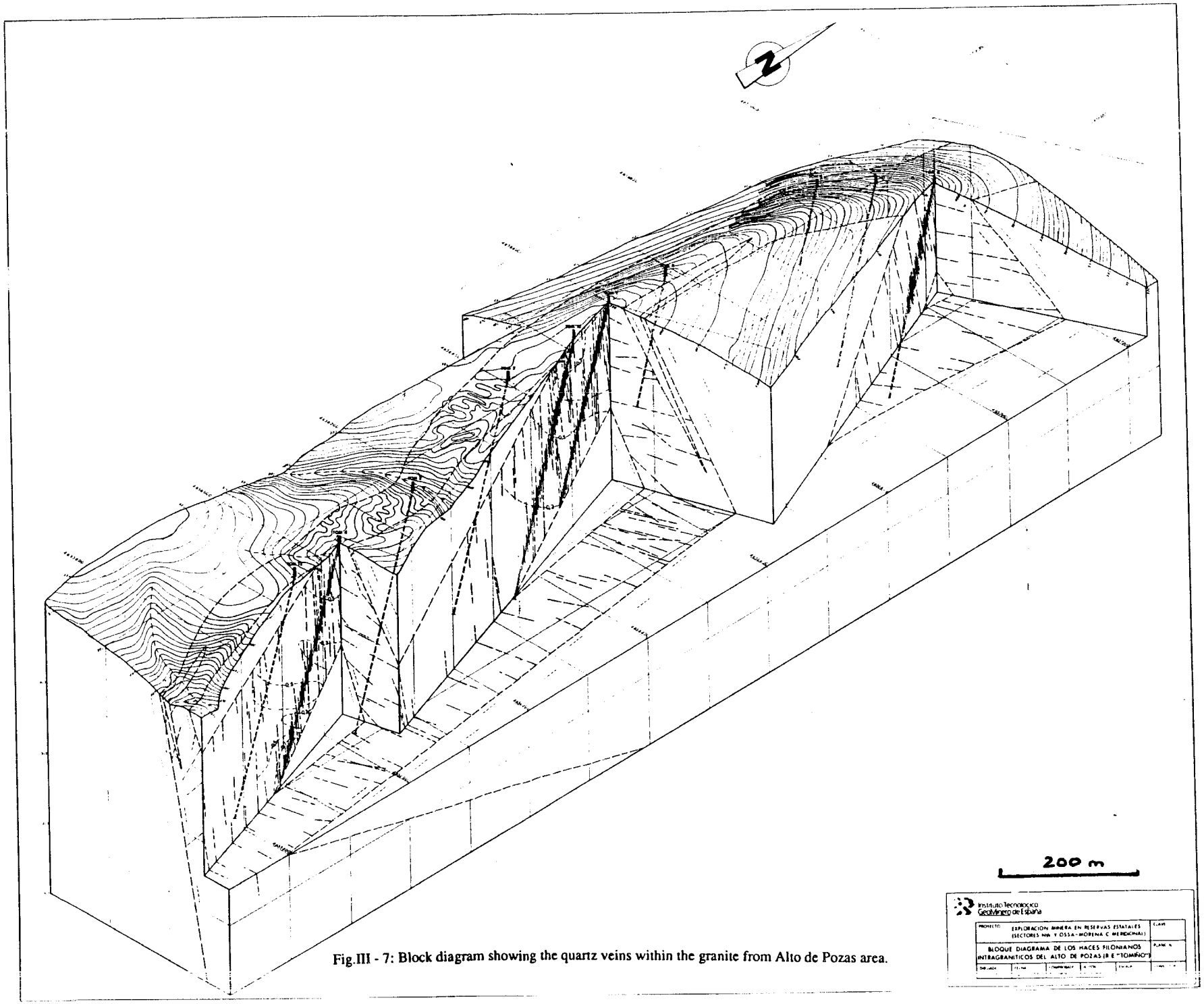

Fig.III - 7: Block diagram showing the quartz veins within the granite from Alto de Pozas area.

to few dm. The maximum lengh of individual quartz vein observed in outcropping and core drilling is about 20 m. Structurally, quartz filling extension gash fractures developped in the last stage of the third phase of deformation. Extensional tectonic regime favoured the earlier greisenization of the wallrock following by hydrothermal alteration with introduction of quartz and sulphides. The width of the alteration zone ranges from 1 cm to more than 1 m and are not proportional to the thickness of the quartz veins, and are assumed as earlier than quartz.

The geometry of the mineralized structures is relative simple, but the faulting and microfissuring processes are relatively complex in detail and correspond to a long lived tectonic activity. This has encouraged a multiscale study of the geometry of the brittle deformation structure by field and laboratory studies.

Ductile deformation

The foliation in the Pedrada granite is parallel to the schistosity an correspond to the third phase of the hercynian deformation. The foliation is oriented N140°-N180°E. The mean direction is N 160°-170°E (Fig. III-8). The foliation planes are generally dipping around 50° NE but are mostly straight N70° to 90° NE.

Brittle deformation

Two types of gold bearing mineralizations can be distinguished :

-Individual quartz-veins filling C-planes of earlier brittle-ductile shear-zones have formed within the metasediments band. The main mineralization consists of locally disseminated to massive-narrow bands of sulfides (arsenopyrite, pyrite) with occasionally native gold. The emplacement of quartz-veins are accompanied of wall-rock alteration (silicification, sericitization, chloritization).

-Intragranitic quartz-vein systems filling shear-fractures or tension gashes, accompanied by greisenization and hydrothermal alteration of wall-rock. Sulfide mineralization with associated gold occurs in quartz-filling and greisened zones.

Different types of structures have been observed in the Pedrada granite :

- Fracture with greisenization ;
- Mineralized quartz veins ;
- Mineralized quartz veins with greisenization ;
- Metric fractures.

These structures are related with several tectonic episodes developed after D3, which have special interest because they act as structural control of gold mineralizations. Some brittle-ductile shear zones and faults appear, usually with a N-S strike, parallel to main foliation. Two shear episodes, sometimes overprinted in the same structure, can be distinguished: first, shear zones with a normal slip component are developed, followed by dextral strike-slip shear zones.

GEOMETRY OF THE MINERALIZED QUARTZ VEINS (PEDRADA MASSIF)

Orientation and dip of the vein network

In the Urgal granite which extends the Pedrada granite in the north, the major direction is N80°±20°E whether the considered structures (Fig. III-9).

In the central part of the massif, the N 10°-40°E direction becomes more important for all the structures, but the N80°±20° E direction is always dominant. In the center and in the south of the massif, the two directions (N 80°±20°E and N10°-40°E) are coexisting with the same importance.

The dip of the brittle structures and of the veins are generally ranging from 70° to 90° (subvertical) but are sometimes observed between 50° and 70°. In the different cases, dip is oriented N or S for the principal direction and SE or NW for the secondary NNE direction.

Some pluridecametric to kilometric faults are croscutting the Pedrada granite. Their directions are mostly N70°-100° E, and sometimes N30°-40°E and N130°E.

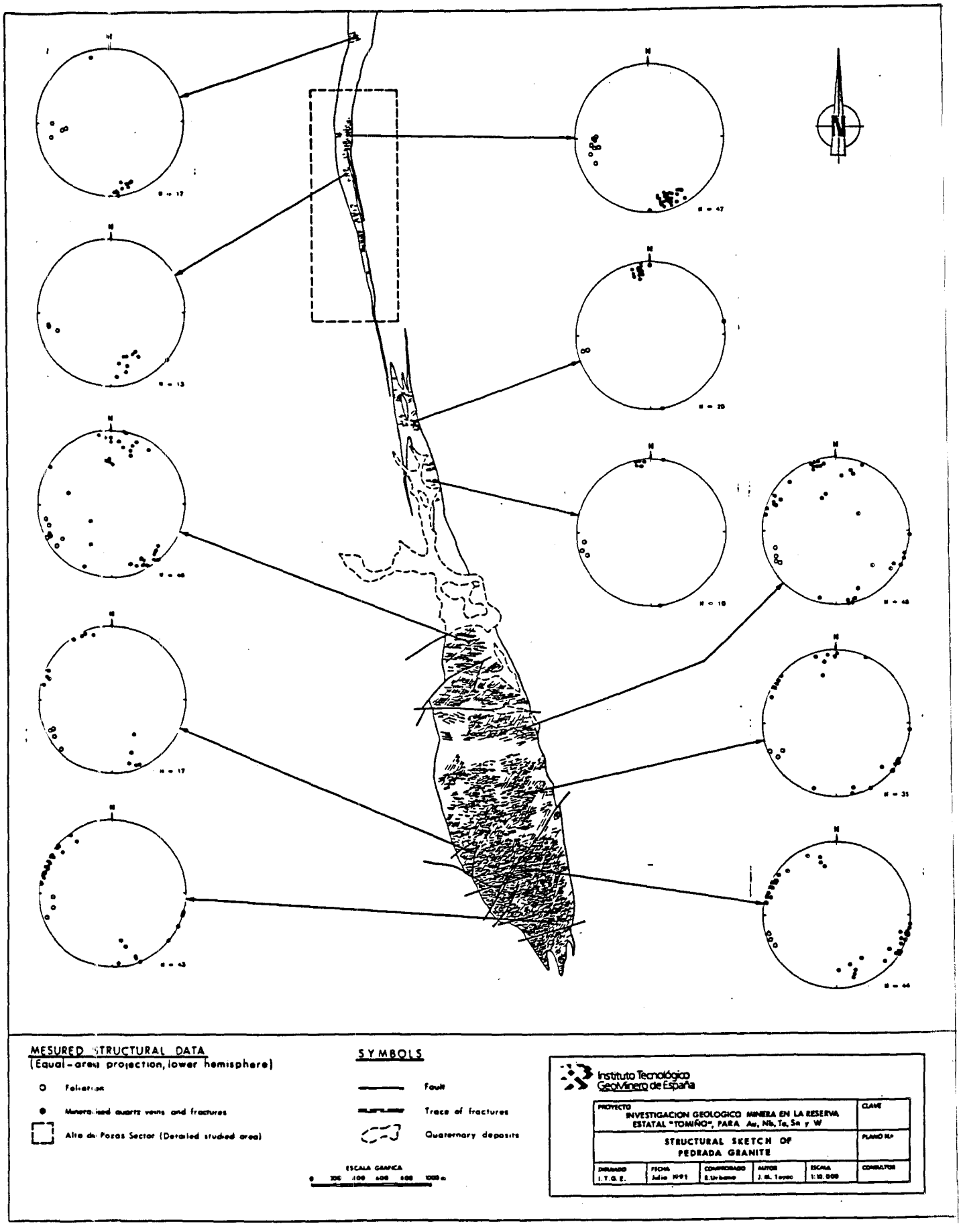

Fig.III - 8 : Ductile and brittle macrostructures in the Tomino area.

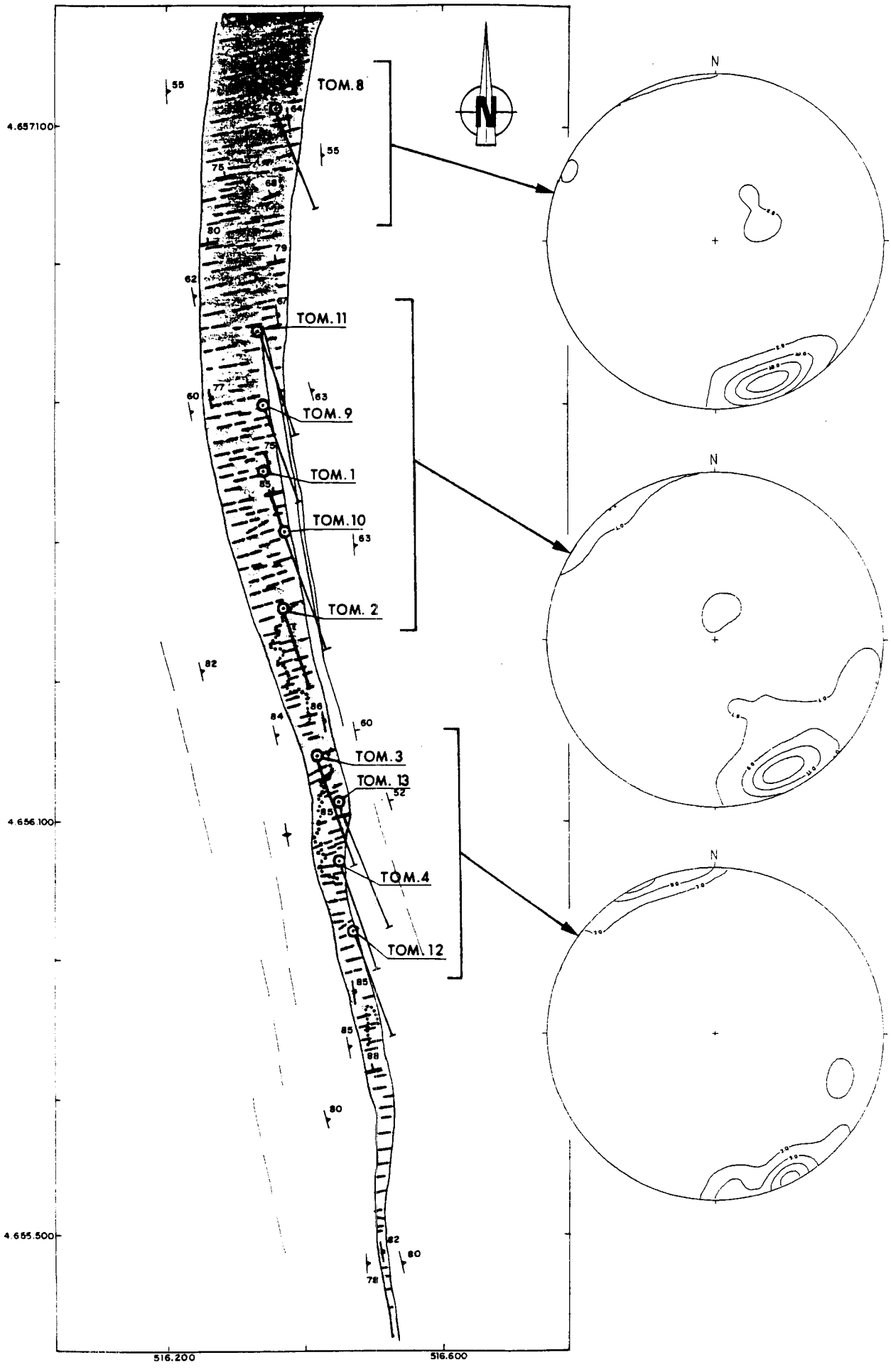

Fig.III - 9 : Mineralized structures from drill cores. Urgal granitic dyke, Tomino area.

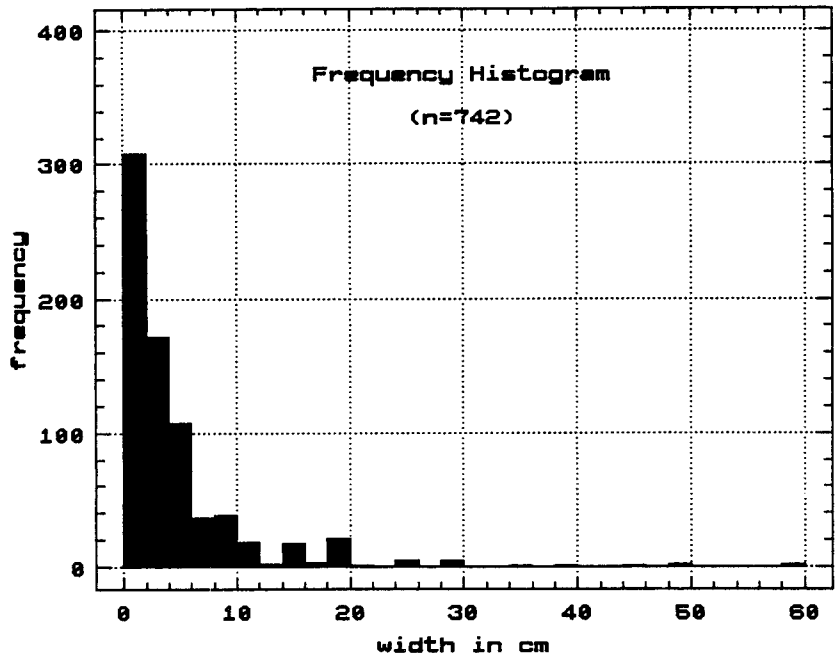

Fig.III - 10 : Histogram of thickness of quartz veins from drill hole data of Tomino area (n : number of quartz veins)

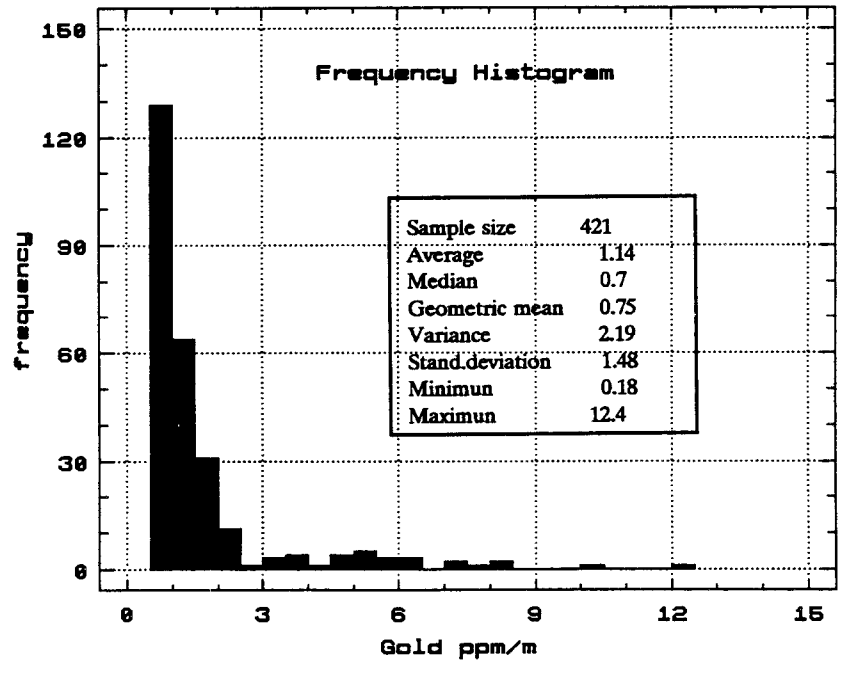

Fig.III - 11 : Histogram of gold contents in quartz veins extended to 1m thickness, from drill-core samples of Tomino area.

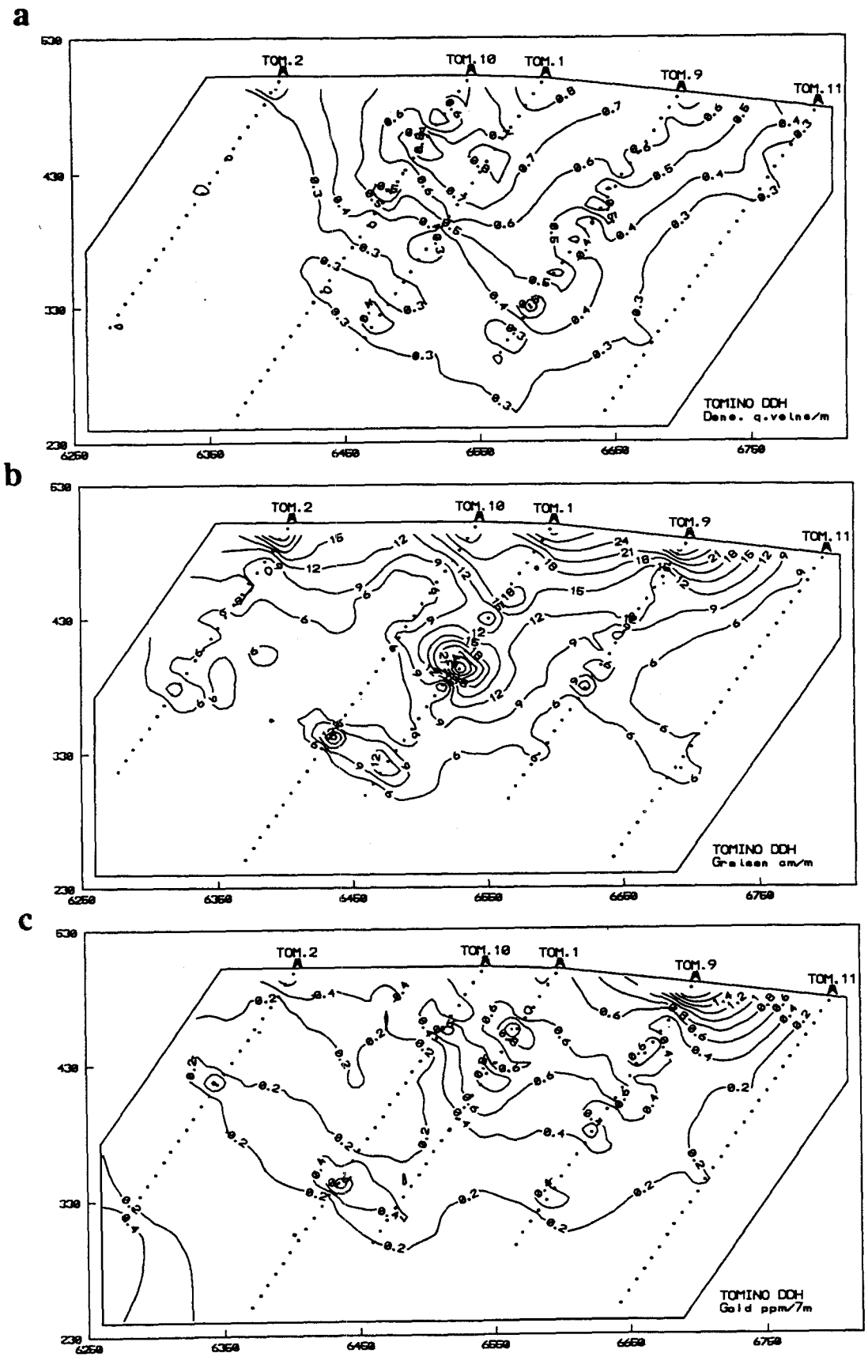

Fig.III - 12: Sections showing iso-values curves inferred from drill hole data of Tomino area.
a : density of quartz veins, b : density of greisen, c: gold content.

Thickness and frequency of the quartz veins

The thickness of mineralized veins intercepted in the drill holes ranges from simple fissures to decimetric quartz veins. The histogramm of figure III-10, based on 742 quartz veins, shows that 90% are lower than 10 cm width, 75% are lower than 5 cm and the maximum frequency is about 1 cm width. In relation with the development in depth and lateral extension of the individualized quartz veins, it can be inferred a length ranging between several meters and tens of meters, following a "en echelon" pattern. The orientation of quartz veins is fairly uniform, most of them being comprised between 60°E and 80°E, dipping a average of 78 °N .Gold content in quartz veins extended to 1 m thickness may reach 12,4 g/t but most of the data are ranging from 0,18 to 2,4 g/t (Fig. III-11).

The density or spacing between quartz veins ranges from short sections of higher density with decimetric to metric intervals, to sections with quartz veins at several meters distance. Figure III-12 shows the space distribution of the density of quartz veins inferred from the drill core information, refered to sections of 10 meters wide, and assigning to each section the average expressed in number of quartz veins by meter. It can be observed a higher density in the central part of the granite dyke, between DDH TOM.2 and TOM.11, decreasing from 100 m depth approximatly. In the southern part, it can be observed a more irregular distribution, with maximum concentration of quartz veins in the last sections of DDH TOM.4.

Geometric relationships between greisens and quartz veins

The greisenization of host rock adjacent to the quartz vein ranges from few millimeters to more than 1 meter, without existing any correlation between the width of the alteration zone and the width of the quartz vein. In the section of figure III-12 was attempted to represent the greisenization, inferred from data of drilling, assigning to each section of drill core of ten meters length, the average expressed in cm of greisen by meter.

Geometry of the late microfissuring

Orientated samples have been taken along a profile in the zone 3 of the Urgal zone, as well in two other places around 50 m to the south of zone 3 and in the Pedrada massif. Microfissuring is only represenred as fluid inclusion trails either in the granite or in the major quartz tension gashes.

The figure III-13 shows the application of the above mentionned methodology to the Tomino profile (zone 3) of the Pedrada massif. In the granite, at the vicinity of a mineralized greisen (0-3 meters from the vein) occupied in its middle place by a quartz vein, the geometry of the dominant fluid inclusion trails is clear, and dominated by the N80±10° direction. At 4 meters, the geometry changes slightly with the a sub-East- West dominant network (N110± 20°E).

In the vein itself, the geometry of the late microfracturing (microfissures formed after the vein N60° E) is dominated by fissures parallel or sub-perpendicular to the (N150°E) to the vein direction.

In the greisen sampled at 5 m to the south from zone 3, microfissures are orientated N120° and N40°E.

The number of cracks decreases from the vein towards the granite, indicating that the early alteration (greisen + quartz vein) has been produced by dense localized microfissuring N60-N70°E probably produced by local compression of the same direction (tension gashes). Therefore the density of cracks is dominated by the lithology. In the greisen, a part of the early cracks have disappeared due to the recrystallization of the quartz.

The chanellized fluid migration through cracks is at the origin of the granite alteration, and then of the quartz crystallization as sealing of major tension gashes.

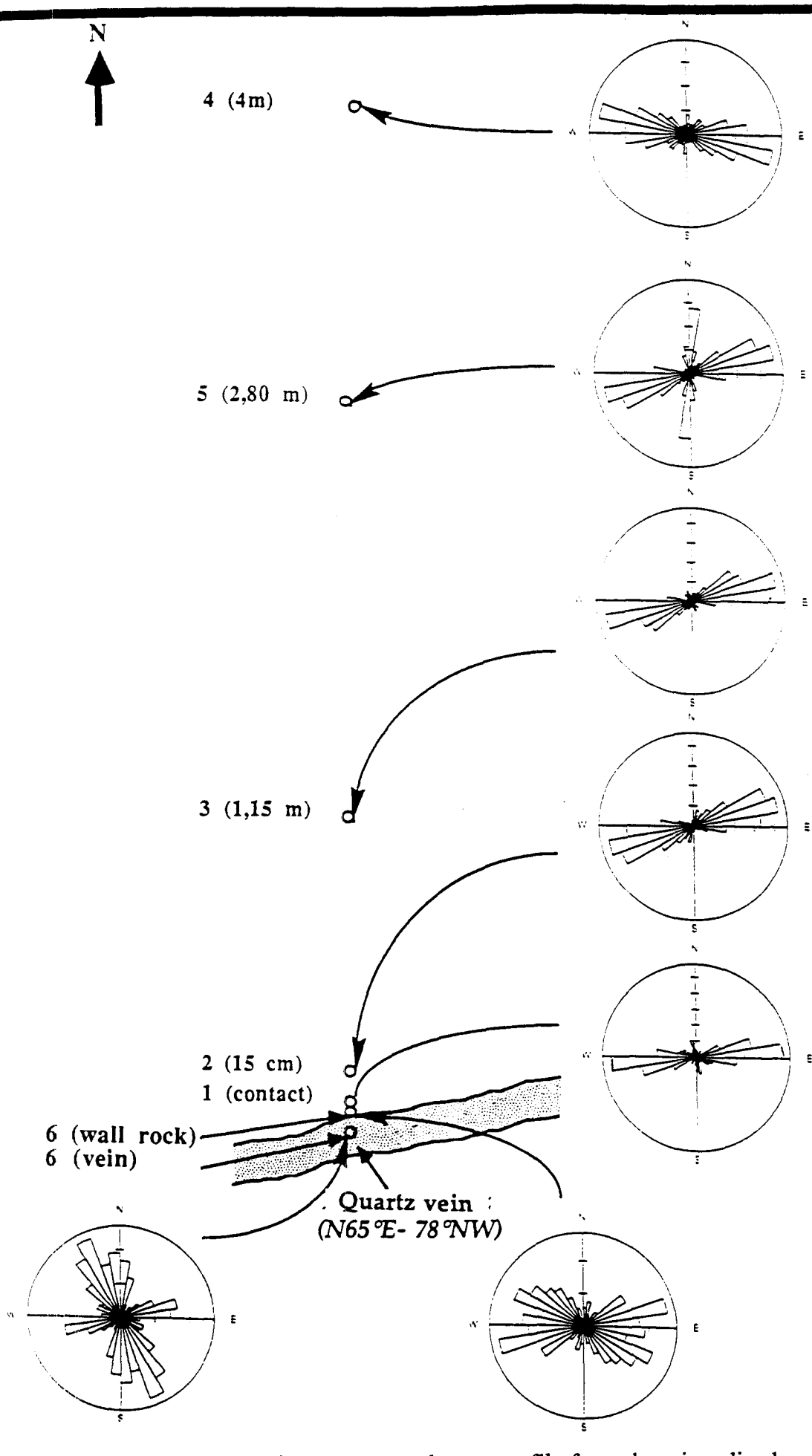

Fig.III - 13: Orientation of microstructures along a profile from the mineralized zone towards the granite from the Tomino area.

New reactivation produces the arsenopyrite crystallization, but a late brittle event is needed to get new microfissuring and mineralization.
At each stage there is a constant orientation of the microcrack network indicating a probable permanence of the major stress direction all along the hydrothermal history of the granite.

b- PENEDONO

Regional setting

The gold mineralization in the Penedono area is scattered among three important sectors that gave place formerly to three mine zones with underground labor. They are lined up along an axis striking NW-SE, corresponding to the edge of an hercynian antiform of the third phase (D3) with a regional extension of 30 km, from Armamar to Penedono. The center of this antiform is intruded by a composite granite massif and preserves small metasedimentary screens from the Douro Group of Cambrian age.

An extensive shear zone between Tomino - Braga - Amarante and Moimenta da Beira controls the regional structures: 1) during the D 1 deformation event, the wrench senestral component of shear in the socle gives rise to the typical arc pattern of the Variscan Fold Belt, the structural imbrication in the overlying formations and emplacement of the NW Iberian nappe system; 2) the dextral wrench regime in the D3 event gives place to a partial melting of crustal portions and produces in the covered formations folds "en echelon" with horizontal axis and sub vertical planes that forms variable angles relatively to the major shear; at last, during D4 event, the regional metamorphism decay implies a brittle dextral deplacement, conjugated of the N.NE-S.SW late hercynian faults.

Local controls of the ores

The three gold mines of the region: i) Vale de Peneda-Dacotim, ii) Laboreira-St Antonio and iii) Ferronha, are structurally controlled by minor senestral shear zones oriented E-W to E.NE-W.SW. These structures form conjugated systems of the regional major shear lineament Tomino - Braga - Amarante - Moimenta da Beira, dextral during D3, oriented N 65°W, sub vertical and located 10 km west to Penedono (Fig. III-14). The non-coaxial character of the induced shear deformation was put in evidence in other regions (Berthe et al, 1979; Iglesias and Chouckrounne, 1980). This fact is evidenced by the continuous change of the angle between the strike of the folds and the major shear plane, decreasing as they approach each other.

Each shear set controlling the referred mines have a ductile-brittle behavior and they are responsible by a fracture system, following the classic experimental models (Tchalenko, 1970), or based in field observations (Gamond and Giraud, 1982). The deformation within these bands is polyphased. We have established a coherent model consisting of three main phases of deformation (D3, D'3, D4) which is consistent with the paragenetic analysis found by Sousa and Ramos (1991). The amount of movement along the shear zones and their ductility increase towards NW, representing each of the three mines a particular model of the same major process:

i) - Vale de Penela - Dacotim (Fig.III-15)

The intragranitic vein field is developed by a ductile shear zone with very close C and S planes (Fig.III-16), oriented N80E and N (70-80)W, respectively, both sub vertical. The strike-slip ductile displacement (D3) engendered a traction gashes system with an "en echelon" distribution (Fig.III-17). Five of these gashes are the main veins, with metric width and hectometric extension and As-Au mineralization. The successive movements and correlative incremental deformation ( ) along the shear zone deflects the "T" gashes with a decreasing in the angle with "C" planes. A system of secondary gashes R, R' and P, develops a slight opening and in spite of this large distribution in the area the mining potential is very limited (Fig.III-18).

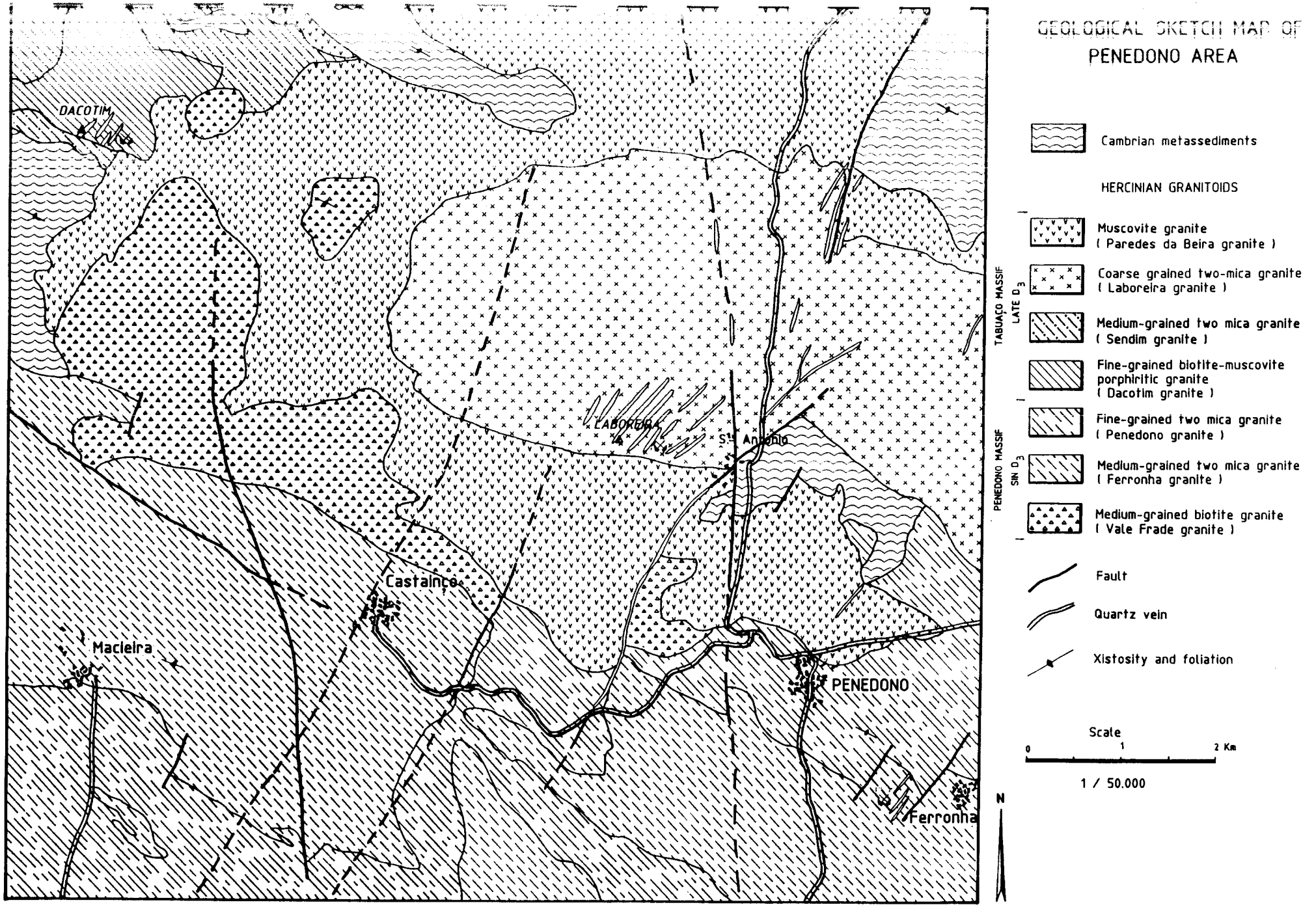

Fig.III - 14: General geological map of Penedono area

DACOTIM MINE (PENEDONO)

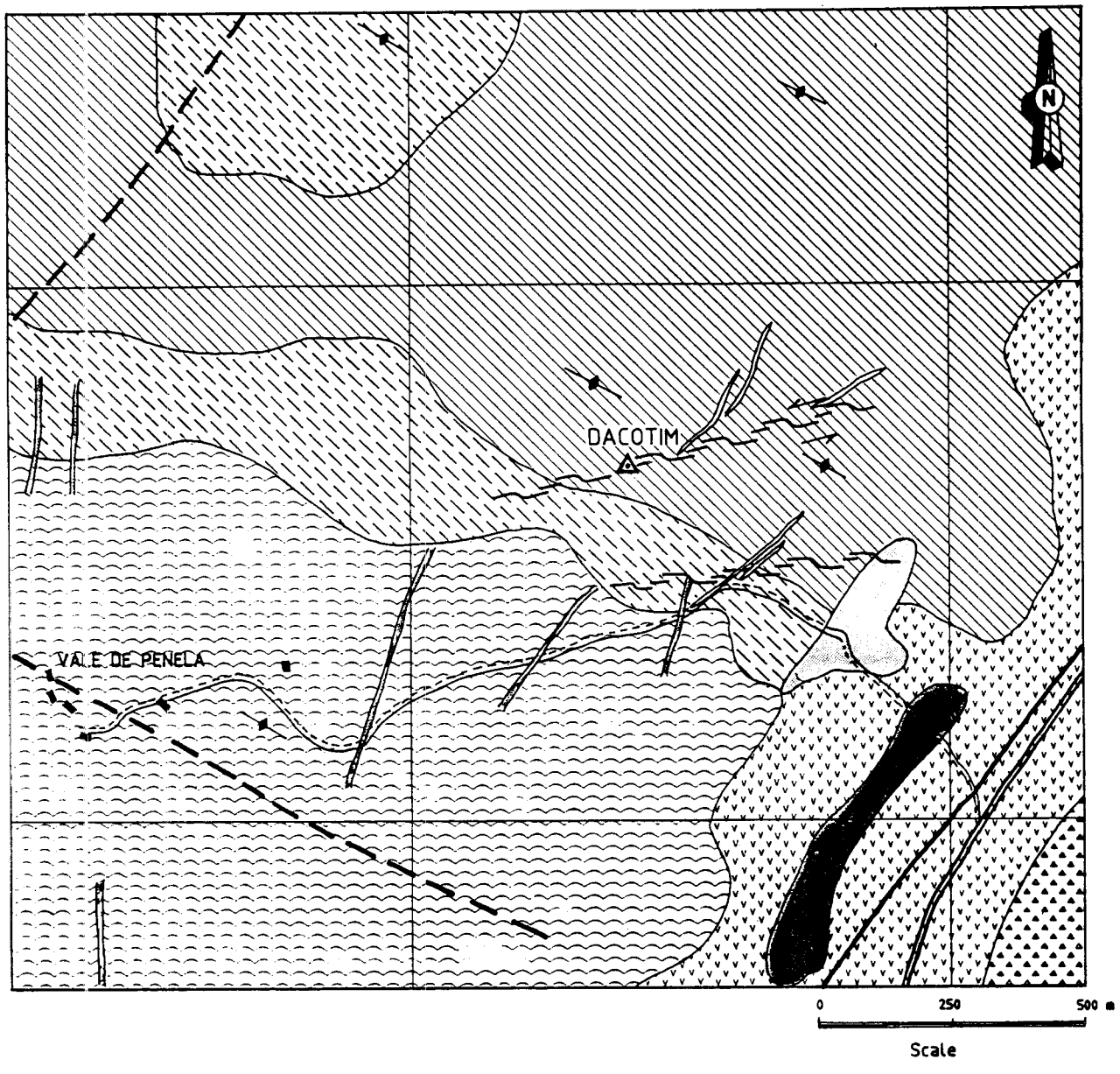

LEGEND

- Alluvium
- Cambrian metassediments (Douro group)
- Dacotim granite porfiritic fine grain with biotite-muscovite
- Paredes da Beira granite medium grain with muscovite, turmaline, scorzalite and trifillite
- Sendim granite medium grain and two mica
- Vale Frade granite porfiritic, medium grain, biotite-moscovite
- Aplite and aplopegmatite veins
- Quartz veins
- Observed / Infered Fault
- Shear zone (sense of movement)
- D_3 foliation

Fig.III - 15 : Sketch geological map of Vale de Peneda-Dacotim

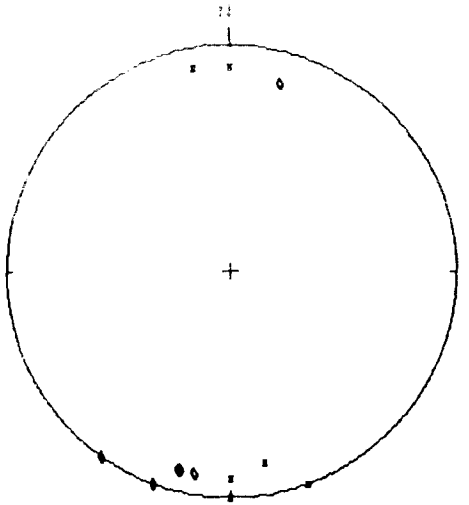

x "C" plane n = 14
◊ Granit foliation n = 12

Fig.III - 16 : Schmidt net, lower hemisphere projection for Dacotim area, with indication of the orientation of "C" plane and granite foliation .

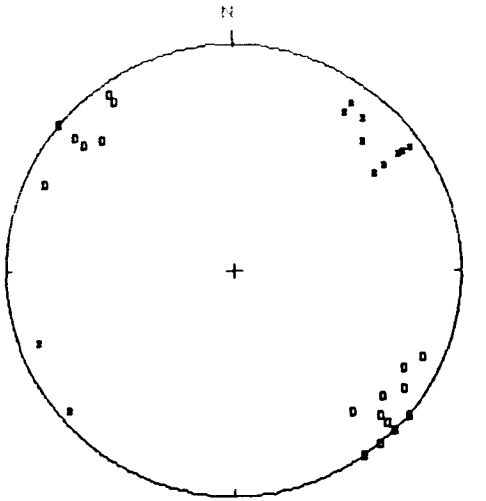

▯ Tension gashes n = 44
▮ Striae on the tension gashes n = 22

Fig.III - 17 : Schmidt net, lower hemisphere projection for Dacotim area, with indication of the orientation of tension gashes and sense of striated planes.

n = 34

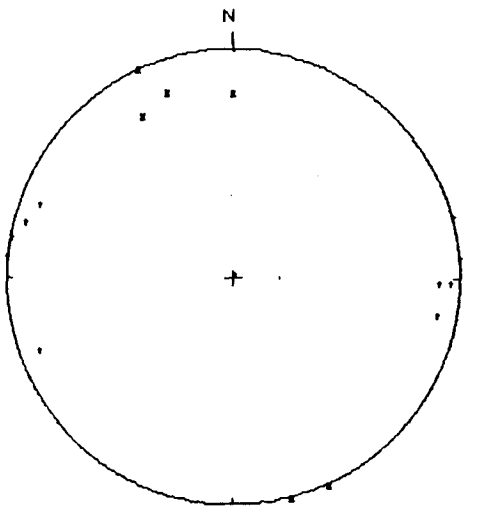

◊ Riedel conjugated fractures n = 22
x Riedel Fractures n = 12

Fig.III - 18 : Schmidt net, lower hemisphere projection for Dacotim area, with indication of the orientation of R, R' fractures.

Fig.III - 19 **GEOLOGICAL SKETCH MAP**

LABOREIRA - MONTE AIROSO - ARCAS

(PENEDONO)

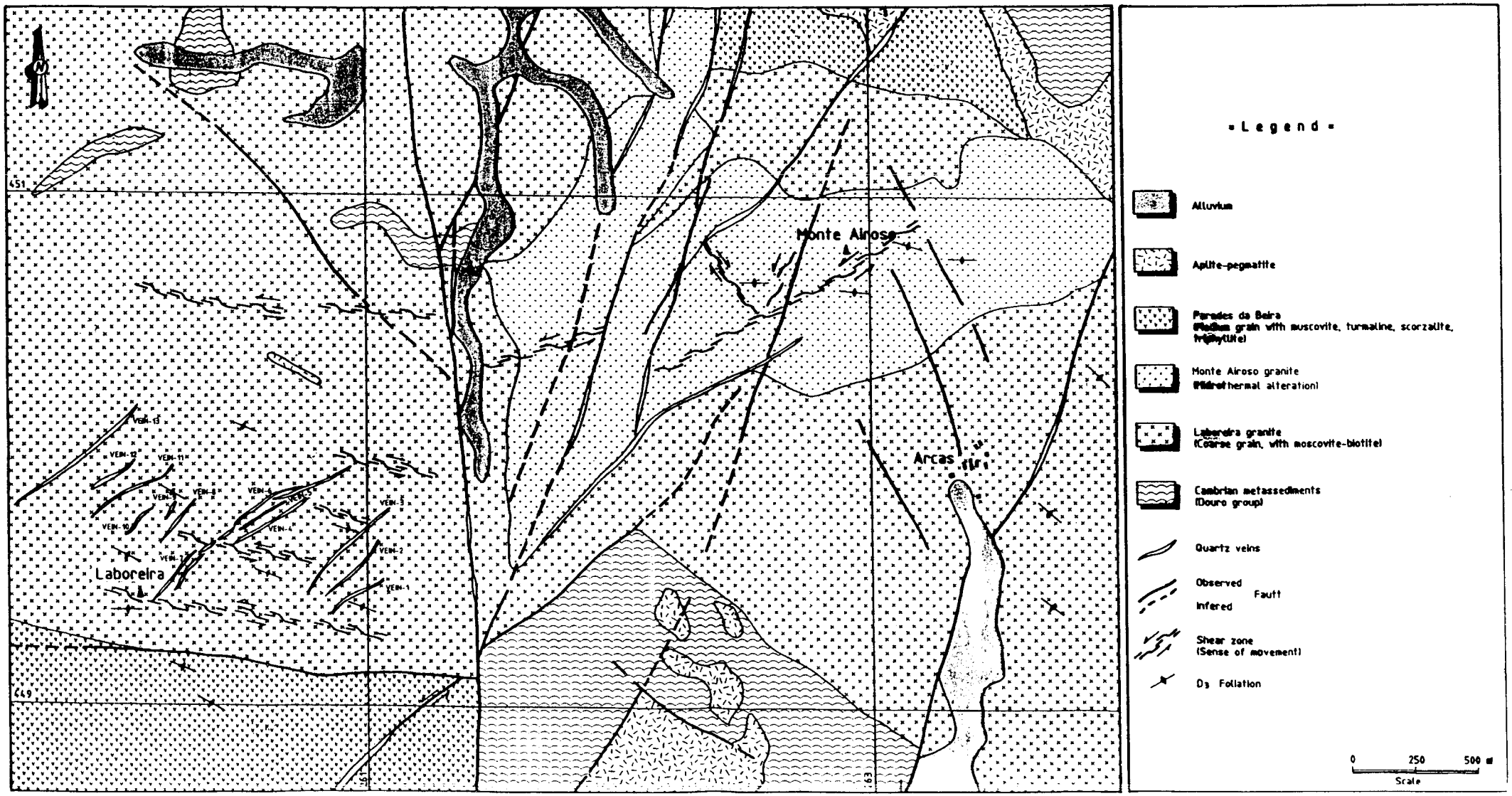

1:45

ii) - Laboreira - St Antonio (Fig.III-19)

St Antonio mine is located at Laboreira granite (Fig.III-19), within a senestral E-W sub vertical shear, with kilometric width and 4-5 km of extension. The shear is responsible by the opening of 13 traction gashes oriented N45W, 0.5-1 m width (Fig.III-20) where is emplaced a first phase of quartz, arsenopyrite pyrrotite and gold.

The shear is a senestral conjugate of the big dextral shear Tomino - Moimenta da Beira. The movement along this last shear is more intense in D3, affecting all the west part of the hercynian chain. In consequence the minor shear of Laboreira - Arcas is successively reactivated with senextral movement after the opening gashes and formation of minor fractures Riedel and X-P (Fig. III-21)

The progressive senestral of the primary gashes in D'3, produces the fracturation of all the system, creating new secondary tension gashes as well as new riedel systems, that can also be open.

This kind of transitional ductile-brittle movement is well seen at Monte Airoso. Here the senestral shears are oriented N55°E and occur also the conjugated N45°W, dextral (Fig.III-22). In a way, this corresponds to a late eastern extension of the Laboreira shear zone.

The ductile-brittle process induces a second phase of mineralization with the fracturation of the preliminary one and deposition of a second generation of quartz, gold, pyrite, wolframite and intense greisenisation.

A late hercynian brittle phase (D4) affects all the system. This last one due to the rotation of the maximum stress G1 to approximately N-S, creates senestral transcurrent faults oriented N20°E , subvertical. The rotation of the G1 to north produces either reactivating of all preexisting fractures with senestral movement when they are in the E quadrant, or dextral movement when situated in the W quadrant; at the same time the associated transcurrent faults produce the rotation of inter fault blocks within the granitoids. This fact is emphasized in Monte Airoso by the general rotation of the granitoid foliation to W.

This brittle movement fractures the former mineral phases followed by the deposition of bismutinite, bismuth, galena, electrum, sulfosalts and tellurides identified by Sousa and Ramos (1991) and confirmed by the present work.

iii) - Ferronha (Fig.III-23)

The vein field is located along the contact between two different granitic facies, one medium and the other fine grained, both exhibiting strong muscovitization and turmalinization. The system of mineralized veins with W, As and Au, corresponds to four major Riedel gashes (R), with metric opening and kilometric extension (Fig.III-24) The shear responsible for the gashes is dominantly brittle, with C and S planes having angles with more than 30° (Fig.III-25), producing a system of traction fractures T, almost closed, sometimes with a millimetric filling of quartz, with wolframite and arsenopyrite.

The granite that contacts these gashes is strongly greisenized, occurring, by differential erosion, as small crests of greisen. They have an " en echelon" distribution, and they are located at the end of the R fractures, or in distensive blocks between the gashes (Fig.III-26). The successive movements react along the R gashes sub parallel to C planes producing the brecciation of the filling material and cementation by later hydrothermal phases (Fig. III-27).

Microstructural study

Oriented samples have been taken along a profile from the vein towards the granite in the Dacotim area. Microfissuring is represented by fluid inclusion planes either in the granite and in the quartz veins

In the quartz vein and in the closed host rock, the major direction is EW. In the granite, located at around 30 meters from the quartz vein, a more complex distribution of fluid inclusions planes have been observed (Fig. III-28). A major direction oriented N 120-130°E, and an E-W direction are observed. Other fluid inclusion planes with intermediate directions from NS to EW are present but remain minor.

The major direction orientated E-W correspond to a major event of fluid circulation in the quartz vein and in the host rocks recognized at a relatively large scale.

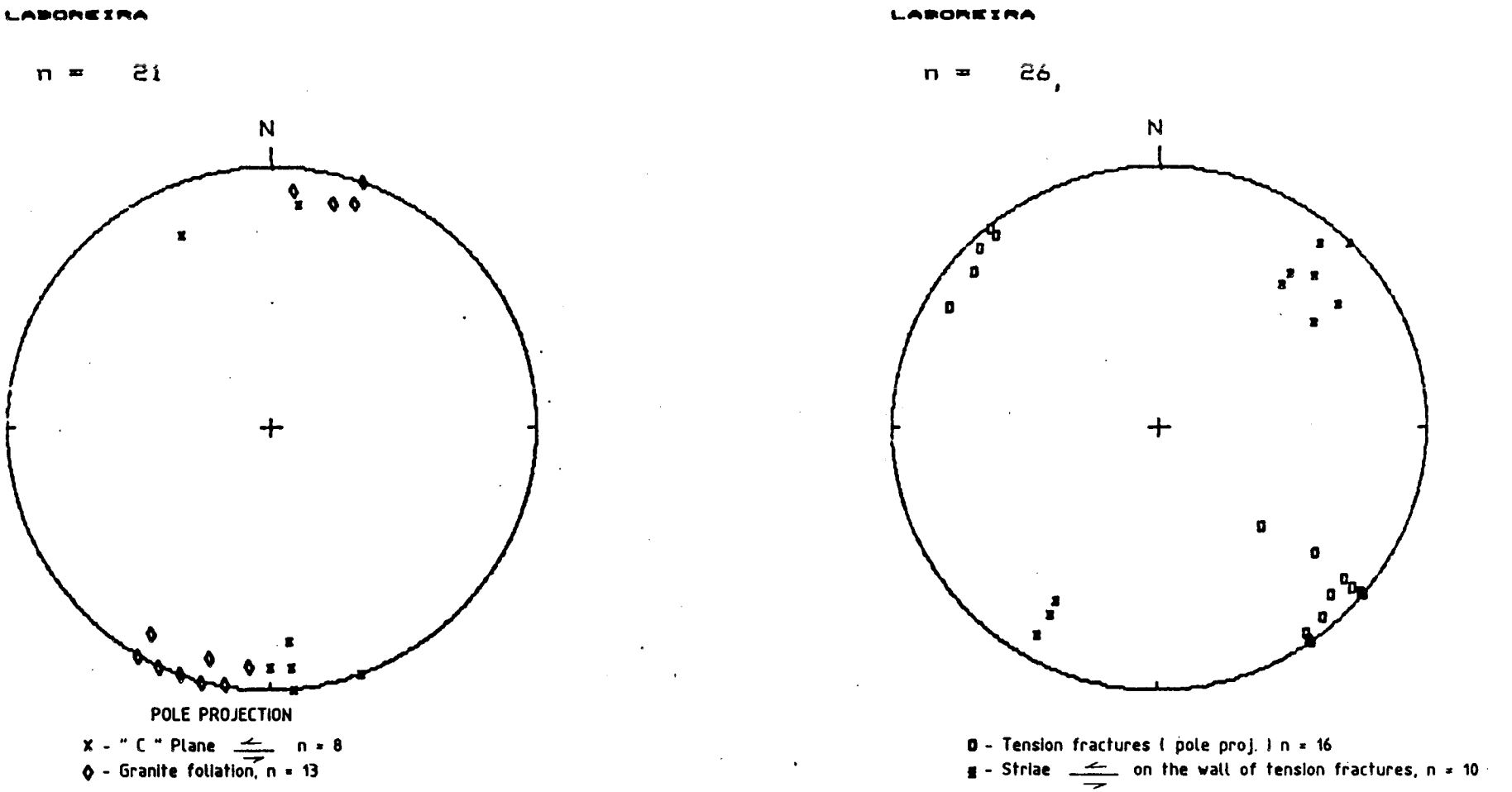

Fig.III - 20: Structural projections of St Antonio, Schmidt net, lower hemisphere projection.

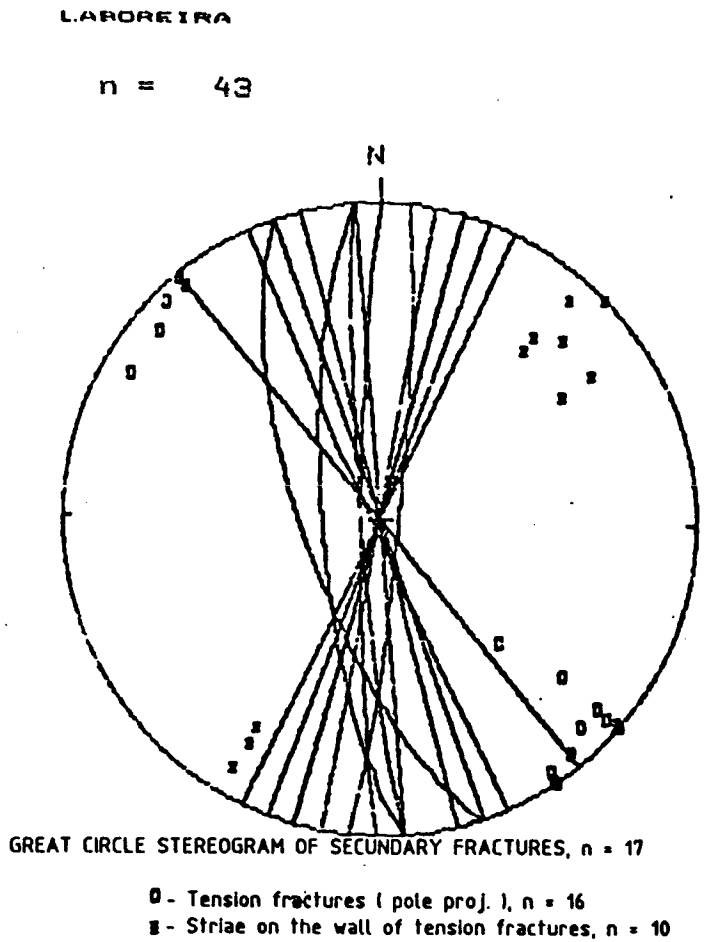

Fig.III - 21 : Structural projections of St Antonio, Schmidt net, lower hemisphere projection.

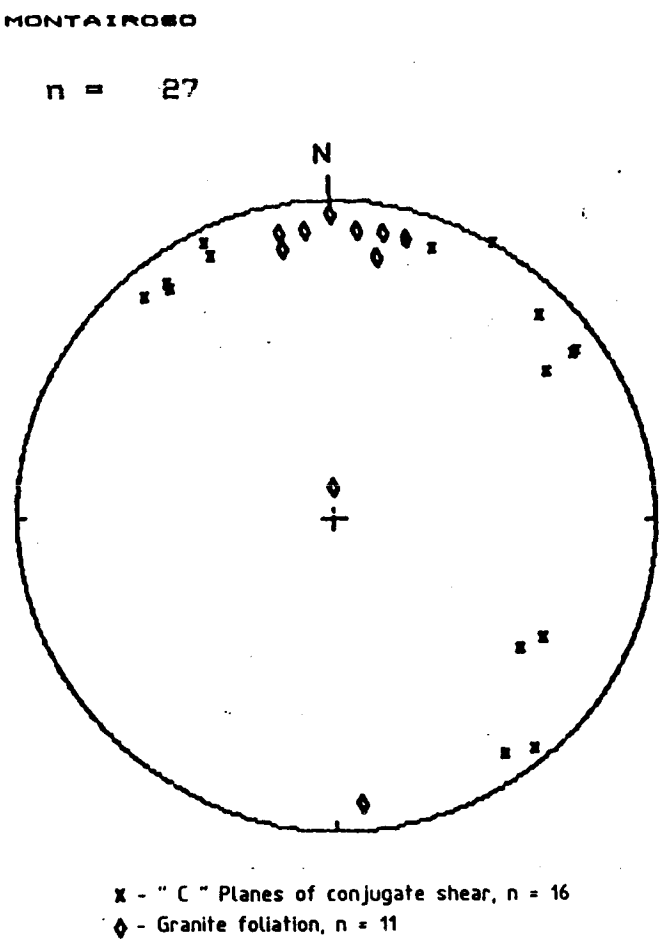

Fig.III - 22 : Structural projections of Montairoso, Schmidt net, lower hemisphere projection.

FERRONHA MINE (PENEDONO)

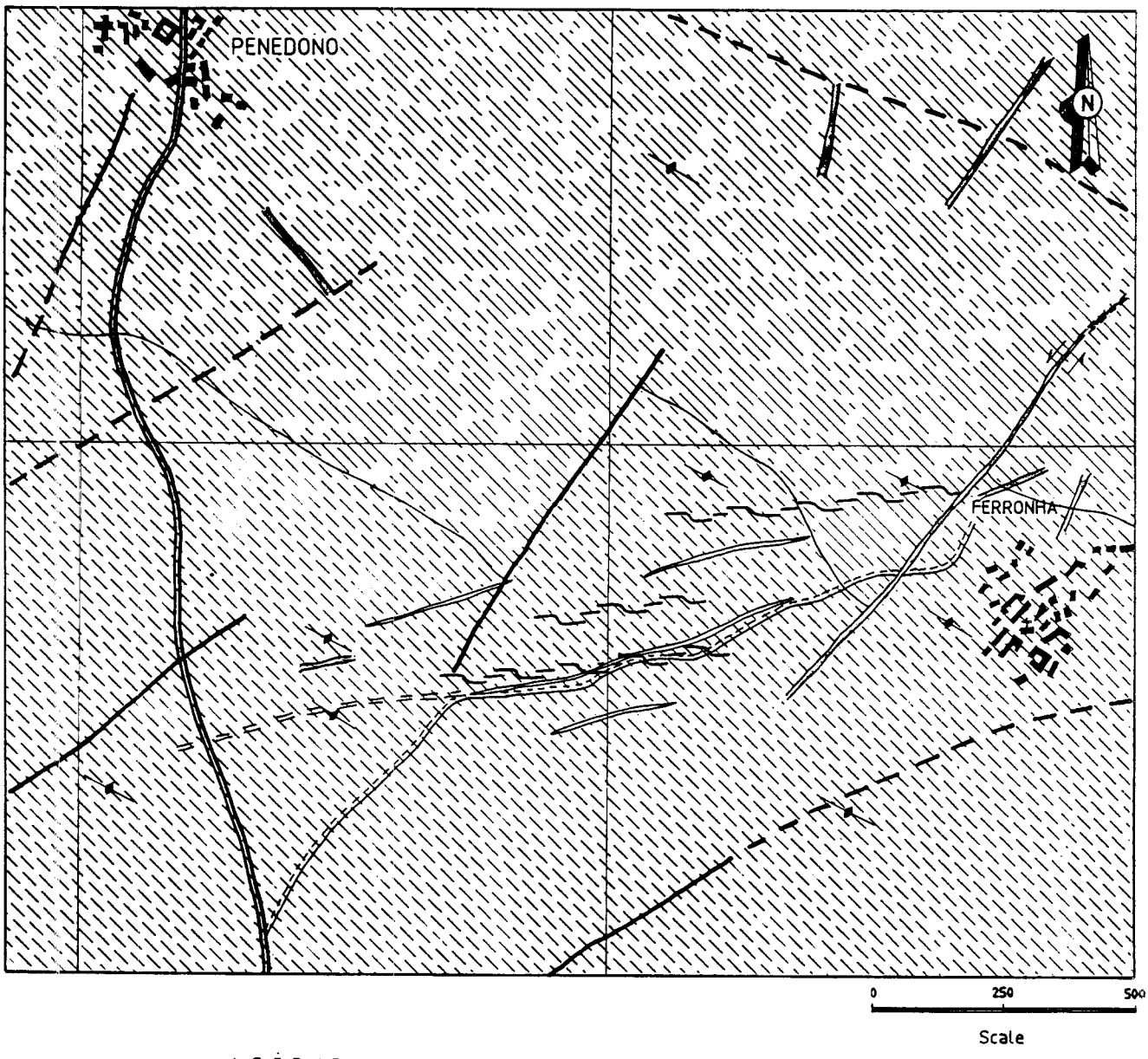

LEGEND

- Ferronha granite
  medium grain, with moscovite-biotite
- Penedono granite
  fine grain, with moscovite-biotite
- Quartz veins
- Aplite or aplopegmatite veins
- Observed / Infered Fault
- Shear zone
  (sense of movement)
- D foliation

Fig.III - 23 : Sketch geological map of Ferronha

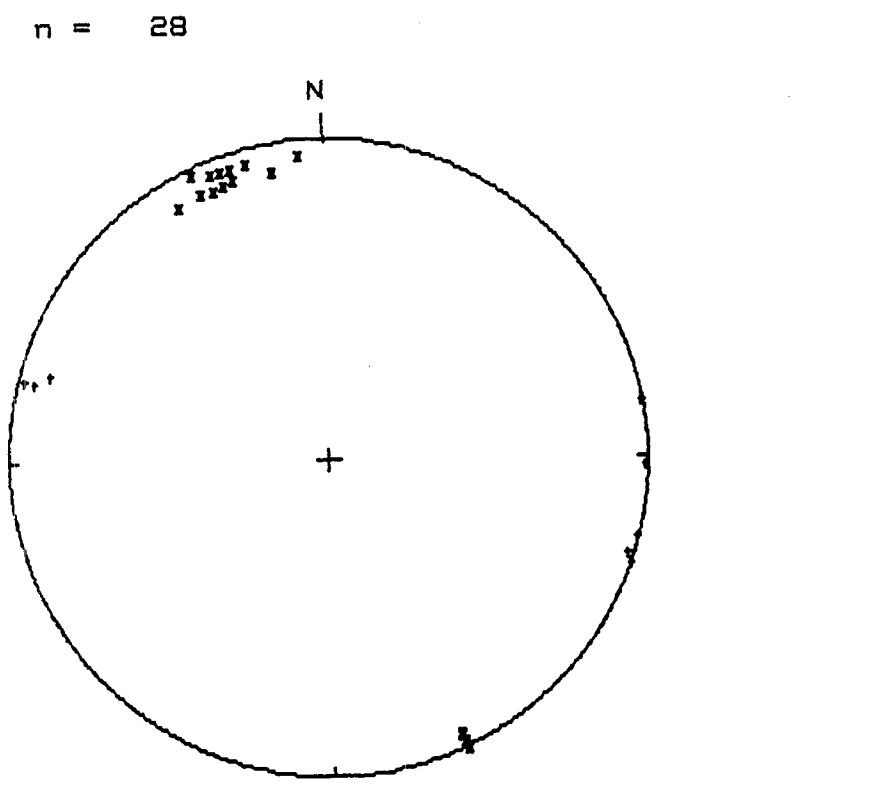

Fig.III - 24: Schmidt net, lower hemisphere projection for Ferronha area, with indication of the orientation of R, R' fractures.

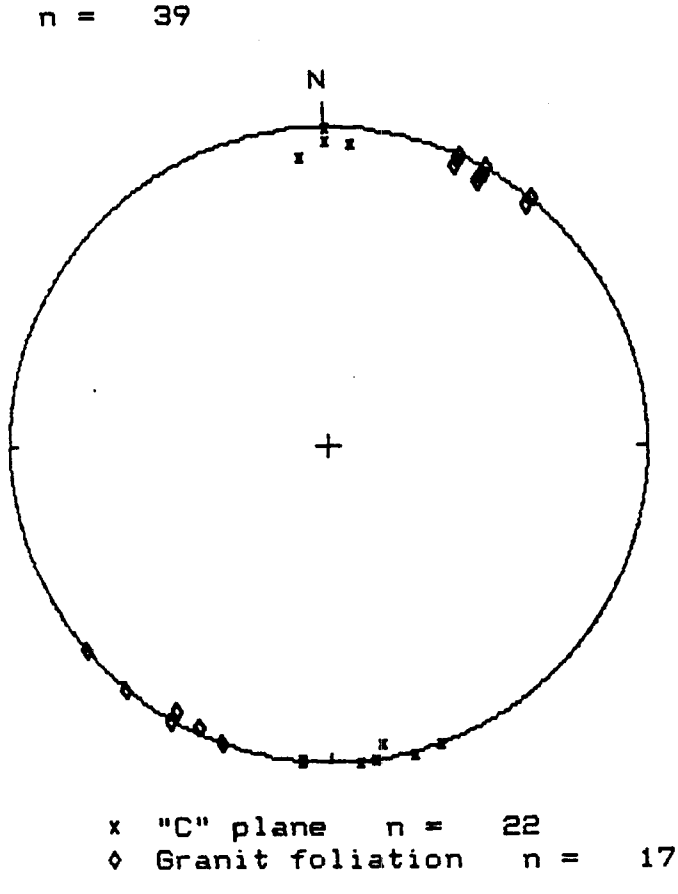

Fig.III - 25: Schmidt net, lower hemisphere projection for Ferronha area, with indication of the orientation of "C" plane and granite foliation .

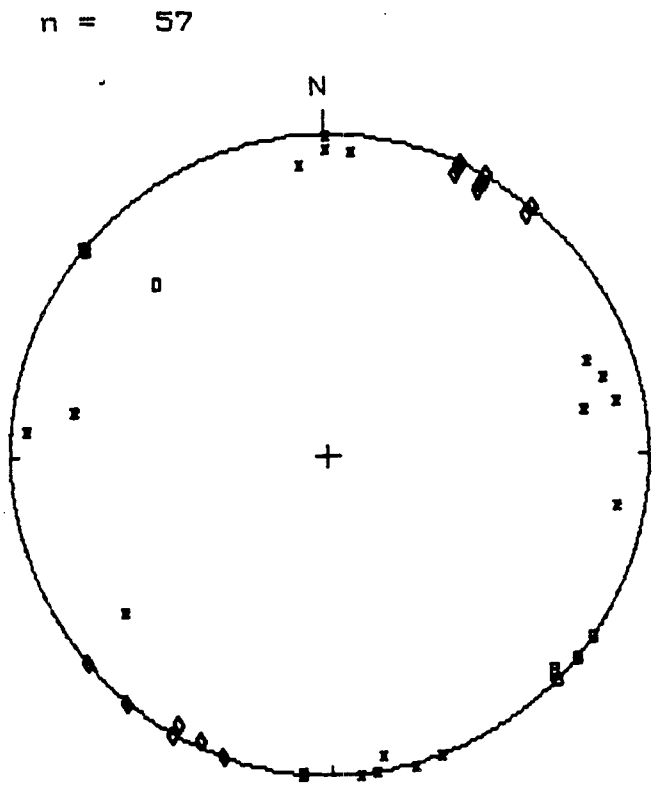

Fig.III - 26: Schmidt net, lower hemisphere projection for Ferronha area, with indication of the orientation of "C" plane, tension gashes, striated planes and granite foliation .

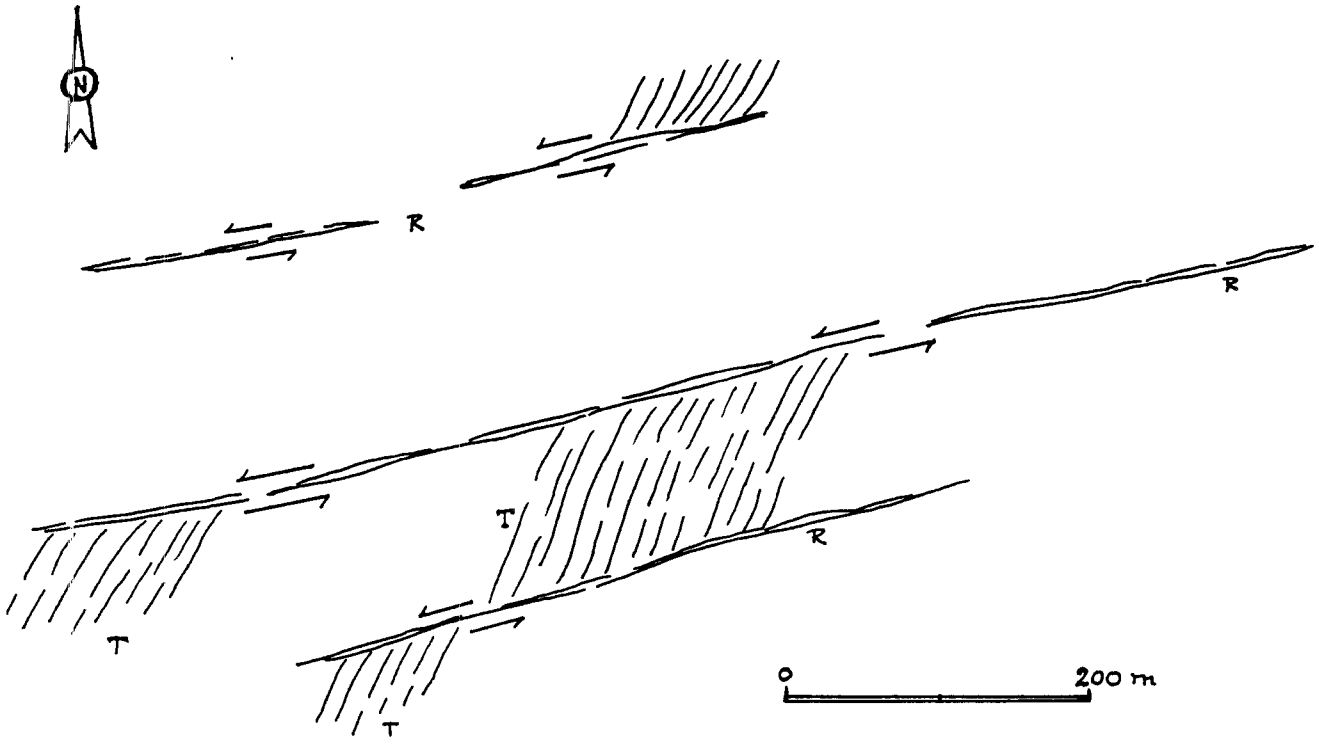

Fig III - 27 : Ferronha area - plane of the R, T gashes.

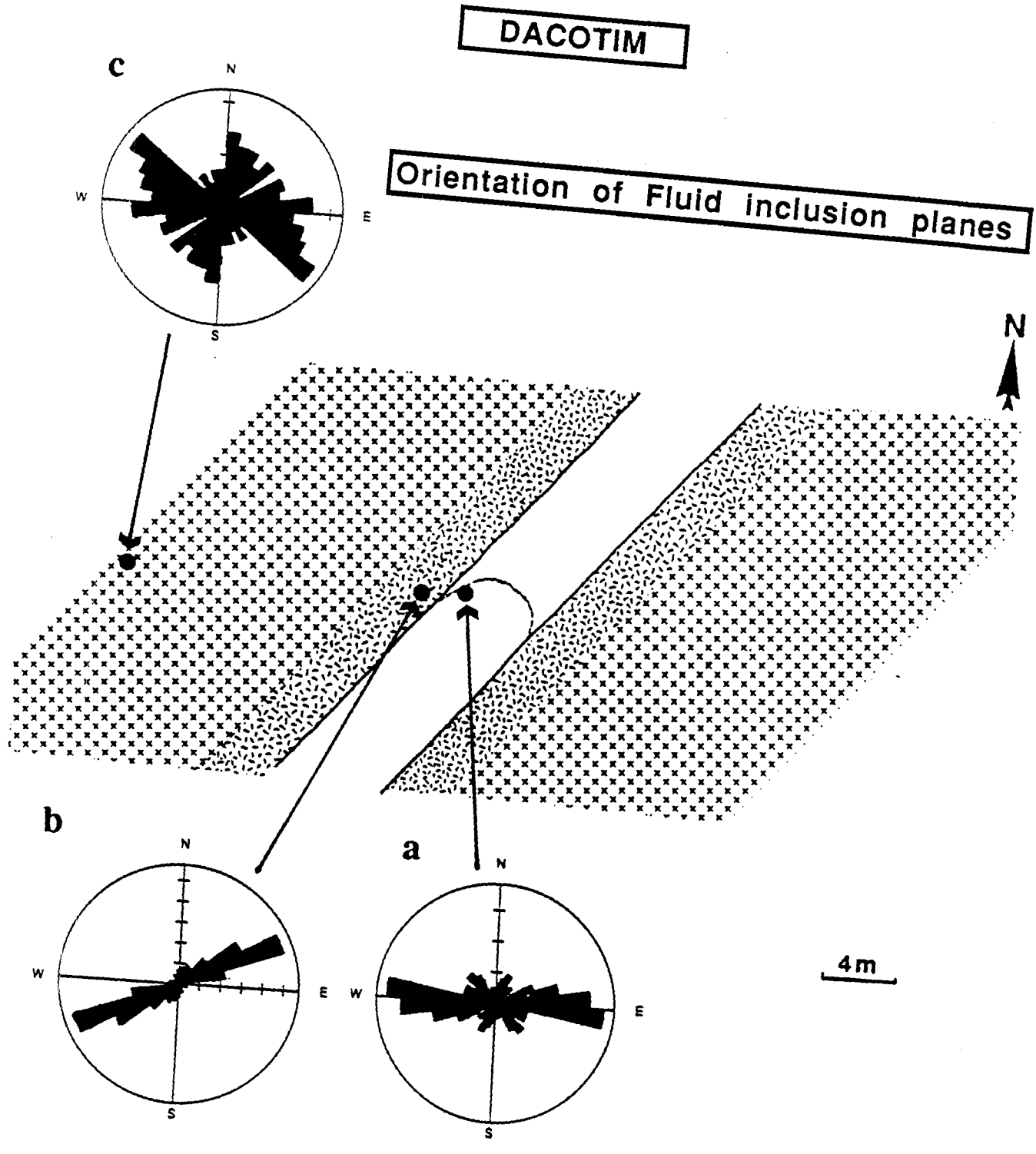

Fig III - 28: Orientation of fluid inclusion planes along a profile from the mineralized zone toward the granite from the Dacotim area. a : quartz vein, b : altered granite at the wall of the quartz vein.

C - STRUCTURAL CONTROL OF THE MINERALIZATION IN THE FRANÇA AREA.

1 - REGIONAL STRUCTURAL FEATURES.

A ductile-brittle regime during D1 was responsible for the development of N20°W and N80°E shears, dextral and senextral respectively (Pereira, et.al. 1984; Ribeiro, 1974). The former sttructures show an important rotation towards SE with a change in strike to N60°W, attributable to the variscan virgation.

Associated to the regional strain and to the beginning of the thrust nappes emplacement, the D1 deformation phase is marked by inclined folds with vergence to NE, recognized at different scales. A penetrative axial planar slaty cleavage was developed associated to this deformation event. It shows a N110°E/60°SW average atitude. In the D1 variscan phase the maximum strain had NW direction with the XY plan dipping to SW (Fig. III-29 and 30).

With the emplacement of the Bragança allochthonous terrains, important D2 thrusts are developed in the authocthonous metasediments. The D2 phase is linked to these thrusts and is characterised by kink band or shear kink band folds with vergence to the SW. An axial planar crenulation cleavage, subhorizontal or gently dipping to NE is associated to these folds. Generally only one fold system is present but it is possible to find locally the conjugate fold system (Fig. III-31).

The morphology of these kink folds with the thrust planes was already referred in Ribeiro (1974). In general the occurrence of antithetic folds both in the hangingwall and in the footwall of the thrust plane are more common in the studied area. Some situations of antithetic folds in the hangingwall and synthetic in the footwall also occur.

The third phase of deformation (D3), coaxial with the other cleavages, is expressed by the upright of the former structures and the development of ductile-brittle shears, specially reworking the D2 N120° thrusts with dextral movement.

This transpression movement produces open, vertical folds with the regional bending of the former cleavages. A vertical axial planar fracture cleavage is associated with these folds (Fig. III-32). In some cases this refolding is so intense that even the D2 cleavage suffers a change in its dipping (Fig. III-30 and 31).

During D4 all these structures are rotated to N70E in a band 2 Km width. To the East of this fault those structures recover their original strike. Within this mega kink band all the former lineaments are reworked with senextral movement and thrust faulting associated. This regional, brittle and late deformation events is responsable for the late - variscan fracture network, which includes the Vilariça strike-slip fault system.

B - GEOMETRY OF THE DEPOSIT AND ITS RELATIONSHIPS TO GENERAL GEOLOGY.

All the Variscan deformation phases have significant hydrothermal activity. From the field observation of the local geology it seams clear the role of these structures in the control of the ore, namely the most brittle phases, D3 and D4.

The first deformation phase is distinguished by centimetric/decimetric white-grey segregation quartz veins. Some of them have the same strike of the slaty cleavage and are folded by it. A second set of quartz veins are N50°E and probably related to the N80°E shear. The Sn quartz veins of the Montesinho mine are the best known example of quartz veins generated in the semi-ductile D1 shears.

These veins are affected by the subsequent deformation phases. In the Ordovician slates, on the road between França and Montesinho, some examples of quartz veins deformed by D2 can be seen. Examples of these veins deformed by D3 occurs namely at 1 Km south of v.g.

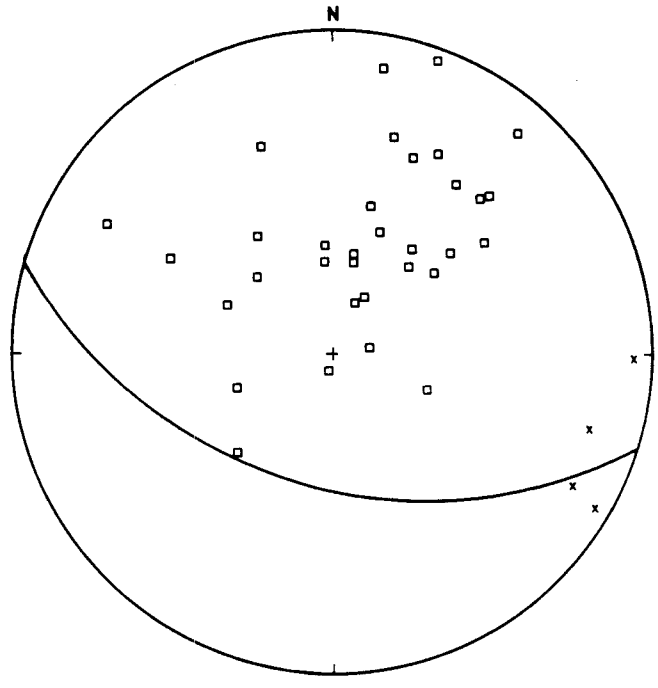

□ - Poles to bedding

x - Poles to fold axis

Average plane = N 104 E/56 S

Fig III - 29: Polar projection for ore bedding and fold axes in França. Schmidt net, lower hemisphere.

FRANÇA SLATY CLEAVAGE S_1 AND STREACHING LINEATION L_1

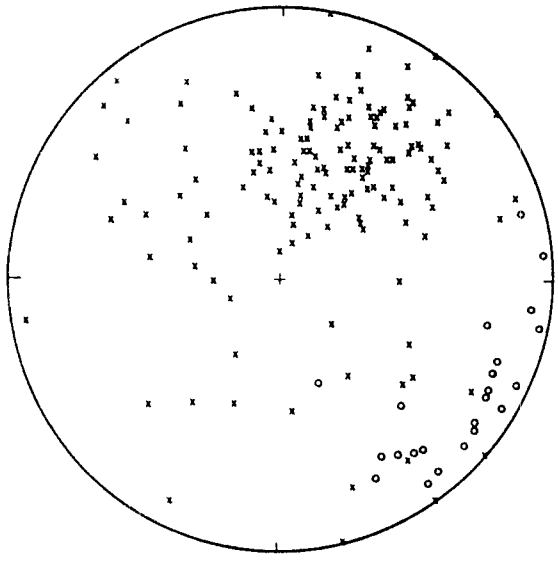

x - n = 156 poles to cleavage

o - n = 24 poles to lineation

Schmidt net, Lower hemisphere projection

a)

FRANÇA S_1 CONTOUR DIAGRAM

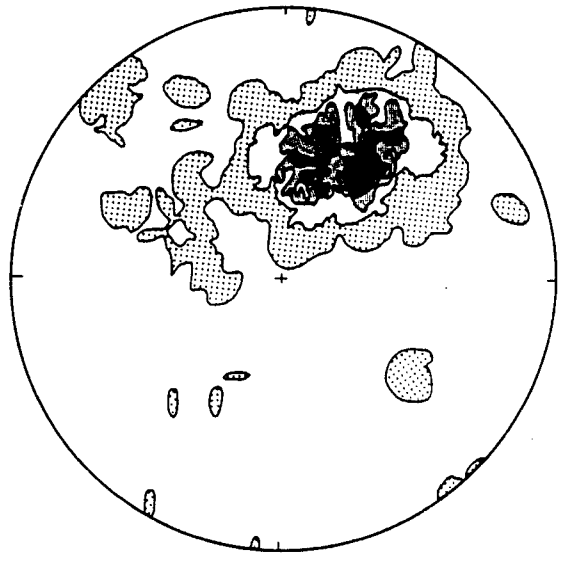

Schmidt net, Lower hemisphere projection

Contours at 1% 4% 6% 8% 10%

max. 12,2% dip 47% towards 38,7%

b)

Fig III - 30: S1 polar projections for França structures. a : slaty cleavage S1 and streaching lineation L1, b : S1 contour diagram.

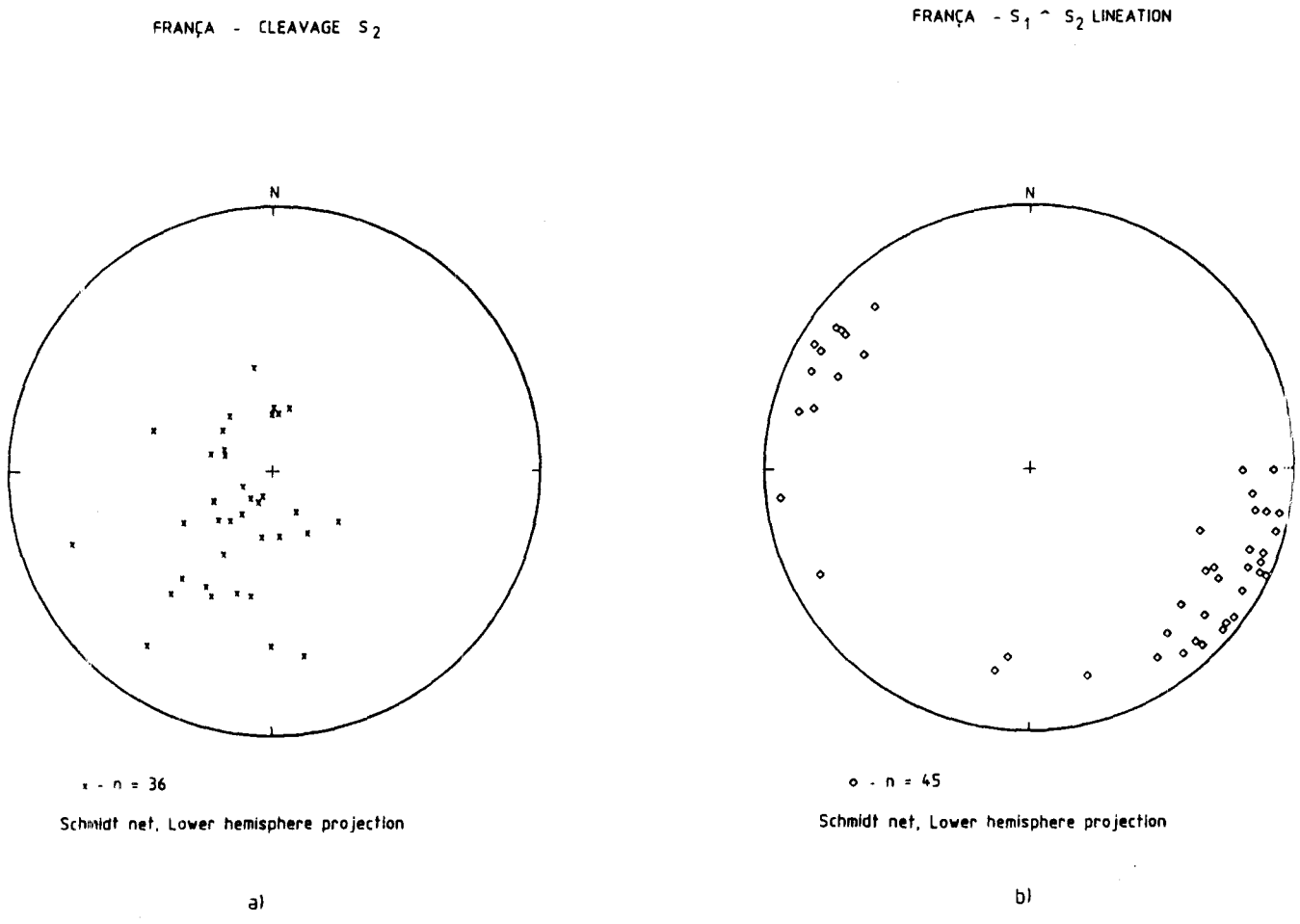

Fig III - 31 : S2 polar projections for França structures. a) S2 cleavage, b) S1-S2 lineation.

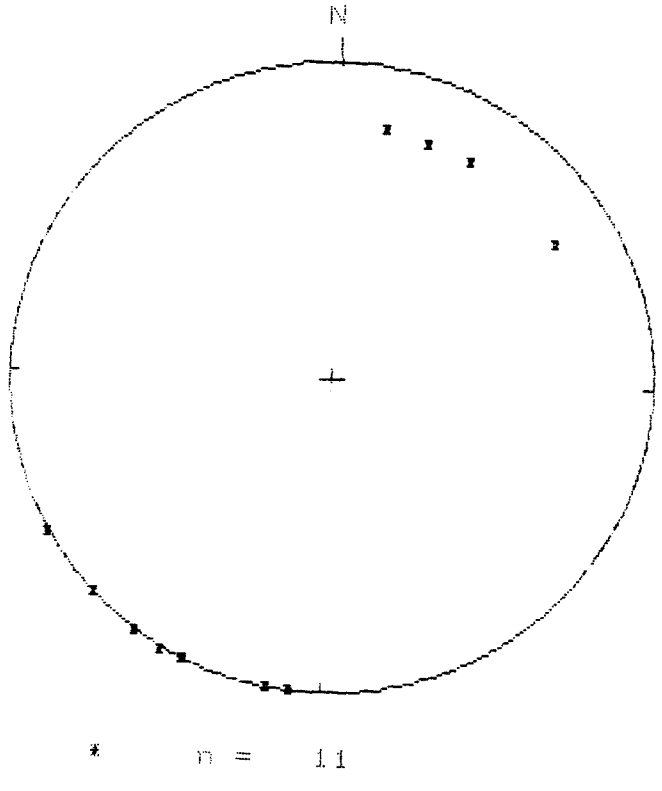

Fig III - 32 : Polar projection for França D3 cleavage.Schmidt net, lower hemisphere

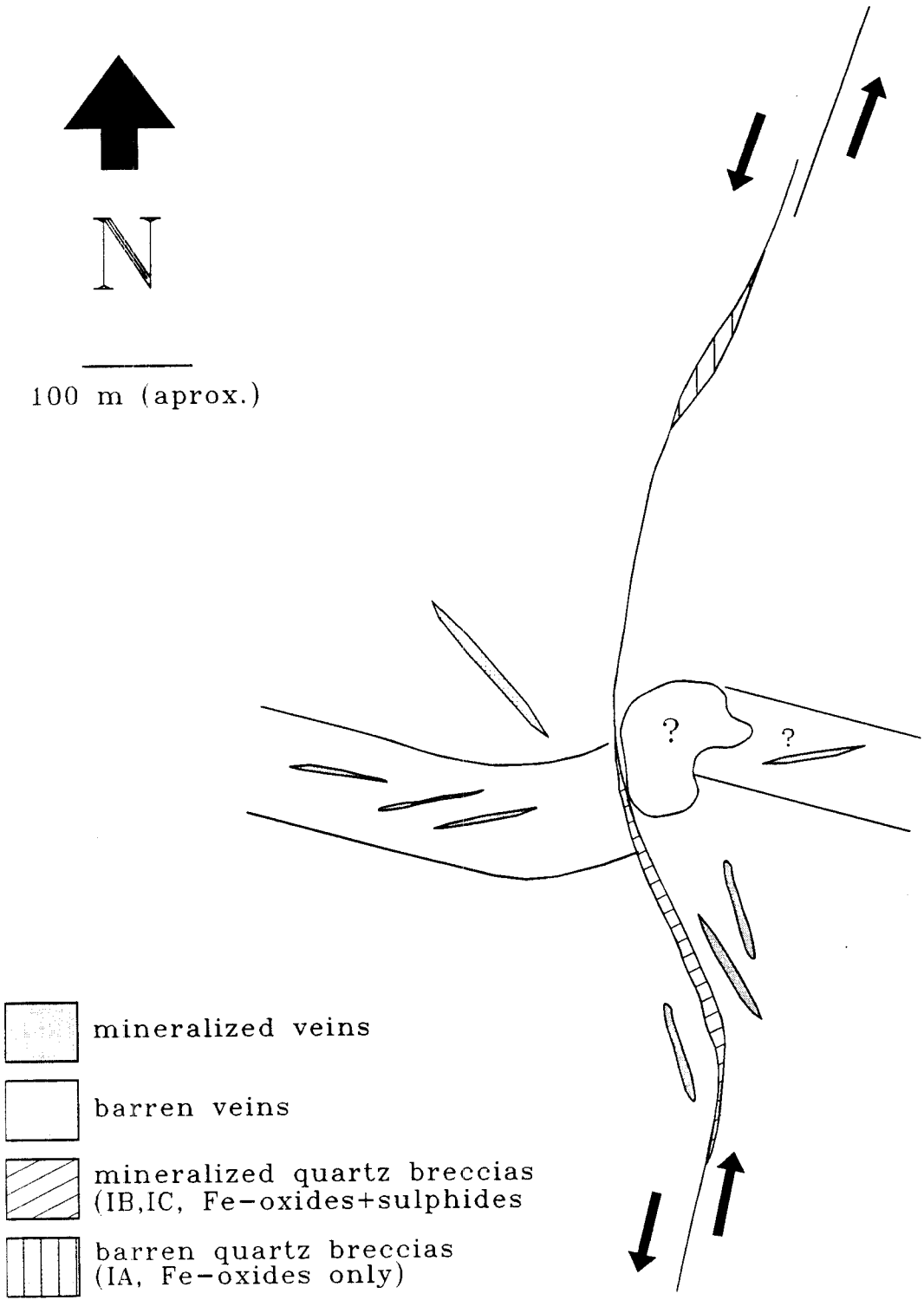

Fig III - 33: Structural interpretation of the Variça fault with indication of the mineralized or barren veins.

Coroto, where is evident the "boudinage" of the vein caused by the D3 dextral shearing along the slaty cleavage.

The NW-SE D2/D3 shears have fault gouge with an iron rich matrix. Large white quartz veins related to a lake of compression in the D3 phase also occurs.

Field mapping and the photointerpretation confirms that the D1/D3 N80°E lineaments are more common in the Ordovician metasediments. The N60°W conjugate set have also a good regional expression, even affecting the Montesinho granite. In the Silurian metasediments this D3 dextral lineament is more evident. Yet the conjugate fault and related tension fractures are also present and probably responsible for the Vilariça fault bending N40-60°E, that occurs between França and Rabal villages.

At a regional scale, it is impossible to precise at the moment if the Au occurrences known in the França area are just associated to the Vilariça fault or similar D4 brittle structures. During the field mapping made in this project, a small ancient mining work was discovery in the same lineament of "Boca da Caborca" open pit (300 m long * 100 m width *70 m depth). They are 2 Km W far away from the influence of Vilariça fault system, clearly implaced in one of the N80°E sinistral shears. The enigmatic "Boca da Caborca" open pit is now understood by the example of "Pena de eguia" where the shear is still preserved and the brecciated, highly oxidized, infill was the main target.

The structural analysis of the França lode gold–silver deposit indicates that the setting and geometry of the main mineralized veins are controlled by the Vilariça, NNE–SSW, strike–slip fault system (Fig. III-33). As a matter of fact, the irregular N15–30W quartz–siderite veins are subsidiary structures of the Vilariça accident related to a major releasing bend, where the fault zone trends N20–30W, on average. These veins show discontinuous development and, in general, exhibit centimetric length (70–80 cm, on average) and thickness (5–15 cm); they are often cut by late subvertical fracture arrays trending N30–40E, sometimes accompanied by a second late system (N60–80W, 55–65SE).

In the mine area, the Vilariça fault system intersects a nearly perpendicular (N70–80W, subvertical) auriferous sinistral D3 shear zone, which rotates towards N50–60E in the vicinity of the Vilariça fault zone. As already mentioned, the N70-80°W shear corresponds to a local variation in strike of a regional N80°E shear, probably due to the influence of its dextral conjugate. Minor NW–SE – NNW–SSE dextral shears, probably representing the D3 conjugate, are also common in the mine area, and are usually underlined by siliceous fillings where quartz exhibits strong plastic deformation. Near these shears, N40–45W barren quartz veins can be found.

In the França Mine, two sets of veins were exploited by the romans and in the modern times: 1) N80W/subv in "Covas Altas" concession and 2) N80E or E/W in "Pingao dos Quintais" concession. The first ones may correspond to P fractures of the D1/D3 sinistral shear (Fig. III-34).

Within the N70–80W shear, the mineralization occurs generally along the footwall of thin (< 10 cm) and irregular quartz veins oriented N80–100°E, 40–50°S, which usually exhibit en echelon disposition and sometimes, horizontal left displacement, typical of classification as hybrid Riedel fractures (Gamond, 1983, 1985; Hancock, 1985).

Extremely brecciated quartz fillings with roughly rhombohedral morphology and variable extension underline many fault segments of the Vilariça fault. These quartz breccia bodies, characteristic of dilatant jogs in strike–slip brittle fault systems, show often prominent enrichment in iron and other metals (breccias of type IA), and in the mine area, one can put in evidence the relation between these fault rocks and their deeper mineralized equivalents (breccias of type IB and IC), which were probably object of Roman exploitation.

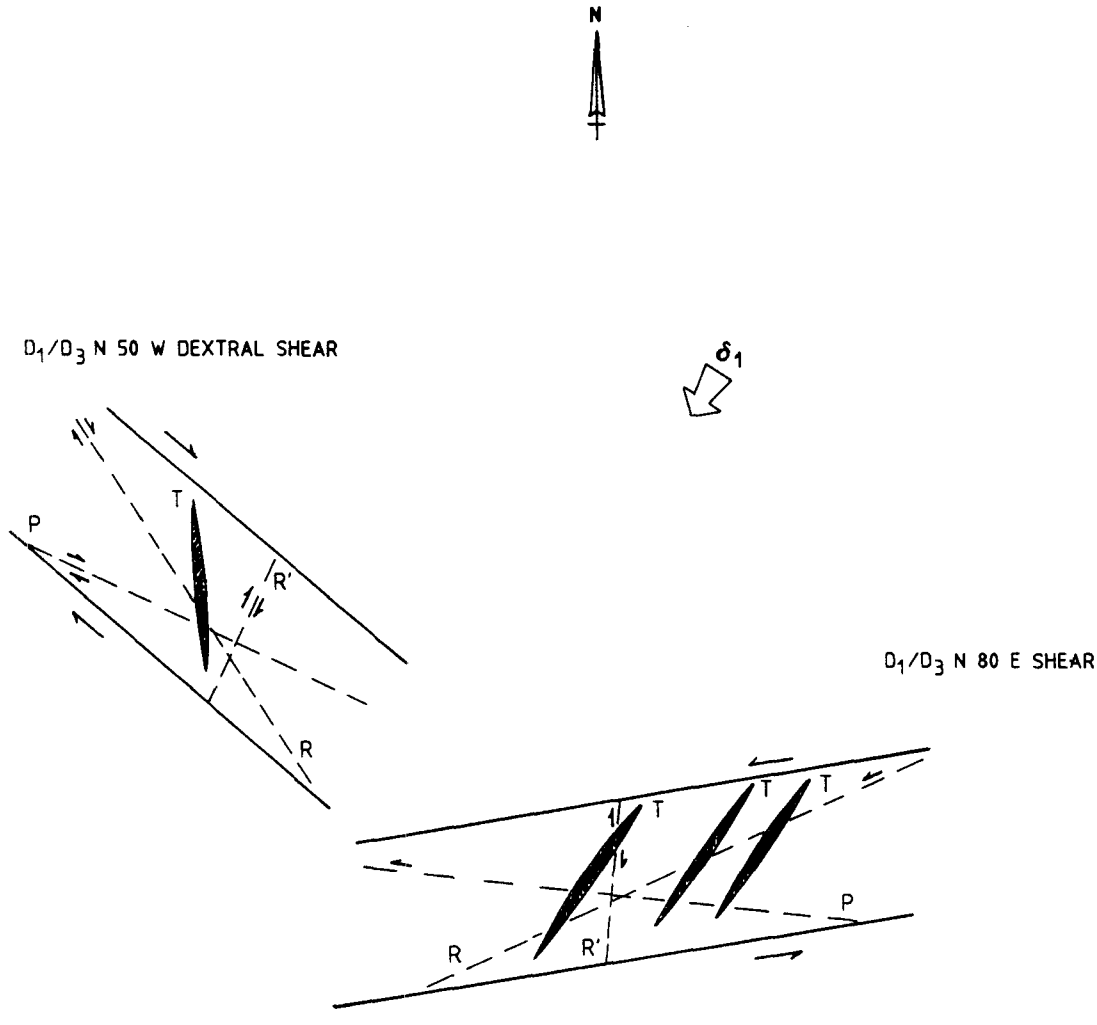

Fig III - 34 : R and P mineralized structures from Covas Altas and Pingao dos Quintais area.

DISCUSSION

Three successive deformational stages are at the origin of the formation of most studied gold-bearing quartz veins. The order of succession knows no exception.

Early stage : shearings and and formation of early structures (milky quartz veins)

The formation of the main channels in generally in relation with major shear zones : the complex superimposition of early deformations from D1 to D4 are responsible for specific structures which have in turn evolved from ductile to britlle regime and are associated with the main shear zones affceting the Gallicia area. The earliest quartz deposition, which create the specific potential trap for later mineralizations are formed at that stage (D3 to D4). They formed mostly after the emplacement of late peraluminous granites (probably Westphalian); they also post-date some subsolidus alteration affecting these granites (albitization-tourmalinisation at Penedono, quartz dissolution at Pino, greisenisation at Tomino).

Quartz fills in general relatively small structures (from the tension gashes of 1dm to 1m length to structures of a few hundred m). These structures may be affected by local ductile deformation , frequently on the wall-rock. Diffuse alteration, and sulphide crystallization in some instances (pyrite, then barren arsenopyrite) in the surrounding rocks seem to preceed the deposition of massive milky quartz in open space (tension gashes at Corcoesto and Tomino, filling of earlier structures at Penedono). High P-T conditions (pressures above 1Kb and temperatures of 350° to 550°C, see later in ChapIV) are recorded and are roughly the same as those which prevailed during the late metamorphic stage in the Variscan terranes during or just after the hyper-collision event

Although the initiaition of the process may be related to nearby regional ductile shearings, no true mylonites were developed in the surroundings of the quartz veins. These features are at variance with those of typical Late Variscan shear-zones which are generally observed nearby at a regional scale.

Intermediate stage:

Due to repeated tectonic reactivation, early milky quartz veins were strongly reworked. A first event resulted in brecciation, or at less healing of the early quartz , leading to the present shape of the massive quartz lenses which are the host for later ore deposition. Earlier pyrite and arsenopyrite were brecciated as well. Sulphide deposition (barren arsenopyrite) locally took place in the microcrystalline quartz, but was never massive.

Later on, these lenses were repeatedly subjected to intense fracturation; there was several alternances of micro-crack formation and healing or sealing by hyaline or clear quartz.

Formation of the most efficient trap fro ores when Au is mobilized

A renewal of tectonic reactivation (frequently a compressive regime characterized by new specific directions of major stresses) under quite different P-T conditions resulted in the main stage of gold ore deposition associated with strong microcrack formation . Such microfracturing is extremely complex in detail, and results from the superimposition of successive brittle stages on the early quartz matrix (milky quartz cemented by microcrystalline quartz).Native gold deposition took place, together with sulphides and sulphosalts (Pb-Ag dominated), along these cracks, especially when they crosscut earlier sulphides.

At each of the two last stages, strong rheological heterogeneities have specific and favourable effects on the intensity of the permeability formation. Main rheological heterogeneities are the followings : granite sills within metamorphic units, quartz veins within granite, silicified schist within shists, etc..

In the case of metric quartz lenses within micachist, finite element modelizations (Lespinasse, 1990) have shown that stress intensities are higher in the quartz vein, in the center

and near its boundaries, this explaining a more intense fracturing of the vein than the host rock, and the lack of mineralization outside the quartz vein. Such modeling have shown also that no strong reorientation of stresses occur within the quartz vein : this implies that the orientation of microcracks and veinlets in the early quartz matrix may be used as markers of the regional stress orientations since they are perpendicular to the $\sigma 1$-$\sigma 3$ plane. In a french deposit (the Aurieras), Essarraj (1989) has shown that quartz vein (Northern Massif Central) was thus affected by two late and successive compressional events, which are in agreement with the regional events determined at the regional scale, by using reverse methods (Lespinasse, 1990).

Therefore, the early quartz matrix (milky quartz cemented by microcristalline quartz) acquires its permeability at the favour of further stress reactivations, which yield higher fluid flows within the veins than in the surroundings. This process explains that only quartz veins are mineralized although the gold inputs are late compared to the quartz matrix formation.This is clearly shown by the Tomino and Penedono examples.

IV - RECONSTRUCTION OF THE PHYSICAL CHEMICAL CONDITIONS

The reconstruction of the conditions of metal transport and deposition is of critical importance to define the major factors controlling the formation of the economic ores. As Au bearing quartz veins are characterized by fairly complex succession of quartz crystallization, deformation, and healing, it is necessary to develop a multidisciplinary approach yielding to a complete characterization of the paleofluid pathways, the reconstruction of physical-chemical conditions, and the identification of the gold-bearing assemblages. Studies have included :

- the characterization of the distribution, the state, and the content in combined and metallic gold, the geometric traps for native gold, and the relationships between gold and sulphides, especially arsenopyrite which is a bearer of combined gold.

- P-T-X-V reconstruction of the properties of migrating paleofluids from microthermometric, Raman and crush-leach data, and from data obtained on alteration minerals.

- ore forming processes and physical chemical conditions favourable to gold depositio using data from fluids, and mineral assemblages together with geological, structural and geochemical data already presented in the previous chapters.

A- GOLD BEARERS AND TIME/SPACE INTRODUCTION OF GOLD IN THE SYSTEM

Gold occurs in most cases as isolated grains of native gold in quartz veins or a silicate matrix, or intimately associated with sulfides. The occurrence of tiny gold particles disseminated within massive pyrite veins are, in some instances, interpreted as resulting from a gold release from the sulfide lattice, during microfracturing and recrystallization stages posterior to the early sulfide crystallization (Romberger, 1986). Such a process is considered as a prerequisite for significant gold enrichment from the previous disseminated ores. Thus, the study of sulphides free of visible native gold is of great interest for the knowledge of the process at the origin of a possible Au-release and reconcentration. Such study has also been encouraged by a renewal in the recent years of the mining of deposits where gold is mostly borne at a combined state by sulfides. Such deposits have been discovered in Australia (Plimer,1982), Spain, and France (Boiron, 1987, Boiron and Cathelineau, 1988, Bonnemaison and Marcoux, 1987, Marion, 1988, Boiron et al., 1989) where the Chatelet deposit (Massif central) has been mined till 1955 (Zappettini, 1983).

Paragenesis, crystal-chemistry and genesis of low grade Au-bearing sulfides are relatively poorly documented in comparison to the increasing data concerning the native Au bearing ore assemblages. Such a situation comes partly from the difficulty of gold analysis and mapping at low concentrations. In this study, multidisciplinary studies of arsenopyrite samples have focused on two points :i) on the analytical problem of gold location, mapping and analysis within crystals at low concentration, extending previous investigations carried out in the recent years (Cathelineau et al., 1988, 1989, Marion et al., 1991), in order to detect possible preconcentration of gold in the vein sequence,

ii) on the study of the relative importance of the gold amount introduced at the different stages of the mineralized vein formation.

1-COMBINED GOLD AND ARSENOPYRITE CHARACTERIZATION

Studies carried out on gold bearers included the following stages : .

i) arsenopyrite parageneses have been studied by reflected microscopy.

ii) then, the Au state within sulfide separates was investigated in some samples using Mössbauer spectroscopy (in collaboration with Prof. Wagner, München Tech.Univ.).This non-destructive method yields information on the chemical state of gold without chemical

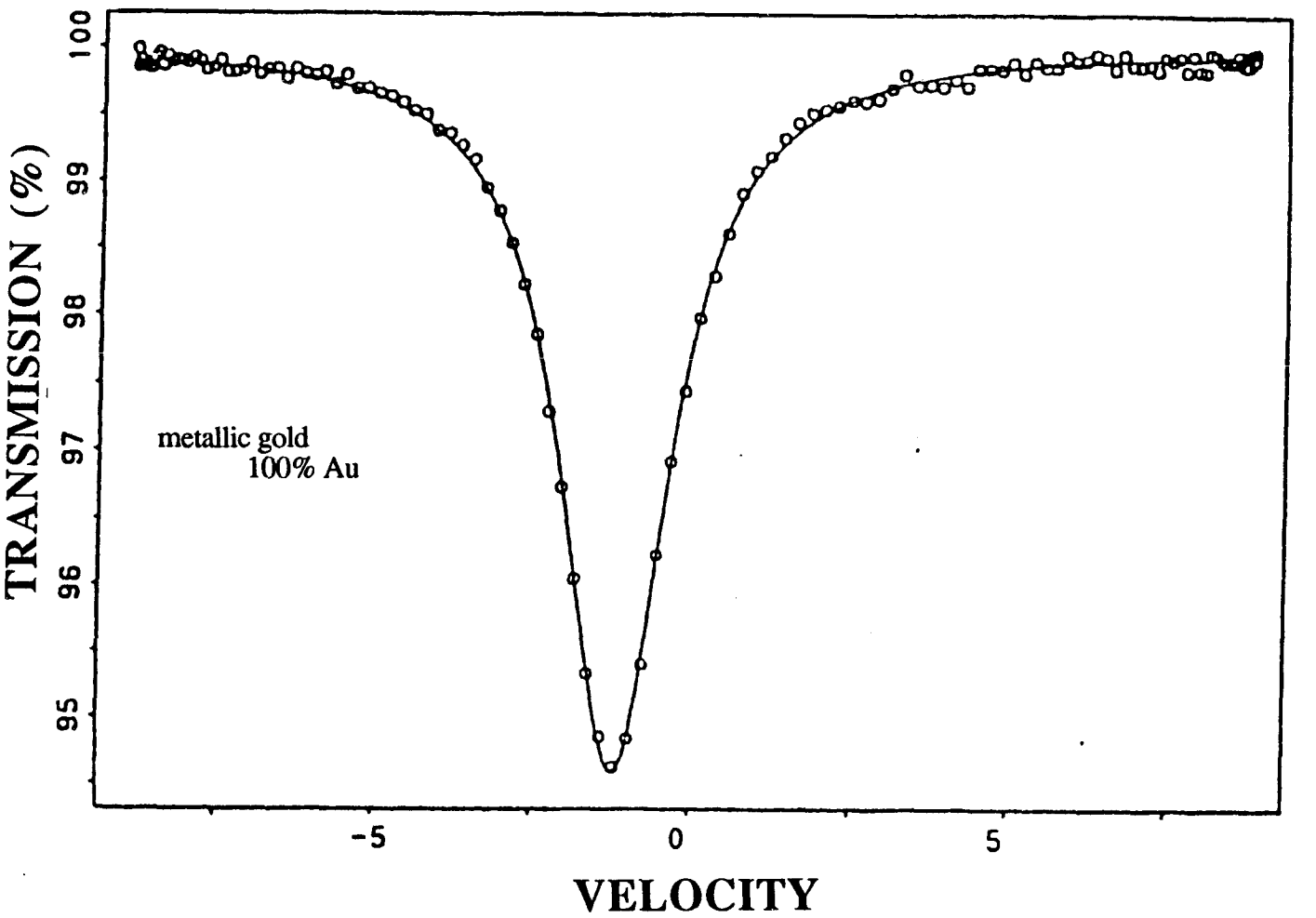

Fig IV - 1 : Mössbauer spectrum of pure metallic gold.

processing of the samples. Metallic gold can easily be distinguished from chemically bound gold, and its relative amount can be determined. Moreover, specific compounds of gold can be identified if suitable reference data are available (Wagner et al, 1986 ; Marion et al, 1986, 1988). Figure IV-1 shows the reference spectrum of pure gold which is typical of most gold ores studied

iii) gold is also present at a combined state in Au-rich arsenopyrites, but represents in that case, a small part of the gold content (< 5%). Further investigation was done on the gold distribution and crystal chemistry of such arsenopyrites. Crystals were polished and examined by scanning electron microscopy (S.E.M., secondary and backscattered electrons) and then analyzed using an electron microprobe. Contrarily to that proposed by Bonnemaison and Marcoux (1989), the Au distribution in crystals enriched in Au cannot be investigated by systematic mapping using grids of electron microprobe analysis because of the strong limitations due to the relatively high detection limit for gold (400 ppm for long counting times around 200s), and to the complex mineral growths and chemical zonings revealed by the SEM images, forbiding the interpolation between two analysis spots distant of more than 2 μm. The Au distribution was thus investigated by a more sensitive method, the secondary ion microscopy, which gives ion images at very low gold concentrations down to a few ppm.

CRYSTAL-CHEMICAL FEATURES OF ARSENOPYRITES

CRYSTAL GROWTH (SEM DATA)

Samples from most localities have been prepared for microscopic examination (thin polished sections, polished sections, polished grains included in conductive resines).

Arsenopyrites have been examined by scanning electron microscopy (S.E.M.) using secondary electron as well as the backscattered electron mode, which reveals very small differences around 0.1 in the distribution of the average atomic nunber (Z).

S.E.M. microphographs in the backscattered electron mode show that crystals exhibit complex chemical zonings due to variations especially in As and S contents. These microphotographs reveal rythmic chemical changes in the crystals from one growth zone to another. In arsenopyrites from the Cointadina deposit for instance, frequent increasing average atomic number from the center to the periphery of the crystals have been observed as shown by figure . Such an increase is due, in that case, to a progressive enrichment in As, correlatively to a decrease in the S (and Sb) contents from a given growth band to the following. In other cases, very complex patterns indicate breaks in the crystal growth followed by new growth characterized by significantly distinct chemical compositions of the new growth bands. Arsenopyrite crystals may be highly microfaulted or brecciated and surrounded by new arsenopyrite cement. A series of photographs taken using the backscattered electron mode of the SEM are presented plate IV- 1.

At Franca, arsenopyrites from the second generation (Aspy II) comprises fine–grained (< 0.5 mm) euhedral undeformed crystals in textural equilibrium with electrum, pyrite Ib and late carbonates (Carb IV). Crystals show evidences of multistage crystallization (Plate IV-1, photo 1 and 2) :

1- rythmic oscillation in major elements (As, S) characteristic of continuous growth with alternated changes in the fluid chemistry (Franca A and B)

2- brecciation events with confuse patterns indicating cementation of earlier arsenopyrite cores (Franca A and B)

3- microfracturing with filling and healing by arsenopyrite frequently richer in As (Franca A and B)

4- possible invading by diffusion (?) of the early complex core by As rich zones (appearing as clearer than the arsenopyrite matrix, (Franca A).

At Montemor (Ecoural W of Evora), arsenopyrites display complex features of crystallization and microfracturing.

At Coitadinha (Tras-os Montes), two generations of arsenopyrites are demonstrated

1- a first one with no compositional changes

2- a second one as small crystals showing clear growth bands, with relatively regular zoning, especially a late overgrowth enriched in As (white growth band) (plate, IV - 1, Photo 3).

At Penedono, arsenopyrite have suffered complex deformation (ductile?, to brittle) and alteration as shown by photograph 4 from plate IV - 1.

At Tomino, zones enriched seem to invade early arsenopyrite cores such as observed at Franca, whilst at **Corcoesto**, very little compositional differences characterize the studied grains.

At **Pino**, arsenopyrites display relatively homogeneous backscattered images with no clear zonation.

ARSENOPYRITE ANALYSIS BY QUANTITATIVE ELECTRON MICROPROBE (PORTO AND LISBOA UNIV AND CREGU)

Quantitative electron microprobe analyses have been carried out in order to determine the major element (Fe, As, S) contents in the different deposits.

- at Porto University for samples from the Vila Pouca de Aguiar zone (Vale de campo, Vale de Egua, Tres Minas, Jogadourao, Velhaquinhas), using a CAMEBAX electron microprobe routinely operated at 15 kVand a beam current of 20 nA.
- and at Lisboa University for França samples using a 3–channel JEOL JCXA 733 electron microprobe routinely operated at 25 kV. All analyses were performed with a beam current of 25 nA, a beam diameter of 5µm and counting times of 20 seconds.

In CREGU, systematic investigations have been carried out on arsenopyrite concentrates previously examined by scanning electron microscope from most deposits (Coitadinha, França, Montemor, Penedono, Pino, Tomino and Corcoesto) through quantitative electron microprobe along profiles chosen on the basis of the backscattered electron images. Systematic quantitative electron microprobe (Q.E.M.) analyses were performed on a SX Cameca probe (Nancy University), using a specific analytical program under the following analytical conditions : accelerating voltage : 30 kV, 40 nA, counting time : 60 s for gold and antimony and 10 s for the other elements. The detection limit for gold is around 500 ppm wt (0,01 ppm at) and 200 ppm wt (0,01 ppm at) for Sb under these analytical conditions,and were calculated using counting statistics models proposed by Ancey et al. (1978).

Data are presented in table IV-1, with indication of the range of the different element content, mean, mode, standard deviation and number of analysis for each deposit, depending of the available data according to their textural and chronological classification. Q.E.M analyses have been carried out with the help of the S.E.M. microphographs to interpret quantitatively the changes of average Z as the result of specific changes in the element contents. As and S are strongly negatively correlated as shown by figure IV-2, following roughly the classical substitution : Fe As_{1-x} S_{1+x}.The data show also that Sb are found exceptionnally on the contrary of most arsenopyrites found for instance in french Hercynian deposits.

Arsenopyrites from the Vila Pouca de Aguiar zone (Porto Univ.)

Generally, arsenopyrites have a quasi-stoichiometric composition, being nevertheless, sulphur-rich. Three different compositional groups of arsenopyrites are distinguished : (i) sulphur-rich and poor in As (Três Minas large crystals of earlier arsenopyrite); (ii) rich in As and less rich in S (Jogadouro); (iii) an intermediate composition (all other occurrences).

Comparison of arsenopyrite compositions (from the literature) from Jales mine is presented. At Jales they are, generally, richer in S (namely the latter anhedral "A" crystals) but in the other examples the compositions are very similar to those of the Vale de Campo, Vale d'Egua and Velhaquinhas.

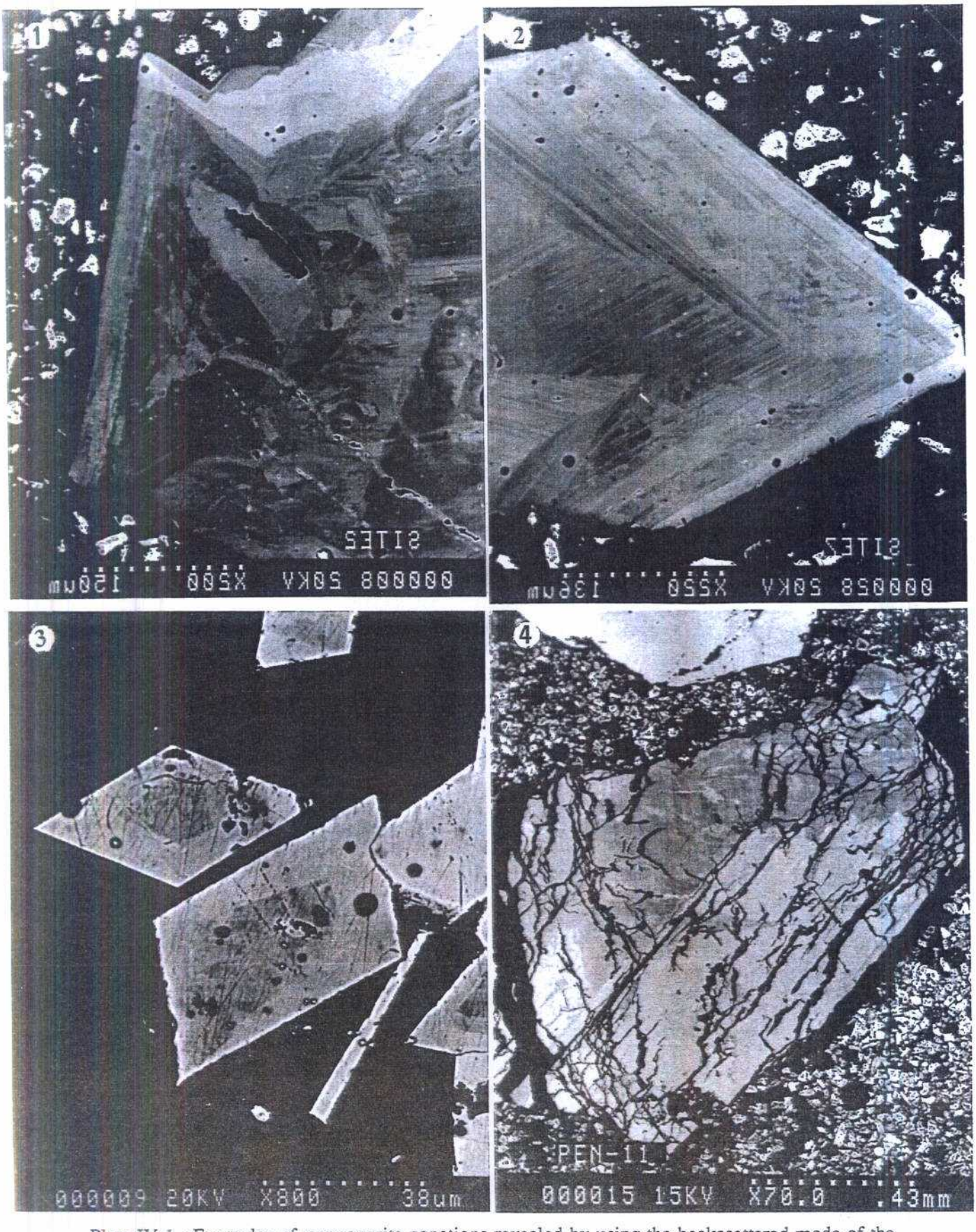

Plate IV-1 : Examples of arsenopyrite zonations revealed by using the backscattered mode of the scanning electron microscope. 1 and 2 - arsenopyrite II from the França area; 3 - arsenopyrite from Coitadinha (Morais zone); 4 - highly factured arsenopyrite from Penedono.

	Deposit	n		As %at	Fe %at	S % at	Au %at	Sb %at
CREGU								
	COITADINHA	50	range	27,3 - 32,2	32,2-34	34,8-39,3	0 -0,02	0,02-0,5
			mean (mode)	30,8 (31)	32,8 (33)	36,1 (36)	0,004	0,198
			std. dev.	*1,8*	*0,3*	*2*		*0,257*
	FRANCA	201	range	30,2-37,4	32,4 - 33,4	29,4 - 37,3	0 - 0,02	0 - 0,07
	Arsenopyrite II		mean (mode)	32 (31,5)	32,8 (33)	35,1 (35,5)	0,003	0,016
			std. dev.	*1,4*	*1*	*1,5*		*0,012*
	MONTEMOR	309	range	29,9-37,8	32,4 -34,7	28,7 -37,3	0 - 0,018	0 -0,071
			mean (mode)	34,2 (36)	33,3 (33)	32,5 (30,5 -33,5 -35)	0,0013	0,01
			std. dev.	*2,2*	*0,4*	*2,4*		
	TOMINO	260	range	29,6 -37,1	31,5 - 35,3	29,1 - 37,9	0 - 0,02	0 - 0,02
			mean (mode)	32,9 (32,5-36,5)	33,9 (33,5)	33,2 (33,5)	0,0018	0,016
			std. dev.	*1,8*	*0,8*	*1,6*		
	CORCOESTO	329	range	29 - 36,7	31,7-35,3	29,2 - 37,9	0 - 0,02	0 - 0,02
			mean (mode)	32 (33,5)	34 (33)	35,5 (33,5)	0	0
			std. dev.	*2,8*	*1*	*1,7*		
	PENEDONO	208	range	32,8-35,3	32,8-34	31,1-34,1	0-0,02	0-0,03
			mean	34,1	33,3	32,5	0	0
			std. dev.	*0,48*	*0,21*	*0,53*		
	PINO	15	range	32,7-33,5	32,7-33,4	33-34,5	0-0,01	0,04-0,23
			mean	33,1	33,1	33,7	0	0,11
			std. dev.	*0,26*	*0,2*	*0,36*		*0,06*
PORTO Univ.	VILA POUCA							
	Vale de Campo	43	mean	31,5	34,2	34,2	<dl	0,02
			std. dev.	*0,96*	*0,42*	*1,81*		
	Vale de Egua	44	mean	31,5	34	34,4	<dl	0,02
			std. dev.	*0,52*	*0,3*	*0,86*		
	Tres Minas	20	mean	32,5	34	33,3	<dl	0,02
	large cristal		*std. dev.*	*0,27*	*0,28*	*0,37*		
	Tres Minas	20	mean	30,4	33,88	35,61	<dl	0,02
	small cristal		*std. dev.*	*0,53*	*0,31*	*0,78*		
	Jogadouro	44	mean	34,15	34	34,74	<dl	<dl
			std. dev.	*0,38*	*0,28*	*0,57*		
	Velhaquihas	44	mean	32,8	33,7	33,4	<dl	0,02
			std. dev.	*0,63*	*0,37*	*1,17*		
LISBOA univ. França	Arsenopyrite Ia	20	range	29,1-31,5	31,6-34,25	35,3-38,9	0-0,02	0-0,03
			mean (mode)	30,7 (30,9)	33,65 (32,75)	36,3 (36,5)		
			std. dev.	*0,51*	*0,59*	*0,81*		
	Arsenopyrite Ib	12	range	29,7-31,9	31,75-34	35,1-38,3	< dl	0-0,02
			mean (mode)	30,5 (31,1)	33,5 (33,6)	36,7 (36,5)		
			std. dev.	*0,56*	*0,64*	*0,88*		
	Arsenopyrite II	9	range	29,2-30,6	33,4-34,4	36,5-39	0-0,012	0-0,08
			mean (mode)	30,1 (29,9)	33,8 (33,9)	37,2 (36,9)		
			std. dev.	*0,5*	*0,35*	*0,8*		
	Arsenopyrite	11	range	30,2-31,3	32,7-33,9	34,7-37,4	0,-0,012	0-0,03
	NW-SE shear zone		mean (mode)	30,9 (30,8)	33,4 (33,1)	36,4 (36,4)		
			std. dev.	*0,3*	*0,42*	*0,24*		
	Arsenopyrite	11	range	29,1-30,22	32,8--34,1	37,4-39	0 -0,012	0-0,02
	in quartz breccia		mean (mode)	29,8 (29,8)	33,6 (33,6)	38,7 (37,4)		
			std. dev.	*0,33*	*0,32*	*0,66*		

Table IV -1 :Arsenopyrite compositions from the different studied deposits .

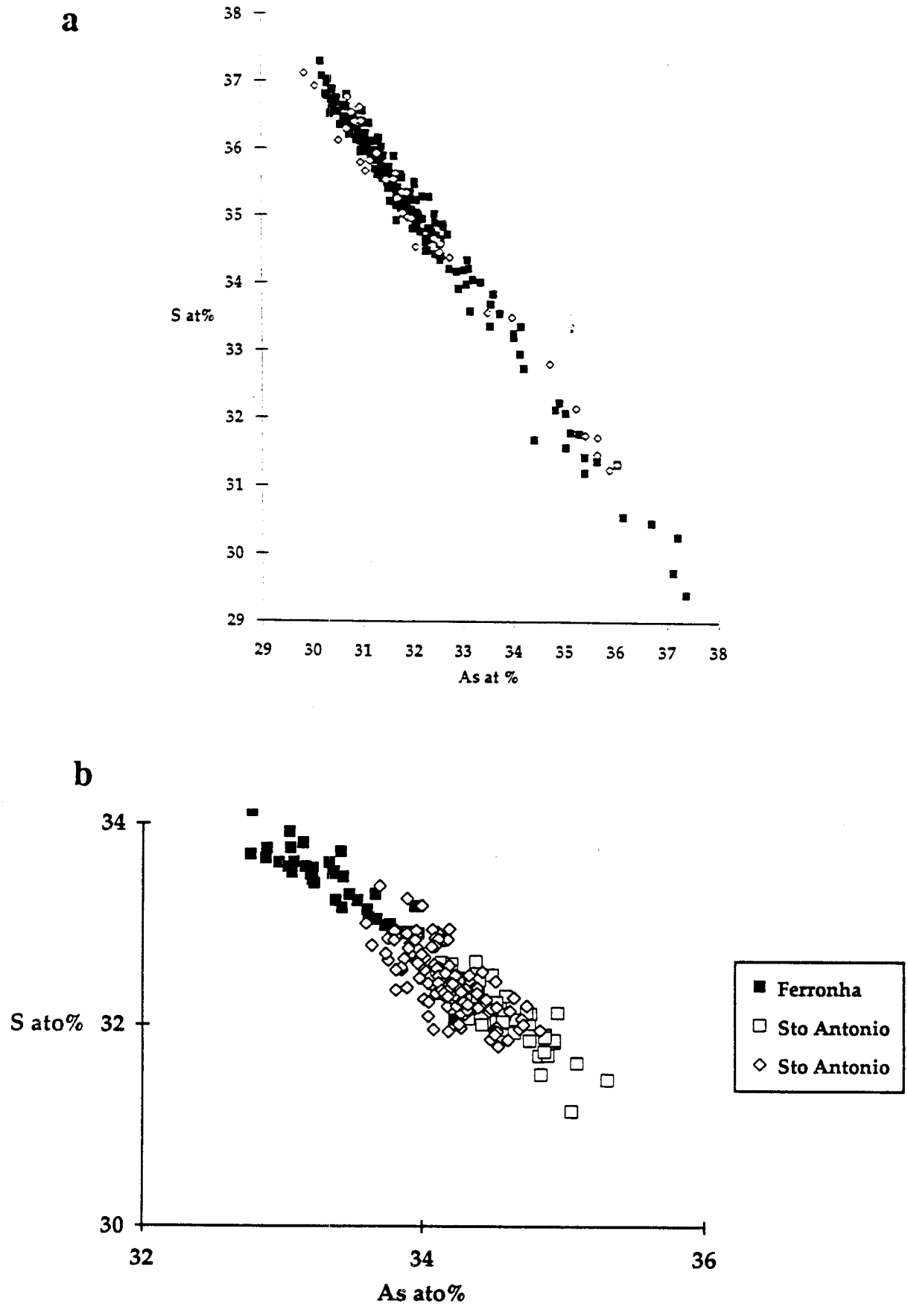

Fig IV - 2 : As-S correlation diagram applied to electron microprobe analyses of arsenopyrites. A : França (black symbols) and Montemor (white symbols) deposits ; B : Penedono area.

Arsenopyrites from the França zone (Lisboa Univ.)

As and S wt% can be used to distinguish the main arsenopyrite families: Aspy I(a,b) shows in general lower sulphur values (with a mode around 21.51 wt%) and arsenic contents scattered in the range 41.01–44.46 wt% (mode : 43.51 wt%); this compositional field comprises also the characteristic arsenopyrites of the mineralized veins along the reactivated shears (for that S and As modes are 21.37 and 43.38 wt%, respectively), and is slightly different from the one obtained for Aspy II and arsenopyrite relics in quartz breccias (with S and As modes of 21.73 and 42.15 wt%, and of 21.99 and 42.06 wt%, respectively, Table IV-1, annexe).

Minor amounts of Pb and Sb were detected in some of the arsenopyrites examined, as well as traces of Au (Ag). Representative analyses of generations Ib and II exhibit, in general, Pb concentrations with modes around 0.17 and 0.10 wt%, respectively, which contrast with the lower and quite constant Pb content (0.07 wt% on average) of the arsenopyrites Ia. Moreover, the available chemical data suggests that Pb abundances in the Ib family are usually higher than the typical content showed by the characteristic samples of generation II, although in both cases one can qualitatively appreciate the tendency for a positive covariance between the Pb and As wt% values. It is also important to point out that for Ib samples, higher Pb values seem to correlate well with iron content of the order of 35 wt%. The Sb wt% of the arsenopyrites II is always greater than 0.10 (with a mode of 0.14 wt%), while for Ia and Ib generations it remains typically below 0.05 wt% (mode values are 0.01 and 0.00 wt%, respectively); values around 0.03 and 0.02 wt% are characteristic of arsenopyrites in mineralized veins along the reactivated shear zones and in quartz breccias of the Vilariça fault, respectively. Thus, from the analytical results obtained, it seems that the Pb and Sb minor contents of the analyzed arsenopyrites can be used as a diagnostic criterion for their chemical distinction.

Arsenopyrites from the Montemor zone (Lisboa Univ.)

Representative microprobe analyses and structural formulas (on the basis of 3 ions), as well as the obtained compositional range of the analyzed arsenopyrites are reported in Table III, according to the above mentioned textural and chronological classification. Arsenopyrites of type I show arsenic and sulphur contents scattered in the ranges 44–47 wt% (mode of 46 wt%) and 18–20 wt% (mode of 18 wt%), respectively. Similar As and S modes (45 wt% and 19 wt%, respectively) characterize arsenopyrite II, although representing a wide range of arsenic and sulphur contents (ranging from 42 to 45 wt% and 13 to 22 wt%) (Table IV-1, annexe). The absence of Sb, and the relative proportion of the Fe, As and S ions per formula unit, suggest that the composition of these sulphides is close to ideal $FeAs_{(1-x)}S_{(1+x)}$. The relationships between arsenic and sulphur contents display the expected inverse linear correlation.

Traces of Cu, Ag and Au (with average values of 0.02, 0.01 and 0.11 wt%, respectively) are characteristic of arsenopyrite I, while solely traces of Ag and Pb (0.02 and 0.06 wt%, on average, respectively) are reported for arsenopyrite II. This points to a possible chemical distinction of the two generations based mainly on the Au and Pb contents.

Other deposits and intercomparison of arsenopyrite crystal chemistry (CREGU)

In most of the deposits, As and S are strongly negatively correlated as exemplified by the As-S diagram (Fig IV-3) or by the profile caaried out through a grain. Examples of chemical zonations observed in arsenopyrite grains from the Montemor area or from the Penedono area are given in Figures IV-4 and 5. As and S display a large range of concentrations as previously assumed when looking at the important zoning of the crystal on backscattered images. Fe is relatively constant.

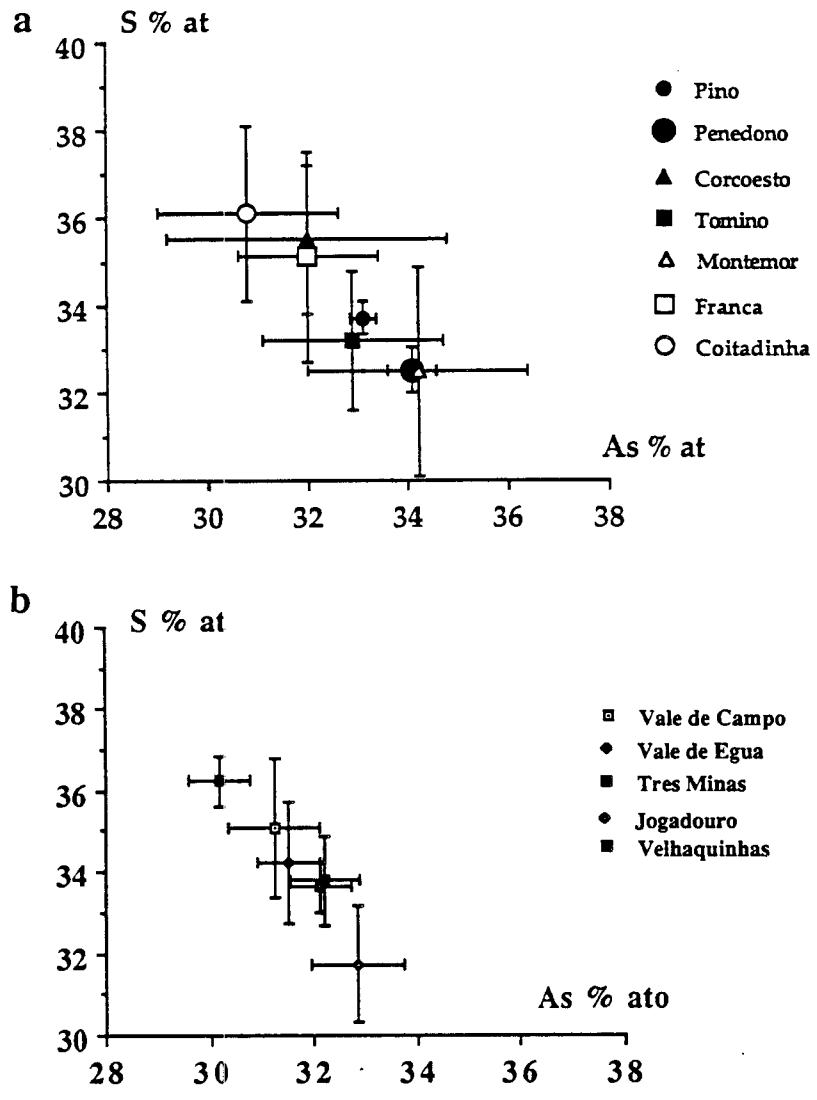

Fig IV - 3 : As-S correlation diagram applied to electron microprobe analysis of arsenopyrites from all the studied deposits with indication of composition ranges for As and S content.

Deposit	n	As %at	Fe %at	S % at	Au %at	Sb %at
COR 111 m	34	32,7-34,6	32,3-33,1	32,4-34,5	0-0,02	0-0,024
COR 147 m	34	32,6-36,5	31,6-33,3	31,4-34,8	0-0,013	0-0,17
COR 189 m	213	29-36,6	31,7-35,9	31-38,5	0-0,025	0-0,9
COR 236 m	29	33,3-35,7	32,2-33,5	31,9-33,9	0-0,019	0-0,047
COR 318 m	14	33,5-34,6	32-33	32,7-34,1	0-0,014	0-0,14

Table IV -2 : Arsenopyrite compositions from the Corcoesto drill hole. For each element, the composition range is given.

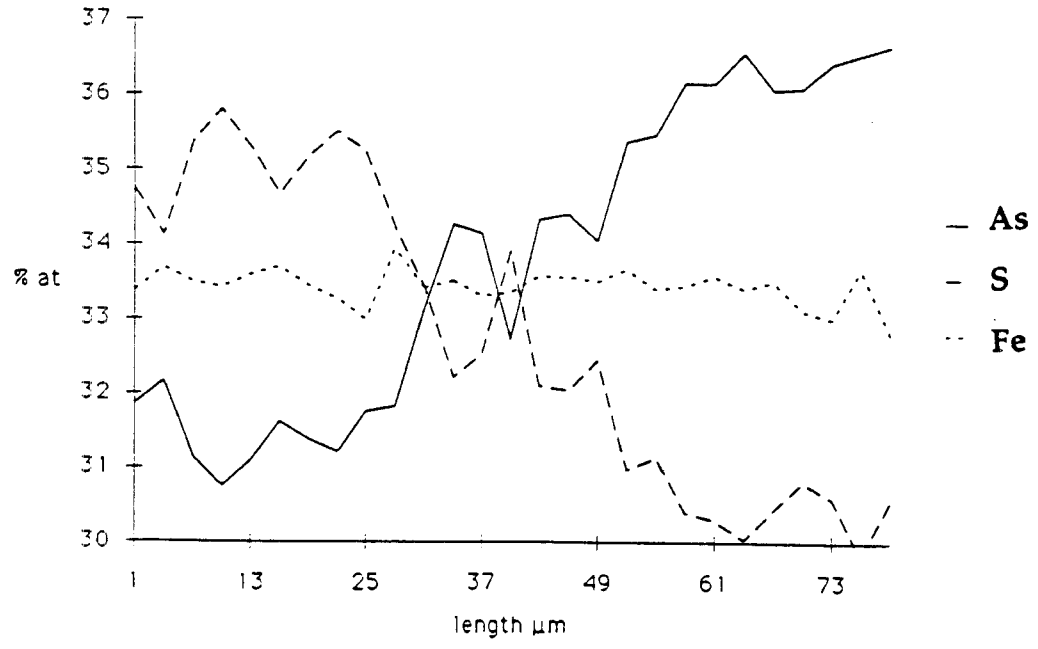

Fig IV - 4 : Profile of electron microprobe analysis of arsenopyrites from Montemor deposit showing the As-S zoning.

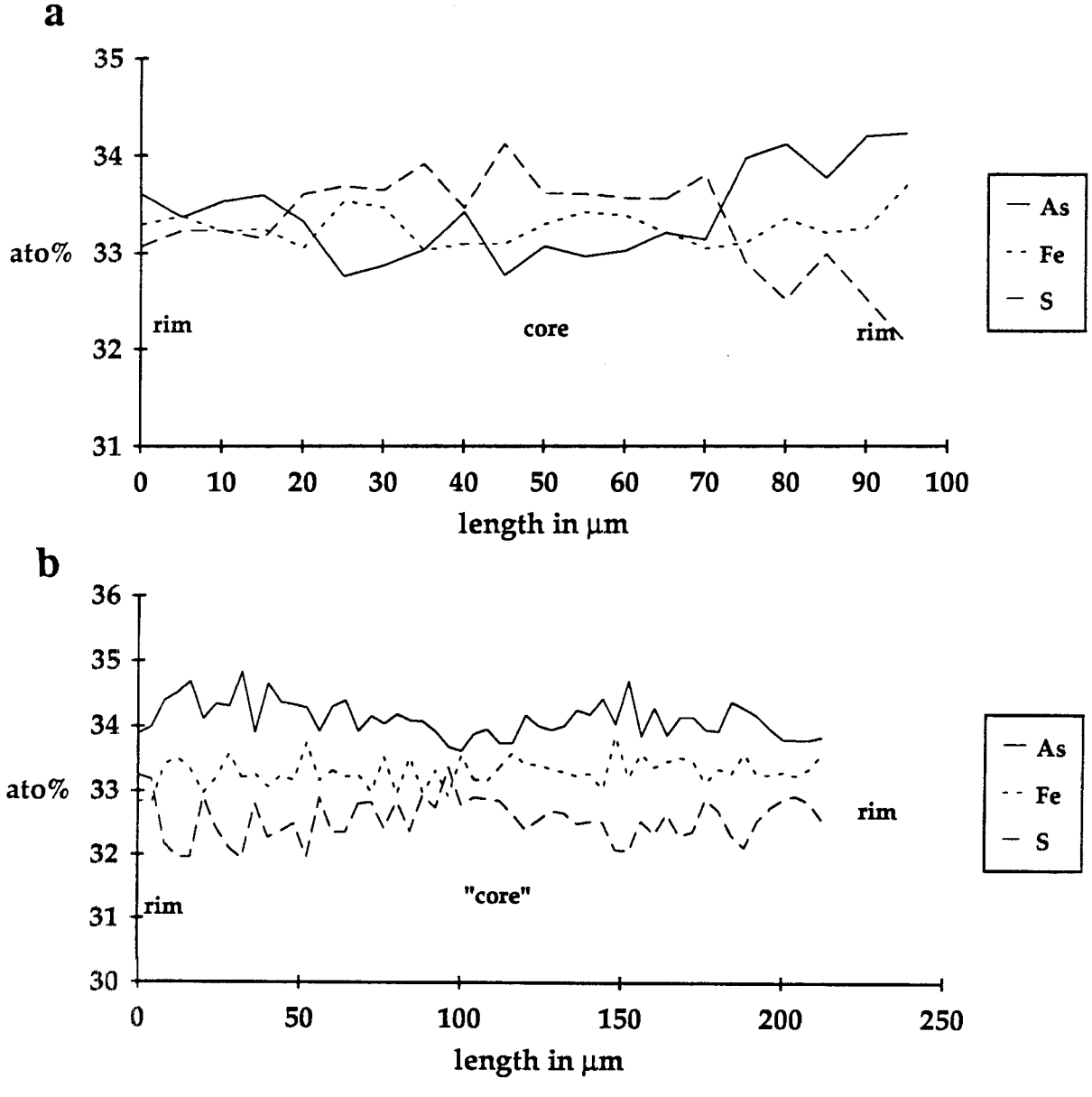

Fig IV - 5 : Profile of electron microprobe analysis of arsenopyrites, for As, S and Fe content from Penedono area . A : arsenopyrite from Ferronha ; b: arsenopyrite St Antonio

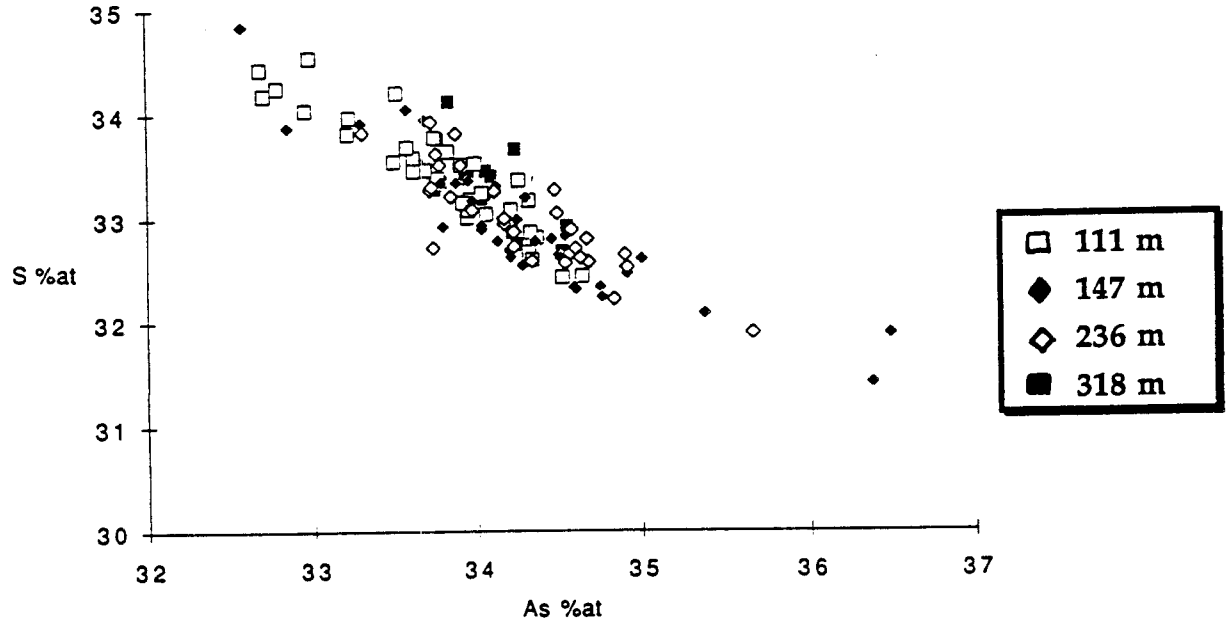

Fig IV - 6 : As-S correlation diagram applied to electron microprobe analyses of arsenopyrites from Corcoesto drill hole.

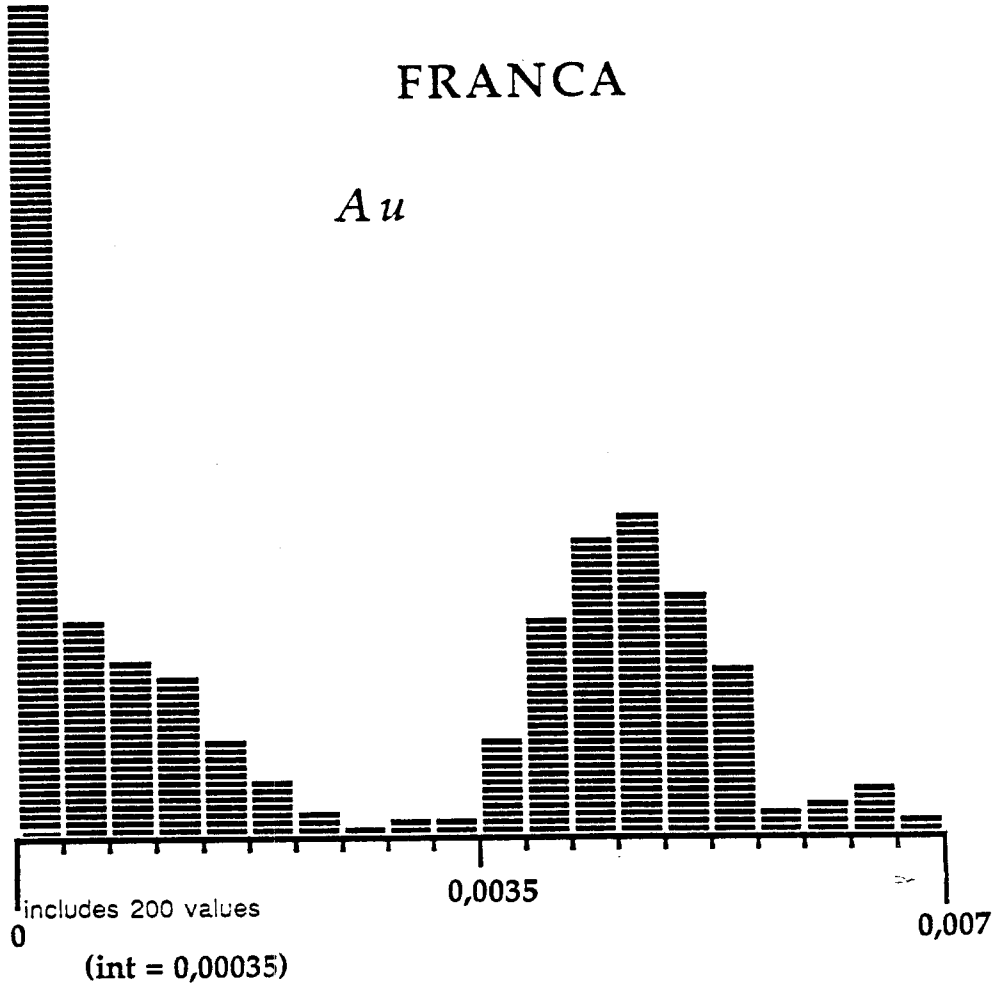

Fig IV - 7 : Histogram of Au concentrations (% at) in arsenopyrites from the França deposit (electron microprobe analysis)

In the specific case of Corcoesto, no significant changes have been observed in the different samples from the Corcoesto drill hole, as a function of the arsenopyrite location (disseminated in the granite or in veinlets) or depth. As and S are covering a large range of composition (Fig. IV-6 and table IV-2). Gold has not been clearly detected in the Corcoesto arsenopyrite. Compared to arsenopyrites from other deposits such as França, the Corcoesto arsenopyrite display rather homogeneous compositions in the whole studied drill cores, confirming the lack of clear chemical zoning and probable similar physical-chemical conditions of crystallization.

trace elements : Au and Sb have been systematically analysed.
Au content is for most of the analyses lower than the detection limit of the microprobe (400 ppm weight, 0,01 % at).

In some cases, as in França zone, Au content is very closed to the QEM detection limit as shown by the histogram (Fig IV-7) which displays a mode centered on 0,005 % at. (200 ppmwt). These data can suggest than gold is present in arsenopyrite at a relatively low content. This hypothesis has been confirmed by ion probe analysis (see next section).

Sb content has been detected at a significative content in Coitadinha deposit where it ranges from 0,02 to 0,5 % at. High Sb content are observed in zones enriched in S and depleted in As.

It has been also detected in the França sample (arsenopyrite II) confirming the data obtained at Lisboa on the same kind of arsenopyrites.

These data indicate that the latest stages of arsenopyrite crystallization are characterized by nearly euhedral crystals of small size containing low but detectable Au and Sb contents. These features are very similar to those described in other deposits from the Varsican chain, especially in the Marche Combrailles deposits (Villeranges-Chatelet deposits, Boiron et al., 1989, Cathelineau et al, 1989) where late epithermal mineralization are characterized by high Sb-high Au contents which could reach, in that cases contents about 10 to 100 times higher than in Galicia.

It can be also noted that deposits characterized by rather long-lived hydrothermal activity display a variety of crystal features, and clear multistage deposition with successive stages of deformation of the earliest arsenopyrite.

- at Penedono and Corcoesto , arsenopyrite may be deformed and brecciated, and crystallized during a series of stages but display limited chemical changes, indicating rather constant crystallization conditions,
- in most other deposits, extreme scattering in the As/S values are recorded in zoned crystals or crystals resulting from multistage crystallization. Extreme zoning are especially found in Franca , Montemor and in some Tomino crystals. These values cannot be used for arsenopyrite geothermometry using the Kretschmar and Scott data (1976). The probable lack of equilibrium with other mineral phases may be at the origin of such changes in the As/S ratio, even in single arsenopyrite grains.

- at Franca and Coitadinha, clear late stages of crystallization, not observed elsewhere, have been detected and could correspond to low temperature conditions (Au, Sb incorporation).

- SULPHIDE ANALYSIS BY SECONDARY ION MASS SPECTROMETRY (CREGU)

As gold is detected at a very low content in the Galicia arsenopyrites, further investigations have been carried out using SECONDARY ION MASS SPECTROMETRY (SIMS) which is the only technique making possible the in-situ quantitative determination of gold at low content in minerals (Cathelineau et al., 1989). New improvements concerned the calibration of the technique using standards, and digital imaging.

Experimental procedure

The SIMS studies have been carried out on a CAMECA IMS 5F equipped with a resistive anode encorder (RAE) elaborated by Charles Evans & associates. Improvements have been carried out in order to quantify with the best accuracy both digital images and ion measurments acquired with the electron multiplier, some changes in the operating conditions previously described (Cathelineau et al, 1989). A 10 keV Cs^+ primary ion beam (10-50 nA) was used and 14,5 keV negative secondary ions were detected. Measurements were acquired with no voltage offset at a mass resolution of 2000. This resolving power is enough for eliminating the molecular interferences $FeAsS2^-$ and $CsS2^-$ on ^{197}Au in gold bearing sulphides analysis (Marion, 1988, Cathelineau et al, 1989). The matrix ion intensities were monitored on the isotopes $^{109}AsS^-$ and $^{90}FeS^-$ for arsenopyrite and pyrite respectively.

Imaging using RAE

The RAE secondary ion detector is a device incorporated into the Cameca IMS 5f as a separate detector which uses microchannel plates to convert ions into a pulse of 10^6 electrons which the impact the resistive surface of an anode. It acts just as an electron multiplier ; however its deadtime of 3 µs limits the instantaneous countrate to 3×10^4 cts/s. It is a position sensitive detector capable of generating (x,y) coordinate for each ion detected : it allows digital images to be stored rapidly without intermediate steps in the RAE directory of the hard disk. Afterwards coordinates can be selected to define areas or line scans; this option constructs and displays a plot of ion intensity versus distance based on the define line coordinates and its width (in pixels). A pixel (the image unit) is equal to an elemental square of 0,6 and 1,5 mm side for images representing analyzed areas of 150 µm and 400 µm respectively. The software allows images to be displayed on the photographic reproduction with both logarithmic and linear pseudo color versus intensity scales.

The ion microprobe with RAE digital imaging equipment provides informations that may be directly used for quantitative determination of the accumulation of trace elements in minerals or in parts of these minerals.

- Gold implant and quantification

Ion implantation seems to be the best way to obtain quantitative elemental SIMS measurements in sulphide minerals. Calibrations of the ion microprobe for gold have been carried out using internal and external standards (Chryssoulis et al, 1989, Cook and Chryssoulis, 1990). In internal standardization, a known amount of gold is implanted into the matrix to be analysed. In external standardization, selected standards or synthetic minerals are used to produce specific calibration curve on the ion microprobe depending on the mineral, the amount of implanted gold and the operating conditions. In our case, we have chosen to use external standardization which appears more reliable for quantitative analysis. This method does not disturb the sample, and is less dependant of the mineral structures (micro-faults, inclusions, hole where gold can diffuse during ion implantation). Direct analysis of the samples can be obtained without preliminary ion implantation as for internal standardization.

The implant of gold has been done at 2 Mev and with a dose of $1{,}09\ 10^5$ at/cm^3 on natural minerals (pyrite and arsenopyrite) by Ion Beam Services Laboratory. These minerals were polished sections of monocristals which are perfectly homogeneous optically under the microscope and under SEM and QEM analysis.

The Relative Sensity Factor (RSF) used to quantify SIMS data can be calculated from ion implant SIMS depth profile using the following equation :

$RSF = Im\ (Dose / \sum i\ c(Zi)$ where Im is the matrix isotope intensity in counts/second and c (Zi) the concentration of gold (at/cm3) at the depth Zi in the standard.

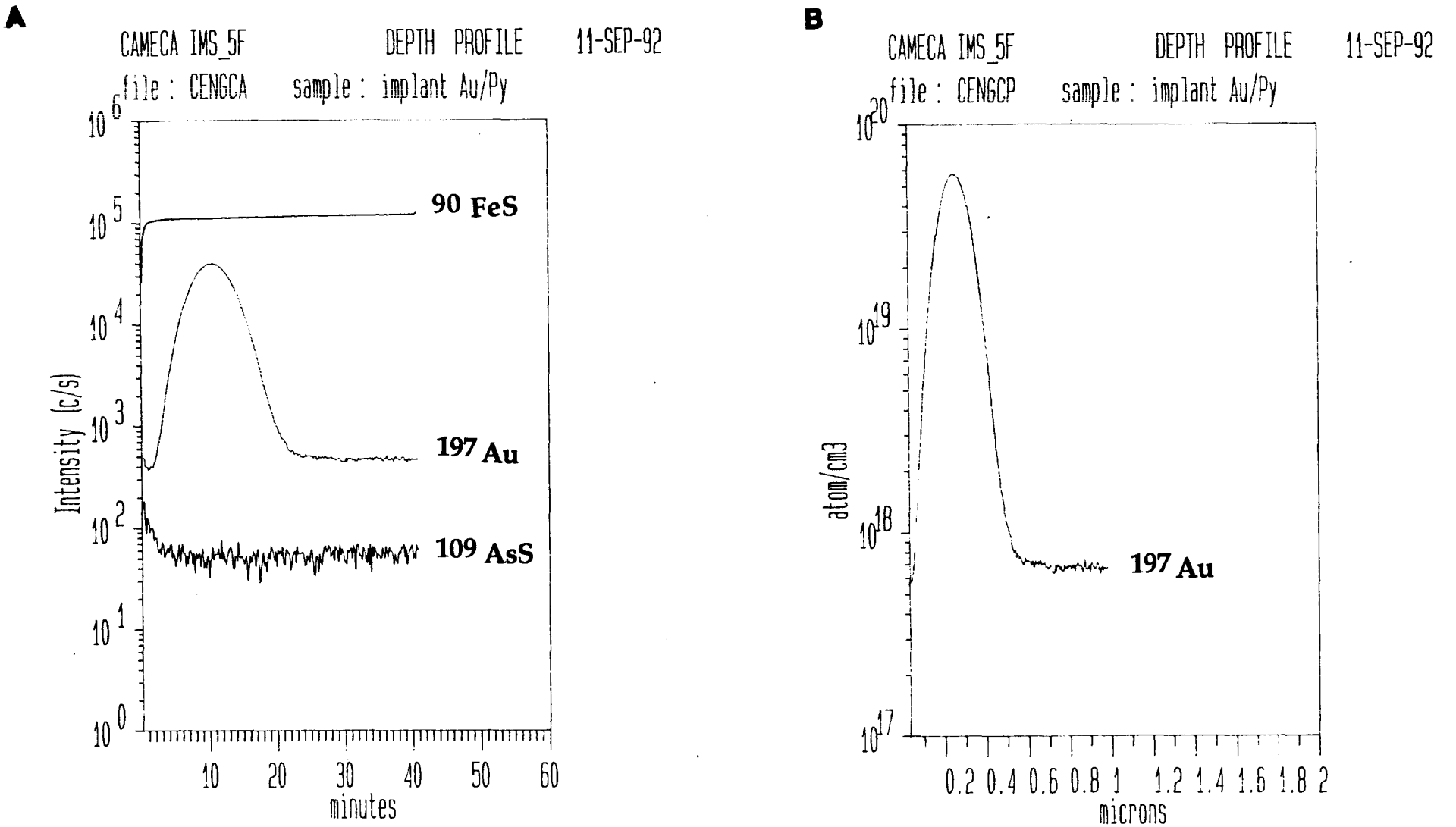

Fig IV - 8 : Implantation profile for arsenopyrite standard. A : Depth profile, Intensities of the different ion mass (^{109}AsS, ^{90} FeS and ^{197} Au) are recorded as a function of depth. B : Calculation of the Au concentration with depth.

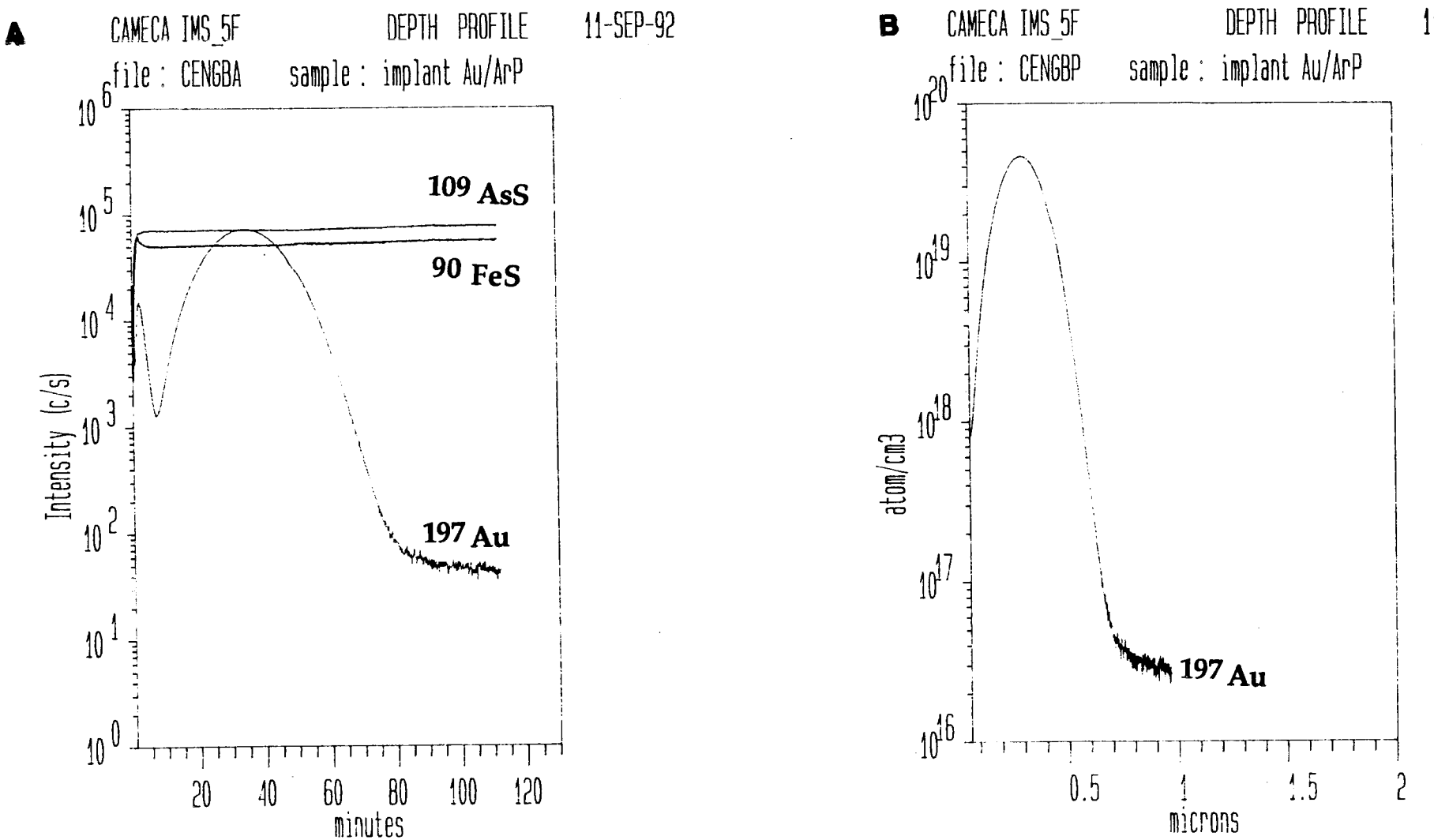

Fig IV - 9: Implantation profile for pyrite standard. A : Depth profile, Intensities of the different ion mass (^{109}AsS, ^{90} FeS and ^{197} Au) are recorded as a function of depth. B : Calculation of the Au concentration with depth.

A

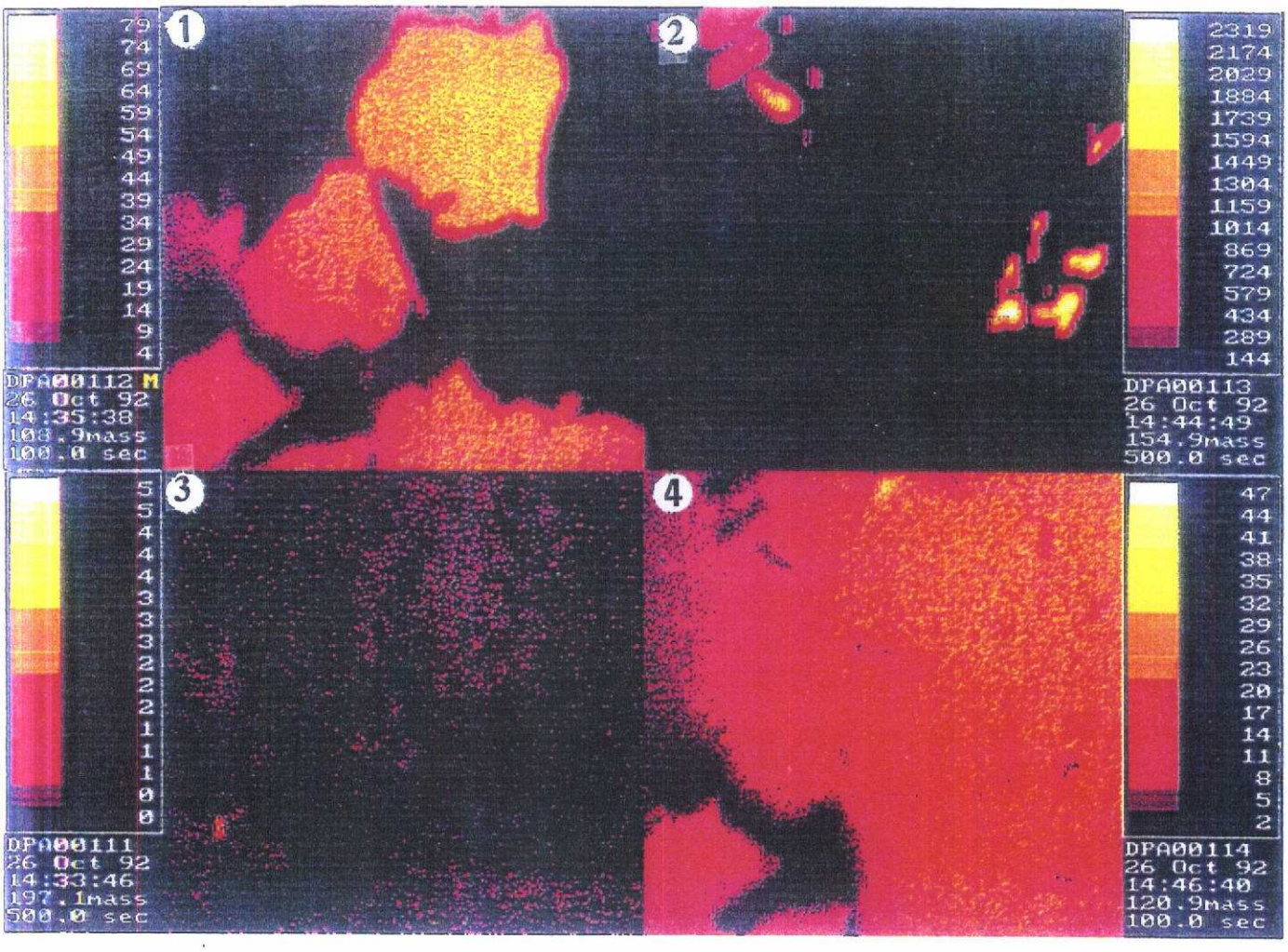

B

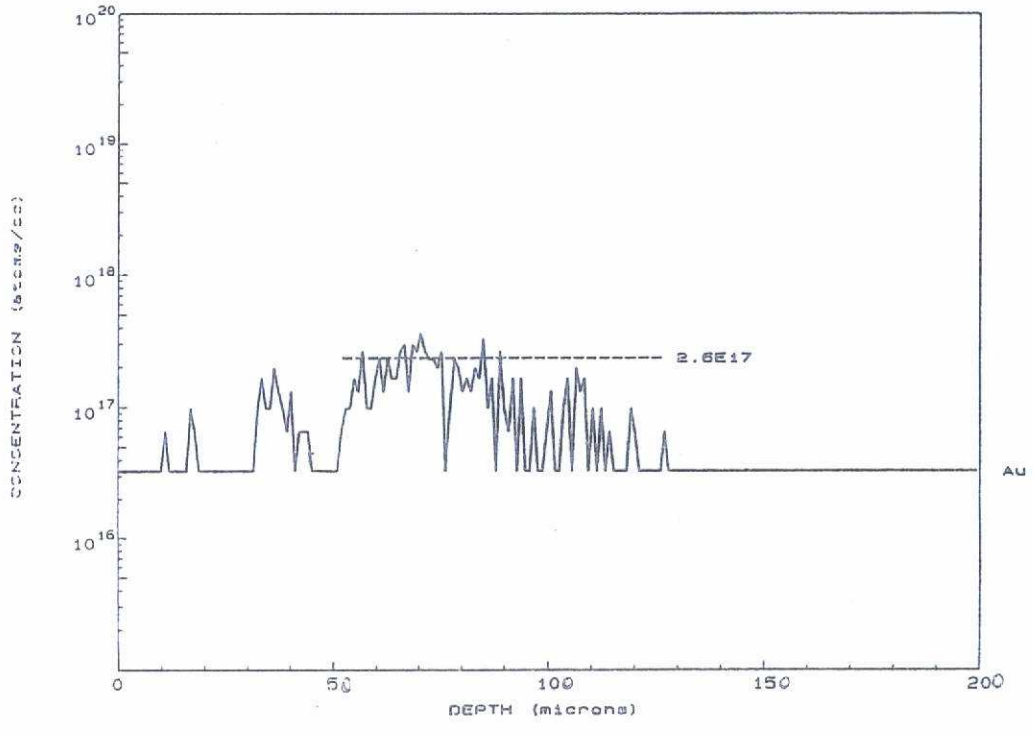

Plate IV-2 : A - Ion images corresponding to the secondary emission of ^{107}AsS (1), ^{155} SbS (2), ^{197} Au (3), ^{120} Sb (4) obtained on arsenopyrite crystals from Corcoesto (deep drilling, 348,50m). The side of the image is 250 µm. B - Profile of Au concentration across the arsenopyrite crystals . The maximum Au content in the crystal is 2. 10^{17} at/cm^3.

A

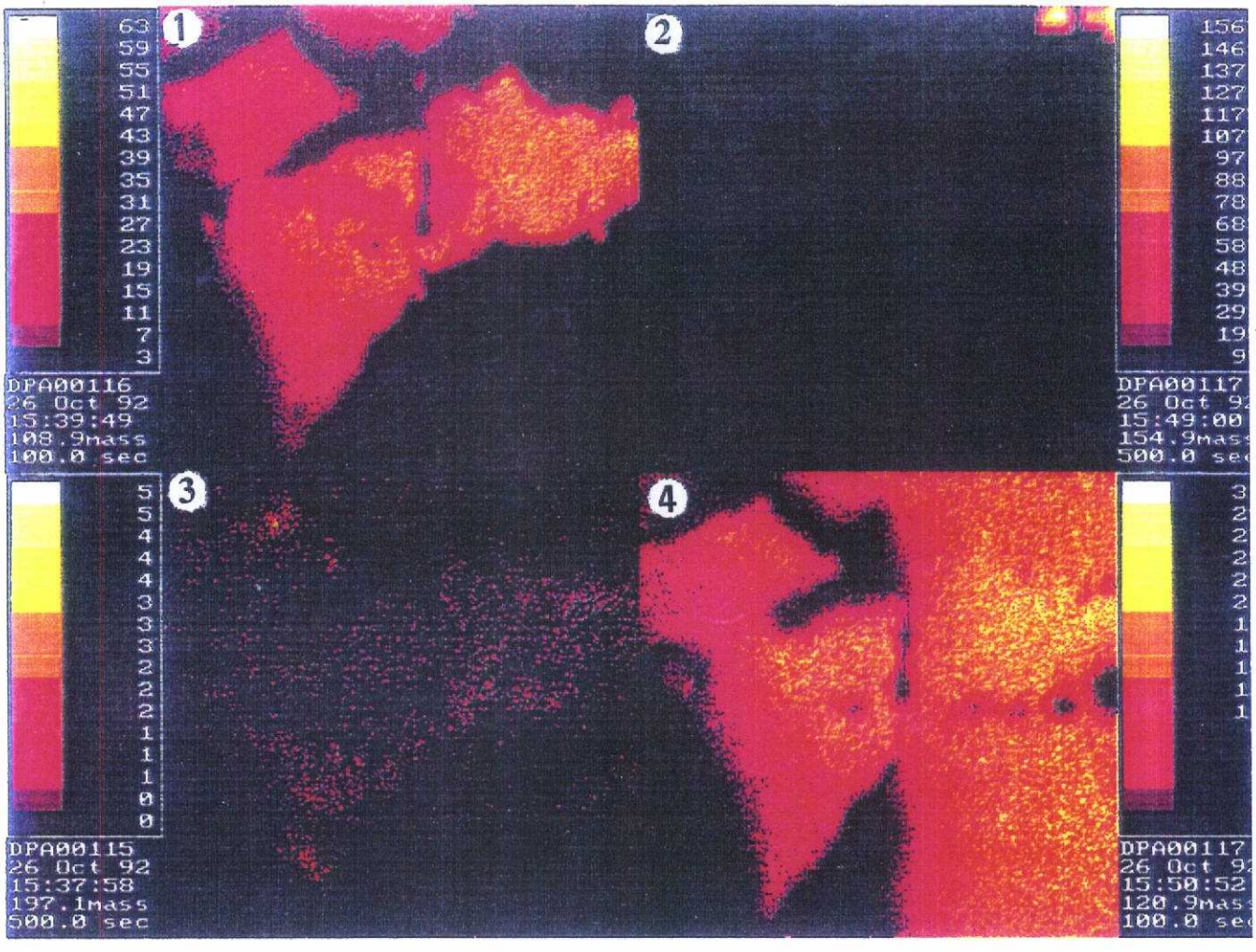

B

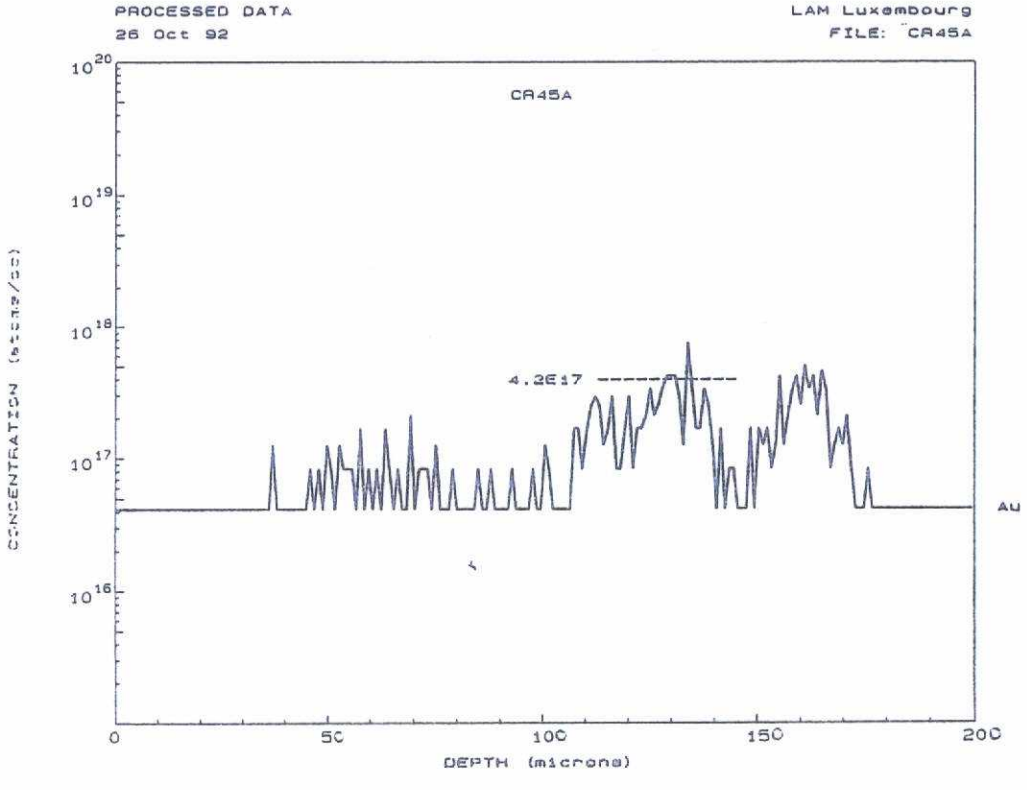

Plate IV-3 : A - Ion images corresponding to the secondary emission of ^{107}AsS (1), ^{155}SbS (2), ^{197}Au (3), ^{120}Sb (4) obtained on arsenopyrite crystals from Corcoesto (deep drilling, 348,50m). The side of the image is 250 µm. B - Profile of Au concentration across the arsenopyrite crystals . The maximum Au content in the crystal is 4.2. 10^{17} at/cm^3.

A

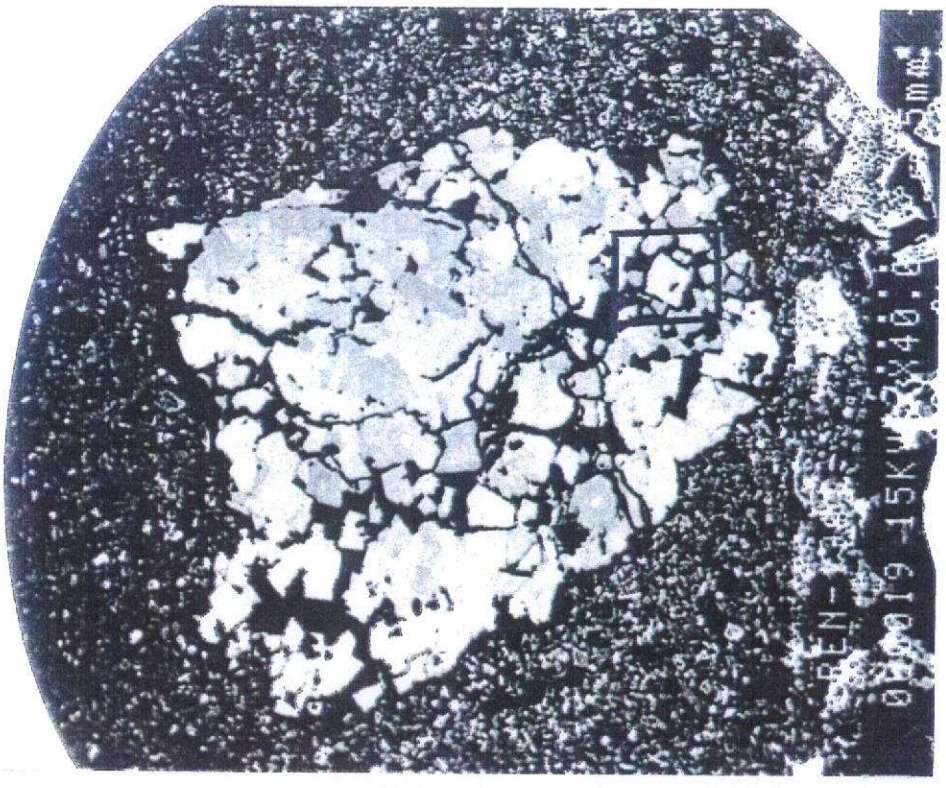

B

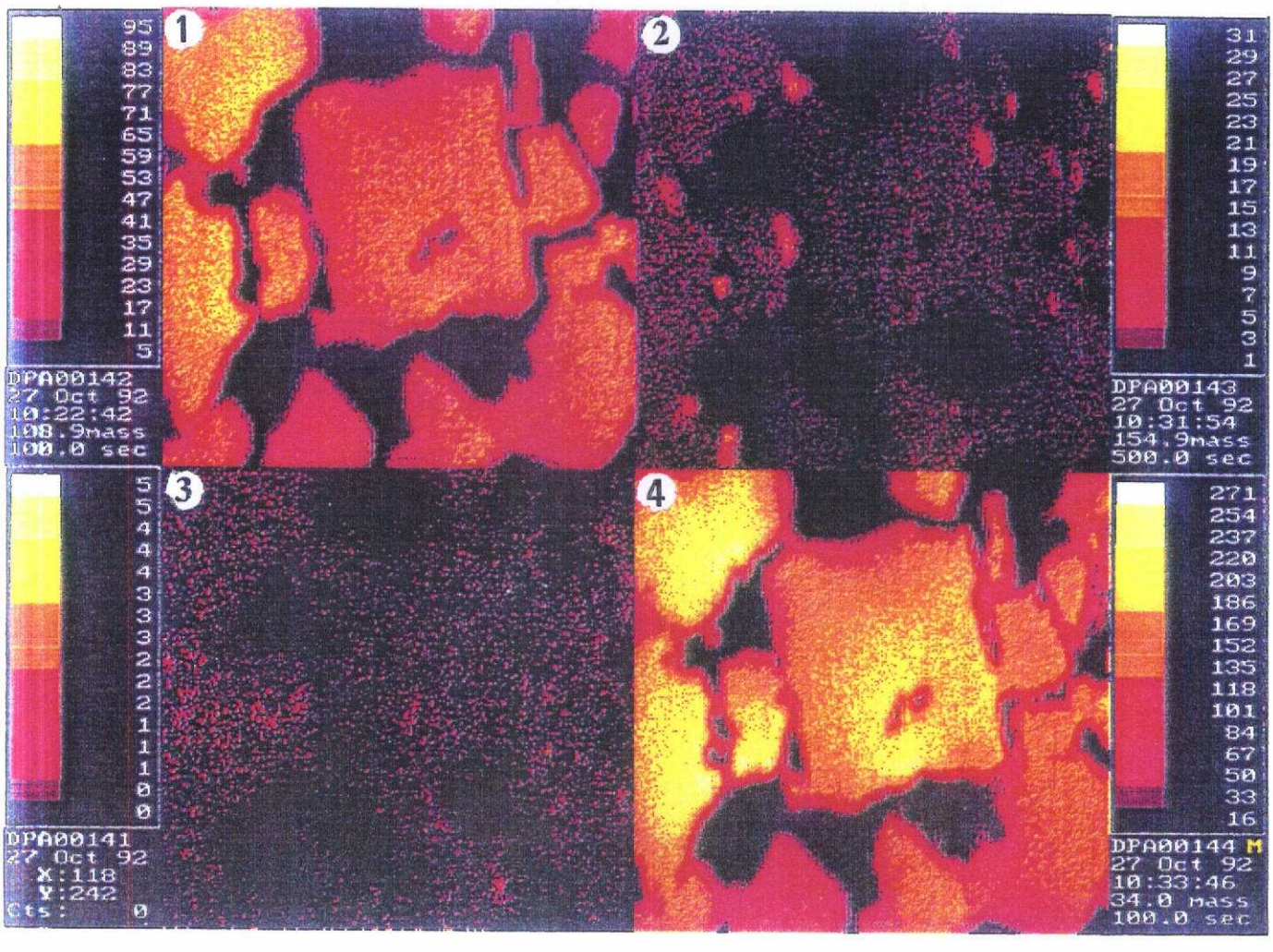

Plate IV-4 : A - Backscattered image of arsenopyrite crystals from Penedono area (Ferronha zone). B : Ion images corresponding to the secondary emission of ^{107}AsS (1), ^{155} SbS (2), ^{197} Au (3), ^{120}Sb (4) obtained on the arsenopyrite crystals mentioned in photo A. The side of the image is 250 µm. The maximum Au content in the crystal is 4.5. 10^{17} at/cm^3

A

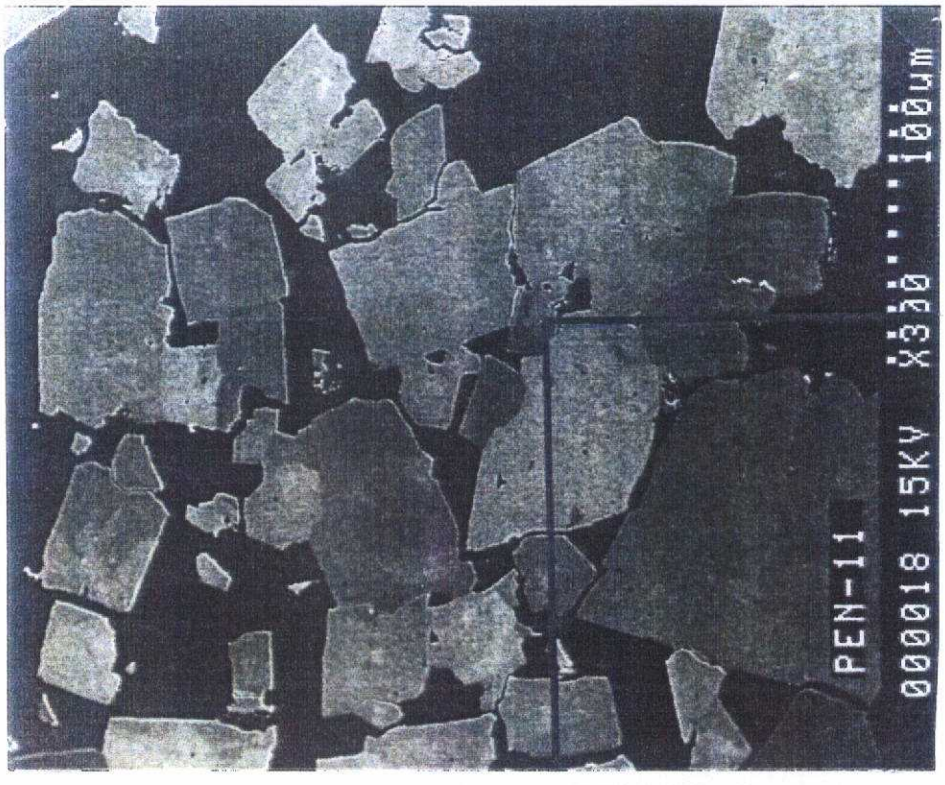

B

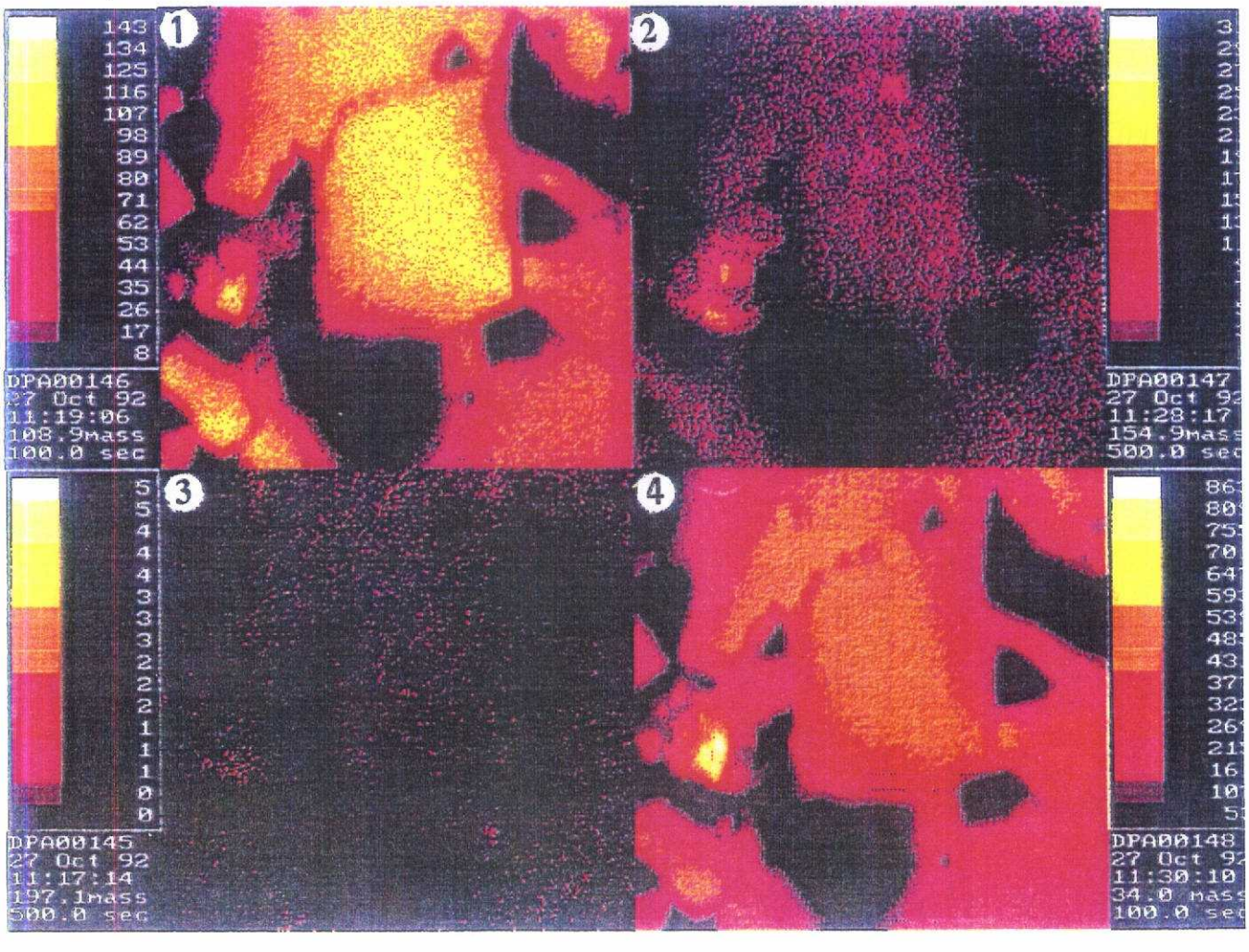

Plate IV-5 : A - Backscattered image of arsenopyrite crystals from Penedono area (St Antonio zone). B : Ion images corresponding to the secondary emission of ^{107}AsS (1), ^{155}SbS (2), ^{197}Au (3), ^{120}Sb (4) obtained on the arsenopyrite crystals mentioned in photo A. The side of the image is 250 µm. The maximum Au content in the crystal is 7. 10^{16} at/cm^3

A

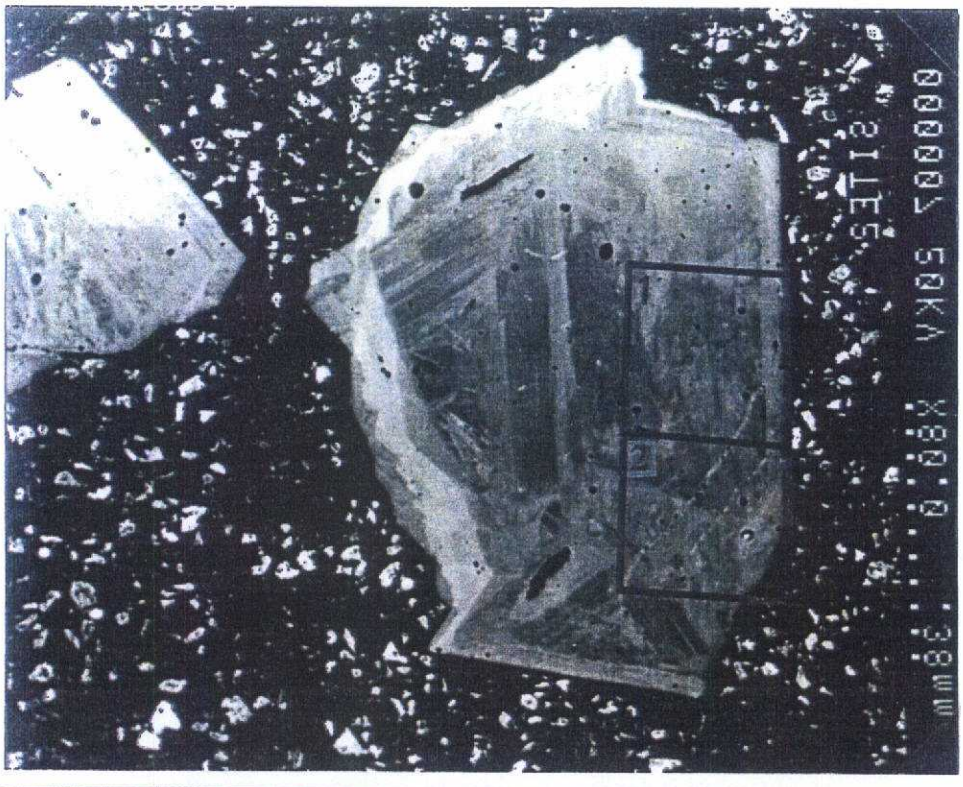

B

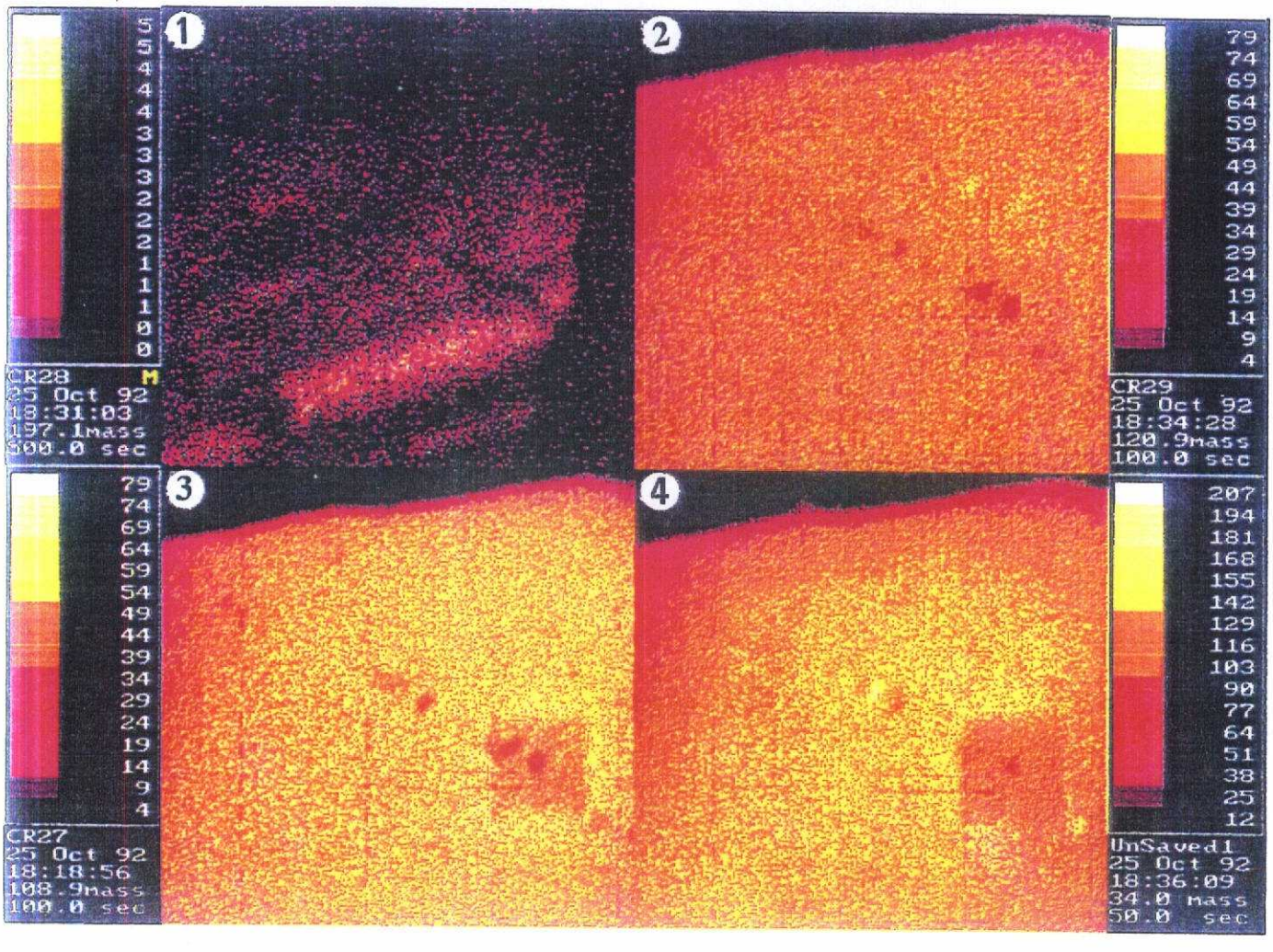

Plate IV-6 : A - Backscattered image of arsenopyrite crystals from França area . B : Ion images corresponding to the secondary emission of ^{107}AsS (1), ^{155}SbS (2), ^{197}Au (3), ^{120}Sb (4) obtained on the arsenopyrite crystals mentioned in photo A, zone 1. The side of the image is 250 µm

A

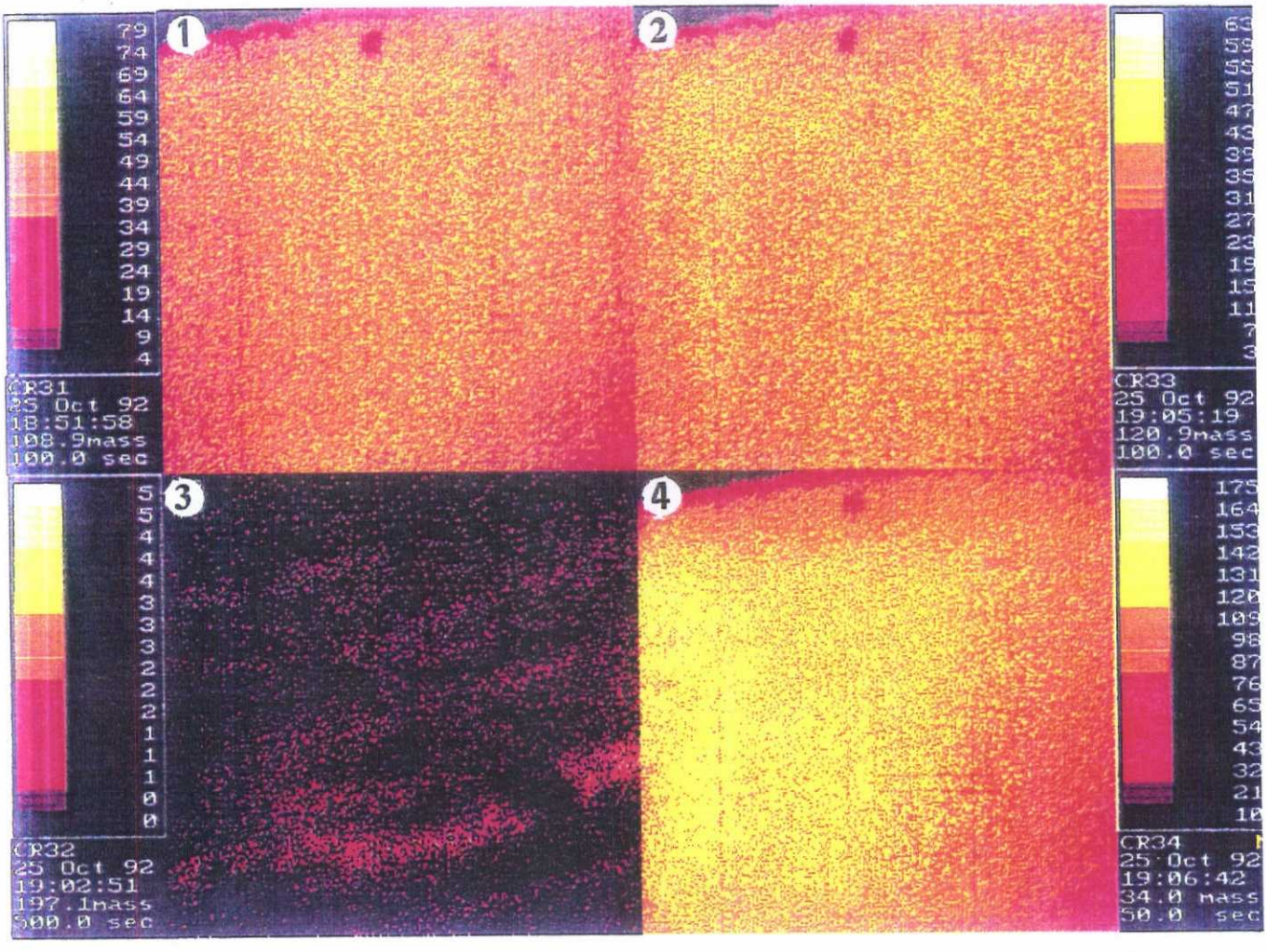

B

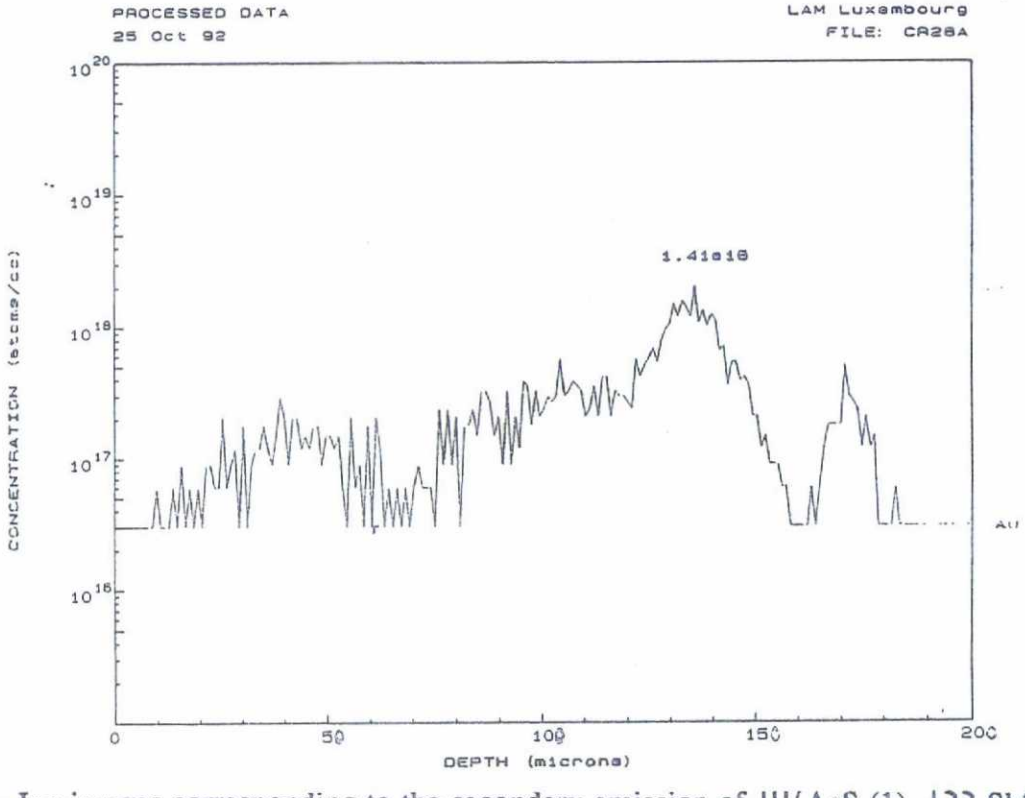

Plate IV-7 : A - Ion images corresponding to the secondary emission of ^{107}AsS (1), ^{155} SbS (2), ^{197} Au (3), ^{120} Sb (4) obtained on arsenopyrite crystals from França area (zone 2 in plate IV-6-A) The side of the image is 250 µm. B - Profile of Au concentration across the arsenopyrite crystals (Zone 1, in plate IV-6-A and ^{197} Au image). The maximum Au content in the crystal is 1.41. 10^{18} at/cm^3.

A

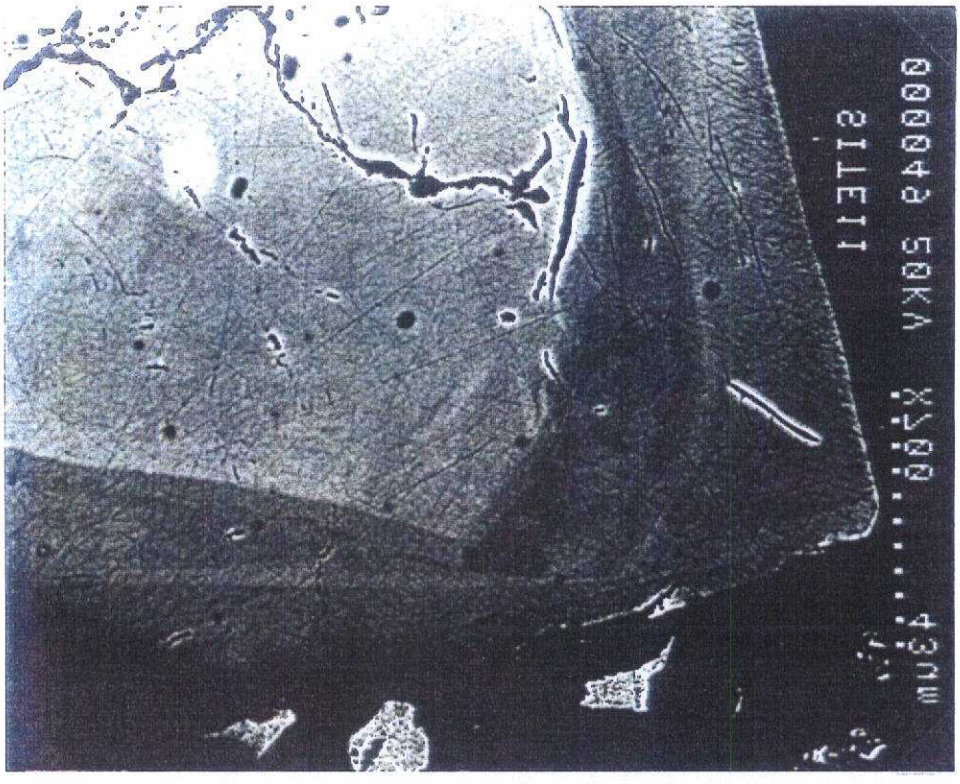

B

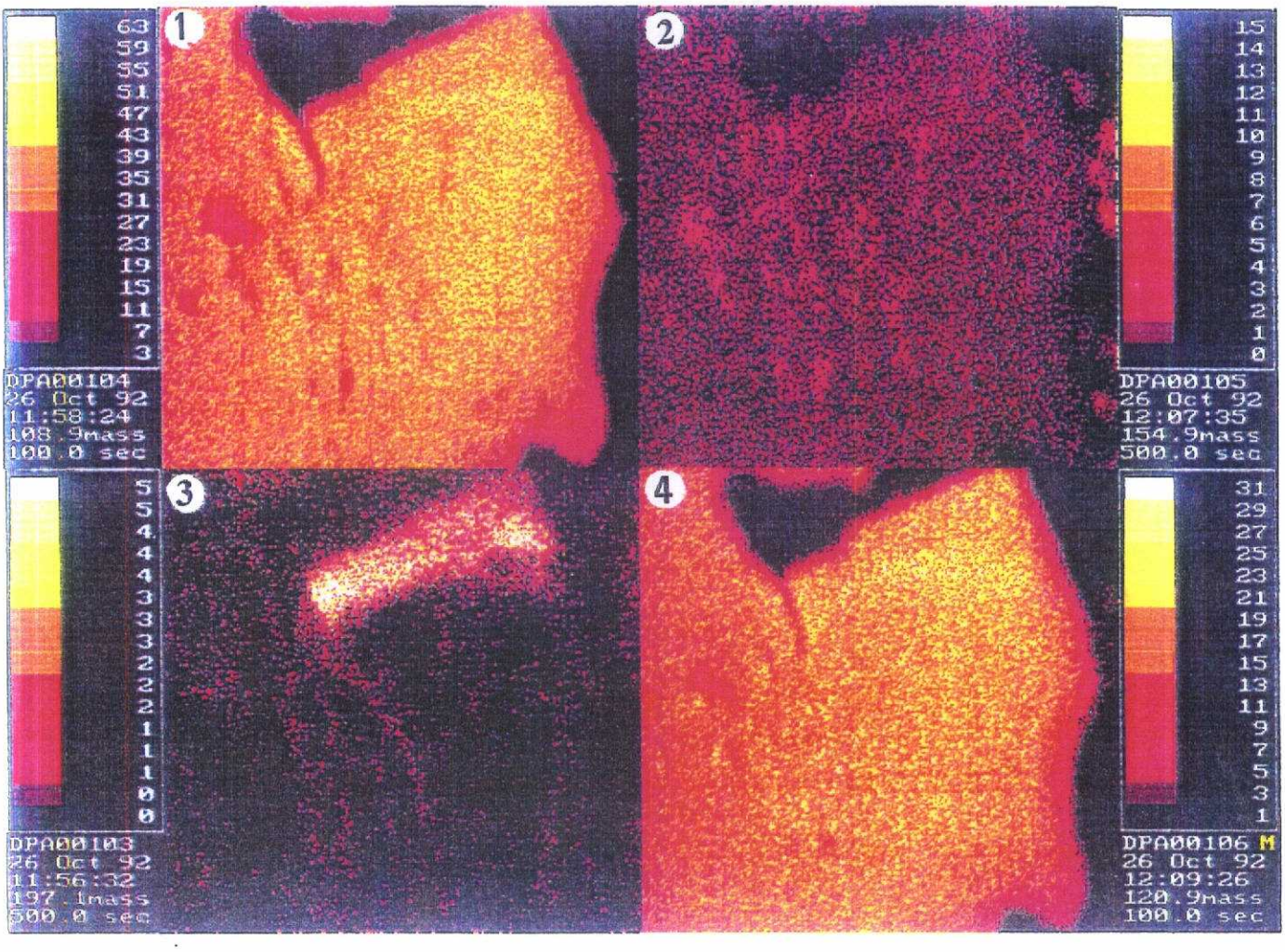

Plate IV-8 : A - Backscattered image of arsenopyrite crystals from Montemor area . B : Ion images corresponding to the secondary emission of ^{107}AsS (1), ^{155}SbS (2), ^{197}Au (3), ^{120}Sb (4) obtained on the arsenopyrite crystals mentioned in photo A. The side of the image is 250 µm. The maximum Au content in the crystal is 4.75. 10^{18} at/cm^3.The profile is given in figure IV -9b.

A

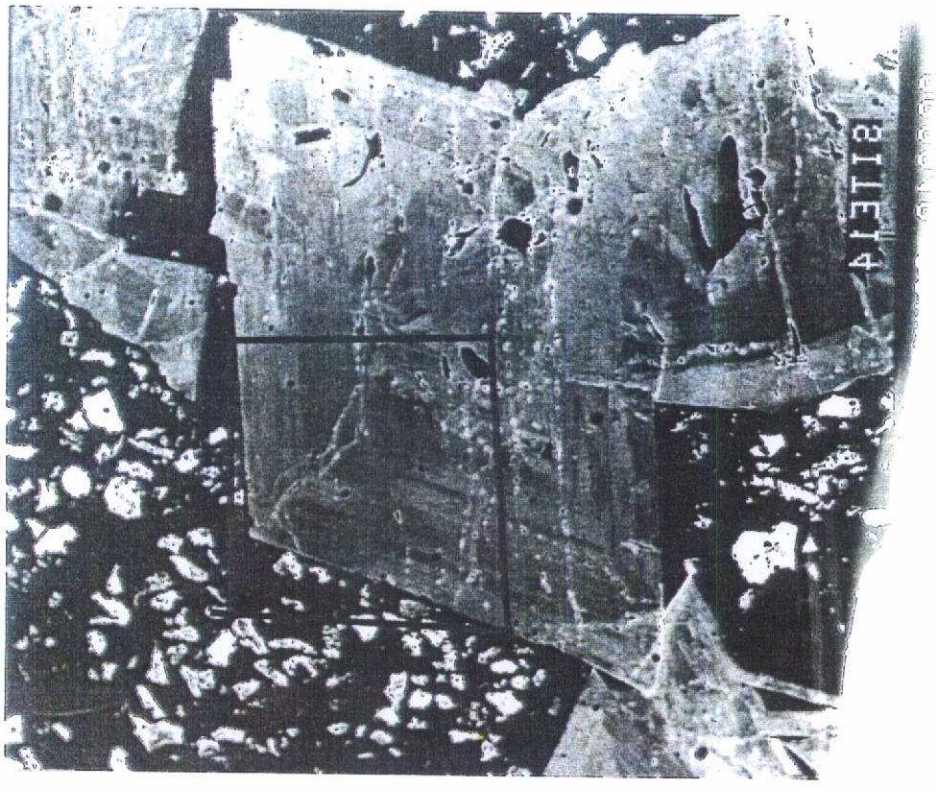

B

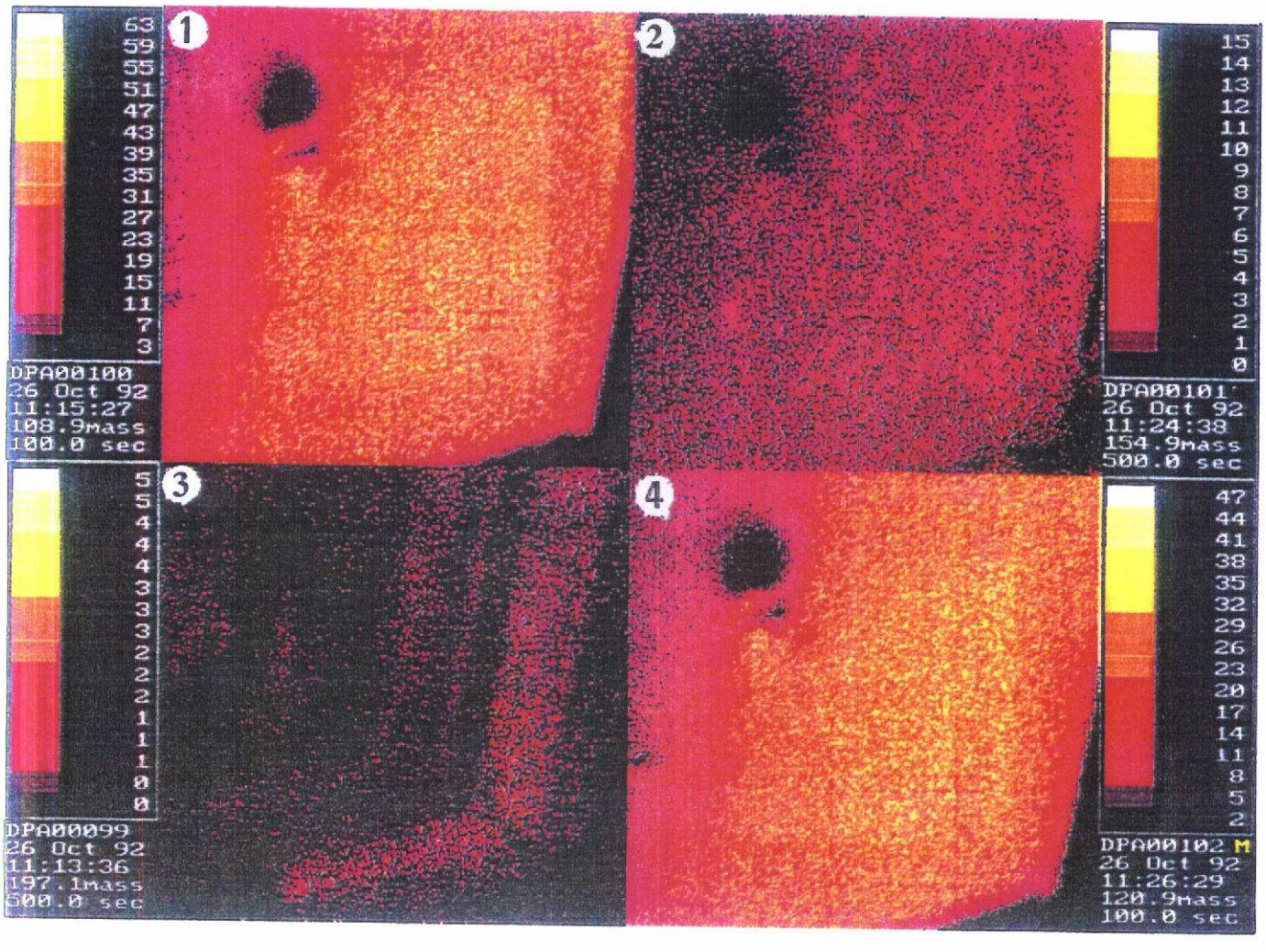

Plate IV-9 : A - Backscattered image of arsenopyrite crystals from Montemor area . B : Ion images corresponding to the secondary emission of ^{107}AsS (1), ^{155}SbS (2), ^{197}Au (3), ^{120}Sb (4) obtained on the arsenopyrite crystals mentioned in photo A. The side of the image is 250 µm. The maximum Au content in the crystal is 1. 10^{18} at/cm^3.

A

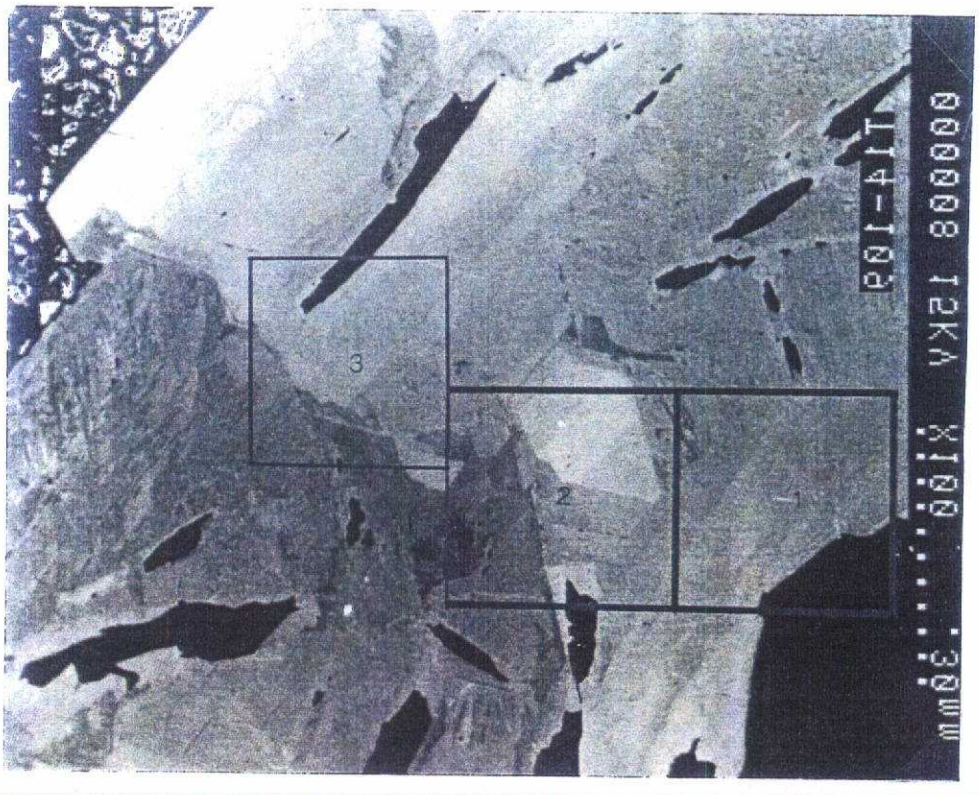

B

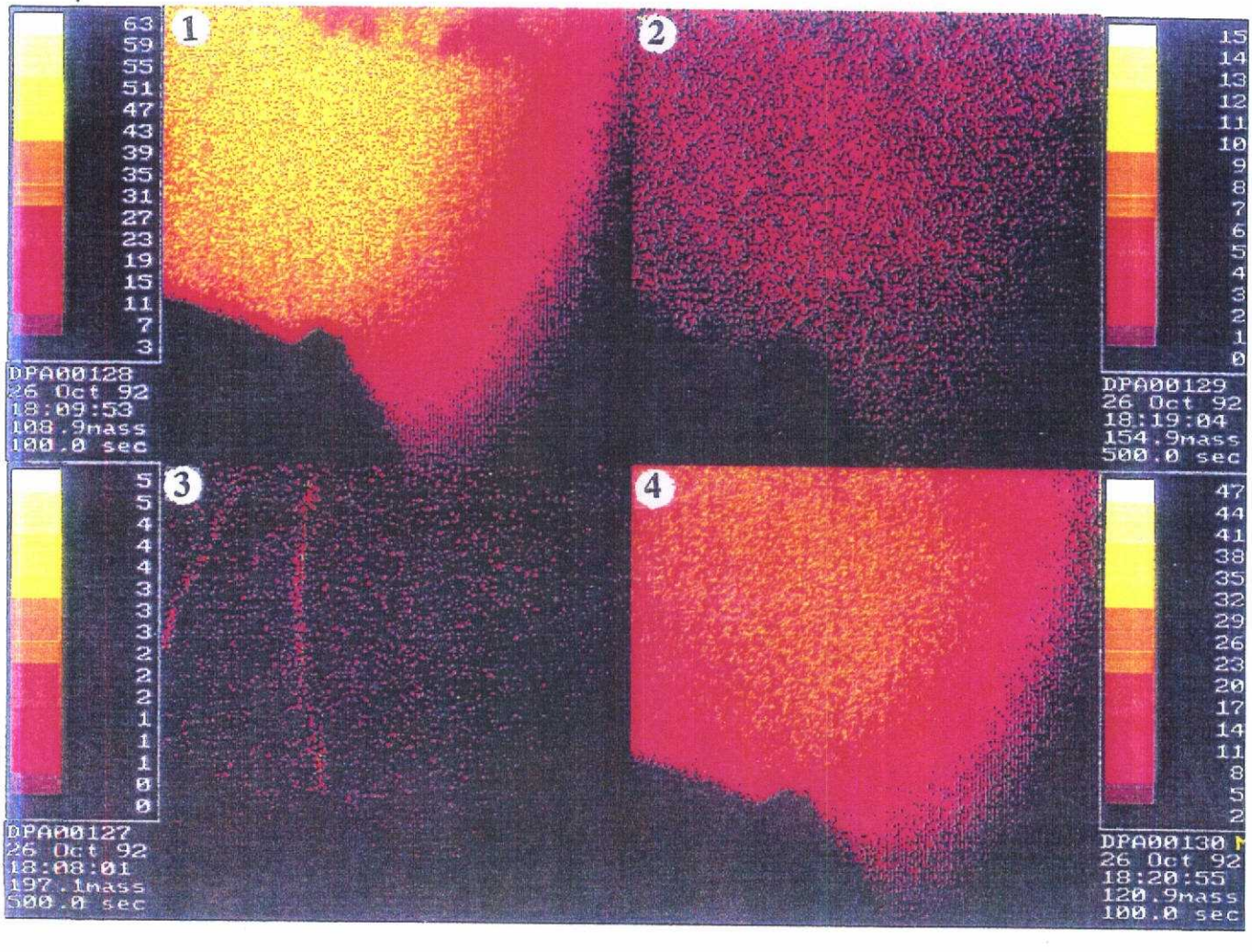

Plate IV-10 : A - Backscattered image of arsenopyrite crystals from Tomino area with indication of the 3 studied zones . B : Ion images corresponding to the secondary emission of ^{107}AsS (1), ^{155}SbS (2), ^{197}Au (3), ^{120}Sb (4) obtained on the arsenopyrite crystal, zone 1, mentioned in photo A. The side of the image is 250 µm.

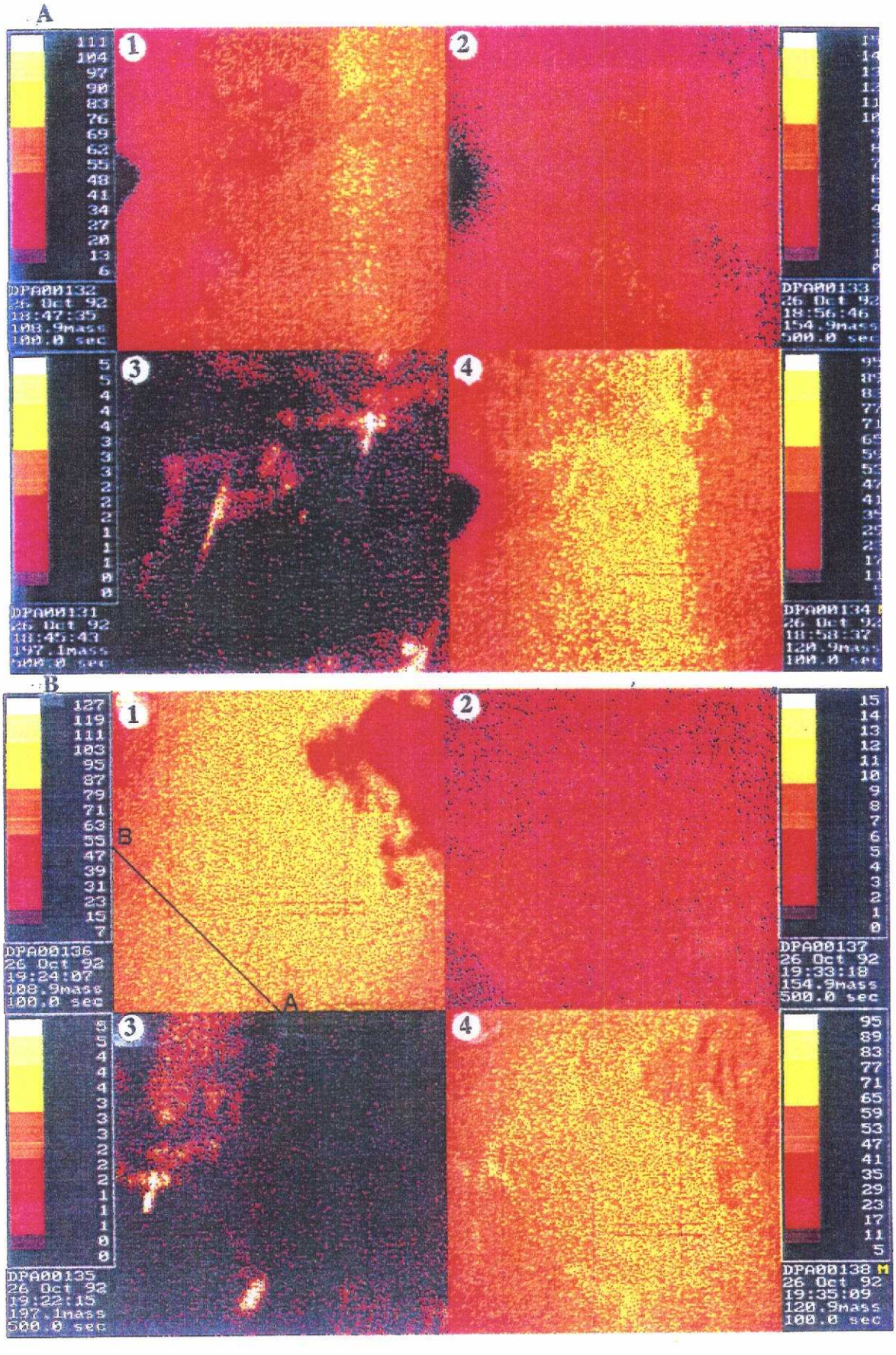

Plate IV-11 : A - Ion images corresponding to the secondary emission of ^{107}AsS (1), ^{155}SbS (2), ^{197}Au (3), ^{120}Sb (4) obtained on the arsenopyrite crystal, zone 2, mentioned in photo A, plate IV-10. B : Ion images corresponding to the secondary emission of ^{107}AsS (1), ^{155}SbS (2), ^{197}Au (3), ^{120}Sb (4) obtained on the arsenopyrite crystal, zone 3, mentioned in photo A, plate IV-10.. The side of the image is 250 µm. The maximum Au content in the crystal (zone 3) is 2.1. 10^{18} at/cm^3. The profile is given in figure IV -9a.

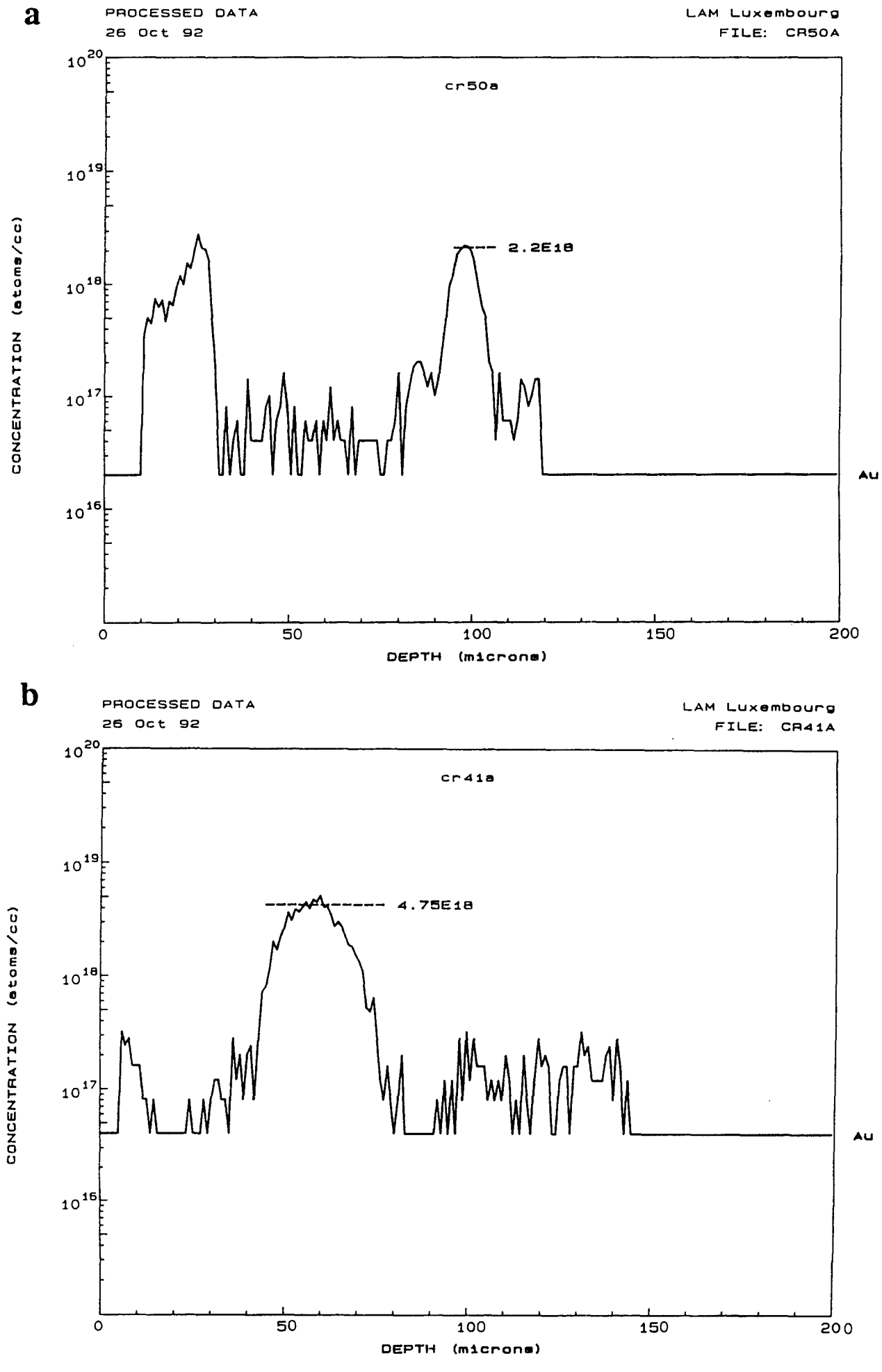

Fig IV - 10 : Profile of Au concentration in arsenopyrite crystal obtained by ion microprobe analysis. a : arsenopyrite from Tomino (Plate IV-10), b : arsenopyrite from Montemor (Plate IV-8).

For arsenopyrite, the molecular ion ^{109}AsS (^{75}As and ^{34}S) presents a good and stable emission (Fig IV-8). The ^{109}AsS ion emission can therefore be chosen as matrix isotope. Using the implantation profile of gold in the arsenopyrite standard (Fig IV-8), the RSF is 1,51 10^{20} at/cm^3 . This has been calculated for the maximum Au implanted at a depth of 3200 Å. This depth has been measured and then used in the computer simulation of the implantation.

The same calculation can be done for pyrite standard. The RSF is 3,43 10^{20} considering the ^{90}FeS ($^{56}Fe^{34}S$) matrix isotope (Fig IV-9).

Gold content distribution using RAE imaging

Ion images have been obtained for most deposits although clear Au distribution have been mostly found in the Tomino, França and Montemor arsenopyrites. The line scans obtained on enriched zones allowed us to quantify gold contents on the basis of results obtained on standards.

Deposits may be classified in two groups :

i) those where no clear Au distributions have been found in growth bands , but only patches and fissures of arsenopyrite slighlty enriched in Au : Corcoesto, Penedono. In these cases, characterized by rather homogeneous major element distributions. Au is found at a low content, generally below 10 ppm, and may reach 20-25 ppm in thin growth bands or in badly defined areas within the crystals. At Corcoesto, the highest contents (40 ppm) have been found in a late growth band of tiny euhedral crystals from the -348 m sample.

ii) those where arsenopyrite display clear incorporation of gold at a combined state during the crystallization of specific growth bands of the crystal : França, Montemor, Tomino. In these deposits, different cases can be distinguished. The best examples of Au distributions are presented in plates IV - 6 to 9:

- late growth bands with high Au content reaching 200-250ppm, crystallized on a crystal containing around 20 ppm Au (Montemor) (Fig.IV-10b).
- alternate enrichments along growth bands, with values oscillating around 50 ppm in the richest zones and 15 ppm Au in the poorest ones (Montemor samples).

Similar patterns are found at França, where the richest Au rich arsenopyrite growth bands reach 70 ppm for an arsenopyrite Au background of around 15 ppm.

In these three deposits, the crystallization of late Au-rich arsenopyrite display similarities to the case of the Laurieras deposit in France where only the latest growth (or overgrowth) bands contain detectable Au (up to 1000 ppm).

More complex patterns are found in the Tomino samples where relatively scarse and localized Au enrichments characterize some growth bands which are relatively difficult to relate to a specific stage in the arsenopyrite sequence. In these zones, Au content may reach 100 ppm.

2- PLACE OF NATIVE GOLD IN THE PARAGENETIC SEQUENCES

Paragenetic sequences in intragranitic deposits

Most reconstructed paragenetic sequences show that metallic gold is for its most part born by early sulphides (especially arsenopyrite) but trapped in vugs and cracks, indicating a probable late Au particle formation. It is rather difficult to assess that gold was introduced early in these veins, as native gold particles or within Au precursors; however, the latter cannot be considered as a significant source for gold, since these sulphides are stable, and display rather low Au contents.

Au occurs mostly as electrum particles, of variable size. Figure IV-11 shows typical EDS spectrum of electrum from Penedono, whilst photographs (Plate IV-12)show typical features of electrum grains.

The association Au- (sulphosalts, Bi-Bism, chalcopyrite) is relatively common (Tomino, Penedono) although native Au may precipitate alone, on arsenopyrite surface, without any accompanying elements (case of Corcoesto and Pino).

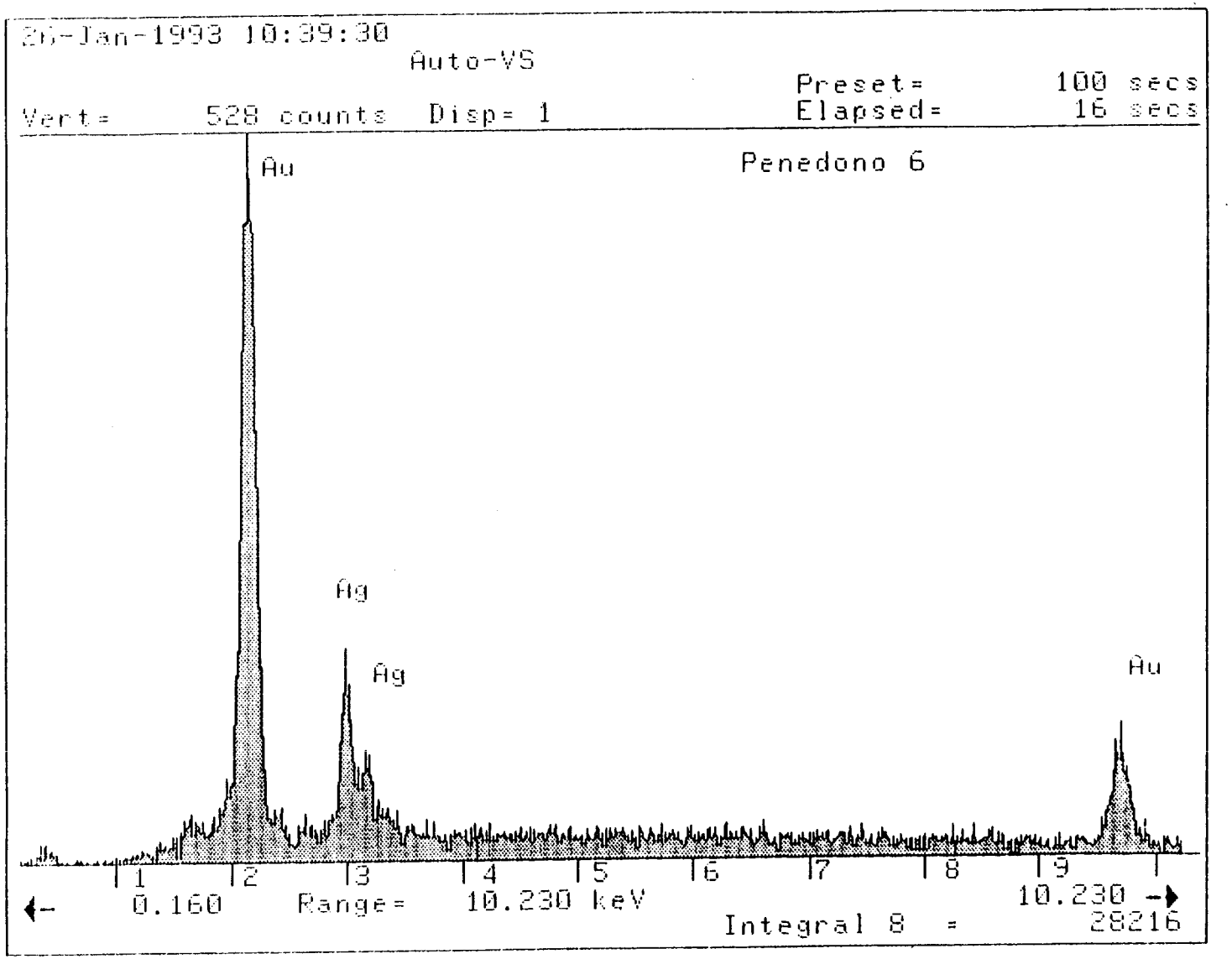

Fig IV - 11 : EDS spectrum of electrum from the Penedono area. Quantification indicates that Au and Ag content are respectively 89 % at and 11 % at.

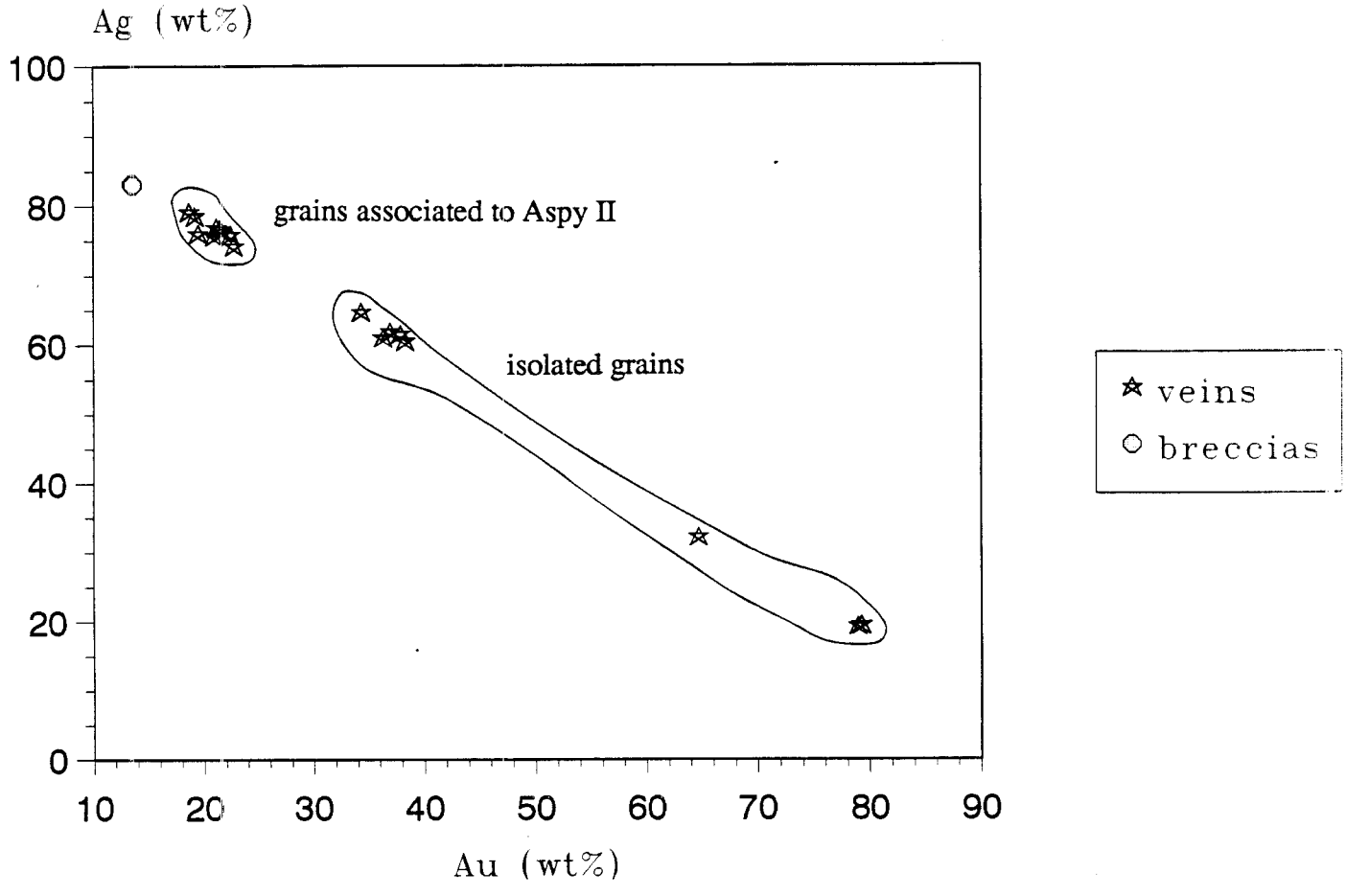

Fig IV - 12 : Au-Ag diagram applied to electrum composition from the França deposit.

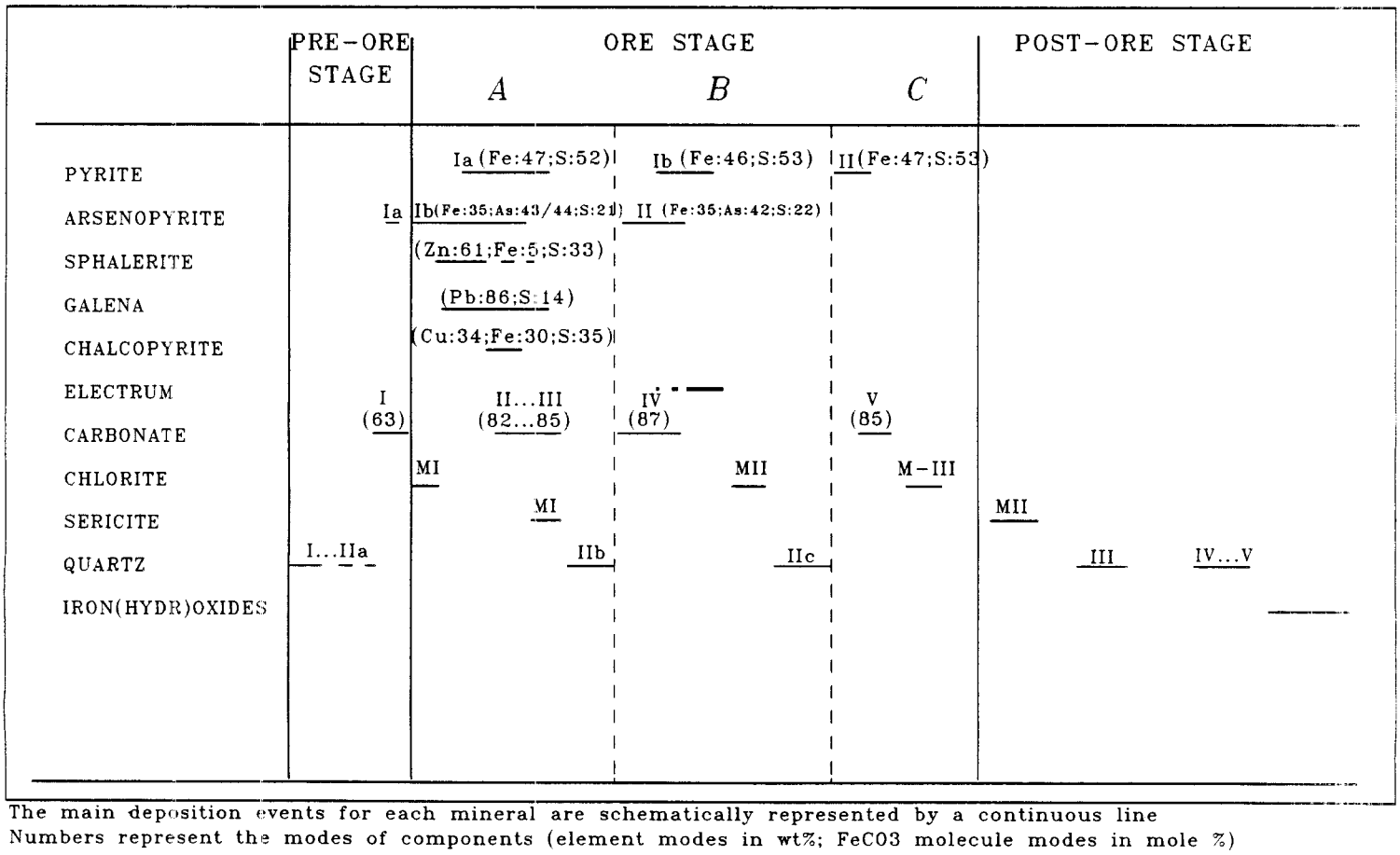

Fig IV - 13 : Paragenetic sequence for mineralized veins of the França ore deposit with indication of the mineral compositions.

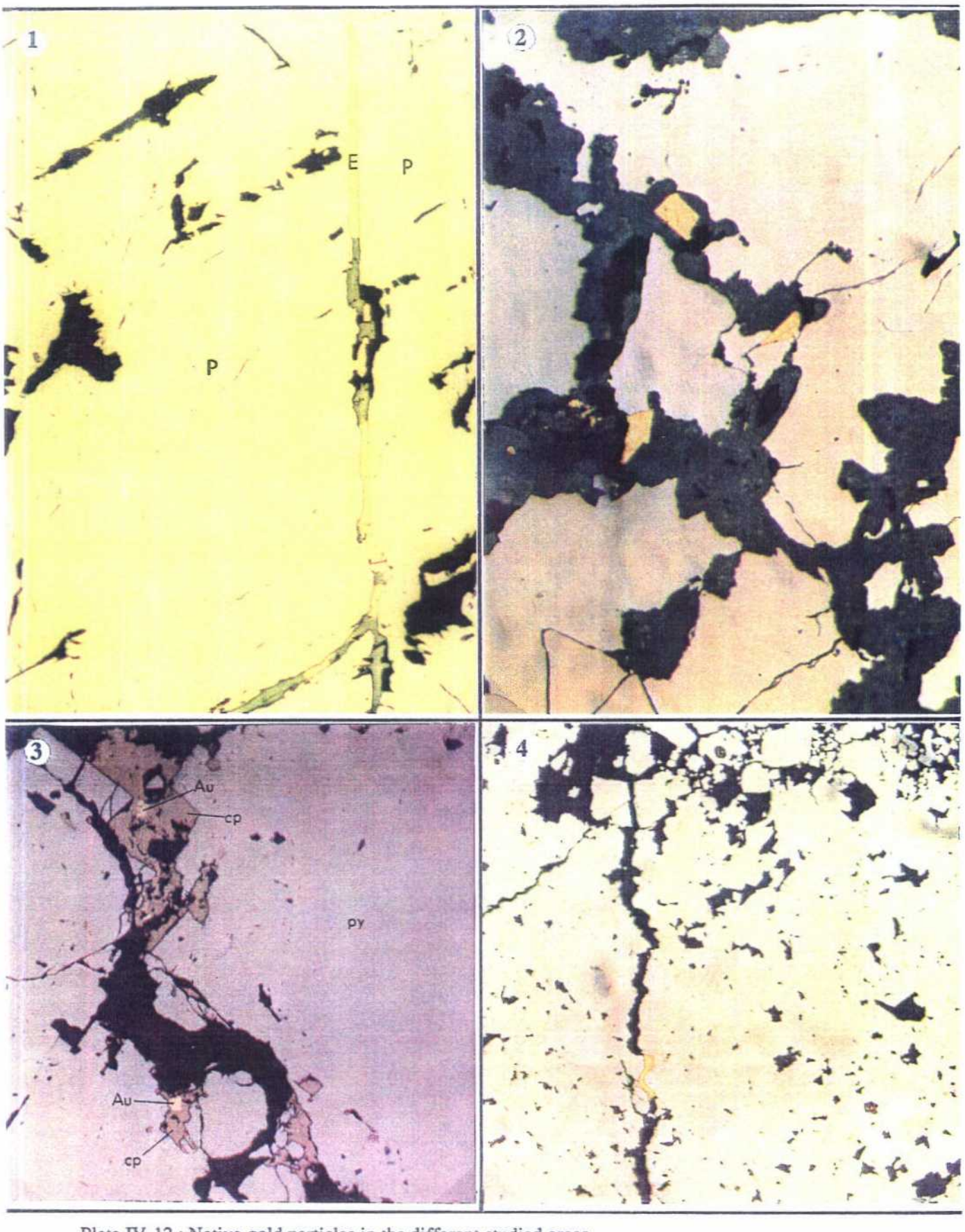

Plate IV-12 : Native gold particles in the different studied areas
1- Electrum (E) and Ag sulfosalts in microfracture within pyrite (P) (Vila Pouca de Aguiar area). 2- Native gold in late quartz croscutting early sulphides (Penedono area). 3- Native gold (Au) inclusions in chalcopyrite (cp) filling microfissures of pyrite (py) (Tomino). 4 - Native gold in microfissures within arsenopyrite from Corcoesto.

Paragenetic sequences in intrametamorphic deposits

Similar observations have been made at Vila Pouca de Aguiar and França where gold or electrum occurs as late particles posterior to most sulphides, and is associated to Pb-Sb-Ag sulphosalts.

At França, mineralized quartz–carbonate veins display electrum particles of variable size (usually ranging from 20 to 150 μm). They occur both close to Aspy II boundaries and as isolated grains. Analytical results of electrum particles are summarized in Table IV-3, (annexe). Besides the expected inverse relationships between Ag and Au contents (Fig. IV-12), widely variable levels of Sb, Fe, Cu, Pb and S were also determined. According to the available data, electrum grains close to Aspy II are extremely rich in silver (70–80 wt%, on average), and show often Sb contents greater than 0.50 wt%. On the contrary, (later) isolated electrum grains, are characterized by gold concentrations ranging from 30 to 80 wt% and traces of Sb (commonly lower than 0.20 wt%) (Fig. IV-13). Within quartz breccia matrices, electrum grains show typically silver contents of the order of 83 wt%, and the deficient totals usually obtained are probably due to the high porous texture exhibited by these particles, since successive microprobe standardizations and qualitative analyses were done in order to check up both the analytical results obtained and the possibility of the presence of other metals.

3- CONCLUSION

Most deposits display a rather similar sequence of gold introduction in the veins :

- gold is mostly observed as native gold in the latest mineral assemblages in most deposits. It is accompanied by specific paragenesis and element associations as shown by the synthetic map from figure IV-14. The Bi-Cu-Pb (Sb) association is one of the most significative.
- it is rather difficult to assess that gold was present or not during earlier stages, since it always observed in vugs or fissures affecting the early sulphides.
- gold is introduced in the veins, at a combined state in small quantities (less than 70 ppm in the richest cases) during a relatively late stage of arsenopyrite deposition :
  - at Franca and Montemor, in the late growth zones from the latest arsenopyrite II (up to 700 ppm)
  - at Tomino and Corcoesto, in arsenopyrite from veinlets , but at low contents

Comparison with french hercynian deposits

A schematic sequence summarizes the mineralogical data obtained on the most significative occurrences the Armorican Massif (La Lucette, La Bellière deposits) and Massif Central (Le Bourneix deposit, Hubert, 1986), and gold showings (Vaulry, Ambazac, Janaillac) from the Limousin area.(Table IV-3). Three major stages of arsenopyrite crystallization may be distinguished. They are characterized by specific mineral assemblages, alteration mineralogy in the host rocks, and physical-chemical conditions. Native gold has been found associated with these different mineral assemblages. However, there are many difficulties in the determination of its cogenetic relationships with the observed paragenesis since gold is several times reworked within a given deposit. Nevertheless, native gold is undoubtably associated with the three late stages, characterized by the sulfide assemblage crystallized in the range 300-400°C as shown by the fluid inclusion data (Hubert, 1986, Cathelineau and Boiron, 1988, Boiron et al, 1988), the late sulphide-sulfosalts assemblages and the supergene events. These deposits display numerous similarities with the Spanish and Portuguese deposits

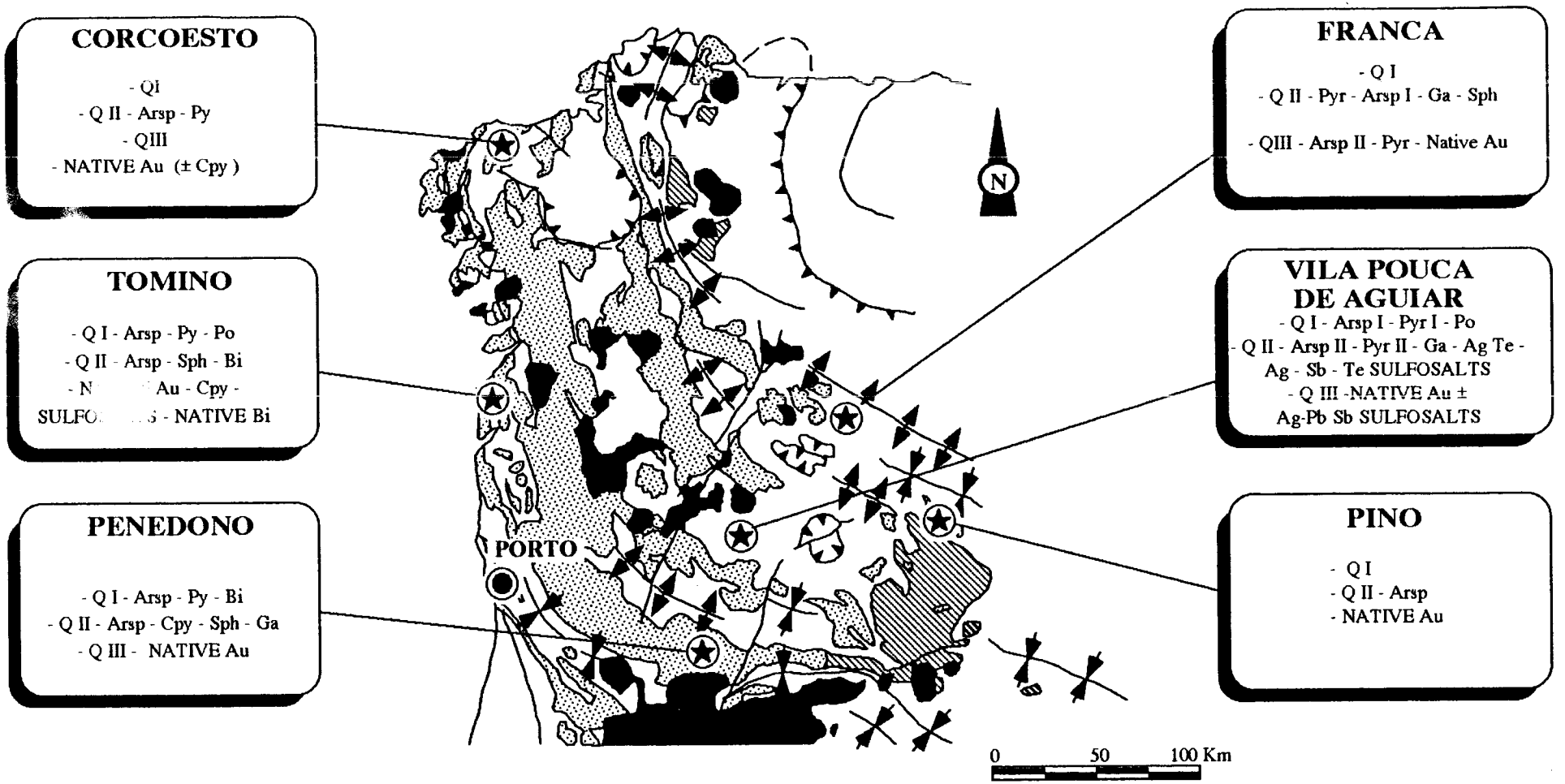

Fig IV - 14 : Paragenetic sequences and place and state of gold in the sequences

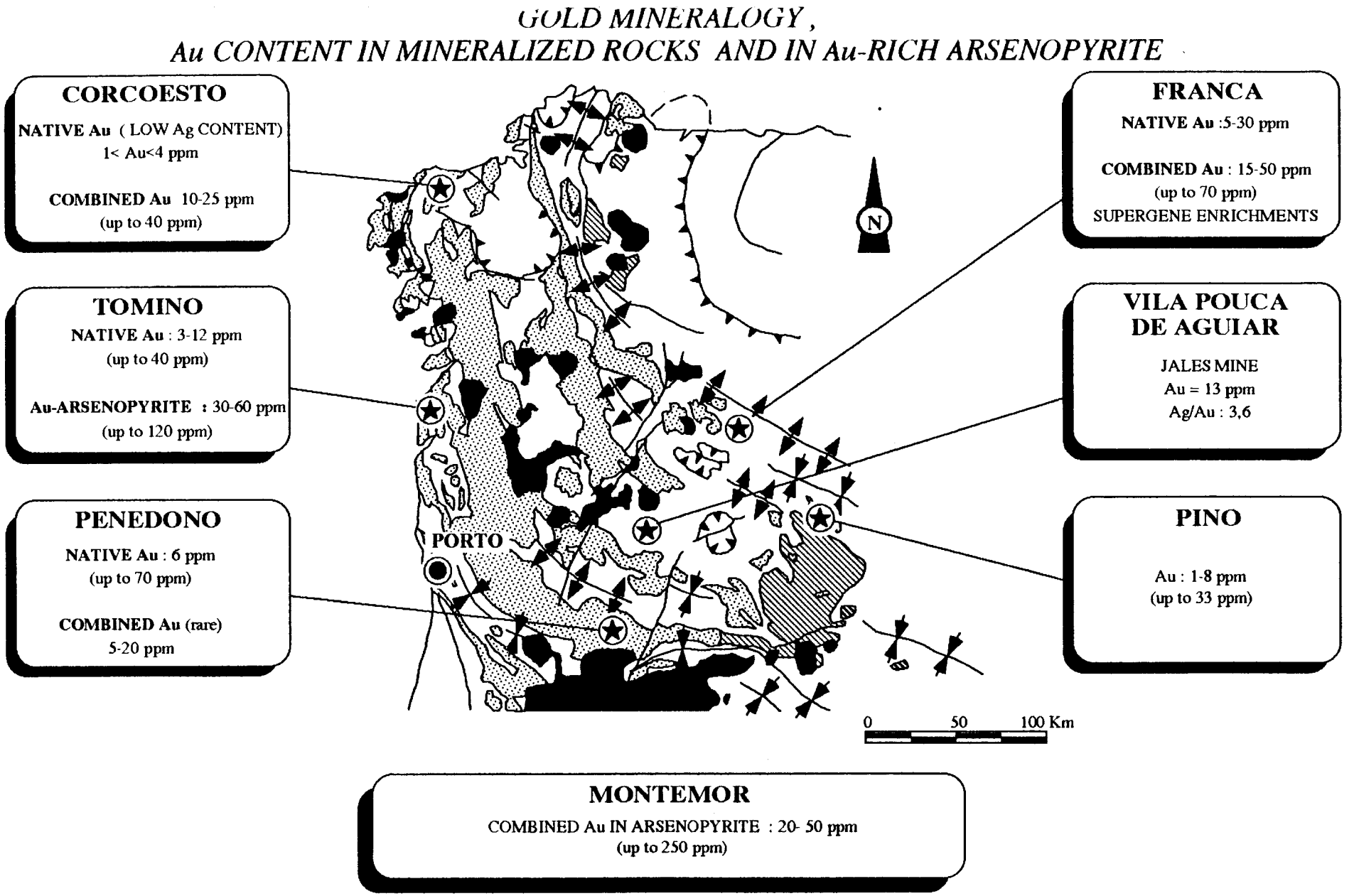

Fig . IV -15 : Gold mineralogy, contents in ores and in gold bearers.

			BELLIERE	MONTAGNE NOIRE	LIMOUSIN district	MARCHE COMBRAILLES VILLERANGES	MARCHE COMBRAILLES CHATELET
Native gold	Qtz veins breccia microsaccharoid qtz		arsp - pyr (?)		arsp - pyr		
Native gold	Microfracturing recrystallized qtz	* P.F.I	sph -gal-cpy	arsp - pyr	arsp		
Combined gold	qtz veinlets	* P.F.I	Au		Au- Arsp		(?)
Native gold		* F.I.T.	(?)	cpy-Au-Bi-bism	gal - cpy sulfosalts		
Combined gold	Authigenic qtz combs	* P.F.I.				Au-arsp-pyr-qtz-ank qtz - stib	Au-arsp-pyr-qtz-ank

Table IV - 3 : Mineralogical assemblages for the gold bearing quartz veins. Arsp : arsenopyrite, Au-arsp : gold bearing arsenopyrite, pyr: pyrite, cpy : chalcopyrite, sph sphalerite, gal : galena, stib : stibine, bi: native bismuth, Au : native Gold, bism : bismuthinite, P.F.I. : primary fluid inclusion, F.I.T. : fluid inclusion trail. (from Boiron et al, 1990).

The Au-rich arsenopyrite deposits are exemplified by the Marche-Combrailles district (North western part of the French Massif Central) which displays a wealth of Au (Sb)-deposits, gold showings, the location of which is spatially related to the so-called "Marche-Combrailles" regional shear zone. Among these Au-occurrences, the Châtelet deposit is the only one to have been mined extensively and produced around 10 metric tons of gold till its closing in 1955. In these deposits, gold is almost entirely borne by sulfides, mostly arsenopyrite and at a lesser degree pyrite. Arsenopyrite crystallizes at a specific stage in the mineral sequence of the deposits together with quartz and ankerite (Boiron, 1987, Boiron et al, 1988). Ore fluid circulation is related to the late magmatic stages of the Hercynian activity, and to late britlle deformation affecting earlier shear zones (Boiron et al, 1989). At that time, heat flows necessary to fluid convection were related to late thermal anomalies which are distributed along deep crustal structures and were probably favoured by the presence of numerous high heat production granites (Vigneresse et al., 1987, 1988). This kind of deposit have not been encountered in north western iberic peninsula.

B-INTEGRATED STUDIES ON THE DETERMINATION OF INDIVIDUAL FLUID INCLUSION COMPOSITIONS

Fluid inclusions are extremely useful geochemical markers : i) they are the only samples available of the paleofluids, ii) their density and composition give minimal estimates of the P-T conditions of their trapping, iii) their trapping in healed microfissured makes possible the reconstruction of the geometry of the paloefluid pathway geometry. This is the reason why they have been extensively studied in close relation with the mineralogical and deformational features of the vein to get significant constraints on the conditions of Au concentration formation.

a-METHODOLOGY AND IMPROVEMENTS

MICROTHERMOMETRIC MEASUREMENTS

Microthermometric characterization of the fluid inclusions was performed on wafers (300µm thick) using a heating-freezing Chaixmeca stage (Poty et al., 1976). The stage was calibrated with melting-point of solid standards at T > 25°C and natural and synthetic inclusions at T< 0°C. The vertical gradient is less than 0.1°C at low temperatures within 40µm below the wafer's surface (Dubois, 1992) . The rate of heating was monitored in order to get an accuracy of ± 0.2°C during freezing, and ± 1°C when heating over the 25°-400°C range and ± 4 °C over the 400°-600°C range. Salinity, expressed as equivalent weight % of NaCl and fluid density of volatile-free fluid inclusions in quartz, were determined by microthermometry (Potter, 1977 ; Potter et al., 1978).

In volatile-bearing fluid inclusions, CO_2 was identified by melting of a solid below -56.6°C. The volumetric fraction of the aqueous liquid (flw) and the volumetric fraction of the volatile-rich liquid in the volatile-rich phase (flc) have been estimated at room temperature by reference to the volumetric chart of Roedder (1972).

RAMAN DATA

Molar fractions of CO_2, CH_4, H_2S and N_2 were determined in individual inclusions by micro-Raman analysis performed on a DILOR X-Y multichannel modular Raman spectrometer (Dhamelincourt et al., 1979).

Bulk composition and molar volume were computed from the P-V-T-X properties of individual inclusions in the C-O-H-S system (Dubessy, 1984 ; Ramboz et al., 1985 ; Dubessy et al., 1987 ; Dubessy et al., 1989, Dubessy et al., 1992).

The P-T properties of aquo-carbonic inclusions were modelled for the system H2O-CO2-CH4- NaCl using the V-X data and the equation of state of Kerrich and Jacobs (1981) and Jacobs and Kerrich (1981)

WATER CONTENT IN FLUID INCLUSIONS

Although water is a very common component in fluid inclusions, the water content in fluid inclusions cannot be accurately determined. If water is visible, the determination of the bulk V-X properties is based on the visual estimation of the volume proportion of the aqueous and non aqueous fluid phases, under optical microscope . If water is not visible, the estimation of the water content is quite difficult especially for inclusions with diameter smaller than 8 µm. The spatial resolution of a good optical microscope is 0.5 mm and thus fixes the maximum thickness of the non visible water film coating the wall of the inclusion. Other investigation methods for the single phase non aqueous inclusions are required to estimate the water content in fluid inclusions.

Infrared spectroscopy is known to be very sensitive to water and OH groups. The wavelength of the water stretching vibration band of liquid water, extending from 3100 to 3800 cm^{-1}, is in the range 2.5-3 µm. Therefore, light diffraction makes difficult the identification of water film with a thickness smaller than 3 µm.

The Raman spectrum of liquid water is also rather weak and thus cannot be obtained if water is not visible. Phase diagrams of water-gas systems show that bulk homogenization to the vapour phase of water-poor fluid inclusions are expected to occur at rather low

temperatures, always below 300°C. Water fills all the volume of the fluid inclusion at temperatures above the temperature of the L + V ---> V phase transition and thus is expected to provide better optical conditions for its detection by micro-Raman spectroscopy. This was done on several fluid inclusions with size down to 10 µm. The water spectrum recorded at 200°C is characterised by a single symmetric band at 3636 cm^{-1} with a width at half height of 12 cm^{-1} in all the inclusions with no visible water at room temperature. No effect of temperature has been noticed. Results of composition calculations will give an order of magnitude of the water concentration in water-poor inclusions till the Raman scattering cross-sections of water-gas systems will not be calibrated as a function of composition and bulk density. Results obtained on several inclusions indicate mole fraction of water in the range 0.1 to 1 mole %. Water has been found for the first time by this method in fluid inclusions from mantle xenoliths and in metamorphic fluids from gold bearing quartz veins (Salsigne district).

The second case deals with inclusions in which water is visible under microscope, corresponding to water concentrations usually larger than 20 mole % . Spectra obtained in water-rich fluid inclusions are completely different. The wavenumber at maximum intensity is shifted towards lower values (3630 cm^{-1} for $X(H_2O) = 0.5$ and 3575 cm^{-1} for $X(H_2O) = 0.7$), the shape of the band is less symmetric and the width at half height is larger (40 to 45 cm^{-1} for $X(H_2O) = 0.5$ and 150 cm^{-1} for $X(H_2O) = 0.7$). These spectroscopic features are a clear indication of increase of water-water interactions. By contrast, the spectrum of CO_2 does not vary as the Raman spectrum of water. The Raman spectrum of CO_2 exhibits a small broadening of the diads of the Fermi resonance and a smaller intensity of the low frequency line of the diad for $X(H_2O) = 0.7$. This pattern is similar to the difference between the spectrum of pure CO_2 and CO_2 dissolved in water at room temperature, indicating that water-CO_2 interactions become noticeable from the Raman spectrum of CO_2 for $X(H_2O) > 0.3$-0.5. Thus, the approximation of the Raman scattering cross section of vapour water cannot be used in water-rich fluid inclusions. A thorough calibration should be made before any use for quantitative analysis. In addition, salts are also expected to complicate the analytical use of Raman spectra because of the ion solvatation by water molecules and structure breaker effects of chloride .

NOMENCLATURE AND CLASSIFICATION OF FLUID INCLUSIONS

CO2-rich fluids

Lc : CO2 dominant monophase inclusions with liquid CO2-CH4 (-N2) (at room temperature), without any visible water.

Lc - w : two or three-phase inclusions (aqueous phase>20%). Global homogenization in the liquid or critical phase.

Vc - w : H2O-CO2-CH4-(N2-H2S) two-phase inclusions which global homogenization in the vapour phase.

Lw - c : two-phase liquid-rich inclusions, in which CO2 is only detected by the presence of clathrates (global homogenization in the liquid phase).

CH4-rich fluids

Vm - w : two-phase CH4 dominant inclusions (at room temperature), with the occurrence of a third phase when freezing below -100 °C.

Vm - w - S : inclusions characterized by the presence of solid inclusions (graphite), with vapour CH4-N2 at room temperature.

Lw - m : two-phase inclusions (aqueous phase dominant), which temperature of final clathrate melting is > +10 °C (CH4 is known to raise the temperature of clathrate melting).

Lw - m - S : two-phase inclusions with a solid phase dominant (graphite). The presence of CH4 and graphite has been confirmed by Raman spectroscopy.

Aqueous inclusions

Lw : H2O-NaCl inclusions, (global homogenization in the liquid phase).

These classification and nomenclature will be used in the following description of the fluid inclusion data for all the studied deposits.

b - FLUID INCLUSION DATA

MINERALIZATIONS IN GRANITE

1 - CORCOESTO (CREGU AND PORTO UNIV.)

Fluid inclusions from Corcoesto drill core samples have been studied in mineralized quartz (MQ) and barren quartz in twelve samples from the surface to 540 m depth at CREGU (levels : surface, 66.5m, 70.85m, 147m, 189m, 256m, 346m, 365m, and 414m) and Porto University (levels 67m, 91m, 540m).

Different types of quartz have been distinguished in mineralized zones (Fig. IV-16):

(i) quartz lenses in metamorphic schists, and quartz associated with deformed pegmatoïds,

(ii) early quartz parallel to the granite foliation generally barren;

Quartz veinlets mineralized in arsenopyrite composed of

(iii) Q1 quartz enriched in abundant by small fluid inclusions ;

(iv) clear overgrowths Q2 preceding the arsenopyrite deposition;

(v) clear euhedral quartz or clear quartz cementing arsenopyrite crystals (Q3) prior to chlorite-carbonate veinlets .

Late barren quartz veinlets :

(vi) quartz comb veinlets Q4 associated with fluorite and kaolinite.

In mineralized quartz Q2-Q3, three major types of fluids have been recognized depending on the microthermometric and Raman data (Barakat, 1992).

- aquo-carbonic fluids with dominant CO2 (Vc-w and rare Lc-w)

Most of them have three phases at room temperature. They have been observed as fluid inclusion planes in Q 1 and MQ 2 or as primary or pseudo-secondary fluid inclusions in MQ-2.

TmCO2 are ranging from -57,1 to -60,5°C but most of the data are in the range -59,0; -57,5°C (Fig. IV-17). Melting temperature of ice is difficult to measure in such inclusions. However, salinity has been estimated in the range 7-8,5 % eq. wt.%NaCl considering the available data. Tm cl are observed beetween 4 and 11°C with a mode around 8°C (Fig. IV-17 and 19). Homogenization temperature of CO2 occurs in the liquid phase between 9° and 30,3°C. ThCO2 in the vapor phase is ranging from 9° to 30,5°C with two modes at 24°C and 31°C (Fig. IV-18). Global homogenization have been recorded in the range 280-390°C either to the liquid or to the vapour phase.

- aquo-carbonic fluids with dominant H2O (Vw-c and Lw-c)

Fluid inclusions are scattered in euhedral quartz crystals within arsenopyrites or display fluid inclusion planes in clear quartz overgrowth (Q3) near the arsenopyrite.

Liquid CO2 content is very low and is only detected by the presence of clathrates. Tm CO2 when visible is in the range -63 ; -57°C (Fig IV-17 and 19). Tf cl is in the range 6-15°C with a mode at 8°C (Fig IV-17 and 19). Global homogenization temperature occurs in the 280-400°C range either to the liquid or the vapour phase. No significant differences have been observed in the different samples.

- aqueous fluids

They are always observed as fluid inclusion planes in Q2 or Q3 croscutting aquo-carbonic fluid inclusion planes. Depending on melting temperature of ice two groups have been distinguished :

- low salinity fluid inclusions (Lw1) displaying TmH2O in the range -6 ; -1°C (Fig. IV-20 and 21) (salinity : 2-9 eq. wt.%NaCl). Such fluid inclusions are very abundant and very small. Global homogenization temperatures are in the range 150-350°C with a mode at 240°C and 300°C (Fig. IV-20 and 21).

-higher salinity fluid inclusions (Lw2) in planes croscutting the Lw1 fluid inclusion planes. TmH2O is in the range -24 ; -12 °C (Fig) and salinity is estimated between 16 and 24 eq. wt.%NaCl). Homogenization temperatures are in the 100-150°C range with a mode around 120°C (Fig. IV-20 and 21).

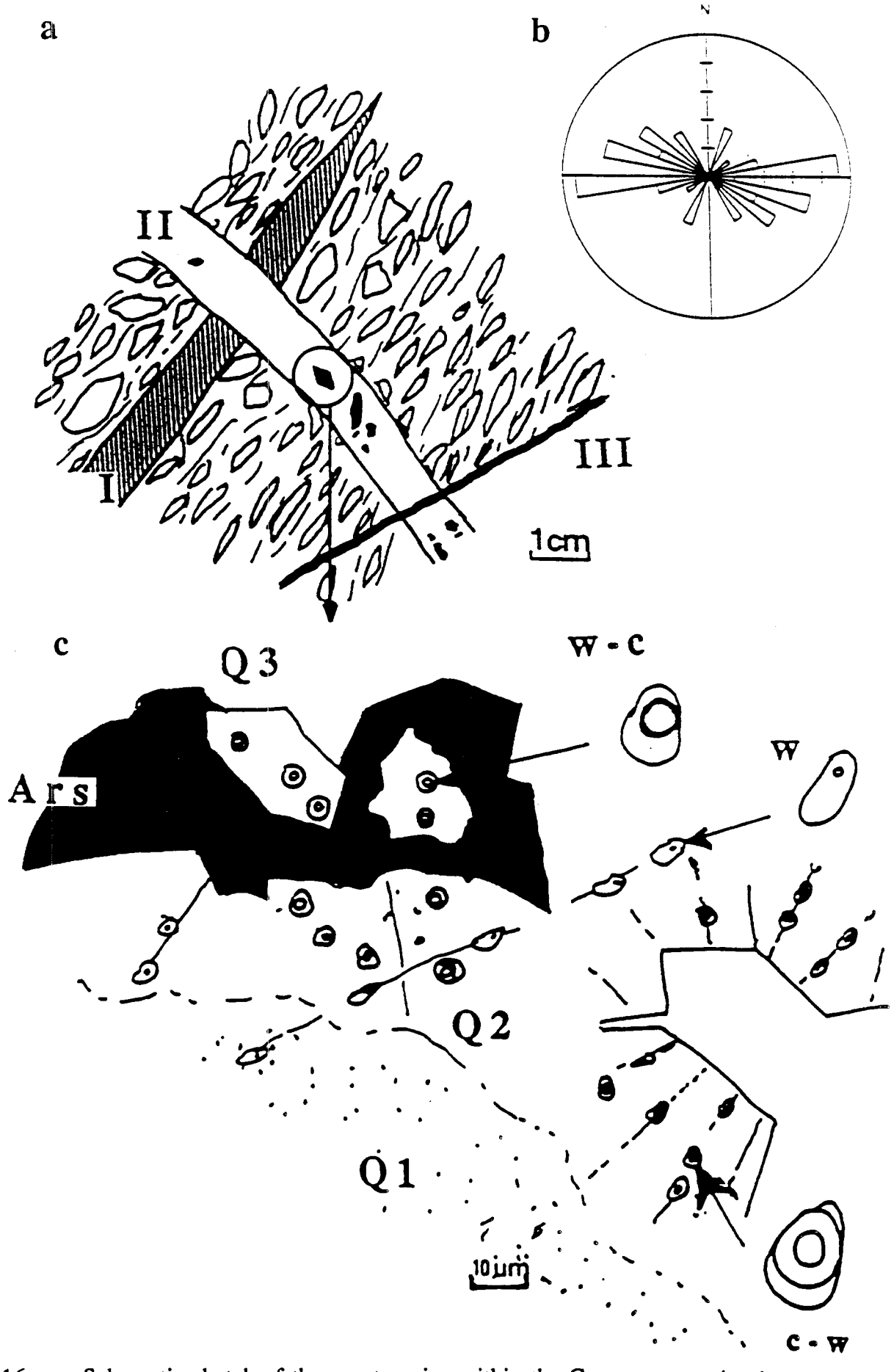

Fig IV - 16 : a : Schematic sketch of the quartz veins within the Corcoesto granite. b : rose diagram showing the orientation of quartz veins. c : different types of quartz with indication of the differents fluid inclusion types. Ars : arsenopyrite, Q1 : quartz 1 enriched in fluid inclusions, Q2 : clear overgrowths of quartz 2, Q3 : clear euhedral quartz 3, cementing arsenopyrite. c-w , w-c and w refer to fluid inclusion typology defined in the text.

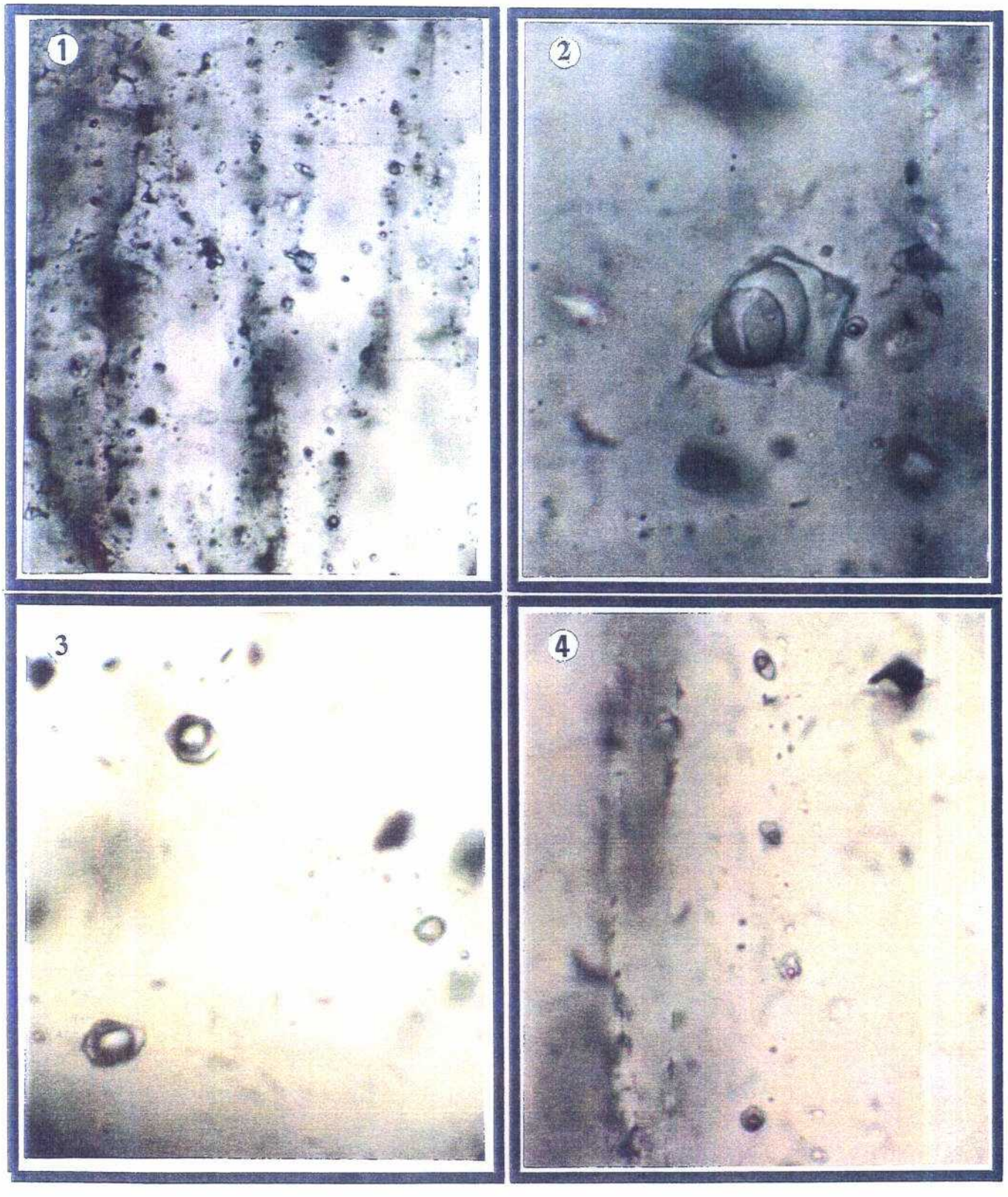

Plate IV-13 : Fluid inclusion features from Corcoesto quartz veins.
1 - Lc-w aquo-carbonic inclusions (three phase inclusions) in trails in Q2 quartz (X 200).
2 - Lc-w aquo-carbonic inclusions in Q2 quartz, detail of photo 1, (X 1000).
3 - Lw-c aquo-carbonic inclusions in Q3 euhedral quartz (X 1000).
4 : Lw aqueous inclusions in trails in quartz Q3, (X 1000).

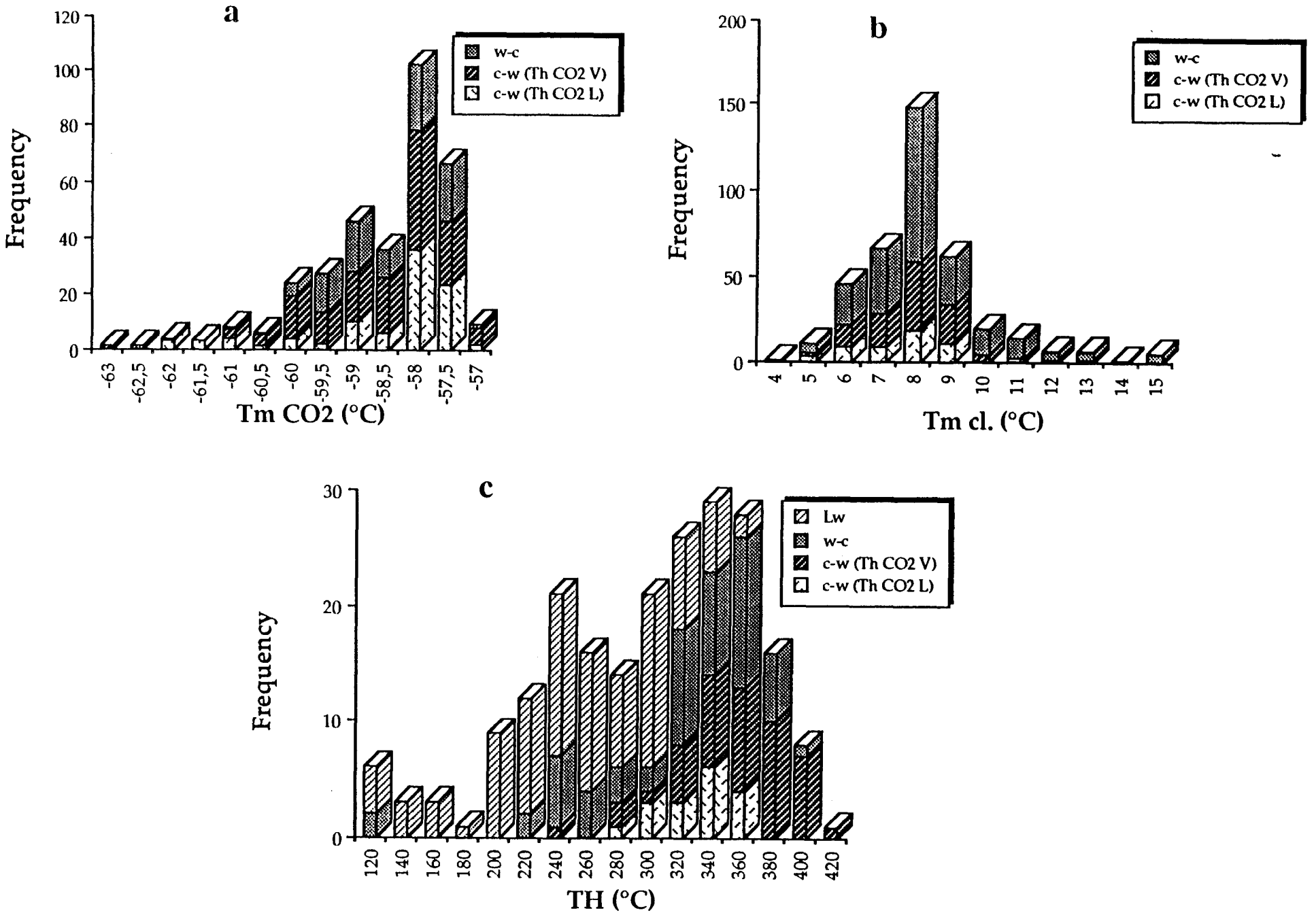

Fig IV - 17 : Corcoesto fluid inclusion data presented as a function of fluid typology. a : histogram of melting temperature of CO2 (TmCO2) ; b : histogram of melting temperature of clathrates (Tm cl),.c : Histogram of global homogenization temperature (TH).

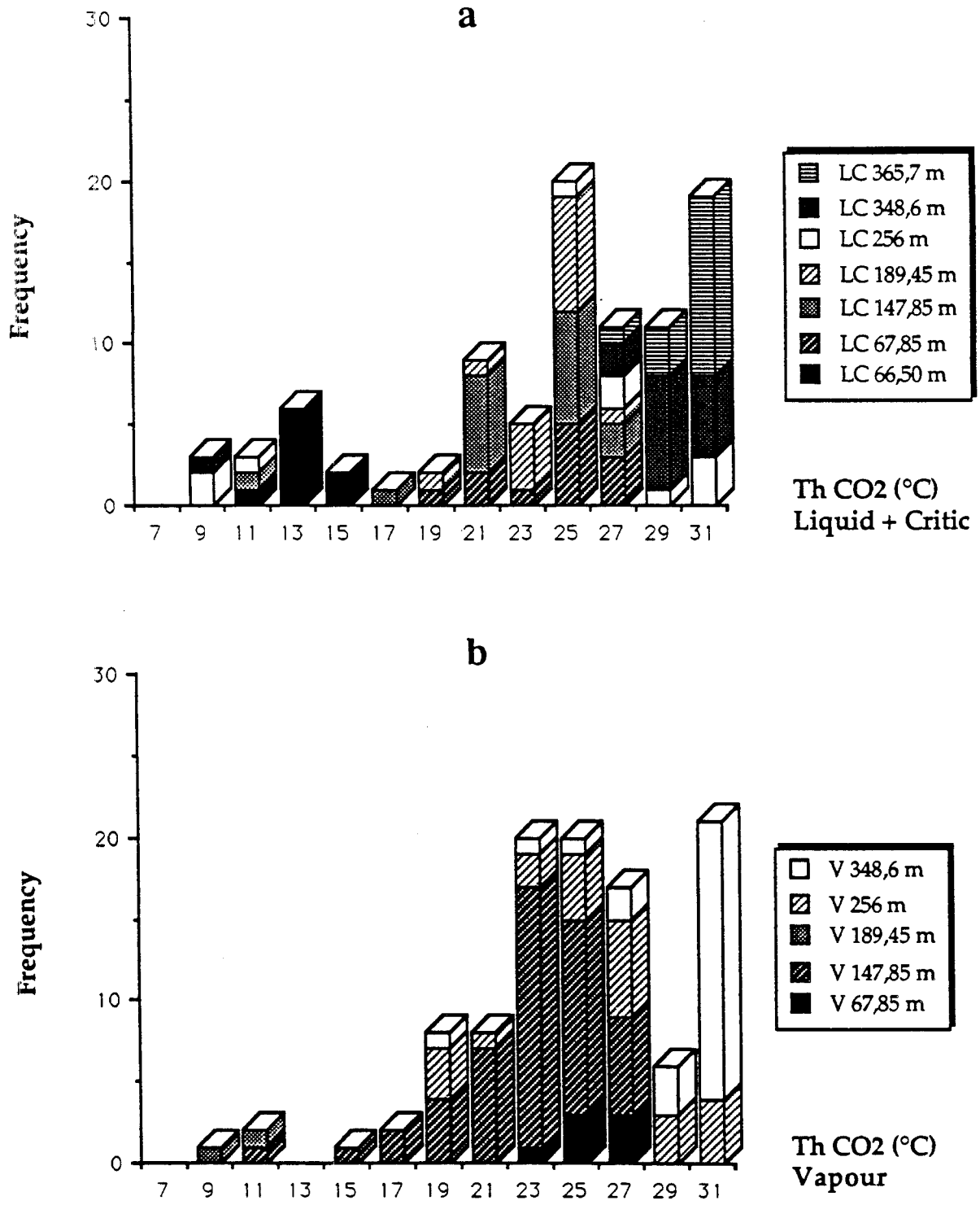

Fig IV - 18 : Corcoesto fluid inclusion data presented as a function of fluid typology. Histogram of homogenization of CO2 (Tm CO2). a : In the liquid or critic phase, b : in the vapor phase.

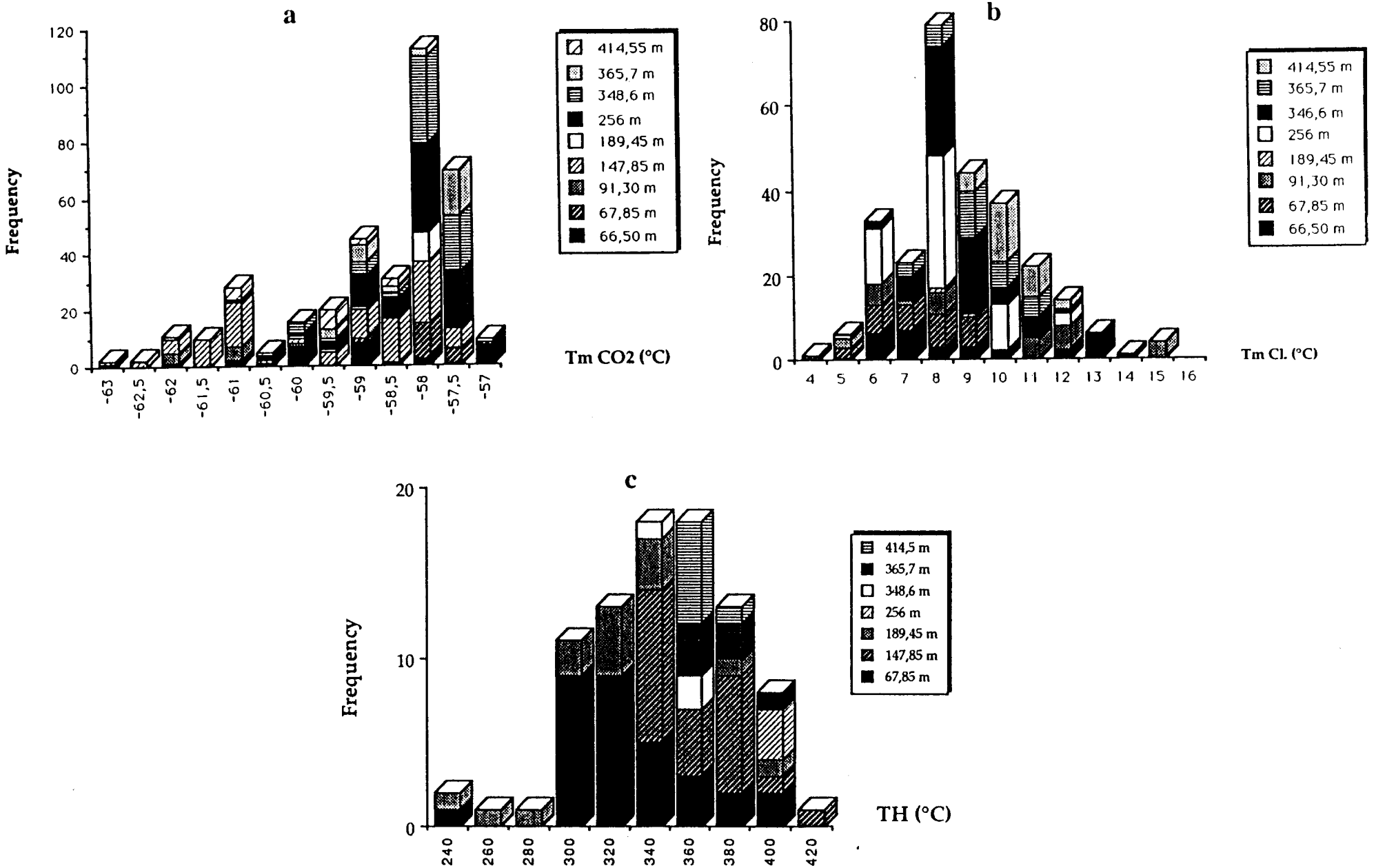

Fig IV - 19 : Corcoesto fluid inclusion data presented as a function of samples at different depths. a : histogram of melting temperature of CO2 (TmCO2) ; b : histogram of melting temperature of clathrates (Tm cl), c : Histogram of global homogenization temperature (TH).

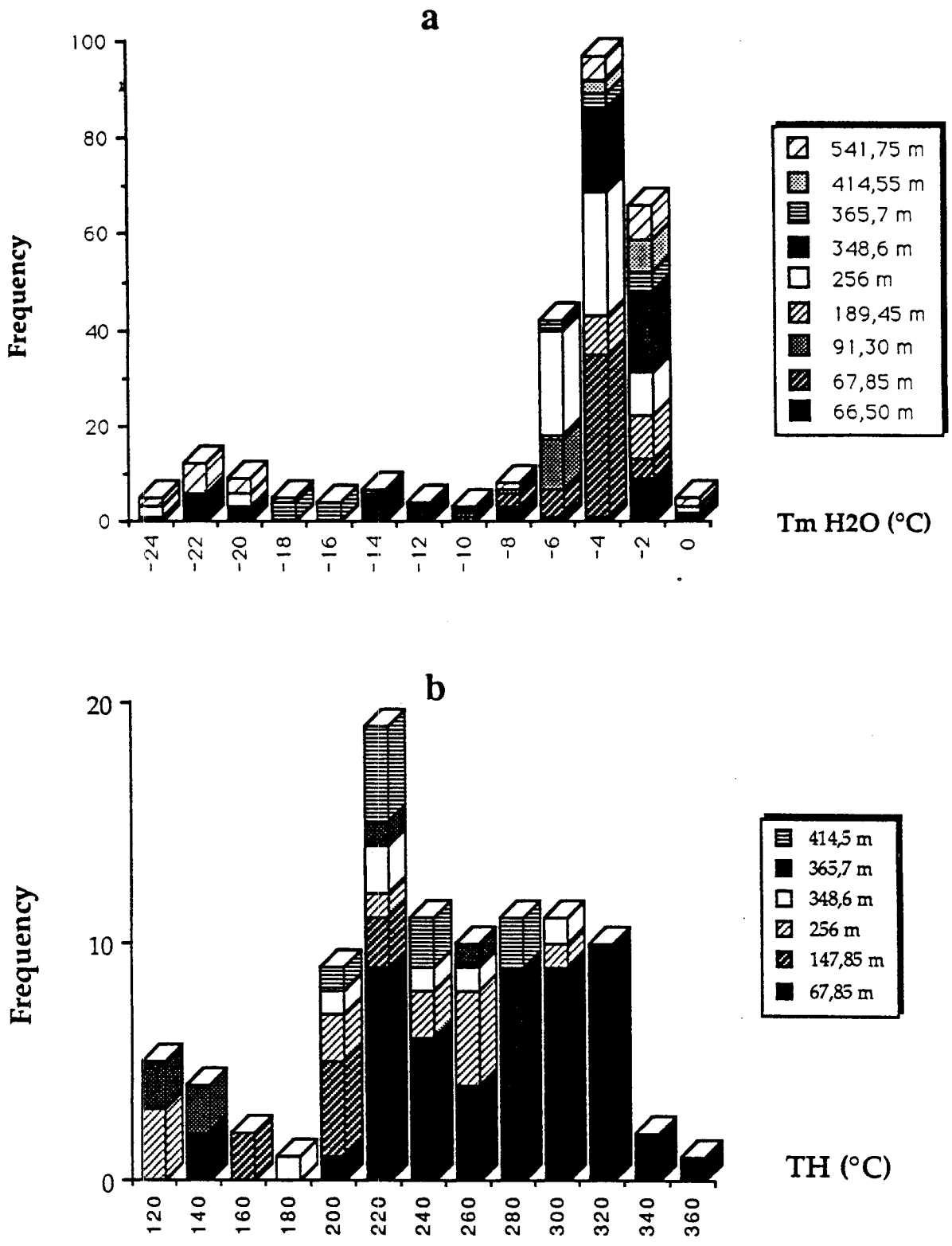

Fig IV - 20 : Corcoesto fluid inclusion data for aqueous fluids presented as a function of samples at different depths. a : Histogram of melting temperature of H2O (Tm H2O), b : Histogram of global homogenization temperature (TH).

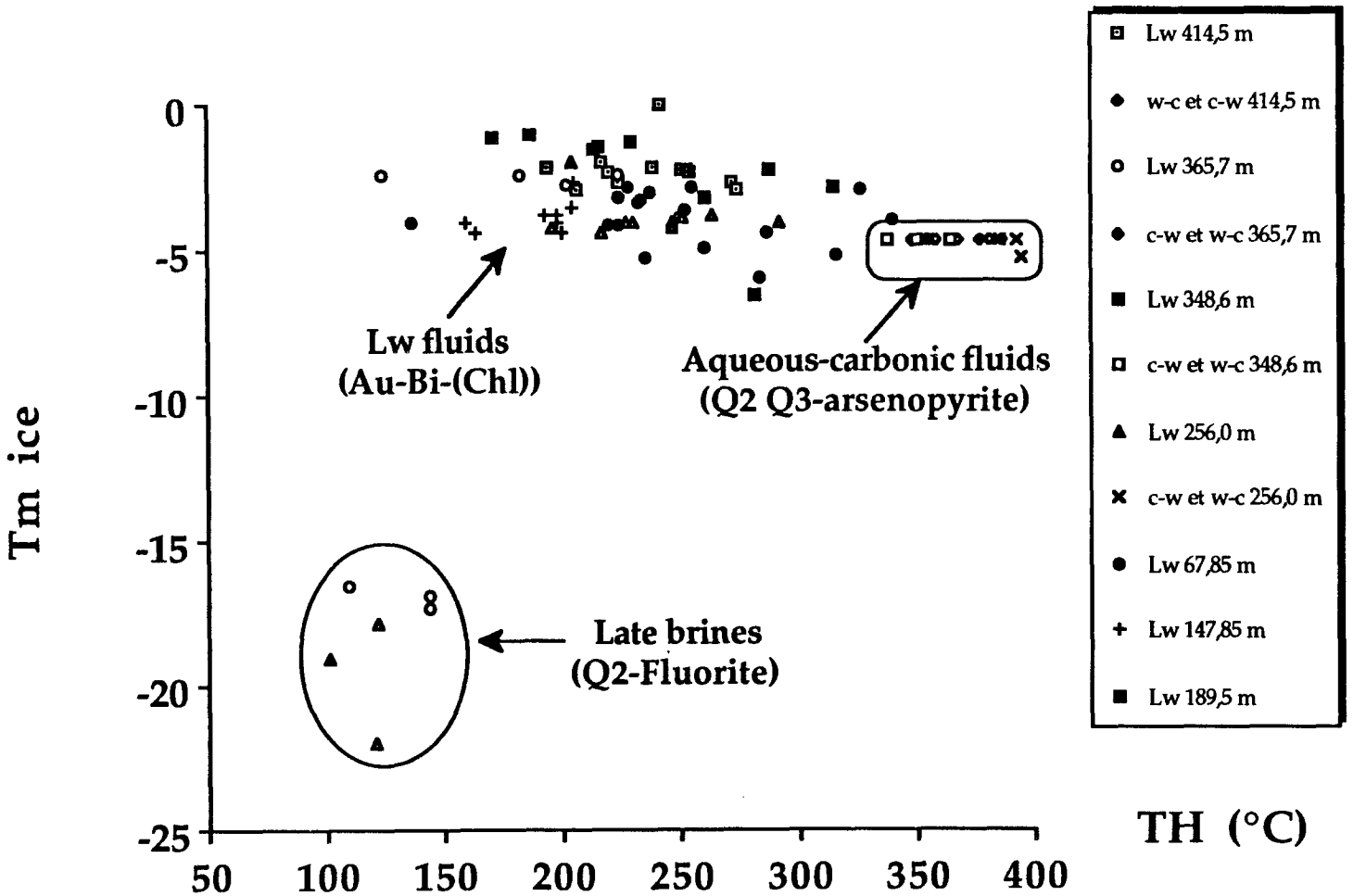

Fig IV - 21 : Tm ice -TH diagram for aquo-carbonic and aqueous fluids from the Corcoesto quartz veins.

In early quartz lenses and barren zones, different quartz generations with a great variety of fluids present are distinguished :
The early quartz lenses and quartz aggregates from pegmatoids display generally :

(i) most frequently, a deformed milky quartz (BQ 1) present within all levels of the drilled structure display all kinds of inclusions as fluid inclusion planes;

(ii) and a quartz with recrystallization-linked contours (BQ2) dsiplying sometimes euhedral shapes;

These quartz display motsly Lc-w and Vw-c inclusions as fluid inclusions planes and later Lw fluid inclusion planes and seem to have recorded most stages of fluid migration distinguished in the mineralized veins as shown by figure . In deep levels, clear quartz are found.

(iii) clear euhedral crystals in comb structures (Q 4) and veinlets show mosaïc textures, and contain mostly Lw inclusions, displaying very low values of Tme and Tmi probably related to the presence of Ca salts (deep levels at 541.75m).These fluids are similar to the Lw2 fluids from the FIP found in mineralized veinlets, indicating the discrete but relatively extended migration of late saline fluids in the whole lithological sequences.

Raman data

Gas phase of the aquo-carbonic fluids in the CH4-N2-CO2 diagram (Fig.IV-22) is lying in the CO2-CH4 axis with a relatively low N2 content (<10 mol%). The CH4 content is lower than 50 mol.% and the CO2 content ranges from 50 to 98 mol.%. Fluids found in Q2 are clearly distinct from fluids in Q3 :

in Q2 : two groups can be distinguished based on the type of CO2 homogenization (liquid, vapor) :

-inclusions with ThCO2 in the liquid phase indicating a rather dense volatile phase (CO2 : 80-100 mol % ; CH4 : 0-18 mol.% ; N2 : 0-8 mol.%)

- inclusions with ThCO2 in the vapor phase (CO2 : 78-95 mol % ; CH4 : 2-18 mol.% ; N2 : 0-10 mol.%)

c-w inclusions with CO2 homogenization in the vapor phase show intermediate densities in the range 0,3-0,9 g/cm3 ; those with CO2 homogenization in the liquid phase display higher densities ranging from 0,5 to 1 g/cm3.

in Q3 : only Lw-c inclusions (with no observed ThCO2, this indicating a low homogenization of the CO2 phase to the vapour phase) are found ; they contain : CO2 : 50-100 mol % ; CH4 : 5-45 mol.% ; N2 : 0-8 mol.%. Lw-c type density is relatively constant with depth and is in the 0,4-0.8 g/cm3 range.

In barren quartz from level 70.85m , monophase CO2-N2 inclusionshave been observed. They display the following compositions : CO2 : 30-33 mol % ; CH4 : ≈1 mol.% ; N2 : 66-68 mol.%.

Bulk chemical evolution

Early stages

The CO2-CH4-N2 ternary plot shows the composition of the three main types of fluids related to the arsenopyrite deposition. A rather clear evolution characterized by an increasing CH4 content is recorded from the densest and earliest fluids Lc-w displaying a rather pure CO2 rich volatile phase towards Vc-w fluids in Q2, and then Lw-c fluids in Q3, of the fluids, (at constant N2 content).

The CO2-CH4-H2O ternary plot (Fig.IV-23) shows that the changes in composition from c-w fluids with ThCO2 (L), to C-w fluids with ThCO2 (V), and Lw-c fluids is mostly characterized by an increase in water content, the w-c inclusions being enriched in water up to 80-90 mole % H2O.

In baren quartz, Raman analyses have shown that most aqueous-carbonic fluid types have the same features than in the mineralized quartz.

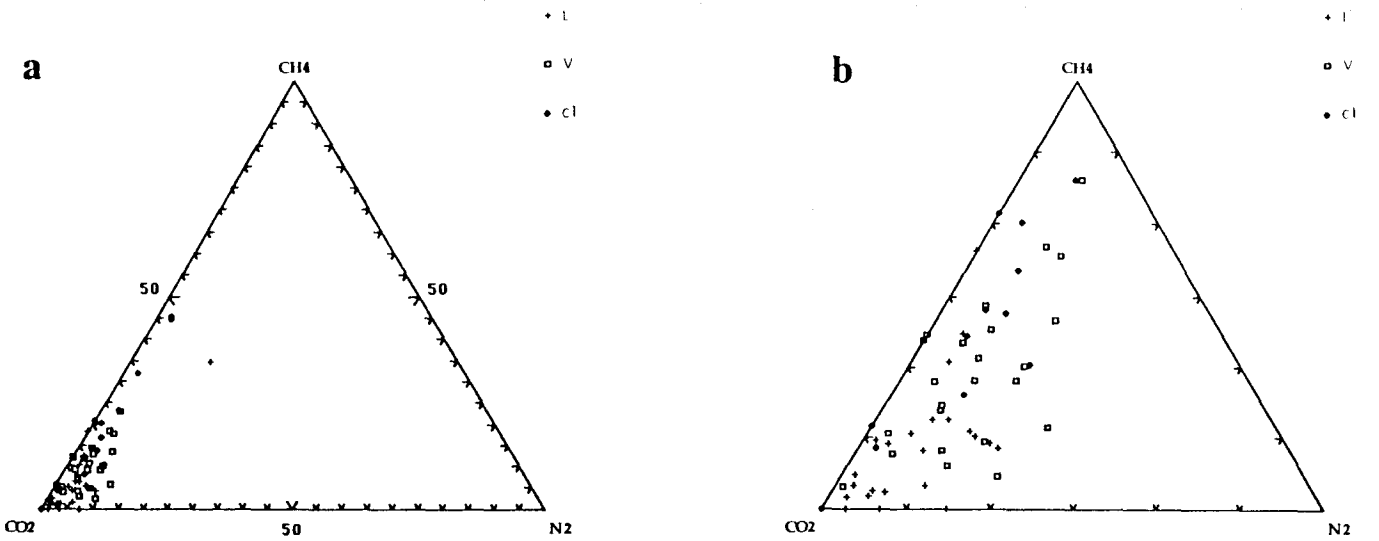

Fig IV - 22 : a : Ternary plot in the CO2-CH4-N2 diagram of the volatile composition for the aquo-carbonic fluids from the Corcoesto drill hole. b : detail of a.
c-w fluids : L : CO2 homogenization in the liquid phase, V : CO2 homogenization in the vapour phase. w-c fluids : cl

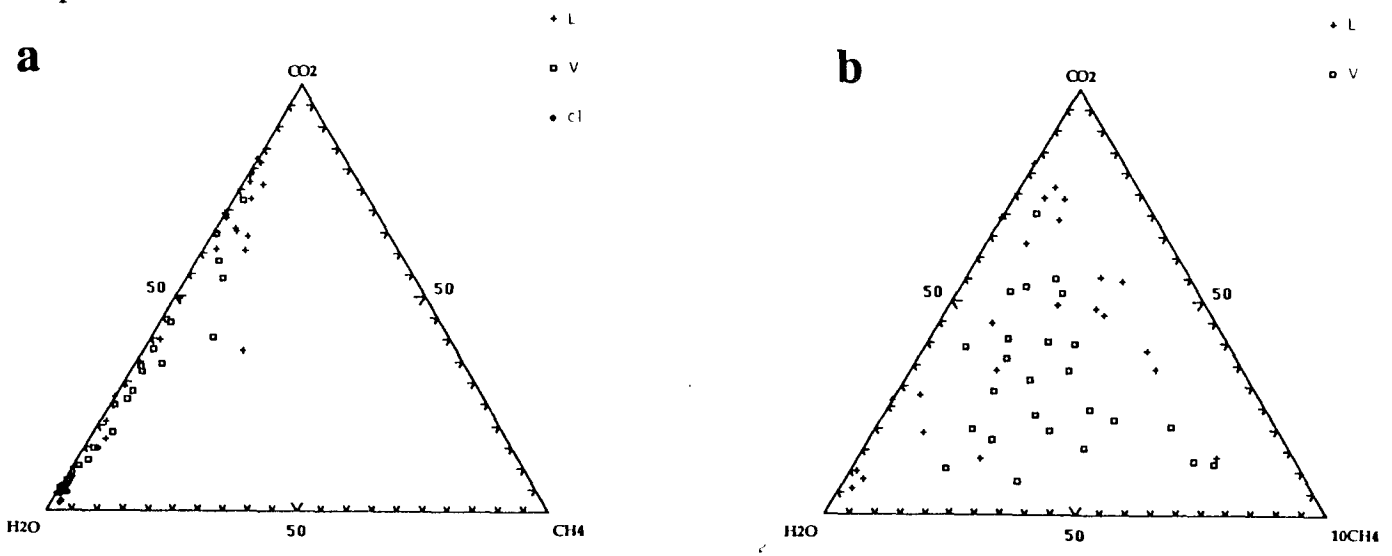

Fig IV - 23 : Ternary plot of the global composition for the aquo-carbonic fluids from the Corcoesto drill hole. a : in the CO2-CH4-H2O diagram, b : in the CO2-10CH4-H2O diagram.
c-w fluids : L : CO2 homogenization in the liquid phase, V : CO2 homogenization in the vapour phase. w-c fluids : cl

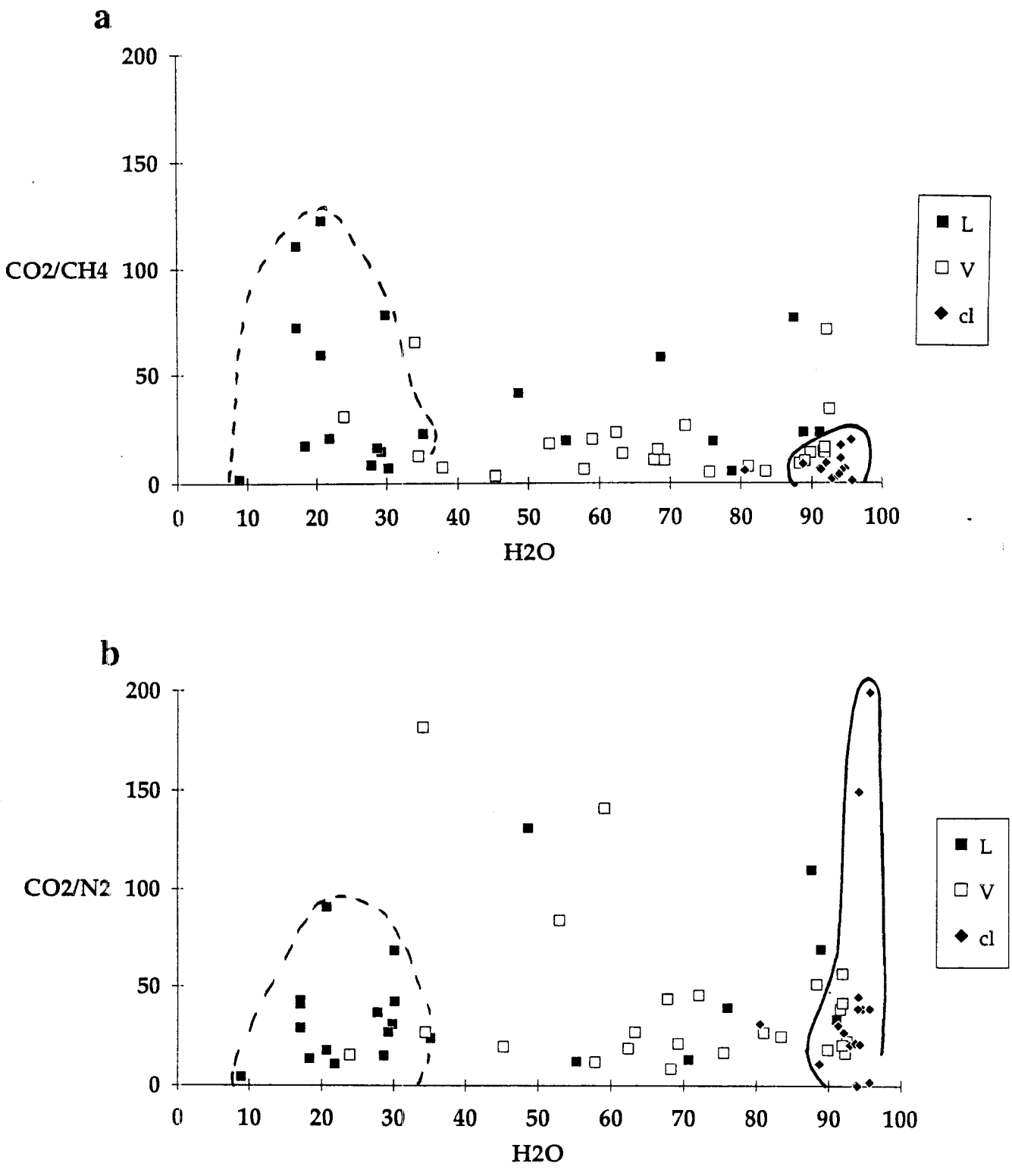

Fig IV - 24 : Global composition of aquo-carbonic fluid from Corcoesto quartz veins in : a: CO2/CH4 versus H2O diagram, b : CO2/N2 versus H2O diagram
c-w fluids : L : CO2 homogenization in the liquid phase, V : CO2 homogenization in the vapour phase. w-c fluids : cl

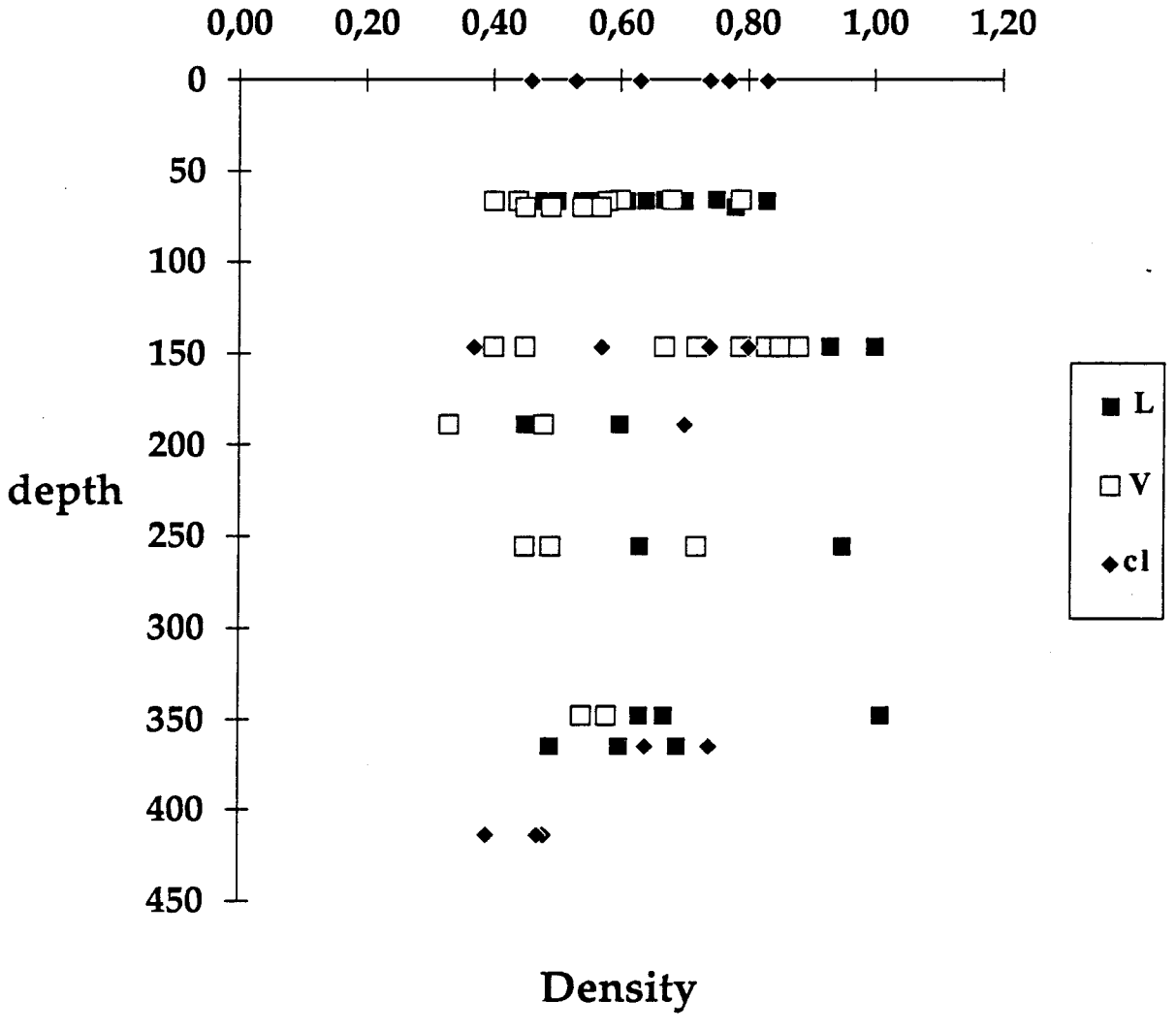

Fig IV - 25 : Density versus depth plot for the aquo-carbonic fluids from the Corcoesto quartz veins.
c-w fluids : L : CO2 homogenization in the liquid phase, V : CO2 homogenization in the vapour phase. w-c fluids : cl

Lc-w and Vc-w inclusions display variable CO2/CH4 and CO2/N2 ratios, especially for the inclusions displaying rather high CO2 contents,which are characterized by CO2/CH4 ratio in the range 1-125. Vc-w inclusions are characterized by more constant values in spite of their scattering of the H20 content (CO2/CH4 between 1 and 35). (Fig. IV-24)

CO2/CH4 ratio for Lw-c is subconstant in the range 1-20 and is homogeneous at the sample scale. CO2/N2 does not exhibit strong variation (12 to 45). The volatile phase of such type of fluid is thus relatively homogeneous.

No clear difference in the fluid compositions appears with depth. The three types of fluids have been recognized in the different studied samples. There is thus no clear relationships between composition, density (Fig. IV-25) and gold content, probably due to the fact that gold is not related to this major fluid stage, but only arsenopyrite. However, it is clear that arsenopyrite crystallized during a major physical-chemical change of the system, characterized by dilution of dense carbonic fluids by dilute waters, correlatively to a change in the CO2-CH4 ratio in favour to CH4 probaly in relation with the unbuffering of the fluids by graphite.

Late stages

Sulphide-Au stage
The evolution of the Lw fluids is shown by the Tm H2O-Th plot (Fig.IV-21). Series of fluids are trapped as fluid inclusion in microfissures (FIP) and document a cooling of the system from the Lw-c stage (Q3) towards relatively low temperatures. Fluid circulation ends with relatively dilute fluids (2- 9 wt%eq.NaCl) at temperatures of 200 to 250°C. This stage is related to end of the intense microfissural activity in most mineralized samples.

Quartz-fluorite-kaolinite stage
A late and totally disconnected stage of fluid migration is recorded in several samples (some FIP) and in the euhedral clear quartz combs. This stage is characterized by saline fluids of low temperatures (100-150°C) which could be of sedimentary origin.

2 -TOMINO (CREGU)

Fluids from Tomino have been studied in the mineralized quartz veins (quartz Q1 and Q2), in the host granite, and in some metamorphic rocks outside the granite (C-rich units). In all studied samples aqueous-carbonic are the earliest fluids, and are synchronous of the most important early events (metamorphic rock devolatilization, quartz crystallization). Later fluids are only trapped in fluid inclusion planes crosscuting all earlier quartz.

Early aqueous-carbonic fluids

On the basis on microthermometric data (TfCO2), and Raman analysis two group of fluid have been distinguished (Essarraj, 1992) :

-CH4 rich fluids : this type of fluid has been observed as primary inclusions in the granites (Urgal granite), in the graphite rich rocks and in quartz crystals (Q1) in quartz veins. Different fluids have been observed :

- L or V (c-m)-w characterized by the presence of important contents of N2 and CH4 in the volatile phase; they display different features at room temperature depending on the presence or the lack of water (two-fluid phase inclusions and monophase inclusions respectively)

TmCO2 are scaterred in the range -60,5 ;-65,5°C. ThCO2 are in the range -16 ; 14°C. The lowest TfCO2 and the more dense fluids have been observed in graphite rich rocks. Melting temperature of clathrates are obse. ed in between 8 and 14°C (Fig. IV-26 and Table IV-4). Homogenization temperature ranges are different depending on the samples :
- 300-320°C in quartz (Q1) from quartz veins;
- 370-410°C in quartz crystal from the granite;
- greater than 510°C in graphite rich rocks.

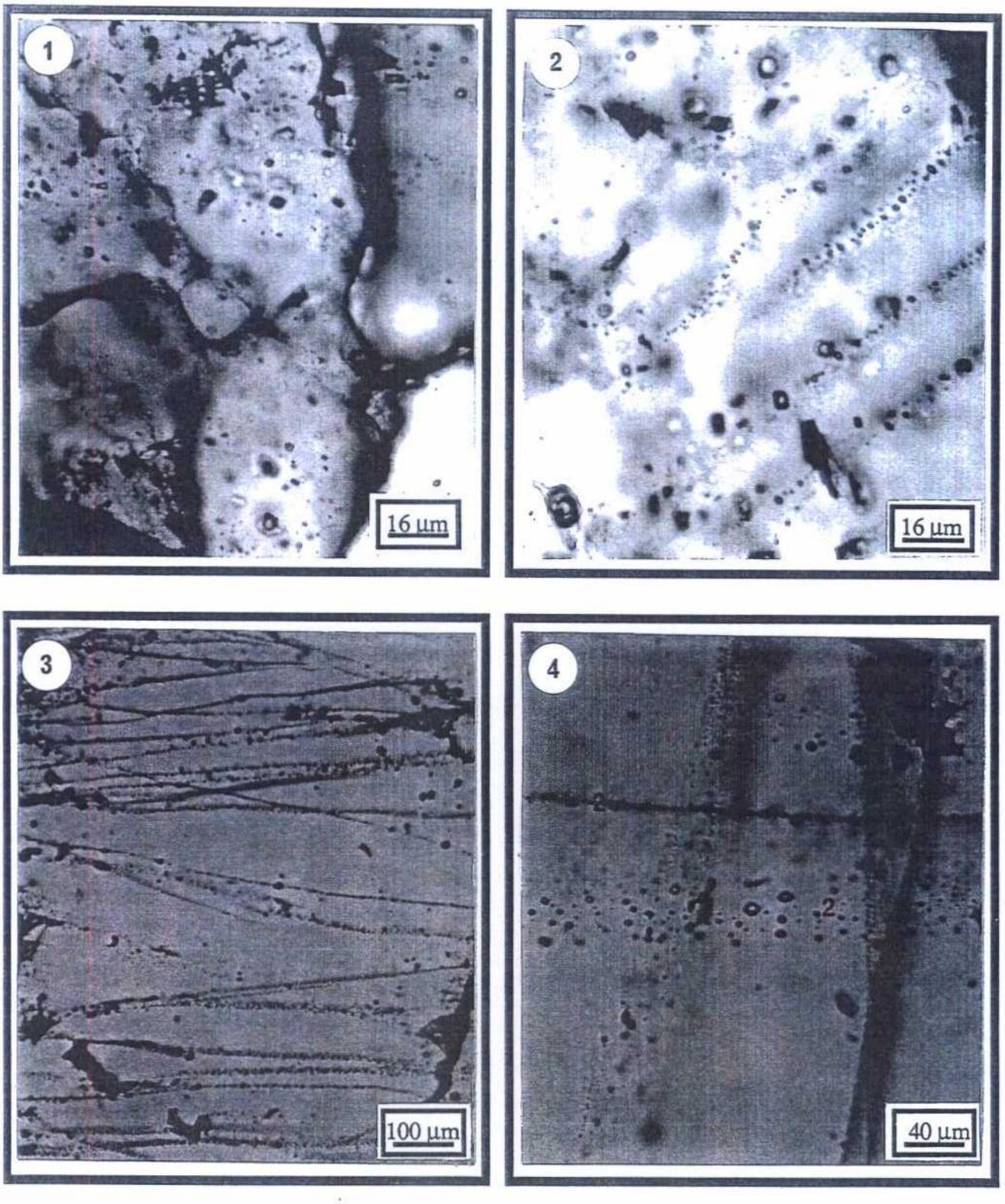

Plate IV-14 : Fluid inclusion features from Tomino area.
1 - early aquo carbonic inclusions (enriched in CH4) in quartz Q1.
2 - aquo carbonic inclusions (depleted in CH4) scattered or in trail in quartz Q2.
3 - network of fluid inclusion planes, (aquo-carbonic fluids depleted in CH4).
4 - Trails of aqueous fluid inclusions (1) croscutting trails of aquo-carbonic fluid inclusions (2).

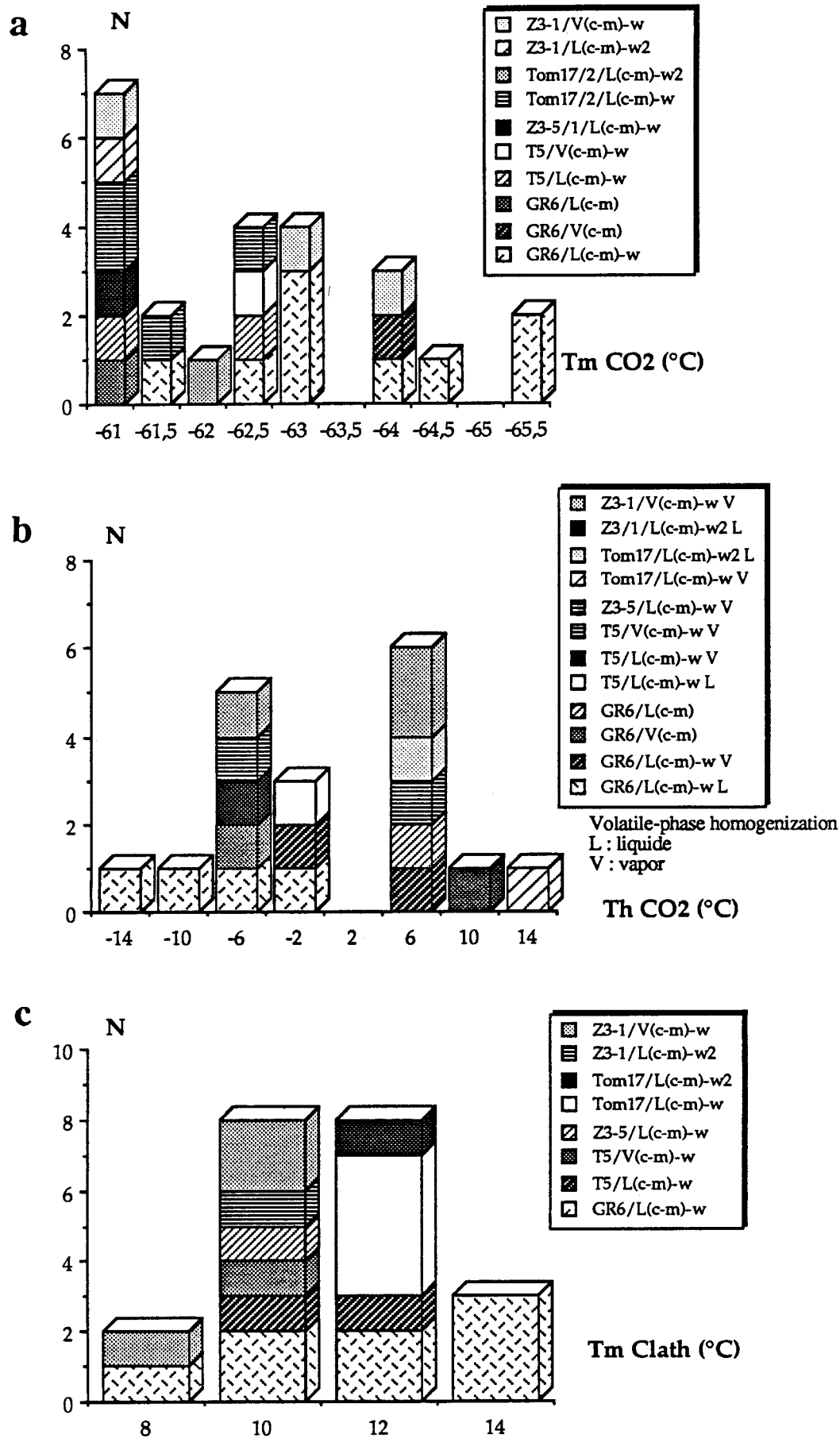

Fig IV - 26: Tomino fluid inclusion data for CH4 rich fluids. a : Histogram of melting temperature of CO2 (Tm CO2), b : Histogram of homogenization temperature of CO2 (ThCO2), c : histogram of melting temperature of clathrates (Tm clath)

-CH4 poor fluids : this type of fluid has been observed in all the studied samples. They are very abundant in quartz (QII) and are mostly observed as secondary fluid inclusions in NS, EW and N 40°E microfractures. In granite, they are primary but sometimes may occur as secondary fluid inclusion in NS fractures (Z3-5).

Microthermometric characteristics are the followings : Tm CO2 are in the range -56,6 ; -60,5°C (Fig..IV-27); ThCO2 are ranging from 4 to 30°C in the liquid phase (Fig. IV-28) ; Tmcl are observed from 4 to 12°C (Fig. IV-29). Salinity deduced from melting temperature of clathrate is in the range 3-7 eq. wt % NaCl.

Global homogenization temperatures are in the 220-420°C range with a mode between 280°C and 380°C (Fig. IV-30). Depending on the mode of the global homogenization two subtypes Lc-w and Lc-w2 have been distinguished : the Lc-w2 type display rather unusual homogenization of the dense volatile phase (ThCO2 to the liquid phase) by increasing the size of the bubble at the depends on the liquid aqueous phase. However, the two types are not rather different from the point of view of their composition and density. Lower homogenization temperatures correspond to EW fluid inclusion planes.

The Raman data confirm the distinction between two contrasted end-members in the aqueous-carbonic fluid series, with nearly continuous mixing yielding to intermediate compositions.

-CH4 rich fluids : CO2 is the dominant species in the gas phase as shown by the Raman data. CO2 content is in the 54-71 mol. % range. CH4 is abundant ranging from 23 to 46 mol.%. Rare fluid inclusions have a CH4 content reaching 60 mol.%. N2 content ranges from 0 to 9,5 mol.% but most of the data are in the 0-5 mol% range. Fluid density is decreasing from L(c-m)-w inclusions to the V(c-m)-w, L(c-m)-w2, L(c-m) and V(c-m) inclusions, ranging from 0,85 to 0,45 g/cm3.

- *CH4 poor fluids* : CO2 is the dominant componant , with a content ranging from 76,5 to 100 mol.%. CH4 is in the 0 - 15 mol % range, but most of the data are ranging from 0 to 5 mol. %. N2 content are lower than10 mol. %. Important quantities of H2S have been detected by Raman microprobe in fluid inclusions in QI and QII and may reach 1 mol. %. Fluid density splits into two groups: 0,85-0,95 g/cm3 and 0,65-0,75g /cm3.

The ternary plots and the binary plots from figures IV-31 and 32 show two dilution trends from CO2 rich fluids by waters, with two distinct end-members :

- a CO2-(CH4)-H20 end-member displaying rather usual compositions of fluids equilibrated with metamorphic host-rocks (CO2/ gas ratio around 10-20);
- a CO2- CH4-N2 end member, with a ratio CO2/ other volatiles around 1.6, which is probably linked to the local chemical equilibrium in the lydites.

Aqueous fluids associated to the gold stage

Aqueous fluids have been studied as a function of the fluid inclusion plane directions determined by the study of microstructures. Major directions are NS and EW. Sometimes the N40-50 °E direction appears in some samples. Different groups have been distinguished :

- NS direction : TmH2O are in the range -4,5 ; -0,2°C. Three modes can be distinguished depending of the samples : -0,5 ; -0,2°C / -2 ; -1,5°C / -3,5 ; -2,5°C. Homogenization temperatures ranges from 130°C to 240°C (Fig. IV-33).
- E-W direction : TmH2O are in the range -3,5 ; -0,1°C, but most of the data are ranging from -0,1 to -0,5 °C. Salinity can be estimated around 0,2 to 0,9 eq. %wt NaCl. Homogenization temperatures are observed from 140 to 260 °C with a large mode in the range 140-220°C. These EW fluid inclusion planes are croscutting the other fluid inclusion planes and dilution processes appear in superimposed zones. The more dilute fluids are observed as primary fluid inclusion in late quartz growth zones crystallized around arsenopyrite and pyrite, (e.g. after the sulphide crystallization).
- N40-50 °E direction : in this minor direction, fluid inclusion have a low salinity with TmH2O in the range -1 ;-3,5 °C . Homogenization temperature is recorded between 140 and 200°C.

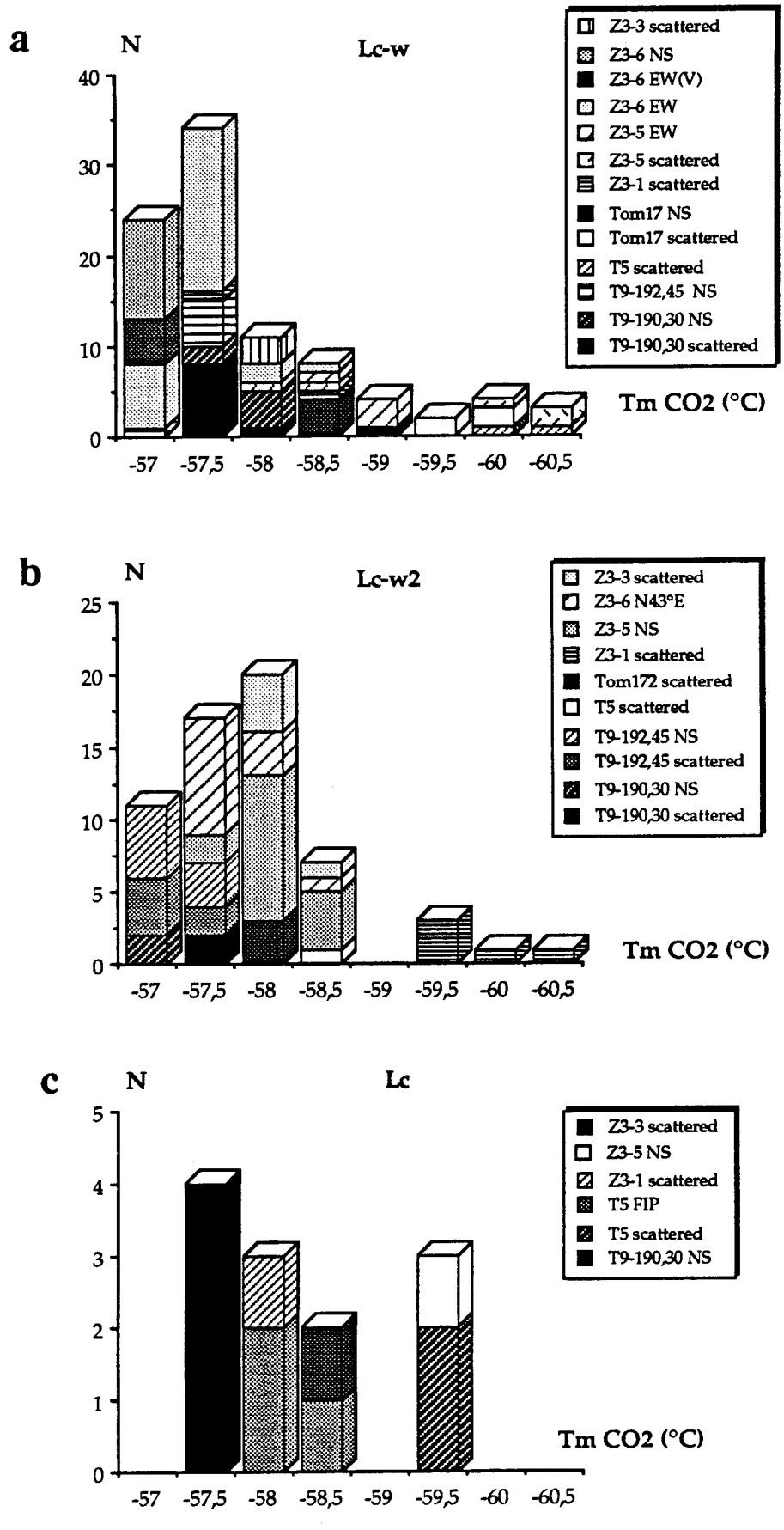

Fig IV - 27: Histograms of melting temperature of CO2 (Tm CO2). a : Lc-w fluids, b : Lc-w2 fluids, c : Lc fluids.

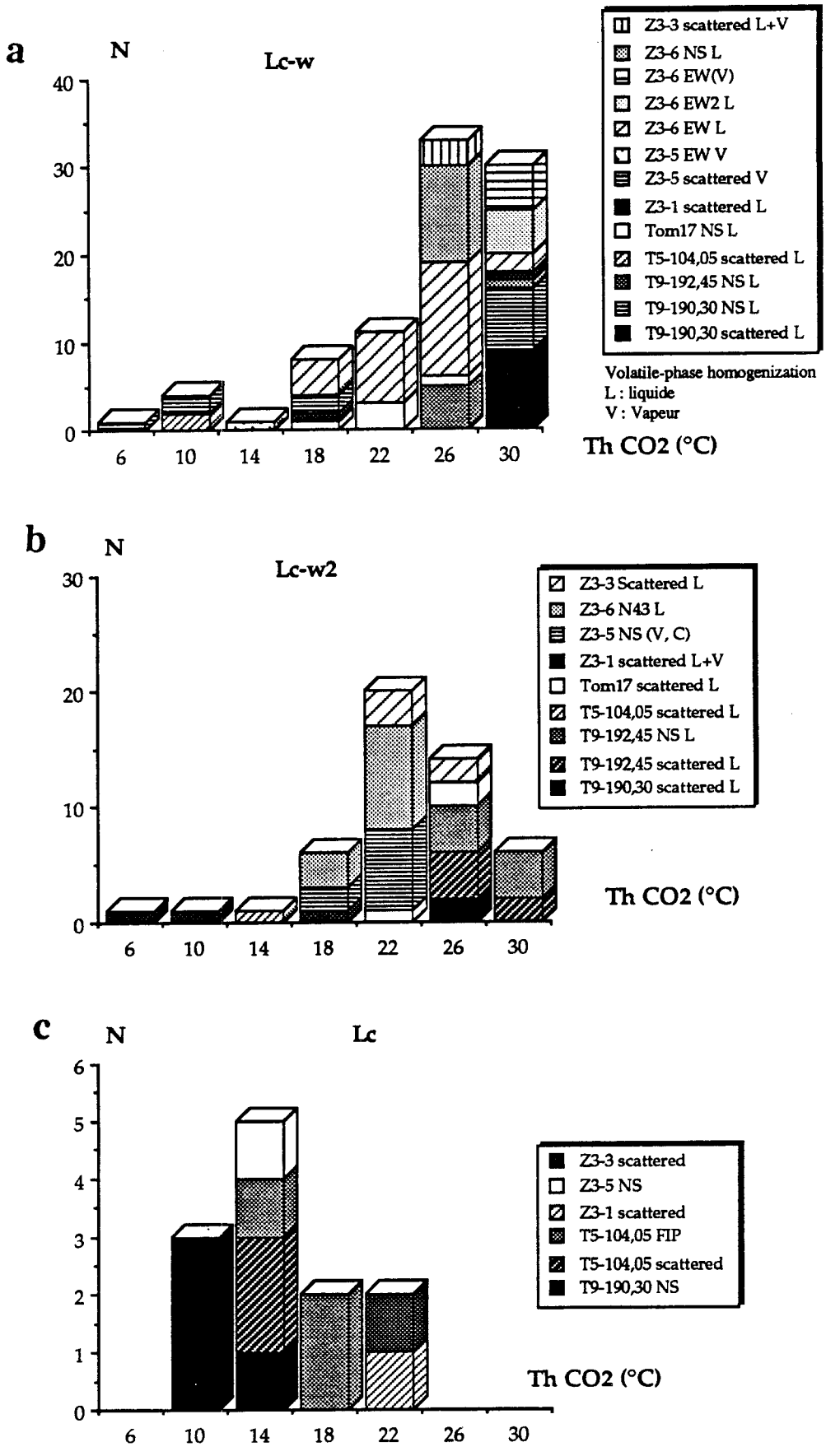

Fig IV - 28: Histograms of homogenization temperature of CO2 (ThCO2). a : Lc-w fluids, b : Lc-w2 fluids, c : Lc fluids.

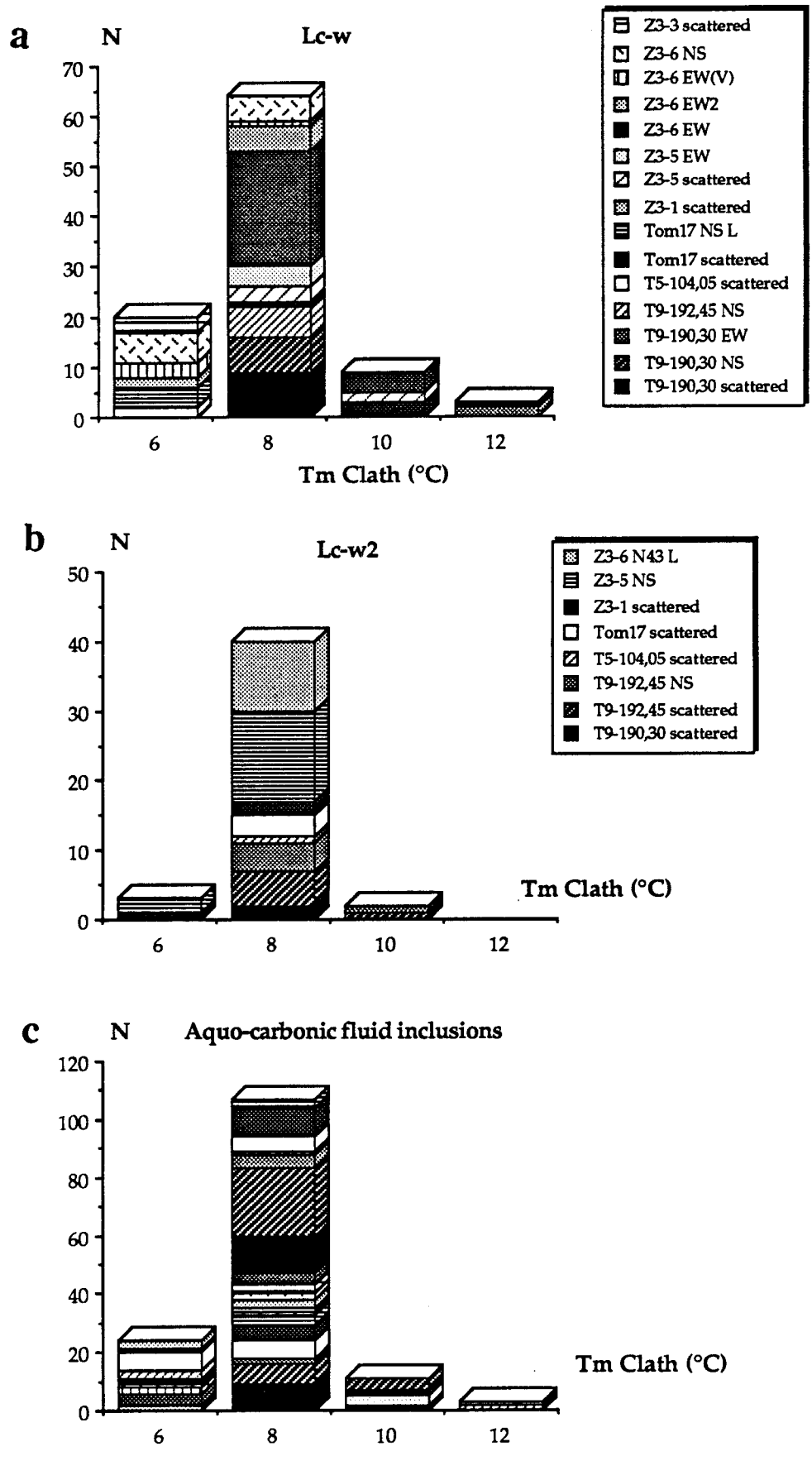

Fig IV - 29: Histograms of homogenization temperature of clathrates (Tm clath), a : Lc-w fluids, b : Lc-w2 fluids, c : Lc fluids.

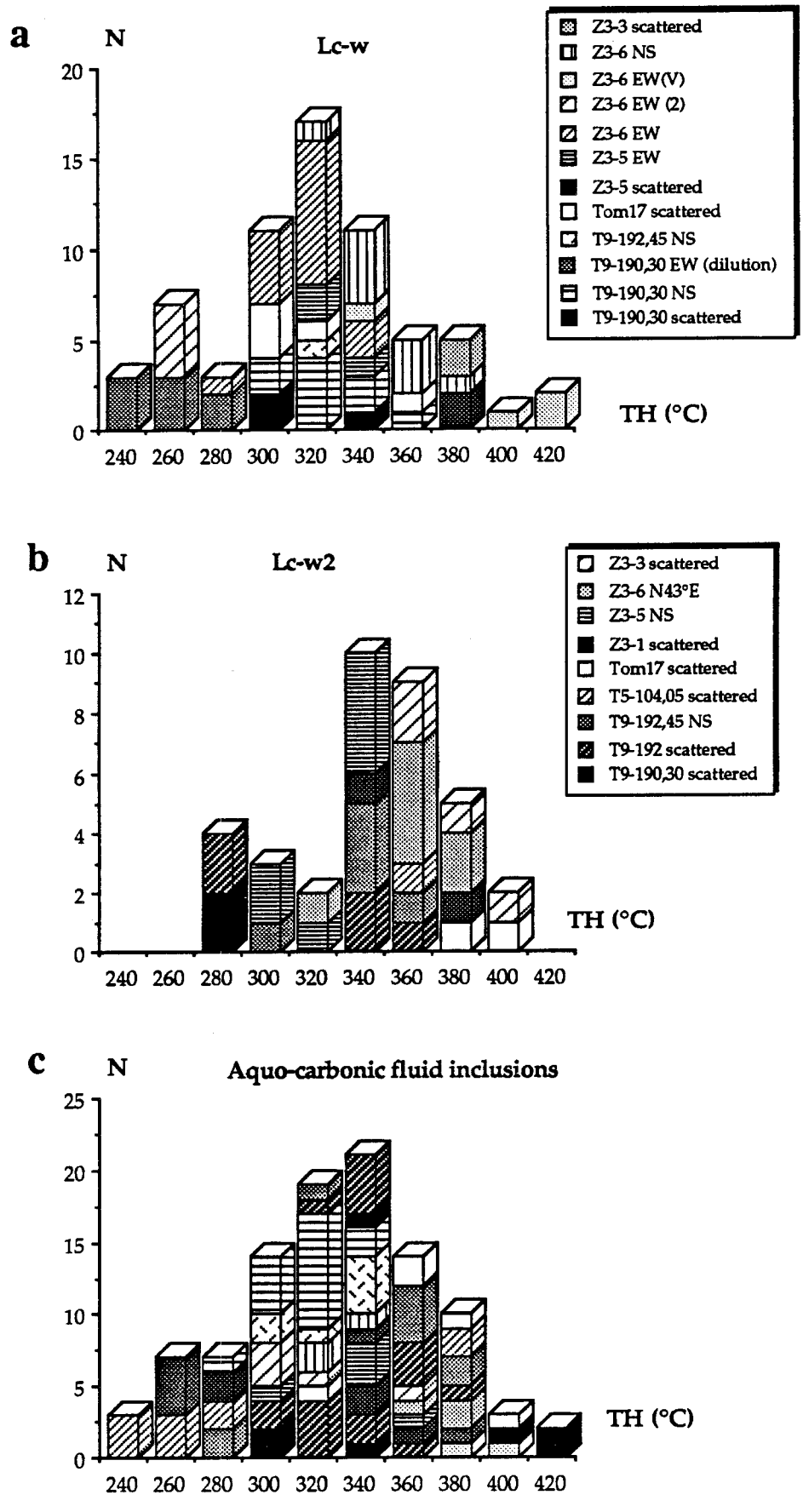

Fig IV - 30: Histograms of global homogenization temperature (TH), a : Lc-w fluids, b : Lc-w2 fluids, c : Lc fluids

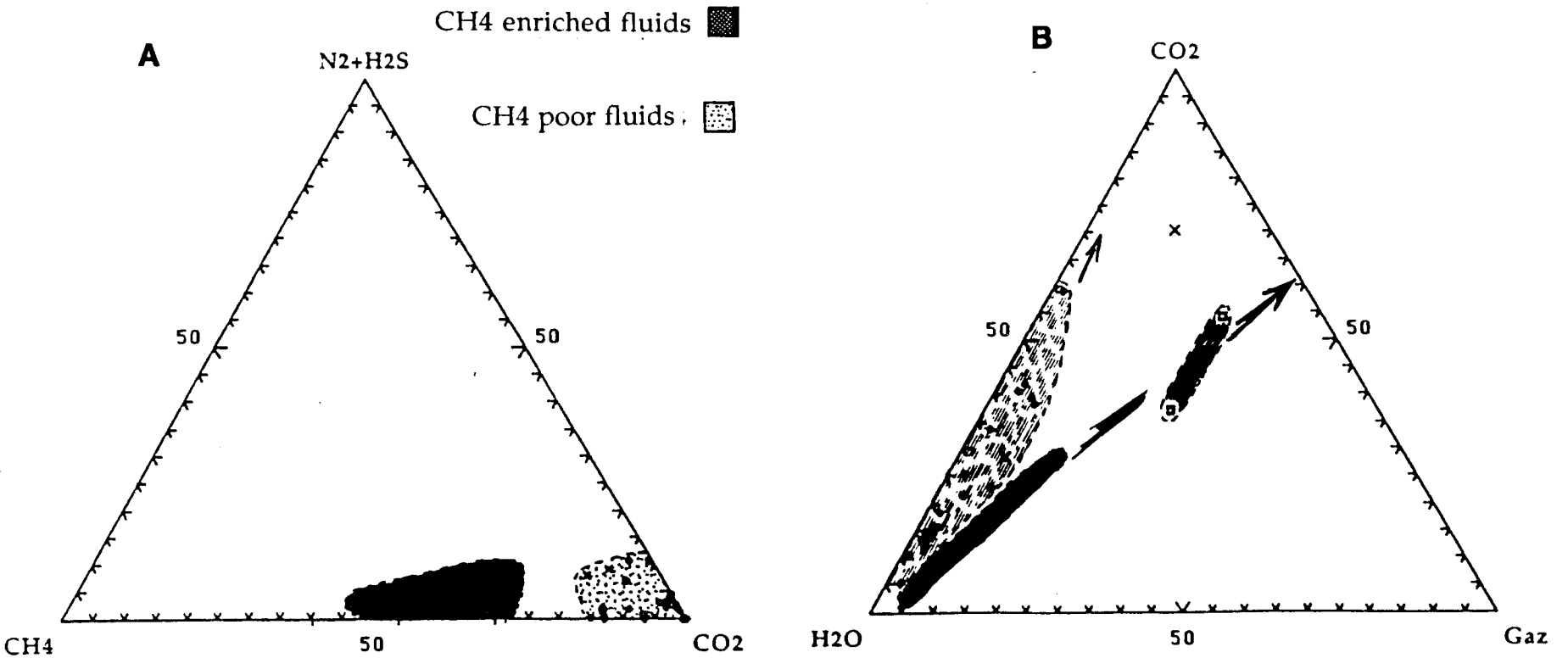

Fig IV - 31: A : Ternary plot in the CO2-CH4-N2+H2S diagram of the volatile phase determined by Raman microprobe analysis for the aquo-carbonic fluids in the Tomino area.
B- Ternary plot in the CO2-gaz (CH4+N2+H2S)-H2O diagram of the global composition for the aquo-carbonic fluids in the Tomino area.

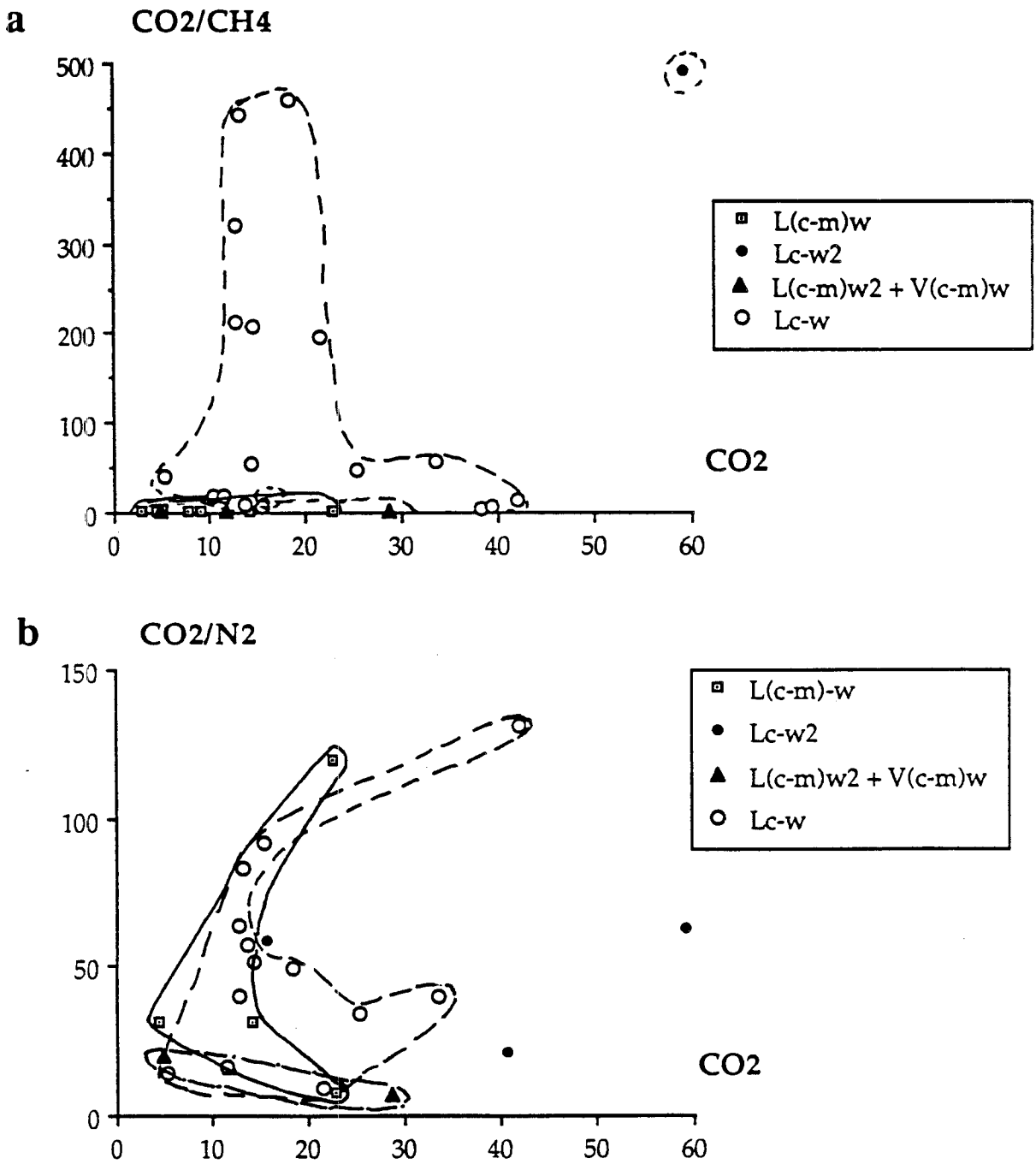

Fig IV - 32 : Global composition of aquo-carbonic fluid from Tomino area in : a: CO2/CH4 versus CO2 diagram, b : CO2/N2 versus CO2 diagram

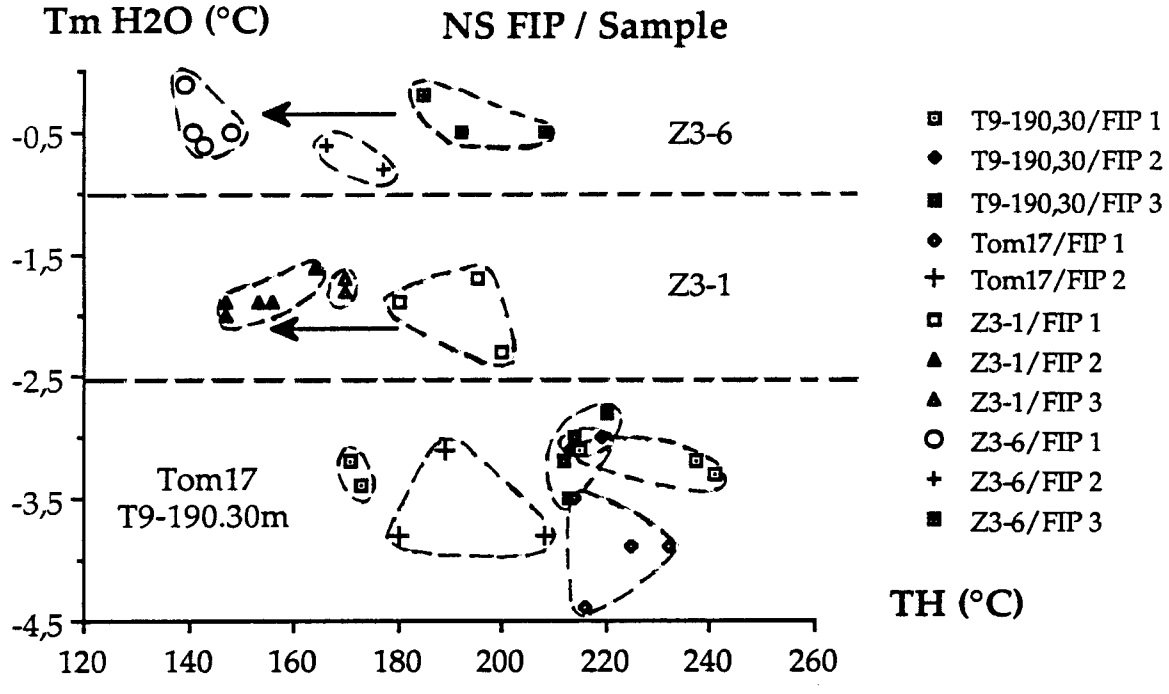

Fig IV - 33 : Tm ice -TH diagram for NS aqueous fluid inclusion planes from the Tomino area.

Quartz	FI type	Tm CO2	Th CO2	Tm Clat	Tm ice	TH
Aquo-carbonic fluids						
Lydite, Granite and Q1	CH4-rich fluid inclusions	'-65.5 / -60.5°C	'-16 / 14°C L or V	8 / 14°C (8 /12°C)	nd	300 / > 510°C
Q2	Lc-w and Lc-w2	'-60.5 / -56.6°C (-57.5/-56.6)	4 / 30°C (18/30°C) L	4 / 12°C (6/8°C)	nd	220 / 420°C (280/380°C) L
	Lc	'-59.5 / -57°C	6 / 22°C			
Aqueous fluids						
Fluid inclusion planes	Lw NS				'-4.5 / -0.2°C	130 / 240°C
	Lw EW				'-3.5 / -0.1°C (-0.5/-0.1°C)	140 / 260°C (140/220°C)
	Lw N40-50°E				'-3.5 / -1°C	140 / 200°C

Table IV - 4 : Recapitulative microthermometric data for the different types of fluids in the Tomino area TmCO2 : melting temperature of CO2, Th CO2 : homogenization temperature of CO2, Tm cl : melting temperature of clathrates,. Tm H2O : melting temperature of H2O, TH : homogenization temperature

Dilution process at decreasing temperature is shown by figure IV-33 drawn for NS fluid inclusion planes. Similar features are observed for EW F.I.P.

These data indicate clearly that the style of microfissuring changed in between the QII-arsenopyrite II stage and the later stage of microfissures probably linked to the gold deposition.

Conclusions

The fluid evolution at Tomino reflects a complex series of fluid migration and production :

- Stage 1 : fluids enriched in CH4 are mostly observed in the granite and in quartz veins. They can be probably compared to those observed in graphite rich rocks located at a few hundred meters from the granites contact, around two kilometers from the quartz veins. They are associated to the deposition of the N80°E quartz Q(I) veins and to the pyrite - pyrrhotite - arsenopyrite I crystallization.

-Stage 2 : Aquo-carbonic fluids depleted in CH4 are related to the major deposition of quartz Q(II) in veins. They are associated to the deposition of arsenopyrite II. Such fluids are observed as secondary fluid inclusions planes orientated EW (N80 ± 20 °E) and rarely N10°E. Dilution processes at decreasing temperature can be assumed.

- Stage 3 : Aqueous fluids are observed in different directions (NS, EW and N40-50E) and show specific characteristics. Dilution processes associated to a slight decrease of temperature are observed from N45° fluid inclusions to EW or NS fluid inclusion in samples where the three directions are coexisting. Late fluids (EW and locally NS) are observed in late overgrowths of quartz formed at the contact between pyrite and arsenopyrite. The similarity of the fluids found in the EW and NS directions seem to indicate that the permeability at that stage was resulting from the good interconnectivity between the two networks. They are related to the deposition of the late paragenesis with chalcopyrite, sulfosalts and native gold. Salinity is in the range 0,2-0,9 wt% eq NaCl. and global homogenization temperature is ranging from 140 to 220°C.

3- PENEDONO (Porto Univ. and CREGU)

Three main stages of fluid migration into the quartz veins can be distinguished at Penedono. Each fluid has its own inprint on quartz matrix. Different fluid types can be related to different types of quartz. The relations fluid/ore is also accomplished with our studies, leading to a good knowledge of the interactions fluid-ore deposition.

Quartz types

QI - Deformed quartz in big grains : this quartz type is the main type, constituting the support of all other types of quartz and also for the ores. Its deformation is marked by wavy extinction and deformation bands. The formation of sub-grains is also found in various samples, exhibiting uniform extinction and triple junction points. A great number of inclusions is observed in this quartz which thus acquires a milky appearance. It is the oldest type of quartz, and registers the different fluid inprints as trails of secondary fluid inclusions. No clear link between quartz and the type of fluid can be made.

QII - Microcrystaline quartz in c-planes : this quartz crosscuts the QI, and represents a new silica input into the vein system. It is usually related with shear planes (c-planes) which crosscut the veins ; it is not deformed and individual grains are no longer than 100 µm. It is a clear quartz with scarse inclusions.

QIII - Hyaline quartz filling tension gashes and geodes : this type of quartz is usually found as a filling of open spaces in the veins. It is an hyaline euhedral quartz, not deformed and only found in a few places. The inclusions are always in trails, in small quantities and size (d <10µm).

The figure IV- 34 shows the global relationships between the types of quartz and the inclusions found for each type.

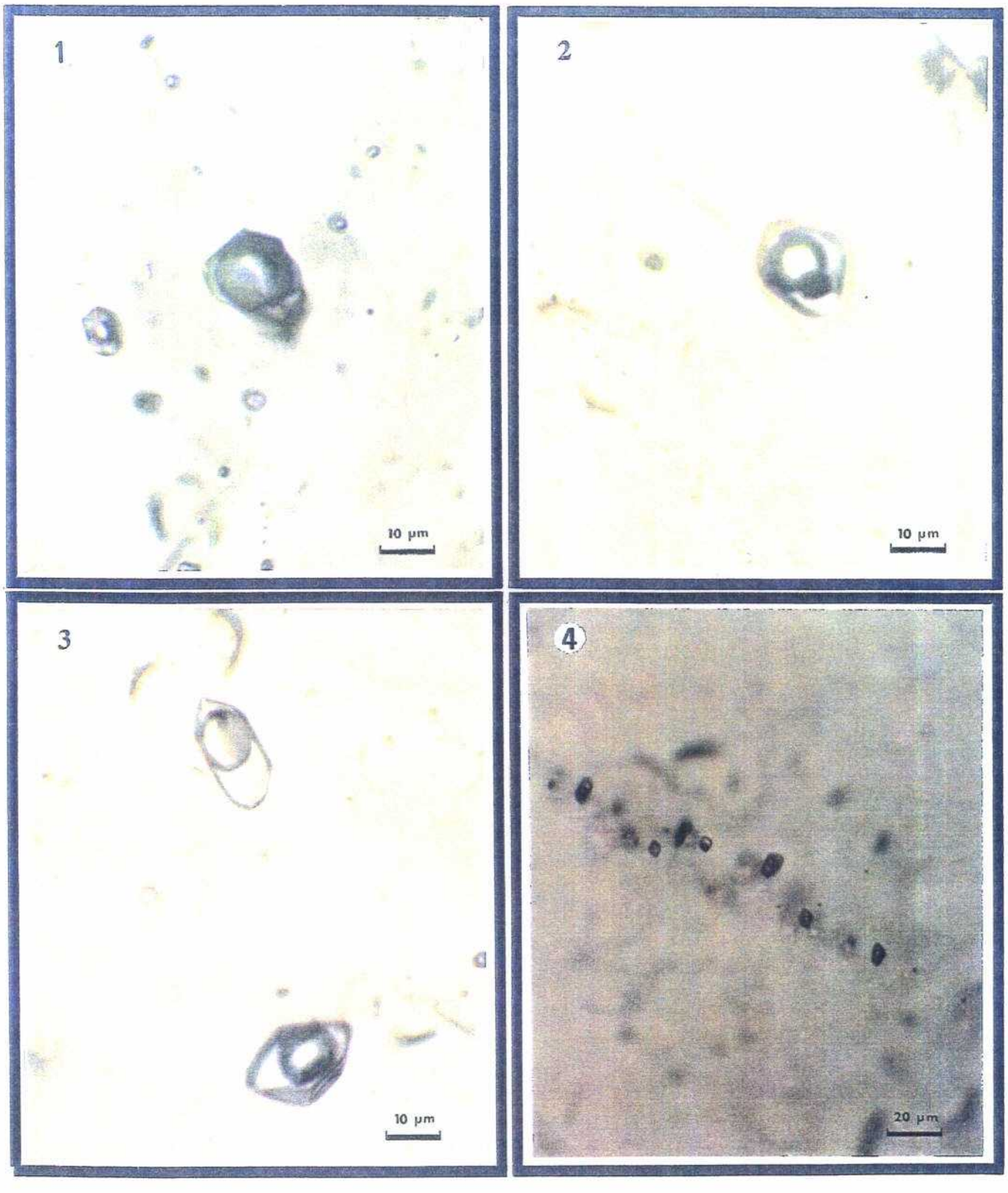

Plate IV-15 : Fluid inclusion features from Penedono area (Dacotim and St Antonio Mine);
1- Lc-w aquo-carbonic inclusions
2- Lc-w aquo-carbonic inclusions with graphite.
3- Lc-w and Lw-c aquo-carbonic inclusions
4 - Planes of aqueous fluid inclusions .

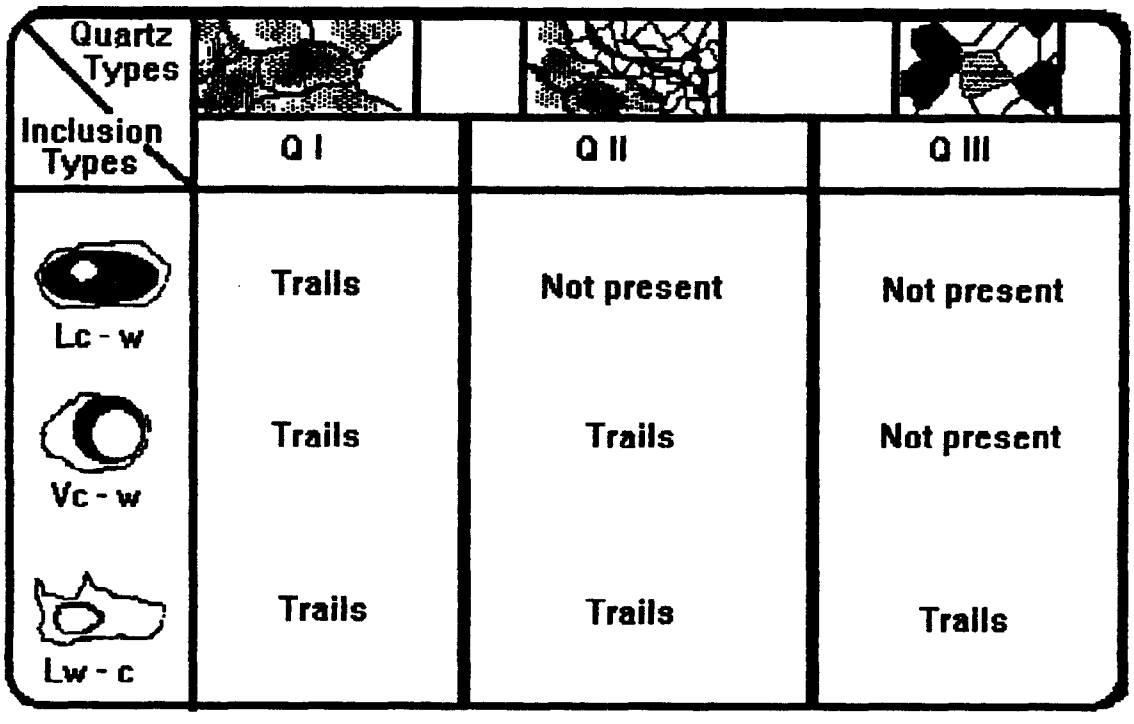

Fig IV - 34 : Relationships between quartz type and inclusion type in Penedono.

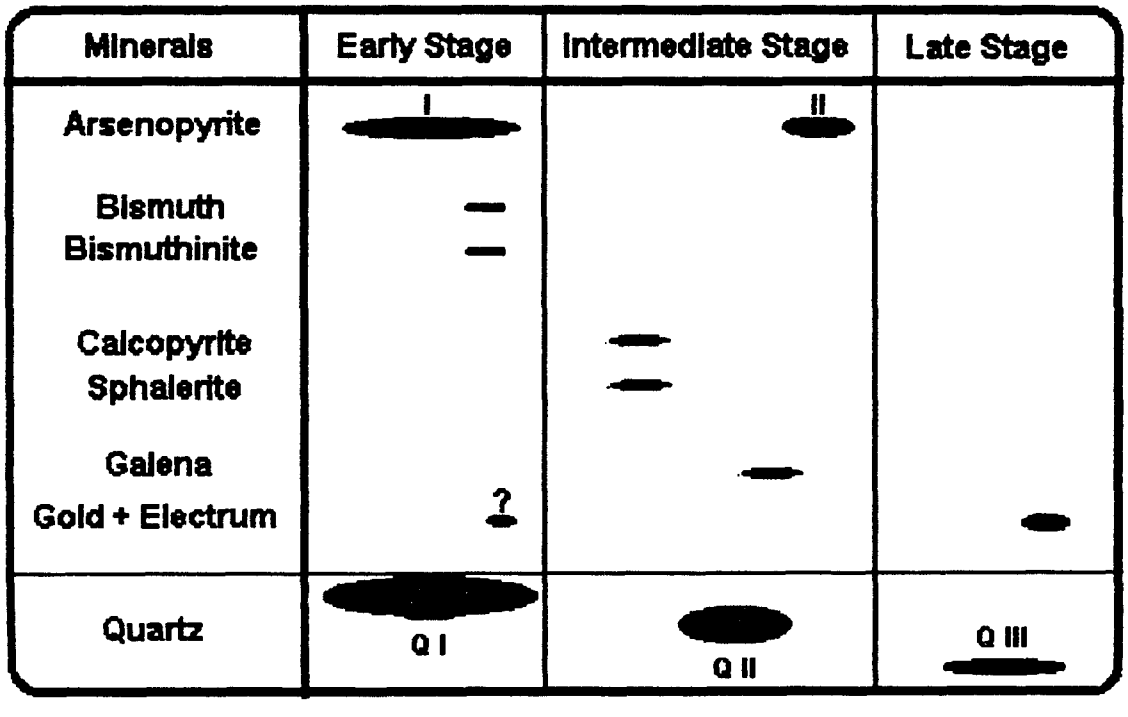

Fig IV - 37 : Schematic association of minerals in Penedono.

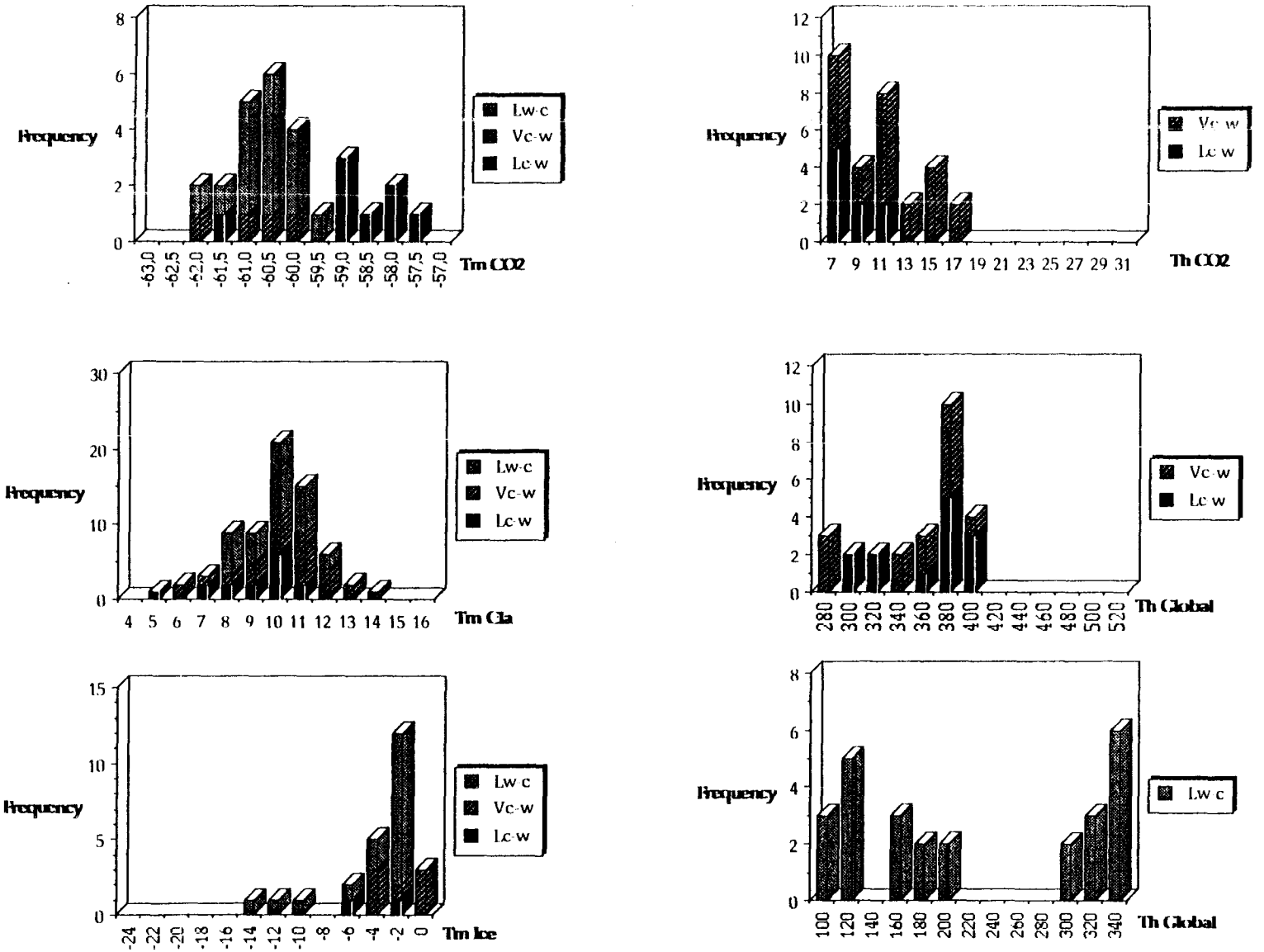

Fig IV - 35 : Histograms of microthermometric data from Penedono.

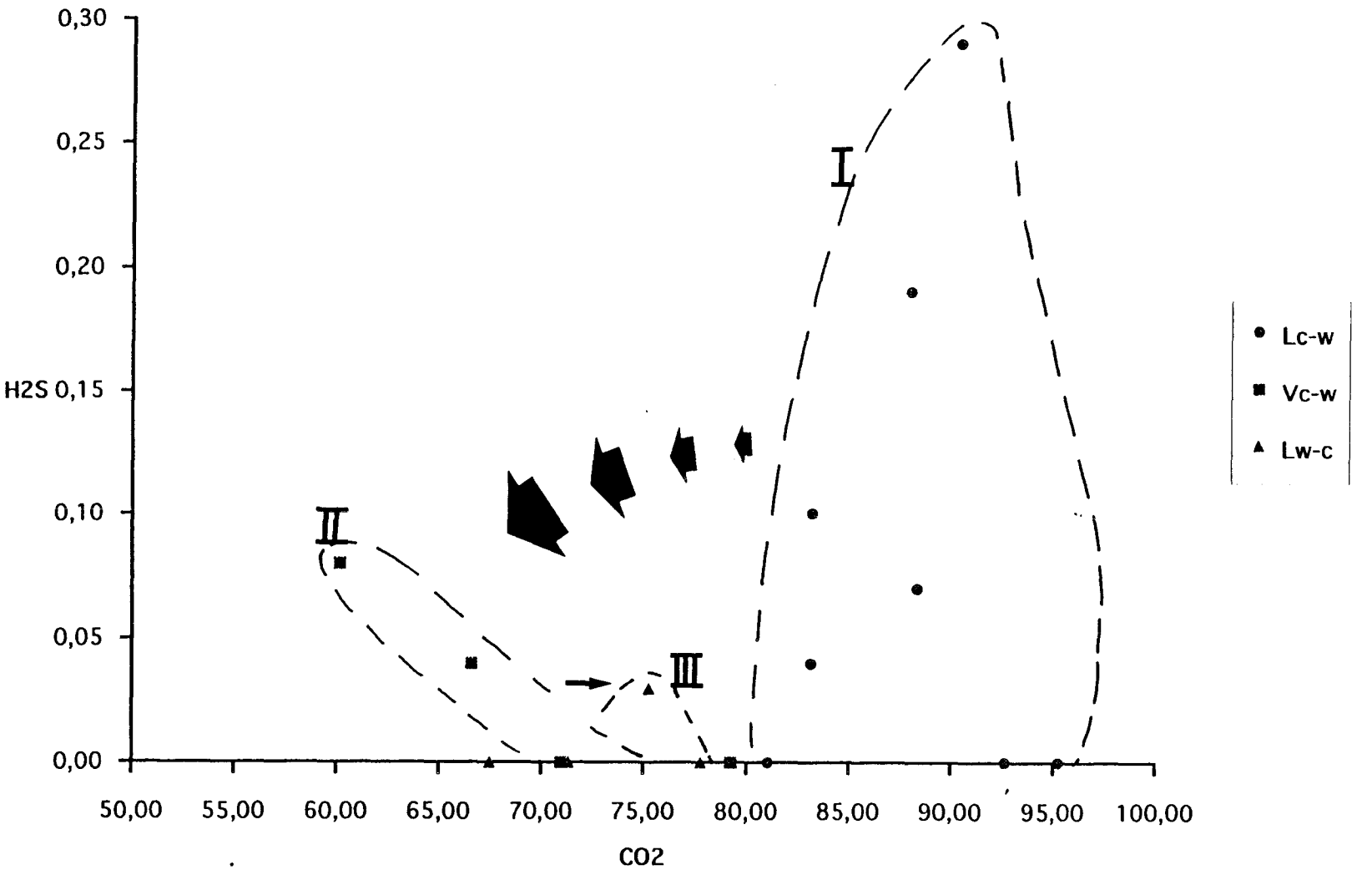

Fig IV - 36 : CO_2-H_2S chart which illustrates the evolution from higher contents in H_2S in the earlier stages.

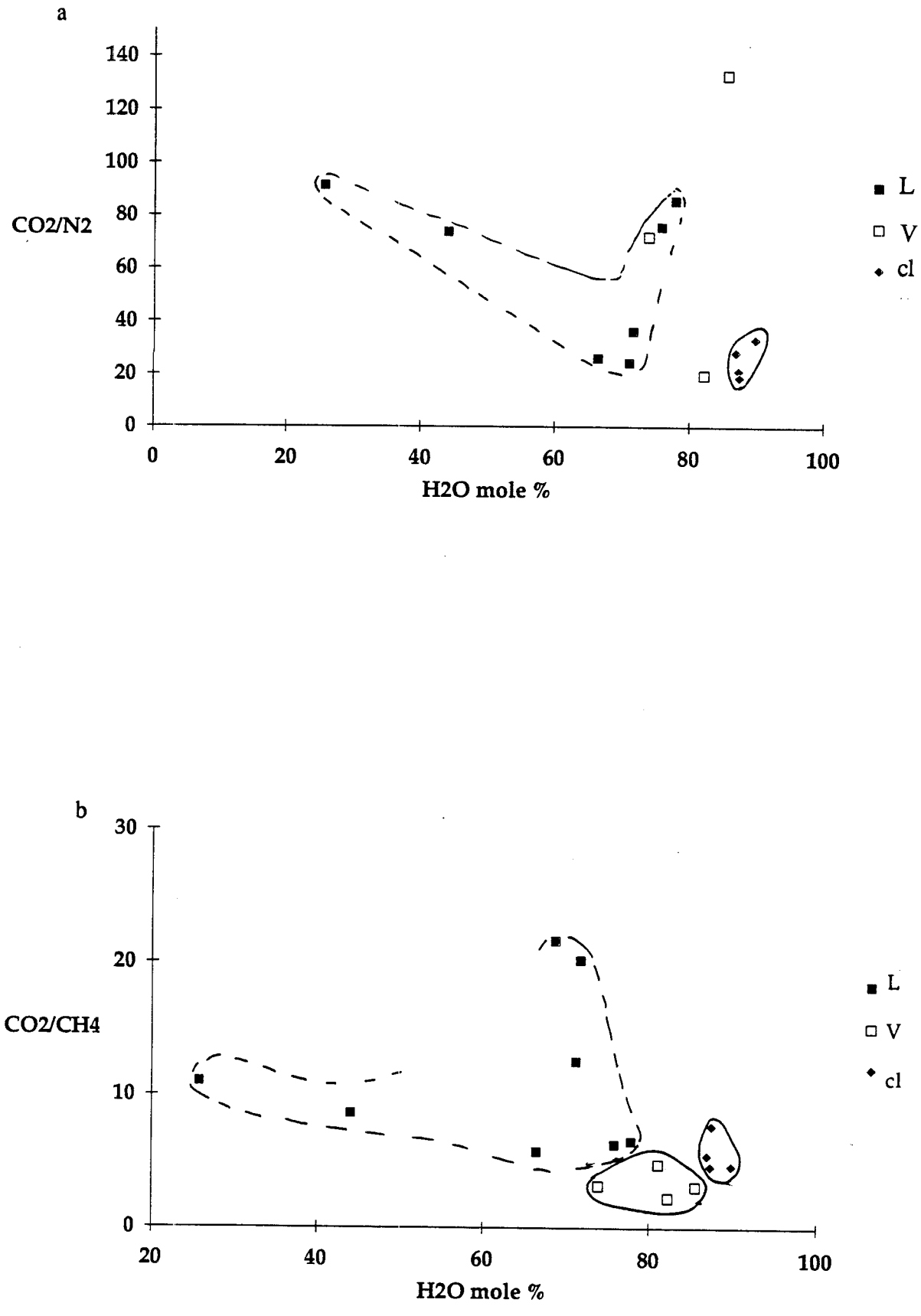

Fig IV - 38 : Global composition of aquo-carbonic fluid from Penedono area in : a: CO2/CH4 versus H2O diagram, b : CO2/N2 versus H2O diagram
c-w fluids : L : CO2 homogenization in the liquid phase, V : CO2 homogenization in the vapour phase. w-c fluids : cl

Fluid types

Three types of fluids were defined for describing the main fluid circulation in the vein systems. The types of fluids were distinguished mainly based on data obtained from microthermometry and Raman analysis, and by microscopic observations .The relations between quartz types and types of fluids describing the mode of occurrence of the inclusions are shown in figure IV - . The microthermometric data are presented in the form of histograms in figure IV- 35. The Raman analyses of the volatile phase, and the calculated bulk composition of inclusions are shown in table IV-6 (annexe).

Microthermometric data

Temperatures of melting and homogenization of carbonic and aqueous phases depend on type of inclusion studied.

Lc-w inclusions : This fluid is mostly found in trails of inclusions in the QI type, but can also be found in QII type as primary or pseudo-secondary in origin. This first type with a high degree of filling in carbonic phase, (liquid), displays Tm CO_2 in the range -61.5,-57.5 °C, Tm cl in the range 5.0,11.0 °C. Tm H_2O is very difficult to observe. For all the inclusions, Th CO_2 is in liquid phase (except one in critic phase), in the 7.0, 11.0 °C range. The global homogenization is in liquid phase in the 300, 420 °C range.

Vc-w inclusions : As most of the fluids, they can be found mainly in QI type. In QII, they were found as primary inclusions and never found in QIII type.They are characterized by a lower degree of filling in CO_2 phase. Tm CO_2 is lower, in the -62.0,-60.0 °C range. Such temperatures indicate a higher content in volatile component than in Lc-w inclusions. Tm ice is in the -6.0, 0.0 °C range indicating a low salt content for the inclusions. Th CO_2 is always in vapour phase, in the 7.0, 17,0 °C range. Global Th is in the 280, 380 °C range.

Lw-c inclusions : they are the richest in aqueous phase (Flw > 50%). In most cases, the density of the gaseous phase is small. In some cases, Tm CO_2 might be observed, but the Th CO_2 is never observed, indicating a low density of CO_2. Tm CO_2 is in the -62.0,-59.5 °C range, indicating a CH_4/CO_2 ratio similar to the previous types. Tm H_2O is in the -14.0,-2.0 °C range, indicating the presence of significant salt content. Tm cl ranges from 8.0 to 12.0 °C; the highest Tm cl confirms the presence of CH_4. The global Th is in the 100, 340 °C range.

Inclusions with solid phases : Though other uncommon fluids were found in QI quartz type, namely inclusions with solid salts (NaCl?), solid C (graphite?) and hydrocarbons, they are not described because of their ambiguous relations with the other fluids, quartz types and ores.

Raman data

Lc-w inclusions : Aquo-carbonic fluid with high CO_2 density.

The gas composition, analyzed by Raman spectroscopy, reveals the presence of CO_2 with smaller amounts of CH_4 (5-15 mole %), N_2 (0-4 mole %) and H_2S (0-0.5 mole %) (see table IV-6, annexe). Anyway, H_2S has higher values in this type of fluid in comparison to the other types (max. 0.29 mol.% bulk composition). (Fig. IV-36). The salinity is always very low (0 -2.9 wt % eq. NaCl) and the degree of filling in aqueous phase never reaches values higher than 50%. The fluid displays densities in the 0.6- 0.9 range.

Vc-w inclusions : Aquo-carbonic fluid with low CO_2 density

The density of the fluid is in the 0.4 - 0.7 range. The Raman spectroscopy shows a higher % mol. of CH_4 (20-35 mole%) and a lower content of H_2S than Lc-w fluids. The variation of N_2 is not significant.The content in CH_4 and its position in the history of the vein system appears to support a metamorphic origin for this type of fluid.

Lw-c inclusions : Aqueous fluids with small amounts of C-phases

Their density is in the 0.6 -0.7range. The salinity is very low in most cases; never higher than 0.7% wt eq. NaCl. N_2 content is slightly higher than in the other cases.

The CH_4, H_2S and CO_2 contents in the volatile phase are very similar to the Vc-w inclusion type.

Relationships between fluids and ore mineralogy

No extensive studies were carried in Penedono, as several previous works (Sousa and Ramos,1991) describe the ore mineralogy for Penedono veins. Three main stages can be distinguished (Fig. IV-37):

- *First stage (I):* during this stage, the main deposition of quartz and arsenopyrite occur. Small amounts of bismuth and bismuthinite and gold are found in arsenopyrite. However their genetic relationships with arsenopyrite are unclear.
- *Intermediate stage (II) :* some chalcopyrite-sphalerite grains formed, and later on galena and some arsenopyrite in the form of small crystals.
- *Late stage (III) :* in this stage, the formation of small fractures in the ores yields to the main deposition of gold (namely in the sulphurs). These fractures are in most of the cases observed easily, although they might be very small. This fact might lead to some misinterpretations of the relationships between the ores and gold.

Each of these stages can be respectively related with some degree of confidence with the different fluid types, Lc-w (I), Vc-w (II) and Lw-c or Lw (III).

Chemical evolution of the system

The global composition of the system varies from a CO_2- rich system (I), to a system with a higher content in CH_4 (II) (Fig. IV-38). This relation of high content in CH_4 and the gold mineralizations has already been noted by other authors. The last phase (III) corresponds to a fluid with low volatile phase density, and a higher salinity which corresponds to a shallower surface source of fluids.

4- PINO (CREGU)

Fluid inclusions have been studied in mineralized quartz (MQ) from the surface samples from the Llago de las Mosas area (table IV-5):

- mineralized episyenites with cavities resulting from quartz dissolution filled by quartz Q1 and Q2,
- pyrite bearing veinlets parallel to the main structure
- fluid inclusion planes from the host granite.

In the mineralized episyenite, most fluid types have been recognized. Their microthermometric and Raman data are the followings :

- aquo-carbonic fluids with dominant CO2 (Lc-w and rare Vc-w)

A part of them have three phases at room temperature. They have been observed as primary fluid inclusions in Q 1.

Tm CO2 are ranging from -57.0 to -59.5°C but most of the data are in the -58.5; 57.5°C range (Fig. IV-39a). Tm ice ranges mostly from -4 to -6°C (Fig. IV-39c) corresponding to a maximum salinity (overestimation due to dissolved CO2) in the range 6.5-9 % eq. wt.%NaCl. Tm cl are observed between 7 and 9°C with a mode around 9°C ((Fig. IV-39d). Th CO2 occurs in the liquid phase between 19 and 27°C and for other inclusions Th CO2 is in the vapor phase and ranges from 17 to 29°C with a mode at 27°C (Fig. IV-39b). Global homogenization have been recorded in the range 180-360°C, with a mode around 320-340°C (Fig IV-40).

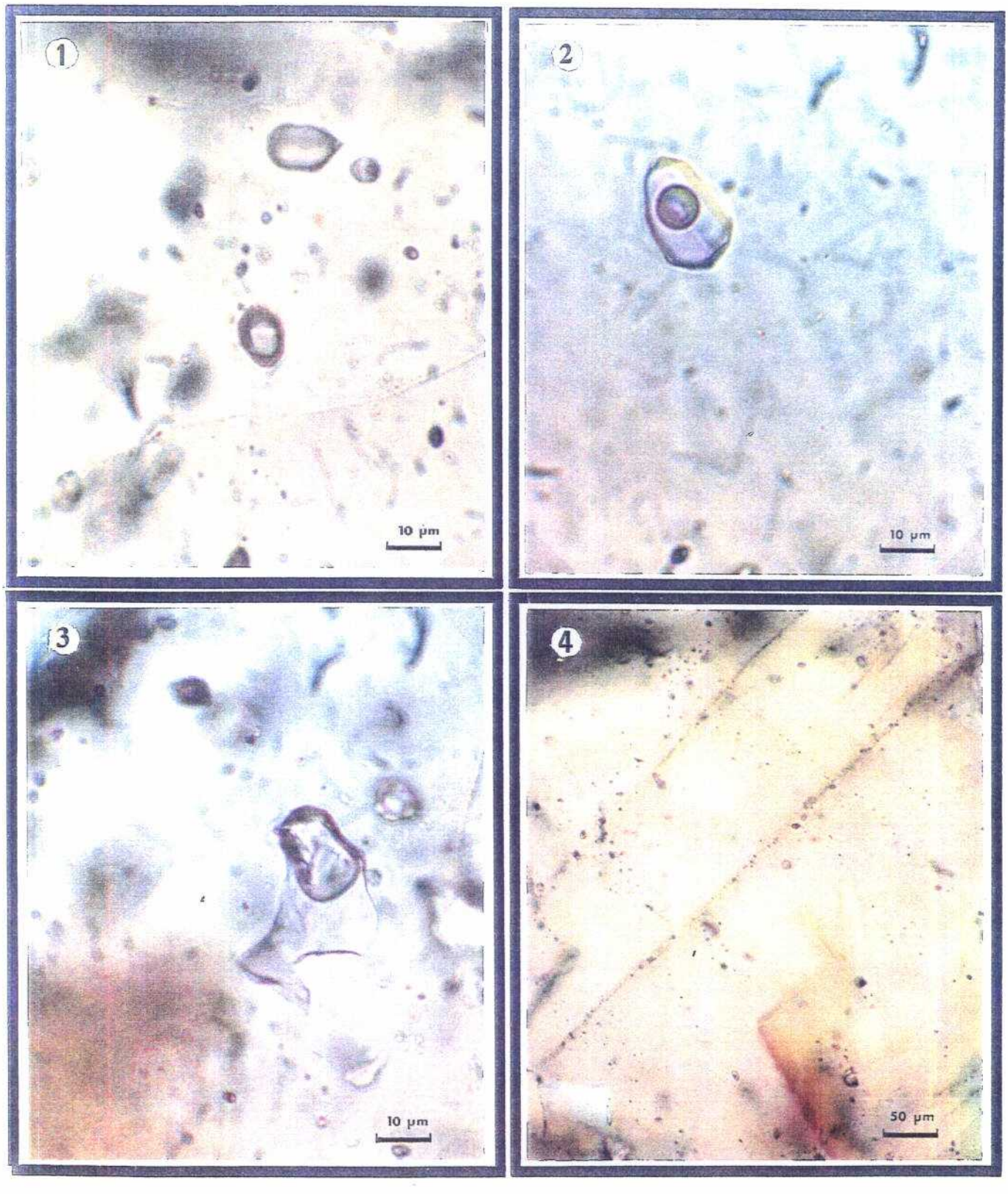

Plate IV-16 : Fluid inclusion features from Pino area;
1- Lc-w aquo-carbonic inclusions in authigenic quartz filling episyenites;
2 - Lw-c aquo-carbonic inclusions in clear authigenic quartz (2) from episyenites.
3 - Lw-c aquo-carbonic inclusions in authigenic quartz from episyenites where the inclusions are characterized by low CO_2 content only detectable by Raman microprobe analysis.
4- network of aqueous fluid inclusions trails in the vein quartz.

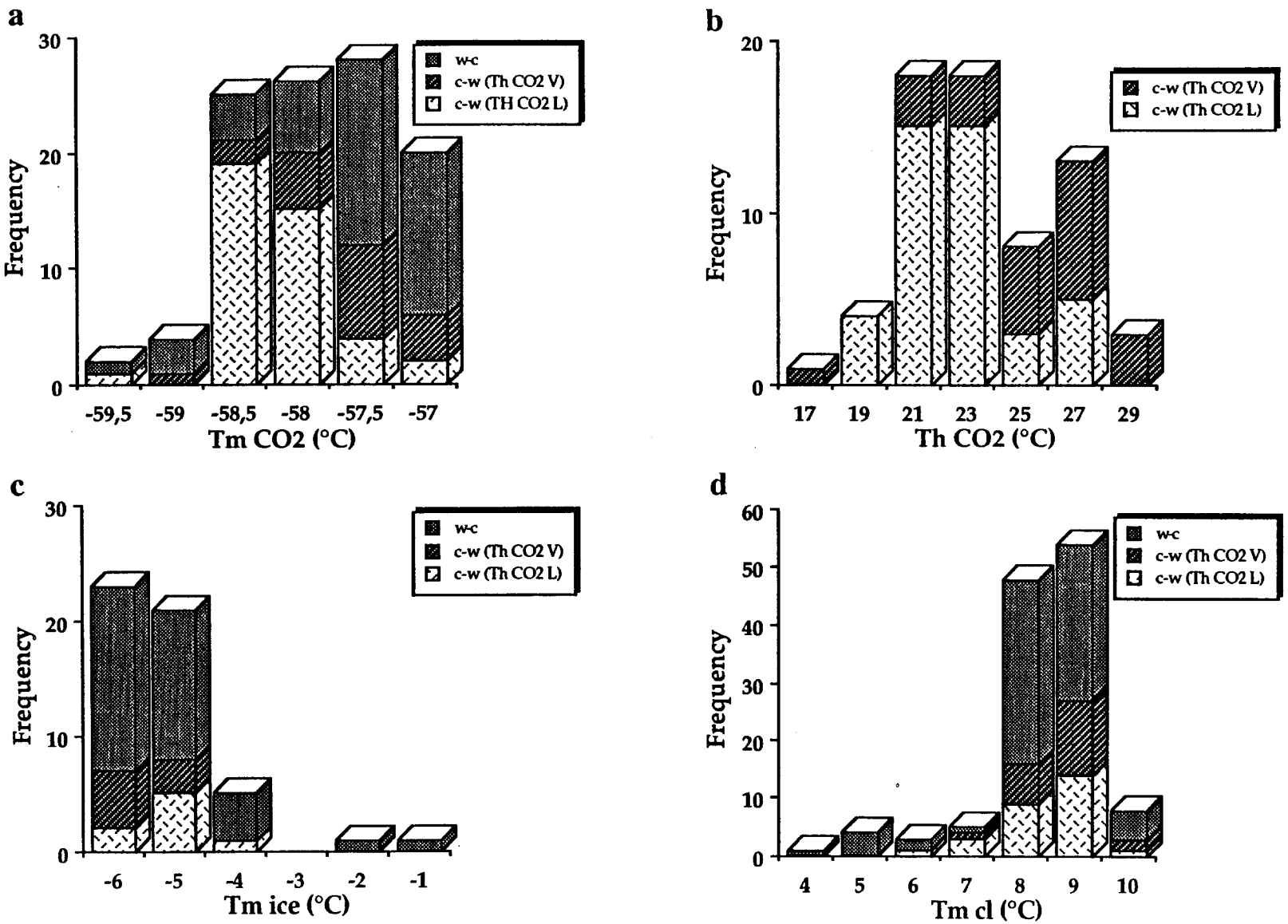

Fig IV - 39:Aquo-carbonic fluid inclusions in episyenites from Pino area. a : histogram of melting temperature of CO2 (TmCO2); b : histogram of homogenization temperature of CO2 (Th CO2), c : histogram of melting temperature of ice (Tm ice) d : histogram of melting temperature of clathrates (Tm cl),.

- *aquo-carbonic fluids with dominant H2O (Lw-c)*

Fluid inclusions are scattered in clear quartz Q2 infillings.
Liquid CO2 content is very low and is only detected by the presence of clathrates. Tm CO2 when visible is in the range -57 ; -59.5°C (Fig IV-39a). Tm cl is in the range 4-10°C with a mode at 8°C (Fig. IV-39d). Global homogenization temperature occurs either in the liquid phase or in the vapor phase in the 220-380°C range with a mode around 260°C (Fig. IV-40).

Gas phase of the aquo-carbonic fluids is dominated by CO2 with a relatively low CH4 (<15 mol% in the volatile phase) and N2 content (<15 mol% in the volatile phase) as shown in the CH4-N2-CO2 diagram (Fig. IV-42a). Three groups can be distinguished based on the type of CO2 homogenization (liquid, vapor or Th not visible and presence of clathrate) and the CO2 content (bulk composition) :

- Lc-w inclusions : CO2 : 20-80 mol % ; CH4 : 1-5 mol.% ; N2 : 1-5 mol.%; H20 : 15-75 mol.%
- Vc-w inclusions : CO2 : 5-25 mol % ; CH4 : 0.2-3 mol.% ; N2 : 0.4-2 mol.%, H20 : 70-90 mol.%
- Lw-c inclusions : CO2 : 2.5-16 mol % ; CH4 : 0-1.2 mol.% ; N2 : 0-0.5 mol.%; H20 : 85-97.mol.%

- *aqueous fluids*

They are always observed as fluid inclusion planes in Q1 and Q 2 , croscutting aquo-carbonic fluid inclusion planes, as well as in the granite quartz grains and vein quartz. They are also found as scaterred inclusions, but are interpreted as badly defined fluid inclusion planes, and are never primary. Depending on the samples (mineralized episyenite, or quartz vein/host granite) two groups have been distinguished :

- in episyenites, aqueous fluids are characterized by TmI12O in the -9 ; -1°C range wtih a mode at -6°C corresponding to a salinity of 9 eq. wt.%NaCl and homogenization temperatures in the range 140-300°C with a mode around 250°C (Fig. IV-41).

in the quartz veins and their host granite, fluids of lower salinities have been found; TmH2O are in the -4 ; -1 °C range with a mode at -3;-4°C and -1;-2 °C in the vein and in the granite respectively (Fig IV-43a and b), corresponding to salinities of 6,5 and 3,3 eq. wt.% NaCl. Global Th are in the 140-240°C range with a mode around 200°C (Fig. IV-43c).

Geometry of fluid circulation

Fluid inclusion plane orientations have been measured on oriented thin sections in different samples : episyenites, granite and quartz veins. Data are presented as rose diagramm in figure IV-44.

In episyenites, a dominant N40-60 °E direction is observed, which is nearly parallel to the major vein direction (N70° E) . The N100-110°E direction is minor. Aquo-carbonic and aqueous fluids are recognized in the two directions.

In quartz vein oriented N 70°E, fluid inclusion planes display a major N10-30°E direction. The N60-70°E is observed but is minor.

In the granite, two major directions have been recognized : a major N130-150°E, roughly perpendicular to the major vein network and a minor N10-30°E direction.

In the granite and in the quartz vein only aqueous fluids as fluid inclusion planes are observed. This tends to indicate that the carbonic fluids have circulated in the altered wall rocks of the vein and are responsible of the arsenopyrite deposition in the episyenite and the vein. Aqueous fluids have then migrated through the veins and rocks in distinct crack networks.

Bulk chemical evolution

The CO2-10CH4-H2O ternary plot shows the composition of the three types of fluid inclusions (Fig. IV-42b) with increasing water contents from Lc-w to Vc-w and Lw-c, confirming a possible dilution process of the early aqueous)-carbonic fluids by aqueous fluids.

CO2/CH4 ratio for Lc-w and Vc-w inclusions is subconstant in the 7-55 range and is homogeneous at the sample scale (Fig. IV-45a). The CO2/N2 ratio does not exhibit strong variation (1 to 30) (Fig. IV-45b). The volatile phase of such fluid type is relatively homogeneous.

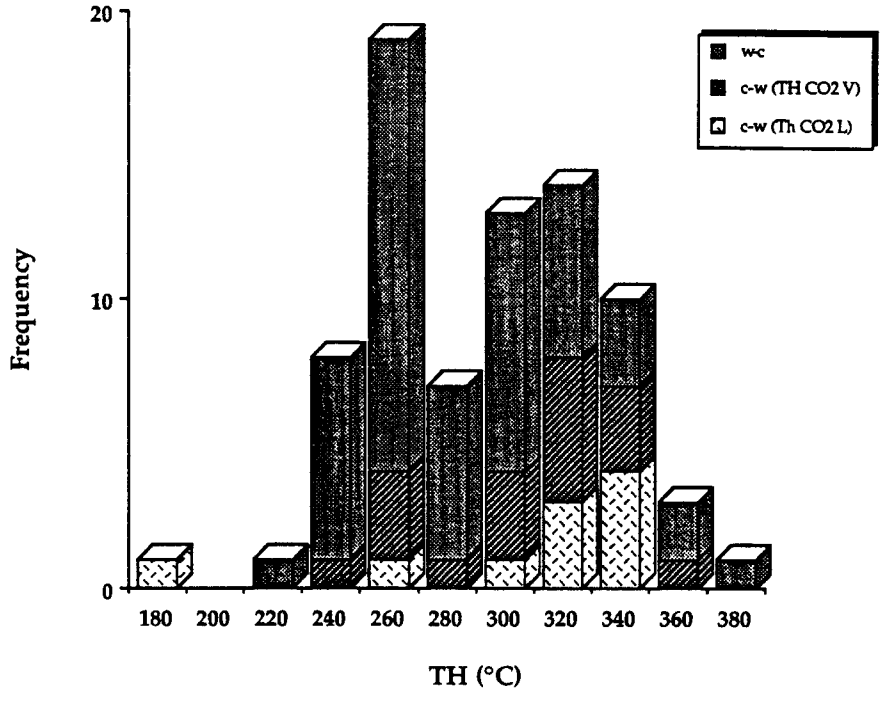

Fig IV - 40 : Histogram of global homogenization temperature of aquo-carbonic fluid inclusions in episyenites from Pino area.

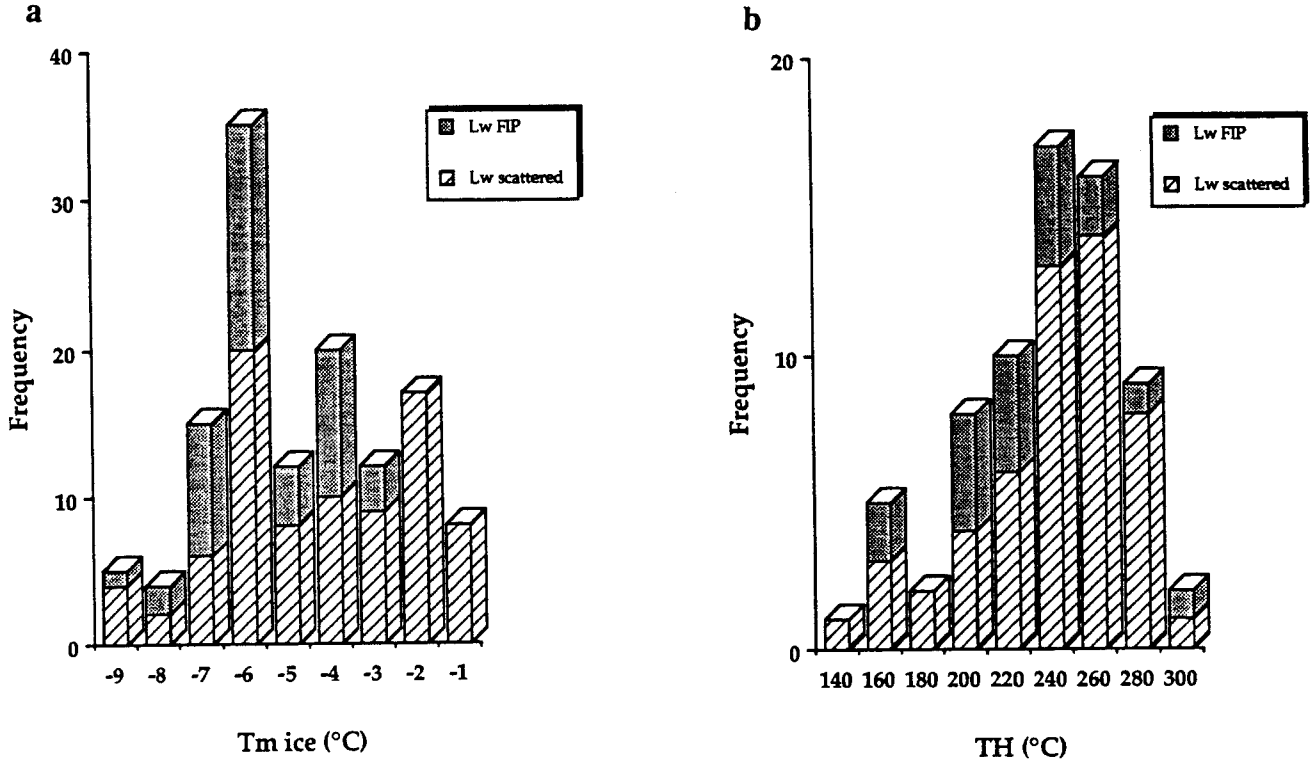

Fig IV - 41 : Aqueous fluids in episyenites from the Pino area. a : histogram of melting temperature of ice. b : histogram of global homogenisation temperature.

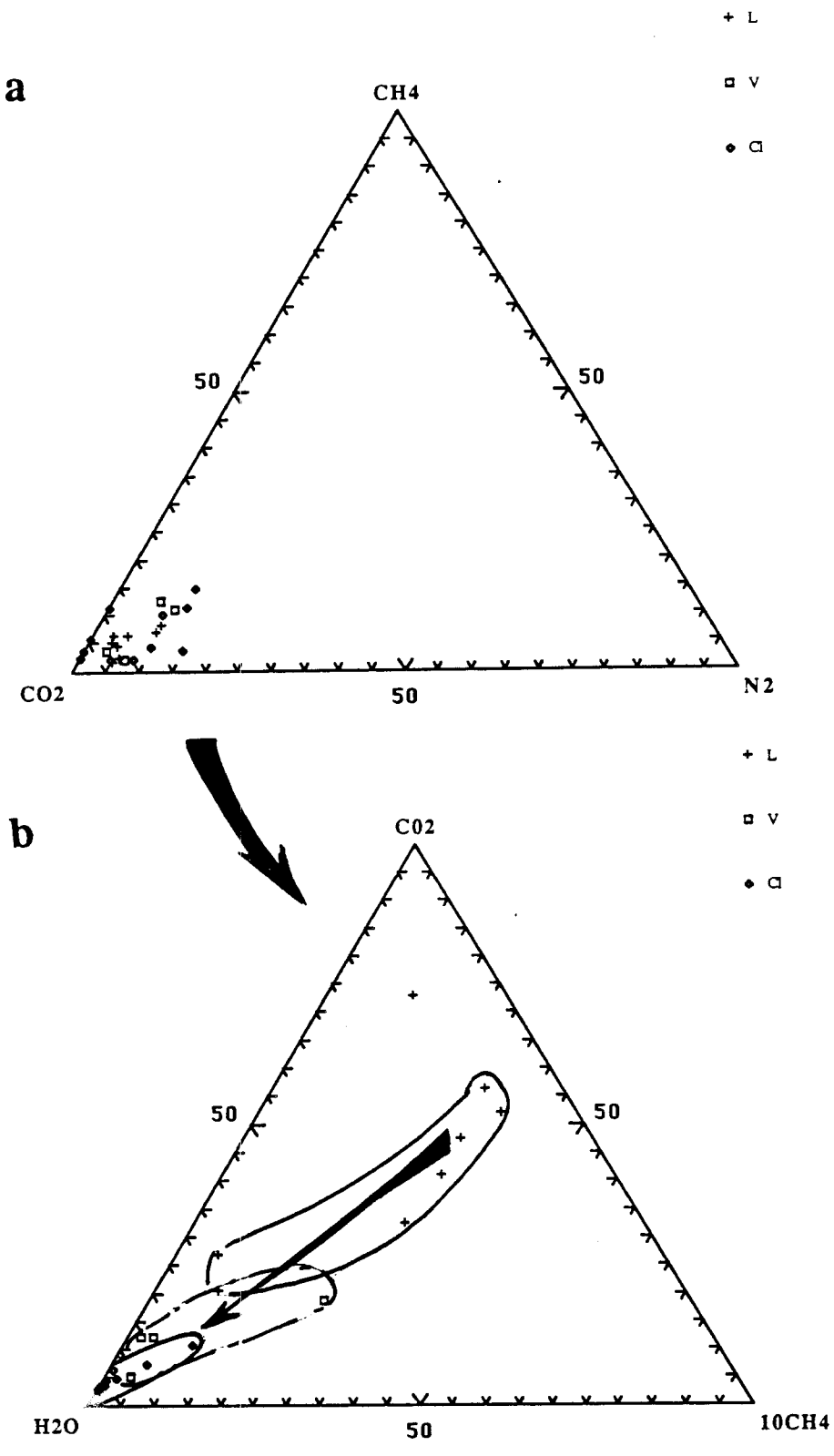

Fig IV - 42 : Ternary plot of the global composition for the aquo-carbonic fluids from the Pino area. a : in the CO2-CH4-N2 diagram, b : in the CO2-10CH4-H2O diagram.
c-w fluids : L : CO2 homogenization in the liquid phase, V : CO2 homogenization in the vapour phase. w-c fluids : cl

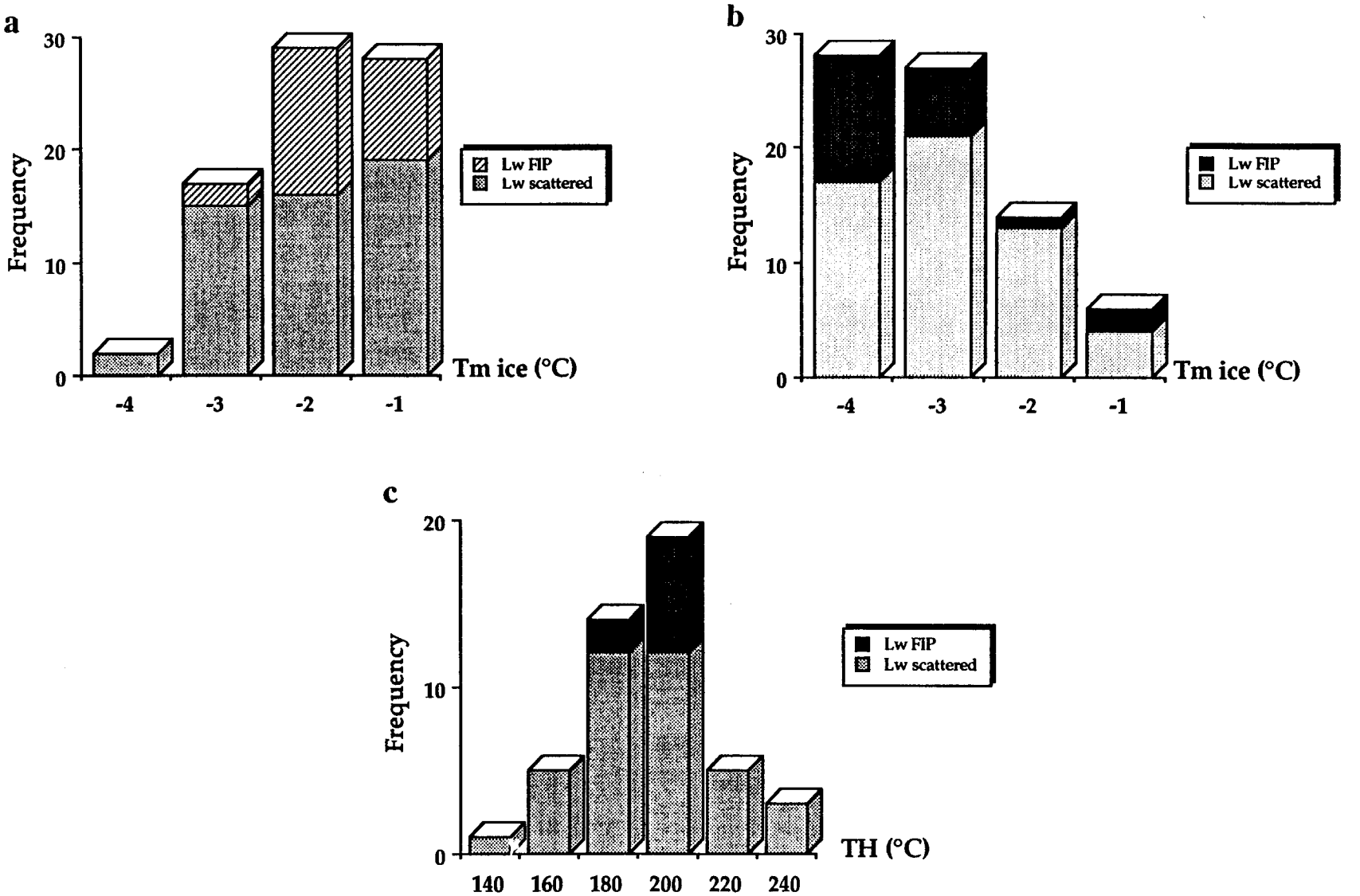

Fig IV - 43 : Aqueous fluids in quartz vein and granite from the Pino area. a : histogram of melting temperature of ice for fluid inclusions in the granite. b : histogram of melting temperature of ice for fluid inclusions in the quartz vein. c : histogram of global homogenisation temperature.

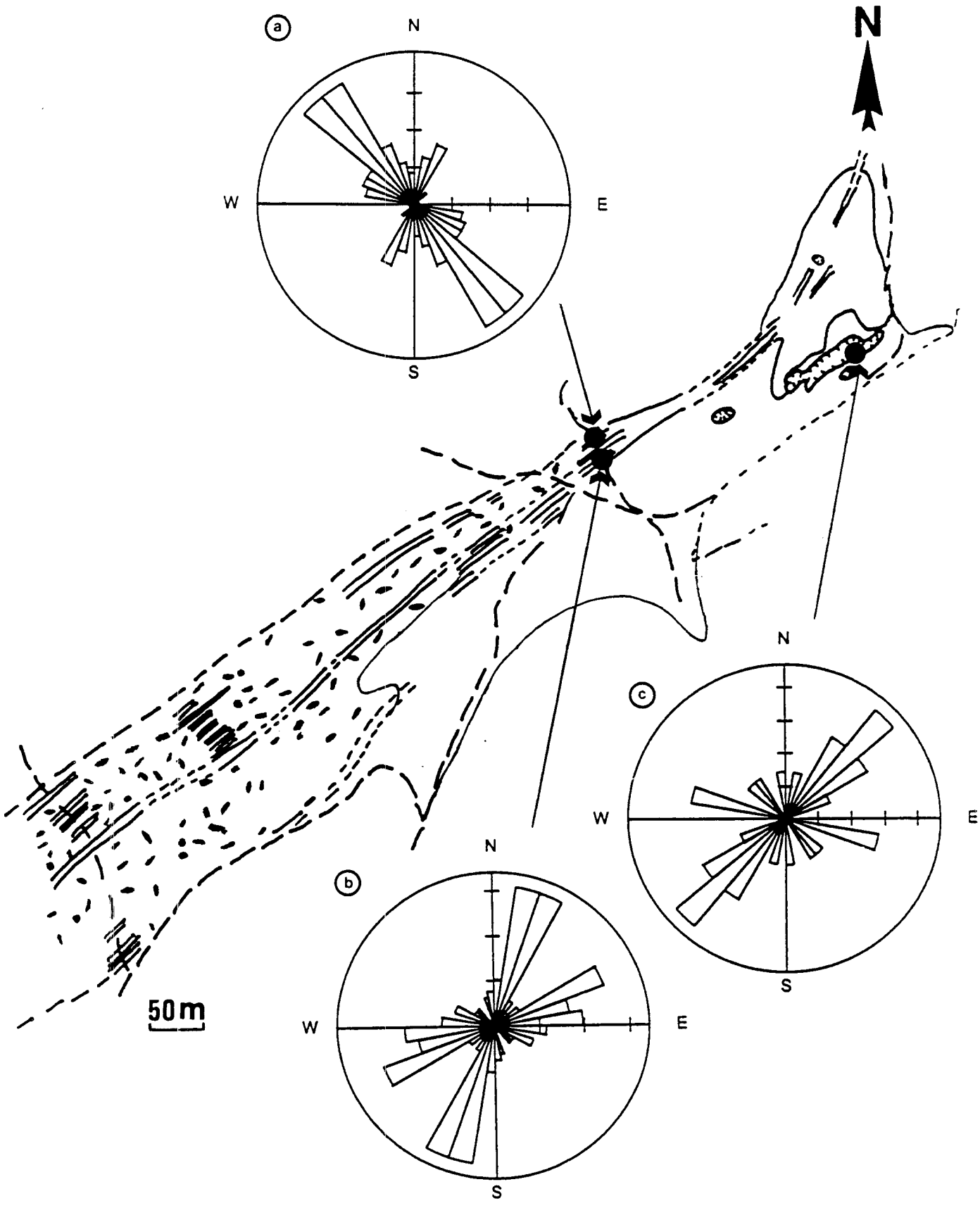

Fig IV - 44 : Rose diagram showing the orientation of fluid inclusion planes.
a : granite, b : quartz vein, c : episyenite

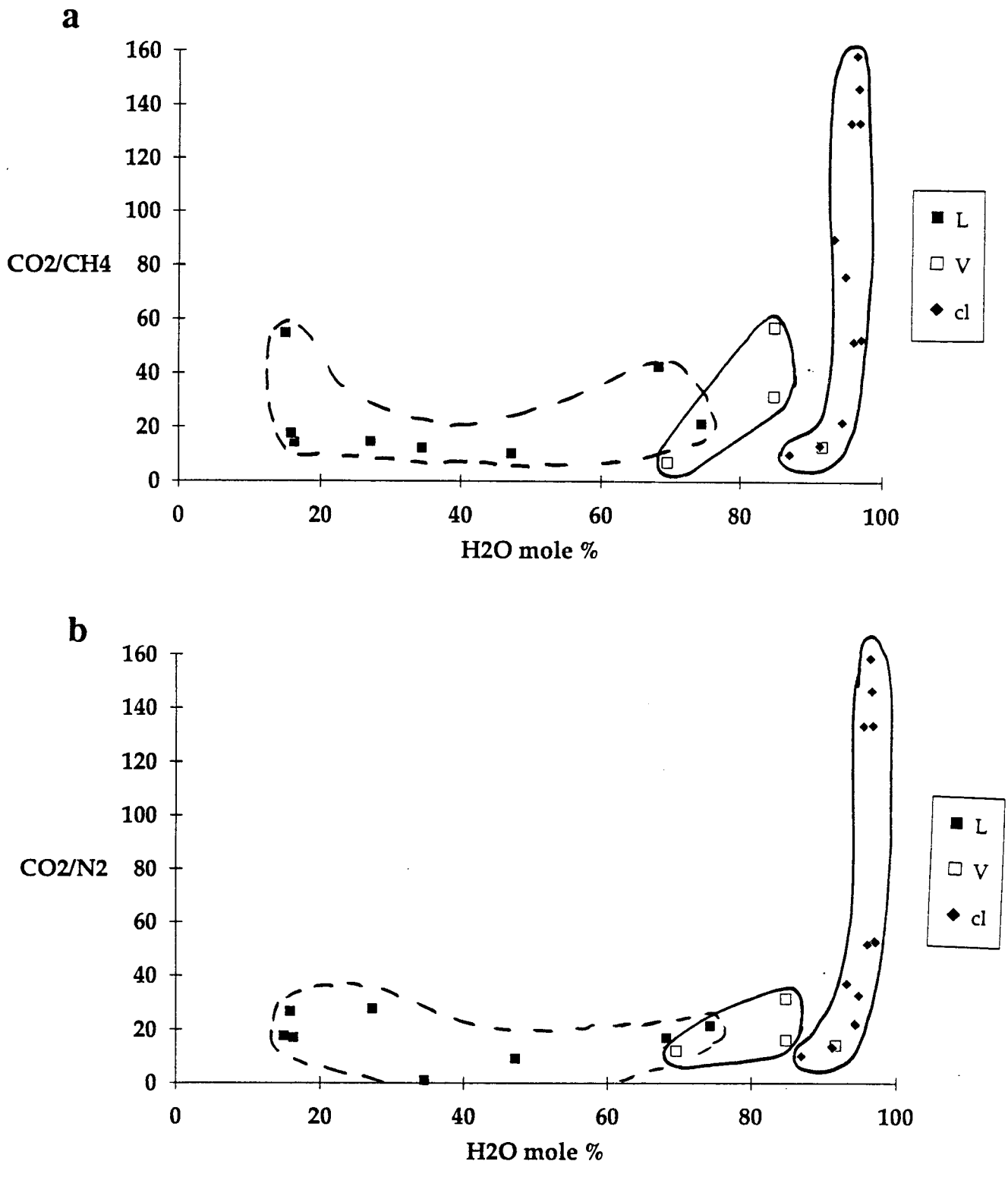

Fig IV - 45: Global composition of aquo-carbonic fluid from Pino area in : a: CO2/CH4 versus H2O diagram, b : CO2/N2 versus H2O diagram
c-w fluids : L : CO2 homogenization in the liquid phase, V : CO2 homogenization in the vapour phase. w-c fluids : cl

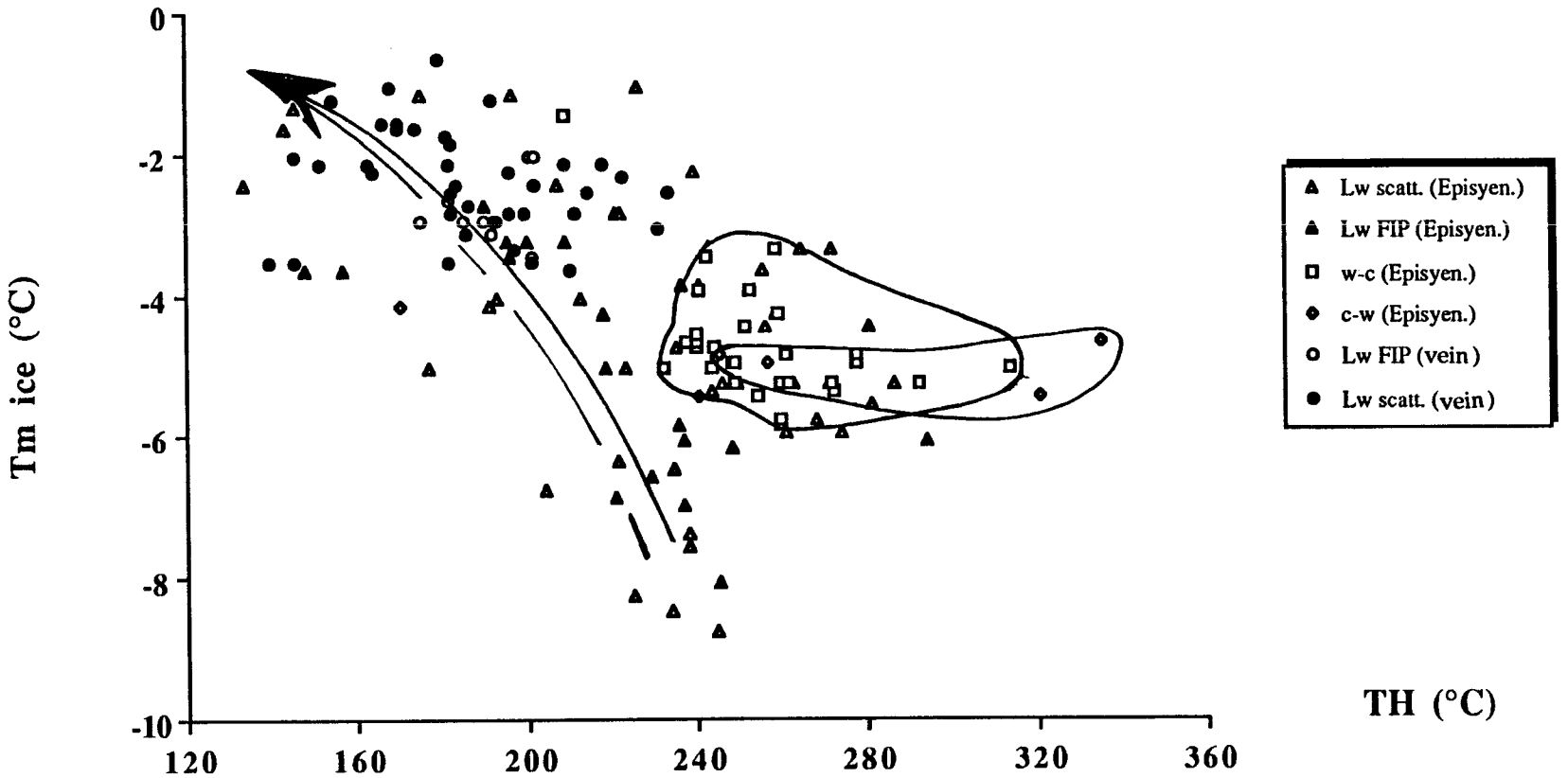

Fig IV - 46 : Tm ice -TH diagram for aquo-carbonic and aqueous fluids from the Pino area.

Lc-w and Vc-w inclusions display more constant CO2/CH4 ratio than CO2/N2 ratio than Lw-c fluids which are characterized by highly variable CO2/CH4 and CO2/N2 ratios covering values from 10 to 160.

Two groups are distinguished among Lw-c fluids : some inclusions noted Lw-c 2 appearing as trapped later on than other, noted Lw-c 1 are characterized by almost no detectable CH4 and N2.

The Tmice-TH plot shows that (Fig. IV-46):

- there is an apparent coincidence between the fluid data concerning the primary Lw-c, Lc-w and some Lw fluids, suggesting a possible evolution from the earliest aqueous-carbonic fluids towards the hot aqueous fluids through a dilution process.
- this important stage is followed by series of trapping of aqueous fluid showing a dilution-cooling trend from fluids of medium salinities (13eq. wt.%NaCl) and Th around 240°C towards dilute fluids displaying lower Th (160°C). These fluids are the only fluids found in the granite and the veins in the studied samples.

METAMORPHIC AREAS

1-FRANÇA (Lisboa Univ)

In order to characterize the typology of fluid inclusions of the different quartz generations in mineralized and barren veins associated both to the Vilariça fault and reactivated D3 shear zones, 20 oriented polished sections were produced and examined. Microthermometric analyses were performed at the Centro de Geologia da Universidade do Porto with M. Armanda Doria, and also at the Dep. Geologia da Universidade de Lisboa, using in both cases Chaixmeca stages. Raman microprobe spectrometry was done at CREGU with M. Christine Boiron.

Quartz typology

As already mentioned, mineralized, N15–30W, veins comprise in general five different types of quartz, although solely two (undeformed quartz IIb and IIc) are related to sulphides and electrum deposition. In some ore samples, quartz I, typically the major generation in the N40– 45W barren veins, may be present, and is characterized by optical features, as well as several microstructures, attributed to intense work–hardening followed by notorious dynamic recovery. Quartz IIa is intimately associated to domains where recovery microstructures of quartz I are neglegible. The distinction between these two quartz types is not always clear, since the generation IIa displays also optical features of (slight) work–hardening; in some domains, quartz IIa may be interpreted as the result of incipient dynamic recovery of quartz I, or simply a different feature of the heterogeneous deformation of quartz I. Nevertheless, it should be noted that quartz IIa is, at least partially, coeval with carbonate I deposition. Quartz type III represents the main post–ore generation, and the remaining quartz generations usually seal late N15W – N30E veinlets.

Quartz lenses along some secondary (N–S, on average) branches of the Vilariça strike–slip fault are mainly composed by two different generations that, in general, are optically similar to quartz IIa and IIb.

Mineralized N80–100E,40–50S veins within the WNW–ESE shear that outcrops in the França mine comprise essentially undeformed quartz, optically similar to quartz IIb and IIc. On the contrary, the main quartz generation associated to regional NW–SE shears exhibits strong plastic yielding and dynamic recovery, and contrasts with the late quartz types that fills both the earlier N55–60E veinlets and the late N25–35W veins. Similar quartz types can be found along the siliceous fillings of the NNE–SSW – NE–SW shear zones, although the prevailing generations are mainly composed by undeformed quartz.

Type		Quartz		Rock	Location	Tm CO2	Th CO2	Tm cl	Tm ice	TH
C-W	Th CO2 L	Q1		Episyenite	scatt. (FIP)	-59,5/-57 -58,5	19/27 22	7 / 9 9	-6/-4 -5	180/340 340
	Th CO2 V				scatt. (FIP)	-59/-57 -57,5	17/29 27	7 / 10 9	-6/-5 -6	240/360 320
W-C					scatt. - FIP	-59,5/-57 -57,5	___	4 / 10 8	-6/-1 -6	220/380 260
Lw					scattered	___	___	___	-9/-1 -6	140/300 260
					FIP	___	___	___	-9/-3 -6	160/300 220
			Q2	Granite	scattered	___	___	___	-4/-1 -1	___
					FIP	___	___	___	-3/-1 -2	___
				Quartz vein	scattered	___	___	___	-4/-1 -3	140/240 190
					FIP	___	___	___	-4/-1 -4	180/200 200

Table IV - 5 : Recapitulative microthermometric data for the different types of fluids in the Pino area. TmCO2 : melting temperature of CO2, Th CO2 : homogenization temperature of CO2, Tm cl : melting temperature of clathrates,. Tm H2O : melting temperature of H2O, TH : homogenization temperature. L : Liquid, V: Vapour, FIP : fluid inclusion plane, scatt : scattered.

Fluid inclusion data

In general, the main types of quartz exhibit specific associations of fluid inclusions, and, according to the microthermometric data, it is possible to put in evidence three distinct groups of inclusions: (1) Lc-w), (2) Lw–c , and (3) Lw. Figures IV-47 to 49 illustrate the obtained range for TmCO2, TmH2O, TmClt, ThCO2 and TH.

Q1 quartz : The main family of fluid inclusions in quartz I occur in clear domains near the boundaries of the deformed crystals where small (<5μm) and deformed inclusions are absent. The width of these domains is typically of the order of 0.25–0.5 mm, and their lateral continuity could usually be followed along a trend subparallel to the intergranular boundaries, suggesting a genetic relation between the development of these irregular bands and the circulation of fluids along intergranular fractures. Therefore, the examined isolated inclusions or clusters of inclusions in clear bands of quartz I have probably a secondary origin. This interpretation is also consistent with the notorious compositional similarities between these fluid inclusions and those along well defined trails, representing, perhaps, healed cracks of contemporaneous age. The examined isolated fluid inclusions are usually of type Lw–c with three phases at room temperature, for which the Th CO2 occurs to the vapour in the range of 15 – 22°C; inclusions along trails have higher ThCO2 (ranging between 22.2 and 26.9°C) and, with the exception of inclusions of trails A (N–S, subvertical), homogenize in vapour phase. The Tm CO2 for the two main groups of inclusions, ranging from –59.4 to –57.5°C and from –59.6 and –56.8°C, respectively), is typically between –58.5 and –58°C; these values, lower than the Tm of pure CO2, as well as the range of Tm cl (8.5–11.2°C), suggests the presence of other volatile compounds (like CH4 and N2), besides CO2. There is no significant difference between the TmH2O of isolated inclusions and the values obtained for inclusions that occur in trails C (N70–80°E,50–60°NW), which are usually in the range –4.3/–2.0°C; for inclusions in trails A and B (N20–30°W,65–75°E), the melting temperature of water is typically between –2 and –1°C. Global homogenization for the different groups of inclusions were recorded in the range of 280–330°C.

QIIa stage : Characteristic inclusions of quartz IIa are, in general, quite similar to those present in quartz I; the major difference is given by the Th which occurs between 270 and 280°C.

Like quartz I, the main quartz generation present along the siliceous fillings of the NW–SE regional shears shows strong plastic deformation, and the isolated inclusions of Lw–c type occur always within irregular bands of clear quartz in the vicinity of the boundaries of deformed crystals. Tm CO2 is typically around –58°C, and Th CO2 occurs to the vapour in the range of 16–20°C. Tm cl is in general close to 10.5°C, although it may be observed at lower temperatures (5–7°C). The characteristic Tm ice is, on average, –3°C. Flw is in the range of 0.50–0.70% and Th (to the liquid) varies between 250 and 310°C. Similar fluid inclusions occur along trails of types A (N10–15°W,70– 80°W) and B (N30–35°W,80–85°E), although one can put in evidence slight differences in Tm cl and ThCO2 ranges. The remaining trails, as well as some inclusions of trails B, are composed by aqueous inclusions with a global homogenization to the liquid between 150–180°C; Tm ice is scatered in the range of –3.8/–0.6°C, and clathrates were detected for the majority of the examined inclusions (Tm cl around 2–3°C), denoting the presence of a (low–density) CO2 phase.

QIIb stage : In ore samples, the prevailing quartz generation (IIb) shows abundant inclusions of Lw–c type with variable shape and dimension (10–30 μm). These inclusions occur usually in clusters and, at room temperature, exhibit in general two phases. Melting and homogenization temperature of CO2 are scatered in the ranges of –59.1/–58°C and 17.3–23.4°C, respectively. Tm cl occurs typically between 7.6 and 9.1°C. Flw is quite constant, in the 0.40–0.55%range, and Tm ice is observed between –4.2 and –2.9°C. The characteristic Th of these inclusions are 270-300°C.

Inclusions from quartz I, IIa, and IIb display compositional similarities as shown by Raman analyses from table ; isolated inclusions in the earlier quartz generation present along

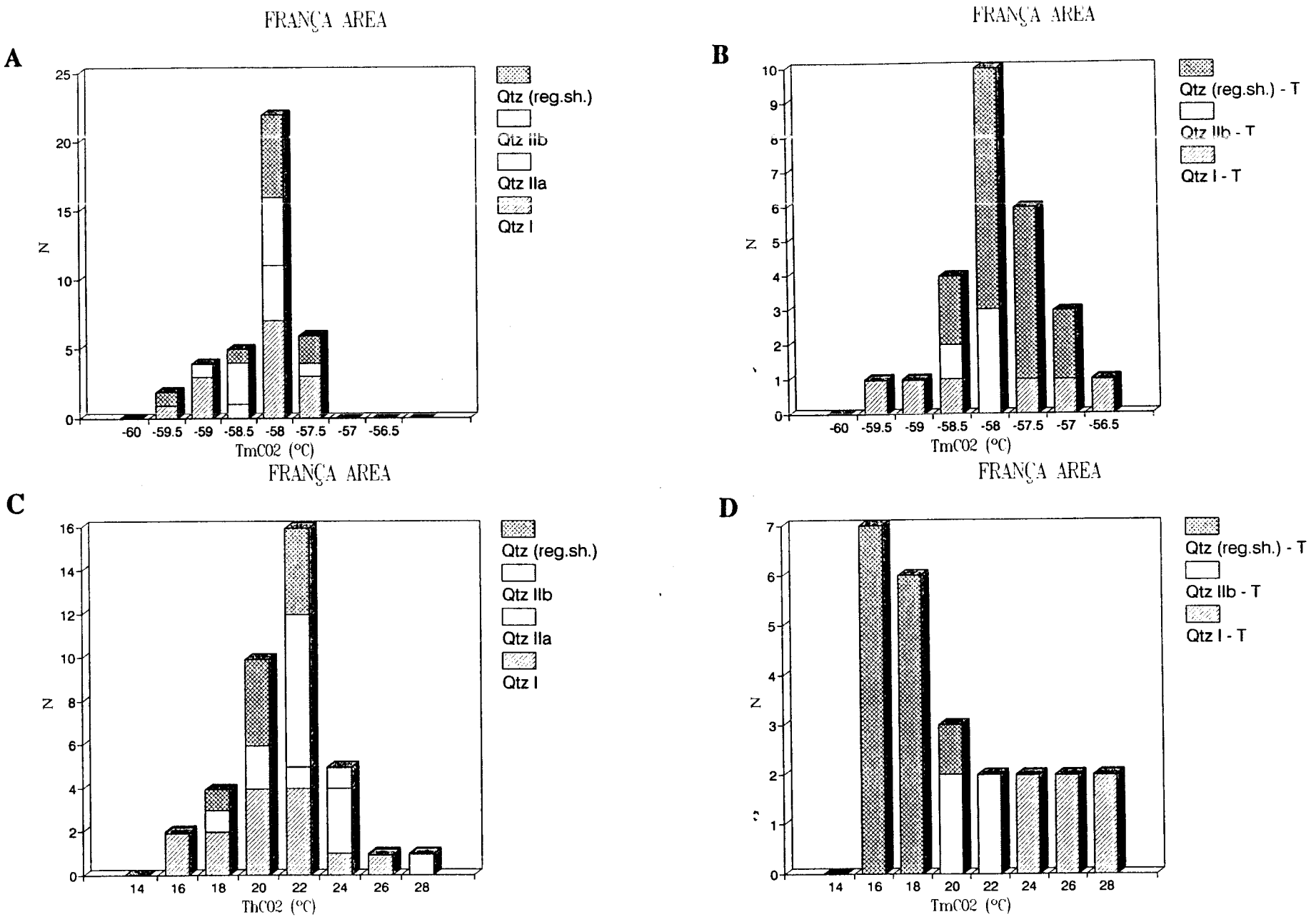

Fig IV - 47 : Inclusions of Lc-w type from the França sector. Histograms illustrating the temperature variation of CO_2 melting (Tm CO_2) (isolated inclusions - A - and trails of inclusions - B), and CO_2 homogenization (ThCO_2) (isolated inclusions - C - and trails of inclusions - D).

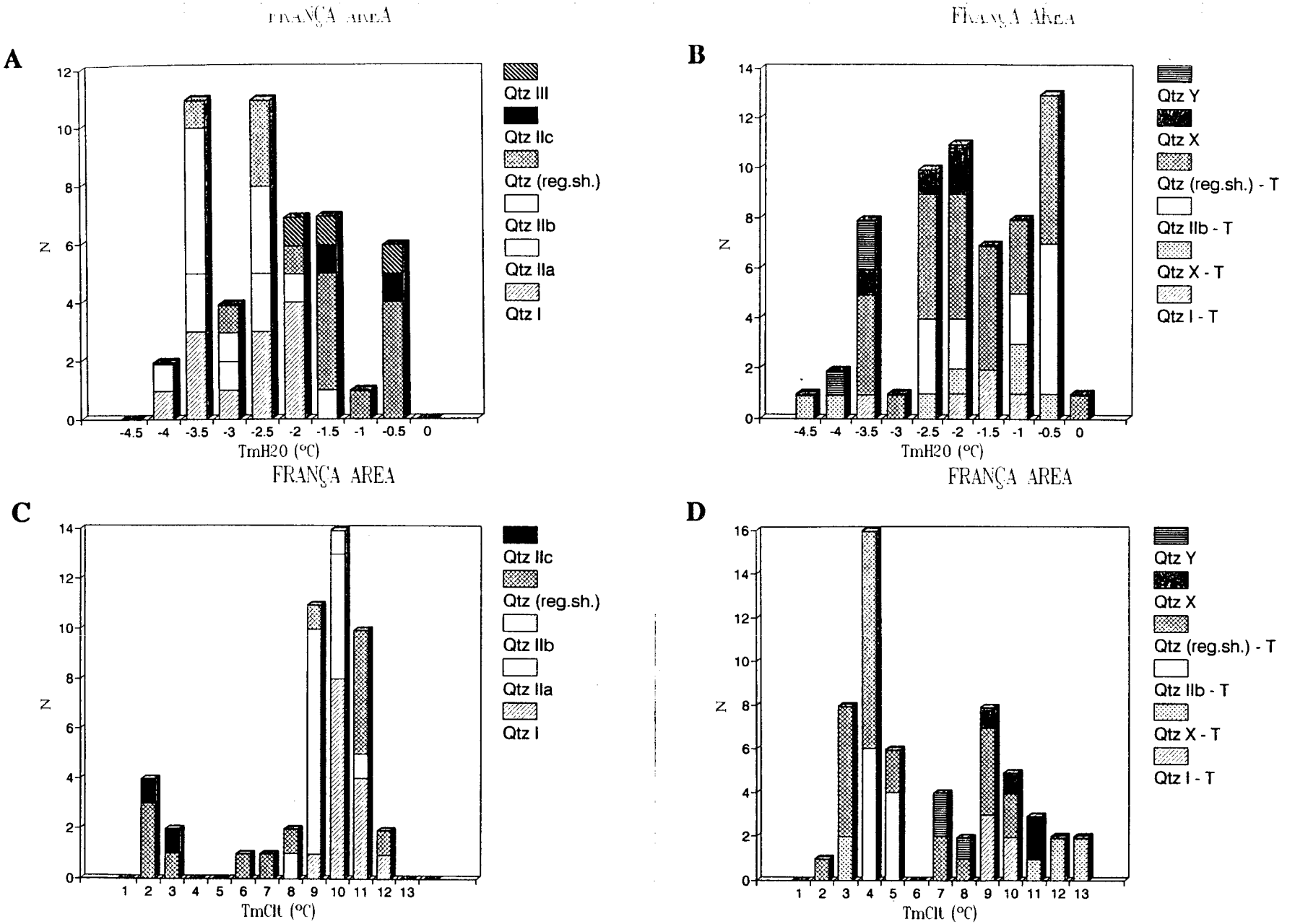

Fig IV - 48 : Fluid inclusions from the França sector. Histograms illustrating the temperature variation of ice melting (Tm H_2O) - A, B - and clathrate melting (Tm Clt) - C, D.

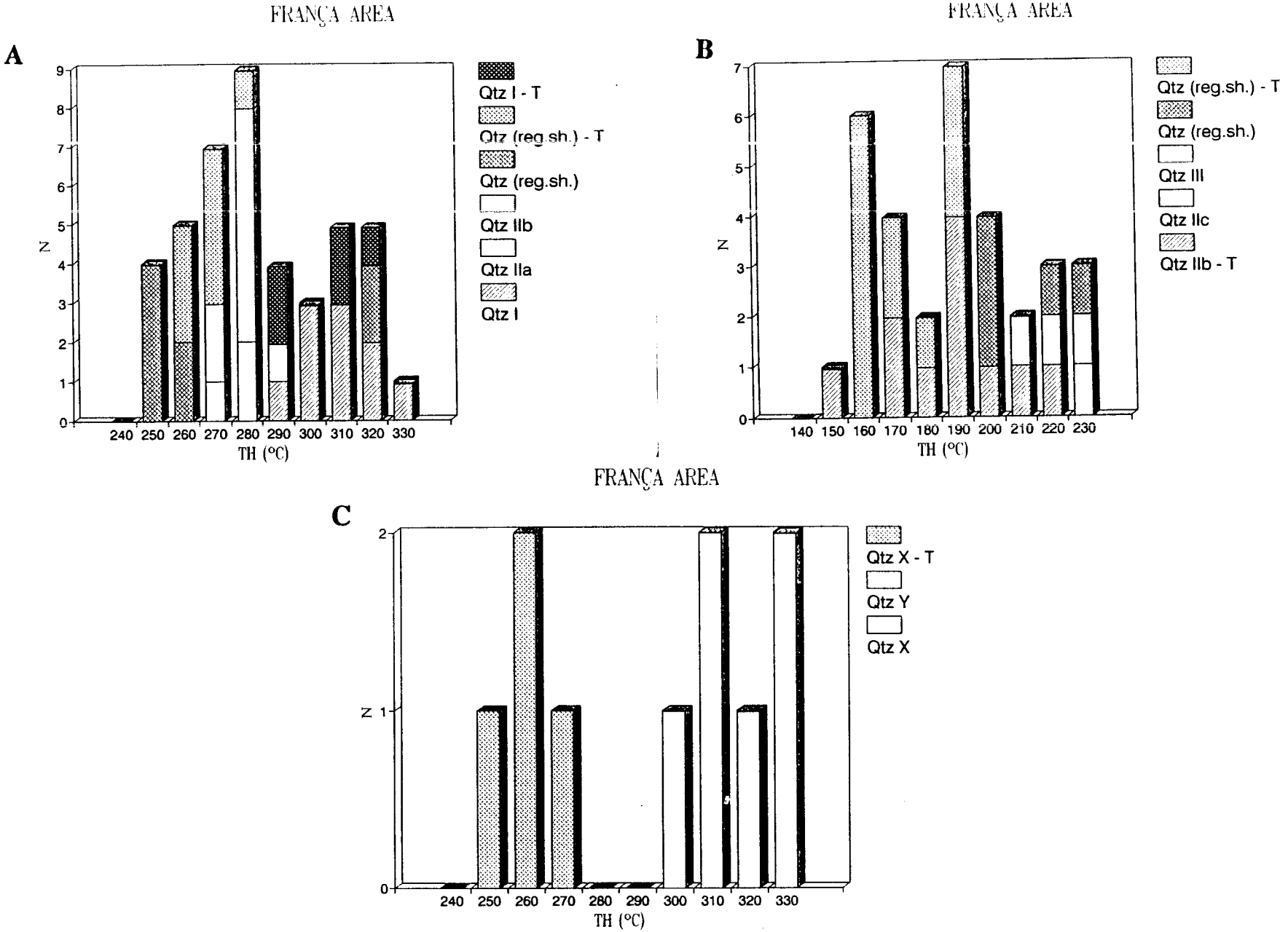

Fig IV - 49 : Variation of the global homogenization temperature (TH) for the characteristic fluid inclusions in each quartz type.

NW–SE shears exhibit also an identical volatile composition. As a matter of fact, comparing the Raman data obtained for isolated inclusions in these three types of quartz, one can conclude that CO2 ranges typically between 75 and 93 mole % (with a mode around 80–85 mole%), CH4 varies between 5 and 20 mole % (although ranging typically from 10 to 15 mole % in quartz IIa and IIb), and N2 is scattered in the range 2–9 mole % (with a mode around 3–4 mole %). These results are clearly illustrated by data projection on a CO2–CH4–N2 ternary diagram (Fig IV-50), as well as plotting CO2 versus CO2/CH4 and CO2/N2 ratios (Fig. IV-51and 52), which enable also the characterization of the compositional deviations obtained for inclusions along the different trails. At this point, it should be noted that the inclusion trails in deformed quartz of NW–SE shears exhibit an enrichment in CH4 and N2, particularly notorious for the N35W direction.

The characteristic inclusions of the barren quartz lenses along the secondary branches of the Vilariça fault show a gas phase quite enriched in CH4 and N2, ranging between 30–50 mole % and 20–40 mole %, respectively, in quartz X, and between 30–60 mole % and 40–70 mole % in quartz Y. Gas composition of inclusions along trails in quartz X is quite variable, and may be just CH4 (N10W trails), or slightly CO2 enriched (around 40 mole %; E–W trails).

Quartz IIC and III : Isolated inclusions in quartz generations of type IIc and III are, in general, very small (<5μm) and therefore of difficult analysis. Nevertheless, the available data suggest that they have strong similarities with the above mentioned secondary fluid inclusions, particularly with those that characterize trails A, D and E.

Quartz IIb exhibits also different trails of secondary fluid inclusions. Trails of type D (N30°W,70°S) and E (N10–15°E,70–80°NW) comprise similar aqueous inclusions with slight different Th (around 170°C and ranging from 150 to 160°C, respectively) and a variable Flw between 0.40 and 0.80%; in these inclusions, TmH2O is in the range –2.9 to –0.7°C, and the presence of a (low–density) CO2 phase may be inferred by the clathrate melting (typically between 3 and 5°C). Fluid inclusions along trails A (N60–70°E,55–70°NW) and B (N40–50°E,60–65°NW) show Tm ice around –1°C, and global Th to the liquid between 150 and 165°C; their water content is commonly around 0.50%. Finally, trails of type C (N20°NW, subvertical), representing probably the earlier system of healed cracks in this quartz generation, are composed by Lw–c (two phase) inclusions with Th of the order of 200°C.

Late quartz generations associated to the NW–SE and WNW–ESE shears, specially the quartz type associated to mineralized veins, comprise abundant inclusions of small size (<10μm) with a characteristic homogenization temperature ranging from 195 to 215°C. The water content of these regular inclusions is, usually, high (Flw between 0.55 and 0.80%), and the recorded TmH2O is in the range –2 to –0.6°C. In these fluid inclusions the presence of a (low–density) CO2 phase may be inferred by the clathrate melting (typically around 2°C).

Finally, it should be noted that the characteristic inclusions of the barren quartz lenses along some secondary (N–S, on average) branches of the Vilariça strike–slip fault show significant differences from the remaining inclusions studied. As a matter of fact, besides the frequent presence of graphite crystals, these inclusions exhibit high Tm cl (in the range 7–11°C) and a typical TmH2O between –4 and –2°C. Melting temperature of carbon dioxide was not observed, and the abundancy of clathrates suggests that other volatile species are dominant (specially CH4 and N2). Global homogenizations to liquid occur between 200 and 220°C for isolated inclusions, and between 140 and 160°C for inclusions along E–W,50–60°N and N55–60°E,60– 65)NW trails.

Bulk evolution

Two main trends can be put in evidence on a H2O–CO2–(CH4+N2) ternary diagram (Fig. IV-53), enabling the distiction between the characteristic fluid inclusions of quartz generations related to mineralized structures (with X(CO2) and X(CH4) typically ranging from 6 to 18 mole %, and from 0.2 to 4 mole %, respectively), and the common fluid inclusions associated to the barren quartz lenses of the Vilariça fault (with X(CH4) and X(N2) scattered in the range 3–5 mole % and 1–8 mole %, respectively). X(H2O) increase (>80 mole %) is the

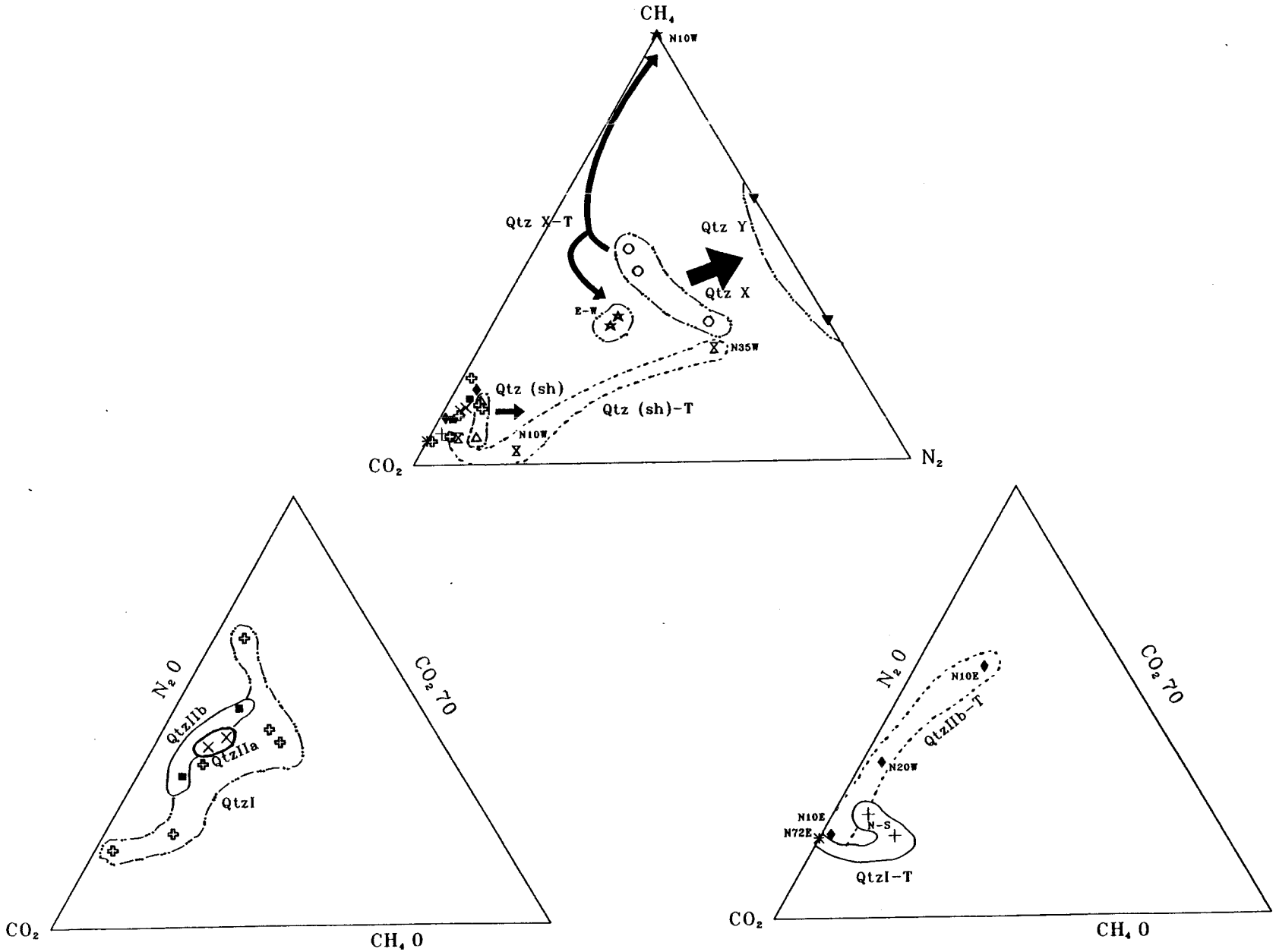

Fig IV - 50 : CO_2-CH_4-N_2 diagram of the volatile phase determined by Raman spectroscopy in representative fluid inclusions of different types of quartz present in mineralised and barren structures in the França area.

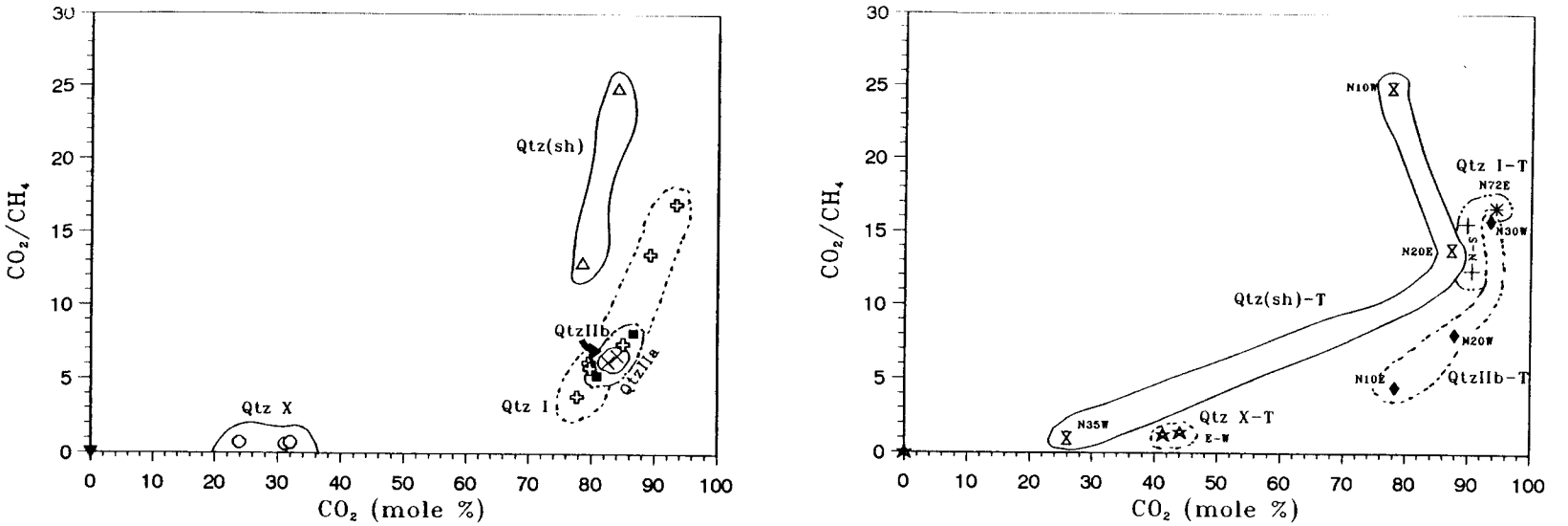

Fig IV - 51 : CO_2/CH_4 versus CO_2 plots for isolated inclusions and trails of inclusions in different types of quartz present in mineralized and barren structures in the França area.

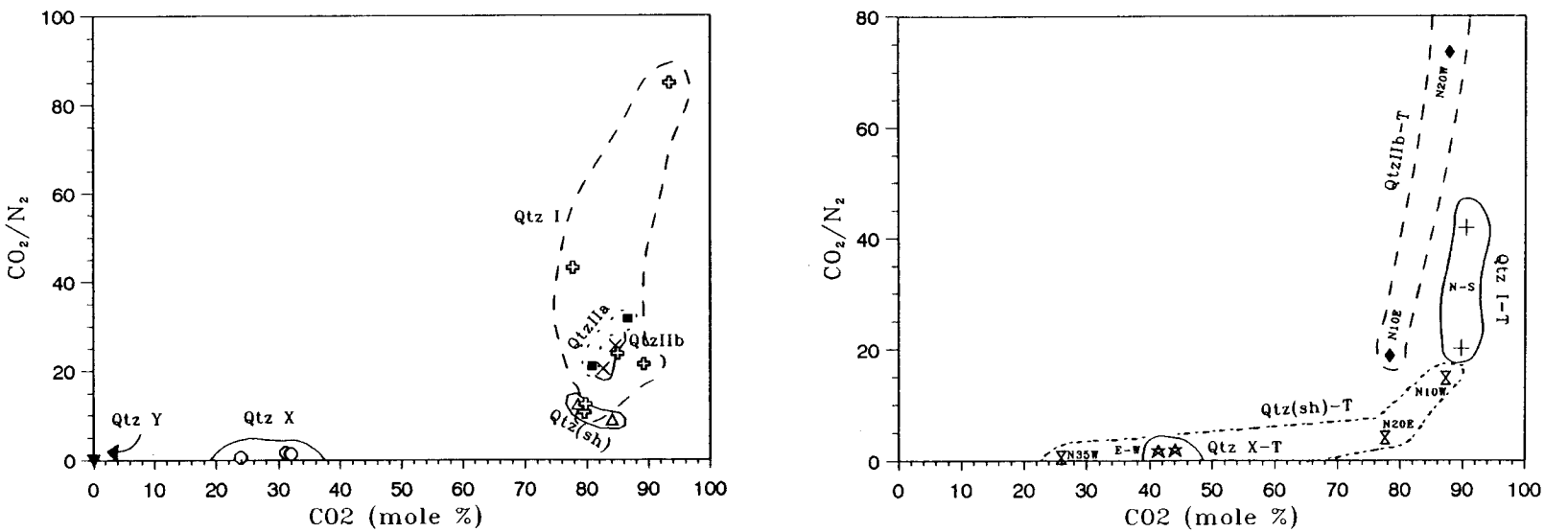

Fig IV - 52 : CO_2/N_2 versus CO_2 plots for isolated inclusions and trails of inclusions in different types of quartz present in mineralized and barren structures in the França area.

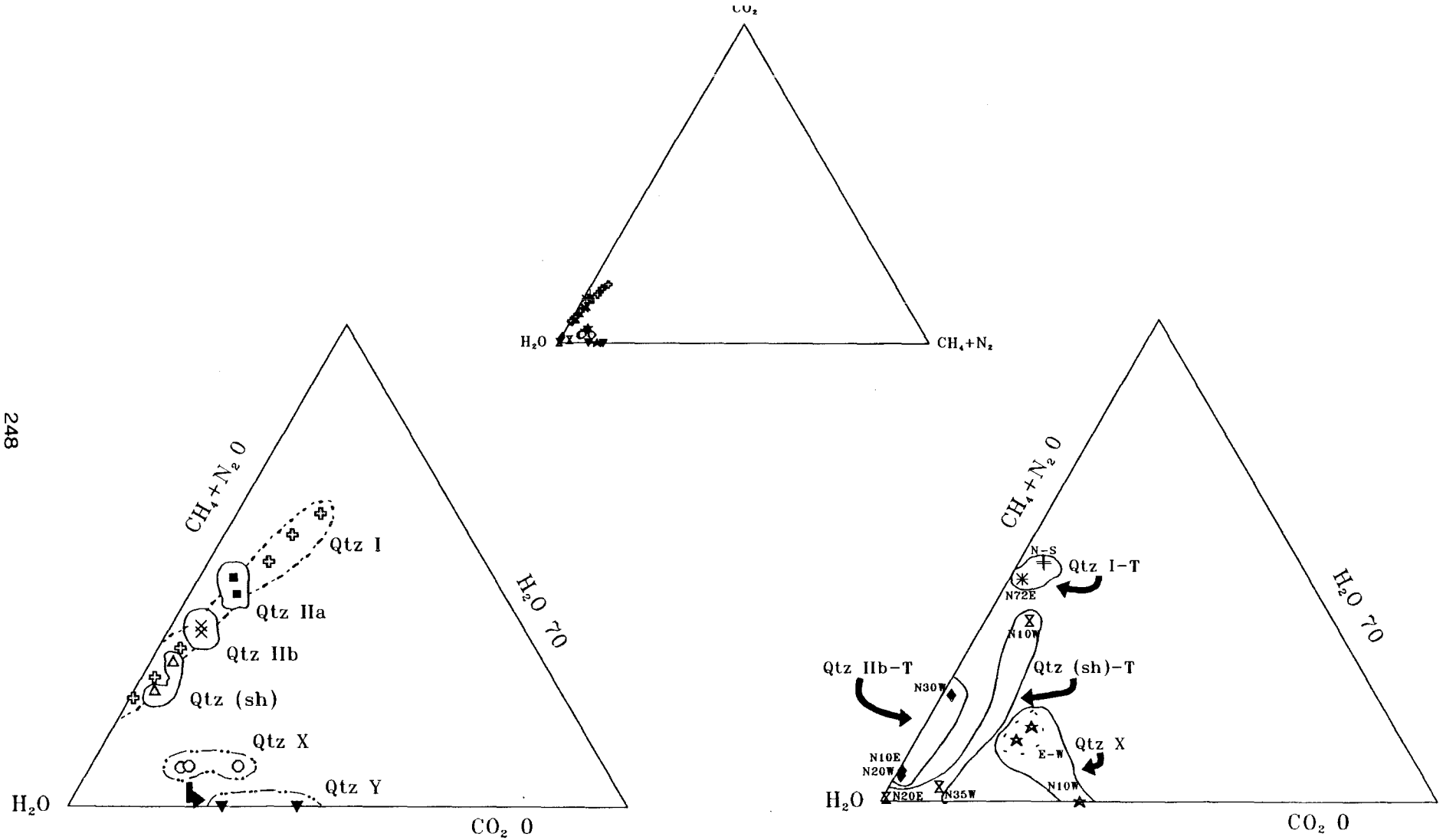

Fig IV - 53 : H_2O-CO_2-(CH_4 + N_2) diagram of the volatile phase determined by Raman spectroscopy in representative fluid inclusions of each type of quartz present in mineralized and barren structures in the França area.

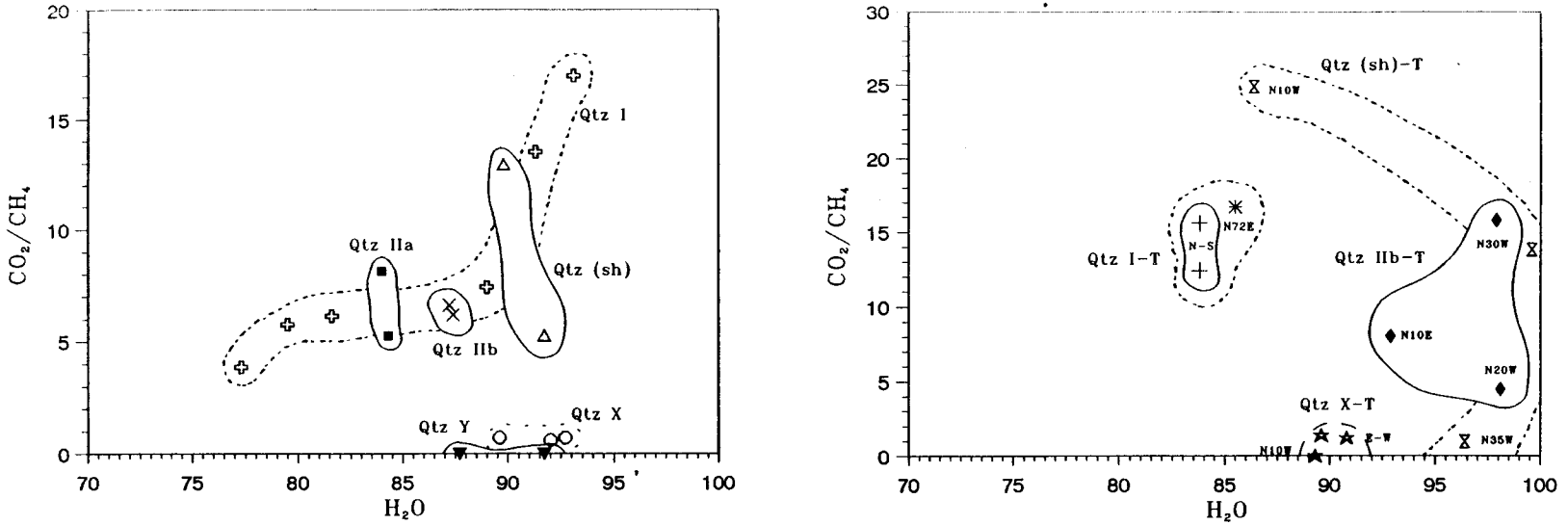

Fig IV - 54 :CO_2/CH_4 versus H_2O plots for isolated inclusions and trails of inclusions in different types of quartz present in mineralized and barren structures in the França area.

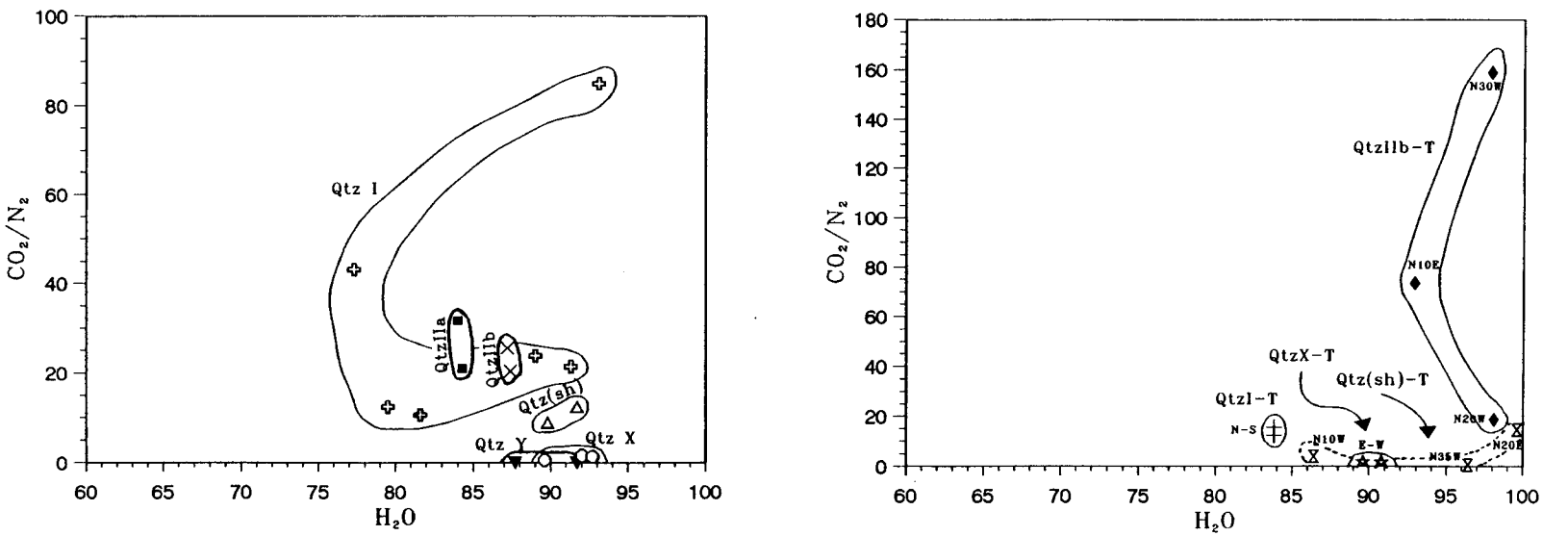

Fig IV - 55 : CO_2/N_2 versus H_2O plots for isolated inclusions and trails of inclusions in different types of quartz present in mineralized and barren structures in the França area.

prevailing characteristic of inclusions along the secondary trails in quartz types of the mineralized structures.

Similar conclusions can be inferred by plotting the H2O content versus CO2/CH4 and CO2/N2 ratios (Fig. IV- 54 and 55). In CO2/CH4 – H2O plots one could observe the distinct compositional fields defined by Lw–c and Lw–m/n isolated inclusions or clusters of inclusions; trails of inclusions in quartz I, clearly different from the remaining trails of inclusions, define a graphical field close to the obtained for isolated inclusions in quartz I and IIa. The CO2/N2 versus H2O plots show that isolated inclusions in deformed quartz of the NW–SE shears have a slightly different CO2/N2 ratio, which enable the definition of an isolate compositional field on that diagram; for secondary trails of inclusions, the main feature is given by the variable CO2/N2 ratio in quartz IIb.

Fluid salinity is also quite distinct for inclusions related to mineralized and barren quartz types. Thus, for inclusions in quartz I and in deformed quartz along regional shears, the calculated salinity ranges from 3 to 5 wt% NaCl, while 5–8 wt% NaCl is the typical variation in inclusions of quartz IIa and IIb; salinity values in inclusions along trails in these quartz types are scatered in the range 0.1–2 wt% NaCl. For the barren quartz lenses of the Vilariça fault, the obtained salinity ranges from 0.3 to 1.5 wt% NaCl.

Summary

From the above considerations one may conclude that three main types of fluids are present in the examined quartz generations of the França sector (Fig. IV-56 to 58):

(1) -- aquo–carbonic fluids (inclusions of types Lw–c and Lw–(c)): observed in inclusions of quartz generations I, IIa, IIb, IIc and of deformed quartz that filled NW–SE regional shears. According to microthermometric and Raman data, it is possible to put in evidence:

(a) aquo–carbonic fluids enriched in CO2 and CH4 (X(CO2) and X(CH4) scaterred in the range 13–17 mole % and 2–4 mole %, respectively), representing probably an earlier stage of fluid circulation along intergranular and transgranular cracks in quartz I and IIa at minimal temperatures of 280 to 310°C. The salinity of these metamorphic fluids is of the order of 3–5 wt% NaCl, and their density 0.7 g/cm3 on average.

(b) aquo–carbonic fluids typically with X(CO2) ranging from 8 to 11 mole % and X(CH4) of the order of 1–1.5 mole %, characteristic of the prevailing quartz generation in ore samples (IIb) and also present in the quartz fillings of the regional shears. This kind of fluid is also represented by secondary inclusions along the trails N20W, subvertical (in quartz IIb), N20–30W,65–75E and N70–80E,50–60NW (in quartz I), and N10–15W,70–80W and N30–35W,80–85W (in deformed quartz of the regional shears). That represents probably the main hydrothermal fluid influx at temperatures ranging from 250–300°C, although with a mode around 260–270°C. Fluid salinity ranges typically from 4 to 7 wt% NaCl, and its density is scaterred in the range 0.6–0.8 g/cm3.

(c) aquo–carbonic fluids where the carbonic phase is inferred by clathrate melting only (X(CO2) and X(CH4) are scaterred in the range 0.2–1.5 mole % and 0.1–0.9 mole %, respectively). This type of fluid, testify the circulation of metamorphic solutions at 150–200°C (with a mode around 180–200°C) and is represented by primary inclusions in quartz IIc and in late quartz fillings of NW–SE shears, as well as by the secondary trails N30°W,70°S and N10–15E, 70–80°NW (in quartz IIb), and N40W,subvertical and N20°E,70–80°E (in deformed quartz of the regional shears). Fluid salinity is quite low (0.3–1.7 wt% NaCl) and its density of the order of 0.50 g/cm3.

(2) - aquo–methan/nitrogen fluids (inclusions of Lw–m(c) type) characteristic of the barren quartz lenses associated to some secondary branches of the Vilariça strike–slip fault, with salinities ranging from 0.3 to 1.5 wt% NaCl and densities scaterred in the range 0.45–0.75 g/cm3. The calculated fO2 (10^{-45} , 10^{-37} see below) is compatible with the circulation of metamorphic fluids CH4 and N2 enriched (X(CH4) and X(N2) in the range 3–11 mole% and

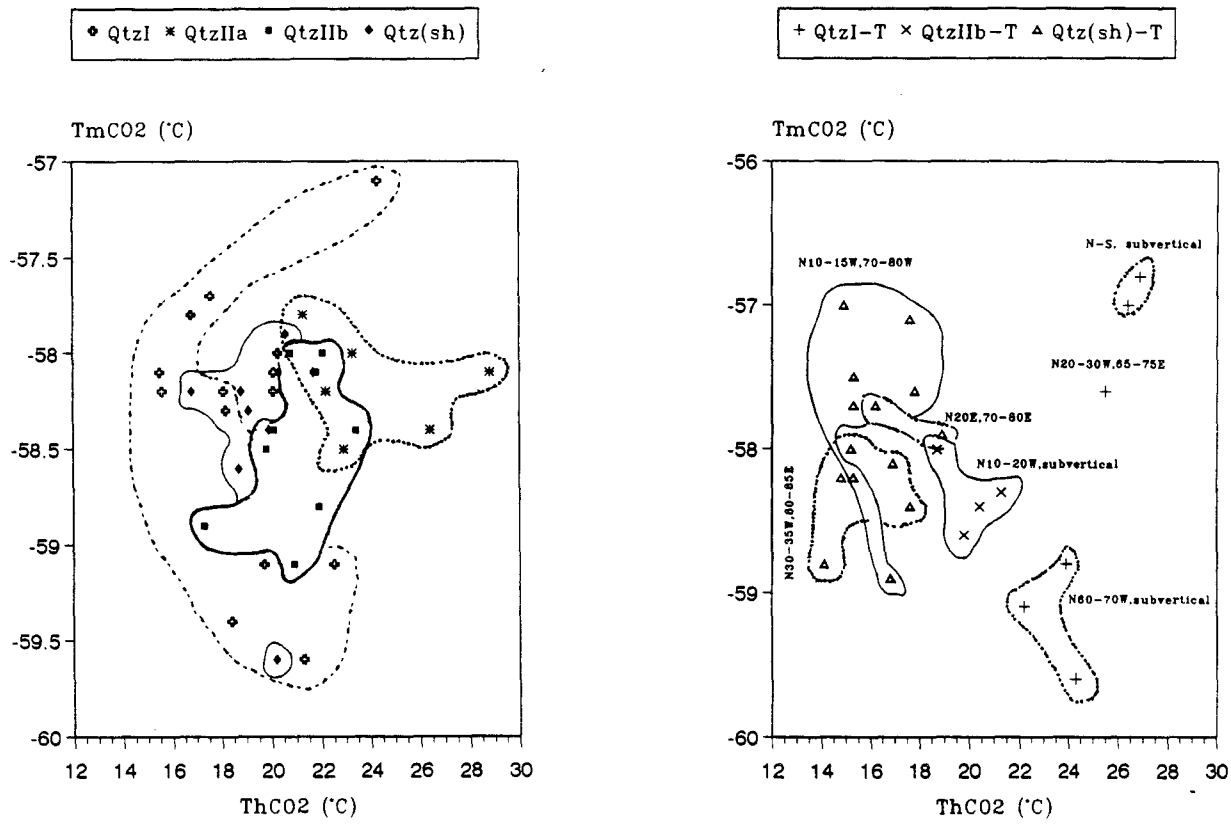

Fig IV - 56 :$TmCO_2$ versus $ThCO_2$ plots for isolated Lw-c inclusions and trails of Lw-c inclusions in different types of quartz present in mineralized and barren structures in the França area.

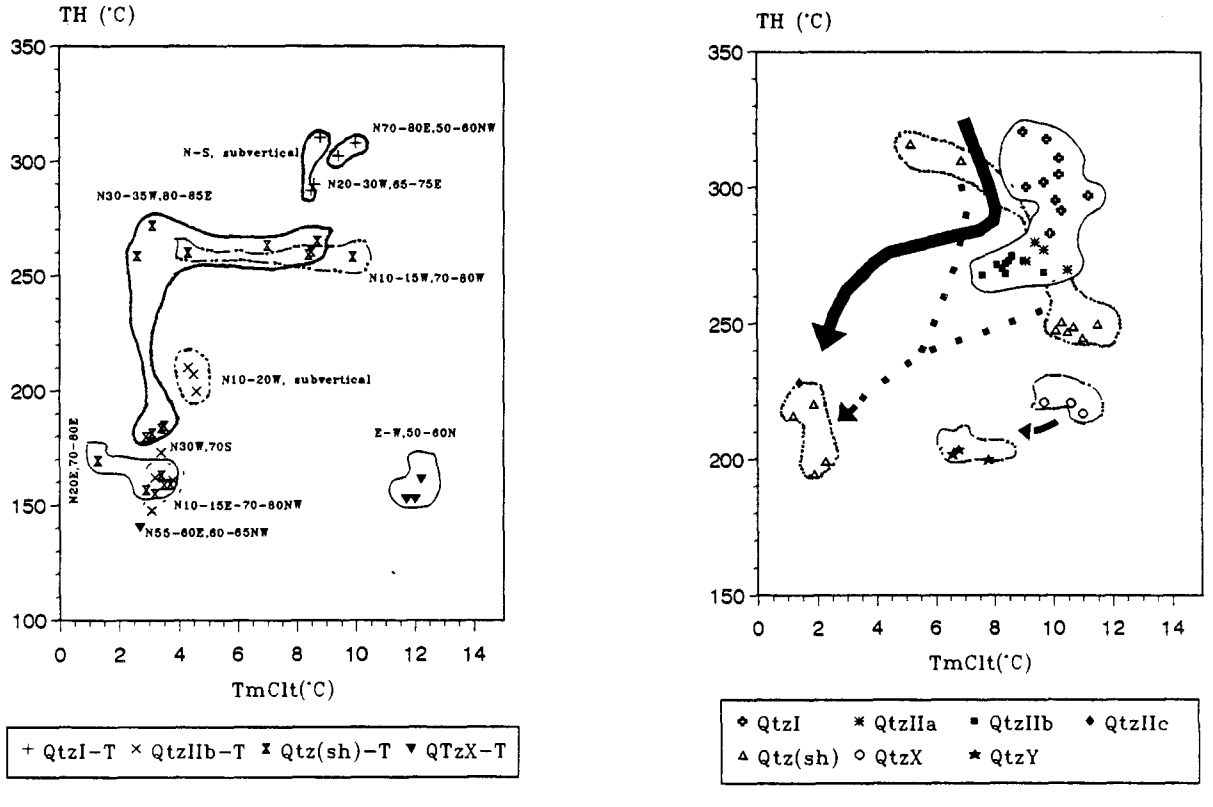

Fig IV - 57 : TH versus TmCl plots for isolated inclusions and trails of inclusions in each type of quartz present in mineralized and barren structures in the França area.

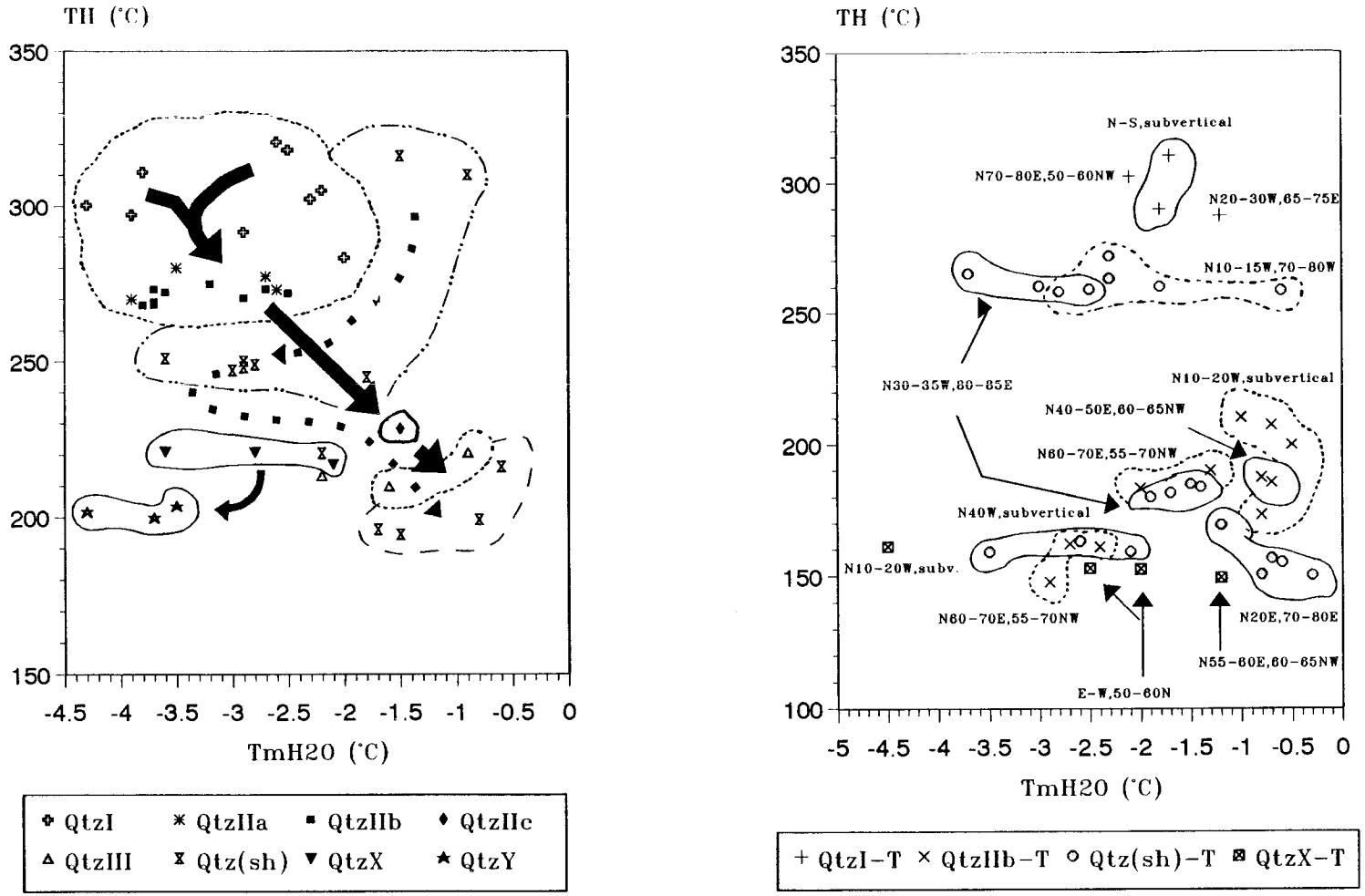

Fig IV - 58 : TH versus TmH_2O plots for isolated inclusions and trails of inclusions in each type of quartz present in mineralized and barren structures in the França area.

1.5–8 mole%, respectively), in equilibrium with carbonaceous rich rocks, at lower temperatures (< 220°C). The source of this type of fluid is certainly local, and its circulation circumscribed to highly fractured domains of the fault zone within the Upper Ordovician units.

(3) – aqueous fluids (inclusions of Lw type): observed in quartz III, and secondary trails N40–50°E,60–65°NW and N60–70°E,55–70N°W (in quartz IIb), and N60–70°W, subvertical (in quartz I). These late hydrothermal solutions are characterized by lower Th (150–165°C) and salinities ranging from 1 to 4 wt% NaCl.

2-VILA POUCA (PORTO UNIV)

In attempting to characterize the fluids from mineralized and barren structures, as well as those from the host metasediments, microthermometic and Raman spectroscopy fluid inclusions studies in quartz from the different samples were carried out (Table IV-6). Nomenclature, microthermometric and Raman data of the fluid inclusions from VPA area are given in table IV-7.

Two major types of fluids have been recognized in barren and mineralized structures, respectively the **aquo-carbonic** (H2O-CO2-CH4-N2-(H2S)) and the **aqueous** (H2O-NaCl).

Aquo-carbonic fluids

Combining data of melting temperatures of solid CO2 (TmCO2), and of clathrate (TmCl), with Raman analyses, two groups of fluids could thus be distinguished: *CH4-rich* and *CO2-rich* fluids. Based on water content, on the presence of C-H-O-(N-S) volatile species detected by microthermometric and /or Raman analyses, and the mode of homogenization of CO2 (L, C, V), the latter fluids can be subdivided altogether into eight sub-groups (Table IV-7).

CH4-rich fluids

This type of fluids has been found as primary inclusions in syn-metamorphic quartz (Q II) from black-shales (barren structures) and in quartz (Q II TM, Q III TM) from Três-Minas, and as secondary inclusions (trails) in quartz (QI TM) from silicified mineralized metasediments.

CO2-rich fluids

This type of fluids occurs in segregation metamorphic quartz (Q I) as inclusions clusters, and as secondary inclusions (trails) in clear quartz (Q III).

In mineralized veins these fluids have been observed in milky quartz (Q IV) as inclusions trails and/or clusters, and as secondary inclusions (trails) in hyaline quartz (Q V). They are mostly observed as secondary fluid inclusions (trails) in milky quartz (Q I TM) and hyaline quartz (Q IV TM) in mineralized structures from Três-Minas.

Aqueous fluids

Lw fluid type has been observed in all samples, being essentially the last fluids from mineralized structures and the only one in posttectonic barren quartz veins.

Monophase or two-phase Lw (H2O-NaCl) rich inclusions occur mostly as secondary inclusions (trails) in barren syn-metamorphic and mineralized structures healing microcracks.

A - FLUID INCLUSION STUDIES

A summary of microthermometric and Raman data from the different samples from all the studied examples are present in table IV - 7.

a-Barren structures

1-Segregation quartz in schists

The primary fluid inclusions of this type of quartz are essentially characterized by CO2-rich fluids in Lc-w and Vc-w types.

Comparing the Vc-w and Lc-w inclutions, the water phase is more dominant in the first type (Flw 50-80%) than in the second (Flw 20-30%), being the Lc-w more abundant in the clear quartz (QIA). There is a significant difference between the TmCO2 of Lc-w (-58,5° to -

Type of quartz / Type of fluids	Barren syn-metamorphic structures			Mineralized structures						Barren post-tectonic veins
				Silicified metasediments				Quartz veins		
	Q I	Q IA	Q II	Q I TM	Q II TM	Q III TM	Q IV TM	Q III	Q I V	Q V
Lc								+ (trails)		
Lc - w		+ (trails)						+ (clusters/trails)	+ (clusters)	
Vc - w	+ (clusters)			+ (trails)				+ (clusters/trails)		
Vm - w						+				
Vm - w - S			+							
Lw - c		+					+		+	
Lw - m			+	+ (trails)	+	+				
Lw - m - S				+ (trails)						
Lw			+ (clusters/trails)				+ (trails)	+ (trails)	+ (trails)	+ (clusters)

Table IV - 6: Quartz and fluid inclusions types from VPA

		Quartz type			MICROTHERMOMETRY								VOLATILE PHASE COMPOSITION			
				Incl. type	Occurrence	Flw	ThCH4	TmCO2	Tml	TmCl	ThCO2	TH	CO2	CH4	N2	H2S
BARREN SYN-METAMORPHIC STRUCTURES	SEGREGATION QUARTZ IN SCHISTS	Milky deformed	Q I	Vc-w	clusters	0,5/0,7		-59,9/-59,4	-11,6/-9,3	7,1/9,6	16,3/18,0 V	309/330 L	77,9/84,9	10,3/14,0	4,8/8,1	
		Clear	Q I A	Vc-w	isolated	0,7/0,8		-59,6/-58,4	-9,6/-5,5	4,2/8,5	7,0/15,0 V	265/280 L	77,9/97,8	2,2/11,1	0/12,5	0/0,4
		subeuhedral		Lw-c	isolated	0,6			-4,0	8						
		"		Lc-w	trails	0,2/0,3		-58,5/-57,7		6,5/8,5	19,0/22,1 L	325/340 L	88,1	9,6	2,3	
	VEINLETS IN BLACK-SHALES	Recrystalized	Q II	Vm-w-S*	isolated		-102/-84,9 V		-1,7/-1,2	10,3/14,5		290/297 L		89,3/90,7	8,7/10,0	0,5/0,7
		poligonal		Lw-m	isolated				-2,9/-0,9	7,2/14,5		317/330 L				
		"		Lw	clusters				-1,2/-1,0							
MINERALIZED STRUCTURES	QUARTZ VEINS	VALE DE CAMPO Milky deformed	Q III	Lc	trails			-57,5/-57,1			19,1/21,3 L					
		"		Lw	trails	0,8/0,9			-3,4/-1,2			130/280 L				
		Hyaline	Q IV	Lc-w	clusters	0,2/0,4		-59,5/-57,6		7,3/9,0	19,0/23,3 L	300/360 C	87,5/90,9	5,5/7,1	3,1/5,2	0,3/0,4
		"		Lc-w	clusters	0,5/0,7		-57,4/-57,0		6,0/8,9	22,6/27,0 L,C	280/360 L,C	97,3/98,2	1,8/2,7		
		"		Lw	trails	0,8/0,9			-3,4/-1,2			130/280 L				
		VALE D'ÉGUA Milky deformed	Q III	Vc-w	clusters	0,4/0,8		-59,0/-57,0	-7,2/-4,6	8,6/9,9	16,8/24,2 V,C	280/300 L	77,5/83,4	13,3/22,0	0,1/3,3	0/0,5
		"		Lc-w	clusters	0,4/0,5		-58,2/-57,0		8,3/8,6	18,0/18,3 L	276/340 L	98,4	1,6		
		"		Lc-w	trails	0,3/0,5		-59,0/-57,2	-6,1/-4,4	6,4/9,8	20,9/24,8 L	300/320 L	84,0/93,0	5,7/11,7	1,3/4,3	0/0,2
		"		Lc-w(?)	trails	0/0,1		-57,4/-57,0			10,8/23,8 L					
		VELHAQUINHAS Milky deformed	Q III	Lc-w	clusters	0,4/0,5		-61,0/-58,0	-3,0/-1,2	7,2/11,8	8,2/18,8 L	290/360 L	80,2/80,3	15,7/16,7	2,9/3,9	0,1/0,2
		"		Lc-w(?)	clusters	0,1					10,0/12,0 L	300/350 L				
		"		Vc-w	clusters	0,4/0,5		-60,0/-58,0	-3,0/-1,0	6,5/12,2	7,0/21,0 V	280/360 L	78,2/83,5	14,3/17,1	2,1/4,7	0/0,2
		"		Lw	trails	0,7/0,8			-3,0/-0,8			220/280 L				
	SILICIFIED METASEDIMENTS	TRÊS MINAS Milky deformed	Q I TM	Lw-m-S*	trails	0,2/0,6			-2,3/-2,1	11,0/12,0		260 L	21,7/27,8	55,6/78,3	0/16,0	0/0,6
		"		Lw-m	trails	0,5/0,7			-6,0/-1,8	11,5/14,1		285/357 L	30,3	69,7		
		"		Vc-w	In trails	0,2/0,7		-65,7/-61,8	-6,4/-3,1	10,7/14,3	-21,2/-11,8 V	302/328 L	47,8/79,8	20,2/43,0	0/9,1	
		Recrystallized	Q II TM	Lw-m	Isolated	0,6/0,7			-3,1/-3,0	12,0/12,5		351 L	28,0	70,4	0,7	0,8
		Mycrocrystalline	Q III TM	Vm-w	Isolated or in clusters	0,7/0,8	-95,5/-93,0 V		-2,0/-0,9	7,5/8,0			0/21,9	63,6/89,5	3,9/14,5	1,3/1,4
		Hyaline	Q IV TM	Lw-c	Isolated or in trails	0,7/0,8			-3,8/-3,6	6,5/8,0	260/284 L		89,6	7,1	3,3	
BARREN POST-TECTONIC VEINS		Milky	Q V	Lw	clusters	0,7/0,8			-3,1/-0,8			210/275 L				

Table IV - 7 : Fluid inclusion data from Vila Pouca de Aguiar area.

57,7° C) and of Vc-w inclusions (-59,9° to -58,4°C) indicating the significant addition of other volatile compounds, such as CH4 and N2 (Fig. IV-59A). ThCO2 of Lc-w inclusions occurs between 19,0° and 22,1° C and, within a higher range (7,0°-18,0°C) in Vc-w type (Fig. IV-59B). Tm ice is difficult to measure both in Lw-c and Lc-w inclusions; in Vc-w Tm ice is observed between -11,6° and -5,5°C (Fig. IV-59C). Tm cl range from 6,5 and 8,5 in Lc-w and Lw-c inclusions and from 4,2° to 9,6°C in Vc-w (Fig. IV-59D). Global Th occurs always into the liquid phase (265 to 340 °C) (Fig. IV-59E).

2-Veinlets in black-shales

The primary fluid inclusions in the recrystallized quartz (QII), the more representative in the veinlets, are essentially characterized by CH4-rich fluids in Vm-w-S and Lw-m types. Lw fluids are present in secondary inclusions.

The only observed volatile Th is the ThCH4 between -102° to -84,9°C in vapour from Vm-w-S inclusion type (Fig. IV-60A). Tm ice is similar in all inclusion types and range between -2,9 to -0,9 C (Fig. IV-60B). Tm cl range from 7,2° to 14,5°C in Lw-m and Vm-w-S inclusions (Fig. IV-60C). Global Th occurs always into the liquid phase between 290°and 330°C (Fig. IV-60D).

B-Mineralized structures

1-Quartz veins

For characterizing the fluids of the mineralized veins we have studied three occurrences: Vale de Campo, Vale de Égua and Velhaquinhas. The microthermometric and Raman data are presentend on table VIII. The fluids present on the different examples are similar. In the early milky quartz (Q III), the primary inclusions are from Vc-w and Lc-w types; in the hyaline quartz (QIV), Lc-w inclusions are also present as primary but with different characteristics from the precedent ones. Lc inclusions are present in trails in QIII. Lw inclusions are always observed as secondary in both quartz types.

In Vc-w inclusions (from QIII) TmCO2 ranges between -60,0° and -57,0°C. Lc-w presents a more significant difference between the TmCO2 when primary in QIII (-61,0° to -57,0°C) from the ones that are primary in QIV (-59,5° to -57,0°C); this fact indicates more significant content of other volatile compounds such as CH4 and N2 in early quartz (QIII) (Fig IV-61A). Th CO2 presents a wide range in all fluid inclusion types (7,0° to 27,0°C) (Fig IV-61B). Tm ice occurs essentialy between -3,4° and -1,0°C, suggesting a low salinity (Fig. IV-61C). Tm cl range from 6,0° and 12,0°C in Vc-w and Lc-w (Fig. IV-61D). Th occurs mainly into the liquid phase between 240° and 360°C (Fig. IV-61E).

2-Silicified metasediments

The four generations of quartz described for Três-Minas silicified mineralized metasediments exhibit a great variety of fluids namely CH4-rich fluids (Vm-w, Lw-m,Lw-m-S) and CO2-rich fluids (Vc-w, Lw-c).

In the early milky quartz (Q I TM) the different type of fluids (Vc-w, Lw-m, Lw-m-S) are always present as secondary inclusions in trails. Both the recrystallized quartz (QII TM) and the micocrystalline quartz (QIII TM) are characterized by CH4-rich fluids present in primary inclusions; however, the Vm-w type is only present in QIII TM. The hyaline quartz (QIV TM) is characterized by CO2-rich fluids, being Lw-c inclusions present as primary. Lw inclusions are always observed as secondary in all quartz types.

In Vm-w inclusions, ThCH4 ranges between -102° and -84,9°C (V) (Fig.IV-62A). Vc-w present a TmCO2 between -65,7° and -61,8°C (Fig. IV-62B) and CO2-homogenization ranging from -21,1° to -11,8°C (V) (Fig. IV-62C). Tm ice occurs essentialy between -6,4° and -0,9°C, suggesting a low salinity (Fig. IV-62D). Tm cl ranges from 6,5° to 8,0°C in Lw-c inclusions and from 10,7° to 14,3°C in the other types (Fig. IV-62E). Th occurs mainly into the liquid phase between 260°and 357°C (Fig. IV-62F); Th is difficult to reach in Lw-m-S inclusions due to decrepitation.

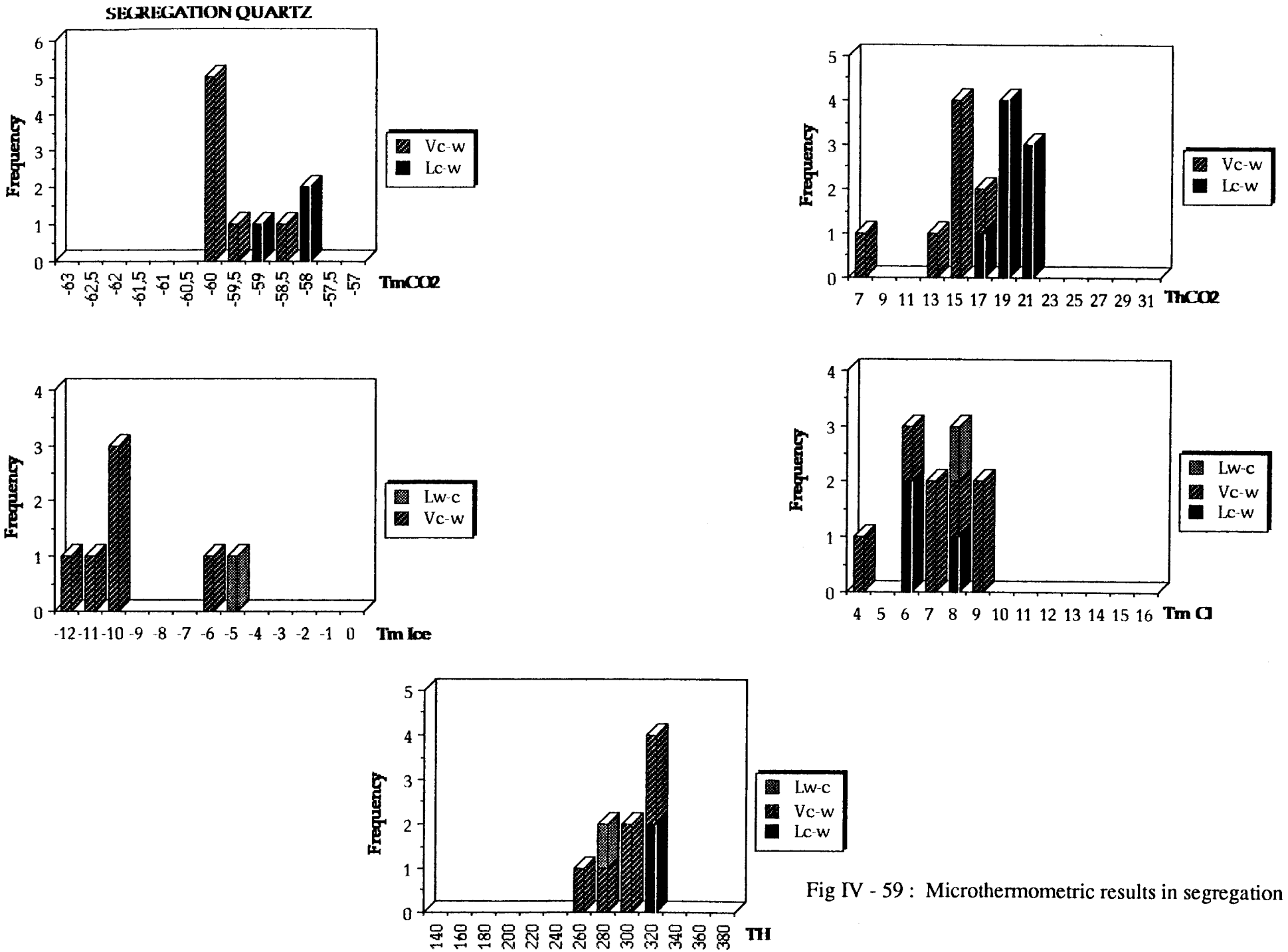

Fig IV - 59 : Microthermometric results in segregation quartz

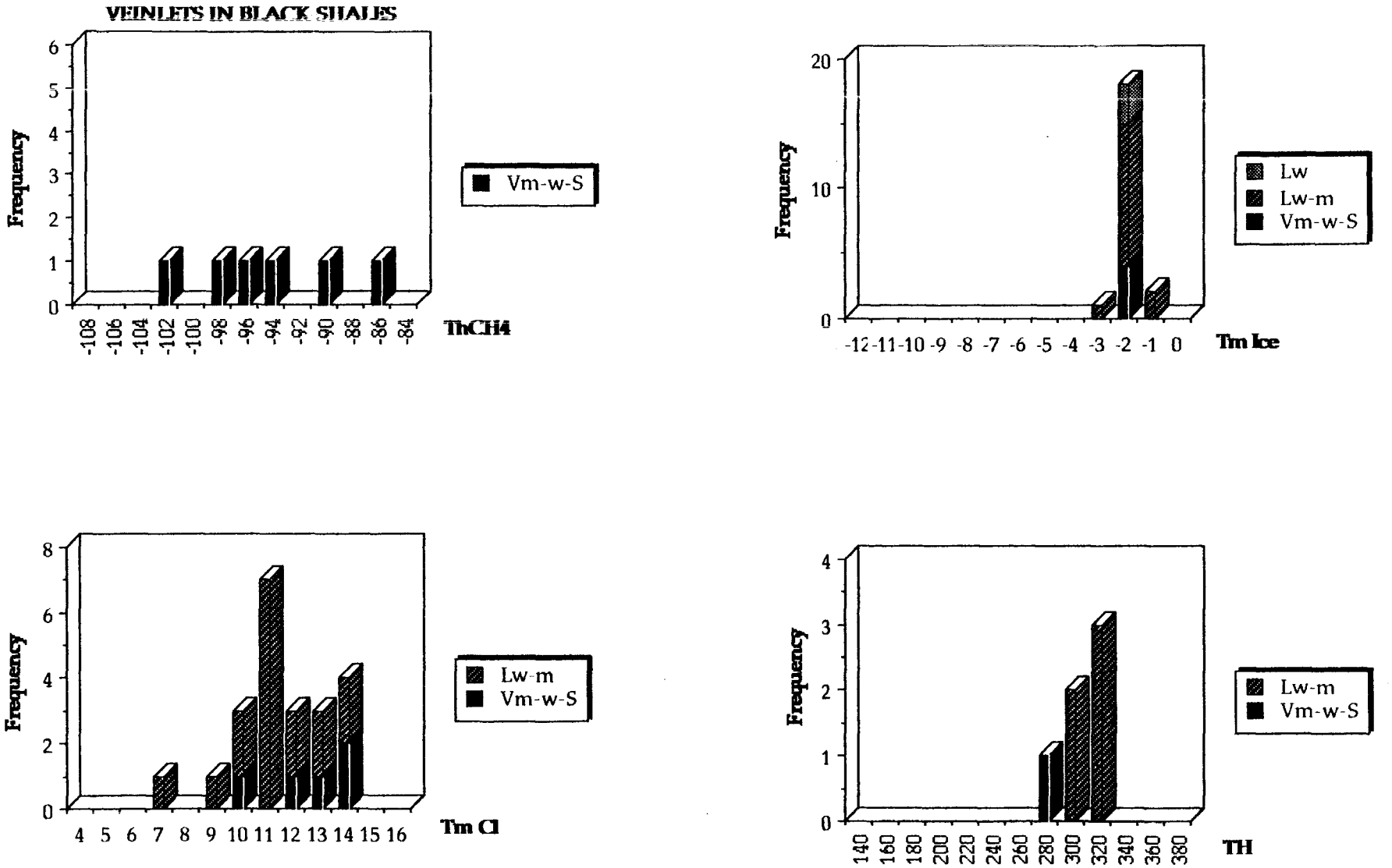

Fig IV - 60 : Microthermometric results in quartz from black-shales

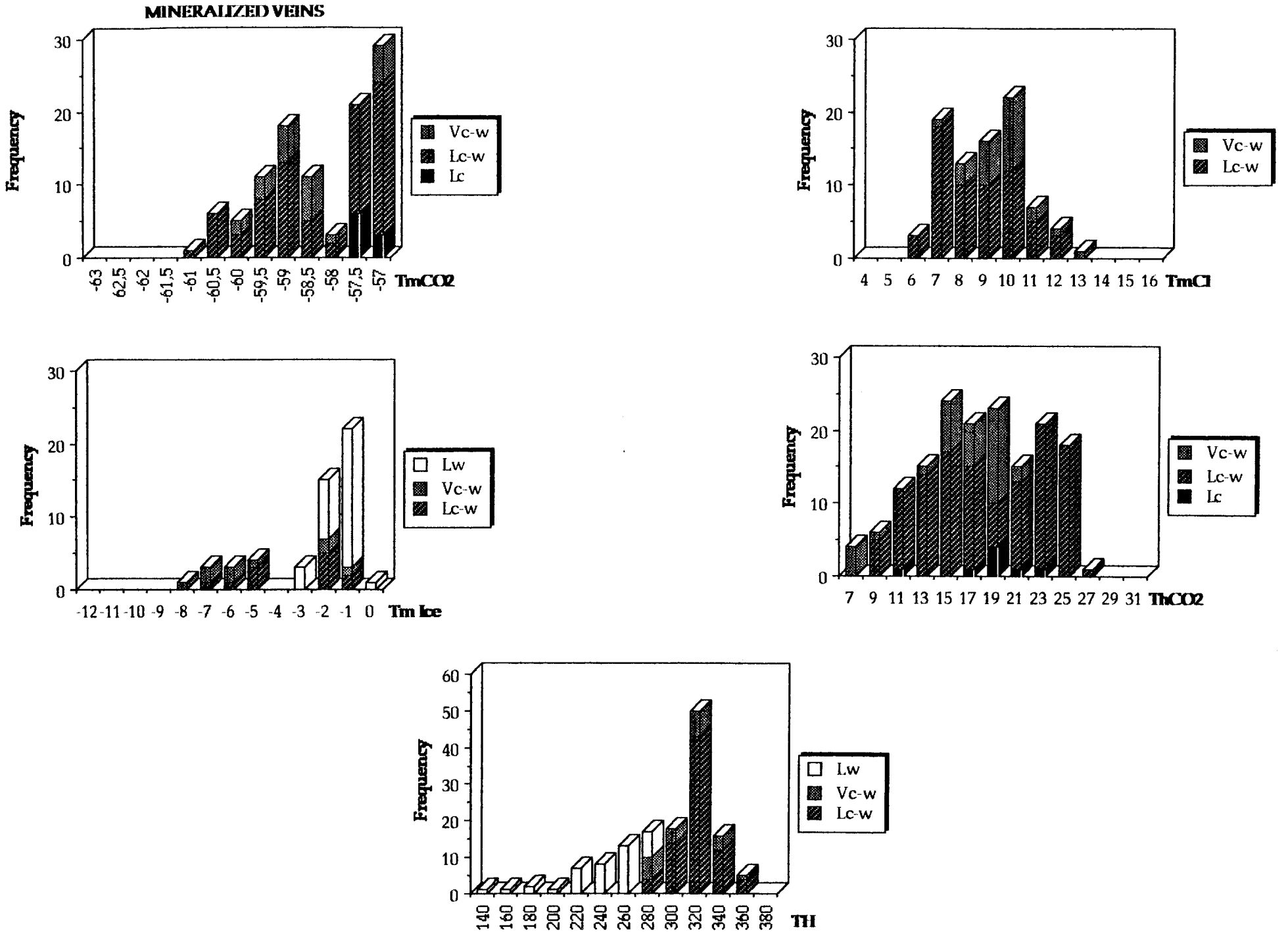

Fig IV - 61 : Microthermometric results in quartz from mineralized veins

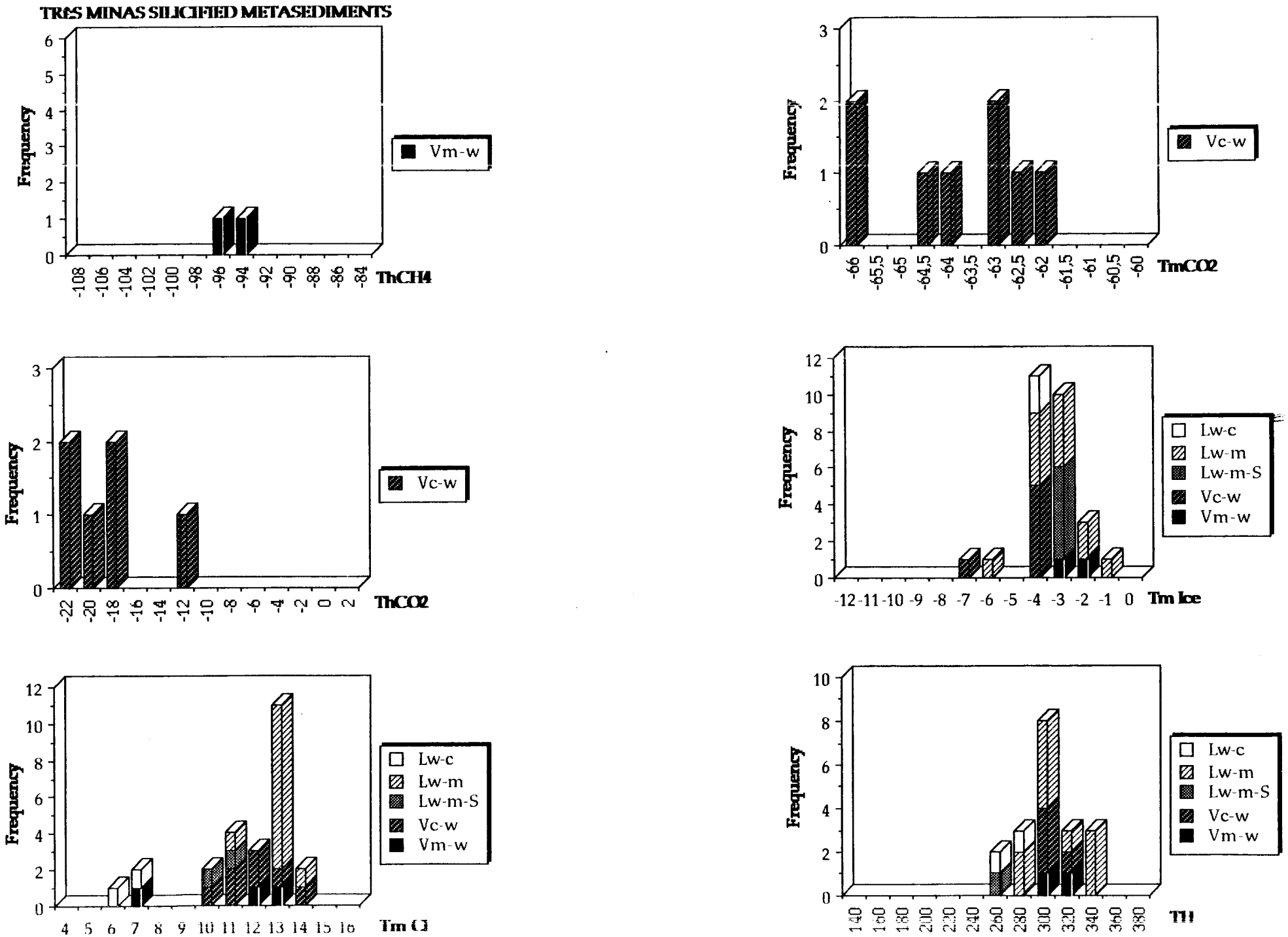

Fig IV - 62: Microthermometric results in quartz from Três-Minas silicified metasediments

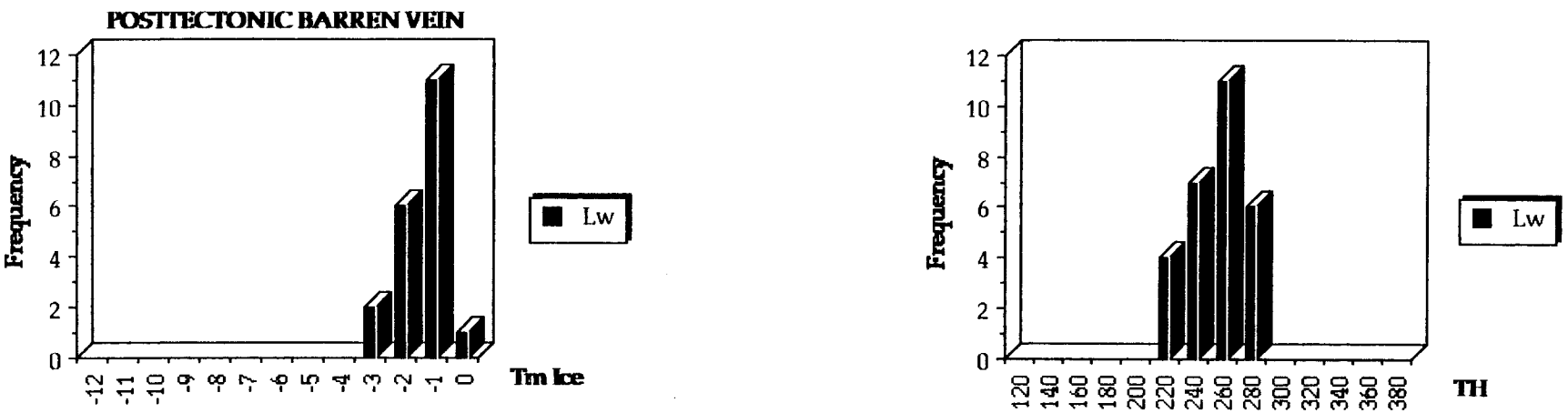

Fig IV - 63: Microthermometric results in quartz from post-tectonic barren veins

C-Barren post-tectonic veins

The quartz (QV) from these veins is characterized by the exclusivity of the Lw fluids. Tm of ice ranging from -3,1° to -0,8°C (Fig IV-63A), suggests typical aqueous fluids. Th are in the range 210-275°C (Fig. IV-63B).

B - GEOCHEMICAL EVOLUTION

The different groups of C-H-O-N-(S) fluids, distinguished on the basis of the microthermometric data and Raman analysis (Table IV-9, annexe) on the different types of quartz, exhibit significant compositional variations, namely those from the volatile phase, which are essentialy characterized by different CO2 contents and CH4/CO2 ratios (Fig. IV-64).The N2 contents are generally low (0 to 15%) and H2S is absent.There are also relatively important differences in the H2O content and bulk densities which increases to the latter fluids (Fig. IV-65). The fluids have always relatively low salinities and the low content in NaCl has a very little variation.

Observing the compositional variation of the volatile phase (Fig. IV-64) we can distinguish: (i) the primary fluids in the segregation quartz are dominated by CO2 (77,9 to 97,8%), the maximum of CH4 is 14%; (ii) in the black-shales on the other hand, the fluids are essentially CH4 -rich (~90%) and CO2 is absent; (iii) on the mineralized quartz veins the fluids do not exhibit significant compositional variations, CO2 is dominant; however the earlier fluids are richer in CH4 than the later ones (Fig. IV-66); (iv) Três-Minas exhibits a very peculiar evolution,with an association of earlier fluids, similar to that present in metamorphic veinlets syn-D3, with latter fluids similar to that present in mineralized veins (Fig.IV-67). The earlier are rich in CH4 (69 to 89%), the later ones rich in CO2 (~89%) or dominantly aqueous with low salinities.

Três-Minas can be interpreted as an example of a long and continuous fluid evolution, where CH4-rich fluids have an important role, which culminates with the gold deposition associated to the later aqueous fluids.

It must be emphasized that gold mineralization only occurs when different fluids are expressed, but the essential of deposition is contemporaneous to the later episodes characterized by the transition from aquo-carbonic to aqueous fluids.

In quartz from the latter veins (barren postectonic veins) no volatile carbonic component was detected. Contrarily to the mineralized structures, they only exhibit aqueous fluids with very low salinities, attesting a very short fluid evolution, on the strong overprint of late fluids (quartz recrystallization during late retrograde metamorphism events).

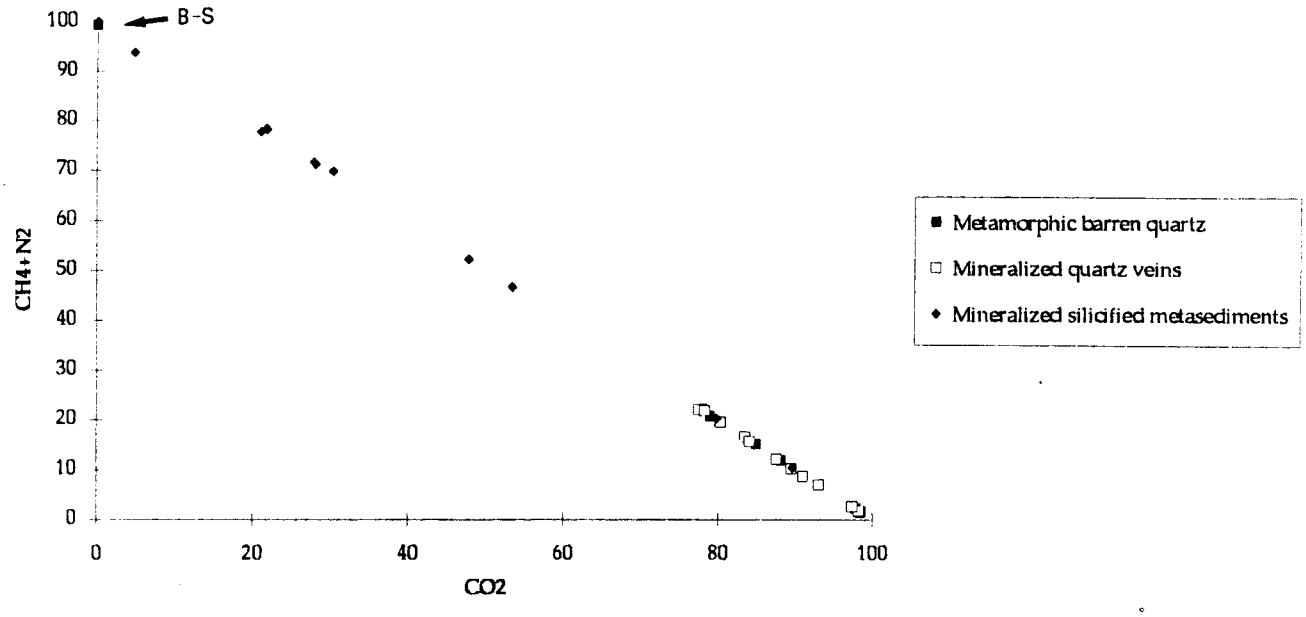

Fig IV - 64 : CH4+N2/CO2 diagram for quartz from VPA area

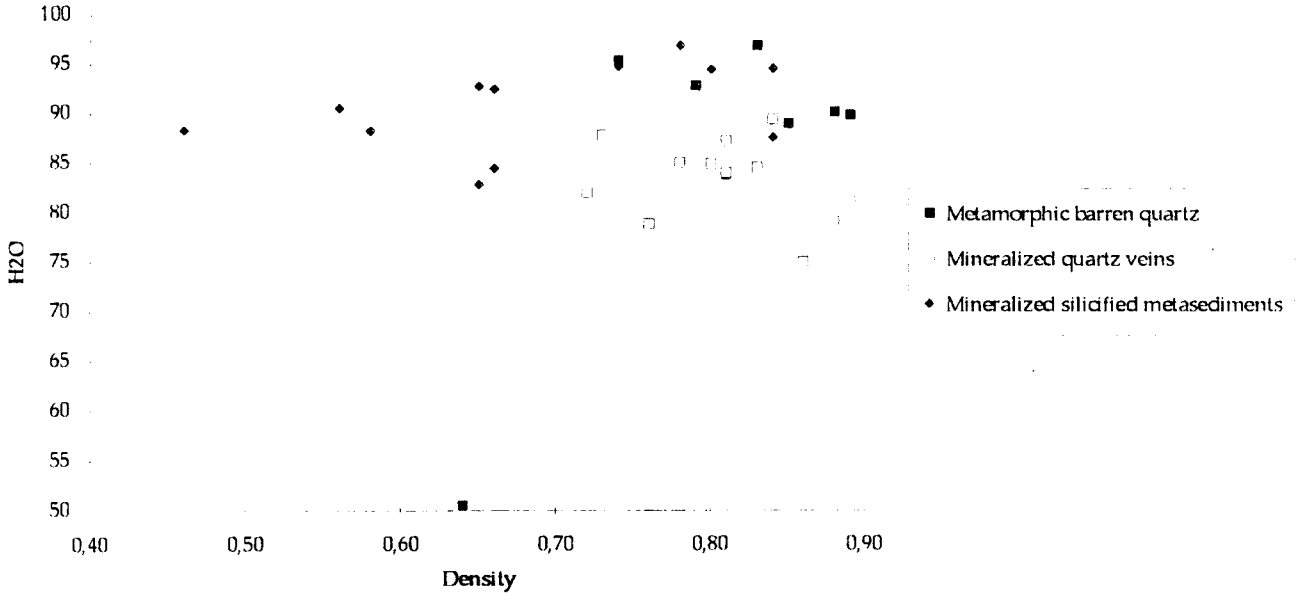

Fig IV - 65 : H2O/d diagram for quartz from VPA area

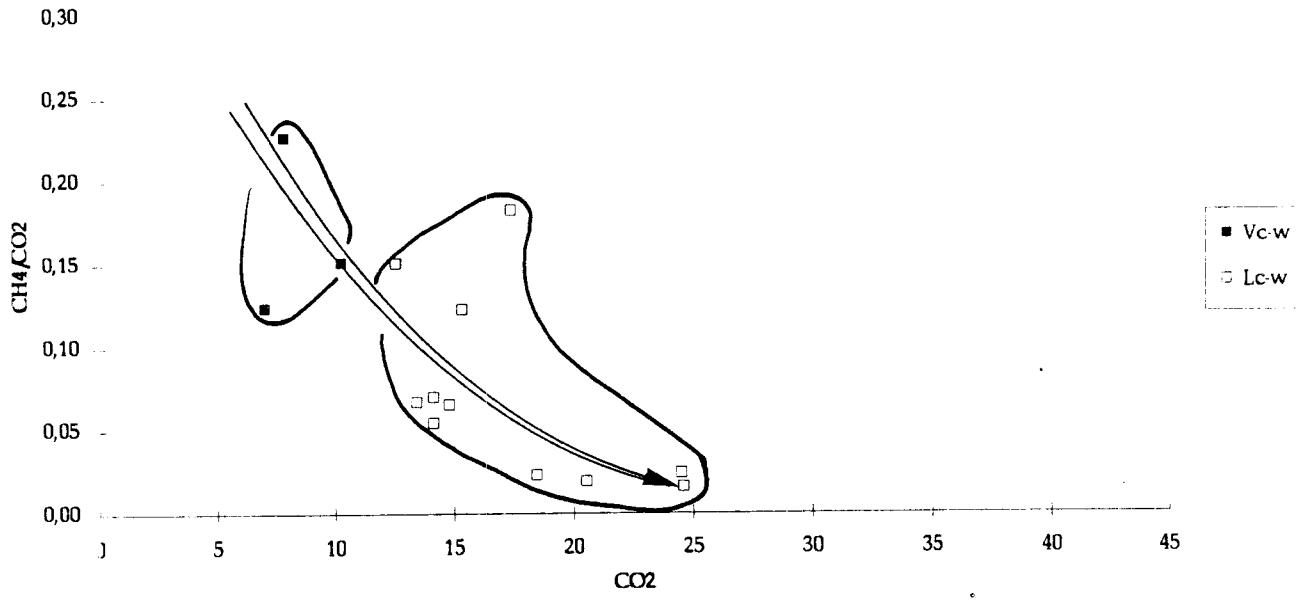

Fig IV - 66 : CH4/CO2- CO2 diagram for quartz from mineralized veins

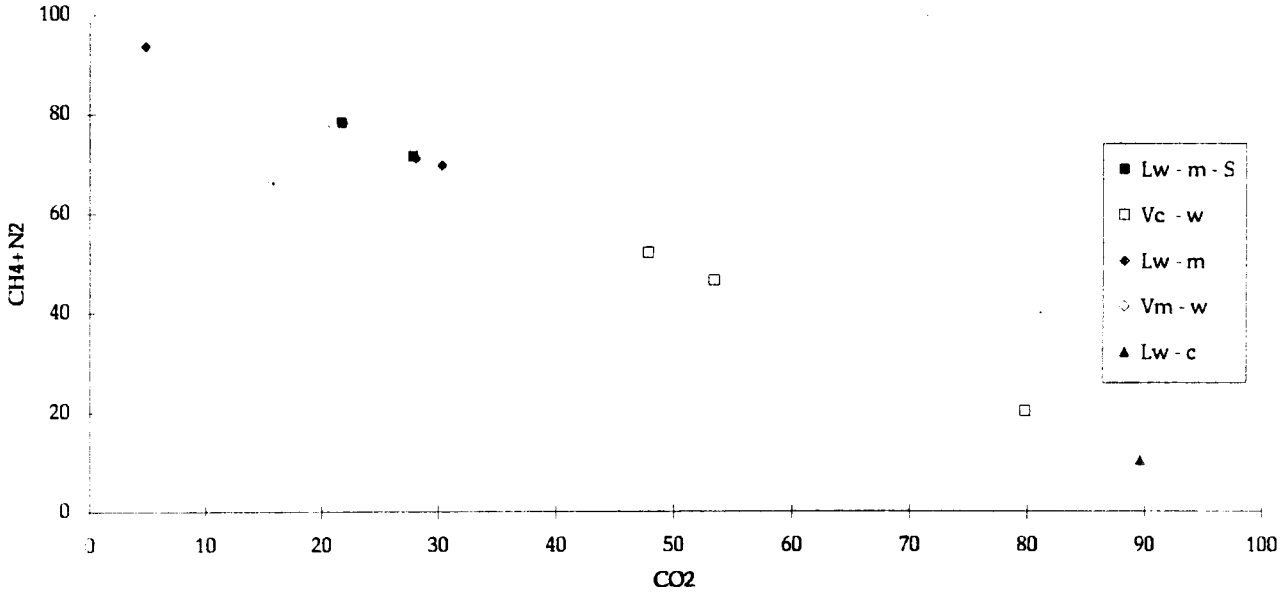

Fig IV - 67 : CH4+N2/CO2 diagram for quartz from Três-Minas area

C – ALTERATION MINERAL ASSEMBLAGES AND CHLORITE/PHENGITE CRYSTAL CHEMISTRY

The hydrothermal alteration exhibited by the wall–rocks of the mineralized quartz veins comprises the deposition of quartz, K–micas and chlorites, locally associated with sulphides (and sulphosalts) and carbonates depending of the deposit.

K- micas and chlorite have analysed by electron microprobe, since they may provide interesting geothermometric constraints for the P-T reconstruction.

1-PHYLLOSILICATE CRYSTAL-CHEMISTRY

Phyllosilicate compositions were determined using

- a 3–channel JEOL JCXA 733 electron microprobe routinely operated with an acceleration voltage of 15 kV, an excitation current of 25 nA, and counting times of 20 seconds at Lisboa
- a CAMEBAX electron microprobe (Nancy Univ.)using the following analytical conditions : acceleration voltage : 15kV; counting time : 6s ; excitation current 6 nA.

Before each analytical session a standardization of the microprobe was achieved and checked by analyzing a set of suitable standards. The typical analytical error is 2% of the amount reported (for major elements).

Structural formulae have been calculated on 11 and 14 oxygen basis (half formulae) for K-micas and chlorite respectively. The main crystal-chemical features and subsitutions have been described in binary or ternary plots. All iron was assumed to be Fe2+ and tetrahedral sites were filled by Si and Al with the remaining Al allocated to octahedral sites.

2- K-MICAS

Dioctahedral K- mica series may be described by three end members :

- Muscovite K (Si3Al) Al2O10 (OH)2
- Celadonite K (Si4) (Al R2+) O10 (OH)2
- Paragonite Na (Si3Al) Al2O10 (OH)2

Between these three poles, different substitutions controlling mass and electric balance are possible. Solid solutions such as the muscovite - celadonite (phengite series) and muscovite - paragonite series are the main ones.

Structural formula for di-octaedral K- mica can be written :

$(Na, K)\ (Si_{3+x}\ Al_{1-x})\ (Al)_{2-x-y}\ R^{2+}{}_{x+y}\ Ti_y\ O_{10}\ (OH)_2$

Phengitic substitution

A part of the Al iv is replaced by Si in the muscovite structure. Thus, the subsequent electrical charge excess is compensated by the entrance of divalent cations in the octaedral site replacing Al.

$$(Si_3\ Al)_{iv} \qquad (Al_2)_{vi} \quad \text{----------} > \quad (Si_{3-x}\ Al_{1-x})_{iv} \qquad (Al_{2-x}\ R^{2+}{}_x)_{vi}$$

The Si-3+Ti versus R2+ diagram illustrate this substitution (Fig IV-68a.) : the upper triangle correspond to micas having an excess of tetrahedral charge compensated by a deficit in the interlayer charge (illite-smectite series). The lower triangle does not correspond to any possible compositions. If the sum $Mg^{2+} + \Sigma$ Fe/Si values plots within this triangle, it indicated that the Fe is in part trivalent.

Na-K substitution

The interlayer site is occupied by K or Na (interlayer charge CI = Σ Na+ K + 2 Ca) which contribute to the charge compensation of the layer. To describe the muscovite (K end member)-

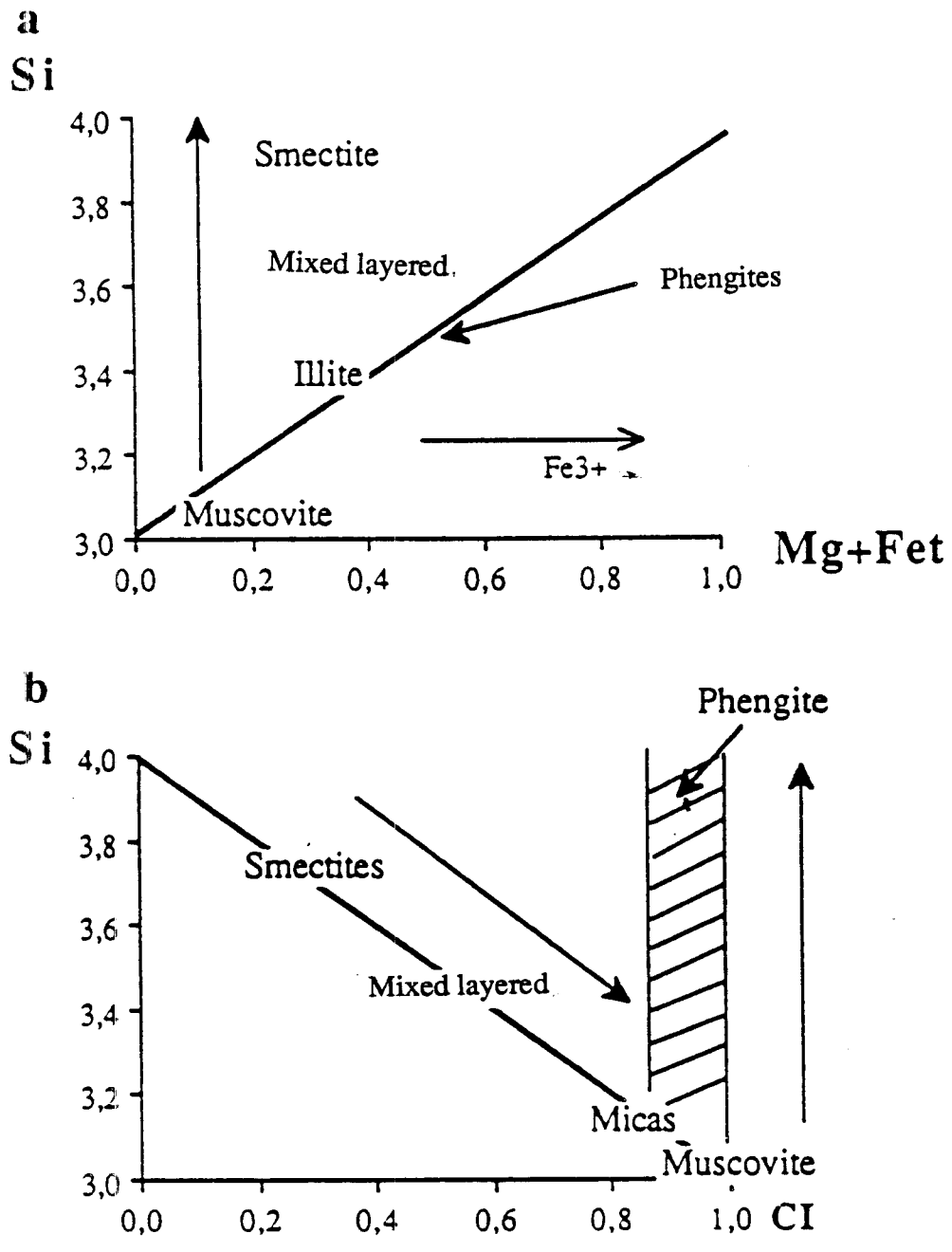

Fig IV - 68 : Si - R^{2+} (Fe+Mg) diagram (a) and Si - Interlayer charge (b) diagram with indication of the location of the theorical end members for dioctaedral K-micas

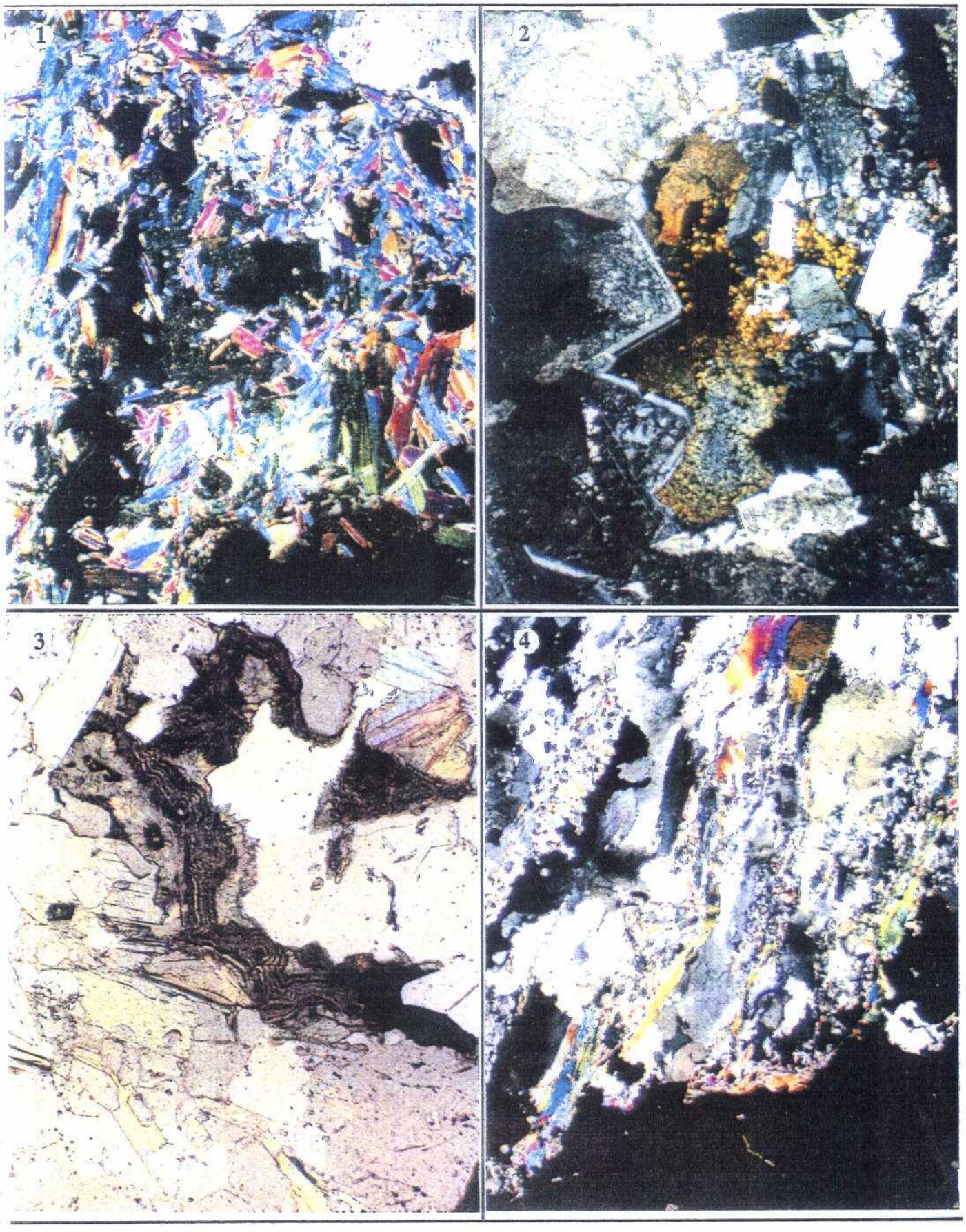

Plate IV 17 - Alteration minerals
1- Important muscovite alteration within the granite from Dacotim (Penedono area); 2- Authigenic euhedral albite crystals and vermicular chlorite in a quartz dissolution vugs from the Pino episyenite. 3- Hydrothermal chlorite in the Tomino granite hosting mineralized quartz veins. 4 - Discrete K- mica alteration associated to arsenopyrite within the deformed granite (Corcoesto drill hole).

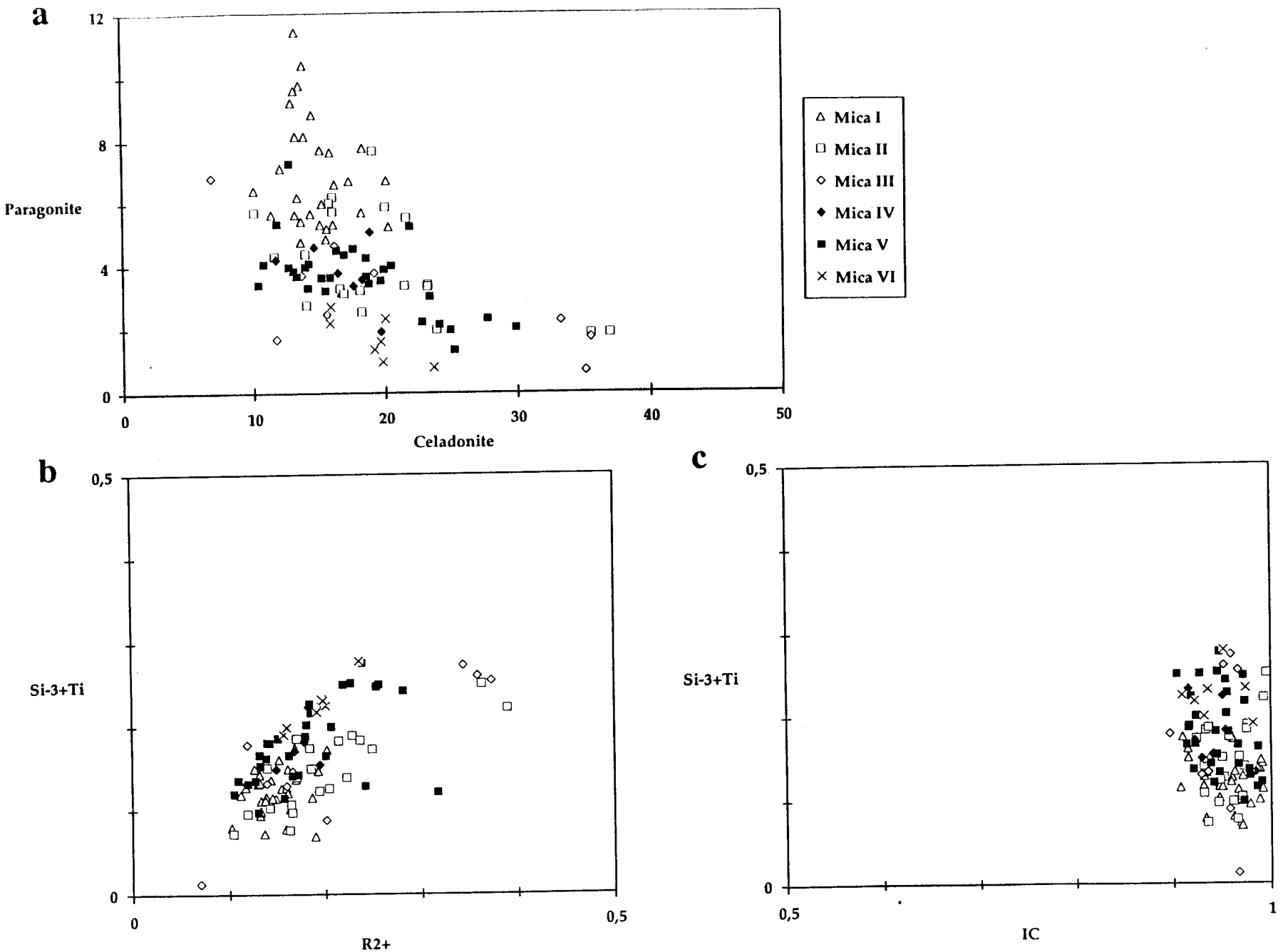

Fig IV - 69: K-micas from Penedono. a : Paragonite versus celadonite diagram. b : Si-3 +Ti versus R^{2+} diagram. c : Si-3 + Ti versus interlayer charge (IC).

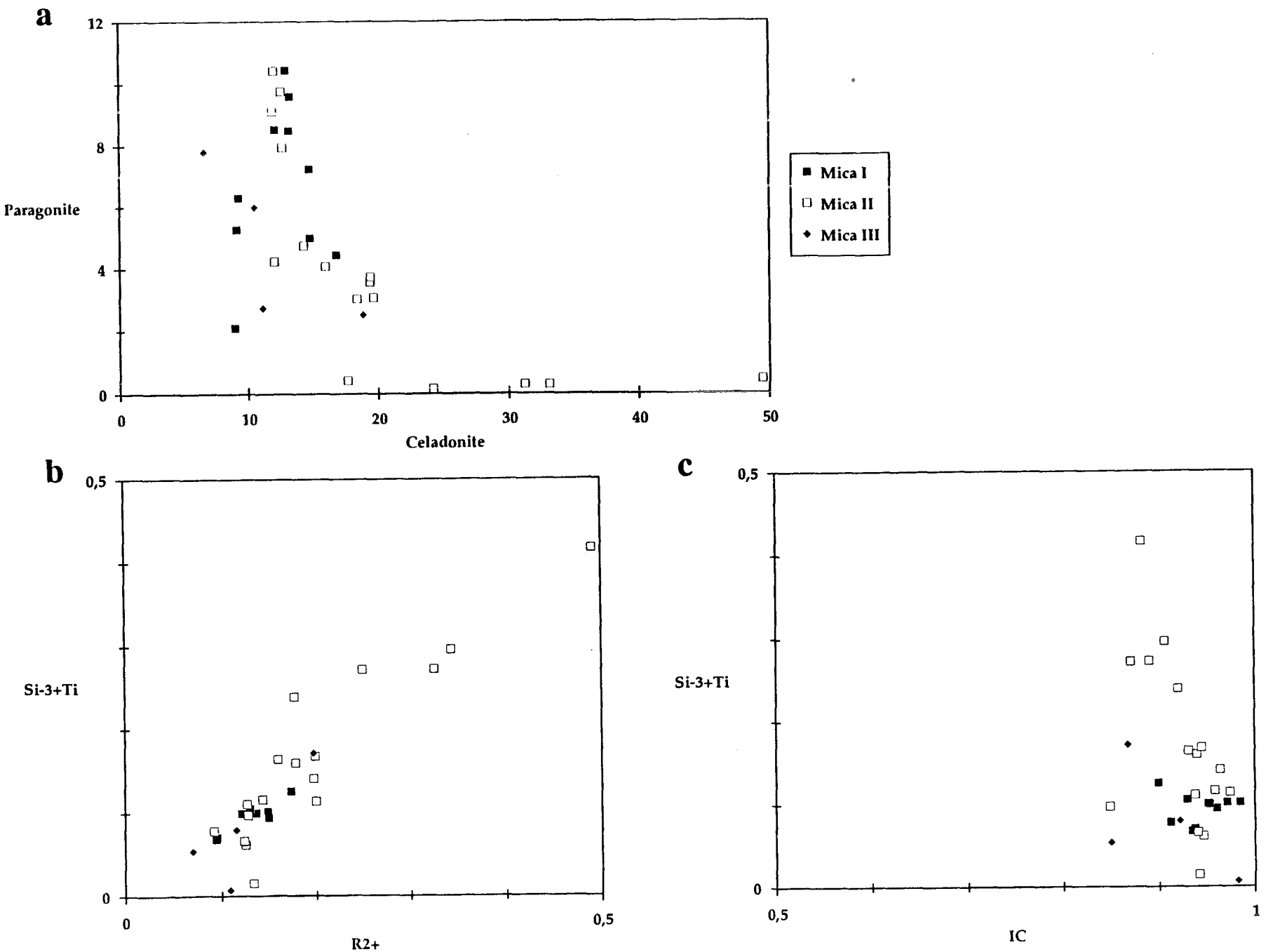

Fig IV - 70: K-micas from Pino a : Paragonite versus celadonite diagram. b : Si-3 +Ti versus R^{2+} diagram. c : Si-3 + Ti versus interlayer charge (IC).

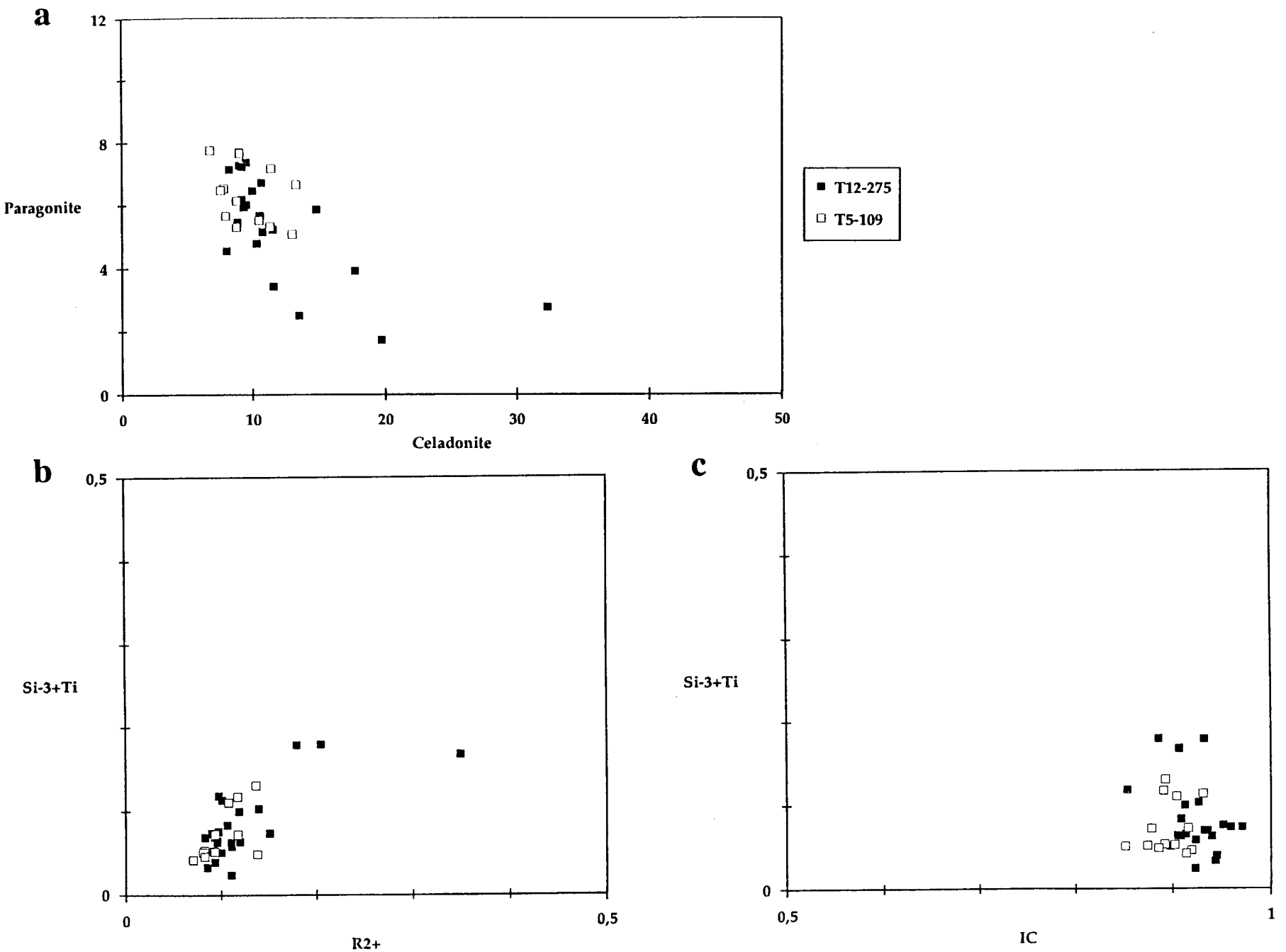

Fig IV - 71: K-micas from Tomino a : Paragonite versus celadonite diagram. b : Si-3 +Ti versus R^{2+} diagram. c : Si-3 + Ti versus interlayer charge (IC).

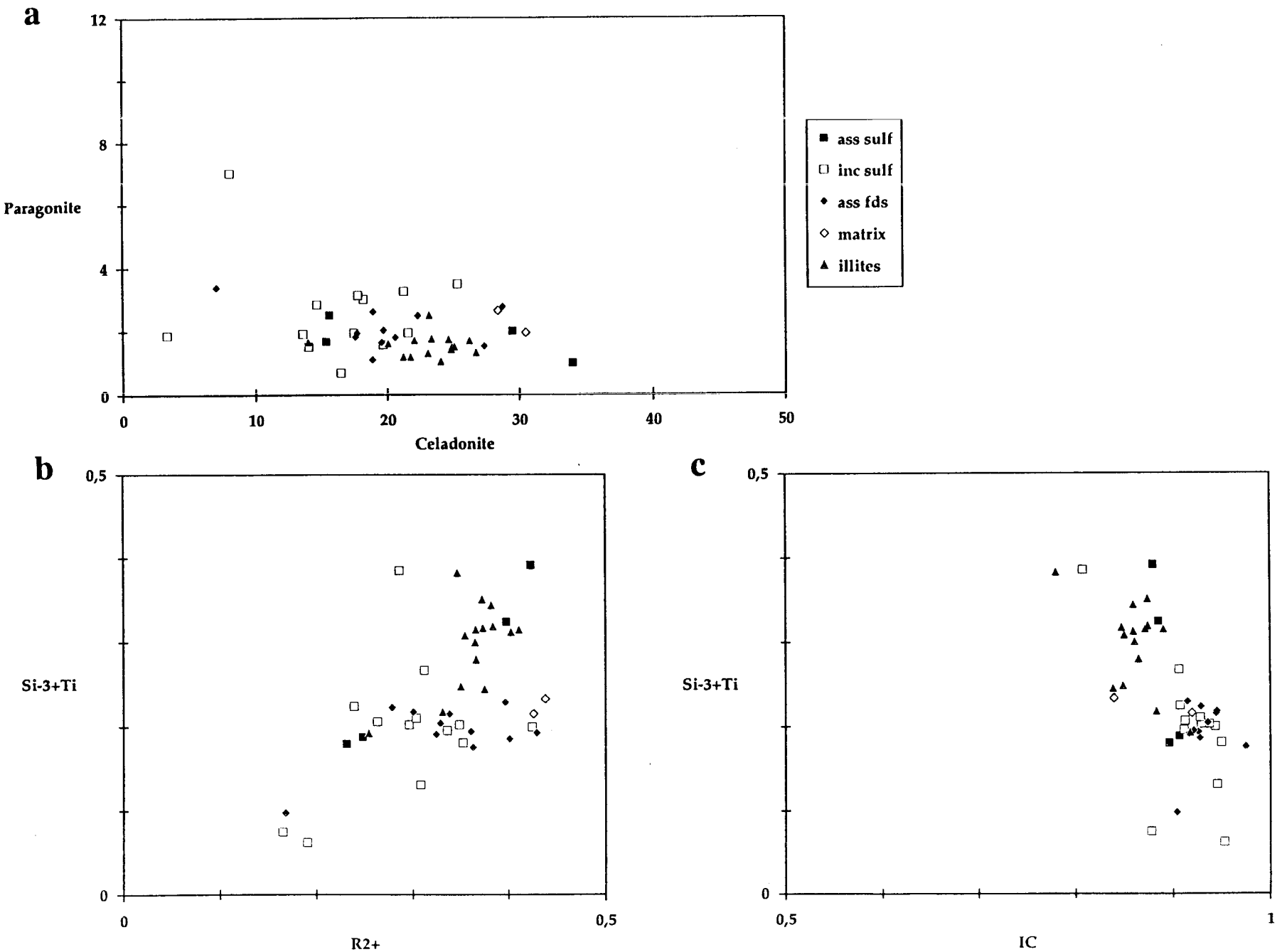

Fig IV - 72 K-micas Corcoesto a : Paragonite versus celadonite diagram. b : Si-3 +Ti versus R^{2+} diagram. c : Si-3 + Ti versus interlayer charge (IC).

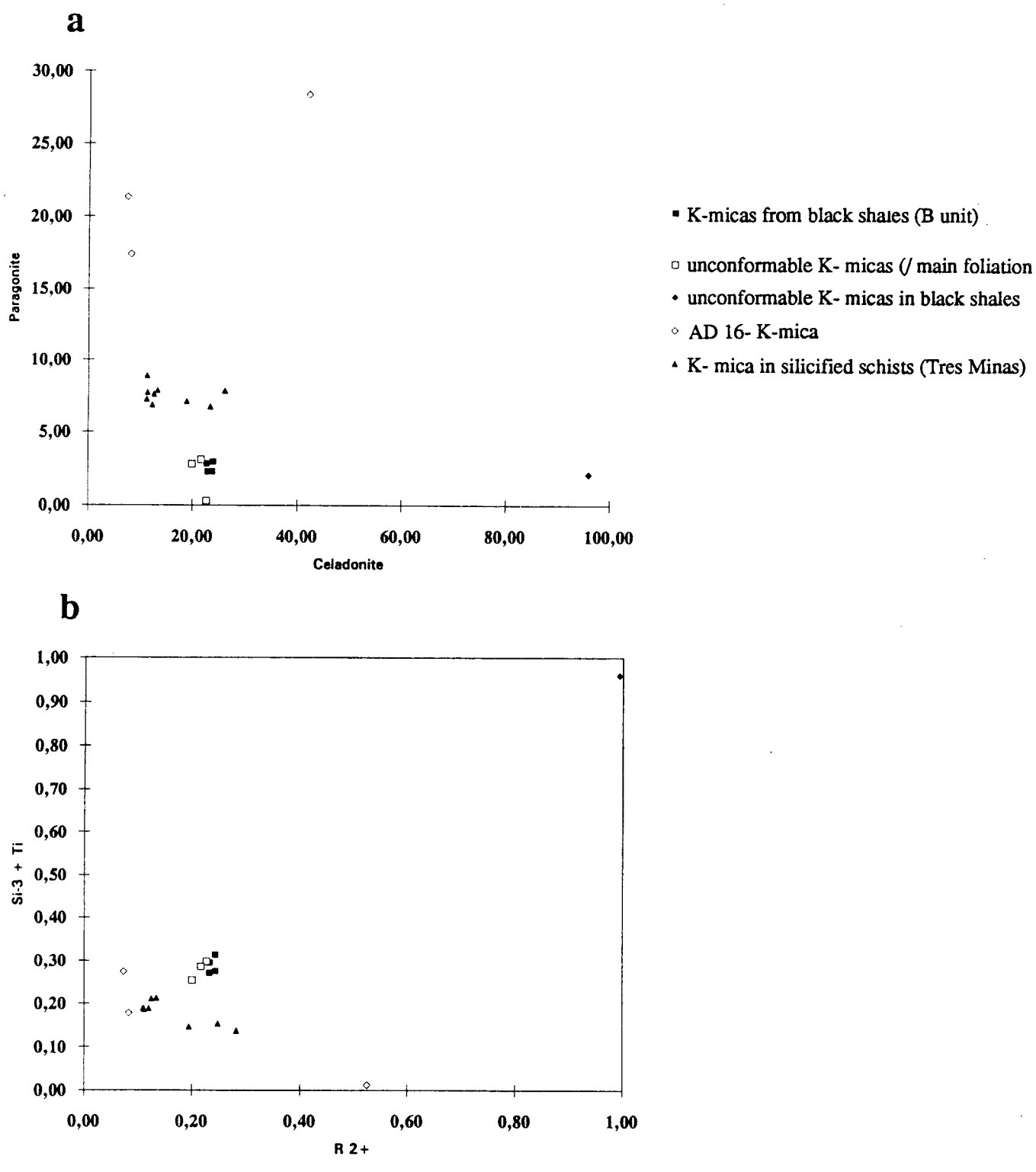

Fig IV - 73 K-micas from Vila Pouca a : Paragonite versus celadonite diagram. b : Si-3 +Ti versus R^{2+} diagram.

paragonite (Na end member) series, the percentage of paragonite is calculated from the Na/Na+K ratio.

"Illitic" substitution
The Si-3 versus interlayer charge diagram shows two trends : the "phengite" series at constant CI and variable Si content between the muscovite and celadonite end-members, and the illitic substitution from the muscovite end members to the pyrophyllite (Si_4, no interlayer charge) (Fig. IV-68b)

These three diagrams have been used to describe the main substitutions of K-micas.

Crystal-chemical data

In the intragranitic deposits, K-micas have been analysed as a function of the alteration stage. different K-micas have been distinguished :

Mica I : primary mica from the granite
Mica II : neoformed mica
Mica III : mica resulting from feldspar alteration
Mica IV : mica resulting from greisenization
Mica V : mica associated with sulfide (arsenopyrite mostly)
Mica VI : mica associated with tourmaline.

At Penedono, all the previous type are observed. Mica I have a high interlayer charge ranging from 0,9 to 1. Paragonite content is variable (5-11,5 %) while celadonite content remains more constant (15-20 %). Mica II, III and V display rather similar features : a rather high interlayer charge (>0,9), an evolution along the phengitic substitution line (Fig. IV-69) and an increase of the celadonite content, at low paragonitic content (<5 %).

At Pino, similar evolution is observed from the primary K-mica in the granite with high interlayer charge to the K-mica associated with arsenopyrite or recrystallized in the host rocks showing phengitic substitution (Fig. IV-70).

At Tomino, K-mica associated with arsenopyrite from two drill hole have been analysed. Interlayer charge is ranging from 0,85 to 0,98. Celadonite content is ranging from 10 to 20 % for a paragonite content in the range 2-8 %. K- micas associated with sulphides are phengites as shown in figure IV-71.

At Corcoesto, K-micas associated with sulphides display low paragonite content (<4 %), a celadonite content ranging from 15 to 35 %. The interlayer charge is variable and is lower in the case sample from depth 414m. K-micas resulting from felspar alteration display large celadonite content and interlayer charge mostly in the range 0,9-0,98 (Fig. IV-72).

In intrametamorphic deposits :

At Vila Pouca, an evolution of the paragonite content is observed from the sericites in the black shales to those analysed in the silificed schists from Tres Minas(Fig. IV-73a). Such K-micas are lying along the phengitic substitution line (Fig. IV-73b).

At França, carbonate veins comprises the deposition of quartz, fine–grained white–micas (E–I and E–II) and chlorites of type E–I, locally associated with sulphides (mainly pyrite) and carbonates (mostly Mg–siderites). The deposition of sericite (E–IIIa, b) and fine–grained chlorite (E–II) along late veinlets and fractures, as well as the development of aggregates of vermicular chlorite (E–III) filling voids and replacing altered sulphides and carbonates, are characteristic of the late hydrothermal assemblages.

Dioctahedral K–micas of M–I type are the prevailing phyllosilicates in ore samples, although chlorite M–I might be present in some veins, particularly those that exhibit abundant Carb I. The deposition of late sulphides is locally followed by chlorite M–II, which surrounds

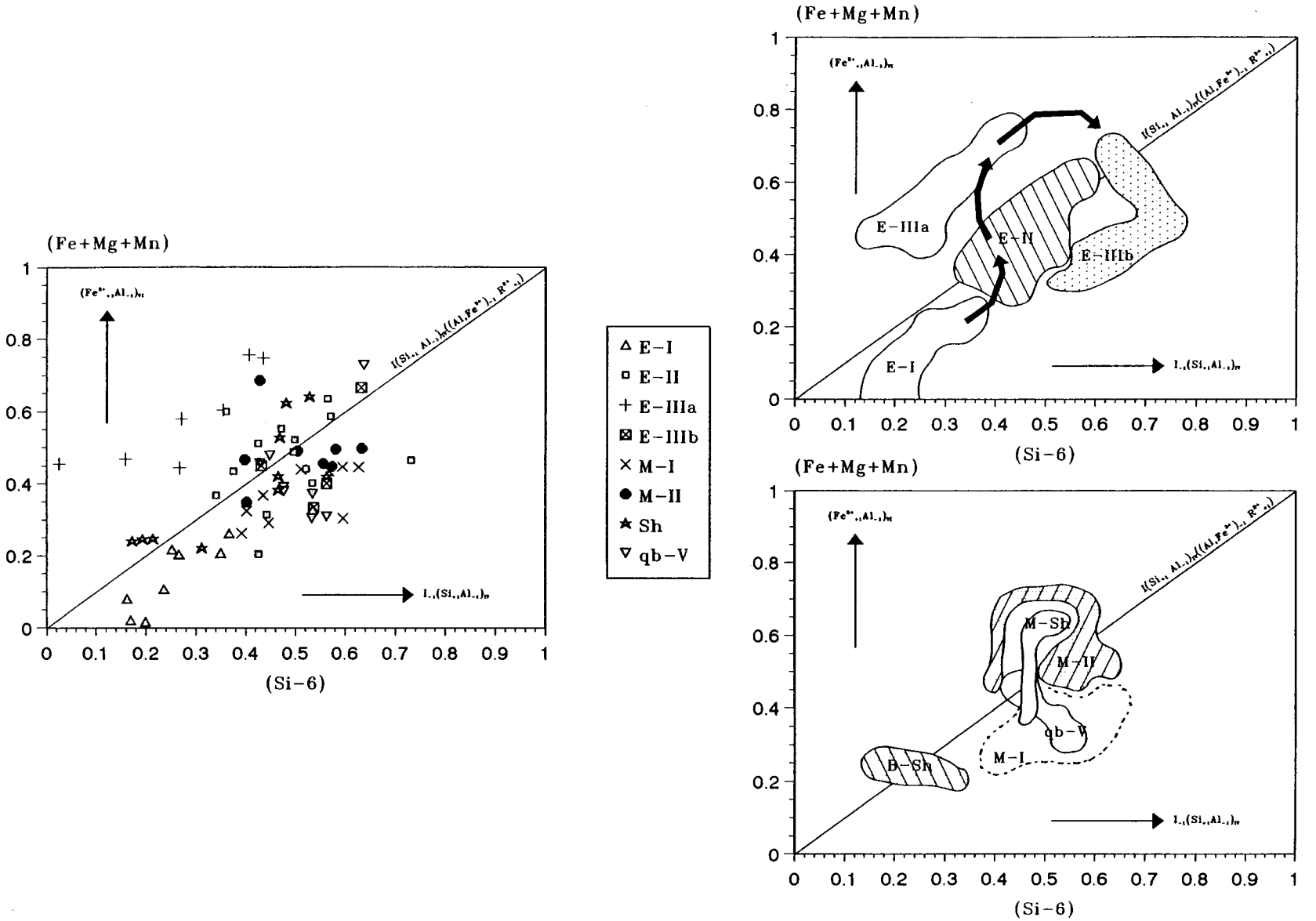

Fig IV - 74 : (Fe+Mg+Mn) versus (Si–6) plot of dioctahedral K–micas from the França area. Symbols represent the different K-mica families, according to the observed textural relationships. B-Sh : barren quartz veins along regional sheas; M-Sh : mineralized quartz veins along regional shears; qb-V : quartz breccias along the Vilariça fault zone.

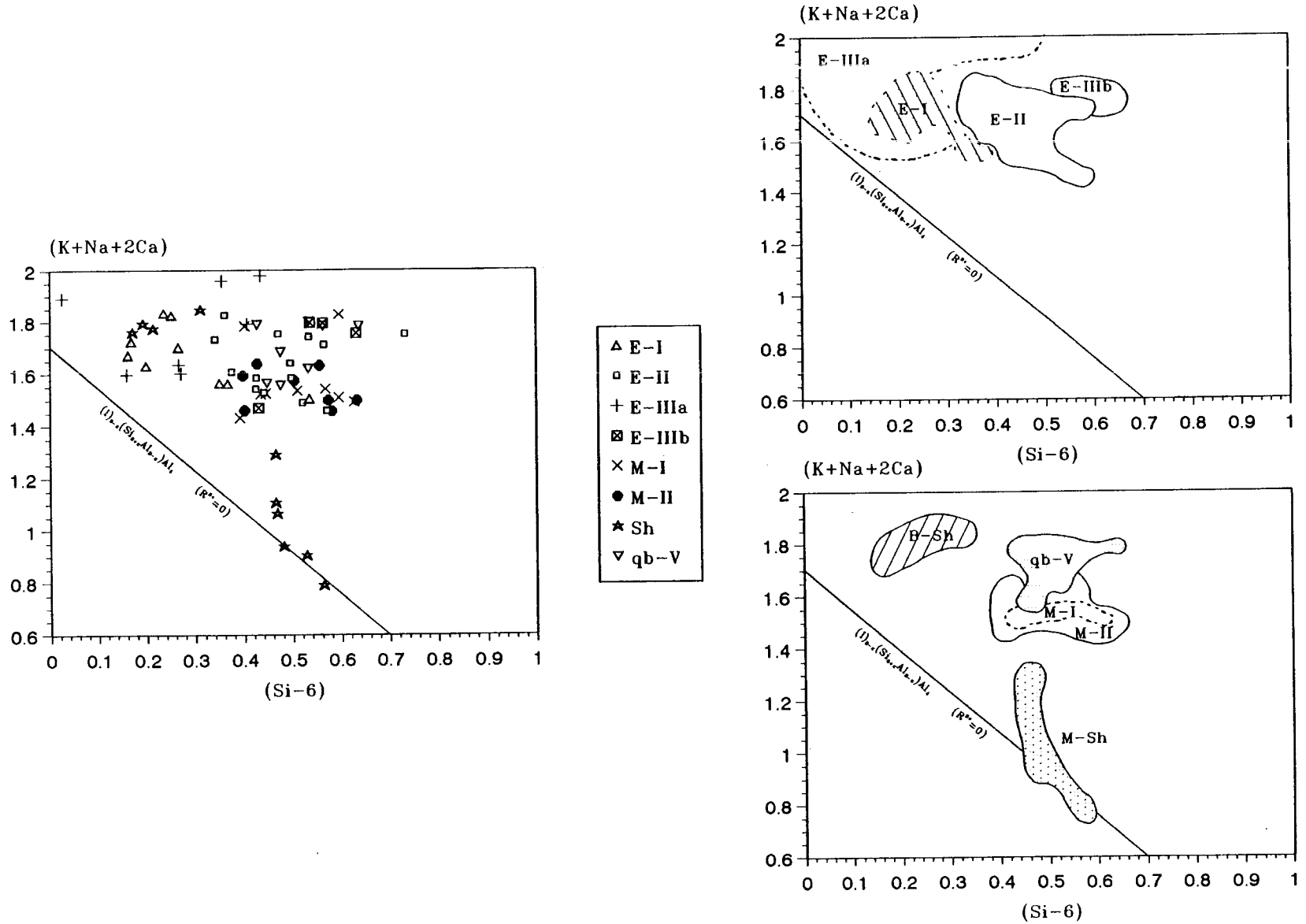

Fig IV - 75 : (K+Na+2Ca) versus (Si-6) plot of K-micas from the França area. It is also plotted the ideal line corresponding to the substitution I-1 (Si+1,Al-1) iv (Muscovite - Pyrophyllite) for R2+ = 0 (i.e., no muscovite -celadonite substitution). Symbols as in figure IV-74.

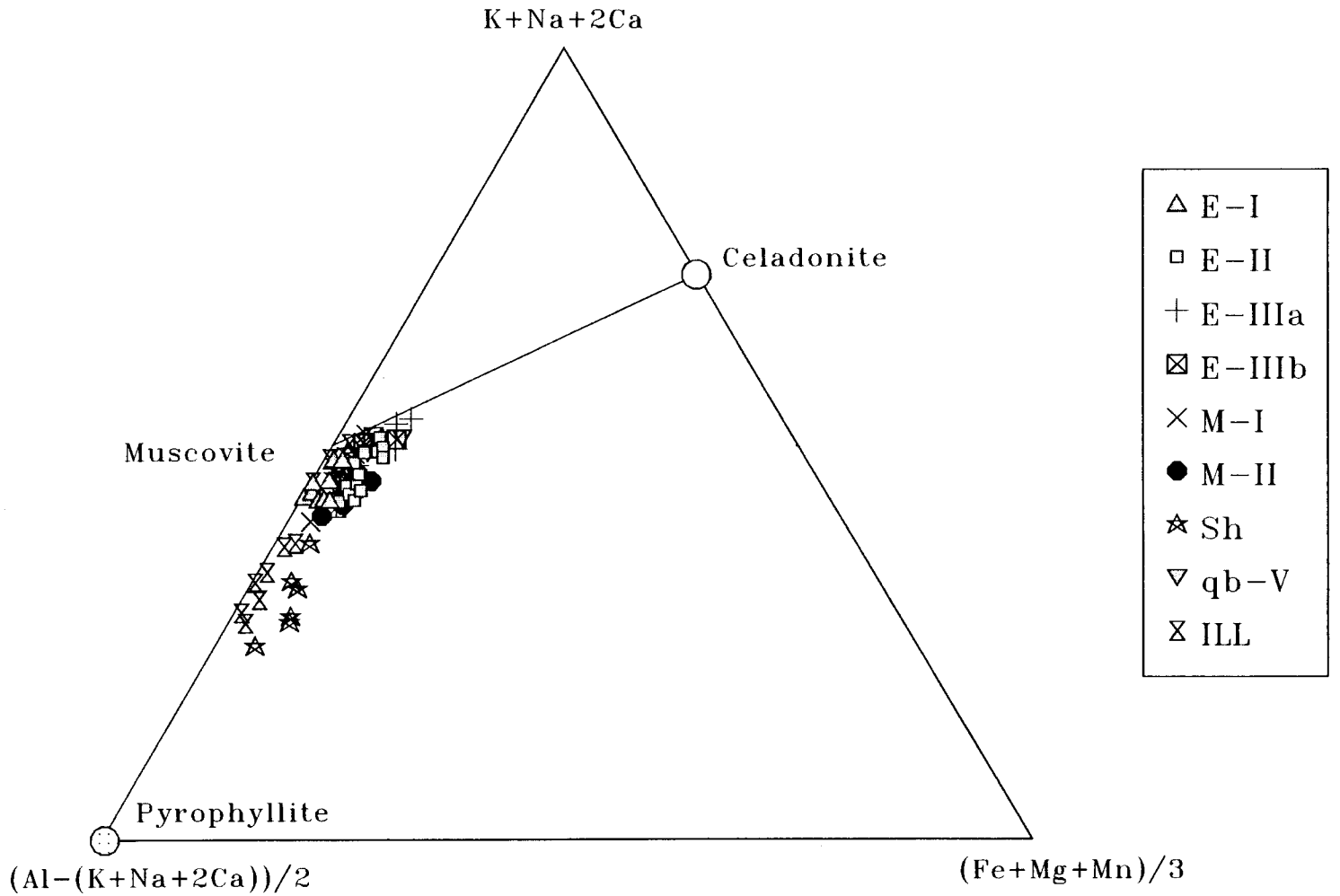

Fig IV - 76 : Plot of the examined sericites and illites (observed within the characteristic matrices of the oxidized quartz breccias along the Vilariça fault) in the MR3-2R3-3R2 diagram from Velde (1977). Symbols as in figure IV-74.

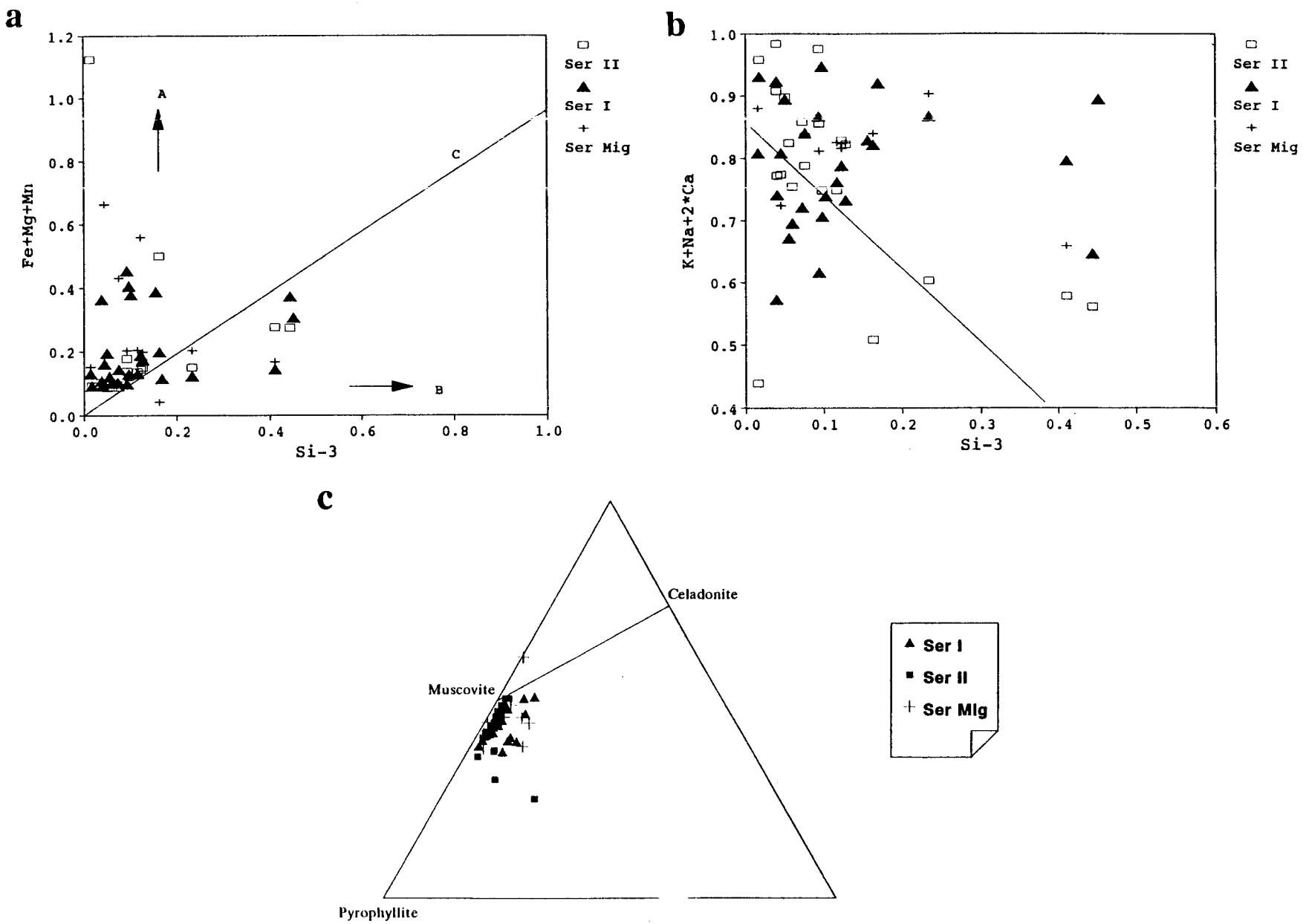

Fig IV - 77 : K-micas from Montemor. a : Si-3+Ti versus R^{2+} diagram.. b : Si-3 +Ti versus interlayer charge (IC). c : MR3-2R3-3R2 diagram from Velde (1977).

carbonate IV. Late fractures filled with chlorite and sericite of M–III and M–II types, respectively, are quite common.

Chemical variations and representative analyses of sericites show that paragonite content of sericites E–II and M–I is quite variable (ranging from 0.5 to 7.25 mole % and 1.5 to 6 mole %, respectively), while values between 1.6 to 3.4 mole % are characteristic of M–Ib sericites. Margarite content is usually below 0.5 mole %, but values above 1 mole % can be observed in sericites of mineralized samples.It should be noted that sericites of mineralized samples in which the Fe2+ content is usually greater than Mg, suggesting that the chemistry of these micas was controlled by the bulk rock composition and mineralogy, especially the presence or the absence of coexisting Fe2+–rich minerals (Fig. IV-74). Finally, the Na/(Na+K) ratios for K–micas in mineralized samples, range from 0.004 to 0.04, and are similar to those characteristic of sericites E–II; on the contrary, the typical Na/(Na+K) ratios for sericites E–I and K–micas in barren quartz veins associated to regional shears are scattered in the range 0.03–0.06 (Fig. IV-75).

Minor amounts of hydrous–phyllosilicates (hydrosericites ? illites, and sparse smectites) were also identified within the characteristic matrices of the quartz breccias associated both to the Vilariça strike–slip fault and to the reactivated D3 shears. For some K–micas in mineralized veins along regional shears, the main substituion seems to be that of Si by Al in tetrahedral sites which is negatively correlated with the whole interlayer occupancy, at nearly constant R2+ content (phengite-illite series, Fig. IV-75 and 76).

At Montemor, the hydrothermal alteration exhibited by the wall–rocks of the mineralized veins comprises mainly the deposition of quartz, fine–grained white–micas (sericites I and II) and arsenopyrite II. Their development postdates an earlier episode of alteration characterized by the assemblage quartz I + chlorite I + rutile , albite , arsenopyrite I.
In ore samples, where arsenopyrite and pyrite are the prevailing sulphides, the major association of non–metallic minerals comprises quartz, sericite II, and minor amounts of chlorite (M – see Fig. IV-77).Later stages of alteration are essentially represented by the association of chlorite (see Fig. IV-77, usually along late veinlets) and covellite, usually followed by scorodite and iron (hydro)– oxides development.

The compositional variation of the examined K–micas is, in general, quite similar for the different groups,and characterized by a low celadonitic exchange. Nevertheless, for a significant number of K– micas (mainly of types I and II) the importance of the exchange Si,Al(iv), negatively correlated with the whole interlayer occupancy for a constant R2+, is clearly illustrated by the relationship between the (K+Na+2Ca) content versus (Si–3) values per formula unit (Fig. IV-77b). Therefore, since the celadonitic exchange is low and quite constant, data plotting on a MR3–2R3–3R2 diagram (Velde, 1977) is concentrated near or slightly below the ideal muscovite, along the muscovite–pyrophyllite line (Fig.IV -77c).The Na/(Na+K) ratio is quite variable for K–micas I and II (ranging from 0.005 to 0.12), and typically around 0.04-0.01 for sericites in migmatites.

Conclusions

In most deposits, the inverse relationship between (Si–6) per formula unit and the ratio Na/(Na+K) can be used in order to distinguish the main groups of phyllosilicates, especially the early ones and those associated with mineralizing events.
The lack of low temperature minerals (illite-smectite series) is noteworthy, since such minerals are extremely abundant for instance in the french Au deposits. Therefore, most K-micas are nearly true phengite with very low "illitic" substitution, indicating that the hydrothermal K-mica crystallization stopped at relatively high temperatures (above 250°C)

2-CHLORITE

Structural formulas were normalized to 14 oxygens, according to the ideal stoichiometry of these phyllosilicates, i.e., (R2+(6–x),R3+(x))(Si(4–x),R3+(x))O10(OH)8 (Foster, 1962, Bailey, 1987, Bryndzia and Scott, 1987) and all iron is assumed as ferrous.

Variations of chemical compositions can be described by the following substitutions :
-The Tchermack substitution (T) (Si-1Al+1)iv (Al+1 R2+–1) iv
- The substituion in octaedral site.(O) : (Al R2+ -3/2 vac 1/2)vi

The rnain diagrams used in this study are the followings :

Si versus Fe/Fe+Mg diagram : this diagramm from Foster (1962) discriminates the chlorite populations in chemical domains which have been defined arbitrarily.

Fe- Mg substitution : the Fe-Mg diagram shows different tendencies depending of the Fe- Mg substitution in the R^{2+} site.

Al iv -Al vi substitution : Al iv -Al vi diagram is useful to describe the major substitutions T , O and their combinaition The theoretical poles and the major substitution vectors are reported on figure IV-78.

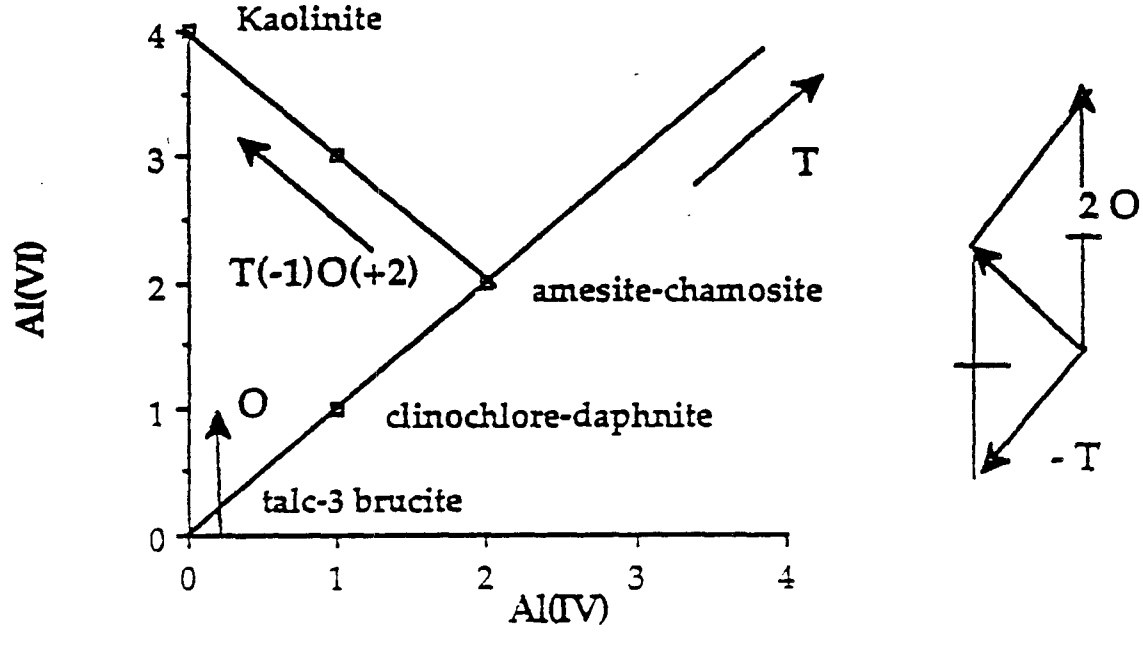

Fig IV - 78 : Aliv -Alvi diagram applied to chlorite analysis with indication of the location of the theorical end members and the possible substitutions.

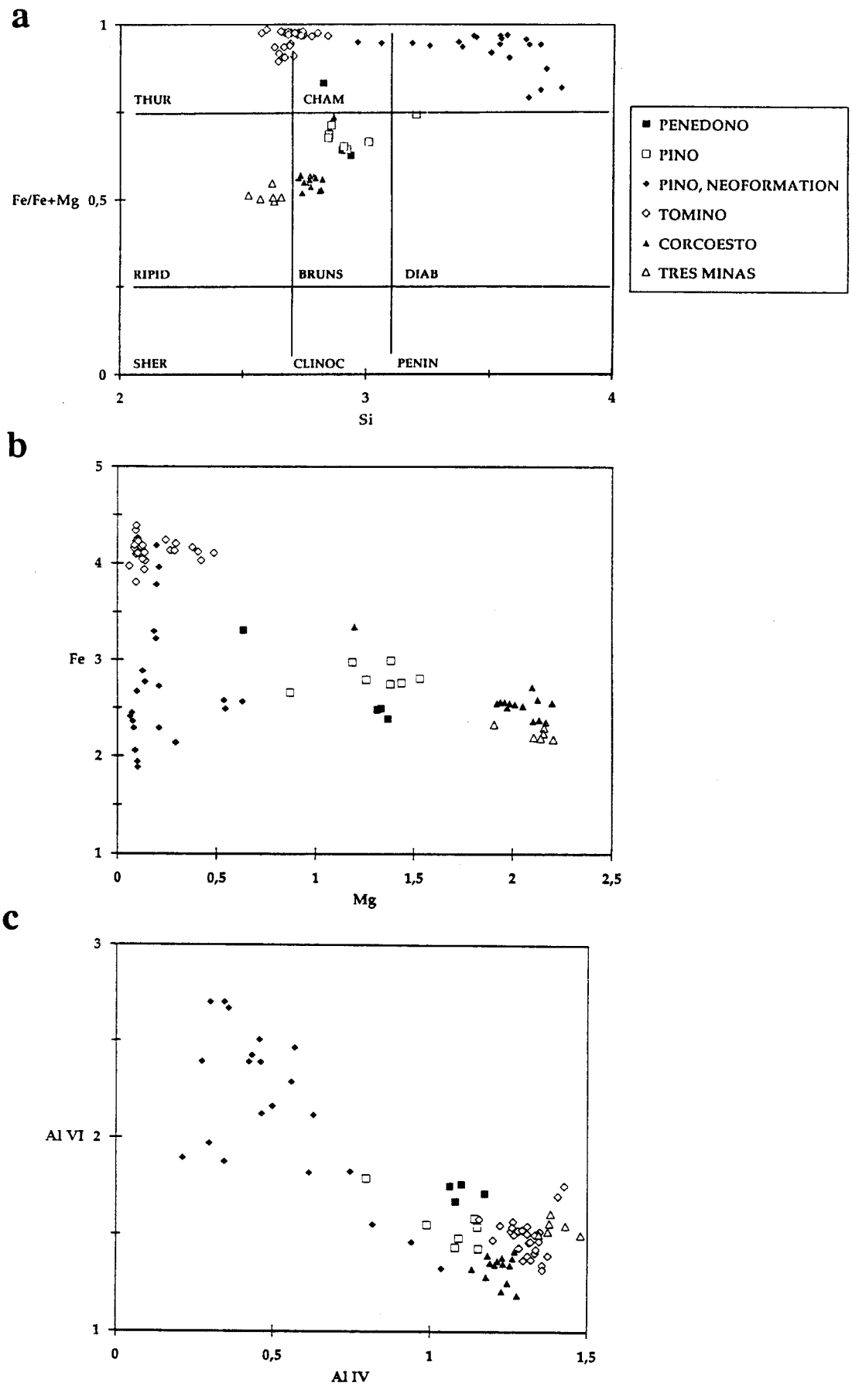

Fig IV - 79 : Chemical analyses of chlorites from Penedono, Pino, Corcoesto, Tomino and Tres Minas. a : Fe/Fe+Mg versus Si diagram (Foster,1962) b : Fe versus Mg diagram c: Aliv versus Alvi diagram.

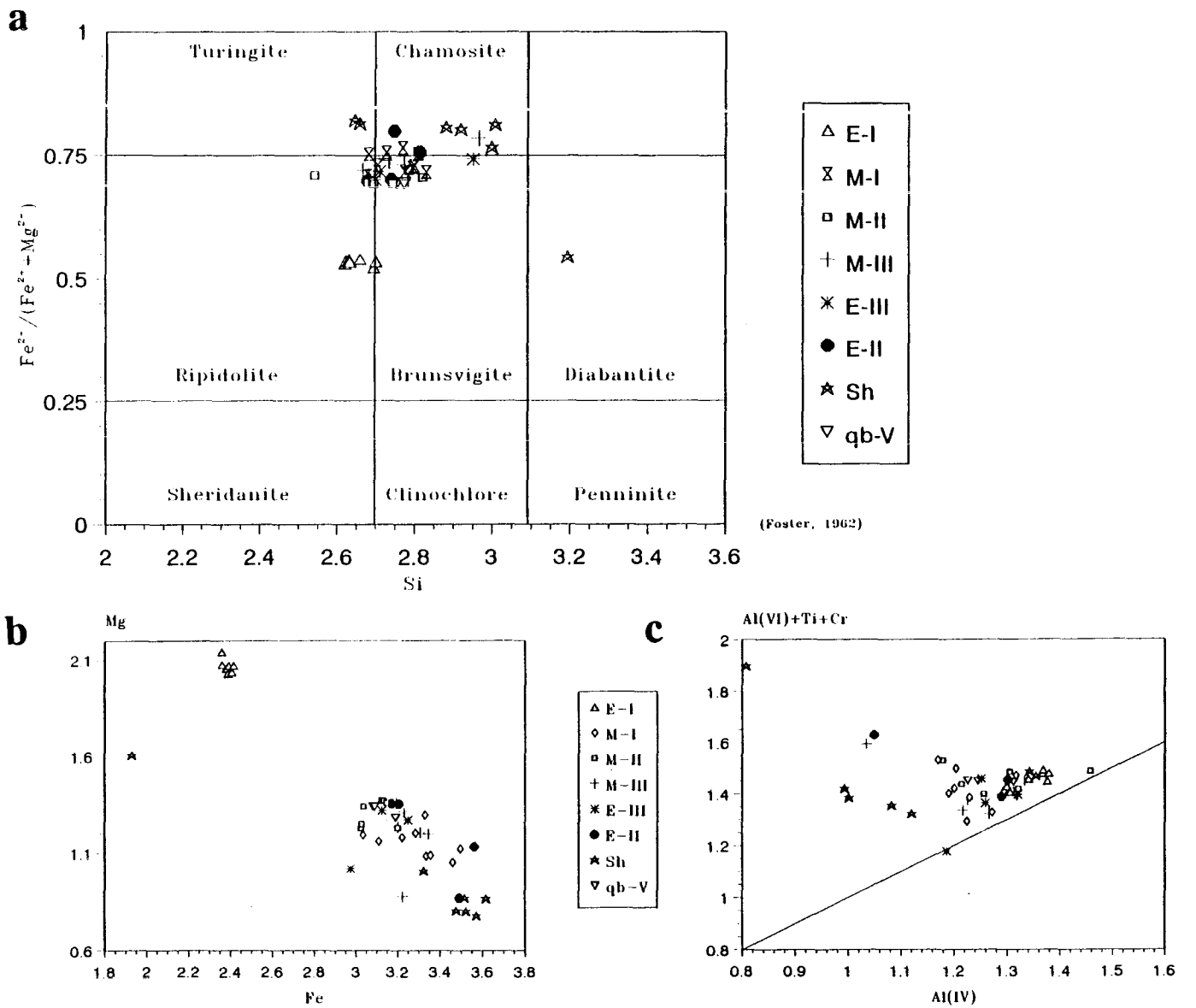

Fig IV - 80 : Chemical analyses of chlorites from França area. a : Fe/Fe+Mg versus Si diagram (Foster,1962). b : Fe versus Mg diagram. c: Aliv versus Alvi diagram.

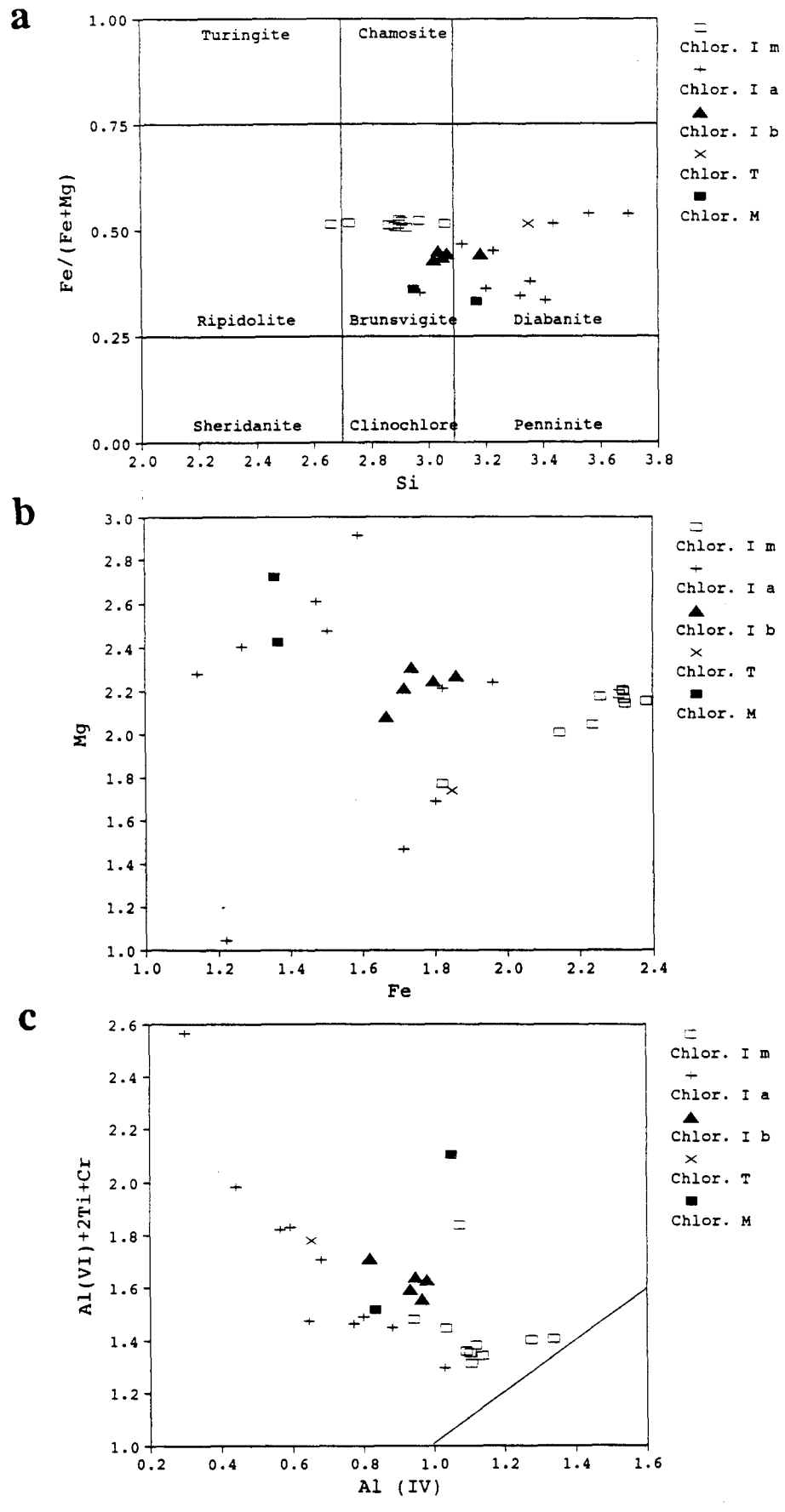

Fig IV - 81: Chemical analyses of chlorites fromMontemor area. a : Fe/Fe+Mg versus Si diagram (Foster,1962) . b : Fe versus Mg diagram. c: Aliv versus Alvi diagram.

Crystal-chemistry data

Chlorites from the different studied deposits (Corcoesto, Tomino, Penedono, Pino, Tres Minas) have been analysed by electron microprobe in Nancy. Data from França and Montemor area have been performed at Lisboa university.

Two major type of chlorites have been recognized :

- *chlorite from altered biotite*

Chlorites resulting from biotite alteration are mostly observed in Penedono and Pino area. They display rather similar characteristics. They are brunsvigites in Foster (1962) diagram (Fig. IV-79a). The Fe content is lower at Penedono (2,3 - 2,5 at) than in Pino (2,7-3 at) for the same Mg content (1,2-1,6 at). Aliv is ranging from 1,1 to 1,25 atome/ half formula.

- *neoformation of chlorite*

At Corcoesto, chlorite are observed as late veinlet infillings, as well as sub-pervasive alteration in the microfissured zones (bleaching zones). They present the characteristics of brunsvigites. The ion content ranges from 2,5 to 3 at. and the Mg content is relatively high compared to the other chlorites (Fig. IV-79b), ranging from 1,8 to 2,3 at.

At Tomino, neoformed chlorites display contrasted composition compared to the others. They are very enriched in Fe (4-4,5 at) and depleted in Mg (<0,5 at). They are located at the boundary Thuringite - Chamosite in the Foster diagram. The Al iv content is ranging from 1,2 to 1,45 at (Fig. IV-79c).

At Pino, neoformed chlorite fills vugs resulting from quartz dissolution in episyenites. The chemical composition show scattered features from chamosite to chlorite with high Si content.(Fig. IV-79a) However, a contribution of expandable layers resulting from supergene alteration is suspected. The Mg content is relatively low (>0,75 at).

At França, the compositional data and representative analyses for the examined chlorites (Tables III and IV) can be classified mainly as ripidolites, brunsvigites and chamosites (Foster, 1962), and a general observation of the Fe/(Fe+Mg) versus Si plot (Fig. IV-80a) suggests that there is a gradual increase of Fe and Si contents towards the late generations. However, this conclusion is only valid if we consider all data points of mineralized samples as an unique generation representative of the ore stage. Nevertheless, it is possible to explain the distribution obtained for M–I, M –II and M–III chlorites assuming that the composition of these minerals was sensitive to slight chemical fluctuations of the medium during their deposition and/or were influenced by the chemistry of the neighbouring, contemporaneous minerals.

The analyzed chlorites show usually an Al content greater than 1.650, one late–chlorite excepted, where Al=1.363 (ions per 14 O). Significant exchange of Fe2+ for Mg2+ occurs (Fig. IV-80b) coupled with the strong covariance between (Fe+Mg) and [Si – ([](vi). 2)].

At Montemor, the chlorites from wall– rock samples close to and far from mineralized veins (Ia and Ib); the chlorites in migmatite samples(Im), and for those in mineralized veins and in late alteration paragenesis (M and T, respectively)have been analyzed. They are mainly as brunsvigites and diabantites . The observation of data scatter in the Fe/(Fe+Mg) versus Si plot (Fig. IV-81) suggests a tendency to a relative increase in Si content, probably coupled with a slight Fe/(Fe+Mg) decrease, towards the mineralized bodies.

It should also be noted that possible mixed–layer sericite–sudoite may also be present in some samples (not considered above), given K_2O values up to 3 wt% in grains optically resembling chlorite.

D- GENERAL P-T RECONSTRUCTION

1 - DATA FROM MINERAL GEOTHERMOMETRY

Two sets of geothermometric data are used :
- for K-Micas, the stability curves of Mg-pengites by (Velde, 1965) which are based on the Si content per formula unit (celadonite content).
- for chlorites : according to Cathelineau and Nieva (1985) and Cathelineau (1988), one can determine the formation temperature of chlorites on the basis of their octahedral vacancies and Al(iv) contents per formula unit. In order to use this geothermometer, modes of site occupancy concern Al(iv) and octahedral vacancy, were calculated for each chlorite family.

Other minerals or mineral assemblages may also be considered :
- the stability of muscovite (in presence of quartz) and the lack of andalusite (+ feldspar) which indicates that temperatures do not reach more than 550°C at 1 Kb.
- the stability of biotite in some instances (Corcoesto) which may indicate temperatures above 450°C
- the graphite-fluid equilibrium which is effective for Lc-w fluids, and may indicate a temperature for these fluids above 350-400°C.
- the arsenopyrite crystal-chemistry : however, the Kretschmar and Scott (1976) geothermometer gives unrealistic temperatures ranging from 300 to 500 °C when applied to the compositional range of a single arsenopyrite crystal. Such temperature discrepancies may result from the presence of trace elements in the arsenopyrite crystals or from the lack of chemical equilibrium between arsenopyrite and other minerals, which forbides a correct use of the geothermometer.

2 - P- T DIAGRAMS

All mineralogical and geochemical constraints have been gathered together in the P-T diagrams. The P-T properties of representative C-H-O inclusions and aqueous inclusions from selected quartz were modelled for the system H2O-CO2-CH4-NaCl using the data obtained from microthermometric studies and from Raman analysis. Sets of isochores give an estimation of pressure of trapping at a given temperature.

CORCOESTO

At Corcoesto, most phengites have a celadonite content a little higher for the fine grain micas (0.2-0.3 in felspars) than for euhedral micas crystallized within arsenopyrite (0.17 ± 0.03); the intersection of the Velde's curves with the isochores of the Lc-w inclusions (L and V CO2 homogenization type) may indicate a P-T pair around 1500 ± 250 bars, and temperatures around 400°C.

The evolution shown by the three series of CHON fluids (Fig.IV-82) indicate that during the veinlet network formation (Q2, Q3) , the P-T conditions were around 450°C for the early stage, and 1500 ± 300 bars , and that pressure decreases significantly between the two major stages of quartz deposition down to 600 ± 200 bars, at nearly constant to slightly decreasing temperature. This pressure drop may correspond to the transition to the hydrostatic pressures, since at the time of the Q3 crystallization, the system was opened (free crystallization of euhedral quartz crystals).

Therefore, the depth of formation of the veinlet network could have been around 5 to 6 kilometres.

TOMINO

The density of the fluids trapped in microfissures from the host metamorphic rocks or in the granite is high. As the Th are above 350°C in the granite and 500°C in the lydites, high P estimates (2000 ± 500 bars in the granite , 3500 ± 500 bars in the lydites) are recorded during

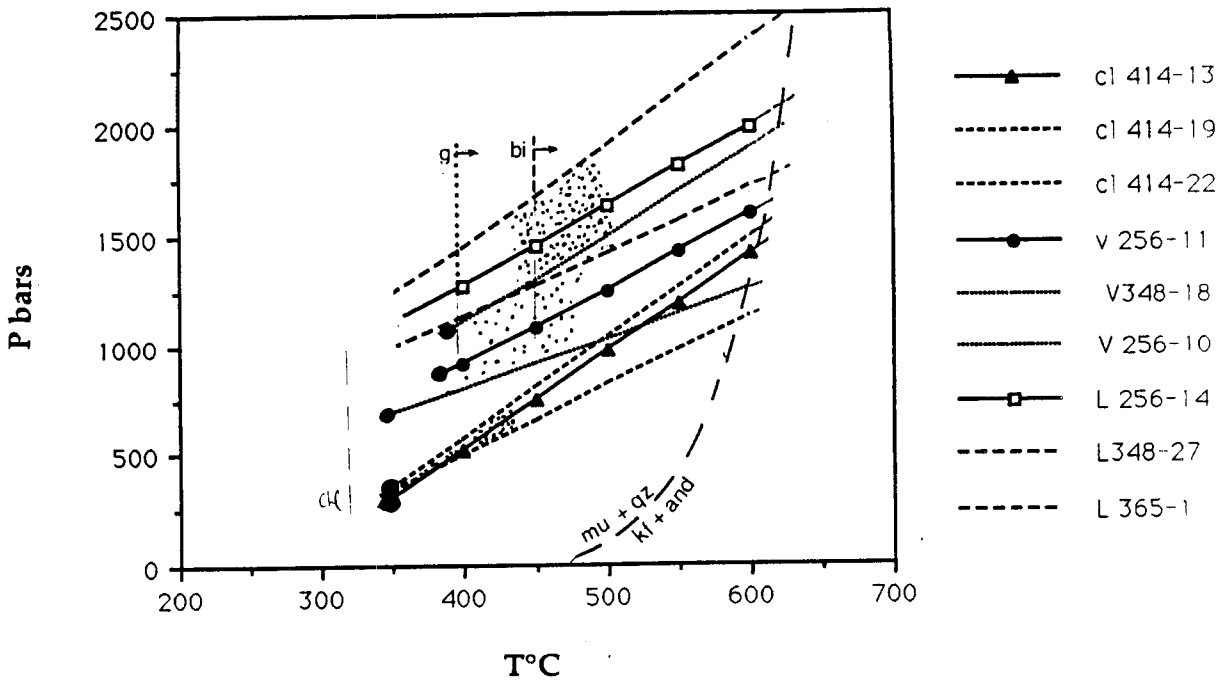

Fig IV - 82 : Pressure - temperature reconstruction of the conditions prevailing in the Corcoesto area.

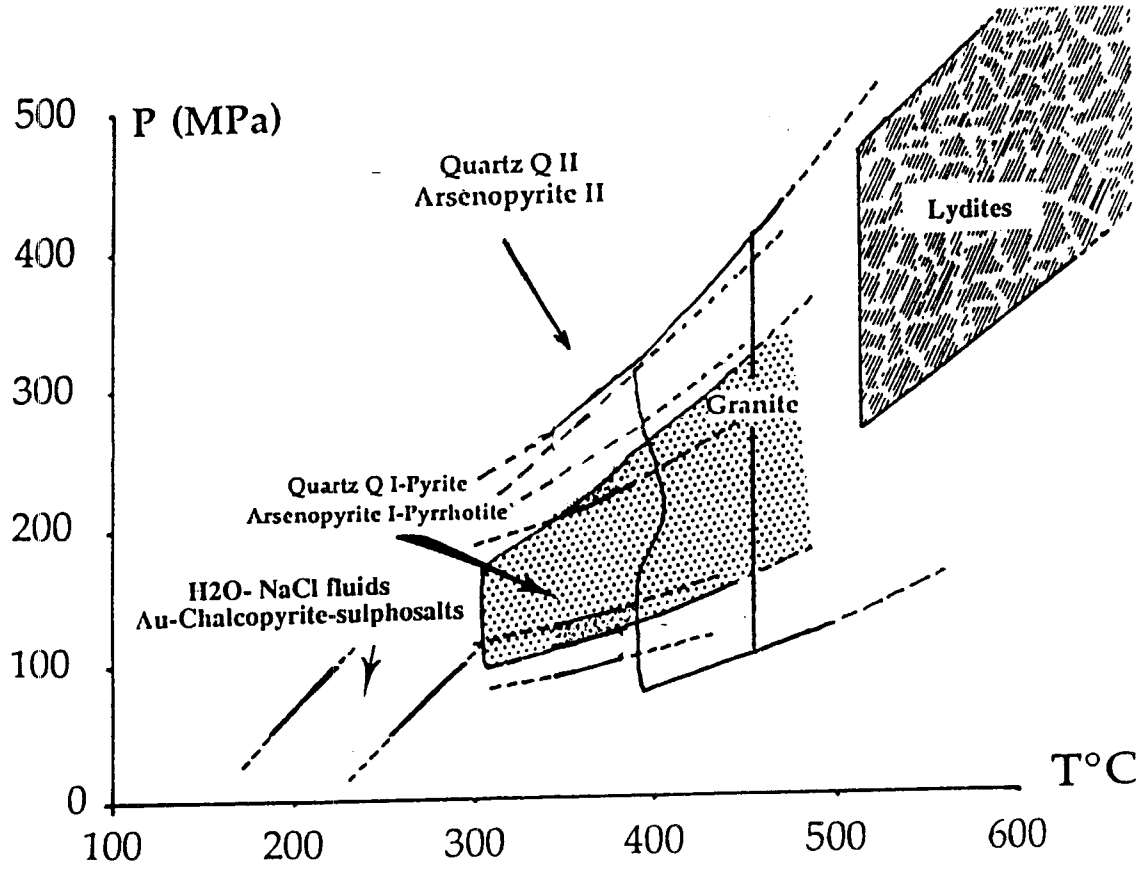

Fig IV - 83 : Pressure - temperature reconstruction of the conditions prevailing for the Tomino area.

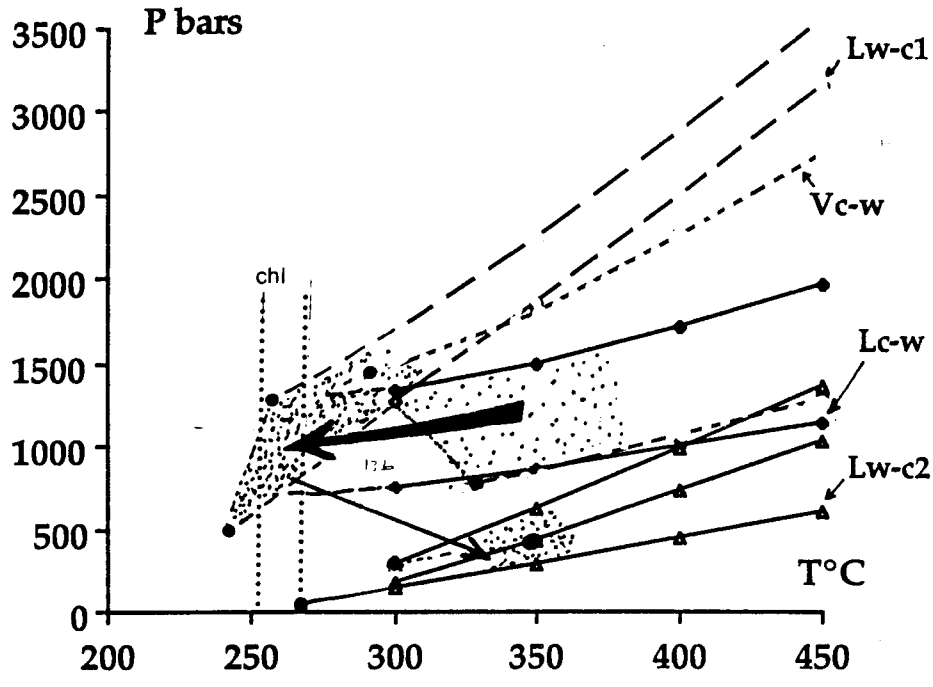

Fig IV - 85 : Pressure - temperature reconstruction of the conditions prevailing in the Pino area.

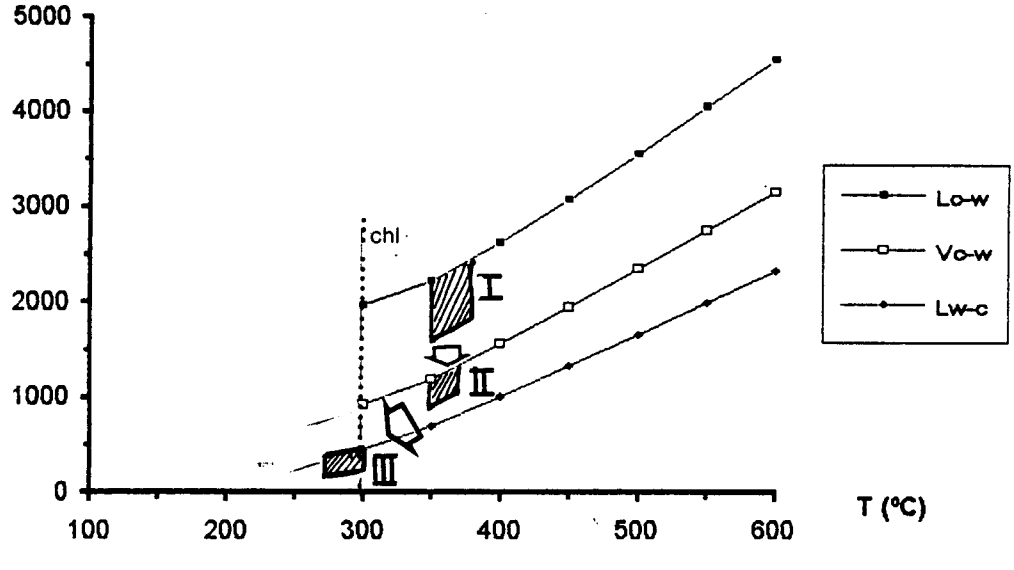

Fig IV - 84 : Pressure - temperature reconstruction of the conditions prevailing in the Penedono area.

the early fluid migration stages. The data for the granite fluids are compatible with the T estimate issued from the use of phengite geothermometry applied to the greisen assemblage.

In quartz QI and Q2, fluids display lower densites yielding to lower minimal P estimates in the 1000-2200 bars range. If the chlorite temperature constraint for this stage is valid, an average estimate of the quartz-arsenopyrite stage could be 360° ± 20°C, 1500±500 bars (Fig.IV-83).

For the late stage a mimimal P-T estimate is 200 ± 20°C, a few hundred bars, although the real P-T pair could have been slighltly higher depending on the pressure.

PENEDONO

The initial temperatures as shown from the isochore representation (Fig. IV-84) evolve from conditions of metasomatic alterations in the granite, (370°C as calculated by Silva et al, 1990), which agrees with our Th. These temperatures correspond to the crystallisation of the QI type of quartz. Pressure is in the range 2-1.5 Kbar, although large variations might occur in the systems (Cathelineau et al, 1993).

- the second phase corresponds to a drop in pressure in the system, at least in what concerns the crystallisation of the quartz as shown by the isochores. The control of the temperature in this case is made only from fluid inclusion data.
- the last phase is characterized by the lowest temperatures, and pressures (below 0,5 Kbar). Gold deposition occured during or after this stage, e.g. in between the Lw-c nd Lw stages.

PINO

The mineralogy of the altered granites at Pino does not offer possibilities of precise mineralogical contraints. However, the albite-"chlorite" (chemically reequilibrated at low temperature) formation after quartz dissolution is generaly considered to occur in the 350° ± 50 °C, in most of the equivalent occurrences from the Variscan range (Cathelienau, 1986). These T estimates correspond to the highest homogenization temperatures obtained on the Lc-w type inclusions.

The evolution shown by the three first groups of CHON fluids (Fig.IV-85) indicate that during the filling of the dissolution vugs of the granite by quartz (Q1, clear quartz Q2), the P-T conditions were around 300°, 350°C for the early stage, and 1100 ± 200 bars. The evolution between the different fluid generations is likely interpreted as quasi-isobaric, at decreasing temperature , down to 250°C. Then, the major stage of fluid trapping in clear quartz (L-w-c 2 fluids) corresponds to pressure decrease (down to around 400 bars), and a temperature increase (new heat input) up to 300-350°C.

The depth of formation of the quartz matrix is around 4.5 kilometres, assuming a lithostatic pressure, indicating a possible transition lithostatic-hydrostatic between the stages Lw-c1 and Lw-c2 at nearly constant depth.

FRANÇA

Temperature constraints

K-micas : The P–T stability fields of dioctahedral K–micas in mineralized samples (M–I, M–II) and altered host rocks (E–I, E–II, E–IIIa/b) on the basis of Velde's curves is illustrated on figure IV-86a, and shows good agreement with the isochore diagrams obtained for fluid inclusions.

Chorite data : in the hydrothermally altered wall rocks, there is a gradual decrease on Al(iv) from the E–I to E–III generations (i.e., from 1.341 to 1.049 cations per formula unit) which is followed by a slight, non–linear, decrease in octhaedral occupancy (0.076, 0.035 and 0.068 vacancies on the basis of 14 oxygens for chlorites E–I, E–II, and E–III, respectively); the Al allocated to the tetrahedral positions, as well as the calculated octahedral vacancy for the characteristic chlorites in ore samples, are in general higher and scattered in the ranges 1.205–1.257 and 0.052–0.094 per formula unit, respectively, and there is not any continuous trend

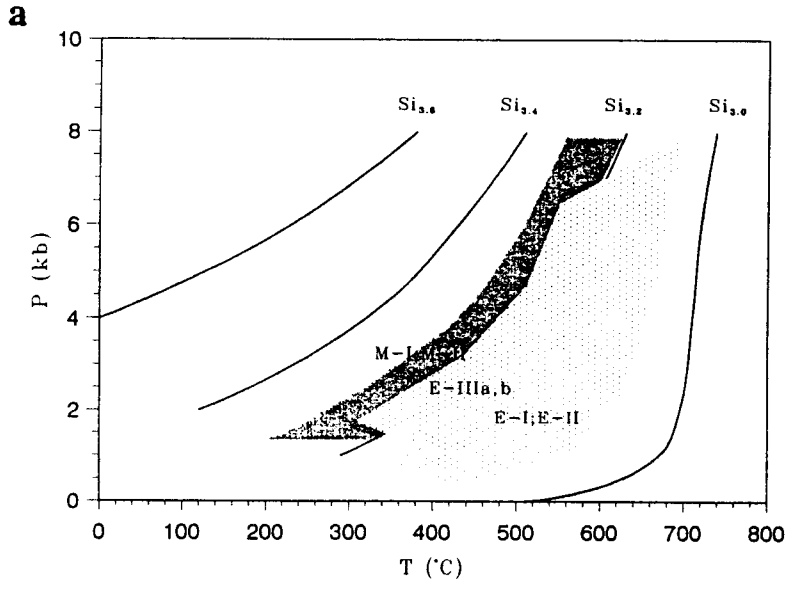

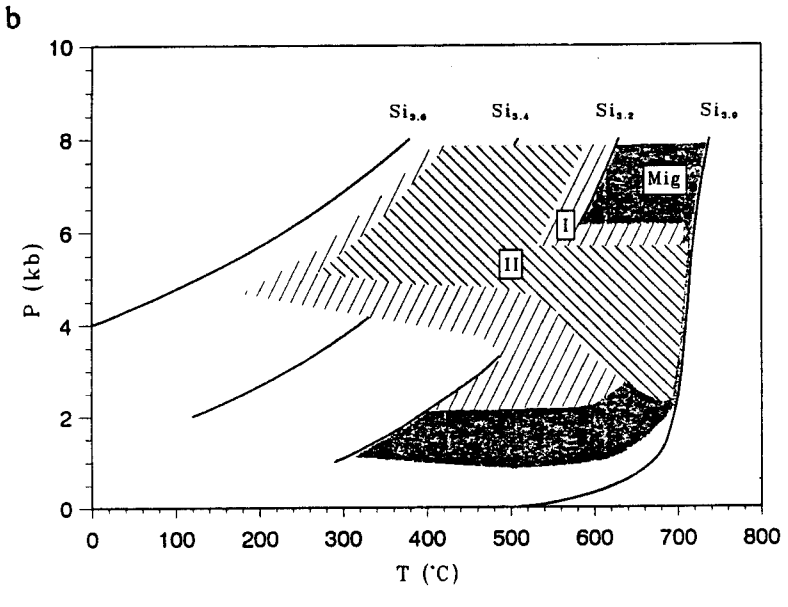

Fig IV - 86 : Pressure - temperature estimation using Si content of phengite (Velde 1965).
a : França area; b : Montemor area.

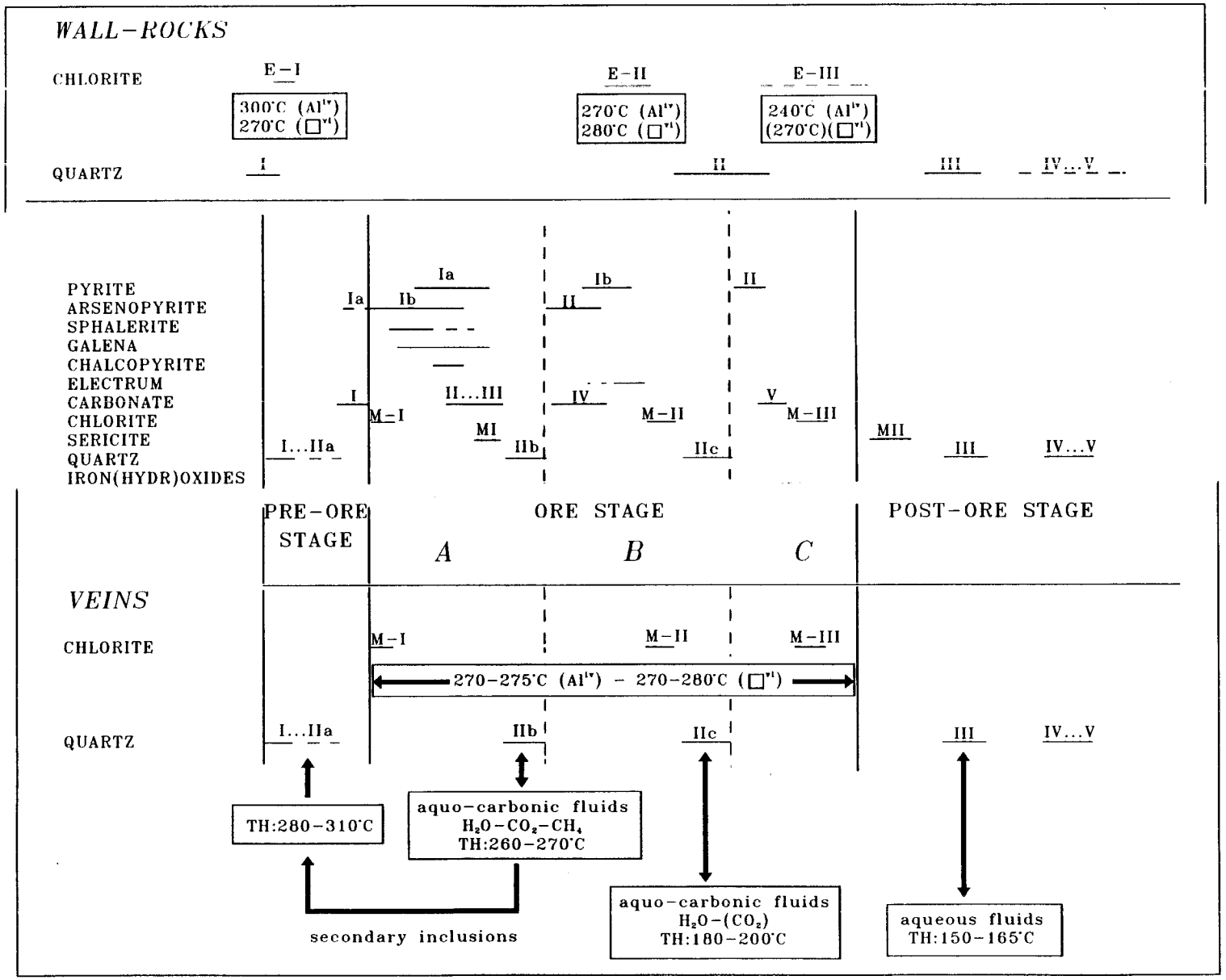

Fig IV - 87 : General comparison of fluid inclusion data and chlorite geothermometry results for the França ore deposit;

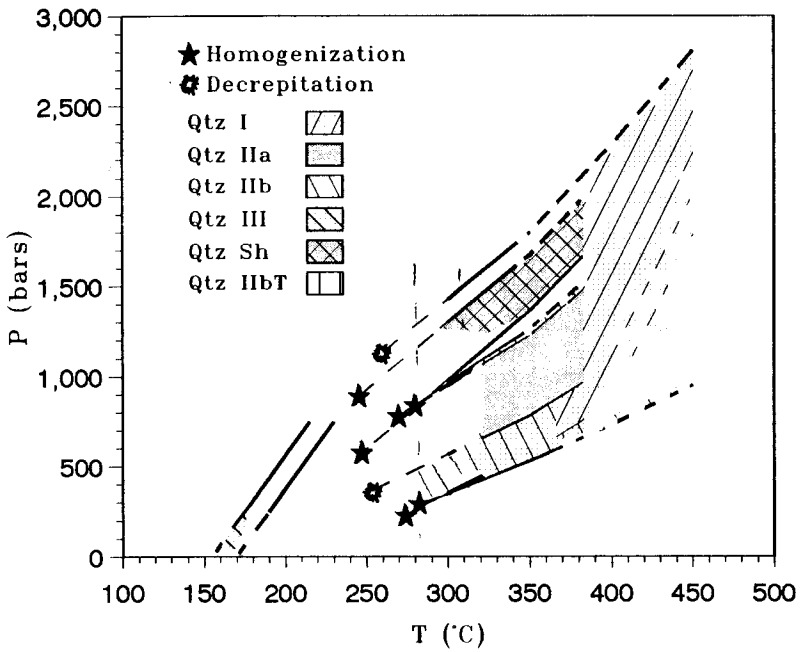

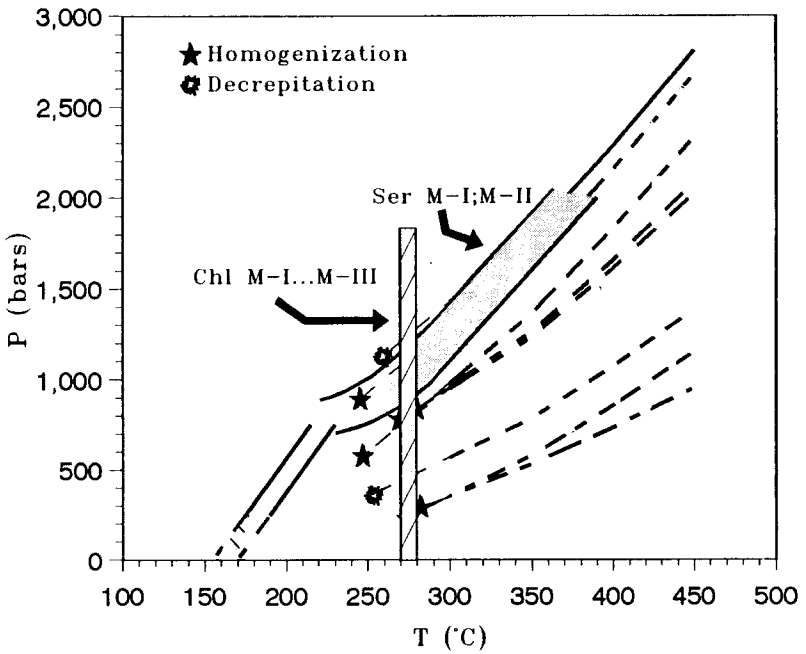

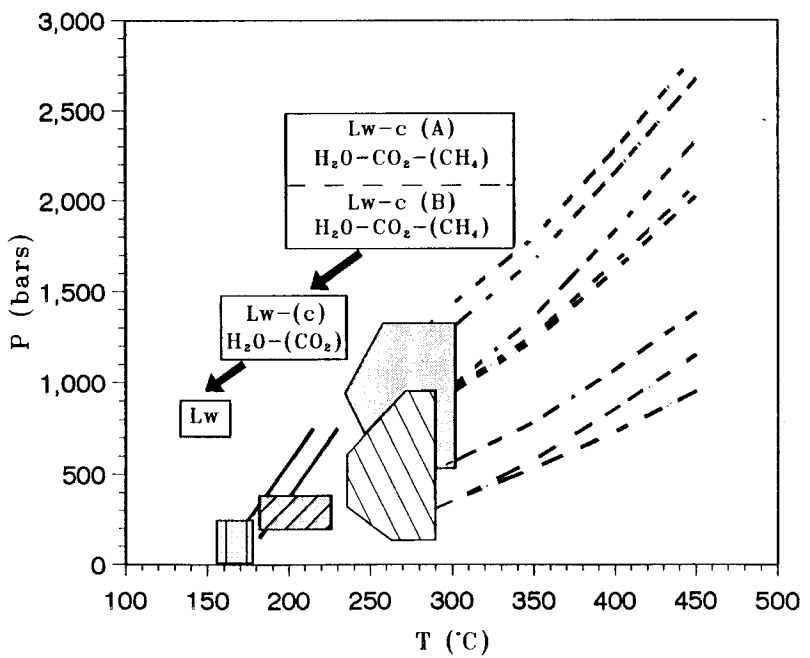

Fig IV - 88 : Pressure - temperature reconstruction of the conditions prevailing in the França area.

with time; chlorites in mineralized veins along regional shears exhibit octahedral vacancies around 0.109 and Al(iv) contents of the order of 1.082 cations per formula unit.
Using the Al(iv) and the octahedral vacancy temperature–dependence equations (see Cathelineau and Nieva, 1985, for details), one may conclude that the T values obtained on the basis of the aluminium content are systematically higher, although never greater than 30°C, from those calculated on the basis of the octahedral vacancy; usually, temperature differences are lower than 10°C. For chlorites in ore samples, the formation temperatures are, in general, quite similar and scattered in the range 270–280°C. Major differences on T values occur for chlorites in altered host rocks, particularly if we take into account the temperatures obtained on the basis of Al(iv) content, and the time sequence of chlorite deposition in that rocks is compatible with a temperature decrease, ranging from 300°C to 240°C. At this point, it should be noted that there is a strong similarity between the estimated formation temperature for chlorites E–II (around 270–275°C) and chlorites M–II (270–280°C). Temperature values ranging from 250 to 260°C are characteristic of chlorites in mineralized quartz veins along regional shear zones.

P-T reconstruction

Good accuracy of temperature estimation on the basis of chlorite chemical composition, is suggested by the comparison between this T values with the ranges of the homogenization temperature of fluid inclusions (Fig. IV-87). This suggests that for the ore stage (QIIb, chlorite MI to III) the pressure corection was relatively low.

The P-T estimate for the ore stages are the followings (Fig. IV-88) :

- IIa : 300-400°C range, pressures around 1000 ± 200 bars, e.g. probably lower than the pressures recorded during stage I (1500± 250 bars).

-IIb (prior to the main stage of electrum deposition) is therefore around 290°C ± 30°C , and 500 ± 100 bars indicating a pressure decrease.

- III : temperature is much lower (180°C ± 15°C), the pressure beeing the same or slighlty lower than during stage IIb.

VILA POUCA DE AGUIAR AREA

The knowledge about the metamorphic conditions on Iberian Massif, supported by the petrographic studies of the area, suggest P-T conditions compatible with a regional metamorphism of intermediate temperature and low pressure on a chlorite zone (300<T<500°C and P~400 MPa). The petrographic studies of organic matter in metasediments suggest temperatures around 300°C. These data are compatible with recent estimations, based on mineral compositions, obtained by Neiva et al. (1990) at Jales area (the granitic area that limits to the south the VPA metasedimentary studied area) suggesting that the syntectonic (relatively to D3 phase) two mica granite was emplaced at ~300 MPa and 690°C and hydrothermally altered at 200 to 400°C and < 100 MPa to 200 MPa. The micaschist was hydrothermally altered at 200 to 480°C and < 100MPa, and the authors reported rock alteration with gold quartz vein deposits. As there are no reasons to admit that all gold mineralizations in gold district of Vila Pouca de Aguiar correspond to the same metallogenic period, we can assume a range of T from 400 to 200°C and P from <100 to 350 MPa as the most probable for the fluid evolution begining with the metamorphic events up to the gold deposition.

On the studied cases the maximum conditions of T - P have occurred during the metamorphic events registered in segregation quartz and in the recristallyzed quartz from the veinlets in black-shales; the TH ranging from 265 to 330°C (with an average of 300°C) constrains the minimal values of P. If we assume a maximum of 400°C, we have the pressure ranging from 200 to 400 MPa (Fig.IV-89) which agrees with the metamorphic conditions known for the area. In the mineralized veins, if we assume that a temperature between 320 (average of TH) and 400°C remained nearly constant during the trapping of the fluids of different densities, the P have changed between 290 and 100MPa during the essential of the vein formation (Fig.IV-89). The gold deposition that occurs associated to latter microfracturing events have probably occured at T~320°C and P<100MPa. The complex tectonic evolution of Três-Minas is well expressed on the variability of fluids densities (Fig. IV-89); the wide density range for CH4-rich fluids can be interpreted as the result of Pf oscilations (Cathelineau et al 1993). However the pressure fluctuated within the ranges already

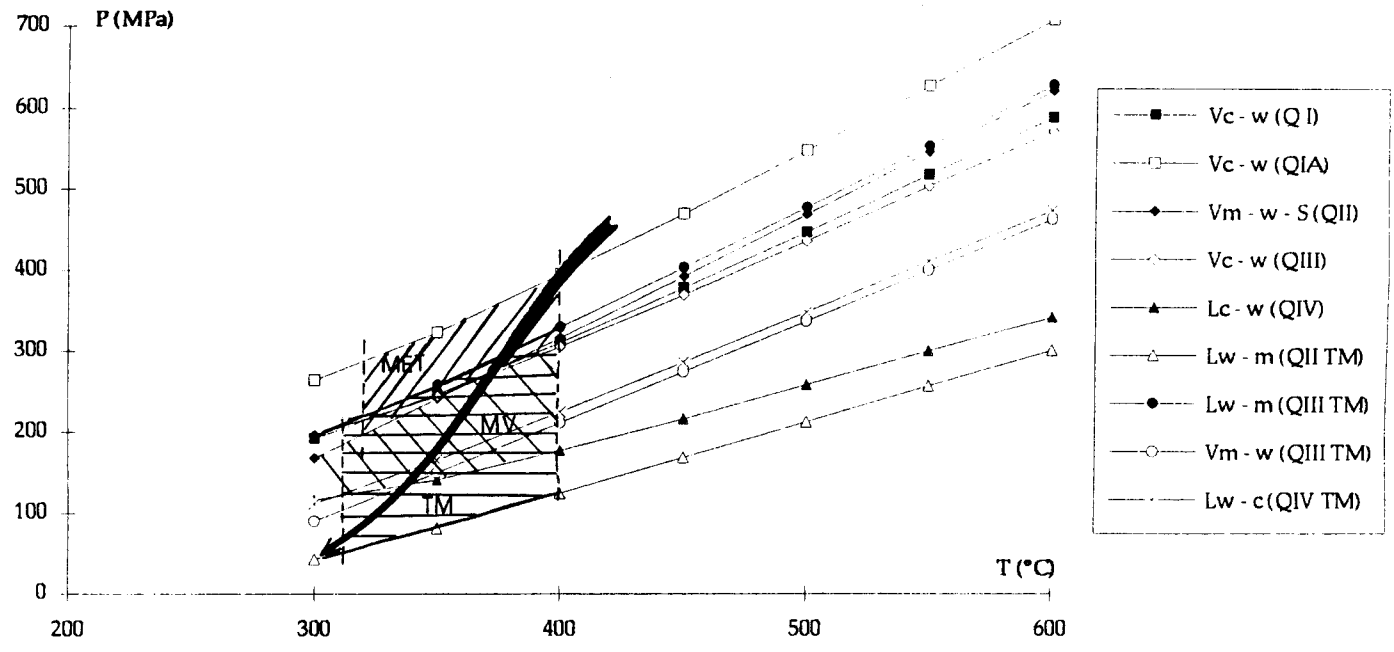

Fig IV - 89 : Pressure - temperature reconstruction of the conditions prevailing in the Vila Pouca de Aguiar area.

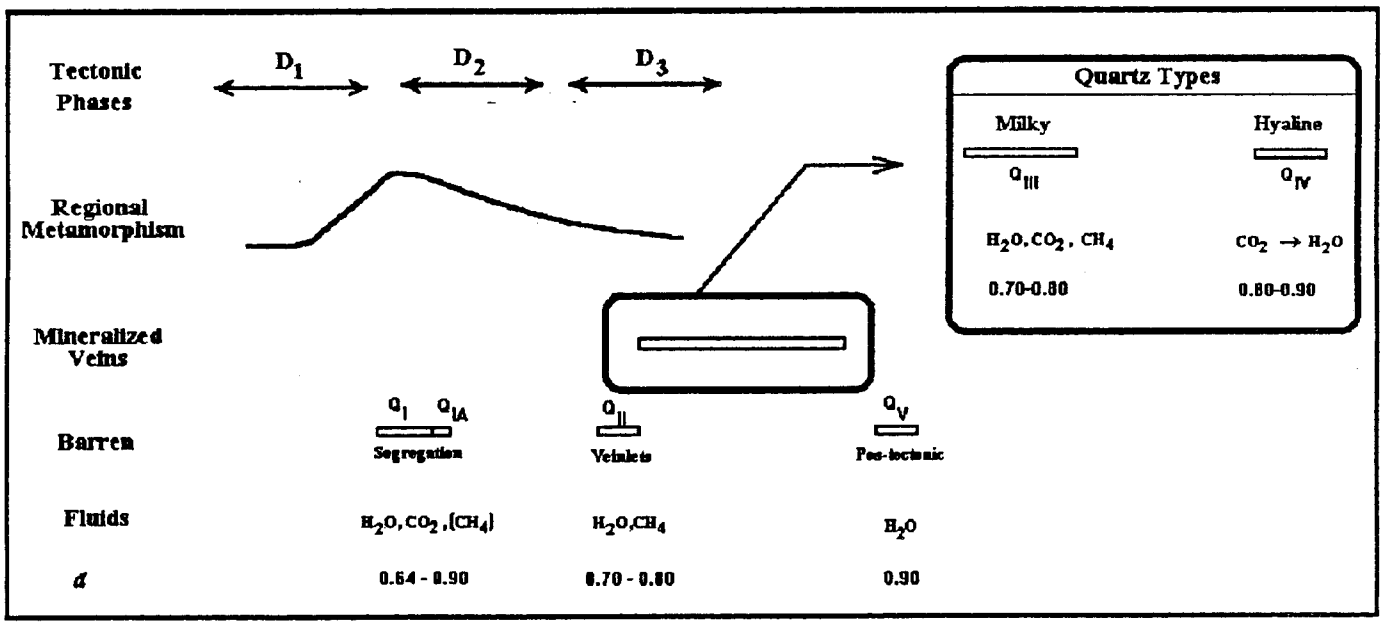

Fig IV - 90 : Fluid evolution in VPA area

indicated for the assemblage of metamorphic and mineralizing events (300 to <100MPa (Fig. IV-89)).

General evolution of the fluids

The studied examples have allowed a good visualisation of the fluid evolution in the course of the geologic history of VPA area (Fig. IV-90).

The fluids comtemporaneous to the metamorphic climax, T~400 C and P~400MPa (Pre- to syn-D2), was dominantly aquo-carbonic (CO2-rich fluids) with a density ranging from 0,6 to 0,9. The later metamorphic fluids, syn-D3, well expressed in veinlets in black-shales had similar densities; in the same time P was already lower (200 to 300 MPa); however in this specific case we can prove the influence of the environment on the fluid compositions (CH4 richness). This influence is still well marked on the earlier fluids, comtemporaneous to the main sulfides deposition, of the mineralized veins and namely at Três-Minas silicified metasediments (P~200MPa). Afterwards, the fluids become dominantly aquo-carbonic (H2O-CO2) and finally, corresponding to a brittle microfracturing, we have the expression of aqueous fluids contemporaneous to the gold deposition.

We must emphasize the importance of the fluids with complex composition (C-H-O fluids) on gold metallogeny because they have certainly a role on gold transport. The gold mineralization only occurs when different fluids are expressed, but the essential of deposition is contemporaneous to the latter episodes characterized by the transition from aquo-carbonic to aqueous fluids.

Três-Minas is considered as an example of a long and continuous fluid evolution, from syn-tectonic and probably metamorphic CH4-rich fluids to late tectonic aqueous fluids, which culminates with gold deposition.

The post-D3 barren veins result exclusively from aqueous fluids attesting a very short fluid evolution.

MONTEMOR AREA

Temperature constraints

K-mica data : the P–T stability fields of dioctahedral K–micas in altered host rocks (I, II), and in migmatites (Mig) on the basis of Si content per formula unit (Velde, 1965) is illustrated on figure IV-86b.

Chlorite data : the highest values of Al(iv) for migmatites were reported, with a range of 0.942 to 1.339 cations per formula unit and an average of 1.123. Simultaneously, these chlorites exhibit the lowest values of octahedral vacancies, with values between 0.038 and 0.934 and an average value of 0.238. In the characteristic chlorites of the wall–rocks, Al(iv) values are in the range 0.301– 1.031 cations per formula unit (both values reported on Ia chlorite). The Al(iv) content shows a tendency to decrease with increasing proximity to the mineralized bodies (averages of 0.930 cations per formula unit, in samples far from the mineralized bodies – Ib – and 0.671 cations per formula unit, in samples collected close to mineralized zones – Ia). This decrease is followed by an increase in octhaedral vacancies from the chlotites Ib (ranging from 0.344 to 0.588, with an average of 0.443) to the chlorites Ia (with values between 0.195 and 1.169, and an average value of 0.607). In chlorites M (ore bodies), the Al allocated to the tetrahedral positions is scattered in the range 1.053–0.833 per formula unit, while the octahedral vacancies show values of 0.598 and 0.403. These ranges are grossly similar to those of chlorites I of the wall–rocks (Ia and Ib). Chlorite T exhibits low Al(iv) (0.657 ions per formula unit), and a high deficiency in octahedral occupancy.

Using the Al(iv) and the octahedral vacancy temperature–dependence equations , one may conclude that some discrepancy exists between the T values calculated both on the basis of the Al content and the octahedral vacancies, with a maximum difference of 50°C for the Ia and T chlorites. For chlorites of ore samples the formation temperatures range, grossly, between 200–240°C, while for T–type chlorite the formation temperature is around 157°C (Al(iv)) or 207°C (octahedral vacancies). For chlorites in wall–rocks the formation temperatures for the Ia family, taking into account the Al occupancies in tetrahedral positions points to 160+45°C,

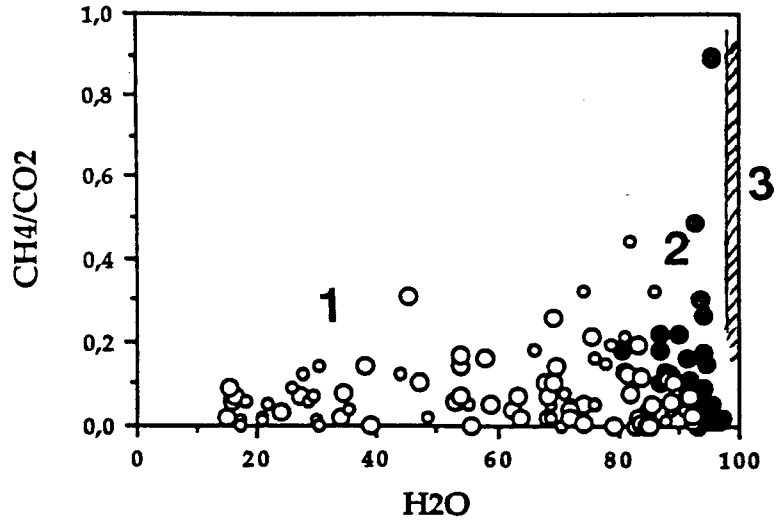

Fig. IV-91 : CH4/CO2 versus H2O diagram applied to individual fluid inclusion composition issued from microthermometric and Raman analyses (Corcoesto, Tomino, Penedono, Pino deposits). 1 : early stages (retrograde metamorphism conditions) - early quartz matrix. 2 : intermediate stage (clear quartz arsenopyrite). 3 : Gold deposition.

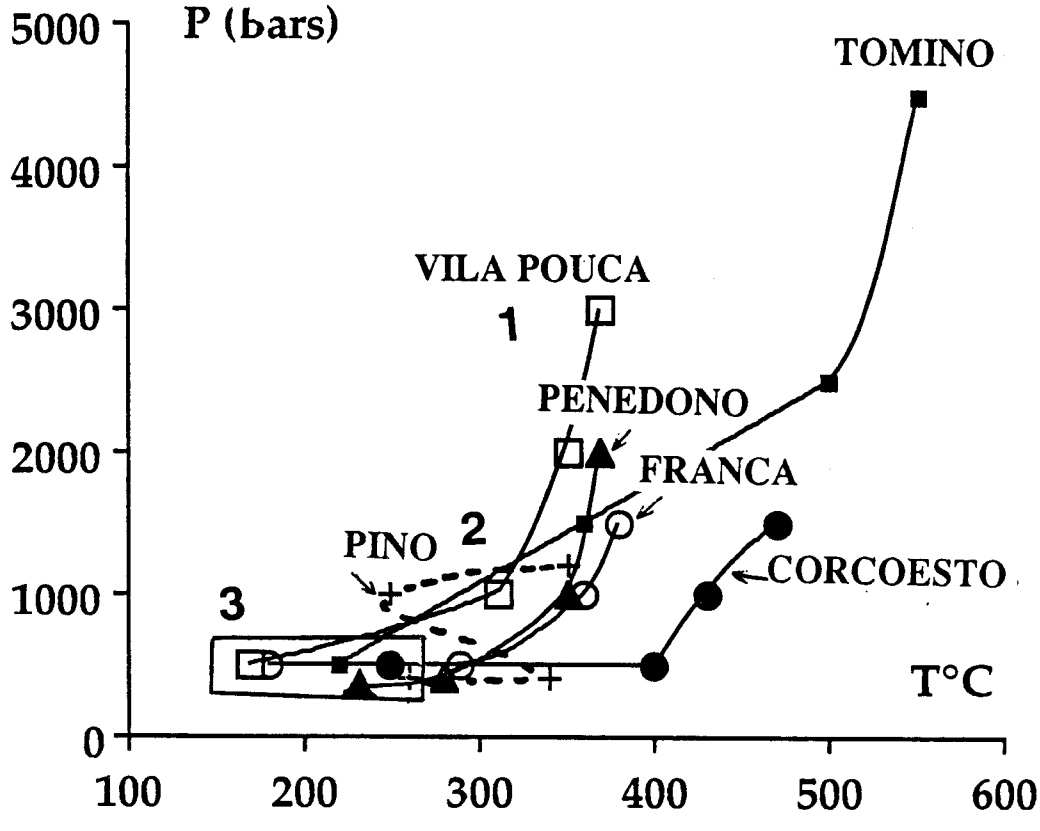

Fig. IV-92 : P - T reconstruction diagram for the studied deposits.
1 : early stages (retrograde metamorphism conditions) - early quartz matrix
2 : intermediate stage (clear quartz arsenopyrite)
3 : Gold deposition.

while for the Ib family the calculated formation temperatures are 215+13°C. The results for chlorites from migmatites (Im) are consistent in both methods, pointing to the highest formation temperatures: 256+24°C.

3 - GENERAL TRENDS OBSERVED IN THE STUDIED DEPOSITS

1 Early stage: formation of milky quartz veins. : milky quartz veins and veinlets formed from early C-H-O-(N) fluids of "metamorphic" derivation . They are dense fluids trapped under pressures above 1Kb (frequently in the 2-4 kb range) and temperatures of 350° to 450°C (ar above at Corcoesto and Tomino). They may be extremely enriched in CH4 and N2, when they mix with fluids produced by the devolatilization of C-rich units (Tomino, VPA, for instance) which are present in most metamorphic series

2 Intermediate stage: Fluids involved in the formation of hyaline quartz (Q2) veinlets or recrystallization zones belong also to the C-H-O-(N) system and are essentially similar to those of the early stage. But at that stage, temperatures range from 250° to 350°C and pressures decreased to 0.5 to 2.0 Kb depending on the localities.

3. Late stage: main gold deposition/enrichment : a renewal of tectonic reactivation (frequently a compressive regime characterized by new specific directions of major stresses) under quite different P-T conditions resulted in the main stage of gold ore deposits formation. The reactivation of early quartz veins (stages 1-2), results in microcracks which were now healed but not sealed by quartz. Native gold deposition took place, together with sulphides and sulphosalts (Pb-Ag dominated), along these cracks, especially when they crosscut earlier sulphides.

Fluids associated with gold deposition are generally aqueous, have relatively low salinities, and were trapped under low temperatures in the 180-250°C range, at nearly hydrostatic pressures (ca. 0.5 kb). They are ubiquitous, were found in all the deposits, but their importance has been largely underestimated in the past as pointed out by Boiron et al.(1990) on the example of the french deposits.

The four figures IV-91 to 94 summarize most of the features of the studied fluids. There are great similarities, at the scale of the studied province, indicating a strong unicity of the processes, from the point of view of the fluid production (e.g. the production zone and related PT conditions), and of the type of fluids able to deposit and transport, first As and then Au.

- transition from lithostatic pressure to hydrostatic pressures, during the major stage of clear quartz-arsenopyrite deposition
- depths around 4-6 km
- progressive dilution of fluids equilibrated with graphite (CHON) by aqueous fluids
- deposition of gold at the ultimate stages of mixing by aqueous fluids

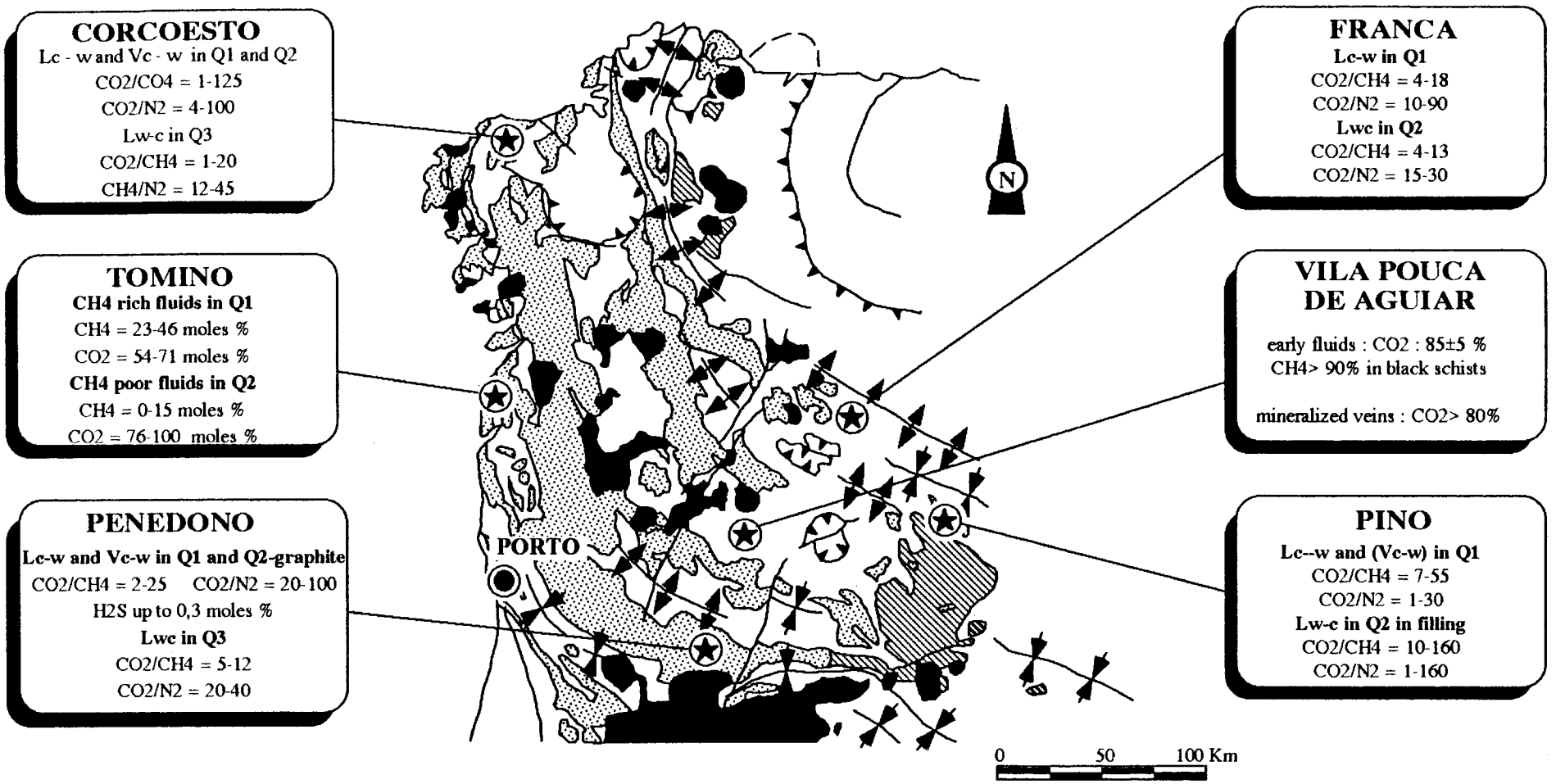

Fig. IV-93 : General comparison of the main chemical features of the CHON components in fluid inclusions (early stages).

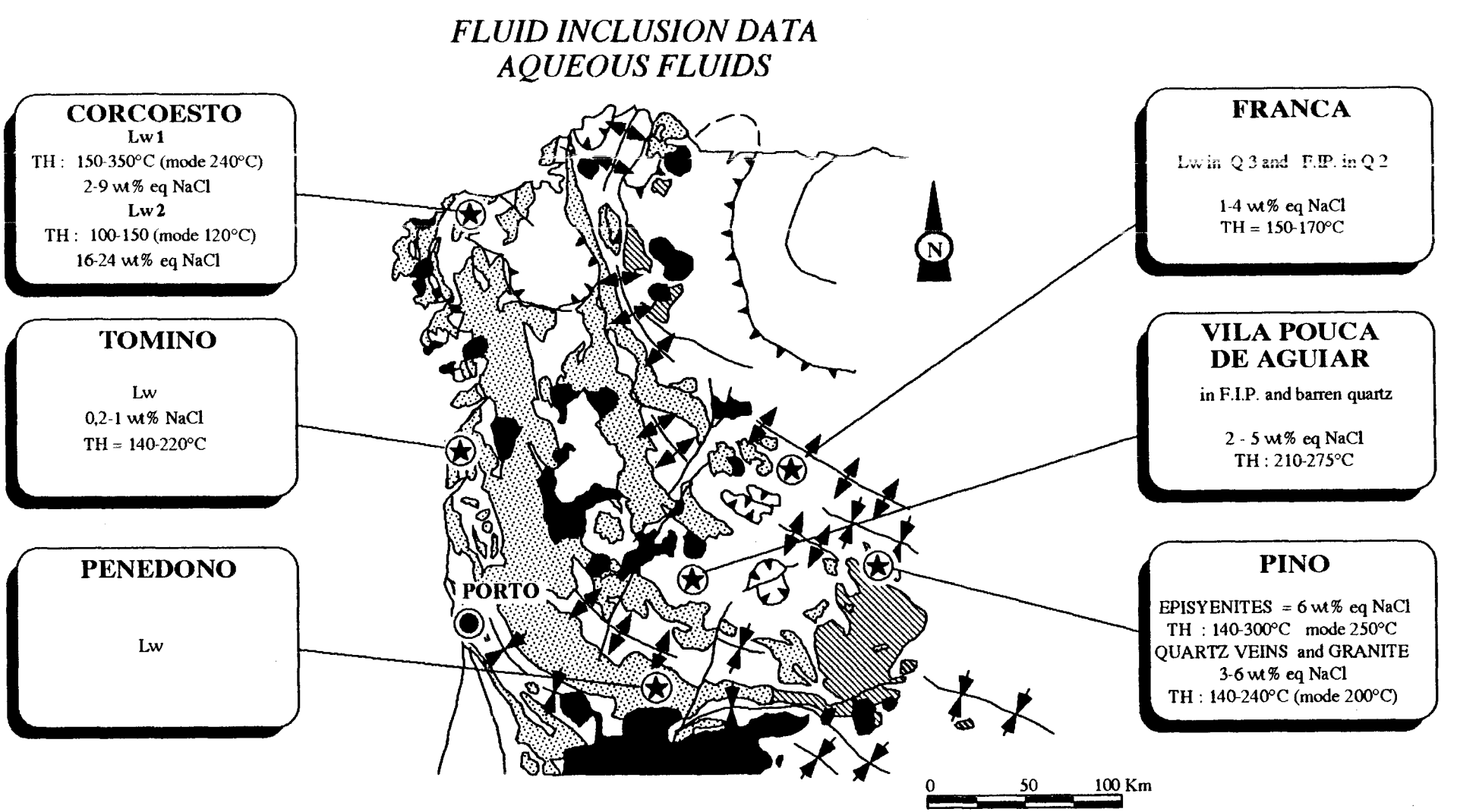

Fig. IV-94 : General comparison of the chemical compositions of aqueous fluids (Gold stage)

E - BULK FLUID INCLUSION VOLATILES

1 - Method.

Fifty two samples of quartz veins from Corcoesto, Tomino, Penedono and Vila Pouca de Aguiar regions have been analysed for their bulk fluid inclusion volatiles, H_2O, CO_2, CH_4 and N_2, using the method described by Shepherd and Miller (1988). Samples of c. 0.2g are heated to 600°C and the volatiles released under vacuum and analysed using a VG Micromass Quadrupole gas mass spectrometer. H_2S is analysed using the method of Bottrell and Miller (1989).The inclusions are decrepitated at 600°C in a stream of N_2 and the H_2S trapped in a NaOH solution. The concentration is determined after the formation and measurement of a fluorescent complex. As the process for liberating the volatiles is identical in both methods it is possible to combine the 2 sets of results.

2 - Results.

Detailed microthermometry and raman analysis has shown that the fluids present in these veins are a complex mixture of H_2O, CO_2, CH_4 and N_2 in a variety of ratios. The bulk analysis of such samples therefore provides an average composition which will only be representative if the different inclusion types are distributed homogeneously within the quartz veins. Multiple analysis (3 - 6) on 4 samples results in relative standard deviations which are generally less than 10% for the aqueous and carbonic components and confirms that the bulk concentrations are true averages of the volatile content of the veins.

Volatile contents of the inclusions presented in Table IV-8 show that the major components are H_2O and CO_2 with lesser CH_4, N_2, which is frequently below detection, and H_2S. The volatile content is quite variable between different samples from the same location ranging from c. 20,000 to 100,000 nmoles per gram of quartz. Covariance between the 2 major components, H_2O and CO_2, would not be expected as they tend to be concentrated in different individual inclusions. This is indeed the case at the 3 locations other than Corcoesto, Figure IV-95, where there is a strong positive correlation between the concentrations of H_2O and CO_2 released from different samples. Covariance between CO_2 and CH_4, Figure IV-96, is observed at Vila Pouca, Corcoesto and Tomino and between CH_4 and N_2 at Tomino, Figure IV-97. The H_2S concentration of samples from Corcoesto and Tomino are quite different. Corcoesto samples have significantly higher concentrations and show a crude positive correlation with CH_4, Figure IV-98, while at Tomino the H_2S concentrations are typically close to the detection limit of the technique. The lack of a correlation with H_2O and the positive correlation with CH_4 indicates that the reduced sulphur is present in the inclusions as H_2S (gas) and not as any reduced sulphur complex in the H_2O phase.

3 - Discussion.

The commonest correlation observed in the bulk volatile data is that between CO_2 and CH_4. This is likely to reflect a relatively narrow range of fO_2 values for the fluids. In many samples the concentration of N_2 is below the limit of detection and it is only at Tomino and Vila Pouca where, with 1 exception, all samples contain N_2 and where there is a positive correlation with CH_4. Its presence is most likely due to the oxidation of NH_3, present in the rocks as NH_4^+ in phyllosilicates, which may have been coupled to oxidation of graphite to CO_2.

In addition to Au mineralisation, other Hercynian and older granites in Iberia, France and SW England contain substantial Sn-W mineralisation. The bulk fluid inclusion volatiles for the deposits of Dartmoor, Bodmin, Carrock Fell, Ballinglen, Montredon, Neuf Jours, Costabonne, Justes and Salau have previously been determined by Shepherd and Miller (1988). They found that there was a strong positive correlation between CO_2 and N_2 and that tungsteniferous fluids were enriched in these 2 components relative to stanniferous fluids. Their data are shown in Figure IV-99 and lie along 2 distinct trends determined by the CO_2/N_2

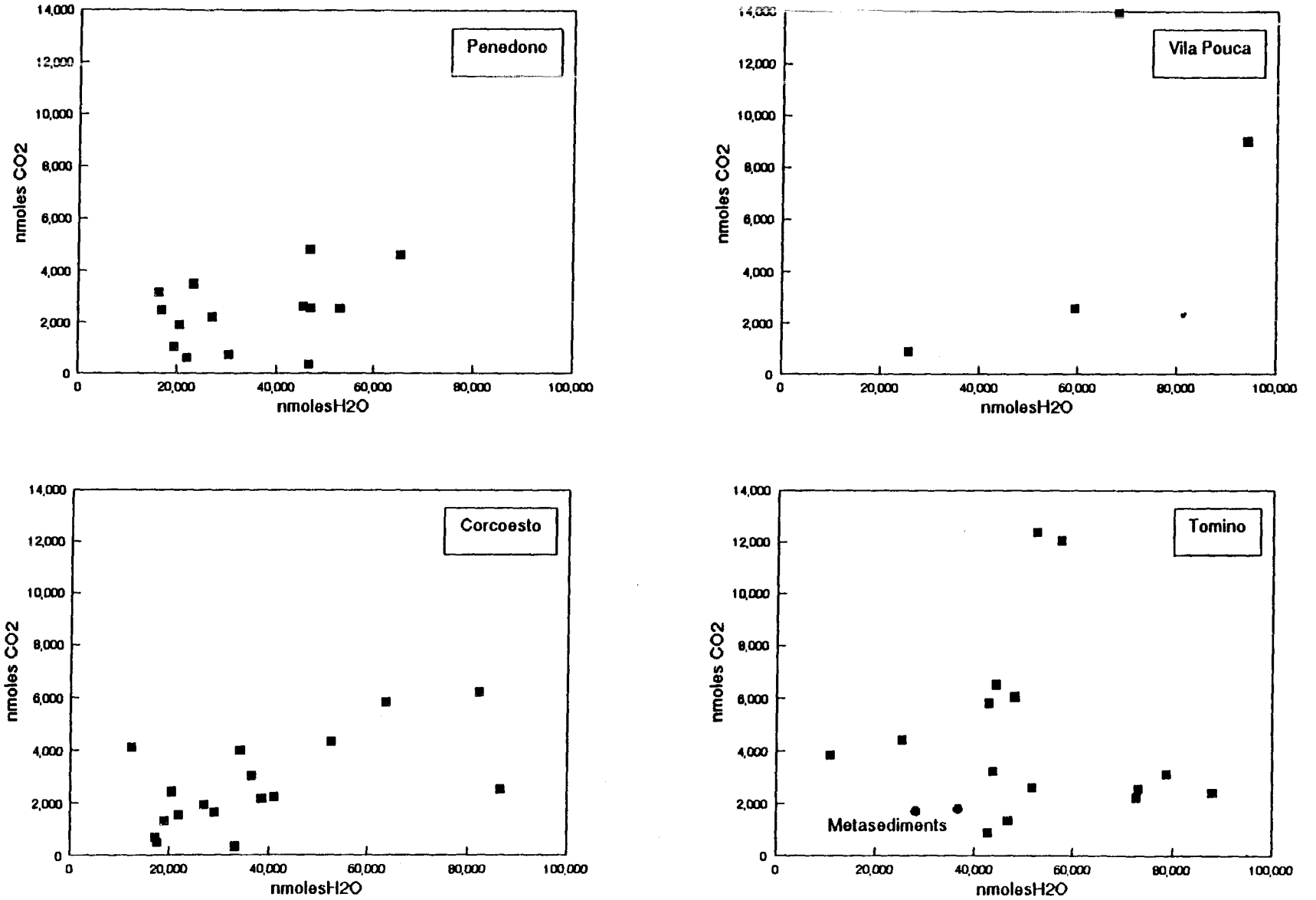

Fig IV - 95· Concentration of H_2O vs CO_2.

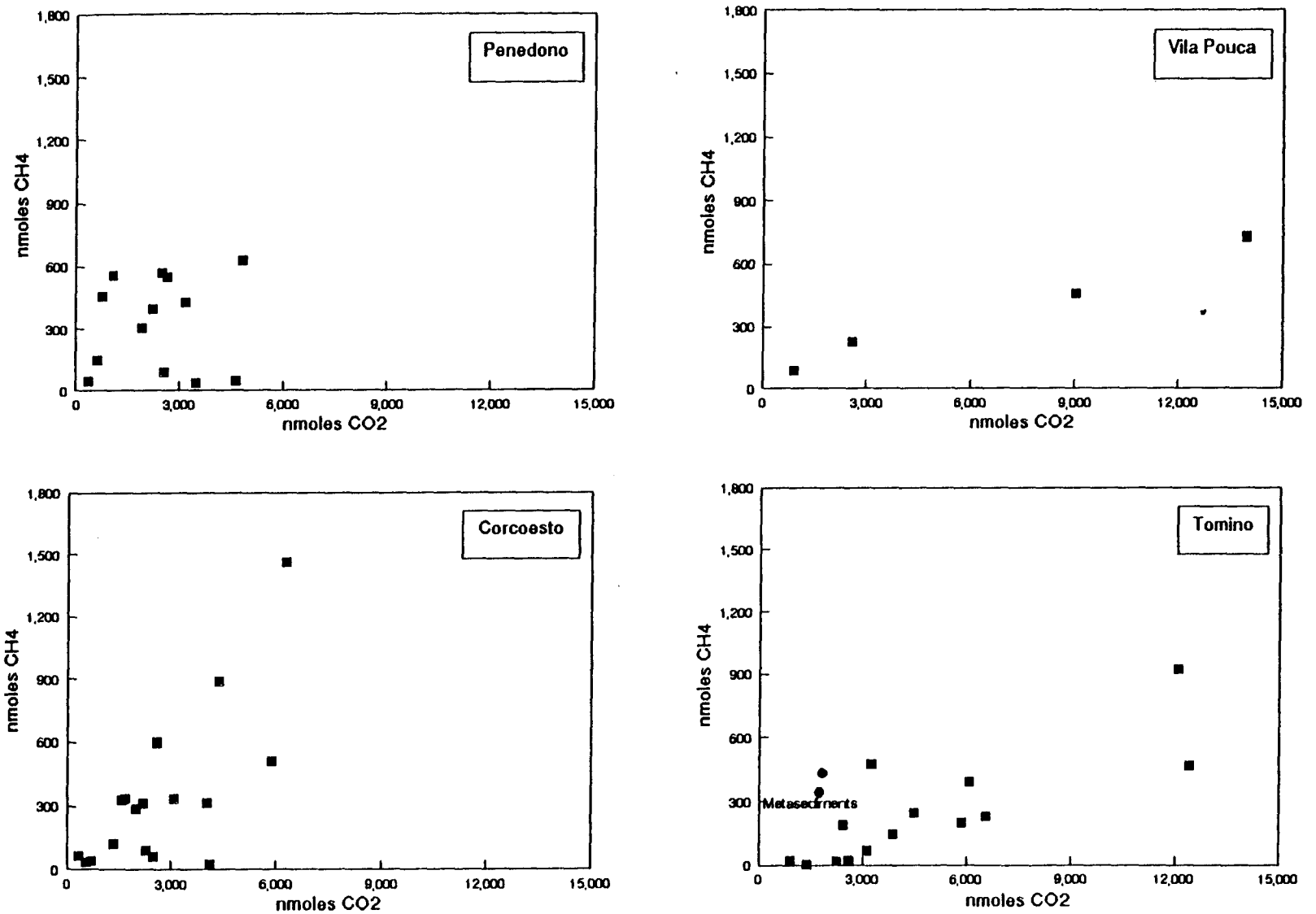

Fig IV - 96 : Concentration of CO_2 vs CH_4.

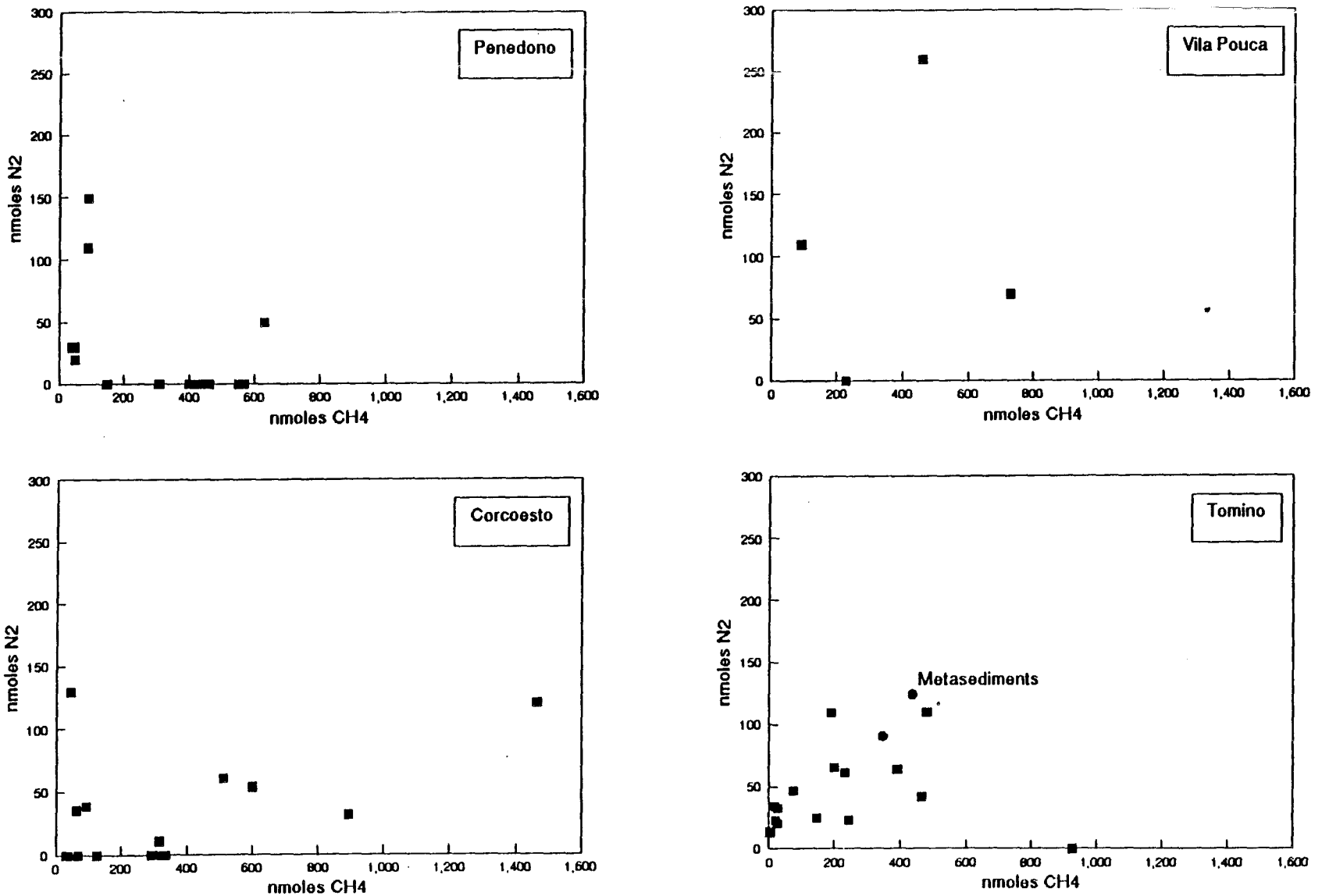

Fig IV - 97: Concentration of CH_4 vs N_2.

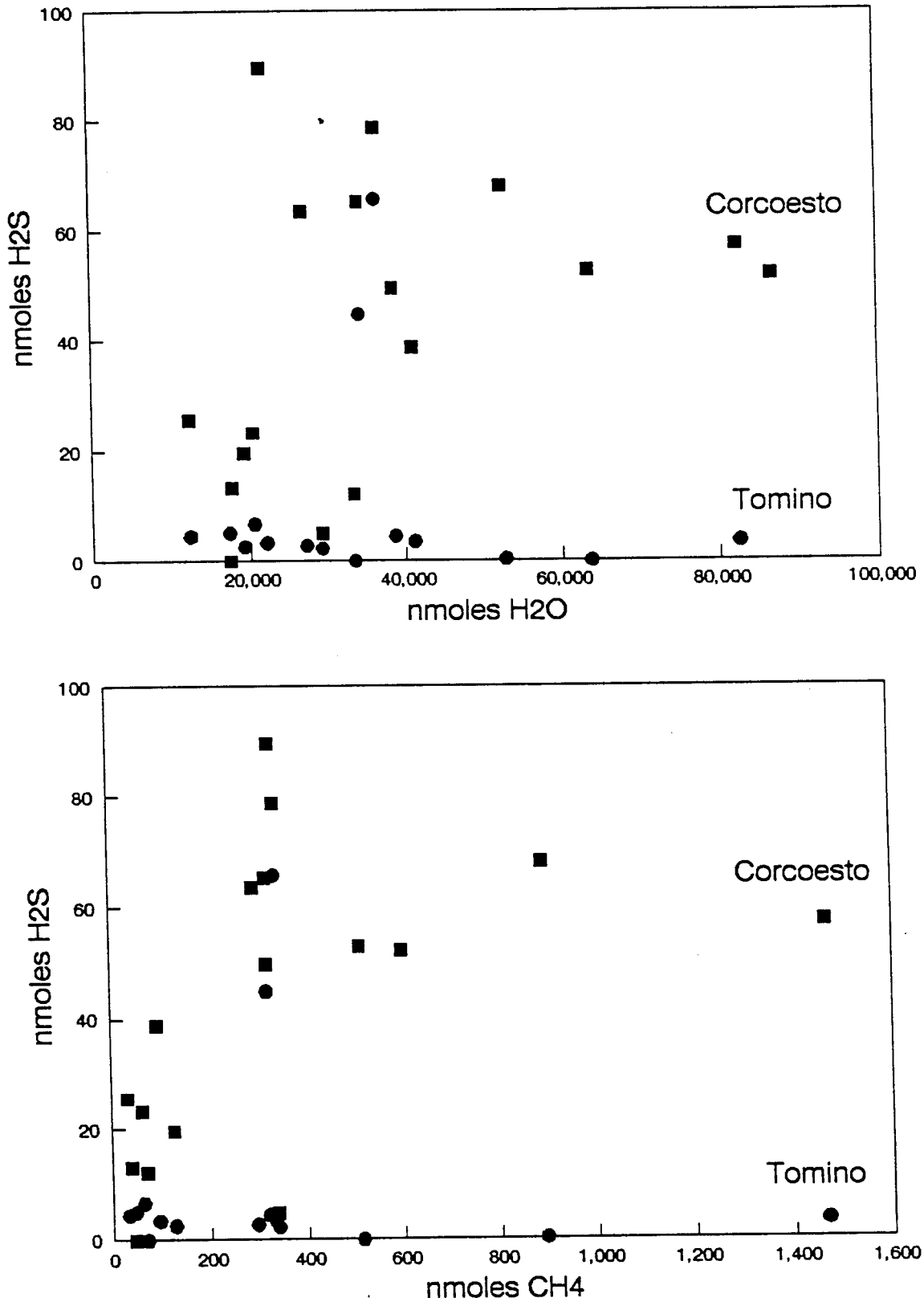

Fig IV - 98: Concentration of H_2O vs H_2S and CH_4 vs H_2S for samples from Tonino and Corcoesto.

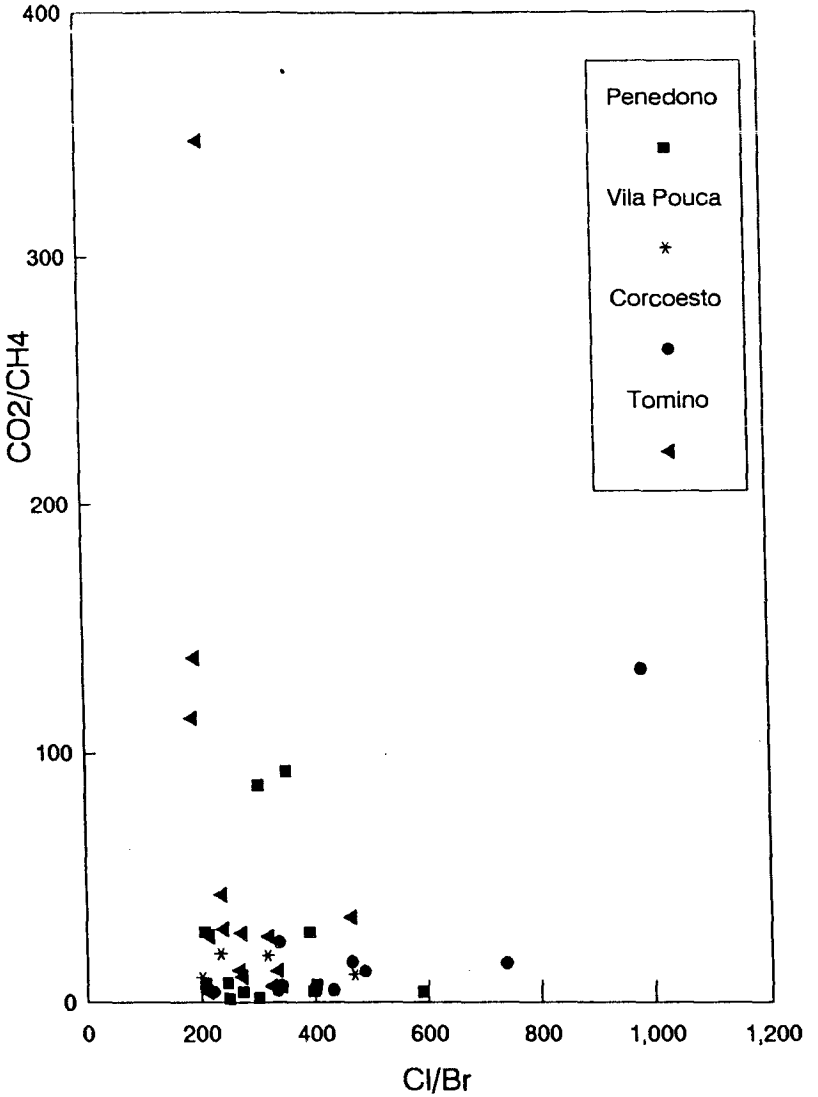

Fig IV -100 : .Cl/Br (crush-leach) vs CO_2/CH_4 (bulk volatiles)

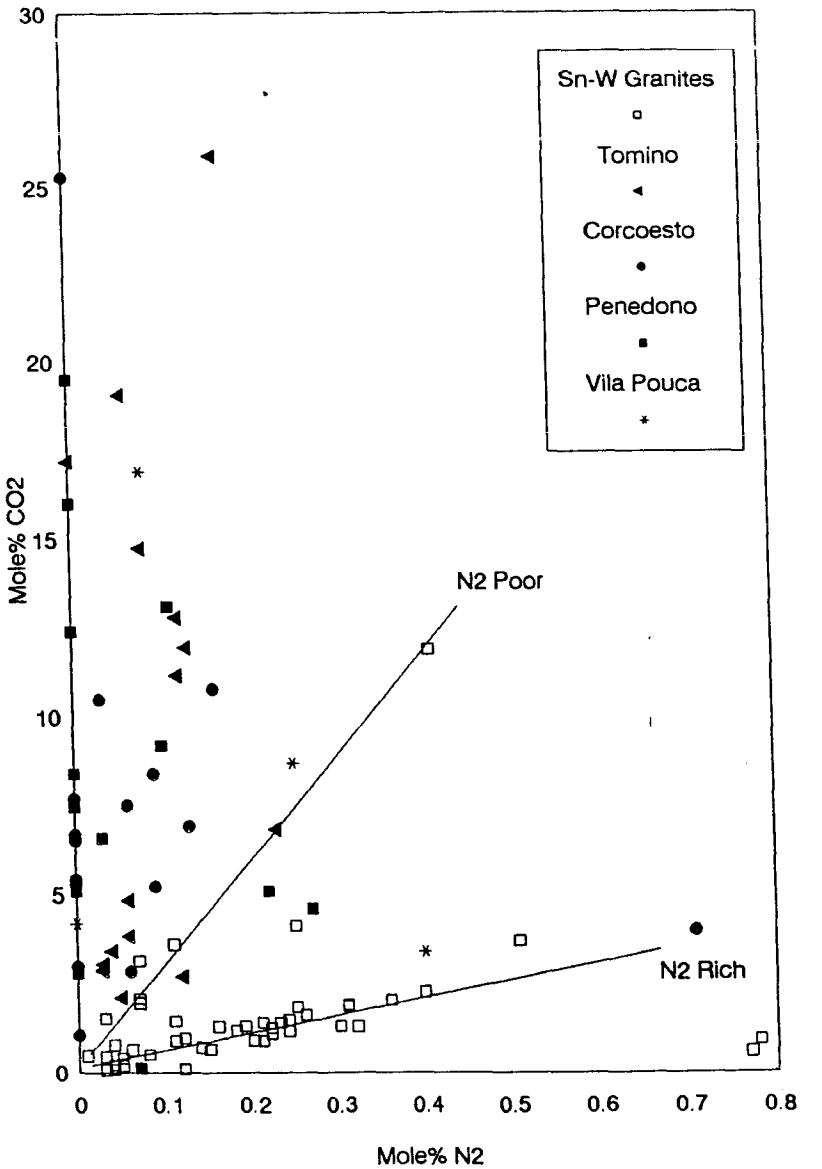

Fig IV - 99 : . Mole % N_2 vs CO_2 (bulk volatiles) of the Iberia Au-granites compared to Sn-W-granites (Shepherd and Miller, 1988).

ratio. The volatile content of the Iberian Au-mineralised granites are distinctly different in that they have elevated CO_2 and depleted N_2 contents relative to the Sn-W granites with almost all the samples lying above the N_2-poor trend. There is no obvious effect related to granite geochemistry, age or location which can account for the observed differences in the gas composition and the conclusion must be that the differences are due to different mineralising systems. Based on dD and $d^{18}O$ measurements, Sn-W precipitation was clearly from "magmatic" fluids whereas Au-mineralisation was clearly not.

F - BULK ELECTROLYTE COMPOSITION

1 - Method

The procedure used is one of crushing bulk samples, c.1g , of cleaned quartz and leaching the contents of the opened inclusions with either double distilled water or acidified lanthanum chloride depending on whether anions or cations are to be analysed. The anions F, Cl, Br, I, SO_4 were analysed using a Dionex ion chromatograph, Na and K were analysed by flame emission spectrometry and the remaining cations, Ca, Mg, Ba, B, Li, Cs, Rb, Sr, Fe, Mn, Pb, Zn, Cu and Bi by inductively coupled plasma mass spectrometry. Full details of the analytical procedure are given in the appendix.

2 - Results

The results of the crush-leach procedures are presented in Tables IV-9 to 12 with the analyses reconstructed to an approximation of the true concentration of the inclusion fluids. This is based on an average salinity of 5 equivalent Wt% NaCl (50000 ppm total dissolved salts) obtained from the microthermometry of individual inclusions. The total of the analysed cations is made equal to the true cation concentration of 19669 ppm (ie. the weight of Na in a 5 Wt.% NaCl solution) and the same multiplication factor applied to the analysed anions. Therefore an approximation of the true fluid composition is obtained. The charge balance (Q^+/Q^-) is obtained by dividing the ppm value of each species by its molecular weight, multiplying by its charge and dividing the sum of the cation charges by the anion charges.

The validity of the analyses obtained from crushing bulk samples is especially difficult to assess where there is more than one fluid present in the inclusions. The detailed microthermometry and raman analysis has shown this to be the situation with the samples used in this study. There are different generations of H_2O-CO_2-CH_4-N_2-salt inclusions but only a single generation of H_2O-salt inclusions, except for Corcoesto where there are 2. However, the observed variations in the aquo-carbonic inclusions are in the relative ratios of the H_2O and the gas species while the salinity remains relatively constant at between 2 and 9 Wt.%. The Cl/Br ratio tends to be conservative in solution and is a good method of detecting different fluids. Combining it with the CO_2/CH_4 ratio, which can be used as a measure of the relative amounts of the variable H_2O-CO_2-CH_4-N_2 fluids in the bulk sample, provides a method for determining if different aqueous fluids were present. In Figure IV-100 there is a factor of 5 variation in the Cl/Br ration of Corcoesto samples which we know to have 2 aqueous fluids present. At Tomino, Penedono and Vila Pouca the variation in Cl/Br is generally only by a factor of 2 while the CO_2/CH_4 ratio varies by several 10's to 100's. Therefore it is probably that, except for Corcoesto, only 1 aqueous fluid was present and the bulk electrolyte composition is that of a relatively homogeneous aqueous fluid component.

3 - Interpretation of the Fluid Inclusion Analyses

There were two reasons for carrying out the programme of fluid inclusion analysis. Firstly we intended to explore the use of halogens as conservative tracer components of the fluid, to identify fluids of common origin and to constrain the source of those fluids. Secondly, we hoped to use the overall geochemical signature of the fluid as an indicator of the types of reactions that had led to ore formation.

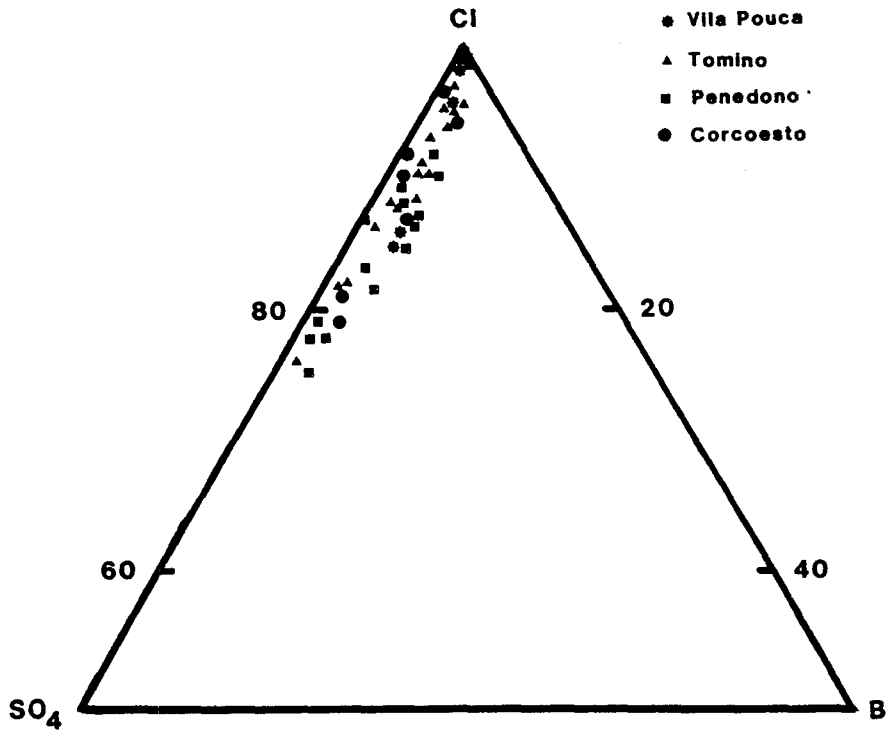

Fig IV -101 : Cl-SO_4-B triangular diagram of the main anionic species in the inclusion fluids.

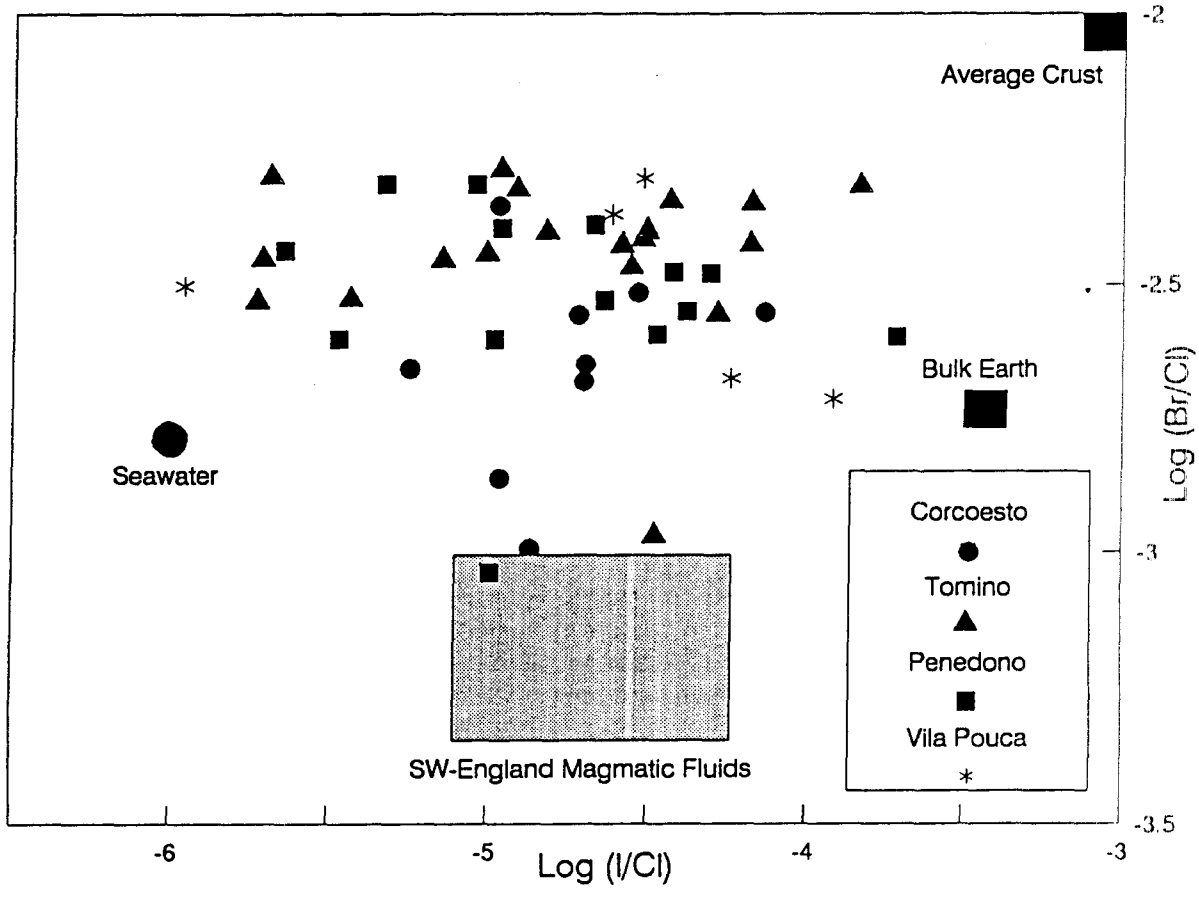

Fig IV - 102 : . Molar Log (I/Cl) vs Log Br/Cl) of the inclusion fluids.

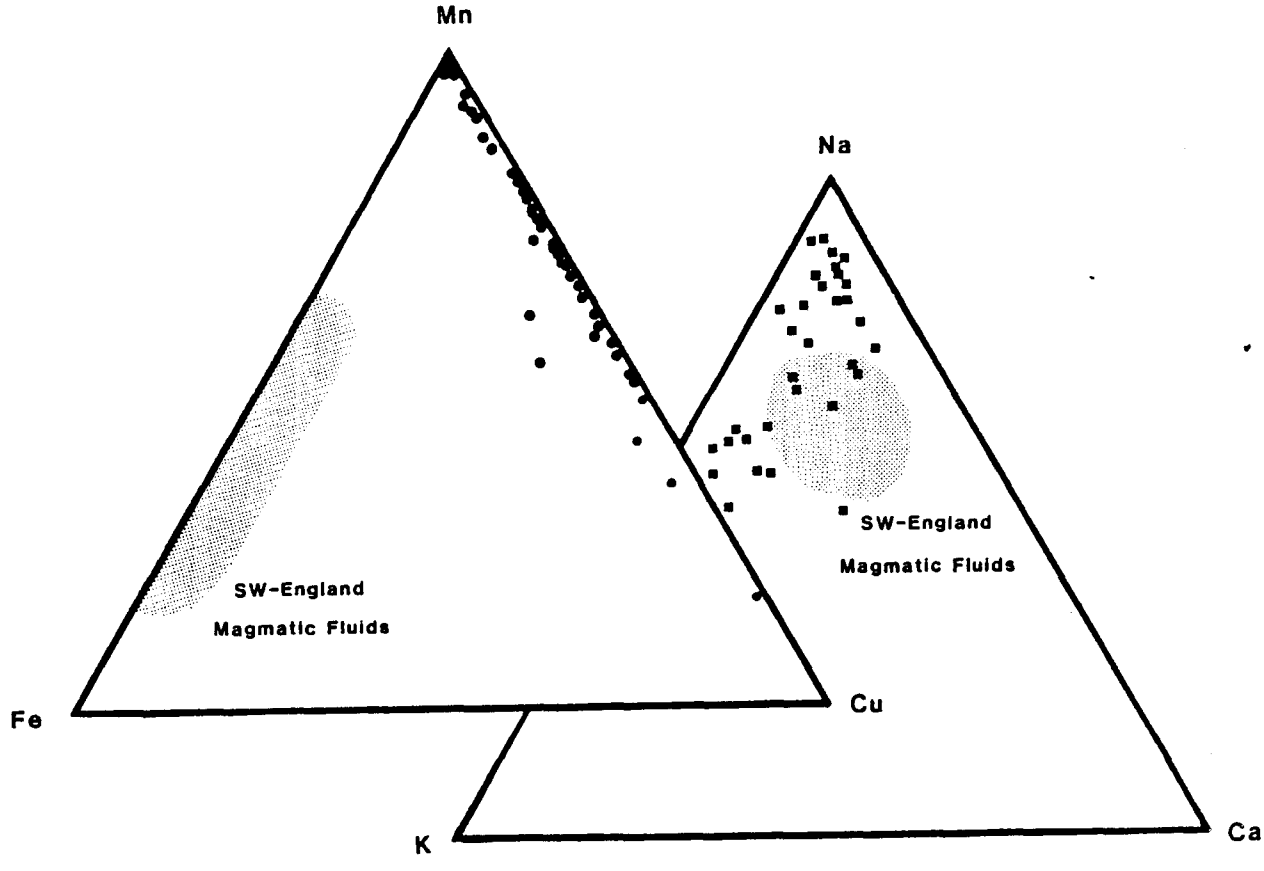

Fig IV - 103 : Na-K-Ca and Mn-Fe-Cu triangular diagrams of the Au-granites compared to SW England Sn-W-granites.

Bulk Fluid Inclusion Volatile Analyses										
Penedono Region	nmoles/g Quartz					Mole % Volatiles				
	H_2O	CO_2	CH_4	N_2	H_2S	H_2O	CO_2	CH_4	N_2	H_2S
St.Antonio-Laboreira -4	30400	747	460	0		79.3	19.5	1.2	0	
-5	16230	3180	430	0		81.8	16.0	2.2	0	
-7	16900	2470	570	0		84.8	12.4	2.9	0	
-8	46800	4820	630	50		89.5	9.2	1.2	0.10	
-9	22050	640	150	0		96.5	2.8	0.66	0	
-10	45560	2640	550	0		93.5	5.4	1.1	0	
-10a	27060	2210	400	0		91.2	7.5	1.4	0	
-11	19390	1070	560	0		92.2	5.1	1.6	0	
-12	20500	1910	310	0		90.2	8.4	1.4	0	
Ferronha -13	47000	2550	90	110		94.5	5.1	0.18	0.22	
-13a	23220	3500	40	30		86.7	13.1	0.15	0.11	
-13b	65220	4640	50	20		93.3	6.6	0.07	0.03	
Dacotim -1	46670	360	50	30		99.1	0.13	0.11	0.07	
-2	53000	2550	90	150		95.0	4.6	0.16	0.27	
Vila Pouca Region										
Vale de Egua	67800	13940	730	70		82.1	16.9	0.88	0.08	
Valhaquinhas	59400	2590	230	0		95.5	4.2	0.37	0	
Segregation veins	25800	910	90	110		95.9	3.4	0.33	0.40	
Vale de Campo	94000	9030	460	260		90.6	8.7	0.44	0.25	
Corcoesto (Drillhole 6281, m-cm)										
110-50	21850	1571	330	0	89.7	91.6	6.6	1.4	0	.04
181-80	40914	2271	93	39	38.8	94.4	5.2	0.21	0.09	.09
211-00/10	20320	2470	62	36	23.3	88.7	10.8	0.27	0.16	.10
323-30/40	34080	4040	318	11	65.3	88.5	10.5	0.83	0.03	.17
330-70/80	28957	1680	336	0	4.9	93.5	5.4	1.1	0	.02
348-30/50	63504	5881	511	61	52.9	90.7	8.4	0.73	0.09	.08
371-50/60	36367	3070	337	0	78.8	91.3	7.7	0.85	0	.20
372-40/60	26917	1960	293	0	63.6	92.1	6.7	1.0	0	.21
419-50/65	52538	4359	891	32	68.1	90.8	7.5	1.5	0.06	.12
419-75/80	82304	6259	1465	121	57.5	91.2	6.9	1.6	0.13	.06
464-30/50	17547	544	37	0	13.2	96.7	3.0	0.20	0	.07
527-60/80	33159	356	69	0	12.2	98.7	1.1	0.21	0	.04
551-30/50	38461	2170	318	0	49.7	93.8	5.3	0.78	0	.12
643-45-60	19050	1340	126	0	19.6	92.8	6.5	0.61	0	.10
678-80/679-00	12179	4140	31	0	25.6	75.4	25.3	0.19	0	.16
Outcrop										
Cor-2	86700	2570	600	54	52.2	96.4	2.9	0.67	0.06	0.06
Cor-10	17200	720	45	130	0	95.1	4.0	0.25	0.82	0

Table IV - 8 : Bulk fluid inclusion volatile analyses for Penedono, Vila Pouca, Corcoesto and Tomino areas.

Bulk Fluid Inclusion Volatile Analyses										
Tomino	nmoles/g Quartz					Mole % Volatiles				
Drillhole (m-cm)	H_2O	CO_2	CH_4	N_2	H_2S	H_2O	CO_2	CH_4	N_2	H_2S
T5 115-05	43600	3250	480	110	3.3	91.9	6.9	1.0	0.23	0.007
T5 115-45	46700	1390	4	14	3.5	97.1	2.9	0.01	0.03	0.007
T8 24-60	47890	6080	391	64	6.7	88.0	11.2	0.71	0.12	0.012
T8 194-60	42780	5850	200	66	44.9	87.4	12.0	0.41	0.13	0.092
T8 210-00	78770	3150	73	47	2.3	96.0	3.8	0.09	0.06	0.003
T9 190-30	88000	2460	190	110	0	97.0	2.7	0.20	0.12	0
T9 192-90	10830	3870	146	25	65.8	72.5	25.9	0.98	0.17	0.44
T12 155-45	51610	2630	19	35	2.8	95.1	4.8	0.03	0.06	0.005
T12 155-70	72800	2280	20	23	0.3	96.9	3.0	0.03	0.03	0.0004
T12 275-45	42560	920	27	21	3.5	97.8	2.1	0.06	0.05	0.008
Outcrop										
Tom-a	25500	4460	246	23	0	84.4	14.8	0.81	0.08	0
Tom-b	52110	12400	467	42	4.5	80.1	19.1	0.71	0.06	0.007
Tom-c	44280	6540	234	62	2.6	86.6	12.8	0.46	0.12	0.005
Locn.41	57170	12070	928	0	4.5	81.5	17.2	1.32	0	0.006
53930	73110	2600	28	33	0.3	96.5	3.4	0.04	0.04	0.0004
Metasediments										
GR-1	28220	1750	347	91	5.1	92.8	5.8	1.1	0.30	0.017
GR-2	36720	1830	436	124	1.3	93.9	4.7	1.1	0.32	0.003

Table IV- 8 (cont.)

Corcoesto Region Reconstructed Fluid Inclusion Compositions (ppm)								
	Drillcore (Hole 6281)							Outcrop
	181-80	323-30/40	330-70/80	419-70/80	464-30/55	527-00	551-30/50	Cor-10
Na	11783	11121	7490	15796	10376	8419	11939	6486
K	5320	6314	8795	1880	6161	9679	4961	11415
Ca	2044	(1482)	(1510)	1404	2335	(994)	(1938)	994
Mg	52	235	918	112	211	152	295	130
Ba	bd	25	133	bd	bd	33	bd	bd
Li	70	25	36	38	32	20	31	86
Sr	121	136	133	88	146	106	155	65
Rb	52	25	73	13	65	67	46	151
Cs	34	25	12	25	32	13	31	21
Fe	bd	12	bd	bd	bd	bd	bd	bd
Mn	156	210	363	163	259	113	217	303
Pb	bd	bd	121	bd	bd	7	bd	bd
Zn	bd	bd	bd	bd	bd	bd	bd	bd
Cu	52	76	96	163	65	79	62	21
Bi	bd	bd	3	bd	bd	bd	6	11
B	260	420	242	526	81	73	450	130
F	bd	914	302	bd	bd	551	bd	bd
Cl	16941	13517	8976	19796	19519	16616	21087	23564
Br	113	62	61	201	92	87	140	72
I	1.81	0.25	2.42	0.76	1.29	1.20	1.40	0.9
SO_4	1666	1557	2126	765	1685	456	4558	bd
Q^+/Q^-	1.31	1.30	1.90	1.15	1.25	1.30	0.96	0.94

bd. Below the detection limit.
Values in ( ) are subject to greater uncertainty than the other analyses.

Table IV - 9 : Reconstructed fluid inclusion composition - Corcoesto area

Penedono Region
Reconstructed Fluid Inclusion Compositions (ppm)

	St. Antonio-Laboreira									Dacotim		Ferronha		
	4	5	7	8	9	10	10a	11	12	1	2	13	13a	13b
Na	14162	11653	12064	15258	7086	10908	10842	6304	7793	13788	7519	12036	9633	12072
K	3079	3496	1056	1781	2362	1850	4844	7656	6829	3011	3619	3661	5478	1155
Ca	462	1568	2888	966	2795	2751	2711	3197	1966	1107	4183	2000	2493	3044
Mg	1109	2241	1357	1195	1339	901	542	450	2550	1125	536	1000	548	682
Ba	31	bd	227	bd	1142	545	24	45	22	36	611	102	114	342
Li	184	90	151	2.3	118	119	189	180	87	91	188	102	114	105
Sr	31	90	76	26	197	71	24	23	43	54	141	51	75	78
Rb	bd	44	37	bd	197	47	bd	bd	43	36	94	34	57	27
Cs	92	44	37	76	157	71	24	45	22	54	47	51	57	52
Fe	bd	44	bd	bd	79	bd	bd	bd	bd	bd	bd	bd	bd	27
Mn	462	269	679	179	709	356	353	293	108	109	423	203	283	577
Pb	bd	bd	1132	bd	2047	949	bd	202	bd	145	2021	323	548	1076
Zn	bd	bd	bd	bd	157	261	bd	698	bd	bd	bd	bd	bd	27
Cu	61	134	528	bd	945	664	118	586	216	36	282	119	246	420
Bi	10	9	bd	bd	354	190	12	4	5	91	19	bd	38	bd
B	585	269	717	966	118	356	401	383	108	598	235	610	529	315
F	bd	bd	bd	bd	bd	bd	bd	671	122	bd	bd	bd	bd	43
Cl	24569	29088	15043	23371	14212	17264	14613	10584	19945	23749	16447	18174	15111	15510
Br	222	317	124	215	55	98	82	79	132	134	180	105	113	99
I	0.92	0.44	0.11	1.79	0.4	11.86	0.24	1.35	1.73	0.91	0.47	2.2	2.65	2.37
SO_4	6250	3173	2051	2620	3829	3154	4407	1991	3004	2631	4093	1389	1738	1134
Q^+/Q^-	0.86	0.92	1.27	0.91	1.42	1.23	1.33	1.53	1.27	0.95	1.22	1.17	1.26	1.50

bd. Below the detection limit

Table IV - 10 : Reconstructed fluid inclusion composition - Penedono area

Tomino Region

Reconstructed Fluid Inclusion Compositions (ppm)

	Drillcore												Outcrop			
	T5			T8				T9		T12						
	104-30	115-05	115-45	24-60	104-30	194-60	210-00	190-45	192-90	155-45	155-70	275-65	Tom b	Tom c	loc. 41	GR-2
Na	10125	9389	13123	15509	11277	11088	13238	9350	13315	14706	14104	9935	10896	16607	15304	16500
K	2855	5821	1357	1312	6079	5976	1091	7756	2860	1244	1649	7097	1765	1513	1928	1218
Ca	2582	730	1674	1408	1569	1017	(2433)	(1274)	1603	1832	1649	1041	2623	296	1195	1035
Mg	587	626	634	834	319	369	1947	468	321	724	1410	615	384	181	631	419
Ba	142	31	91	bd	bd	bd	195	127	bd	113	bd	48	171	bd	bd	53
Li	81	73	68	96	48	92	58	95	99	68	65	94	111	279	90	53
Sr	41	31	91	71	48	62	98	42	75	113	87	48	40	33	90	157
Rb	20	31	bd	bd	bd	bd	bd	22	25	bd	21	bd	21	17	12	bd
Cs	41	41	22	23	48	31	20	32	25	22	44	48	31	66	38	40
Fe	10	10	0	48	bd	bd	bd	bd	bd	bd	bd	bd	21	bd	bd	bd
Mn	2531	2608	2556	214	98	154	331	340	1355	860	652	615	2805	262	269	170
Pb	20	21	22	bd	bd	62	38	22	bd	bd	bd	48	31	66	bd	bd
Zn	152	bd	bd	bd	bd	bd	bd	53	bd	bd	bd	bd	303	bd	bd	bd
Cu	263	229	45	143	48	62	156	96	bd	bd	bd	bd	484	33	116	40
Bi	233	41	bd	23	147	770	78	6	5	bd	3	94	bd	329	8	bd
B	233	208	135	453	98	154	253	159	321	159	130	48	323	362	488	485
F	648	bd	136	bd	3237	bd	bd	5079	112	bd	bd	3477	100	1204	26	bd
Cl	16889	15147	17377	17299	10885	19713	18398	12346	15940	19683	24638	14762	17291	16690	16731	17807
Br	182	105	181	143	98	184	175	107	112	226	292	72	181	138	141	188
I	0.2	0.21	10.37	1.68	0.98	4.3	0.87	0.43	2.96	0.91	0.97	2.14	4.03	0.4	1.81	2.36
SO_4	608	3087	1176	1909	3260	bd	1520	510	1479	2444	3644	3193	464	791	1428	48
Q^+/Q^-	1.37	1.37	1.51	1.33	1.33	1.24	1.46	1.10	1.42	1.34	1.10	1.11	1.38	1.30	1.33	1.33

bd. Below the detection limit.

Value in ( ) subject to greater uncertainty than the other analyses.

Table IV - 11 : Reconstructed fluid inclusion composition - Tomino area

Vila Pouca de Aguiar Region Reconstructed Fluid Inclusion Compositions (ppm)				
	Vale de Egua	**Vale de Campo**	**Valhaquinhas**	**Segn. Veins**
Na	16699	15030	15736	9376
K	1144	1273	949	1959
Ca	618	1112	1474	(1528)
Mg	449	1852	749	5695
Ba	139	bd	bd	153
Li	32	51	124	21
Sr	77	68	76	181
Rb	bd	bd	bd	bd
Cs	15	17	25	7
Fe	bd	bd	bd	bd
Mn	32	179	200	263
Pb	324	bd	124	167
Zn	bd	bd	bd	76
Cu	155	102	225	257
Bi	bd	bd	bd	bd
B	665	407	724	41
F	bd	bd	76	bd
Cl	20378	26416	19658	37810
Br	145	254	94	423
I	0.08	2.3	4.25	4.10
SO_4	2628	839	2648	462
Q^+/Q^-	1.03	1.04	1.08	0.95

bd. Below the detection limit.
Value in ( ) subject to greater uncertainty than other analyses.

Table IV - 12 : Reconstructed fluid inclusion composition - Vila Pouca de Aguiar area

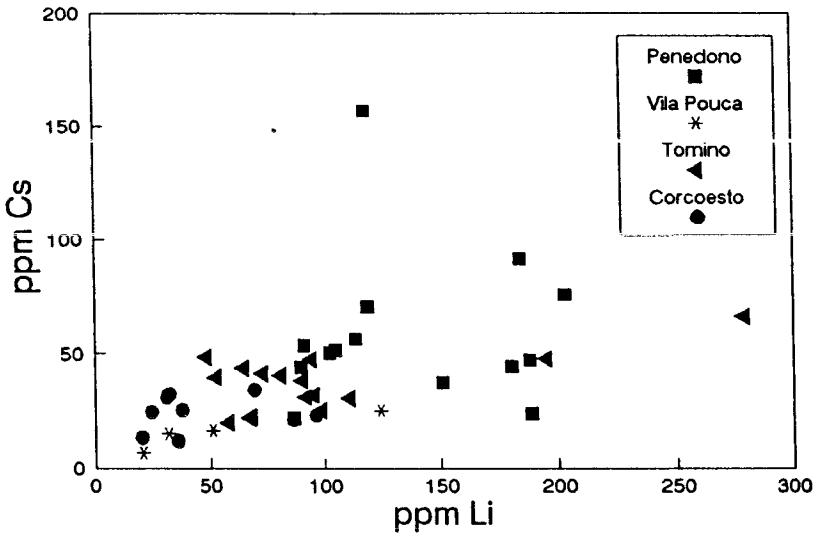

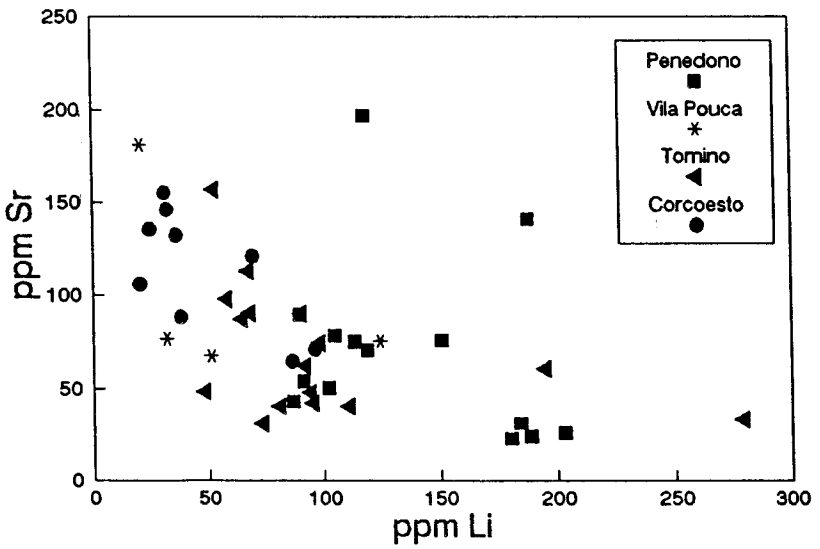

Fig IV - 105 : ppm Li vs ppm Cs and ppm Li vs ppm Sr of the reconstructed fluid inclusion compositions.

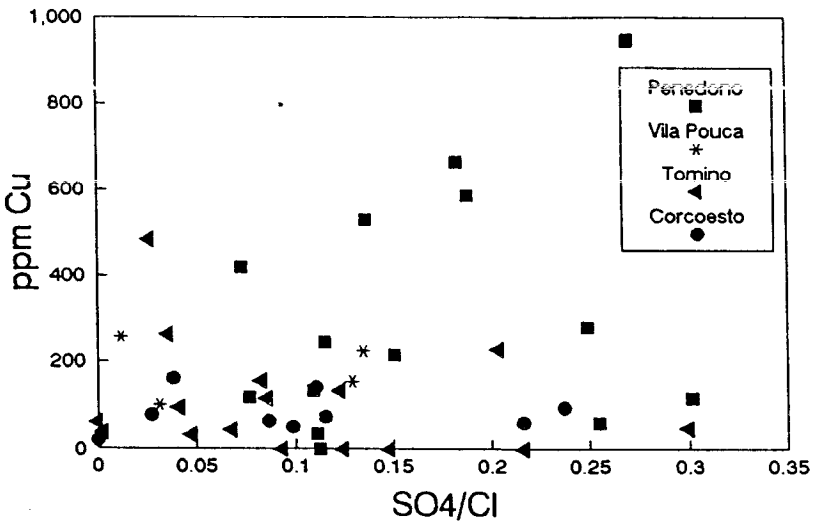

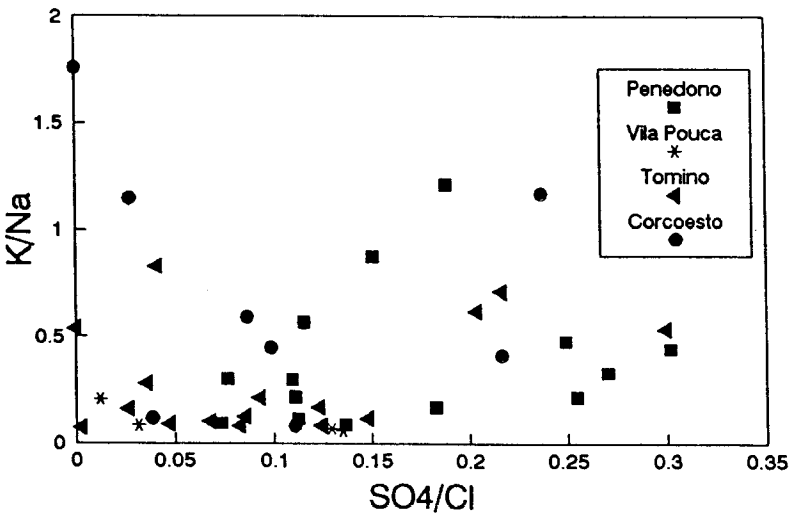

IV - 104 : SO_4/Cl vs ppm Cu and SO_4/Cl vs K/Na of the reconstructed fluid inclusion positions.

a - Anion Chemistry of the Inclusion Fluids

The dominant anion in all the analysed fluids is chloride,but in many cases the next most abundant are sulphate, then borate Their relative abundances are illustrated in Figure IV-101. This is an unusual pattern for analysed deep fluids, where sulphate is usually much less abundant than borate and often less abundant than bromide (e.g. Yardley et al., 1993). When the charge balance is considered (Tables IV-9 to 12), it is clear that most analyses are systematically deficient in negative charges. This is most likely due to the presence of bicarbonate, which cannot be analysed directly. The magnitude of the discrepancy suggests that HCO_3^- may be present at a level of around 20% of the total analysed anions, in equivalents. Thus the analysed fluids are chloride-dominated, but with significant levels of both bicarbonate and sulphate. There are modern analogues for such fluids in some geothermal areas.

The concentrations of the conservative halogens, Cl, Br and I, are shown as a plot of the ratios I/Cl against Br/Cl in Figure IV-102. These ratios, and especially Br/Cl, are relatively unaffected by fluid:rock interaction and therefore provide geochemical tracers that are effective in distinguishing fluids from different sources; indeed this was the rationale behind this aspect of the study in the first instance. It is clear that the fluids from all the deposits studied have a similar range of halogen compositions, and that these are somewhat enriched in Br relative to seawater and bulk earth, and with a range of I/Cl values intermediate between these two points. A few points from Corcoesto that have lower Br/Cl ratios are from deep in the drill hole, and the composition of the Corcoesto fluids appears to change in depth towards lower Br/Cl values.

Also shown in Figure IV-102 is the field of composition of high-T, Sn-W vein fluids from the Hercynian granites of SW England, compiled from our own unpublished data. It is notable that almost all the fluids associated with the Au mineralisation are quite distinct from these high-T, magmatic fluids, although the deeper Corcoesto fluids trend towards them. This result confirms the conclusion from the bulk gas analyses that the ore fluids for the Au mineralisation were quite distinct from the higher-T ore fluids. The source of the salinity in the Au ore fluids is therefore unlikely to be directly linked to the granite magmatism. By comparison with halogen analyses of fluids from a wide range of modern environments (Bohlke & Irwin, 1992), the signature found in the fluids analysed for this study is typical of shield brines, and some oilfield brines, found within the upper few km of the crust today.

Thus the halogen ratios of the Au ore fluids can be interpreted as indicating that they were derived by deep percolation of surface waters. There is evidence for minor mixing with a Br-depleted fluid component, of likely magmatic origin, but only very rarely is this component important. In general, granite-derived fluids do not appear to have played a major role in Au-mineralisation. The high sulphate contents of some fluids are indicative of relatively oxidising fluid, and this would also be consistent with derivation from higher, rather than deeper, structural levels.

b - Cation Chemistry of the Inclusion Fluids

The cation analyses show that the fluids are dominated by Na, K and Ca, sometimes with appreciable Mg. The relationships between the three major cations are shown in Figure IV-103, together with data from the high-T mineralisation hosted by similar granites from SW England. A remarkable feature is the very wide range of K:Na ratios. This ratio is normally buffered by the coexistence of K-feldspar and sodic plagioclase and can be used as a geothermometer; in this suite of analyses, many fluids have anomalously high K:Na ratios. Similar high K contents are found today in geothermal acid sulphate waters, where plagioclase in the host rock has been entirely destroyed by acid attack, however there is no simple relationship between the SO_4:Cl ratios of these ore fluids and their K:Na ratios (Figure IV-104). Nevertheless, it is likely that the K-rich fluids were derived from kaolinised, or otherwise altered granites in which plagioclase had been destroyed. Such fluids are sufficiently common in the data set as to suggest that the Au ore fluids may have also been responsible for hydrolysis of plagioclase in nearby granites and acid-leaching.

Sulphur Isotopic Composition of Vein Sulphides (per mil, CDT)					
Mine and Outcrop Samples			Drill core (Hole, m-cm)		
Sample	**Mineral**	$\delta^{34}S$	**Sample**	**Mineral**	$\delta^{34}S$
Penedono Region			**Corcoesto**		
St.Antonio -4	Arsenopyrite	-3.3	6281, 32-20	Pyrite	-2.3
-6	"	-3.9	6281, 110-50	Arsenopyrite	-2.9
-7	"	-0.1	6281, 146-65	"	-3.6
-8	"	-5.2	6281, 323-35	"	-3.8
-8a	"	-4.0	6281, 348-40	"	-4.2
-9	"	-3.6	6281, 371-55	"	-3.1
-10	"	-2.8	6281, 551-40	"	-3.5
-10a	"	-8.5	5400, 375-35	"	-4.8
-11	"	-5.8	4933, 268-30	"	-4.0
-12	"	-2.6	4924, 90-00	"	-4.2
Ferronha-13a	"	-3.8			
Dacotim-1	"	-3.9	**Tomino**		
-3	Pyrite	-5.9	T5, 115-05	Pyrite	-4.6
Antas-14a	Arsenopyrite	-1.0	T5, 115-05	Arsenopyrite	-4.6
-14b	Pyrite	-3.0	T8, 24-60	Pyrite	-5.5
			T8, 86-50	"	-2.2
Vila Pouca			T8, 117-00	"	-4.2
Vale de Egua	Arsenopyrite	-5.2	T8, 194-00	"	-3.3
			T8, 210-00	"	-0.3
Tomino			T9, 190-30	"	-1.2
Locn.-41	Pyrite	-1.1	T9, 190-30	Arsenopyrite	-1.3
CREGU-13	"	-2.4	T9, 190-45	Pyrite	-1.6
CREGU-13	Arsenopyrite	+1.1	T9, 192-90	"	-3.1
			T12, 118-00	"	-2.6

Table IV - 13 : Sulphur Isotopic composition of vein sulphide from Penedono, Vila Pouca and Tomino areas.

The relatively low Ca content of the Au ore fluids may be most readily explained by their low salinity compared to the SW England fluids. The effect of higher salinity is to increase the proportion of divalent to monovalent cations in fluids buffered by the same mineral assemblage (e.g. Eugster & Gunter, 1981).

The Au ore fluids also contain significant concentrations of Li in many instances, and rather lower concentrations of Sr and Cs. Ba is locally enriched. The Li:Cs ratios of fluids from all the deposits are rather similar, although their absolute concentrations appear to vary (Figure IV-105). In contrast Sr shows a negative correlation with Li (Figure IV-105), and this probably reflects derivation of alkali metals from K-feldspar in the granites, while Sr came from plagioclase. Li, Cs rich fluids attacked K-feldspar more extensively, while the Sr-rich ones interacted more extensively with plagioclase. The variability in these fluid parameters may reflect local wall rock variability.

A second very distinctive feature of the ore fluids in this study is that they have extremely low concentrations of Fe, frequently at the limits of detection. Instead, Mn is commonly the most abundant transition metal, although some samples have high levels of Cu. The relative abundances of these elements is indicated in Figures IV-103 and104. Bottrell & Yardley (1991) noted that fluids from oxidising environments were depleted in Fe and enriched in Mn relative to those from reducing environments, given similar wall rocks. This effect arises because both Fe and Mn occur in reduced form in solution, and the effect of progressive oxidation is to precipitate out Fe before Mn, hence high Mn:Fe ratios are possible provided conditions are not sufficiently oxidising for Mn^{4+} to precipitate. The high Cu contents of some fluids may or may not be accompanied by enhanced Zn and Pb levels.

The Bi content of the ore fluids is generally low, except at Tomino where Bi mineralisation is present. The very variable Bi content suggests that it is being locally controlled in the vicinity of each deposit.

4 - Discussion

Taking the anion and cation chemistry of the fluids together with other geochemical parameters for the ore systems, there are a number of recurrent features which consistently indicate similar conditions for ore genesis. Firstly, it is clear that the fluid chemistry of all the deposits for which it has been studied in detail forms a coherent set that is distinct from fluids associated with other types of mineralisation hosted by Hercynian granites. The microthermometric studies have shown that the ore fluid is dominantly aqueous, with moderate salinity, generally around 2 - 9 wt % NaCl equivalent. The fluids have low N_2:CO_2 ratios and are slightly enriched in Br:Cl relative to seawater, the halogen ratios being similar to many upper crustal fluids.

A number of further inferences can be drawn from the fluid chemistry. Both the high sulphate levels and the high Mn:Fe ratios indicate that the infiltrating fluid was relatively oxidising. This is in agreement with the results of laser-Raman analysis of individual inclusions. The precipitation of pyrite from such a fluid requires that it was also relatively acid. It is clear from the high K:Na ratios of many samples that the fluid had sometimes equilibrated with potassic phases in the absence of plagioclase in its source region, and this would be consistent with an acid fluid which had attacked plagioclase along its flow path.

While some aspects of the source of the fluid can be inferred from its geochemistry, there are also many indicators of the importance of local interactions with nearby wall rocks. For example the concentrations of a number of elements (e.g. Bi) vary significantly between different deposits, suggesting a local input, while the patterns of alkali and alkali-earth metal variability are consistent with interactions with granite feldspars.

Fluid Source.

In some respects, the chemistry of the analysed ore fluids can be compared with modern geothermal fluids at high crustal levels, but there is considerable evidence to suggest that simple parallels are inappropriate because the analysed fluids have interacted with wall

rocks at relatively low fluid:rock ratios. For example, high K:Na ratios in geothermal waters are commonly found in acid sulphate waters, because these are the main type of acid waters in geothermal fields which have been able to destroy plagioclase in their host. In the samples from this study, there is no relation between K:Na and the proportion of sulphate in the fluid (Figure IV-104); furthermore it is clear from the sulphur isotope data that biogenic processes have not played a role in remobilising sulphur from the host granites into the ore bodies.

Instead, it is likely that the ore fluids resulted from slow, deep penetration of surface or sediment-derived waters, possibly accompanied by inorganic oxidation of magmatic sulphide ores to account for the copper-rich fluids.

Mechanisms of Gold Transport and Precipitation.

Although the general chemical and structural controls on the Au ore bodies are well constrained by this study, uncertaities remain as to the precise mechanism of transport and precipitation of Au. In most gold orebodies it is generally believed that Au is transported as sulphide complexes. In the present case however all the indications are that the ore fluid was too oxidising for such complexes to be an effective means of gold transport. While the transport of gold in oxidising and acid fluids is quite well known, there is as yet no consensus on the nature of the most important ligands for mobilising gold in such settings. Given however that the incoming fluid is both acid and oxidising relative to the environment buffered by the wall rocks in all the deposits studied, it is reasonable to suggest that precipitation was linked to neutralisation and reduction of the incoming fluid, and perhaps also its interaction with locally available sulphide.

G-SULPHUR ISOTOPE STUDIES.

1 - INTRODUCTION.

The deposition of gold in Iberia was closely linked to the formation of sulphides, usually pyrite and arsenopyrite. Although in this project it has been determined that deposition of gold was later than the host sulphides, they were closely associated with the concentration of gold. Sulphur was therefore a key requirement of the mineralising system and the identification of potential sources of prime importance. Sulphur isotopes of pyrite and arsenopyrite from granite-hosted quartz veins have been determined on samples from Corcoesto, Tomino, Penedono and Vila Pouca de Aguiar and are presented in Table IV-13

2 - CORCOESTO.

Ten drill core samples were analysed from samples which contained varying concentrations of gold. The values of $d^{34}S$ are between -2.3 and -4.8, average -3.6 per mil. There are no differences in sulphur isotopic composition between barren and Au-bearing samples, different drill holes or with depth.

3 - TOMINO.

Twelve drill core and three outcrop samples were analysed from locations along the length of the mineralisation. Drill core samples have $d^{34}S$ between -0.3 and -5.5, average -2.9 per mil whereas the outcrop samples are between +1.1 and -2.4, average -0.8 per mil. Again there are no differences between barren and Au-mineralised samples, between different drill holes or with depth. The heavier $d^{34}S$ of the 1 outcrop sample may be erronious as the others are within the range of the drill core samples.

4 - PENEDONO.

Fifteen mine and outcrop samples have been analysed from 4 mines in the Penedono region, St. Antonio-Laboreira, Ferronha, Dacotim and Antas. Samples from St. Antonio-Laboreira have $d^{34}S$ between -0.1 and -8.5, average -4.0 per mil. Veins oriented N-S, samples 6, 8a and 10a, show no differences with the other samples which are from veins oriented N45E. The samples from the other 3 mines have $d^{34}S$ values between -1.0 and -5.9 per mil, within the range of those from St. Antonio-Laboreira. No gold concentrations are

available for these samples but it was observed that the small veinlets with a N-S orientation were generally richer in gold. There is therefore no difference in $d^{34}S$ between barren and Au-mineralised samples or between the different mines in the Penedono region.

5 - VILA POUCA DE AGUIAR.

Only 1 sample has been analysed from this region, Vale de Egua, with a $d^{34}S$ of -5.2 per mil.

6 - Source of Sulphur.

Although spread over several hundred kilometres these 4 regions of Au-mineralisation have sulphides with an essentially identical sulphur isotopic composition which indicates a similar sulphide source and process at each of the deposits. Apart from 2 possibly erroneous values the range in $d^{34}S$ is small at only 6 per mil and the average value for all the deposits is -3.3 per mil. Using a fluid temperature of 300-350°C the $d^{34}S$ of the fluid which precipitated these sulphides can be calculated, assuming that the fluids were in the H_2S stability field. At these temperatures the fluid would be only 1 per mil lighter than the mineral values, therefore -4.3 per mil is a reasonable estimate of the $d^{34}S$ of the fluid precipitating the sulphides. Such values are close to, but in some cases slightly lighter, than those normally associated with igneous rocks (-3 to +3 per mil). This could be explained by the loss of a small amount of SO_2 from the magma. We suggest that the occurrence of these sulphides in granite-hosted quartz veins, the narrow range of $d^{34}S$ values and their similarity to magmatic sulphide values, indicates that they derived the majority of their sulphur from pre-existing igneous sulphides via a simple inorganic route.

FIG. V-1 : LITHOSTRATIGRAPHIC CORRELATION OF THE STUDIED METASEDIMENTARY AREAS

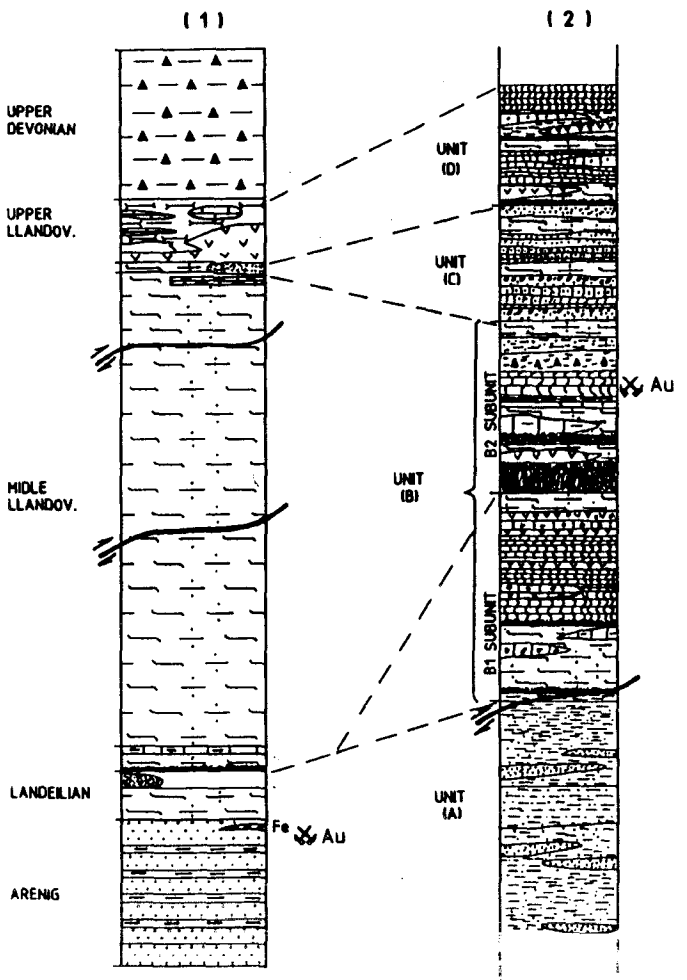

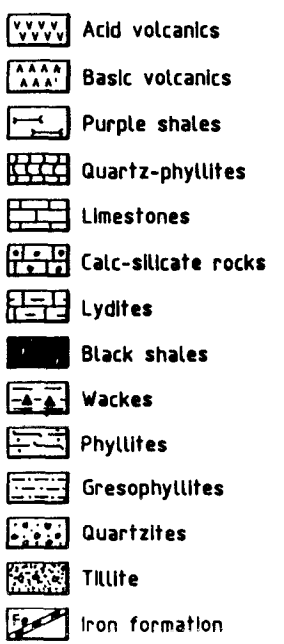

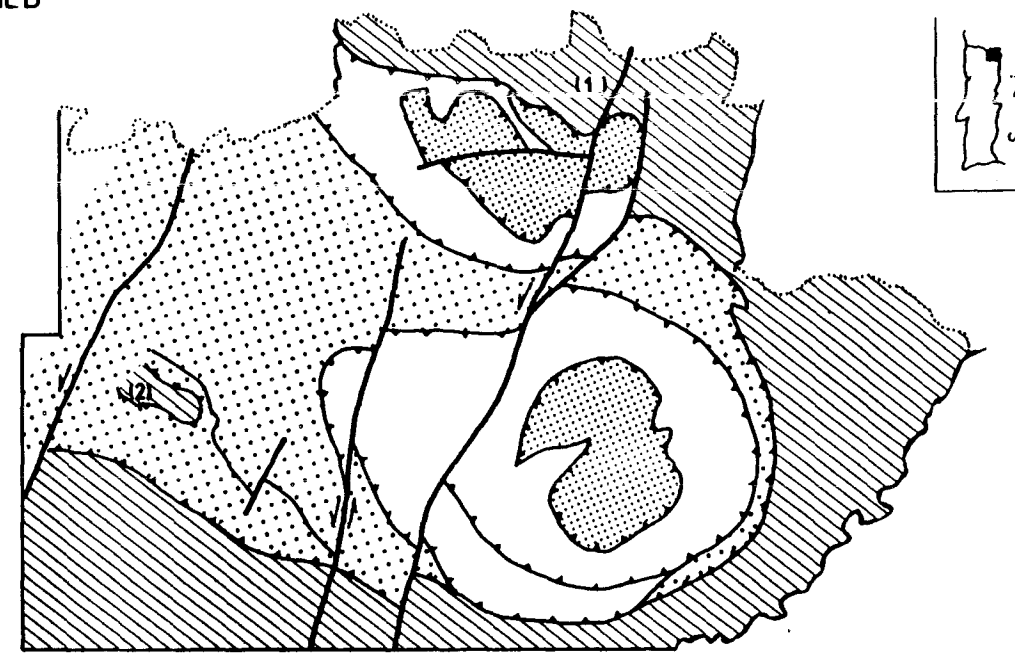

MAP WITH THE LOGS LOCATION

LEGEND

" DOURO INFERIOR " DOMAIN
(AUTOCHTHONOUS)

" PERITRANSMONTANO " DOMAIN
(PARAUTOCHTHONOUS)

" CENTROTRANSMONTANO " DOMAIN
(ALLOCHTHONOUS)

BRAGANÇA AND MORAIS
MAFIC / ULTRAMAFIC MASSIFS

CONCLUSIONS

GENERAL FEATURES OF THE ORE ZONES

GEOMETRIC, LITHOLOGICAL, AND STRUCTURAL CONSTRAINTS IN METAMORPHIC SERIES FROM NORTH-WESTERN PORTUGAL

Important structural studies have been carried out in North-Eastern Portugal (Vilariça fault zone - França deposit - and Vila Pouca de Aguiar area - VPA) in order to reconstruct the evolution in the different deformational stages and their relationships with metallogeny. These two areas are also considered to be the better to give a good image of the relation between metasedimentary host rocks with mineralized structures.

In the França and VPA areas , the admitted regional stuctural models for the Central Iberian Zone appear to be valid. França is situated on the autochthonous "Douro Inferior Domain" and involves host rocks belonging to lower Ordovician (Arenig) to upper Devonian, VPA on the parautochthonous "Peritransmontano Domain" involving host rocks belonging to lower Silurian (Llandoverian) to lower Devonian (Ribeiro, 1974). Cartographic and lithostratigraphic studies in França allowed the individualization of an autochthonous sequence characterized by a predominance of Ordovician and Silurian metasediments. This sequence exhibit from the base to the top: quartzites from Arenig, slates from Landeilian, a Silurian characterized by a basal conglomerate (low Landoverian), greywackes, greyphyllites and a volcanosedimentary sequence (upper Landoverian) and a Devonian essentially characterized by greywackes. The studies on VPA area allowed the individualization of four lithostratigraphic units (A, B, C, D), predominantly constituted by quartzites, chlorite phyllites, black-shales interbedded with acid metavolcanic and calc-silicate rocks. The A unit represents an autochthonous basement and B, C and D units the parautochthonous (Peritransmontano Group).

In the Fig; V-1, we present a correlation essay between the two sequences defined on the studied areas. The B1 subunit can be correlated with the carbonaceous sediments from the Landeilian and the D unit with the volcanosedimentary complex assumed to be of upper Landoverian age at França. In spite of the difficulty of correlating we must emphasize certain similarities between the two environments, namely the presence of black-shales and volcanosedimentary terms.

At least four Hercynian deformational phases are recognized: 1) the D1 characterized by axial planar slaty cleavage (S1) with vergence to the north (domain of the recumbent folds); there is a continuous deformation process between D1 and D2 giving place to important thrust nappes, responsible for the parautochthon character of the "Peritransmontano Group"; 2) the well marked subhorizontal S2 shear cleavage; at França it is overturned to south, with reverse sense of the thrusts; at VPA this phase is not well marked in A autochthonous unit, prevailing a S1 foliation, while in the other units D2 developed a S2 foliation that transposes the S1 , mainly in the most pelitic lithologies; some quartz veins occur in relation to this deformation phase; 3) the D3 event is responsible for large subvertical kilometric folds and for the uplifting of the former structures; these are reactivated with dextral shearing sense. At França, D3 does not produce any penetrative cleavage, besides important shears; these shears are filled up by iron oxides and quartz; in VPA, D3 deformation affects all the units with a subvertical crenulation-cleavage (S3), striking N120, but this S3 cleavage is more penetrative in A unit; a late D3 brittle-ductile deformation is expressed mainly by a tensional fracture system N40 to N50E; the rotation of the greastest principal stress (s1) from NE to NNE induces a sinistral shear sense in this tensional fractures and, in some cases, the earlier subvertical foliation N120 (So//S1//S2) is reactivated with dextral shear sense; in same places this shear deformation is accompained by intense hidrothermal alteration with silicification and chloritization (Três-Minas); 4) the D4 event affects all the former structures; D4 is a brittle phase with two conjugated fracture systems striking N10W to N20E, conditioned by a strain field consistent

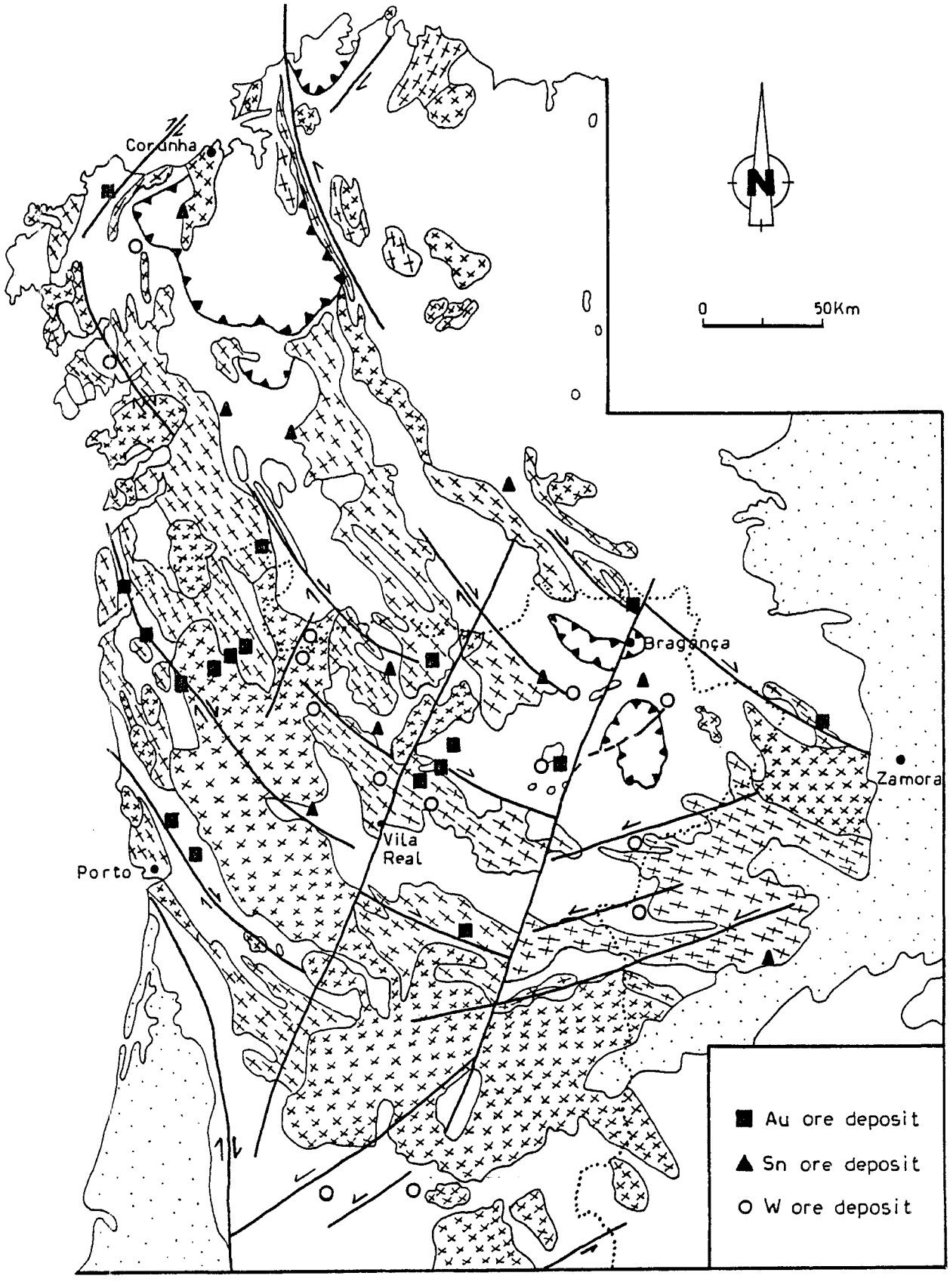

FIG. V-2 : General distribution of the Au -Sn - W ore deposits in the North Western Iberian Massif

with a dextral shearing prevailing in the previous shear planes N120E; Vilariça fault (N10E) in França area and Régua-Verin fault (N15 to N20E) in VPA area are D4 events.

The few geochemical data available attest the particular behaviour of V, Cr and Ni in the two studied areas. Curros autochthonous unit from VPA and the autochthonous from França are richer in those elements and this fact suggests the influence of ultrabasic rocks in the source of the Paleozoic sediments.

Studies of textural and chronological relationships between the different ore minerals have shown that arsenopyrite, pyrite, and galena are the main sulphide minerals in mineralized structures from França and VPA areas and appear associated with late quartz fillings of D3 to D4 stuctures. At França gold appears at a combined state within arsenopyrite II as well as electrum during a relatively late stage (quartz IIb-carbonates-sericite-chlorite) of the vein fillings; in VPA mineralized structures electrum and/or gold occur predominantly, as a latter phase, in intergranular spaces between pyrite and arsenopyrite, or in microcracks inside arsenopyrite/pyrite generally associated with galena and sulphosalts . The later gold is associated with aqueous fluid migration.

Final considerations

The mineralized structures of VPA are hosted by metasediments of lower Silurian to lower Devonian characterized by several different lithologies, namely black-shales, vulcanites and quartzic terms affected, at least, by four hercynian deformation phases.

The mineralized structures are structurally controlled: the mineralized quartz veins occur in traction fractures related to D3; the silicified metasediments (Três-Minas) corresponding to D3 shear-zones. However the essential of gold expression is tardif and related with D4 microfracturing process.

The geochemistry attest an important volcanic contribution with bimodal character. Hoewever the hight contents in V, Cr and Ni, evident in certain terms, suggest the influence of ultrabasic rocks and a sedimentary evolution with geochemical maturity.

The Au geochemical data suggest: a specialised crust in this sector of the Iberian Massif and the inexhistence of specific specialised terms or preferencial concentrators, namely the black-shales; and a very specific behaviour of Au irrespective of other metallic elements, namely As, Ag and W. The differences in the location (granite vs metamorphic series), time (W deposits associated to early granites late calk-alcaline magmatism) and behaviour of sources, in addition of the specific chemical-conditions of mobility and deposition of the metals, explain the distinct location of the concentrations

RELATIONSHIPS BETWEEN GRANITE AND MINERALIZATIONS

Most granites hosting mineralizations are aluminous, and for their most part leucocratic (Fig. V-3). They may be considered as relatively passive traps, as most of these granites are cold and already affceted by several stages of ductile and brittle deformation at the time of the gold introduction. Their spatial association with ores may be the consequence of two factors :

1- the syntectonic granites are emplaced in active zones which are responsible of later tectonic reactivation which are at the origin of a great part of the structures which can be mineralized.

2- as shown in Chap. III the richness in quartz is one of the major parameter in rock deformation; therefore, the granites richer in quartz, which are generally the most differenciated and leucocratic are more susceptible to react positively to britlle deformation in giving series of tension gashes networks (this is the case of the Tomino and Corcoesto leucogranites, rarely in mesocrate granites).

The crustal stock-metal in metamorphic series can be remobilized through successive metamorphism, deformation and fluid migration. Consequently, if the concept of a specialised Paleozoic crust is valid, the role played by Hercynian granites in the gold ore formation is specific The main role of the granite intrusions, in case of being decisive, may have consisted

FIG. V-3 : *ROCK TYPES HOSTING THE AU - VEINS*

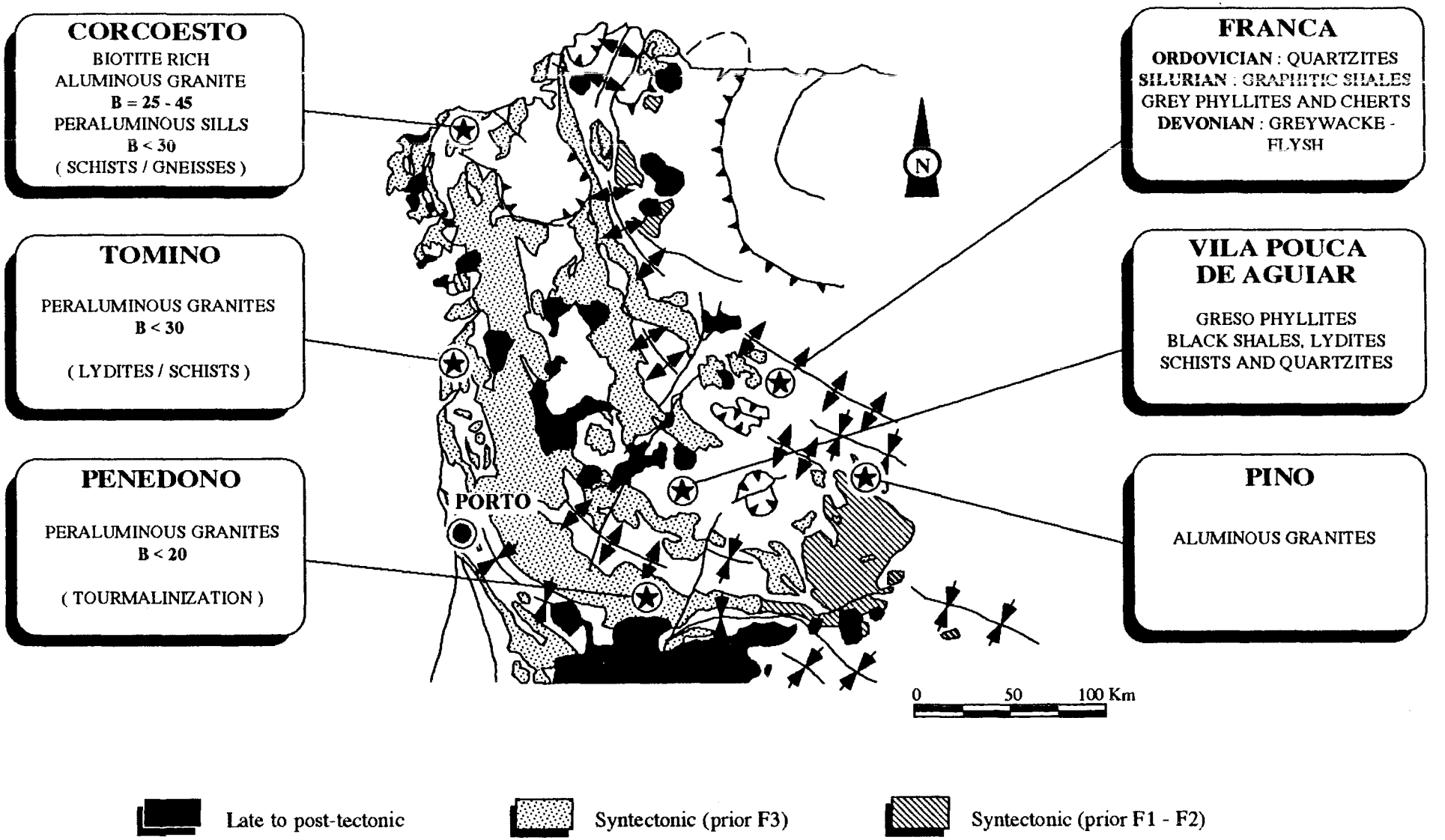

in the subsequent heat source at the origin of fluid circulation and the related Au stock mobilisation (preconcentrations ?).

Such a case is clearly illustrated by the Corcoesto zones, where a complex succession of magma intrusions, from coarse grain Bi-granite, to peraluminous granites, aplites and subvolcanic sills (felsites) are recoreded at the the same place.

Therefore, they act more as an indirect activator rather than a mineralizing agent. **Considering finally, the relationships between the ore formation and granites, it is likely to consider that only the latest stages of granite intrusions (post-tectonic, calc-alcaline type) or other magmatic intrusions could be responsible of the thermal fluxes (or indirect markers) related to the late hydrothermal cells responsible for the Au-ore formation.**These thermal anomalies are predominantly located around major lineaments which correspond to zones of crustal thinning , and which have been subjected to long-lived superimposed magmatic to structural activities.

STRUCTURAL CONTROLS (Fig V-4)

The main structural factors are the following :

1- formation of the main channels in relation with major shear zones : the complex superimposition of early deformations from D1 to D4 are responsible for specific structures which have in turn evolved from ductile to britlle regime and are associated with the main shear zones affceting the Gallicia area. The earliest quartz deposition, which create the specific potential trap for later mineralizations are formed at that stage (D3 to D4). ***Quartz fills in general relatively small structures (from the tension gashes (1dm-1m to a few hundred m) which are in turn mineralized by arsenopyrite and then by gold, at variance of the major shear zones which remain generally barren or display low grade mineralizations.*** These structures may be affected by local ductile deformation , frequently on the wall-rock.

2- formation of the most efficient trap for ores when Au is mobilized

It is linked to the strong microfracturing stages of the previous quartz lenses due to late brittle deformational stages . Such microfracturing is extremely complex in detail, and results from the superimposition of each brittle stage on the early quartz matrix (milky quartz cemented by microcrystalline quartz).

At each of the two last stages, strong rheological heterogeneities have specific and favourable effects on the intensity of the permeability formation. Main rheological heterogeneities are the followings : granite sills within metamorphic units, quartz veins within granite, silicified schist within schists, etc..

Therefore, the early quartz matrix (milky quartz cemented by microcristalline quartz) acquires its permeability at the favour of further stress reactivations, which yield higher fluid flows within the veins than in the surroundings. This process explains that only quartz veins are mineralized although the gold inputs are late compared to the quartz matrix formation.

Similar processes are clearly demonstrated at Tomino and Corcoesto.

Contrary to the "gold bearing shear zone" model (Bonnemaison and Marcoux, 1987, 1989), it is shown that :

- there is **no clear evidences of gold preconcentrations** in relation with the early or intermediate stages prior or contemporaneous of the multistage quartz vein formation (milky quartz, microcrystalline quartz)
- **mineralized faulted areas are not typical shear zones** : major of the shear zones themselves are barren, and the evidence of early ductile deformation due to shears is minor along the mineralized faults in most cases. Economic mineralization results from the existence of strong rheological heterogeneities, such as those produced by the presence of

FIG. V-4 : *STRUCTURAL CONTROLS OF THE MINERALIZATIONS*

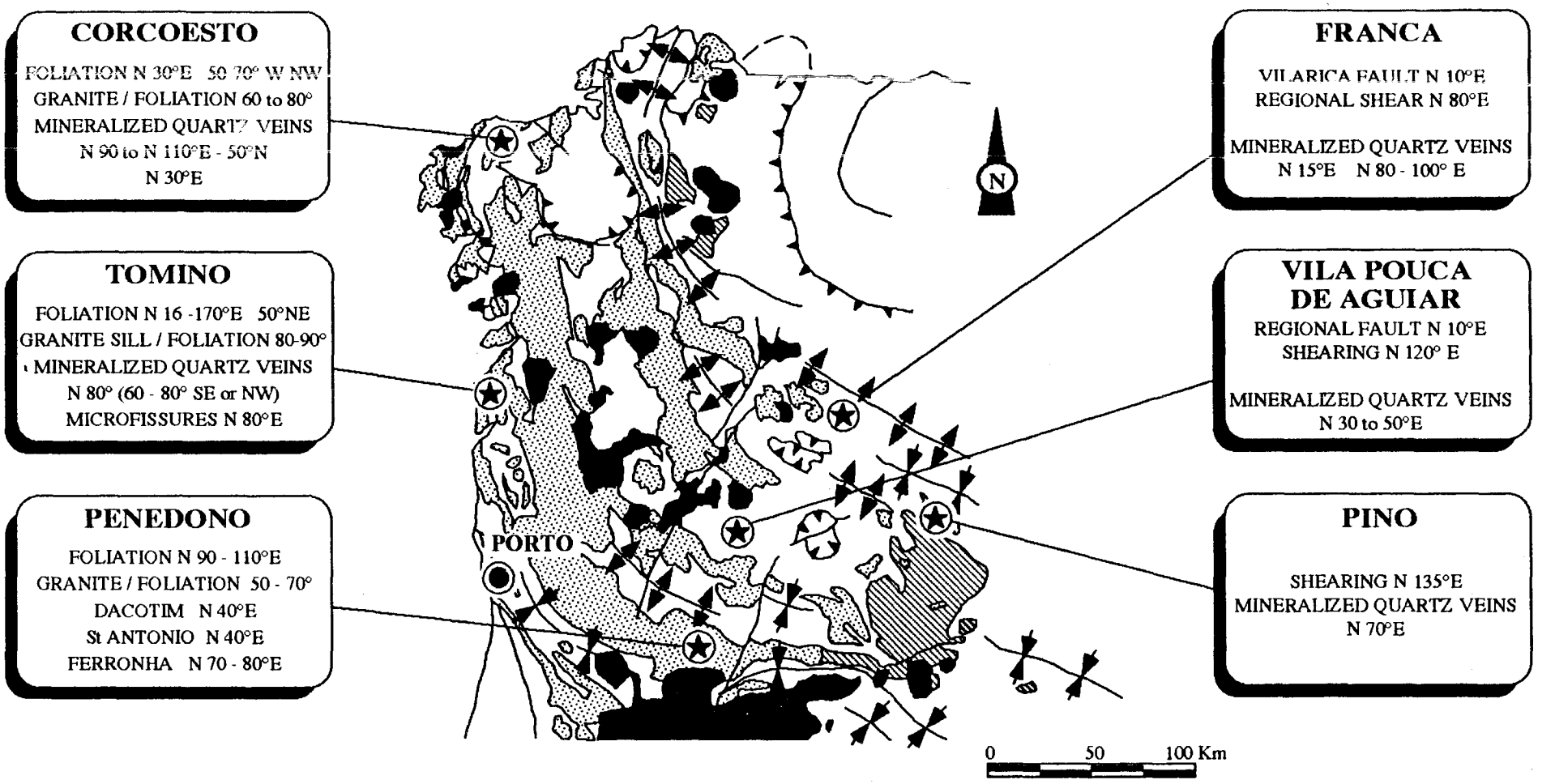

metric quartz lenses within micachist and later strong microfracturing stages of the previous quartz lenses due to late brittle deformational stages.

There are some convergences between our data and the "gold bearing shear zone" model:
- the beginning of the processes at the transition between ductile-brittle conditions ;
- the necessary long evolution of the faulted quartz bearing zones in order to get economic concentrations.

GENERAL RECONSTRUCTION OF FLUID MIGRATION STAGES

Three successive stages are recorded in the formation of the studied Late Hercynian gold-bearing quartz veins, each characterized by its own set of P-T conditions, mineral assemblages, fluid compositions and deformational state (closely related to the fluid flow regime). The order of succession knows no exception.

Early stage: formation of milky quartz veins.

Milky quartz veins and veinlets formed mostly after the emplacement of late peraluminous granites (probably Westphalian); they also post-date the ductile deformation of the granite as well as the early subsolidus alterations affecting these granites (albitization and quartz dissolution at Pino, greisenization at Tomino, albitization at Corcoesto, muscovitization at Penedono, Fig; V-5). Diffuse alteration, and sulphide crystallization (then barren arsenopyrite) in the surrounding rocks seem to preceed the deposition of massive milky quartz in open space (tension cracks at Corcoesto, and Tomino). Locally, a discrete ductile shearing of the early quartz crystals may occur (Tomino, Corcoesto) . But no true mylonites were developed in the surroundings of the quartz veins. These features are at variance with those of typical late Variscan shear-zones. These shear zones may be in some instances at the origin of the early fault formation prior to the quartz matrix formation .

Early C-H-O-(N) fluids of metamorphic derivation are found in the surroundings of the early milky quartz veins, and as rare relics within the quartz itself. These are dense fluids trapped under pressures above 1Kb (frequently in the 1.5-3 Kb range) and temperatures of 350° to 450°C. These conditions are roughly the same as those which prevailed during the late metamorphic stage in the Variscan terranes during or just after the hyper-collision event.

Pyrite and barren arsenopyrite are found in the milky quartz. There is no clear evidence of gold deposition at that stage, even at low concentrations in sulphides (pyrite, pyrrhotite, arsenopyrite)

Intermediate stage

Due to repeated tectonic reactivation, early milky quartz veins were strongly reworked. A first event resulted in brecciation and development of the so-called "microcrystalline quartz" as a cement to the breccias, leading to the present shape of the massive quartz lenses which are the host for later ore deposition. Earlier pyrite and arsenopyrite were brecciated as well. Sulphide deposition (arsenopyrite) locally took place in the microcrystalline quartz, but was never massive.

Later on, these lenses were repeatedly subjected to intense fracturation; there was several alternances of micro-crack formation and healing or sealing by hyaline quartz.

Fluids involved in the formation of hyaline quartz veinlets belong to the C-H-O-N system and are essentially similar to those of the early stage. But at that stage, temperatures range from 250° to 350°C and pressures from 0.5 to 2.0 Kb depending on the localities. The alternances of increasing and decreasing permeabilities recorded by the quartz veinlets formation are reflected in strong pressure variations.

Late stage: main gold deposition/enrichment

A renewal of tectonic reactivation (frequently a compressive regime characterized by new specific directions of major stresses) under quite different P-T conditions resulted in the main stage of gold ore deposits formation. Reactivation of early quartz veins (stages 1-2), results in microcracks which were healed but not sealed by quartz. Native gold deposition took place, together with sulphides and sulphosalts (Pb-Ag dominated), along these cracks, especially when they crosscut earlier sulphides. Most relics of host rocks as well as the wall-rocks are at that stage almost completely altered in a quartz-illite assemblage. In that case, it is difficult to determine wether the native gold deposited results entirely from a new gold input in the structure, or from a partial reworking of early concentrations into new mineral assemblages, although new input is in any case obvious.

GEOCHEMICAL CONSIDERATIONS

Element sources (Au, As, S)

Source of sulphur

The sulphur isotope data presented above is remarkable for the uniformity of the $d^{34}S$ values of sulphide minerals from many, widely spaced deposits. The values are typical of magmatic rocks and are most readily explained by a local source of S from intrusive bodies in the vicinity of each deposit. The data also preclude significant biogenic modification of the sulphur chemistry of the fluid, which is significant in view of the evidence for a high-level fluid source.

Source of gold

The available geochemical data attest the the influence of ultrabasic rocks in the source of the Paleozoic sediments. The Au geochemical data suggest a specialised crust in this sector of the Iberian Massif, but the inexistence of specific specialised terms or preferential concentrators, namely the black-shales. The Au dsitribution seemms to be controlled by very specific factors which are distinct to those controlling other metalic elements, such as As, Ag or W.

Although at the root of the concept of maturation of auriferous shear-zones (Bonnemaison and Marcoux, 1989), the very fact of gold preconcentration in early sulphides could not be assessed in our studies. Gold has been trapped in some instances in arsenopyrite crystals at the combined state, probably within the lattice (Wagner et al., 1986, Marion et al., 1988, Cathelineau et al., 1989). In that case, gold is incorporated in the latest growth band, and is not then released from the lattice (latest arsenopyrite growth zones for instance at França). In other cases, the highest contents do not reach more than a few tens of ppm in some growth bands, and accounts for low average concentrations in the crystals (less than 0.5-5 ppm).

Source of the fluid components (Fig. V-6)

Both the Cl : Br : I systematics and the bulk CO_2 - N_2 relationships demonstrate that the fluid associated with the gold mineralisation in these Hercynian granitoids is quite distinct from that which gave rise to Sn-(W) mineralisation related to peraluminous magmatism (for instance the Sn occurrences from Conrwall).

However, the CO_2 - CH_4 -N_2 relationships for early fluids display numerous similarities with the fluids equilibrated with Hercynian metamorphic rocks, especially C bearing schists. Such fluids are ubiquitous and have been encountered in Au quartz veins or W quartz veins from the french Massif Central. Therefore, the geochemical signatures of early CHON fluids are relatively common ones, and indicated that CHON fluids produced during the

FIG. V-5 : *WALL - ROCK ALTERATION*

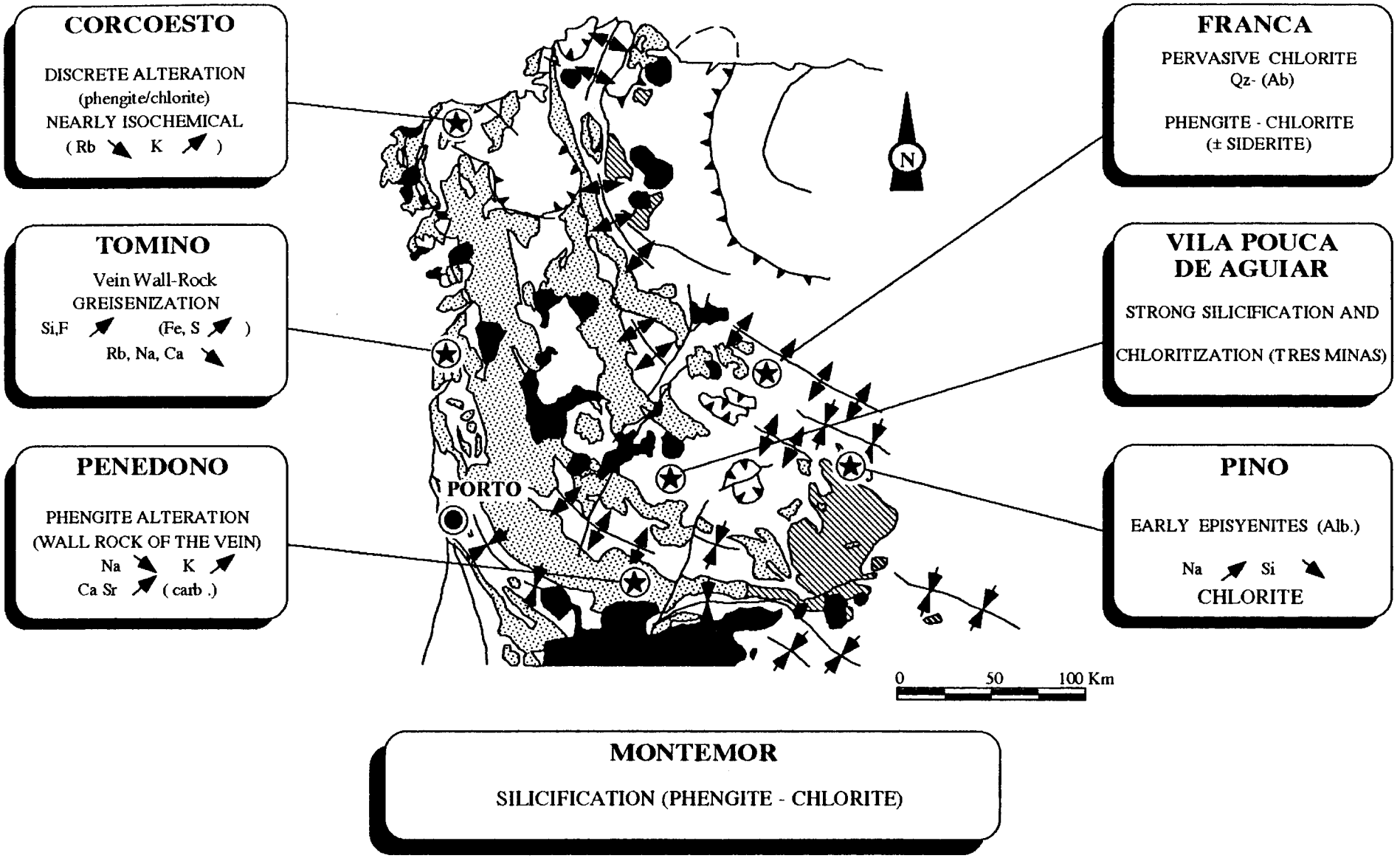

retrograde metamorphism migrate relatively far from their production zones, and especially infiltrate the granites.

The halogen ratios are instead closely comparable to modern shield brines, and only in the deeper part of the Corcoesto drill hole is a halogen input with a magmatic Br : Cl ratio detected.

The high SO_4^{2-} levels also provide evidence for a component of downward-penetrating, surface-derived water. Similar Cl : SO_4 ratios are known from geothermal fluids with a component of acid sulphate water, and, like geothermal acid sulphate waters, many of the analysed inclusion fluids have anomalously high K : Na ratios for their temperature of formation, indicating that their compositions were not buffered by coexistence with plagioclase. An alternative analogue for the sulphate-rich component of the fluids in the development of zones of secondary Cu enrichment below the water table in sulphide or bodies. Here, high sulphate in the fluid is due to near-surface oxidation of sulphide minerals rather than oxidation of volcanic H_2S gas. The very high Cu content of the inclusion fluids relative to many other cations strongly supports this origin for the sulphate-rich waters.

In summary, the halogen data suggest that the salt component of the ore-fluid evolved in a low water : rock ratio setting, as found in modern shield brines, while the high sulphate and copper contents indicate that the water in the source region included a component of downward-percolating ground water whose composition was modified by interaction with primary sulphide minerals.

Physical and chemical conditions of sulphide and gold precipitation from fluids

The role of the physical-chemical conditions as factors controlling the ability of hydrothermal fluids to transport and deposit Au together with As has been studied by estimating T, fO_2, fS_2, pH and fluid composition at different stages of the hydrothermal activity. Such parameters were estimated from the consideration of the mineralogical and geochemical results obtained on natural Au-occurences together with the results of fluid inclusion studies. Fluid composition and density were obtained by microthermometric analysis of the fluid inclusions hosted by the ore gangue minerals. fO_2, fS_2 and pH have been obtained by considering the sulfide and silicate assemblages together with their relative stability diagrams.

Fluid characteristics during milky quartz and arsenopyrite deposition

Ore fluid inclusions are observed mostly within recrystallized zones of the early milky quartz, and are characterized by CO_2 -CH_4 -N2 (± H_2O - NaCl, salinity : 2-4 wt. % eq. NaCl) rich fluids trapped at relatively high temperatures (250 - 450°C), and probably related to the early sulfide (and especially the first arsenopyrite) deposition.

Estimation of the fO_2-fS_2 - pH conditions during the early stages

The redox conditions were calculated from the P–V–T–X properties of individual inclusions in the C–O–H–S system (e.g. Dubessy et al. 1989). Most of the logfO2 obtained, range from –45 to –31 (for a temperature range of 250–450°C), and follows the variation fixed by the Ni–NiO oxygen buffer (fig. 10).

Arsenopyrites crystallize mostly together or in presence of pyrite. This mineral association indicates that fO_2 was close to that fixed by the pyrite-arsenopyrite boundary, or not very far from that fixed by the pyrite - arsenopyrite - pyrrhotite equilibrium, as indicated by the stability of pyrrhotite during the first stage of the arsenopyrite deposition.

FIG. V-6 : *FLUID GEOCHEMISTRY - ION CONTENT*

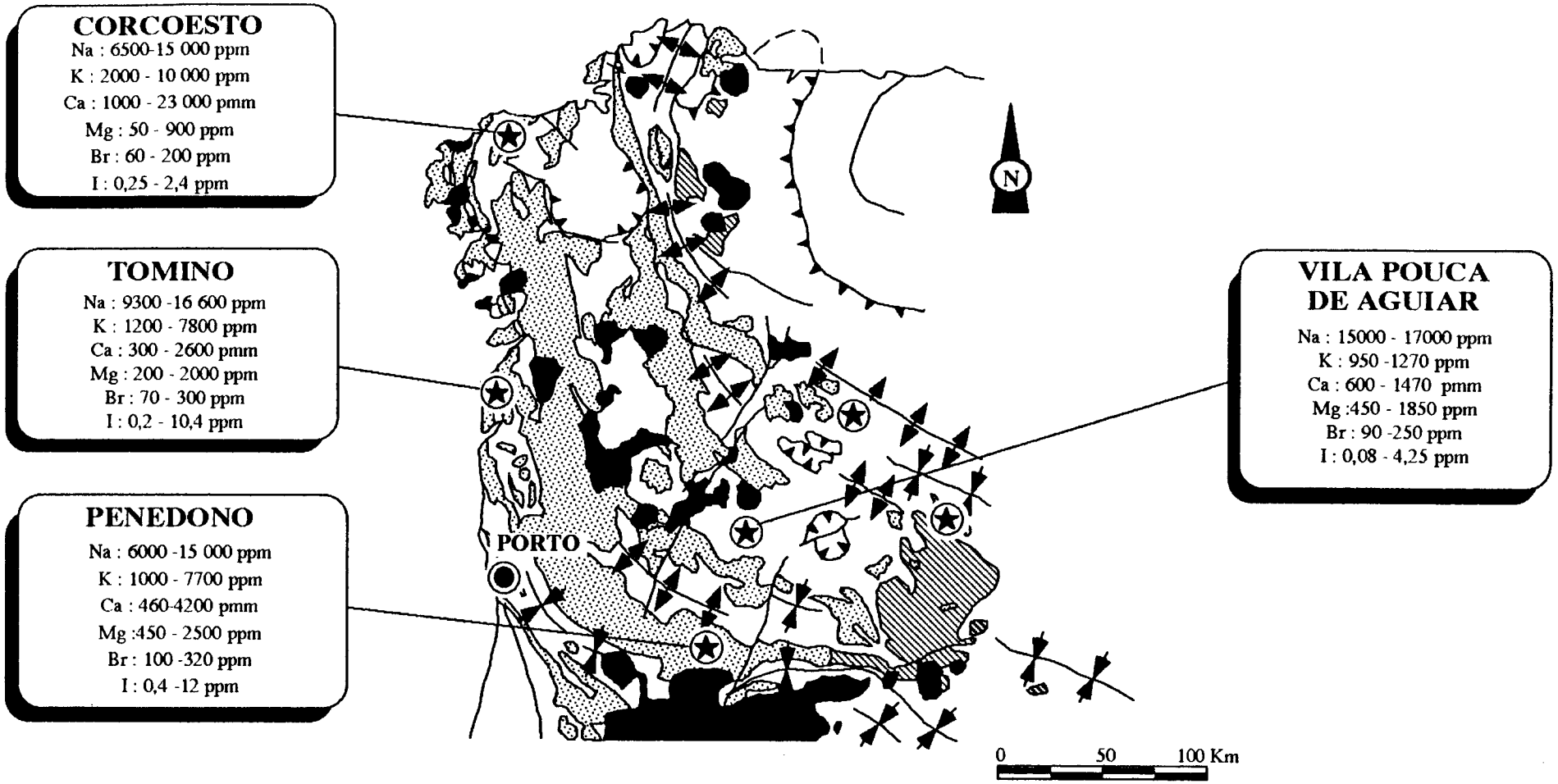

At Tomino for instance, mineralogical data show that fO_2 was around that fixed by the pyrite-pyrrhotite and the fO_2-fS_2 calculated from fluid data is compatible with this association (Bowers et al., 1984), e.g. : a fO_2 closed to that fixed by the Ni- NiO oxygen buffer,.and a rather high fS2.

At França, the ore deposition should have occurred under fO2 conditions near those calculated for quartz II, i.e., around $10^{-35\pm1}$ at 270±10°C. The calculated fS2 is quite high (around 10^{-11}–10^{-10}), and compatible with the stability field of pyrite .

Fluid characteristics during gold deposition

nature of the ore fluid

It is clear from the microthermometric and textural studies that gold mineralisation was associated with the later stages of the hydrothermal activity in which the fluid was predominantly aqueous, and mildly saline (2 to 4 wt. % eq.NaCl). The temperatures are low to moderate, and range from 180 °C to 250°C. These features display strong similarities to many french occurrences (Boiron, 1987, Boiron et al., 1989, 1990).

The crush-leach analyses exhibit several unusual features which distinguish these fluids both from high-T magmatic ore fluids associated with Sn-(W) mineralisation (Bottrell and Yardley, 1989), and from fluids associated with mesothermal Au-quartz veins in metamorphic hosts (Yardley et al., 1993). Both the very low concentrations of Fe relative to Mn (Bottrell and Yardley, 1991) and the high SO_4^{2-} levels are indicative of a relatively oxidising fluid infiltrating the vein system. Oxygen fugacity was significantly above the hematite-magnetite buffer, and the stability of pyrite under these conditions indicates a low pH.

Causes of Au deposition

Although Au is thought to have been transported and deposited under relatively high fO_2 at a temperature around 180-250°C, no significant change in the early mineralogy (stability of arsenopyrite and pyrite) is observed, indicating that the fS_2 was sufficiently high and pH low to preserve these minerals in relatively oxidizing conditions.

At the light of the literature data on gold solubility (Henley, 1973, Seward, 1973, Grigoryeva and Sukneva ,1981) it can be assumed that gold precipitation resulted from the destabilization of Au sulfide complexes, which are the most probable stable species in solution under the mentioned conditions, as the Cl content of the fluids is rather low. Gold solubility is controlled by fO_2 and fS_2 as shown by Romberger (1986) using the data from Henley (1973) and Seward (1973). Considering that the maximum solubility of gold is around neutral to slightly basic pH at low fO_2, it may be recorded that three different mechanisms may be proposed for native gold deposition in the case of gold transport by bisulfide complexes :

a) a fluid oxidation which results in a decrease of sulfide activity in solution and therefore in the destabilization of the bisulfide complexes ;

b) a decrease of the oxygen fugacity;

c) a decrease of pH ; or the combination of the factors b and c. The destabilization of the sulphur complexes is probably enhanced by the pressure decrease which should occur during rock microfissuring and leads to a fH_2S decrease.

The lack of specific mineralogical change (no hematite crystallization, no alteration at low pH and low temperature, such illitization) and of data on the the fO2 of aqueoud fluids (no constraints from the volatile chemistry) makes difficult the choice among one these processes.

However, the fluid mixing generally demonstrated from fluid inclusion studies is in favour of oxidation-reduction processes related to the mixing of relatively oxidizing solutions with reducing ones in zones characterized by the presence of early sulphides.

Electrochemical processes, at the surface of microfissured sulphides, could be, in addition, one of the major cause of Au precipitation, as already demonstrated by experimental studies (Starling et el., 1989, Knipe et al., 1991). In that case, the precipitation of gold results from adsorption (physisorption), followed by reduction (chemisorption) which occurs when the physisorbed precursor exceeds the surface energy barrier via electronic or vibrational processes (allowing electron diffusion). The best sites for the process are the sites of highest charge density and focused conductivity which are located where surface bonding is disrupted (fracture surfaces for instances).

CONCLUSIONS

The integrated studies carried out in this work make possible to set up new concepts about the metallogeny of the north-western iberic peninsula :

- the Au concentrations appears to be extremely specific, especially **not genetically linked to granites**, at variance of the Sn metallogeny.

- there is a **lack of direct link between shearing (especially ductile) and Au enrichment,** at variance of any "shear" model ; the role of mechanical heteogeneities and microfissuration is far important for the formation of the trap, although the early shearings may be at the origin of fault or discontinuities which may be reactivated at the time of the As or Au mobility. Therefore, some spatial link between major shear zones and concentrations are systematically found at the regioanl scale.

- there are strong difficulties to asses direct spatial link between sources and concentrations, at variance of other metals for which sources are correctly identified (Sn, U in granites for instance).

Tonnage/grade contrasts

The best conditions are found in zones where most of the above mentionned conditions are gahered togehter.
The contrasted tonnnage and grades between the different studied depoits argue in favour of the specific effects of each of these factors :

- the relatively high concentrations, at Penedono for instance may be explained by the quality of the mechanical contraSts between quartz veins and the granite,

- the important tonnage at low grade (Corcoesto) may reflect an extremely good potentiality at first in terms of sources, and concentration factors (successive heat flows reated to the complexity of the magmatic history, large scale fluid migration and element concentration along the band (As, Au). However, the low grade may be due to the lack of sufficient tectonic reactivation and of major tectonic trap (meter thick quartz veins for instance), which seems too weak to concentrate gold at high grade in specific zones.

Enrichment process

The early stages (quartz matrix formation, sulphide precipitation) are necessary but not sufficient to get economic concentrations. Therefore , all the factors contributing to the formation of the quartz-arsenopyrite vein are important (early opened zones linked to nearby shear zones, fluid production, and As concentration, ...).

The presence of reducing environments (such as black shale units) seems to have relatively low local efficiency on both stages. However, the graphite-fluid equilibrium is at the origin of most fluid components observed in the stages preceding gold. These fluids, equilibrated with the host metamorphic series, moved and penetrated fissured units such as quartz veins, granites, ...

The enrichments are related to the best structural trap which is characterized by a long lived deformational system, and by the existence of late microfissuring stages necessary to the ore fluid migration;
The most competent units located nearby a major deformation zone are the best candidates to host mineralizations.

Main features of best potential areas

The evolution recorded by Au quartz veins is extremely complete and describes most of the **transition from late metamorphic conditions (retrograde metamorphism) to hydrothermal stages**, which occurred generally during the **basement uplift**. The importance of long lived history of microfissuring and fluid percolation seems absolutely necessary to get ores.

Ores form especiallly

-if early sulphides are present and microfissured (chemical trap responsible of elctrochemical process and Au reduction),

- if percolated host matrix is sufficiently permeable (thanks to a high degree of microfissuring)

-under hydrostatic pressures at depths probably around 3-5 km, by mixing processes (end of the progressive dilution of fluids equilibrated with graphite (CHON) by aqueous fluids)

The indirect marker of such conditions are :

- the intensity of late tectonic reactivation
- the presence of mechanical heterogeneities (quartz veins, silicified rocks) responsible for higher degree of microfaulting
- the avaibility of specialized crustal series (source of Au, As, S)
- the permanence of localized heat flows (late granites or magma injection , abnormal heat flows along shear zones or major lineaments)

Local Au redistribution : the influence of supergene effects

Supergene stages have contributed to the dispersion, or enrichments of the surficial levels. (Bio-)oxidation of sulphides may have liberated some combined gold in some instances, and reconcentrated the gold which has been exploited during Roman times.

The supergene effects are at the origin of dispersion-reconcentration (at depth) mechanisms which could make difficult the ineterpretation of the geochemical anomalies in soils, when the paleorelief features are not taken into account.

REFERENCES

Alonso, P.V., Viruete, J. E. and Matiniez Catalan, J. R.., (1992) - La zona de cizalla de Juzbado - Penalva do Castelo en el sector espanol. Simposios, III Congreso Geologico de Espana y VIII Congreso Latinoamericano de Geologia, Tomo 2: 446-455 , Salamanca.

Ancey M., Bastenaire F. and Tixier R. (1978) - Applications des methodes statistiques en microanalyses In Maurice, Meny, Tixier eds, Microanalyse, microscopie électronique à balayage. Orsay, Les éditions de la Physique., 323-347.

Arenas, R., Ibarguchi, J.G., Lodeiro, F. G., Klein, E.,Catalan, J.R.M., Girones, E.O., Macia, J.G.P. and Peinado, M., (1986) - Tectonostratigraphic units in the complexes with mafic and related rocks of the NW of the Iberian Massif. Hercynica II, 2 : 87-100.

Babin, C.,Chauvel, J.J., Lardeux, H., Paris, H. and Robardet,M., (1976) - Lexique des formations de l'Ordovicien armoricain. Bull. Soc. Geol. Min°ral. Bretagne, n° Special, Rennes.

Badham,J.P.N., (1982) - Strike-slip orogens - an explanation for the Hercynides. J. Geol. Soc. London, 139: 493-504.

Bailey, S. W. (1984) – Crystal chemistry of the true micas. In: Micas (edited by Bailey, S.W.), Reviews in Mineralogy, 13, Mineralogical Society of America, 13–60.

Bailey, S.W. (1987) – Chlorites: structures and crystal chemistry. In: Hydrous Phyllosilicates (exclusive micas) (edited by Bailey, S.W.), Reviews in Mineralogy, 19, Mineralogical Society of America, 347–403.

Barakat A., (1992) - Reconstruction des conditions physico-chimiques de mise en place des filonnets de quartz à arsénopyrite dans la lame de granite de Corcoesto (Galice). DEA, Univ. Nancy I, Juin 1992, 49 p.

Barbey P. and Cuney M., (1982) - K, Rb, Sr, Ba, U and Th geochemistry of the Lapland granulites (Fennoscandia). LILE fractionation controlling factors. Contrib. Mineral. Petrol., 81, 304-316.

Barriga F., Mateus A., Noronha F., (1986), Hydrothermal activity and ore genesis at the Borralha tungsten deposit (Western Tras os Montes). Maleo, 2 (13), 28.

Bart J.P., Capdevilla, R.,Matte, P. and Ribeiro, A., 1973 - Geotectonic modelfor the Variscan Orogen. Nature 241: 50-52.

Bayer R. and Matte P. (1979) - Is the mafic/ultramafic massif of Cabo Ortegal (northwest Spain) a nappe emplaced during a variscan? A new gravity interpretation. Tectonophysics 57, T9-T18.

Berth, D., Chouckroune, P. and Jegouzo,P., (1979) - Orthogneiss, mylonite and non-coaxial deformation of granites: the exemple of the South Armorican shear zone.J. Struct. Geol. 1: 31-42

Berth, H.J., Engel,W., Franke,W.,Giese, P. and Weber,K., (1984) - The variscan belt in central Europe : main structures, geodynamic implications, open questions. Tectonophysics, 109: 15-40.

Bohlke, J.K. and Irwin, J.J. (1992) - Laser microprobe analysis of Cl, Br, I, and K in fluid inclusions: Implications for sources of salinity in some ancient hydrothermal fluids. Geochim. Cosmochim. Acta. 56, 203-226.

Boiron M.C (1987) - Minéralisations à Au, As, Sb, altérations hydrothermales et fluides associés dans le bassin de Villeranges (Combrailles, Massif Central français). Geol. Geochim. Uranium, Mem. Nancy, 15, 310 p.

Boiron M.C. and Cathelineau M. (1988) - Les altérations hydrothermales et les minéralisations associées des tufs viséens du bassin de Villeranges (Massif Central Français). Données géothermométriques déduites de l'études des inclusions fluides. Bul. BRGM, 158, 651-665.

Boiron M.C., Cathelineau M. and Trescases J.J. (1989) - Conditions of gold-bearing arsenopyrite crystallization in the Villeranges basin, Marche-Combrailles shear zone, France. A mineralogical and fluid inclusion study. Econ. Geol. 84, 1340-1362.

Boiron M.C., Cathelineau M., Dubessy J. and Bastoul A. (1988) - Contrasted behaviour of Au and U in French hercynian granites at the hydrothermal stage: The role of fO2 and pH. Soc. Italiana Mineralogia Petrologia, Rendiconti, 43-2, 485-498.

Boiron M.C., Cathelineau M., Dubessy J. and Bastoul A. (1990) - Fluids in hercynian Au-veins from the french variscan belt. Min. Mag., 54,231-243..

Boiron M.C., Essarraj, Sellier E., Cathelineau M., Lespinasse M. and Poty B. (1992) - Geometric and genetic relationships between cathodoluminescent microstructural domains in quartz and fluid inclusions : application to the reconstruction of Au-ore fluid chronology. Geoch. Cosmochim. Acta., 56, 175-185.

Bonnemaison M. (1987) - Les concentrations aurifères dans les zones de cisaillement, métallogénie et prospection: Unpublished Doct. Thesis, Toulouse Univ.

Bonnemaison, M. and Marcoux, E. (1987) - Les zones de cisaillement aurifères du socle hercynien français, Chron. rech. min., 488, 29-42

Bonnemaison, M. and Marcoux, E., (1989) - Auriferous mineralization in some shear zones : A three stage model of metallogenesis. Min. Deposita 25, 96-104.

Bottrell S.H., Yardley B.W.D., Buckley F., (1988) - A modified crush-leach method for analysis of fluid inclusion electrolytes. Bull. Mineral. V. 111, 279-290.

Bottrell, S.H. and Miller, M.F. (1989) - Analysis of reduced sulphur species in inclusion fluids. Econ. Geol. 84, 940-945.

Bottrell, S.H. and Yardley, B.W.D. (1991) - The distribution of Fe and Mn between chlorite and fluid: Evidence from fluid inclusions. Geochin. Cosmochim. Acta. 55, 241-244.

Bouchot V., Gros Y. and Bonnemaison M. (1989) - Structural controls on the auriferous shear zones of the Saint Yrieix district, Massif Central, France : Evidence from the Le Bourneix and Laurieras gold deposits. Econ. Geol. 84, 1315-1327.

Bowers T. S. and Helgeson H. W. (1983) - Calculation of the thermodynamic and geochimical consequences of nonidial mixing in the system H2O-CO2-NaCl on phase relations in geological systems: Equation of state for H2O-CO2-NaCl fluids at high pressures and temperatures. Geochim. Cosmochim. Acta 47, p. 1247-1275.

Bowers, T.S.; Jackson, K.J. and Helgeson, H.C. (1984) – Equilibrium Activity Diagrams (for coexisting minerals and aqueous solutions at pressures and temperatures to 5 kb and 600°C. Springer–Verlag, 397 pg.

Braux, C., Moravek, P., Janatka, J. and Bonnemaison, M., (1991) - Comparaison entre les gites aurifères du socle Varisque francais et du massif de Bohème. Chron.de la Recherche Minière 504: 21-39.

Brimhall, G.H. and Crerar, D.A. (1987) – Ore fluids: magmatic to supergene. In: Thermodynamic Modeling of Geological Materials: Minerals, Fluids and Melts, Ed. by I.S.E. Charmichael and H.P. Eugster. Reviews in Mineralogy, 17, Mineralogical Society of America, 235–321.

Brimhall, G.H. and Dietrich, W.E. (1987) – Constitutive mass balance relations between chemical composition, volume, density, porosity, and strain in metasomatic hydrothermal systems: results of weathering and pedogenesis. Geochim. et Cosmochim. Acta, 51, 567–587.

Brimhall, G.H., Alpers, C.N. and Cunninghan, A.B. (1985) – Analysis of supergene ore–forming processes and ground water solute transport processes using mass balance principles. Econ. Geol., 80, 1227–1256.

Brink, A.H., (1960) - Petrology and geology of the Vila Real - Sabrosa - V.P. Aguiar region, northern Portugal. Com. Serv. Geo. Portugal, T.43.

Bryndzia, T. and Scott,S.D. (1987) – The composition of chlorite as a function of sulphur and oxygen fugacity: an experimental study. Am.J.Sc., 287, 50–76.

Burg J. P. and Iglesias P. L. M. (1985) - Pressure-solution structures in granite. J. Struct. Geol. 7, p. 431-436.

Burnay Bank (1910) - Internal Report of Mining Concessions, (unpublished),in Circunscriçao Mineira do Norte, Porto.

Burnay Bank (1948) - Internal Report of Mining Concessions, (unpublished),in Circunscriçao Mineira do Norte, Porto.

Cabral, J.M. (1985) – Estudos de neotectónica em Trás–os–Montes Oriental. Mc. Sc. Thesis, Geol. Dep. Univ. Lisboa, Portugal.

Capdevila R. and Floor P. (1970) - Les différents types de granites hercyniens et leur distribution dans le Nord ouest de l'Espagne. Bul. Géol. Min. 81, p. 215-225.

Capdevila R., Corretge G. and Floor P. (1973) - Les granitoïdes varisques de la Meseta Iberique. Bul. Soc. Géol. de France 15, p. 209-228.

Carneciro Gomez R. M. A. (1982) - Granitoïdes del centro-Oeste de la provincia de Salamenca. Clasificacion y correlacion. IVe Reunion de Xeoloxia e Mineria do Noroeste Peninsular. Cuad. Trab. Lab. Laxe, p. 45-50.

Carvalho, A.D. (1979) - Breves referencias sobre Jazigos Auriferos Portugueses. Bol.Minas, Lisboa, 16 /(3/4):139-150.

Castro, P. (1992) - Estágio em micro=sonda electrónica. Unpubl. Report, Serv. Geol. Portugal, Lisboa.

Castroviejo R. (1990) - Gold oress related to shear zones, west Santa Comba -Fervenza area (Galicia, Spain). A mineralogical study. Mineral. Deposita, 25, suppl., 42-52.

Cathelineau M. and Boiron M.C., (1988) - Fluid mineral equilibria in French hydrothermal gold veins. Geol. Soc. Australia, 23, 428-430.

Cathelineau M., Boiron M.C., Holliger P., and Marion P., (1988) - Gold rich arsenopyrites : Crystal-chemistry, location and state of gold, and physical and chemical condition of crystallization . Geol. Soc. Australia, 22, 235-240.

Cathelineau, M. and Nieva, D. (1985) – A chlorite solid solution geothermometer. The Los Azufres (Mexico) geothermal system. Contrib. Mineral. Petrol., 91, 235–244.

Cathelineau, M., Boiron, M.C., Essarraj, S., Dubessy, J., Lespinasse, M. and Poty, B., (1993) - Fluid pressure variations in relation to multistage deformation and uplift: a fluid inclusion study of Au-quartz veins. Eur. J. Mineralogy, 5, 107-121.

Cathelineau, M., Boiron, M.C., Holliger, P. and Poty, B. (1990) - Metallogenesis of the french part of the Variscan orogen : Part II : time-space relationships between U and Au - ore deposition and tectonomagmatic events. Tectonophysics, 177, 59-79.

Cathelineau, M., Boiron, M.C., Holliger, P., Marion, P. and M. Denis (1989) - Gold-rich arsenopyrite : crystal chemistry, gold location and state, physical chemical conditions of crystallization: Econ. Geol, Monograph 6 ,"The geology of gold deposits : The perspective in 1988", 328-341.

Cerveira, A., (1947) - Notas sobre uma mina de ouro da serra da Louzã. Bol. Soc. Geol. Portugal, VI, 3, 245-254.

Cerveira, A., (1952) - Relações entre os jazigos hipogénicos portugueses de ouro e tungsténio. Bol. Soc. Geol. Portugal, 10, 133-144.

Charley, J. (1989) - "Montemor Prospect – Mineralogical and petrological descriptions of selected samples from outcrop and the following DDH's: T2, T3, T4, T6, T12, T24, T26, T28, T39, T40". RIOFINEX Internal Report.

Charoy B., (1979) - Définition et importance des phénomènes deutériques et des fluides associés dans les granites. Conséquences crsitallochimiques. Sci. de la Terre, 37, 346p.

Chryssoulis S.L., Cabri L.J., Lennard W. (1989) - Calibration of the ion microprobe for quantitative trace precious metal analyses in ore minerals Econ. Geol. 84, 1684-1689.

Colvine, A.C., (1989) - An empirical model for the formation of archean gold deposits : products of final cratonization of the Superior Province. In : The geology of gold deposits : the perspective in 1988. Ec. Geol. monograph, 6, pp. 37-53.

Condie K. C., (1993) - Chemical composition and evolution of the upper continental crust : Contrasting results from surface samples and shales. Chem. Geol., 104, 1-37.

Coney,P., Jones, D.L., Monger, J.W.H., (1980) - Cordilleran suspect terranes. Nature 288: 329-333.

Cook N.J., Chryssoulis S.L. (1990) - Concentration of "invisible god" in the common sulfides.Canadian Mineralogist, 28, 1-16.

Couto, H., Roger, G., Moelo, Y. and Bril, H., (1990) - Le district a antimoine-or Dúrico-Beirão Portugal: Evolution paragenétique et geochimique; implications metallogéniques. Min. Deposita, 25 (supp), 69-81.

Cuney M., Friedrich M;, Blumenfeld P., Bourguignon A., Boiron M.C., Vigneresse J.L., (1990) - Metallogenesis in the French part of Variscan orogen. Part I : U preconcentrations in pre-Variscanand Variscan formations. A comparison with Sn, W and Au. Tectonophysics, 177, 39-57.

Dallmeyer, R.D., (1989) - Terranes in the Circum-Atlantic Paleozoic Orogens. GSA Spec. Pap. n° 230

Dallmeyer, R.D., Ribeiro, A. and Marques, F., (1991) - Polyphase Variscan emplacement of exotic terranes (Morais and Braganta Massifs) onto Iberian successions: evidence from 40Ar/39Ar mineral ages. Lithos, 27: 133-144

Debon F., and Lefort P. (1983) - A chemical-mineralogical classification of common plutonic rocks and associations. Trans. R. Soc. Edim., Earth Sci., 73, 135-149.

Debon F., and Lefort P. (1988) - A cationic classification of common plutonic rocks and their magmatic associations : principles, mathod, applications. Bull. Mineral. 111,493-510.

Diez Balda, M. A., (1992) - El cizallamiento ductil subhorizontal de la segunda fase Hercinica al sur de Salamanca: engrossamiento y colapso extensional. Simposios, III Congreso geologico de Espana y VIII Congreso Latinoamericano de Geologia, Tomo 2: 365-374, Salamanca.

Diez Balda, M.A., (1990) - Structure of autochtonous sequences of Central-Iberian Zone. In: Dallmeyer, R.D. and Martinez Garcia, E (Eds.): Pre-Mesozoic Geology of Iberia : 172-188.

Diez Balda,M.A.; Vegas, R.; Gonzalez Lodeiro,F. (1990) - Structure of the Central-Iberian zone. In Pre-Mesozoic geology of Iberia. Springer-Verlag, Berlin. pp 172-188.

Dubessy J. (1984) - Simulation des équilibres chimiques dans le système C-O-H. Conséquences méthodologiques pour les inclusions fluides. Bull. Mineral. 107, 157-168.

Dubessy J., Poty B., and Ramboz C. (1989) - Advances in the C-O-H-N-S fluid geochemistry based on micro-Raman spectroscopic analysis of fluid inclusions. Eur J. Mineral. 1, 517-534

Duddy, I.R. (1980) – Redistribution and fractionation of rare–earth and other elements in a weathering profile. Chemical Geology, 30, 363–381.

Essarraj S. (1989) -.Microfracturation et circulation fluide dans les filons de quartz aurifères : Exemple du gisement de L'Aurieras (Massif Central). DEA, Univ Nancy I, 71 p.

Essarraj S. (1992) - Migration fluides, microfissuration et conditions de dépôt de l'or dans les veines de quartz aurifères. Thèse INPL Nancy, 399 p.

Eugster, H.P. and Gunter, W.D. (1981) - The compositions of supercritical metamorphic solutions. Bull. Soc. Fr. Mineral Cristallog. 104, 816-826.

Faria, A.F. (1988) - "Geology of the Montemor gold belt from Tabuleiros to Azinhaga". RIOFINEX Internal Report.

Farias P., Gallastegui,G., Lodeiro, F.G., Marquinez,J., Parra, L.M.M., Catalan, J.R.M., Macia,J.G.P. and Fernandez, L.R.R., (1987) - Aportaciones al conocimiento de la estratigrafia y estrutura de Galicia Central. An. Fac. Cien. Univ. do Porto, Mem. 1: 411-431.

Fernandez Turiel, J.L. (1987). Aspectos geológicos y metalogenéticos del Batolito de Ricobayo y Complejo de Villaseco-Pereruela y sus mineralizaciones asociadas (Zamora). Tesis Doctoral, Univ. de Salamanca. 307 pp.

Ferreira, N., Iglesia, M., Noronha, F., Pereira, E., Ribeiro, A., and Ribeiro, M. L., 1987 - Granotoides da Zona Centro Iberica e seu enquadramento geodinamico. in Geologia de los Granitoides y rocas asociadas del macizo hesperico. Libro homenaja a L. C. Garcia de Figuerola. Ed. Rueda, Madrid.

Ferreira, P., (1971) - Jazigos uraníferos portugueses. Jazigos de Au-Ag sulfuretos do Norte de Portugal. Livro guia da excursão nº 5 I C.H.L.A.G.E., Lisboa

Foster M.D. (1962) – Interpretation of the composition of trioctahedral micas. Geol. Survey Profess. Paper 354–B.

Gamond J. F., Giraud A. (1982) - Identification de zones de faille à l'aide des associations de fractures de seconde ordre, Bull. Soc. Geol. France (7), T XXIV, nº 4, pp.755-762.

Gamond, J. F. (1987) - Bridge structures as sence of displacement criteria in brittle fault zone.,Journal of Structural Geology, Vol 9, nº 5/6, pp. 609-620.

Gamond, J.F. (1983) – Displacement features associated with fault zones: a comparison between observed examples and experiment models. J.Struct.Geol., 5(1),33–45.

Gamond, J.F. (1985) – Bridge structures as sense of displacement criteria in brittle fault zones. J.Struct.Geol., 9(5/6), 609–620.

Garcia Palomero F, Bedia J.L., Garcia M., Sides E., (1986) - Nuevas investigaciones y trabajos de evaluacion de reservas de gossan en minas de Rio Tinto. Bol. Geol. y Minero, Madrid, T XCVII-V.

Garcia Palomero F, Malave J., Garcia M., Sobol F., Sides E., (1988) - Modelos geologicos para la exploracion y calculos de reservas a largo y corto plazo en el yacimiento de cobre de Cerro Colorado (Minas de Rio Tinto) Bol. Geol. y Minero, Madrid, T XCIX-I.

Gonzalez Clavijo, E. (1990) - Estudio geométrico y cinemático de la cizalla de Villalcampo (Zamora). Aplicación a la prospección minera. Tesis de licenciatura, Univ. de Salamanca. 98pp.

Gonzalez Clavijo,E.; Ortega, C.; Florido, P.; Locutura, J.(1991) - El control estructural de las mineralizaciones auríferas en la zona de Pino, provincia de Zamora (España). XI Reunuión de Geología del Oeste Peninsular. Huelva (España). In press.

Gouanvic Y, (1983), Métallogénéèse à tungstène étain et or dans le linéament granitique de Monteneme (NO Galicia, Espagne). These 3° cycle, Univ. Nancy I.

Grant N.T., Banks D.A., Mc Caig A.M., Yardley B.W.D., (1990) - The chemistry source and behaviour of fluids involved in Alpine thrusting of the central Pyrennees. J. Geophys. Res., 95, 9123-9131.

Guidotti, C.V. (1984) – Micas in metamorphic rocks. In: Micas (edited by Bailey, S.W.), Reviews in Mineralogy, 13, Mineralogical Society of America, 357–468.

Hancock, P.L. (1985) – Brittle microtectonic: principles and practice. J.Struct.Geol., 7(3/4), 437–457.

Harris, L.B. and Cobold, P.R., (1984) - Development of conjugate shear bands during bulk simple shearing. J. Struct. Geol., 7 (1): 37-44.

Heier K.S. and Billings G. K., (1970) - Rubidium In : Wedepohl K.H. ed, handbook of geochemistry, Springer Verlag, Vol II/4, 37.

Herranz, P., (1983) - El Precambrico de la Zona de Ossa Morena. In: Geol. de Espana, Libro Jubilar J.M.Rios, I.G.M.E.: 100- 108.

Houston, S. (1989).- "Report on the Montemor gold prospect; Portugal: petrological and geochemical description of host rocks and alteration related to gold mineralization". RIOFINEX Internal Report.

Howel, D.G. and Jones,D.L., (1984) - Tectonostratigraphic terrane analysis and some terrane vernacular. In: Howell,D.G.,Jones,D.L.,Cox, A. and Nur, A.(Eds.): Proc. Circum-Pacific Terrane conference. Stanford Univ. Pub. Geol. Scie. 18: 6-9.

Howel, D.G., Jones, D.L. and Schemer, E.R., (1985) - Tectonostratigraphic terranes in the Circum-Pacific region. In: Howell, D.G. (Eds.): Tectonostratigraphic terranes of the Circum-Pacific region. Houston, Circum-Pacific Coucil for Energy and Mineral Resources, Earth Sciences Series, 1: 3-30.

Hubert, P., (1986) -Textures et inclusions fluides des quartz aurifères. Application au gîte de Cros Gallet (Haute Vienne, France) et au prospect de Sanoukou (District de Kinieba, Mali): Document du B.R.G.M., 114, 350 p.

I.T.G.E. (1992). Ivestigación de detalle en el area de Pino (Zamora). Inédito, Centro de Documentación del I.T.G.E.

Iglesias M. and Chouckroune P. (1980) - Shear-zones in the Iberian Arc. J. Struct. Geol. 2, p. 63-68.

Iglesias M., Ribeiro M. L. and Ribeiro A. (1983) - La interpretacion aloctonista de la estructura del noroeste Peninsular. In: Geologia de Espana Int. Geol. Min. Espana, Madrid, p. 459-467.

Iglesias, M. and Chouckroune, P., (1980) - Shear zones in the Iberian Arc. J. Struct. Geol. 2 (1/2) : 63-68.

Iglesias, M., Ribeiro, M.L. and Ribeiro, A., (1983) - La interpretacion aloctonista de la estrutura del Noroeste Peninsular. In: Libro Jubilar de J.M. Rios, Geologia de Espa±a I, I.G.M.E.: 456-467.

Iglesias, M.P.L., Ribeiro, A. (1981) - La zone de cisaillemente ductile de Juzbado (Salamanca)-Penalva do Castelo (Viseu): Un linéament ancien ractivé pendant l'orogonèse hercynienne? Comun. Serv. Geol. Port., t. 67 (1), 89-93.

Jegouzo, P., (1980) - The South Armorican shear zone. J. Struct. Geol. 2 (1/2): 39-48.

Johnson G.A.L., (1973) - Closing the Carboniferous sea in western Europe. In: Tarling, D.H. and Runcorn, S.K. (Eds.): Implications of Continental Drift to the Earth Sciences, vol.II: 845- 850, London.

Johnson, G.A.L., (1978) - European plate movement during the Carboniferous.

Julivert,M; Fonbote, J.M.; Ribeiro, A.; Conde, L. (1972).- Mapa tectónico de la Peninsula Ibérica y Baleares (1:1.000.000). memoria explicativa (1980). Inst. geol. Min. de España, Madrid.

Junta de Castilla Y Leon (1986) - Estudio gológico-minero en el area de Pino (provincia de Zamora). Fase I. Consejería de Industria, Energía y Trabajo. Dirección General de Política Industrial.

Krestchmar U. and Scott S.D. (1976) Phase realtions involving arsenopyrite in the system Fe-As-S and their application. Canadian Mineralogist, 14, 364-386.

La Roche H. de (1964) - Sur l'expression graphique des relations entre la composition chimique et la composition minéralogique quantitative des roches cristallines. Présentation d'un diagramme destiné à l'étude chimico-minéralogique des massifs granitiques ou granodioritiques. Sci. de la Terre, 9, 293-337.

La Roche H. de, Leterrier J., Grandclaude P., and Marchal M. (1980) - A classification of volcanic and plutonic rocks using R1-R2 diagram and major element analyses. Its relationships with current nomenclature. Chem. Geol., 29, 183-210.

La Roche H. de, Stussi J. M., and Chauris L., (1980) - Les granites àà deux micas hercyniens français. Essais de cartographie et de correlations géochimiques appuyés sur une banque de données. Implications pétrologiques et métallogéniques. Sci. de la Terre,24, n°1, 5-121.

La Roche, H. de, (1968) - Comportement geochimique differentiel de Na, K et Al dans les formations volcaniques et sedimentaires: un guide pour l'étude des formations metamorphiques et plutoniques. C.R.Acad. Sci. Paris, 267, D:39-42.

Lapique F., Champenois M. and Cheilletz A. (1988) - Un analyseur vidéographique interactif description et applications. Bull Mineral. 6, 258-263.

Lefort, J.P. and Ribeiro, A., (1980) - La faille Porto-Badajoz- Cordoue a-t-elle controlé l'evolution de l'océan paléozoique sud- armoricain. Bull. Soc. Geol. France (7) 22 (3): 455-462.

Lespinasse M. (1990) - Les trainées d'inclusions fluides : marqueur microstructural des paléocontraintes et des migrations fluides. Unpubl. Thesis, Nancy I Univ., 288 p.

Lopez Plaza, M. (1982) - Contribución al conocimiento de la dinámica de los cuerpos graníticos de la penillanura salmantino-zamorana. Tesis doctoral, Univ. Salamanca. 332 pp

Lotze, F., (1945) - Zur gliederung der Varisziden der Iberischen Meseta.Geotekt Forsch 6: 78-92 (traduzido: Publicationes Extranjeras sobre Geol. Esp. 5: 149-166.)

Marion P. (1988) - Caractérisation des minerais sulfurés aurifères : mise en oeuvre de méthodes classiques et nouvelles. Unpublished Thesis, INPL, Nancy.

Marion P., Holliger P., Boiron M.C., Cathelineau M., and Wagner F.E. (1991) - New improvments in the characterization of refractory gold in pyrites : An electron microprobe, Mössbauer spectrometry and ion probe study.Brazil gold 91, Balkema Ed.,389-395.

Marion P., Regnard, J.R., and Wagner, F.E. (1986) - Etude de l'état chimique de l'or dans les sulfures aurifères par spectroscopie Mössbauer de 197 Au : premiers résultats: C.R. Acad. Sc. Paris, t. 302, série II, 8, 571-574.

Marques, F.G., Pereira, E. and Ribeiro, A., (1991) - Tectonic evolution of the deep crust: Variscan reactivation by extension and thrusting of Precambrian basement in the Bragan†a-Morais massifs (Tras-os-Montes, NE Portugal). Geodinamica Acta (Paris), 5 (1-2): 135-151.

Marquinez J. L. (1982) - Estudio geologico del area esquistosa de Galicia Central (Zona de Lalin Forcarei-Beariz). IVe Reunion de Xeoloxia e Mineria do Noroeste Peninsular. Cuad. Trab. Lab. Laxe, p. 135-154.

Martinez Garcia, E., 1973 - Deformation y metamorfismo en la zona de Sanßbria (Provincia de Léon, Zamora y Orense). Stud. Geol. V: 7-106.

Mateus, A. and Barriga, F.J.A.S. (1987) - Petrography and microdeformation of selected samples from Braços–Tabuleiros sector". RIOFINEX Internal Report.

Mateus, A.M. (1989) – Petrografia e microdeformação das rochas de falha e litótipos encaixantes do troço transmontano do acidente Manteigas–Vilariça–Bragança. Mc. Sc. Thesis, Geol. Dep. Univ. Lisboa, Portugal.

Mateus, A.M. and Barriga, F.J.A.S. (1990) – Metallogenetic implications of the geochemistry of the Vilariça fault breccias: a preliminary study. Proc. of VIII Semana de Geoquímica, Dep. Geol. Univ. Lisboa, Portugal.

Mateus, A.M. and Barriga, F.J.A.S. (1991) – Gold–silver mineralizations associated with the Vilariça Fault, NE Portugal. Brazil Gold'91 (edited by E.A. Ladeira), Balkema Publ., 615–622.

Matte P. and Ribeiro, A., (1975) - Forme et orientation de l'ellipsoide de deformation dans la virgation hercynienne de Galice. Relations avec le plissement et hypotheses sur la genèse de l'arc Ibero-Armoricain. C. R. Ac. Sc. Paris, Ser. D, 280: 2825-2828.

Matte, P. and Burg, J. P., (1981) - Sutures, thrusts and nappes in the Variscan Arc of Western Europe: plate tectonics implications. In: Mc Clay K.R. and Price,N.J. (Eds.): Thrust and nappe tectonics, London, Geol. Soc., Spec. Pub., 356-358.

Matte, P., (1986) - La chaine varisque parmi les chaines periatlantiques: modèle d'evolution et position des grandes blocs continentaux au Permo-Carbonifere. Bull. Soc. Geol. France, II: 1-24.

Matte,P., 1983 - Two geotraverses across the Ibero-Armorican Variscan Arc of western Europe. In: Rast, N., Delany, M. (Eds.): Profils of orogenic belts. AGU Geodin. Ser. 10: 53-81.

Mehnert, K.R. (1986) – Migmatites and the Origin of Granitic Rocks. Elsevier Publishing Company. 393 p.

Meireles, C. and Carvalho, J.H., em prep. - Enquadramento metalogenºtico das ocorrencias de Au em Portugal.

Moine, B., (1975) - Caractères des sedimentation et de metamorphisme des series précambriennes epizonales a catazonal du centre de Madagascar (region d'Ambaatofinandrahana). Sc. de la Terre. 31, 281p.

Moura, A., (1988) - Caracterizaçao de quartzos filonianos em regiao potoncialmente aurífera. Rel. de estágio Fac. Ciên.Univ.Porto. 132p.

Munha, J., Oliveira,J.T., Ribeiro, A., Oliveira,V., Quesada, C., Kerrich, R., 1986 - Beja-Acebuches Ophiolite: characterization and geodynamic significance. Maleo 2 (13): 31

Neiva, A.M.R., Neiva, J.M.C. and Silva, M.M.V.C., (1990) - Geochemistry of gold quartz vein walls from Jales (northern Portugal).Chem.Geol., 82, 217-251

Neiva, A.M.R.,(1992) - Geochemistry and evollution of Jales granitic system, northern Portugal. Chem. Erde, 52, 225-241

Neiva, J.M.C. and Neiva, A.M.R., (1990) - The gold area of Jales (northern Portugal). Terra Nova, 2, 243-254.

Neiva, J.M.C., (1945) - Alguns jazigos de ouro do alto Minho. Est. Not. Trab. I, 3 e 4, 190-265.

Nicolas A. and Jackson M. (1982) - High temperature dikes in peridodites: origin by hydraulic fracturing. J. Petrology 23, p. 568-582.

Noronha, F., Ramos, J.M.F., Rebelo, J., Ribeiro, A. and Ribeiro, M.L., (1979) - Essai de correlation des phases de deformation hercinienne dans le Nord-Ouest pºninsulaire. Bol. Soc., Geol. Portugal, XXI, 227-237.

Oliveira, J.M.S. and Ramos, J.A., (1987) - Estudos de geoquimica aplicada na regiao aurífera vizinha de Três Minas (Vila Pouca de Aguiar, Norte de Portugal). Est. Not. e Trab., D.G.G.M., 29, 3-25.

Oliveira, J.M.S., (1990) - Geological, mineralogical and lithogeochemical studies in the Gois and Vila Pouca de Aguiar - Vila Real region, Portugal. Est. Not. Trab., D.G.G.M., 32, 35-75.

Pascual,E., (1981) - Investigaciones geologicas en el sector Cordoba-Villaviciosa de Cordoba (Sector Central de Sierra Morena). Thesis, Univ. Granada, 521p.

Paterson M. S. (1978) - Experimental Rock Deformation-The Brittle Field. Springer, Berlin.

Pereira E, (1989) - Carta geologica de Portugal a escuela 1/20 000. Coordenador da noticia explicativa da Folha 1. Servicos geologicos de Portugal.

Pereira, E. and Meireles, C., em prep. - Cisalhamentos Hercynicos e controlo das mineralizases de W-Sn, Au e U na Z.C.I. , em Portugal.

Pereira, E., (1987) - Estudo geologico-estrutural da regiao de Celorico de Basto e sua interpretaçao geodinamica. Serv. Geol. Portugal. 274p.

Pereira, E., Iglesias, M. and Ribeiro, A (1984) - Leucogranitos - "stockscheider" e o controlo estrutural da mineralizaçoo na mina de Montesinho - Bragança. Comun. Serv. Geol. Portugal, t.70, fasc.1, 11-22.

Perez Estaun, A., (1974) - Aportaciones al conocimiento del Carbonifero de San Clodio (Prov. de Lugo). Breviora Geol. Asturica 18 (1): 3-8.

Petit, J. P. (1987) - Criteria for the sence of movement on fault surfaces in brittle rocks., Journal of Structural Geology, vol. 9 nº5/6, 597-608.

Pinto, M.S., Casquet, C., Ibarrola,E., Corregto, L.G. and Ferreira, M. R. P., (1987) - Syntese geocronologica dos granitoides do Maci†o Esperico. In: Libro Homenaje a L. C. Garcia de Figuerola: Geologia de los granitoides y rocas asociadas del Macizo Hesperico, 69-86. Editorial Rueda, Madrid.

Plimer I.R., (1982) - The Hillgrove antimony deposits : Geology of new England region Symposium Armidale N.S.W.July 1982, Proc., 277-284.

Potter R. W., Clime, M. A., Brown D. L. (1978) - Freezing point deposition of aqueous sodium chloride solution. Econ. Geol. 73, p. 283-285.

Potter R.W. (1977) - Pressure corrections for fluid inclusion homogenization temperatures based on the volumetric properties of the system NaCl-H2O. J.res. U.S. Geol. Surv. 6, 245-257.

Potter R.W., Clime M.A., and Brown D.L. (1978) - Freezing point deposition of aqueous sodium chloride solution. Econ. Geol 73, 284-285.

Poty B., Leroy J. and Jachimowicz L. (1976) - Un nouvel appareil pour la mesure des temperatures sous le microscope, l'installation de microthermométrie Chaix - Meca. Bull. Soc. Fr. Mineral. Cristallogr. 99, 182-186.

Prominas, (1988) - Internal Report of the C.M.P./Cercal/Prominas joint venture (unpblished), in Serv. Geol. Portugal, Lisboa

Quesada, C. and Munha, J. (1990) - "(The Ossa Morena Zone) Metamorphism".in :"Pre–Mesozoic Geology of Iberia" (1990). Dallmeyer, R.S. & Martinez Garcia, E. (ed.), pp. 252–258.

Quesada, C. et al. (1990) - "(The Ossa Morena Zone) Stratigraphy: Precambrien".in :"Pre–Mesozoic Geology of Iberia" (1990). Dallmeyer, R.S. & Martinez Garcia, E. (ed.), pp. 314–320.

Quesada, C., Apalatgui, O., Eguiluz, L., Lian, E. and Palacios,T., (1990) - Precambrian stratigraphy (Ossa-Morena Zone). In: Dallmeyer,R.D. and Martinez Garcia, E. (Eds.): Pre-Mesozoic Geology of Iberia, 252-258, Springer-Verlag.

Quesada,C., Larrea, F.J., Forido, P., (1987} - Mapa Geologico-Minero de Estremadura. Dir. Gen. Ind. Energ. Min. Junta de Estremadura : 1-131.

Quinquis, H., Audren, C., Brun,J.P. and Cobold, P.R., (1978) - Intense progressive shear in Ile de Groix blueschists and compatibility with subduction or obduction. Nature, 273: 43-45.

Quiroga, J.L. (1981). Estudio geológico del este de Zamora. Tesis doctoral, Univ. de Oviedo. 210 pp

Quiroga, J.L., (1980) - La sucession sil·rica en tierras de Aliste y Carbajales (Zamora) .Cuad. Lab. Xeol. Laxe 1: 147-156.

Ramboz C., (1980) - Géochimie et étude de phases fluides de gisements et indices d'étain tungstène du sud du Massif Central (France). Thèse 3° Cycle, INPL, 278 p.

Ribeiro, A. (1981) – A geotraverse through the Variscan Fold Belt in Portugal. In Variscan Orogen in Europe (Zwart, H.J. and Dornsiepen, U.F. eds.), Geol. Mijbouw 60(1), 41–44.

Ribeiro, A. and Pereira, E., (1981) - Controlos paleogeo- grßficos, petrologicos e estruturais na genese dos jazigos portugueses de estanho e volframio. Geonovas 1 (3): 23-31.

Ribeiro, A. and Pereira,, E., (1986) - Flacke tectonics in the NW iberia Variscides. Maleo, Bol. Inf. Soc. Geol. de Portugal 2(13): 38.

Ribeiro, A. Quesada, C. and Dallmeyer, R.D, (1990) - Geodynamic evolution of the Iberian Massif. In: Dallmeyer,R.D. and Martinez Garcia, E. (Eds.): Pre-Mesozoic Geology of Iberia: 399-410, Springer-Verlag.

Ribeiro, A. Quesada, C. and Dallmeyer, R.D., 1987 - Tectonostratigrafic terranes and the geodynamic evolution of the Iberian Variscan Fold Belt. Conference on Deformation and Plate Tectonics, Gijon (Spain), Abstract Vol. 60-61.

Ribeiro, A., (1974) - Contribution a l'étude tectonique de Trás-os-Montes oriental. Serv. Geol. Portugal. 24, 168p.

Ribeiro, A., Iglesias, M.,Ribeiro,M. L. and Pereira,E., (1983) - Modèle géodynamique des Hercynides Ibériques. Com. Serv. Geol. de Portugal, LXIX, 291-294.

Ribeiro, A., Pereira E. and Dias, R., (1990) - Structure in the NW of the Iberia Peninsula (Alloctonous sequences). In: Dallmeyer, R.D. and Martinez Garcia, E. (Eds.): Pre-Mesozoic Geology of Iberia: 220-236, Springer-Verlag.

Ribeiro, A., Pereira, E. and Gonzalves, L.S.M., 1980 - Analise da deformatio da zona de cisalhamento Porto-Tomar na transversal de Oliveira de Azemeis. Com.Serv.Geol. de Portugal, 66: 3-9.

Ribeiro, M.L. (1986) - Geologia e Petrologia da Região a SW de Macedo de Cavaleiros (Trás-os-Montes Oriental). Unpubl. Ph.D. Thesis. Serv. Geol. Portugal, Lisboa.

Ries, A. and Schackleton, R., (1987) - Pattern of strain variation in arcuate fold belts. Phil. Trans. R. Soc. A 283: 281-288.

Robardet, M. and Gutierez Marco, J.C., (1990) - Sedimentary and faunal domains in the Iberia Peninsula during lower Paleozoic times. In: Dallmeyer,R. D. and Martinez Garcia, E. (Eds.): Pre- Mesozoic Geology of Iberia: 383-395, Springer-Verlag.

Robardet, M., (1980) - Late Ordovician tillites in the Iberian Peninsula. In: Hamberg, M.J. and Harland, W.B. (Eds.): Eart's pre- Pleistocene glacial records. Cambridge Univ. Press.

Robardet,M. and Dore, F., (1988) - The late Ordovician diamictic formations from southestern Europe : north-Gondwana glaciomarine deposits. Palaeogeogr. Palaeocliatol. Palaeoecol. 66: 19-31.

Roedder E. (1972) - Composition of fluid inclusions. U.S. Geol. Surv., Prof Parper, 440JJ, 164 p.

Roedder E. (1984) - Fluid inclusions. Rev. Mineralogy V. 12, 644 p.

Roedder E. and Kopp O.C., (1975) - A check on the validity of the pressure correction in inclusion geothermometry, using hydrothermally-grown quartz. Fortsch. Mineral., 52, 431-446.

Romberger S.B., (1986) - The solution chemistry of gold applied to the origin of hydrothermal deposits. in Clark L.A. ed. Gold in western shield. Canadian Inst. Mining Metallurgy spec. Vol., 168-186.

Sanderson, D. J. and Marchini, W.R.D., (1984) - Transpression. J. Struct. Geol. 6 (5), 449-458.

Schermerhorn, L.J.C., (1981) - Framework and evolution of hercynian minerallization in the Iberian meseta. Leidse Geol. Med. 52, 1, 23-56.

Senior A. and Leake B.E., (1978) - Regional metamorphism and geochemistry of the Dalradian metasediments of Connemara, western Ireland. J. Petrol., 19, 585-625.

Shelton K.L. and Orville P.M., (1980) - Formation of synthetic fluid inclusions in natural quartz. Amer. Mineral., 65, 1233-1236.

Shepherd, T.J. and Miller, M.F. (1988) - Fluid inclusion volatiles as a guide to Tungsten deposits, Southwest England: Application to other Sn-W provinces in Western Europe. In: Boissonnas, J. & Omenetto, P. (eds) Mineral deposits within the European Community. Springer Verlag, pp29-52.

Silva, J. B., Oliveira, J. T. and Ribeiro, A.,(1990) - Structural outline of the South Portuguese Zone. In: Dallmeyer,R.D. and Martinez Garcia, E. (Eds.): Pre-Mesozoic Geology of Iberia: 348- 362.

Silva, M. M. V. G. and Neiva, A. M R. 1990 - Geochemistry of the granites and their minerals from Paredes da Beira - Penedono, Northern Portugal. Chem. Geol, 85:147-170.

Silva, M.M.V.C. and Neiva, A.M.R., (1990) - Geochemistry of the granites and their minerals from Paredes da Beira-Penedono, northern Portugal. Chem.Geol., 85, 147-170.

Sousa B., 1982 - Litostratigrafia e estrutura do "Complexo Xistograuvaquico Ante-Ordovocico"-Grupo do Douro (Nordeste de Portugal). unpubl. Ph. D. thesis Univ Coimbra. 223 pp.

Sousa,M.B. and Ramos,J.M.F., (1991) - Caracteristicas geologico-estruturais e quimico-mineralogicas das jazidas auriferas da região de Penedono-Tabuaço (Viseu-Portugal), Est. Not. e Trab., D.G.G.M., 33, 71-96.

Sterner S.M. and Bodnar R. J., (1984) - Synthetic fluid inclusions in natural quartz I Compositional types synthetized and aplication to experimental geochemistry. Geochim Cosmochim Acta, 48, 2659-2668.

Taylor S.R. (1964) - Abundance of chemical elements in the continental crust : a new table. Geochim. Cosmochim. Acta, 28, 1273-1285.

Taylor, S.R. and Melennon, S.M., (1986) - The continental crust: its composition and evolution. Blackwell. 312p.

Tchalenko, J. S. (1970) - Similarities between shear zones of diferent magnitudes. - Geol. Soc. of America Bull., vol 81, 1625-1640

Teixeira, C. and Pais, J., (1973) - Sobre a presen†a de Devonico na regiao de Bragança (Guadramil) e de Alcanices (Zamora) .Bol. Soc. Geol. de Portugal 18: 199-202.

Thadeu, D., (1977) - Hercynian paragenetic units of the portuguese part of the hesperic massif. Bol. Soc. Geol. Portugal, 20, 247-276.

Velde, B. (1965) – Phengite micas: synthesis, stability, and natural occurrence. Amer.J.Sci., 263, 886–913

Velde, B. (1977) – Clays and clay minerals in natural and synthetic systems. Dev. Sedimentol., 21, 218

VigneresseJ. L., Cuney M., Jolivet J.,and Bienfait G., (1989) - Selective heat producing element enrichment in a crsutal segment of mid-European Variscan chain. Tectonophysiscs, 159, 47-60.

VigneresseJ. L.,Jolivet J., Cuney M. and Bienfait G., (1987) - Heat flow, heat production and depth of granites in western France. Geophys. Res. Lett., 14-3, 275-278.

Villar, P. (1990) - Estructura del Antiforme de Villadepera (Zamora). Tesis de licenciatura, Univ. de Salamanca

Wagner, F.E., Marion, P. and Regnard, J.R. (1986) - Mössbauer study of the chemical state of gold in gold ores: GOLD 100, Proceeding of the international conference ore gold, Extractive metallurgy of gold, Johannesburg, SAIMM, V. 2,.435-442.

White J. H., Burrows S. E., Carreras J. Shaw N. D. and Humphreys F. J. (1980) - On mylonites in ductile shear-zones. J. Struct. Geol. 2, p. 175-187.

Wu X. and Delbove F. (1989) - Hydrothermal synthesis of gold bearing arsenopyrite. Econ. Geol. 84, 2029-2032.

Wu X., (1989) - L'arsenopyrite aurifère, composition, conditions de genèse : L'apport des synthèses minérales et de l'étude de gisements d'or (Le Chatelet, L'Auriéras, France). Unpubl. thesis, Orléans Univ, 207 p.

Yardley, B.W.D. Banks, D.A. Bottrell, S.H. and Dymond, L.W. (1993) - Post-metamorphic gold-quartz veins fom N.W. Italy: The composition and origin of the ore fluid. Min. Mag. in press.

Zappettini E. O.(1983) - Le gisement d'or du Chatelet (Creuse, Massif Central français). Cadre géologique régional, étude métallogénique. Unpub. Thesis, Limoges, 151p.

Zhang Y. G. and Frantz J.D., (1987) - Determination of the homogenization temperatures and densities of supercritical fluids in the system NaCl-KCl-CaCl2-H2O using synthetic fluid inclusions. Chem. Geol., 64, 335-350.

Ziegler, P.A., (1984)- Caledonian and Hercynian consolidation of western and central europe, a working hypothesis. Geol. mijbouw 63: 93-108.

ANNEX

CHAPTER II

	Tabuaço Massif						Penedono Massif		
Granite type	Sedim	Paredes	Laboreira	Monte Airoso	Greisen (Laboreira)	Dacotim	Penedono	Ferronha	Vale Frade
SiO2	72.68 0.75	72.73 0.85	73.36 1.41	73.20 0.65	62.69	73.05 0.99	71.19 0.75	73.67 2.07	71.32 1.28
TiO2	0.13 0.04	0.02 0.04	0.12 0.02	0 0	0.14	0.12 0.02	0.11 0.04	0.20 0.04	0.29 0.12
Al2O3	14.63 0.56	15.45 0.73	14.33 0.58	14.49 0.41	20.61	15.11 0.33	15.07 0.70	14.16 1.25	15.31 0.47
Fe2O3	0.17 0.12	0.15 0.21	0.25 0.16	0.02 0.03	0.42	0.32 0.20	0.26 0.12	0.22 0.15	0.50 0.38
FeO	0.99 0.07	0.55 0.06	0.72 0.10	0.61 0.16	0.32	0.80 0.10	0.91 0.19	0.99 0.22	1.43 0.39
MnO	0.01 0.01	0.02 0.01	0.03 0.01	0.05 0.00	0.02	0.02 0.01	0.02 0.00	0.02 0.01	0.03 0.01
CaO	0.96 0.63	0.48 0.32	0.58 0.18	0.64 0.01	0.05	0.59 0.15	0.88 0.19	0.06 0.14	0.70 0.17
MgO	0.40 0.21	0.12 0.13	0.17 0.08	0.10 0.01	0.12	0.25 0.10	0.42 0.12	0.28 0.14	0.42 0.16
Na2O	3.38 0.34	4.48 0.68	4.37 1.01	3.87 0.45	1.26	3.37 0.24	4.60 0.84	3.39 0.08	3.35 0.47
K2O	4.80 0.55	4.14 0.45	4.56 0.34	4.17 0.37	7.13	4.45 0.21	5.05 0.42	5.07 0.35	5.02 0.31
P2O5	0.53 0.15	0.48 0.10	0.51 0.05	0.54 0.02	0.67	0.53 0.27	0.50 0.06	0.47 0.07	0.64 0.21
H2O+	0.04 0.19	0.55 0.40	1.02 0.14	0.87 0.37	4.04	1.02 0.07	0.90 0.22	0.93 0.09	0.91 0.08
H2O-	0.15 0.04	0.07 0.05	0.12 0.13	0.07 0.01	0.27	0.14 0.08	0.14 0.10	0.07 0.01	0.11 0.06
Li.	178 96	210 127	200 28		120	234 47	75 30	88 54	164 77
Sn					32				
F	1057 360	1964 504	1294 122		1942	1534 275	943 294	901 300	1557 398
Rb	406 64	658 137	408 23	528 28	530	502 53	363 33	390 34	371 32
Sr	38 8	19 7	40 2	18 4	48	36 7	40 16	55 14	95 34
Y	22 3	22 4	25 0	19 1	35	25 2	20 2	22 2	21 1
Zr	74 6	50 5	72 1	42 8	96	67 8	77 18	89 19	146 62
Nb	22 3	27 5	18 1	23 3	22	25 4	20 2	17 2	16 4
Ba	222 33	119 46	200 1	108 6	219	228 25	235 40	288 20	356 105
Ta	3 2	5 3		13 1	1	1	3 2		

Table II -1 : Average and standard deviation for representative granites of Penedono area.

	SiO2 %	Al2O3 %	Fe2O3 %	MnO %	MgO %	CaO %	Na2O %	K2O %	TiO2 %	P2O5 %	P.F. %	Total	Au ppb	Ag ppm	As ppm	Ba ppm	Be ppm	Br ppm	Co ppm	Cr ppm	Cs ppm	Cu ppm	Ga ppm	Hf ppm	Hg ppm	Ir ppm	Mo ppm	Ni ppm	Rb ppm	Sb ppm	Sc ppm	Se ppm	Sr ppm	Ta ppm	Nb ppm	V ppm	W ppm	Y ppm	Zn ppm	Zr ppm	La ppm	Ce ppm	Nd ppm	Sm ppm	Eu ppm	Gd ppm	Tb ppm	Dy ppm	Er ppm	Yb ppm	Lu ppm	U** ppm	Th** ppm
A UNITY																																																			
MA 59	64,62	17,57	7,13	0,04	1,62	0,08	0,81	3,45	0,83	0,16	3,42	99,73	11	<5	14	603	2	<1	17	96	8	27	24	4,5	<1	<5	<5	53	162	<0,2	12,8	<5	87	<1	8	101	<4	22	105	149	59	110	37	7,4	2		<0,5			3,94	0,59	2,78	13,51
MA 61	54,4	22,71	6,55	0,1	2,27	1r	0,6	3,08	0,96	0,15	4,33	99,33				727	3,69		10	119		25	13					38	234		17,3		91		10	119		23	105	161	39,81	85,61	29,45	5,69	1,13	4,64		4,91	2,9	3,09	0,49	3	18,17
MA 67	64,12	18,28	6,44	0,03	1,41	0	0,3	4,16	0,88	0,15	3,96	99,73				613	2			93		30	25					54	155		11,8		44		9	96		22	156	228											3,53	14,44
MA 117	47,17	25,35	10,25	0,1	2,87	0,04	3,91	3,83	1,27	0,11	4,73	99,65	13	<5	<2	656	3	<1	24	158	10	24	28	12	<1	<5	<5	74	210	1	21,1	<5	227	4	23	152	<4	26	143	275	63	130	41	8,9	2		<0,5			5,94	0,95	4,48	20,09
MA 118	59,5	20,31	7,8	0,08	2,12	0	0,81	3,95	0,93	0,13	4,08	99,71	13	<5	<2	685	2,7	<1	20	124	13	40	27	5,9	<1	<5	<5	45	201	1,9	16	<5	64	1	16	109	<4	26	100	155	66	120	48	9	1,9		1,3			4,24	0,7	2,32	17,29
MA 149	60,9	20,03	7,19	0,03	1,82	0	0,81	3,79	0,96	0,14	4,08	99,75				593	2,2			110		20	25					38	196		14,3		82		9	120		25	100	161											1,92	15,19
MA 150	58,04	21,14	8,03	0,13	1,88	0	0,38	4,83	0,88	0,16	4,23	99,7				789	2,2			113		22	28					48	306		14,8		49		8	107		21	117	140											2,34	15,82
MA 152	55,75	23,78	6,94	0,1	0,8	0	0,25	5,47	0,83	0,2	5,62	99,74				763	2,7			131		49	30					43	224		14,3		65		9	117		6	153	95											1,11	8,97
MA 155	45,42	28,52	9,71	0,12	1,66	Tr	0,43	6,33	1,12	0,2	6,14	99,65				876	4		12	153		35	29					40	283		22,2		108		15	157		25	96	148	52,38	104,1	43,41	8,27	1,61	6,24		5,61	3,16	3,33	0,52	3,41	23,29
MA 159	61,57	19,82	6,94	0,03	1,52	0,19	1,18	3,75	0,93	0,22	3,58	99,73				596	2,9		11	104		18	11					12	187		14,8		118		12	105		30	83	217	67,43	122,4	53,05	10	1,78	8,11		6,78	3,39	3,53	0,51	3,59	17,93
MA 160	56,92	20,75	8,55	1,08	1,67	0,28	0,17	4,75	0,76	0,25	4,51	99,69	<5	<5	83	1069	2,7	<1	13	118	13	37	12	5,4	<1	<5	<5	47	175	<0,2	15,8	<5	53	<1	8	108	<4	37	115	119	64,52	88,26	58,36	11,1	2,25	9,18	2,5	7,47	3,79	3,9	0,59	2,78	14,46
MA 163	54,84	22,57	9,32	0,26	2,04	Tr	0,4	4,69	0,79	0,19	4,61	99,71				987	3,2		36	108		26	16					61	193		17,3		96		6	126		21	96	108	43,97	89,87	37,91	7,46	1,56	5,62		4,94	2,5	2,43	0,38	2,71	14,37
MA 164	53,24	24,48	8,44	0,04	1,28	Tr	0,48	4,65	0,91	0,17	6,05	99,74				671	3,7		16	128		65	20					62	229		19,3		131		12	149		21	117	135	6,63	19,66	5,93	1,82	0,61	2,69		4,07	2,46	2,73	0,43	2,97	19,23
MA 165	64,09	17,96	7,03	0,02	1,62	0,08	1,22	3,2	0,97	0,14	3,23	99,65				513	2,7		16	107		28	12					46	158		13,1		102		15	96		35	98	455	60,23	113,7	48,7	9,69	1,87	7,67		7,35	4,01	4,37	0,64	4,64	21,65
B UNITY																																																				
AD 8	62,82	20,10	2,67	0,02	0,88	0,02	0,16	5,55	0,93	0,2	5,71	99,06	13	<5	4	1417	2,2	<1	<5	87	15	36	28	6,6	<1	<5	<5	12	205	1,6	19,6	<5	38	<1	17	111	<4	34	98	187	63	120	33	7,5	2,2		1,3			4,5	0,63	11,1	21,7
AD 7	70,44	13,48	3,17	0,01	0,89	0,51	0,30	2,90	0,56	0,93	6,45	99,64	9	<5	17	1319	3	<1	<5	112	2	49	24	0,6	<1	<5	11	21	104	0,3	14,3	<5	64	<1	12	457	<4	37	74	98	20	29	17	3,6	1		0,8			3,63	0,59	13,05	10,43
AD 10	91,06	3,49	0,72	Tr	0,10	0,02	Tr	0,88	0,11	0,26	3,22	99,86				271	1,2		<5	99		20	<5					11	35		2,5		<5		<5	682		7	20	<5												
AD 17	77,31	8,21	6,23	Tr	0,72	0,22	0,03	0,81	0,30	0,60	5,34	99,77				308	<,5		16	104		187	11					47	32		5,6		<5		8	147		7	40	41												
AD 31	87,42	6,04	0,64	Tr	Tr	Tr	Tr	1,63	0,56	0,08	3,36	99,73				669	<,5		<5	34		20	11					24	30		2,5		75		6	47		<5	19	451												
AD 59	82,00	6,94	4,08	0,02	0,24	Tr	Tr	0,96	0,20	0,15	5,22	99,81	10	<5	26	243	3	<1	52	139	3	280	<5	1,5	<1	<5	<5	84	38	1	4	<5	12	<1	<5	930	7	54	58	33	40	58	43	8,5	3		2,8			8,97	1,32		
AD 60	96,64	0,79	0,44	Tr	Tr	Tr	Tr	0,16	0,02	0,06	1,79	99,90	20	<5	18	84	<,5	<1	<5	71	<2	9	<5	<0,5	<1	<5	9	5	11	0,9	<1	<5	<5	<1	<5	285	<4	<5	8	<5	7	9	6	1,2	0,4		<0,5			1,35	0,21		
AD 62	93,59	0,75	0,40	Tr	Tr	0,34	Tr	0,15	0,03	0,52	4,12	99,90				61	<,5		<5	116		<5	<5					12	11		1		<5		<5	254		16	8	<5												
AD 63	95,44	0,83	0,26	Tr	Tr	Tr	Tr	0,24	0,02	0,05	3,04	99,88	<5	<5	<2	305	<,5	<1	<5	128	<2	<5	<5	<0,5	<1	<5	9	20	9	0,6	<1	<5	<5	<1	<5	443	<4	5	8	<5	6	15	7	1,6	0,6		<0,5			3,09	0,44		
AD 64	92,96	0,78	0,50	Tr	0,06	Tr	Tr	0,11	0,08	0,13	4,65	99,27				60	<,5		<5	58		7	<5					13	10		1,7		<5		<5	130		4843	14	4848												
AD 65	88,93	6,33	0,27	Tr	0,06	Tr	Tr	1,87	0,20	0,08	2,01	99,75				601	<,5		<5	27		<5	<5					7	38		1,29		<5		<5	52		<5	13	76												
AD 11	95,81	1,06	0,40	Tr	0,04	Tr	Tr	0,32	0,03	0,06	2,10	99,82	<5	<5	17	315	<,5	<1	5	117	<2	19	<5	0,9	<1	<5	14	<5	11	6,1	1,1	<5	<5	<1	<5	342	<4	6	54	<5	10	25	12	2,4	0,8		0,7			2,42	0,35		
AD 12	95,90	0,71	0,45	Tr	0,03	Tr	Tr	0,16	0,02	0,06	2,52	99,85				167	<,5		12	256		19	<5					25	8		<1		<5		<5	232		6	12	<5												
AD 13	95,59	0,76	0,40	Tr	Tr	Tr	Tr	0,20	0,02	0,10	2,78	99,85				309	<,5		14	185		9	17					29	8		<1		<5		<5	430		<5	<5	<5												
AD 18	97,75	0,44	0,24	Tr	Tr	Tr	Tr	0,13	Tr	0,04	1,32	99,92	17	<5	<2	97	<,5	<1	<5	134	<2	11	9	<0,5	<1	<5	6	19	5	0,4	<1	<5	<5	<1	<5	225	<4	<5	11	<5	3	4	<5	0,6	0,2		<0,5			0,61	0,1		
AD 20	97,20	0,72	0,20	Tr	Tr	Tr	Tr	0,17	Tr	0,08	1,47	99,84				143	<,5		<5	70		58	<5					<5	7		<1		<5		<5	367		<5	13	<5												
AD 26	94,64	1,37	0,60	Tr	0,03	Tr	Tr	0,38	0,04	0,08	2,70	99,84	17	<5	22	438	0,6	<1	<5	208	2	8	<5	<0,5	<1	<5	<5	10	16	0,5	1,5	<5	23	<1	<5	506	5	10	16	<5	11	16	12	3,1	0,9		0,8			2,91	0,46		
AD 16	59,92	21,32	5,01	0,06	2,22	Tr	1,10	3,22	0,93	0,17	5,70	99,65				924	2,4		6	149		30	31					17	136		14,6		118		12	188		24	77	102												
AD 9	53,15	19,50	5,04	0,08	2,52	4,26	2,77	2,84	0,96	0,29	8,96	100,37	<5	<5	7	1023	5,8	<1	<5	119	21	38	15	9	<1	<5	<5	22	137	2,3	20,3	<5	325	2	18	257	<4	61	56	209	36	50	27	6,3	1,8		1,6			8,64	1,52	1,35	0,51
AD 15	98,71	0,10	0,50	0,11	Tr	Tr	Tr	Tr	Tr	0,04	0,49	99,95				<5	<0,5		<5	72		5	<5					10	<5		<1		<5		<5	5		<5	<5	<5												
MA 57	73,21	13,35	2,7	0,03	0,94	1,29	2,25	3,89	0,48	0,17	1,41	99,72	<5	<5	3	794	2,2	<1	6	49	4	10	6	8,8	<1	<5	<5	14	107	0,6	7,5	<5	230	2	10	48	4	21	58	214	42	75	27	5,3		1,5		<0,5	3,75	0,54		
MA 39	67,1	17,33	2,61	0,02	3,34	0,05	0,27	3,91	0,22	0,17	4,65	99,67	14	<5	3	1287	2	<1	9	6	10	39	13	6	<1	<5	<5	29	117	0,7	4,5	<5	23	<1	7	12	<4	37	89	143	37	86	36	6,7	1		1,5			5,58	0,8		
MA 26	51,6	24,75	8,28	0,15	2,11	0,15	0,71	5,2	0,97	0,17	4,45	98,54	<5	<5	65	730	4,59	<1	8	118	26	35	29	6	<1	<5	<5	39	270	1,3	23,8	<5	116	<1	14	130	5	35	127	127	97	170	64	11	2,5		<0,5			5,48	0,81		
MA 36	75,47	11,19	2,45	0	0,22	0,22	3,79	1,28	0,45	0,11	2,17	97,35	25	<5	5100	406	2	<1	<5	28	3	5	1	9,2	<1	<5	<5	1	31	<0,2	3,5	<5	109	<1	9	25	24	17	53	229	41	74	29	5,1	1,2		<0,7			2,1	0,37		
MA 121	66,28	16,35	5,5	0,08	1,82	0,32	0,81	4,37	0,81	0,17	3,2	99,71	<5	<5	69	768	2,7	<1	16	109	14	9	23	7,3	<1	<5	<5	49	172	1,6	11,8	<5	82	1	14	83	<4	20	88	208	48	86	33	5,8	1,5		1,1			4,15	0,63	1,65	12,08
MA 122	76,31	11,83	2,77	0,05	0,64	1,1	2,9	1,18	0,48	0,17	2,06	99,51	<5	<5	200	333	1,7	<1	<5	94	3	10	14	12	<1	<5	<5	24	44	0,8	5,8	<5	170	<1	6	41	<4	14	45	199	48	90	33	5,4	1,4		<0,5			2,86	0,52	3,04	13,07
MA 123	74,54	12,66	3,58	0,02	1,2	0,06	2,12	2,47	0,55	0,1	2,51	99,81	<5	<5	83	480	1,29	<1	8	69	7	23	14	4,8	<1	<5	<5	23	92	1,8	7	<5	38	<1	6	52	<4	15	59	207	41	84	25	6,1	1,4		<0,5			3,44	0,53	2,18	9,5
MA 126	67,34	13,88	10,19	0,05	1,2	0	0,1	2,45	0,93	0,08	3,47	99,69	12	<5	16	437	2,58	<1	15	76	7	31	21	21	<1	<5	<5	51	114	0,5	11,9	<5	42	2	20	81	<4	33	120	651	69	130	49	11	2,9		2,5			5,91	0,97	3,55	25,11
MA 127	96,4	1,31	1,04	0	0,22	0	0	0,14	0	0	0,92	99,93	15000	<5	11	1	7,58	<1	<5	5	<2	123	1	<0,5	<1	<5	<5	1	10	0,4	0,5	<5	1	<1	1	1	<4	1	84	1	2	<3	<5	0,4	<0,2		<0,5			0,25	<0,05	0,5	1,27
MA 128	61,45	20,82	6,44	0,03	1,72	1	0,34	4,39	1,02	0,12	4	100,3	20	<5	19	739	3,08	<1	8	60	11	26	1	7,2	<1	<5	<5	8	221	1,1	15,5	<5	93	3	1	11	<4	33	107	205	86	160	68	14	3,6		2,7			6,77	1,03	3,1	17,81
MA 130	71,46	16,91	1,97	0	0,68	0,11	0,08	5,41	0,34	0,11	2,86	99,93	10	<5	58	709	6,58	<1	<5	114	14	27	40	6,5	<1	<5	<5	11	390	3,2	5	<5	29	1	1	81	23	23	38	174	39	87	27	5,4	1,5		1,5			4,11	0,64	1,42	7,63
MA 145	71,96	13,96	4,32	0	1,08	0,11	2,37	2,67	0,64	0,17	2,48	99,76	<5	<5	11	392	1,6	<1	12	55	6	25	12	11	<1	<5	<5	36	104	<0,2	7,4	<5	39	<1	6	58	<4	22	89	265	48	83	31	5,3	1,1		<0,5			2,96	0,57	2,09	12,54
MA 146	74,65	14,16	2,79	0	0,56	0	0,14	3,59	0,64	0,08	3,2	99,81	41	<5	62	490	1,7	<1	<5	74	12	24	14	4,2	<1	<5	<5	10	172	3,8	9,5	<5	24	<1	1	80	5	13	26	85	50	92	28	5,5	1,8		<0,5			3,14	0,49	1,02	10,35
MA 147	88,43	6,66	1,16	0	0,28	0	0,06	1,92	0	0,04	1,3	99,85	22800	<5	12	277	0,8	<1	<5	17	5	8	1	<0,5	<1	<5	<5	1	79	1	0,5	<5	9	<1	1	5	<4	1	27	1	2	5	<5	0,4	<0,2		<0,5			0,6	<0,05	0	0
MA 156	65,96	14,75	3,69	0,08	1,37	10,55	0,48	0,15	0,51	0,16	1,71	99,41				295	5,4		9	303		20	10					71	10		11,7		408		5	66		24	48	209	35,68	62,72	30,56	5,83	1,22	4,58		4,05	2,25	2,29	0,36	2,01	8,91
MA 157	80,96	7,83	4,82	Tr	0,88	0,2	1,12	1,66	0,45	0,8	1,68	99,68				376	1,29		5	78		15	<5					21	74		5		76		<5	44		19	32	617	30,35	64,73	27,16	6,01	1,17	5,1		4,64	2,35	2,52	0,43	2,65	12,98
MA 158	76,54	8,1	7,15	0,02	1,21	0,3	0,86	1,82	0,45	0,17	1,79	98,41				346	1,29		8	97		26	<5					26	99		6		67		<5	55		23	48	523	28,28	70,36	30,39	7,7	1,56	6,9		6,07	2,86	2,77	0,45	2,71	13,64
MA 161	78,31	10,8	2,72	0,03	0,78	0,59	2,72	1,82	0,43	0,11	1,49	99,8				423	1,5		5	62		8	8					17	74		5		98		<5	42		11	32	233	27,12	53,82	20,97	4,07	0,79	2,93		2,5	1,35	1,52	0,24	2,29	10,27
MA 162	79,27	7,91	5,58	0,03	1,12	1,11	1,25	1,87	0,55	0,29	1,06	100				413	1,79		5	144		7	<5					27	57		6,3		262		<5	46		27	38	980	30,46	69,5	28,13	6,5	1,3	5,97		5,7	3,24	3,27	0,56	3,97	16,95
C UNITY																																																			
MA 16	70,42	14,94	4,54	0,05	1,6	0,25	0,65	3,77	0,66	0,22	2,63	99,73				835	1,7			49		21	6					14	121		12,5		87		10	48		29	88	196												
MA 27	72,84	14,06	4,64	0	0,64	0	0,15	3,54	0,68	0,08	3,13	99,76				736	1,2			79		16	13					21	118		8,3		37		7	75		11	69	227											2,44	12,04
MA 120	82,56	8,89	2,17	0	0,27	0,03	0,64	2,17	0,34	0,08	1,96	99,11	14	<5	4	432	1,1	<1	<5	97	6	11	13	6,6	<1	<5	<5	14	73	0,6	4,1	<5	69	<1	1	31	<4	9	27	204	29	56	17	3,5	1		<0,5			2,2	0,35	2,12	8,7
MA 125	64,77	17	5,32	0,07	0,88	0,03	0,38	4,41	0,8	0,1	3,28	99,21	24	<5	42	609	3,7	<1	6	104	22	13	22	5,9	<1	<5	<5	26	179	0,7	13	<5	173	<1	16	89	<4	29	68	171	68	140	42	8,1	2		1,6			4,81	0,88	2,95	17,95
MA 129	53,82	21,35	8,49	0,05	1,97	0,03	0,68	5,48	0,86	0,16	4,74	99,63	13	<5	3	1110	3,4	<1	23	112	13	11	27	4,3	<1	<5	<5	47	192	2,6	16,5	<5	75	<1	15	115	<4	36	124	139	88	150	54	12	3,1		2,2			5,94	0,92	2,69	19,07
MA 132	92,5	4,69	0,32	0	0	0	0,02	1,16	0,16	0	1,02	99,87	<5	<5	5	217	1	<1	<5	53	2	1	1	7,5	<1	<5	<5	1	44	0,3	1,3	<5	24	<1	1	11	<4	1	1	169	15	33	12	2,1	0,7		<0,5			1,31	0,23	1,04	4,48
MA 133	78,99	10,48	3,08	0,03	0,65	0,08	0,85	2,83	0,48	0,11	2,17	99,75	21	<5	15	450	1	<1	<5	66	8	8	10	6,9	<1	<5	<5	17	87	0,5	6,6	<5	39	<1	5	56	<4	12	49	196	28	59	23	3,8	0,8		<0,5			2,52	0,43	1,55	8,45
MA 136	71,53	15,38	7,2	0	0,26	0,05	0,1	2,33	0,86	0,13	1,91	99,75	10	<5	<2	344	2	<1	9	72	24	7	12	8,5	<1	<5	<5	16	122	0,4	12,3	<5	75	2	7	62	<4	25	83	202	53	110	39	8	1,7		1,9			4,85	0,76	2,81	11,29
D UNITY																																																			
MA 20	58,29	18,78	7,41	0,06	3,25	0,6	1,04	6,37	0,78	0,22	2,87	99,67	11	<5	4	955	2,9	<1	<5	105	<2	37	28	<0,5	<1	<5	<5	47	225	0,6	19,2	<5	44	<1	14	112	<4	28	99	150	5	9	<5	1	0,4		<0,5			1,37	0,21		
MA 22	78,05	10,73	2,77	0,05	0,68	0,78	3,29	1,48	0,48	0,13	0,95	99,39	7	<5	2	350	1,2	<1	7	41	5	8	16	17	<1	<5	<5	10	60	0,8	5,9	<5	104	2	11	41	<4	23	42	405	52	100	32	6,3	1,4		1,2			4,37	0,67		
MA 22A	67,96	14,1	4,08	0,53	0,96	9,21	0,64	0,13	0,44	0,17	1,57	99,79	24	<5	2	18	1,7	<1	9	221	22	12	18	5,4	<1	<5	<5	50	9	2,7	10,3	<5	213	<1	14	75	10	28	36	188	41	74	22	5,1	1,3		1,3			4,45	0,62	3,05	9,87
MA 22B	46,82	26,77	8,96	0,14	2,41	0,5	0,96	7,8	1,13	0,24	3,83	99,56	33	<5	<2	1394	3,9	<1	21	142	18	31	37	7,6	<1	<5	<5	52	293	0,6	19,5	<5	98	<1	22	127	<4	34	118	267	96	180	53	11	2,5		<0,5			5,52	0,9	2,68	21,39
MA 24	72,96	12,35	3,42		0,88	2,31	3,7	0,88	0,52	0,16	0,81	98,12				409	2,5			34		15	8					11	6		7		175		10	31		18	60	287												
MA 110	71,62	13,88	4,19	0,03	1,37	0,59	1,38	3,89	0,59	0,22	1,96	99,72	<5	<5	4	616	1,7	<1	8	73	15	16	15	9,7	<1	<5	<5	17	148	1,3	7,5	<5	71	2	7	61	<4	19	64	201	52	100	39	7,2	1,6		<0,5			4,09	0,65	2,64	10,87

Table II -2 : Geochemical data of metasediments from VPA area

Table II - 3

	F 1 43%	F 2 14%	F 3 9%
Al	0,955	0,173	0,028
Fe	0,845	-0,078	-0,016
Mg	0,705	0,196	0,026
Na	-0,323	0,370	-0,222
K	0,881	0,250	0,076
Ti	0,870	0,298	-0,047
P	-0,049	-0,353	-0,034
P.F.	0,609	-0,515	0,363
Ba	0,719	0,128	0,102
Be	0,560	-0,014	-0,237
Co	0,403	-0,663	-0,177
Cr	0,555	-0,419	0,019
Cu	0,063	-0,820	-0,246
Ga	0,825	0,066	0,128
Ni	0,633	-0,549	-0,048
Rb	0,906	0,149	0,108
Sc	0,947	0,082	0,107
Sr	0,278	0,399	-0,191
Nb	0,767	0,121	0,082
V	0,010	-0,834	-0,083
Y	-0,285	-0,132	0,906
Zn	0,889	0,004	0,016
Zr	-0,299	-0,033	0,852

Table II -6

	F 1 40%	F 2 14%	F 3 10%
Al	0,917	0,132	-0,132
Fe	0,803	-0,162	-0,232
Mn	0,206	0,220	-0,145
Mg	0,701	-0,065	-0,152
Ca	-0,217	-0,458	0,314
Na	-0,398	-0,362	0,011
K	0,856	0,214	-0,078
Ti	0,892	0,126	-0,225
P	-0,117	0,285	0,785
Ba	0,700	0,319	0,439
Be	0,199	0,528	-0,168
Co	0,584	0,054	-0,341
Cr	0,621	-0,064	0,296
Cu	-0,009	0,686	-0,104
Ga	0,694	0,288	0,018
Hf	0,166	-0,814	-0,181
Ni	0,677	0,031	-0,226
Rb	0,850	0,170	-0,177
Sc	0,932	0,202	0,085
Sr	0,129	-0,492	0,322
Nb	0,752	0,059	0,104
V	0,407	0,453	0,669
Y	0,758	-0,216	0,426
Zn	0,798	0,225	-0,246
Zr	-0,097	-0,789	0,244
LREE	0,715	-0,443	-0,139
Eu	0,721	-0,392	-0,048
Yb	0,789	-0,371	0,097
Lu	0,750	-0,427	0,105
U	0,285	0,165	0,843
Th	0,782	-0,411	0,129

Table II - 3 : Loading factors for 23 elements and 50 samples considered in the A.C.P. treatment.

Table II -6 : Loading factors for 32 elements and 34 samples considered in the A.C.P. treatment.

	Al	Fe	Mg	Na	K	Ti	P	P.F.	Ba	Be	Co	Cr	Cu	Ga	Ni	Rb	Sc	Sr	Nb	V	Y	Zn	Zr
Al	*1*																						
Fe	0,782	*1*																					
Mg	0,700	0,592	*1*																				
Na	-0,216	-0,274	-0,102	*1*																			
K	0,901	0,635	0,687	-0,361	*1*																		
Ti	0,880	0,780	0,516	-0,247	0,764	*1*																	
P	-0,144	-0,020	-0,028	-0,079	-0,197	-0,254	*1*																
P.F.	0,543	0,406	0,328	-0,489	0,428	0,301	0,269	*1*															
Ba	0,728	0,391	0,624	-0,287	0,782	0,488	0,127	0,566	*1*														
Be	0,480	0,443	0,284	-0,079	0,374	0,706	-0,033	0,212	0,261	*1*													
Co	0,292	0,516	0,211	-0,137	0,169	0,163	-0,038	0,378	0,116	0,236	*1*												
Cr	0,441	0,569	0,257	-0,198	0,347	0,371	0,240	0,542	0,203	0,166	0,428	*1*											
Cu	-0,078	0,096	-0,141	-0,269	-0,183	-0,141	0,195	0,360	-0,104	0,287	0,606	0,201	*1*										
Ga	0,778	0,571	0,532	-0,205	0,722	0,697	-0,044	0,572	0,635	0,350	0,169	0,486	-0,052	*1*									
Ni	0,493	0,699	0,403	-0,189	0,391	0,355	0,000	0,529	0,262	0,275	0,827	0,584	0,482	0,484	*1*								
Rb	0,911	0,745	0,648	-0,401	0,922	0,828	-0,150	0,496	0,633	0,454	0,237	0,448	-0,115	0,727	0,445	*1*							
Sc	0,922	0,799	0,631	-0,272	0,855	0,882	-0,001	0,581	0,685	0,524	0,261	0,548	-0,038	0,767	0,486	0,894	*1*						
Sr	0,369	0,303	0,175	0,509	0,215	0,336	-0,030	-0,139	0,192	0,256	-0,029	0,264	-0,251	0,150	0,059	0,210	0,328	*1*					
Nb	0,699	0,594	0,509	-0,093	0,626	0,693	-0,018	0,451	0,588	0,406	0,176	0,338	-0,034	0,773	0,421	0,585	0,743	0,294	*1*				
V	-0,117	-0,047	-0,201	-0,237	-0,179	-0,280	0,279	0,441	-0,022	0,067	0,480	0,433	0,599	-0,036	0,357	-0,110	-0,013	-0,216	-0,057	*1*			
Y	-0,264	-0,209	-0,218	-0,107	-0,259	-0,288	-0,056	0,137	-0,227	-0,203	-0,099	-0,108	-0,072	-0,175	-0,108	-0,205	-0,179	-0,169	-0,160	0,018	*1*		
Zn	0,844	0,788	0,593	-0,253	0,750	0,811	-0,099	0,512	0,569	0,628	0,373	0,345	0,111	0,711	0,598	0,779	0,807	0,177	0,671	-0,043	-0,199	*1*	
Zr	-0,275	-0,149	-0,207	0,205	-0,286	-0,259	-0,037	0,047	-0,241	-0,232	-0,119	-0,094	-0,138	-0,208	-0,098	-0,225	-0,187	-0,039	-0,146	-0,062	0,965	-0,204	*1*
Moyen.	272,4	59,7	30,5	28,1	65,2	7,9	1,4	3,3	588,7	2,1	8,2	86,0	32,0	13,4	28,2	123,6	9,7	70,7	7,3	116,7	117,1	71,4	295,3
Ec.type	134,3	34,9	19,2	27,3	34,1	3,5	1,2	1,5	320,9	1,3	9,5	34,7	46,5	9,8	18,7	76,4	6,1	57,2	5,4	159,9	675,2	39,3	674,4

Table II - 4 : Matrix of correlations for 23 elements and 50 samples considered in the A.C.P. treatment.

	F 1	F 2	F 3	F 4
Phyllites	2,585	-0,446	0,291	0,103
Phyllites	0,394	0,572	0,486	2,417
Phyllites	3,233	0,750	1,249	2,456
Phyllites	0,176	1,254	-0,025	0,719
Green Schists	5,065	0,812	0,300	-0,320
Green Schists	3,642	-0,291	0,150	-0,544
Green Schists	2,637	0,282	0,203	-0,247
Green Schists	3,878	-0,253	0,464	0,331
Green Schists	3,125	-0,715	0,258	0,516
Green Schists	3,894	-1,358	-0,216	-0,843
Green Schists	4,493	-1,200	0,081	-1,022
Green Schists	1,530	1,602	0,127	0,783
Green Schists	4,633	-0,106	0,356	-0,145
Green Schists	2,825	0,168	0,391	0,029
Gresophyllites	2,140	-0,297	-0,145	-0,706
Gresophyllites	3,740	0,311	0,210	-0,186
Gresophyllites	3,848	-0,622	0,563	0,582
Gresophyllites	1,854	0,871	-0,159	-0,655
Gresophyllites	2,096	0,076	-0,143	-1,557
Gresophyllites	-0,370	0,596	0,339	1,219
Gresophyllites	2,012	1,309	-0,049	-0,522
Banded (qz)phyllites	-1,036	2,247	-0,994	-1,598
Banded (qz)phyllites	2,385	0,242	0,041	-0,373
Banded (qz)phyllites	-2,239	1,353	-0,991	-2,146
Banded (qz)phyllites	-1,373	0,772	-0,378	-0,349
Banded (qz)phyllites	-0,844	0,423	-0,560	-0,952
Banded (qz)phyllites	-2,869	-0,258	-0,375	0,061
Banded (qz)phyllites	-1,972	-0,060	-0,326	-0,616
Banded (qz)phyllites	-2,905	1,390	-0,912	-1,180
Banded (qz)phyllites	-1,863	0,809	-0,555	-2,743
Banded (qz)phyllites	4,108	0,661	0,274	0,409
Banded (qz)phyllites	-2,590	2,437	-1,421	-2,647
Banded (qz)phyllites	-0,425	1,124	-0,273	0,184
Siliceous Schists	-2,853	0,598	-0,243	0,474
Siliceous Schists	-2,065	0,854	-0,100	0,707
Siliceous Schists	-0,170	0,713	-0,245	-0,086
Siliceous Schists	-1,128	0,590	0,138	1,624
Silicified Schists	-4,679	0,918	-0,391	1,835
Silicified Schists	-4,431	-0,446	-1,925	0,460
Quartzites	-5,961	0,110	-0,643	1,085
Quartzites	-5,046	0,798	-0,398	1,265
Wacke	2,177	-0,419	0,458	-0,804
Black shales	1,347	-2,321	0,467	2,298
Black shales	-4,291	-2,638	-0,475	1,679
Black shales	-1,522	-4,367	-0,496	0,761
Black shales	-3,138	0,406	0,319	1,214
Black shales	-1,013	-9,442	-2,147	-1,587
Black shales	-5,049	-2,051	-0,105	1,775
Black shales	-6,419	-1,652	8,975	-1,721
Black shales	-4,537	0,589	-0,089	2,211

Table II -5: Score factors for 50 samples considered in the A.C.P. treatment with 23 elements.

	Al	Fe	Mn	Mg	Ca	Na	K	Tl	P	Ba	Be	Co	Cr	Cu	Ga	Hf	Ni
Al	*1*																
Fe	0,708	*1*															
Mn	0,243	0,315	*1*														
Mg	0,654	0,713	0,219	*1*													
Ca	-0,247	-0,144	-0,067	0,043	*1*												
Na	-0,316	-0,304	-0,245	-0,099	0,331	*1*											
K	0,919	0,560	0,258	0,597	-0,305	-0,463	*1*										
Tl	0,868	0,738	0,038	0,603	-0,181	-0,334	0,738	*1*									
P	-0,230	-0,161	0,037	-0,085	0,132	-0,031	-0,186	-0,271	*1*								
Ba	0,670	0,315	0,313	0,420	-0,129	-0,395	0,777	0,443	0,294	*1*							
Be	0,152	0,156	0,158	0,095	-0,017	-0,315	0,104	0,732	0,044	0,062	*1*						
Co	0,547	0,746	0,233	0,696	-0,367	-0,069	0,423	0,467	-0,140	0,276	0,163	*1*					
Cr	0,607	0,588	0,229	0,498	0,133	-0,207	0,563	0,387	0,150	0,508	-0,107	0,405	*1*				
Cu	-0,022	-0,012	0,166	-0,128	-0,111	-0,284	-0,048	0,453	0,218	-0,002	0,793	0,019	-0,207	*1*			
Ga	0,685	0,370	-0,068	0,329	-0,425	-0,257	0,684	0,550	-0,093	0,608	0,079	0,365	0,498	0,054	*1*		
Hf	0,045	0,370	-0,097	0,051	0,334	0,179	-0,094	0,113	-0,404	-0,243	-0,372	0,197	-0,021	-0,394	0,032	*1*	
Ni	0,629	0,777	0,267	0,645	-0,232	-0,113	0,518	0,529	-0,118	0,333	0,096	0,818	0,619	0,056	0,582	0,289	*1*
Rb	0,912	0,650	0,148	0,662	-0,271	-0,437	0,908	0,807	-0,217	0,604	0,150	0,470	0,538	0,011	0,627	-0,048	0,523
Sc	0,936	0,703	0,228	0,632	-0,227	-0,442	0,868	0,875	-0,031	0,768	0,241	0,518	0,609	0,084	0,654	-0,024	0,575
Sr	0,127	0,207	-0,138	0,116	0,595	0,308	0,004	0,051	0,054	-0,034	-0,011	0,046	0,551	-0,302	-0,102	0,158	0,149
Nb	0,607	0,487	-0,048	0,395	-0,434	-0,241	0,556	0,666	-0,064	0,522	0,243	0,364	0,423	0,070	0,735	0,296	0,514
V	0,358	0,192	0,018	0,180	-0,065	-0,261	0,337	0,208	0,626	0,664	0,139	0,153	0,457	0,191	0,513	-0,311	0,282
Y	0,526	0,581	0,241	0,513	-0,042	-0,188	0,457	0,614	0,253	0,594	0,100	0,328	0,455	-0,102	0,287	0,123	0,352
Zn	0,750	0,695	0,208	0,518	-0,258	-0,326	0,674	0,833	-0,153	0,464	0,425	0,538	0,347	0,383	0,637	0,117	0,683
Zr	-0,341	0,157	-0,189	-0,032	0,343	0,173	-0,349	-0,174	0,173	-0,287	-0,325	-0,039	0,181	-0,308	-0,394	0,917	0,033
LREE	0,597	0,522	0,114	0,469	-0,066	-0,137	0,550	0,663	-0,350	0,357	-0,072	0,286	0,234	-0,365	0,347	0,356	0,225
Eu	0,558	0,541	0,159	0,448	0,046	-0,321	0,543	0,620	-0,243	0,437	-0,032	0,245	0,223	-0,254	0,310	0,314	0,235
Yb	0,611	0,552	-0,030	0,410	-0,003	-0,333	0,581	0,725	-0,151	0,468	-0,031	0,185	0,315	-0,266	0,453	0,337	0,281
Lu	0,569	0,542	-0,051	0,370	0,039	-0,284	0,527	0,666	-0,139	0,404	-0,049	0,167	0,314	-0,299	0,444	0,404	0,295
U	0,142	-0,064	-0,121	-0,024	0,040	-0,148	0,177	0,133	0,574	0,649	0,016	-0,129	0,230	0,090	0,275	-0,148	-0,056
Th	0,617	0,687	-0,041	0,546	-0,009	-0,148	0,516	0,736	-0,143	0,421	0,024	0,398	0,520	-0,166	0,353	0,499	0,498

Moyen.	307,1	70,0	1,3	30,5	5,7	26,2	71,6	9,0	1,4	619,3	2,4	8,8	91,9	25,9	15,3	7,0	30,4
Ec.type	113,0	31,1	2,9	14,0	6,3	24,0	29,2	2,7	1,3	293,9	1,2	7,7	27,5	21,7	8,9	4,3	17,3

Table II -7 : Matrix of correlations for 32 elements and 34 samples considered in the A.C.P. treatment.

	Rb	Sc	Sr	Nb	V	Y	Zn	Zr	LREE	Eu	Yb	Lu	U	Th
Rb	*1*													
Sc	0,867	*1*												
Sr	0,007	0,119	*1*											
Nb	0,491	0,679	0,038	*1*										
V	0,285	0,510	0,003	0,443	*1*									
Y	0,431	0,679	0,278	0,598	0,460	*1*								
Zn	0,669	0,723	-0,117	0,594	0,289	0,430	*1*							
Zr	-0,331	-0,259	0,468	-0,087	-0,220	0,234	-0,239	*1*						
LREE	0,561	0,521	0,139	0,469	-0,085	0,672	0,482	0,066	*1*					
Eu	0,548	0,539	0,060	0,410	-0,010	0,707	0,514	0,103	0,929	*1*				
Yb	0,585	0,614	0,144	0,582	0,165	0,790	0,579	0,127	0,865	0,904	*1*			
Lu	0,525	0,557	0,202	0,575	0,157	0,764	0,532	0,166	0,847	0,869	0,981	*1*		
U	0,076	0,386	0,083	0,397	0,721	0,580	0,106	0,066	0,048	0,133	0,270	0,229	*1*	
Th	0,548	0,695	0,378	0,674	0,173	0,792	0,463	0,364	0,648	0,656	0,701	0,688	0,342	*1*

Moyen.	144,9	11,1	77,6	7,9	88,7	21,6	81,5	238,0	172,9	1,6	3,5	0,6	3,1	13,9
Ec.type	66,0	5,1	49,1	5,5	73,6	9,8	36,4	189,7	76,0	0,7	1,4	0,2	2,4	4,9

Table II -7

	F 1	F 2	F 3	F 4
Phyllites	-0,211	3,481	-0,898	-2,633
Phyllites	3,538	1,436	2,784	3,183
Green Schists	3,672	0,620	-0,906	-0,520
Green Schists	-0,067	2,990	-0,600	-2,896
Green Schists	1,167	3,797	-1,195	-3,282
Green Schists	3,372	1,398	-0,288	-0,946
Green Schists	2,950	2,275	-1,244	-2,895
Green Schists	2,670	3,190	-0,379	-2,800
Green Schists	2,824	-2,402	-0,280	3,421
Green Schists	5,764	-0,152	-0,284	0,791
Gresophyllites	1,775	0,410	-0,848	-0,545
Gresophyllites	2,757	1,831	-0,547	-1,263
Gresophyllites	0,044	4,919	-1,268	-2,611
Gresophyllites	1,611	0,165	0,488	0,163
Gresophyllites	2,513	-0,584	0,343	-0,572
Gresophyllites	-3,448	2,605	-0,322	-0,705
Gresophyllites	2,222	-0,712	0,488	1,515
Banded (qz)phyllites	1,635	0,080	-0,592	-0,714
Banded (qz)phyllites	-3,522	-2,815	0,905	-0,758
Banded (qz)phyllites	-2,520	-0,223	-0,714	0,645
Banded (qz)phyllites	-1,748	-0,858	-1,053	-0,143
Banded (qz)phyllites	-4,121	-0,690	2,061	-0,731
Banded (qz)phyllites	-2,814	-0,969	0,278	-0,717
Banded (qz)phyllites	-5,088	-0,311	0,045	-0,682
Banded (qz)phyllites	-2,511	-3,799	3,035	-2,817
Banded (qz)phyllites	-1,027	-1,051	0,073	0,897
Siliceous Schists	-4,729	-0,135	-0,160	0,612
Siliceous Schists	-3,790	0,041	-0,530	0,907
Siliceous Schists	-0,218	-0,934	-0,553	1,882
Siliceous Schists	-2,256	0,853	-0,852	2,240
Silicified Schists	-8,725	5,085	-2,841	1,143
Quartzites	-7,625	0,061	-1,071	1,481
Wacke	3,693	-3,403	-0,867	0,970
Black shales	0,504	4,177	7,688	0,186

Table II -8 : Score factors for 34 samples considered in the A.C.P. treatment with 32 elements.

	F 1 50%	F 2 10%	F 3 10%
Al	0,951	-0,010	-0,231
Fe	0,871	-0,196	0,140
Mg	0,712	-0,028	-0,215
Na	-0,323	-0,685	-0,144
K	0,868	0,179	-0,363
Ti	0,839	-0,068	-0,311
P	-0,025	-0,003	0,508
Ba	0,706	0,162	-0,246
Co	0,490	-0,100	0,603
Cr	0,584	-0,158	0,519
Cu	0,717	0,201	0,135
Ni	0,768	-0,108	0,390
Rb	0,903	0,146	-0,238
Sc	0,948	-0,001	-0,117
Sr	0,280	-0,827	-0,238
V	0,713	0,103	0,423
Y	0,647	-0,221	0,220
Zn	0,878	0,036	-0,090
Zr	0,021	-0,748	-0,013

Table II - 9 : Loading factors for 19 elements and 49 samples considered in the A.C.P. treatment.

	Si	Al	Fe	Mg	Na	K	Ti	P	Ba	Co	Cr	Cu	Ni	Rb	Sc	Sr	V	Y	Zn	Zr	U	Th
Si	1																					
Al	-0,984	1																				
Fe	-0,851	0,783	1																			
Mg	-0,751	0,700	0,592	1																		
Na	0,190	-0,217	-0,274	-0,102	1																	
K	-0,882	0,901	0,635	0,687	-0,361	1																
Ti	-0,875	0,879	0,780	0,516	-0,247	0,764	1															
P	0,067	-0,144	-0,020	-0,028	-0,079	-0,197	-0,254	1														
Ba	-0,717	0,728	0,391	0,624	-0,287	0,782	0,488	0,127	1													
Co	-0,404	0,350	0,545	0,204	-0,122	0,185	0,203	-0,074	0,137	1												
Cr	-0,508	0,441	0,569	0,257	-0,198	0,347	0,371	0,240	0,203	0,419	1											
Cu	-0,666	0,643	0,517	0,449	-0,283	0,563	0,496	0,182	0,586	0,326	0,366	1										
Ni	-0,696	0,621	0,791	0,550	-0,189	0,532	0,523	0,020	0,367	0,787	0,557	0,566	1									
Rb	-0,897	0,911	0,745	0,648	-0,401	0,922	0,828	-0,150	0,633	0,257	0,448	0,588	0,575	1								
Sc	-0,937	0,923	0,799	0,631	-0,272	0,855	0,882	-0,001	0,685	0,295	0,548	0,659	0,606	0,894	1							
Sr	-0,378	0,369	0,303	0,175	0,509	0,215	0,336	-0,030	0,192	0,045	0,264	0,010	0,136	0,210	0,328	1						
V	-0,673	0,626	0,613	0,338	-0,261	0,478	0,502	0,170	0,408	0,476	0,741	0,533	0,627	0,571	0,697	0,072	1					
Y	-0,805	0,544	0,561	0,488	-0,107	0,430	0,395	0,144	0,510	0,556	0,427	0,468	0,410	0,457	0,598	0,260	0,398	1				
Zn	-0,858	0,844	0,788	0,593	-0,253	0,750	0,811	-0,099	0,569	0,444	0,345	0,673	0,685	0,779	0,807	0,177	0,499	0,547	1			
Zr	-0,024	-0,046	0,239	0,042	0,205	-0,115	0,102	0,072	-0,055	-0,049	0,066	-0,081	0,126	-0,077	-0,017	0,495	-0,150	0,177	-0,013	1		
U	-0,174	0,142	-0,063	-0,024	-0,148	0,178	0,134	0,573	0,649	-0,159	0,230	0,379	-0,056	0,077	0,387	0,083	0,273	0,581	0,107	0,066	1	
Th	-0,681	0,617	0,687	0,546	-0,148	0,516	0,736	-0,143	0,421	0,442	0,520	0,329	0,498	0,548	0,695	0,376	0,578	0,792	0,465	0,363	0,345	1

Moyen.	1143,6	307,3	70,0	30,5	26,2	71,6	9,0	1,4	619,3	9,5	91,9	23,0	30,4	144,9	11,1	77,6	77,5	21,6	81,5	238,0	3,1	13,9
Ec.type	177,6	113,3	31,1	14,0	24,0	29,2	2,7	1,3	293,9	8,1	27,5	13,9	17,3	66,0	5,1	49,1	36,6	9,8	36,4	189,7	2,4	4,9

Table II - 10 : Matrix of correlations for 19 elements and 49 samples considered in the A.C.P. treatment.

	F 1	F 2	F 3	F 4
A UNIT	2,12	-0,14	0,53	0,94
A UNIT	3,63	0,12	-0,62	0,28
A UNIT	2,25	0,62	-0,31	0,46
A UNIT	3,39	0,15	0,55	0,68
A UNIT	2,28	-0,03	-0,58	0,18
A UNIT	3,32	0,90	-0,83	0,16
A UNIT	3,28	1,45	-0,40	-0,14
A UNIT	1,73	-0,84	-0,50	-0,23
A UNIT	3,68	0,80	0,65	-0,52
A UNIT	4,10	0,11	1,23	1,17
A UNIT	4,79	0,13	0,88	0,32
A UNIT	2,25	-1,69	0,46	0,64
B UNIT	2,61	1,65	-1,52	-1,85
B UNIT	0,52	0,98	1,10	-4,87
B UNIT	-4,58	1,84	1,03	-0,36
B UNIT	-1,88	1,14	3,70	-0,15
B UNIT	-3,52	0,18	-0,62	0,07
B UNIT	-2,19	0,20	3,59	1,88
B UNIT	-5,47	1,32	2,27	-1,07
B UNIT	-4,69	2,04	-0,56	0,34
B UNIT	2,49	-0,16	0,14	-0,95
B UNIT	-6,14	1,67	0,73	1,09
B UNIT	-1,27	-2,20	-1,69	-0,55
B UNIT	0,40	1,58	-1,50	-1,33
B UNIT	4,78	-0,06	-0,65	-0,20
B UNIT	1,64	-0,25	0,02	0,67
B UNIT	-2,69	-2,44	-0,34	0,05
B UNIT	-1,49	-0,31	-0,41	0,52
B UNIT	1,83	-1,16	0,83	1,32
B UNIT	-5,87	1,91	-0,55	1,58
B UNIT	1,85	0,18	-2,27	-0,09
B UNIT	-0,70	-0,77	-0,03	0,76
B UNIT	-1,12	1,73	-0,82	0,12
B UNIT	-4,99	2,14	-0,95	0,77
B UNIT	-2,35	-1,67	1,61	-2,58
B UNIT	-1,13	-1,25	0,84	0,10
B UNIT	-2,98	-1,44	-0,73	0,41
B UNIT	-1,19	-5,21	0,63	-1,16
C UNIT	0,14	0,22	-1,51	-1,01
C UNIT	-0,65	0,98	-0,83	0,20
C UNIT	-3,13	0,19	-0,20	0,23
C UNIT	1,22	-0,74	-0,83	0,12
C UNIT	4,00	0,01	0,11	0,56
C UNIT	-5,42	1,21	-0,48	0,87
C UNIT	-2,29	0,47	-0,59	0,35
C UNIT	-0,32	-0,01	-0,24	0,97
D UNIT	3,92	0,72	-0,96	-0,97
D UNIT	-2,98	-3,05	-1,40	-0,21
D UNIT	-0,56	-0,11	-0,69	-0,22

Table II - 11 : Score factors for 49 samples considered in the A.C.P. treatment with 19 elements.

	F 1 44%	F 2 13%	F 3 10%
Si	-0,984	-0,094	-0,058
Al	0,973	0,143	-0,008
Fe	0,904	-0,054	0,084
Mg	0,787	0,125	-0,033
Na	-0,189	0,322	0,235
K	0,876	0,209	-0,112
Ti	0,901	0,236	-0,022
P	0,132	-0,232	0,079
P.F.	0,628	-0,346	0,264
Ba	0,767	0,111	-0,092
Co	0,492	-0,619	0,133
Cr	0,175	-0,497	0,038
Cu	0,113	-0,760	0,050
Ni	0,647	-0,520	0,183
Rb	0,851	0,144	-0,074
Sc	0,954	0,054	0,067
Sr	0,388	0,179	0,143
V	-0,208	-0,789	0,022
Y	-0,191	0,115	0,921
Zn	0,886	0,008	0,024
Zr	-0,143	0,216	0,948

Table II - 12 : Loading factors for 21 elements and 67 samples considered in the A.C.P. treatment.

	Si	Al	Fe	Mg	Na	K	Ti	P	P.F.	Ba	Co	Cr	Cu	Ni	Rb	Sc	Sr	V	Y	Zn	Zr
Si	1																				
Al	-0,987	1																			
Fe	-0,885	0,848	1																		
Mg	0,894	0,754	0,680	1																	
Na	0,065	-0,134	-0,168	-0,006	1																
K	-0,843	0,882	0,712	0,654	-0,320	1															
Ti	-0,920	0,917	0,858	0,670	-0,060	0,778	1														
P	-0,130	0,069	0,137	0,070	-0,103	0,034	-0,010	1													
P.F.	-0,597	0,565	0,472	0,442	-0,224	0,481	0,437	0,319	1												
Ba	-0,733	0,748	0,517	0,643	-0,207	0,826	0,597	0,238	0,619	1											
Co	-0,431	0,397	0,576	0,286	-0,053	0,271	0,301	-0,010	0,338	0,207	1										
Cr	-0,168	0,113	0,173	0,105	-0,188	-0,050	0,003	0,035	0,214	-0,026	0,272	1									
Cu	-0,047	0,011	0,141	-0,067	-0,255	-0,042	-0,005	0,225	0,333	-0,021	0,555	0,042	1								
Ni	-0,604	0,541	0,692	0,494	-0,142	0,367	0,452	0,076	0,432	0,277	0,792	0,498	0,398	1							
Rb	-0,820	0,860	0,720	0,594	-0,330	0,932	0,756	0,019	0,502	0,695	0,277	0,049	-0,010	0,378	1						
Sc	-0,950	0,933	0,856	0,734	-0,136	0,808	0,918	0,159	0,635	0,713	0,366	0,226	0,037	0,558	0,790	1					
Sr	-0,498	0,441	0,350	0,316	0,411	0,133	0,402	0,075	0,105	0,189	0,095	0,351	-0,146	0,323	0,137	0,462	1				
V	0,275	-0,312	-0,226	-0,209	-0,112	-0,304	-0,382	0,120	0,286	-0,118	0,284	0,363	0,453	0,135	-0,238	-0,181	-0,251	1			
Y	0,147	-0,175	-0,142	-0,173	0,039	-0,159	-0,185	-0,033	0,120	-0,167	-0,093	-0,095	-0,060	-0,080	-0,130	-0,119	-0,108	-0,009	1		
Zn	-0,845	0,846	0,839	0,643	-0,142	0,762	0,838	0,053	0,501	0,626	0,499	0,019	0,155	0,586	0,726	0,817	0,224	-0,218	-0,139	1	
Zr	0,086	-0,125	0,046	-0,142	0,222	-0,129	-0,110	0,009	0,060	-0,144	-0,087	-0,124	-0,115	-0,046	-0,104	-0,079	0,010	-0,127	0,959	-0,096	1

Moyen.	1220,5	254,5	54,3	30,0	33,5	58,4	7,4	1,3	3,2	552,6	8,4	100,7	28,8	27,7	114,6	9,1	77,4	144,0	91,8	64,5	251,9
Ec.type	248,5	155,8	38,1	20,5	34,1	41,0	4,2	1,1	1,6	337,5	9,3	53,3	41,1	19,9	91,6	6,8	79,8	163,6	585,0	41,1	590,8

Table II - 13 : Matrix of correlations for 21 elements and 67 samples considered in the A.C.P. treatment.

	F 1	F 2	F 3	F 4
A UNIT	2,222	-0,334	0,073	-0,360
A UNIT	3,758	0,315	-0,048	0,263
A UNIT	2,316	0,204	-0,101	0,665
A UNIT	5,453	-0,194	1,325	-3,440
A UNIT	3,159	-0,510	0,090	-0,151
A UNIT	2,379	0,647	-0,141	0,120
A UNIT	3,409	0,520	-0,294	0,922
A UNIT	3,342	-0,182	-0,137	1,128
A UNIT	5,188	-0,229	0,172	0,490
A UNIT	1,985	0,789	-0,054	-0,110
A UNIT	3,437	-0,501	-0,069	0,825
A UNIT	4,262	-1,319	0,309	-0,225
A UNIT	4,200	-1,247	0,470	-0,093
A UNIT	2,078	0,000	0,461	-0,733
B UNIT	2,631	0,819	-0,477	2,417
B UNIT	1,066	-1,955	0,091	2,319
B UNIT	-3,776	-2,099	-0,697	1,231
B UNIT	-0,728	-3,997	0,340	1,176
B UNIT	-2,471	0,647	-0,272	0,942
B UNIT	-0,597	-9,285	0,955	0,175
B UNIT	-4,825	-0,392	-0,991	0,730
B UNIT	-4,192	-1,287	-0,469	1,030
B UNIT	-4,343	-1,433	-0,759	0,530
B UNIT	-4,978	1,316	10,310	3,323
B UNIT	-3,379	1,004	-1,084	1,471
B UNIT	-4,118	-0,993	-0,925	0,721
B UNIT	-3,998	-2,251	-0,576	-0,685
B UNIT	-4,016	-2,504	-0,551	-0,119
B UNIT	-4,712	-0,763	-0,935	0,083
B UNIT	-4,880	-1,097	-1,009	0,986
B UNIT	-4,027	-1,882	-0,783	0,125
B UNIT	2,328	0,093	-0,030	-0,057
B UNIT	3,232	0,257	1,089	-1,482
B UNIT	-5,074	0,519	-1,119	0,279
B UNIT	-0,394	1,778	-0,212	-1,104
B UNIT	1,310	0,680	-0,527	1,961
B UNIT	4,423	0,357	0,003	0,164
B UNIT	-2,365	2,112	-0,010	-1,154
B UNIT	2,056	0,085	-0,067	-0,151
B UNIT	-1,679	1,183	0,103	-1,910
B UNIT	-0,729	0,817	-0,182	-0,282
B UNIT	1,761	-0,336	0,584	0,109
B UNIT	-4,226	-0,232	-1,041	1,252
B UNIT	2,566	1,444	-0,376	0,999
B UNIT	0,221	0,905	-0,979	1,973
B UNIT	-0,088	0,543	0,111	-0,461
B UNIT	-0,651	0,865	-0,823	1,313
B UNIT	-3,555	1,257	-1,227	1,273
B UNIT	0,349	-1,286	0,641	-4,890
B UNIT	-1,554	0,183	0,353	0,320
B UNIT	-0,905	0,261	0,114	-0,318
B UNIT	-1,880	1,396	-0,171	-1,041
B UNIT	-1,002	0,784	0,856	-2,077
C UNIT	0,726	1,433	-0,518	0,862
C UNIT	-0,017	0,870	-0,565	1,077
C UNIT	-2,290	0,837	-0,594	0,121
C UNIT	1,445	0,846	-0,265	-0,210
C UNIT	4,218	-0,221	0,083	0,302
C UNIT	-4,164	1,156	-1,026	0,700
C UNIT	-1,434	1,061	-0,570	0,484
C UNIT	0,194	0,815	-0,400	0,192
D UNIT	3,582	0,738	-0,368	0,630
D UNIT	-2,058	1,724	0,094	-1,287
D UNIT	-0,890	-0,803	0,260	-3,032
D UNIT	5,870	0,042	0,083	0,390
D UNIT	-1,771	2,114	0,119	-2,016
D UNIT	0,062	1,040	-0,419	0,220

Table II -14 : Score factors for 67 samples considered in the A.C.P. treatment.with 21 elements.

Atomic N°	Element	Analytical Method	Detection Limit
4	Be	Fusion ICP	1 ppm
5	B	Prompt Gamma	0,5 ppm
6	C	LECO	0,01% CO_2
11	Na	Fusion ICP	0.01% Na_2O
12	Mg	Fusion ICP	0,01% MgO
13	Al	Fusion ICP	0,01% Al_2O_3
14	Si	Fusion ICP	0,01% SiO_2
15	P	Fusion ICP	0,01% P_2O_5
16	S	XRF	50 ppm
19	K	Fusion ICP	0,3% K_2O
20	Ca	Fusion ICP	0,01% CaO
21	Sc	INAA	0,1 ppm
22	Ti	Fusion ICP	0,001% TiO_2
23	V	Fusion ICP	3 ppm
24	Cr	INAA	0,5 ppm
25	Mn	INAA (short lived)	1 ppm
26	Fe	Fusion ICP	0,01% Fe_2O_3
27	Co	INAA	0,1 ppm
28	Ni	Fusion ICP	5 ppm
29	Cu	Fusion ICP	5 ppm
30	Zn	Fusion ICP	5 ppm
31	Ga	XRF	5 ppm
33	As	INAA	1 ppm
34	Se	INAA	0,5 ppm
35	Br	INAA	0,5 ppm
37	Rb	XRF	2 ppm
38	Sr	Fusion ICP	1 ppm
39	Y	Fusion ICP	1 ppm
40	Zr	Fusion ICP	1 ppm
41	Nb	XRF	2 ppm
42	Mo	INAA	2 ppm
47	Ag	AAS	0,1 ppm
50	Sn	XRF	50 ppm
51	Sb	INAA	0,1 ppm
55	Cs	INAA	0,2 ppm
56	Ba	Fusion ICP	1 ppm
57	La	INAA	0,1 ppm
58	Ce	INAA	1 ppm
60	Nd	INAA	1 ppm
62	Sm	INAA	0,01 ppm
63	Eu	INAA	0,05 ppm
64	Gd	Prompt Gamma	0,5 ppm
65	Tb	INAA	0,1 ppm
66	Dy	INAA (short lived)	0,5 ppm
70	Yb	INAA	0,05 ppm
71	Lu	INAA	0,01 ppm
72	Hf	INAA	0,2 ppm
73	Ta	INAA	0,3 ppm
74	W	INAA	1 ppm
77	Ir	INAA	1 ppb
79	Au	INAA	2 ppb
80	Hg	INAA	1 ppm
82	Pb	AAS	5 ppm
83	Bi	XRF	5 ppm
90	Th	INAA	0,1 ppm
92	U	INAA	0,1 ppm

INAA - Instrumental Neutron Activation Analysis
Fusion ICP - Fusion Induced Coupled Plasma Emission
AAS - Atomic Absorption Spectrometry
XRF - X-Ray Fluorescence

Table II -1: Analytical method and detection limit for the different element analysed from Montemor and França. (Lisboa Univ.)

Table II -16 : Whole rock geochemistry, Montemor sector.

	(1)	(2)	(3)	(4)	(5)	(6)	(7)	(8)	(9)	(10)	(11)	(12)
SiO_2	53.46	73.42	48.00	42.20	67.00	62.36	71.14	61.00	68.34	63.98	72.54	69.90
TiO_2	0.54	0.26	1.90	1.42	0.53	0.70	0.56	0.70	0.32	0.66	0.28	0.32
Al_2O_3	14.18	6.94	14.58	12.34	16.70	17.12	13.82	18.52	16.94	16.94	12.22	15.24
Fe_2O_3	11.64	7.48	16.38	23.12	4.38	6.34	5.06	6.40	3.28	6.04	3.08	3.16
MnO	0.02	<0.02	0.12	0.14	0.06	0.12	0.04	0.06	0.04	0.06	0.02	0.06
MgO	1.78	0.60	4.92	4.26	2.43	3.44	2.08	2.66	1.66	2.56	1.54	1.18
CaO	0.82	0.36	1.54	1.74	1.25	1.08	0.62	1.22	1.34	1.98	0.64	3.06
Na_2O	4.72	2.38	1.92	1.82	5.05	3.70	2.82	5.78	6.64	5.24	1.48	4.34
K_2O	1.52	0.64	3.32	2.56	1.64	2.12	2.60	2.28	1.00	1.56	4.52	1.20
P_2O_5	0.24	0.08	0.16	0.16	0.26	0.24	0.16	0.20	0.24	0.20	0.40	0.16
LOI	8.68	5.46	5.10	7.98	1.67	3.04	1.92	1.52	0.82	1.16	1.20	0.76
TOTAL	97.60	97.68	97.94	97.70	100.97	100.28	100.80	100.32	100.60	100.38	97.92	99.38
S (wt%)v2	3.03	1.57	3.18	6.66	0.16	0.70	0.064	0.20	0.20	0.12	0.17	<0.005
Be	<2	2	<2	<2	5	3	2	2	2	2	<2	<2
Sc	10	5.2	27	37	11	18	11	15	9.7	15	7.0	8.2
V	65	36	229	154	61	122	66	102	45	94	43	29
Cr	59	42	98	81	60	110	72	90	44	80	36	8.5
Co	91	44	66	150	43	18	11	15	6.4	13	8.6	6.6
Ni	104	50	57	80	56	47	38	46	19	38	30	13
Cu	229	78	241	586	12	46	16	20	11	18	18	5
Zn	20	9	74	66	19	54	32	41	100	51	21	45
Ga	24	<2	21	<2	19	20	15	66	19	20	10	15
As	54000	43000	1250	2400	1400	24	38	28	20	36	32	35
Se	6.2	7.2	<0.5	<1.2	<0.5	<0.5	<0.5	<0.9	<0.5	<0.5	<0.5	<0.5
Rb	29	19	118	87	57	86	92	76	26	45	125	45
Sr	92	66	104	102	143	100	76	142	108	146	46	186
Y	8	12	40	32	20	24	24	32	100	28	12	8
Zr	89	62	132	99	129	168	147	185	130	198	74	72
Nb	9	4	3	<2	15	9	10	9	9	9	5	5
Mo	<2	<2	<2	<2	<2	<2	2	<2	<2	<2	2	<2
Ag	1.4	<0.4	0.7	1.2	<0.4	<0.4	<0.4	<0.4	<0.4	<0.4	<0.4	0.5
Cd	0.5	<0.5	0.6	<0.5	<0.5	0.6	<0.5	<0.5	<0.5	0.5	<0.5	0.5
Sn	<5	<5	<5	<5	<5	<5	<5	<5	<5	<5	<5	<5
Sb	6.2	37	<0.1	<0.1	<0.1	0.4	0.6	0.2	0.1	0.3	1.2	0.2
Cs	1.1	0.9	4.9	3.0	1.3	3.8	2.8	3.6	0.5	1.5	2.3	1.6
Ba	336	222	804	742	286	760	606	858	278	498	1228	256
La	11.4	7.8	8.5	6.0	24.9	33.0	34.0	42.9	21.9	32.7	12.7	7.3
Ce	22	14	20	13	45	65	66	77	43	62	27	14
Nd	10	7	14	8	20	31	30	35	21	29	14	7
Sm	1.7	1.4	4.4	2.7	4.1	5.4	5.1	6.1	4.0	5.2	2.9	1.2
Eu	0.60	0.32	1.19	1.03	0.89	1.25	1.19	1.43	0.70	1.40	1.16	0.76
Gd	1.5	0.5	5.1	3.8	3.3	3.7	4.0	4.4	3.1	4.3	2.3	1.2
Tb	0.2	0.1	0.9	0.7	0.6	0.7	0.7	0.8	0.6	0.7	0.4	0.2
Dy	1.3	0.7	6.0	4.3	3.2	3.6	3.5	2.8	3.3	4.2	2.3	1.3
Yb	0.75	0.51	3.75	3.24	1.90	2.13	2.25	2.32	2.27	2.65	1.27	0.76
Lu	0.11	0.09	0.54	0.51	0.29	0.33	0.35	0.44	0.38	0.39	0.19	0.12
Hf	3.0	2.0	2.9	2.3	3.6	4.6	4.5	5.2	3.6	5.0	2.1	1.7
Ta	1.1	0.8	0.7	<0.3	3.4	0.3	0.9	0.8	1.1	0.9	0.4	0.9
W	15	<3	3	<1	4	<1	2	3	<1	<1	2	<1
Ir	<1	<1	<1	<1	<1	<1	<1	<1	<1	<1	<1	<1
Au (ppb)	6110	11700	246	3500	71	10	30	7	<2	8	24	<2
Hg	<1	<1	<1	<1	<1	<1	<1	<1	<1	<1	<1	<1
Pb	26	8	<5	10	5	10	5	8	16	10	6	15
Bi	9	6	<5	6	<5	<5	<5	<5	<5	<5	<5	<5
Th	7.0	4.5	0.7	0.9	7.0	8.7	9.5	11	8.2	9.0	3.9	1.6
U	<0.4	<0.3	0.9	<0.2	5.5	2.5	2.2	2.9	18	2.9	2.1	0.8

(1),(2) M-I (150XI,MII8ab); (3),(4) M-II (150XXI,150XX); (5) D-I (150XII); (6),(7) D-II (141IV,150II); (8),(9),(10) S-I (150XV,141XII,141IX); (11) S-II (150VII); (12) Mig (S5AII)

%	(1)	(2)	(3)	(4)	(5)
SiO_2	86.23	86.00	90.50	90.20	78.73
TiO_2	0.01	0.03	0.12	0.10	0.01
Al_2O_3	0.50	0.41	0.71	0.85	0.47
Fe_2O_3	10.64	10.10	6.86	6.87	16.68
MgO	0.01	0.33	0.05	0.02	0.07
CaO	0.10	0.51	0.11	0.03	0.02
Na_2O	0.02	0.02	0.05	0.02	0.03
K_2O	0.20	0.06	0.13	0.12	0.12
P_2O_5	0.16	0.17	0.04	<0.02	0.08
LOI	1.67	1.77	1.31	1.31	3.09
Σ	99.54	99.40	99.88	99.54	99.30
ppm					
Be	2	4	2	<1	<1
B	1.4	2.0	2.0	4.0	3.6
C	409.4	431.2	891.3	900.6	409.4
S	<50	<50	<50	<50	8110
Sc	0.3	0.2	1.4	1.1	0.4
V	4	12	12	6	4
Cr	10.0	9.0	11.0	11.0	5.9
Mn	46	110	94	49	50
Co	3.6	4.0	6.0	5.4	0.7
Ni	30.0	7.0	15.0	20.0	20.0
Cu	55	21	55	35	20
Zn	40	73	46	70	170
Ga	<2	<2	<2	<2	<2
As	160	200	4	4	2400
Se	<0.5	<0.5	<0.5	<0.5	<0.5
Br	1.8	6.0	5.0	0.7	<0.5
Rb	<2	16	18	15	15
Sr	261	<1	<1	<1	3
Y	10	9	10	10	8
Zr	456	15	13	<1	3
Nb	3	<2	3	2	<2
Mo	<2	<2	<2	<2	<2
Ag	<0.1	0.5	0.1	0.1	7
Sn	<5	<5	<5	<5	<5
Sb	0.9	0.5	5.3	5.5	11.0
Cs	1.1	1.0	1.0	0.7	1.1
Ba	46	64	101	25	12
La	0.6	0.8	2.5	2.1	0.3
Ce	2	4	6	5	1
Nd	1	2	1	3	<1
Sm	0.15	0.10	0.50	0.56	0.13
Eu	0.05	0.06	0.20	0.13	0.06
Gd	0.2	0.2	0.4	0.4	<0.5
Tb	<0.1	<0.1	<0.1	<0.1	0.1
Dy	0.3	0.3	0.4	0.4	0.6
Yb	0.10	0.10	0.20	0.22	0.47
Lu	0.02	0.02	0.03	0.03	0.07
Hf	<0.2	<0.2	<0.2	<0.2	<0.2
Ta	<0.3	<0.3	<0.3	<0.3	<0.3
W	<1	<1	14	13	1
Ir	<1	<1	<1	<1	<1
Au	0.002	0.010	0.011	0.002	0.475
Hg	<1	<1	<1	<1	<1
Pb	16	10	5	34	32
Bi	10	<5	<5	<5	<5
Th	0.40	<0.10	0.50	0.60	0.20
U	0.40	<0.10	0.60	0.60	<0.10

Quartz breccias IA: (1) F-67; (2) F-67A; (3) F-45A; (4) F-45
Quartz breccias IB: (5) F-27

Table II -17 : Assay data for the mineralized quartz breccias of the Vilariça fault in França sector.

(cont.)

Assay data for the mineralized quartz breccias of the Vilariça fault in França sector

%	(6)	(7)	(8)	(9)	(10)
SiO_2	34.47	33.70	64.08	62.04	57.95
TiO_2	<0.01	0.02	<0.01	0.06	0.02
Al_2O_3	0.36	0.38	0.29	0.75	0.21
Fe_2O_3	44.85	40.60	23.31	21.85	25.24
MgO	0.09	0.37	0.02	0.09	0.02
CaO	0.03	0.10	0.02	0.06	0.04
Na_2O	0.01	0.05	<0.01	0.01	0.04
K_2O	<0.02	0.03	<0.02	0.18	0.04
P_2O_5	<0.02	0.09	0.04	0.06	<0.02
LOI	12.95	16.20	11.03	12.75	14.20
Σ	92.81	91.54	98.83	97.85	97.78
ppm					
Be	<1	1	<1	1	<1
B	2.2	2.0	0.6	3.0	1.5
C	1801.2	535.1	491.2	2592.7	409.4
S	10600	11420	12900	10616	17200
Sc	0.4	1.4	0.1	0.8	0.1
V	16	6	10	22	26
Cr	6.4	50.0	5.7	20.0	5.5
Mn	534	740	47	486	25.6
Co	0.5	4.0	1.0	3.2	4.5
Ni	<10	<10	20.0	<10	<10
Cu	210	290	120	70	45
Zn	350	420	100	25	75
Ga	196	190	33	16	6
As	2000	24000	16000	20000	12000
Se	<0.5	<0.5	<0.5	2.8	5.2
Br	<0.5	<0.5	<0.5	<0.6	<0.5
Rb	<2	<2	6	14	8
Sr	<1	6	<1	8	10
Y	6	5	4	20	14
Zr	14	34	15	15	2
Nb	3	3	3	3	4
Mo	<2	<2	<2	<2	<2
Ag	56	100	97	65	70
Sn	<5	<5	<5	<5	<5
Sb	15.0	61.0	14.0	68.0	78.0
Cs	0.9	<0.2	0.5	<0.2	1.2
Ba	38	154	24	56	61
La	1.0	0.7	0.8	0.7	0.8
Ce	2	3	<1	<1	<1
Nd	1	<1	<1	<1	<1
Sm	0.36	0.20	0.06	0.14	0.15
Eu	0.25	<0.05	<0.05	0.14	0.12
Gd	<0.05	<0.05	0.4	1.6	<0.5
Tb	0.1	<0.1	<0.1	0.2	0.1
Dy	0.9	0.8	0.4	1.5	0.5
Yb	0.77	1.60	0.20	0.63	0.28
Lu	0.12	0.10	0.03	0.10	0.04
Hf	0.3	2.0	<0.2	<0.2	<0.2
Ta	<0.3	<0.3	<0.3	<0.3	<0.3
W	<1	<1	<1	7	<1
Ir	<1	<1	<1	<1	<1
Au	0.797	22.000	3.490	6.950	1.660
Hg	<1	<1	<1	<1	<1
Pb	43900	40000	3900	2810	2500
Bi	<5	<5	<5	<5	<5
Th	0.40	<0.10	0.40	<0.10	<0.10
U	0.30	0.20	<0.10	<0.20	<0.10

Quartz breccias IB: (6) F-23L; (7) F-23L1; (8) F-23C
Quartz breccias IC: (9) F-23; (10) F-11

%	(11)	(12)	(13)	(14)	(15)
SiO_2	63.58	66.06	45.70	92.61	49.42
TiO_2	1.12	0.45	0.86	0.40	0.49
Al_2O_3	17.72	8.67	15.54	1.75	7.83
Fe_2O_3	4.54	15.53	21.07	1.09	35.38
MgO	1.16	0.42	0.43	0.22	0.39
CaO	0.32	0.05	0.38	0.01	<0.01
Na_2O	0.14	0.04	0.04	0.03	0.06
K_2O	4.44	2.04	4.28	0.48	1.34
P_2O_5	0.12	1.16	0.96	0.08	0.66
LOI	4.54	4.71	8.79	0.99	4.31
Σ	98.68	99.13	98.05	98.46	99.89
ppm					
Be	6	14	7	1	4
B	67.3	20.4	105.0	4.6	24.9
C	299.9	409.0	409.0	490.8	409.0
S	730	1065	9600	755	1520
Sc	12.0	7.5	15.0	1.6	6.7
V	450	3700	110	26	500
Cr	62.0	160.0	103.0	13.0	97.0
Mn	<0.3	95.4	258.0	14.0	36.0
Co	0.9	8.1	9.1	0.9	1.2
Ni	<10	60.0	<10	50.0	20.0
Cu	80	350	50	<5	260
Zn	20	250	160	20	35
Ga	26	15	21	<2	9
As	40	96	12000	8100	55
Se	3.6	13	<0.5	1.0	4.6
Br	1.3	<0.5	<0.5	<0.5	1.9
Rb	123	62	155	19	47
Sr	75	88	57	5	33
Y	80	64	42	42	24
Zr	535	124	219	928	190
Nb	73	3	15	7	10
Mo	21	130	<2	<2	23
Ag	0.3	1.6	3.2	0.4	0.1
Sn	<5	<5	<5	<5	<5
Sb	22.0	16.0	30.0	13.0	11.0
Cs	6.5	6.6	35.0	2.5	3.9
Ba	6012	1775	486	123	1737
La	60.2	39.2	36.8	23.5	22.0
Ce	122	57	77	58	40
Nd	56	40	34	22	20
Sm	9.50	9.70	6.50	5.20	3.90
Eu	1.71	2.09	1.92	0.88	0.87
Gd	12.2	13.8	6.4	5.2	4.2
Tb	1.8	2.1	1.2	0.7	0.7
Dy	9.8	13.0	6.7	2.6	3.9
Yb	5.47	4.47	4.94	2.04	2.17
Lu	0.84	0.72	0.77	0.35	0.33
Hf	13.0	2.4	6.2	27.0	4.7
Ta	6.2	0.8	1.2	0.7	1.0
W	4	4	22	<1	<1
Ir	<1	<1	<1	<1	<1
Au	0.015	0.009	0.480	0.038	0.004
Hg	<1	<1	<1	<1	<1
Pb	24	40	410	18	2
Bi	<5	<5	<5	<5	<5
Th	21.00	7.10	11.00	12.00	6.50
U	22.00	42.00	4.30	2.30	10.00

Fault gouges and associated breccias II: (11) F-15A; (12) F-15C; (13) F-16A; (14) F-18B; (15) FM-5A

Table II -18 : Assay data for the fault gouges and associated late breccias of the Vilariça fault in França sector.

(cont.)

Assay data for the fault gouges and associated late-breccias of the Vilariça fault in França sector

%	(16)	(17)	(18)	(19)
SiO_2	3.95	60.54	77.17	77.02
TiO_2	0.03	0.64	0.22	0.15
Al_2O_3	2.32	9.91	3.83	4.25
Fe_2O_3	80.93	16.31	3.81	9.92
MgO	0.08	0.55	0.21	0.19
CaO	0.02	0.02	0.09	0.22
Na_2O	0.01	0.11	0.01	0.03
K_2O	0.12	2.54	1.18	1.02
P_2O_5	0.62	2.16	0.18	1.10
LOI	9.70	4.88	1.69	4.11
Σ	97.78	97.66	88.39	98.01
ppm				
Be	<1	4	<1	6
B	2.2	32.9	26.9	7.4
C	490.8	409.0	54.5	409.0
S	3215	1440	55	<50
Sc	0.9	10.0	2.1	3.4
V	82	570	20	470
Cr	31.0	106.0	23.0	55.0
Mn	16	80	60	1550
Co	2.4	1.8	0.7	14.0
Ni	30.0	20.0	<10.0	70.0
Cu	650	120	5	330
Zn	120	20	<5	750
Ga	<2	11	3	3
As	37	350	29	330
Se	9.7	4.1	<0.5	<0.5
Br	55.0	1.8	<0.5	<0.5
Rb	5	68	47	23
Sr	3	44	10	330
Y	16	32	12	76
Zr	10	63	165	60
Nb	<2	12	5	<2
Mo	INT	95	INT	14
Ag	0.2	0.3	0.1	1.6
Sn	<5	<5	<5	<5
Sb	3.4	11.0	14.0	80.0
Cs	1.2	6.5	1.9	7.3
Ba	183	1855	142	380
La	4.1	31.7	12.8	20.3
Ce	11	60	30	28
Nd	7	28	12	22
Sm	1.9	5.5	1.8	4.9
Eu	0.44	1.10	0.38	1.20
Gd	2.3	5.2	1.8	7.9
Tb	0.3	0.9	0.3	1.2
Dy	1.3	4.4	1.3	7.4
Yb	0.46	2.56	0.89	4.25
Lu	0.09	0.40	0.15	0.72
Hf	0.4	6.6	5.0	0.3
Ta	<0.3	1.3	0.3	<0.3
W	<1	4	3	18
Ir	<1	<1	<1	<1
Au	<0.002	0.004	0.034	0.025
Hg	<1	<1	2	<1
Pb	12	18	12	38
Bi	<5	<5	<5	<5
Th	0.60	8.40	5.00	2.70
U	33.00	26.00	1.90	25.00

Fault gouges and associated breccias II: (16) FM - 5B; (17) FM-5C; (18) FM-6B; (19) FM-7.

%	(20)	(21)
SiO_2	63.48	42.61
TiO_2	0.09	0.29
Al_2O_3	1.62	6.76
Fe_2O_3	27.69	39.18
MgO	0.05	0.23
CaO	0.06	0.03
Na_2O	0.02	0.02
K_2O	0.16	1.20
P_2O_5	0.12	1.96
LOI	4.44	7.49
Σ	97.73	99.77
ppm		
Be	<1	22
B	2.7	34.2
C	300.2	409.4
S	3315	670
Sc	2.4	8.7
V	34	1500
Cr	22.0	130.0
Mn	23	58
Co	0.6	5.7
Ni	20.0	80.0
Cu	75	280
Zn	10	690
Ga	<2	7
As	220	300
Se	21	16
Br	0.8	2.6
Rb	4	34
Sr	32	47
Y	6	84
Zr	84	91
Nb	3	<2
Mo	INT	45
Ag	0.7	12
Sn	<5	<5
Sb	4.8	100
Cs	<0.2	6.6
Ba	56	1071
La	5.9	33.3
Ce	12	46
Nd	5	32
Sm	1.20	6.50
Eu	0.40	1.97
Gd	1.1	8.4
Tb	0.2	1.6
Dy	0.9	8.4
Yb	0.37	7.61
Lu	0.06	1.27
Hf	0.7	1.9
Ta	<0.3	<0.3
W	<1	<1
Ir	<1	<1
Au	0.040	0.024
Hg	<1	<1
Pb	6	28
Bi	<5	<5
Th	2.30	9.70
U	9.40	46.00

(20) - FM-1; (21) - FM-3

Table II -19 : Assay data for late breccias related with the reactivation of the NW-SE regional shears in França sector.

(cont.)

Assay data for late-breccias related with the reactivation of the NNE-SSW - NE-SW regional shears in França sector.

%	(27)	(28)	(29)	(30)
SiO_2	70.83	76.33	58.07	56.15
TiO_2	0.58	0.24	0.95	0.95
Al_2O_3	13.91	13.76	18.26	18.84
Fe_2O_3	4.81	2.06	7.03	9.12
MgO	0.30	0.83	0.77	1.60
CaO	0.09	0.04	0.09	0.14
Na_2O	4.88	0.11	9.24	8.82
K_2O	0.12	3.22	0.22	0.06
P_2O_5	0.16	0.24	0.18	0.30
LOI	2.16	2.75	2.91	3.19
Σ	97.84	99.58	97.72	99.17
ppm				
Be	1	2	3	3
B	6.8	93.2	4.3	7.0
C	900.6	709.6	109.2	109.2
S	13100	<50	3500	700
Sc	6.0	3.7	16	16
V	96	28	130	140
Cr	77.0	11.0	83.5	99.2
Mn	540	67	350	655
Co	8.8	1.8	3.2	5.3.
Ni	50.0	<10.0	<10.0	30.0
Cu	20	10	65	45
Zn	20	15	55	80
Ga	17	14	23	22
As	8	33	35	11
Se	1.2	<0.5	1.7	2.2
Br	<0.5	<0.5	<0.5	<0.5
Rb	8	106	2	<2
Sr	58	19	204	169
Y	16	32	26	26
Zr	110	110	192	162
Nb	11	8	19	17
Mo	<2	INT	INT	INT
Ag	<0.1	<0.1	<0.1	<0.1
Sn	6	11	<5	9
Sb	1.6	3.5	1.2	0.9
Cs	<0.2	5.8	<0.2	<0.2
Ba	51	1220	191	784
La	17.3	21.0	29.5	52.1
Ce	39	45	58	98
Nd	19	2	24	37
Sm	3.30	4.70	3.90	6.30
Eu	0.78	0.68	0.64	1.04
Gd	2.9	5.4	2.7	4.7
Tb	0.5	1.0	0.5	0.7
Dy	3.6	5.3	2.9	3.9
Yb	1.88	3.02	2.14	2.63
Lu	0.27	0.44	0.38	0.43
Hf	3.4	3.4	5.2	4.5
Ta	0.9	1.1	1.4	1.5
W	<1	1	<1	<1
Ir	<1	<1	<1	<1
Au	0.003	<0.002	0.006	0.003
Hg	<1	<1	<1	<1
Pb	4	20	20	12
Bi	<5	11	<5	<5
Th	9.10	12.00	18.00	17.00
U	3.30	8.10	6.50	5.90

Quartz breccias and associated fault gouges of type IV: (27) FM-10A; (28) FM-10B; (29) FM-11; (30) FM-11B (fault gouge).

%	(22)	(23)	(24)	(25)	(26)
SiO_2	56.40	63.36	63.81	58.29	93.22
TiO_2	0.92	0.80	0.81	0.95	0.03
Al_2O_3	14.12	15.81	17.01	17.94	1.04
Fe_2O_3	9.80	7.73	6.36	6.37	1.64
MgO	2.78	2.23	1.45	1.87	0.11
CaO	0.10	0.31	0.37	0.36	0.23
Na_2O	3.95	5.13	3.35	8.69	0.04
K_2O	1.44	0.32	2.60	0.38	0.32
P_2O_5	0.48	0.24	0.30	0.22	0.24
LOI	3.94	3.66	4.01	2.40	1.09
Σ	93.93	99.59	97.07	97.47	97.96
ppm					
Be	5	4	4	3	1
B	12.5	3.5	52.0	4.0	19.3
C	409.4	409.4	1009.8	409.4	409.4
S	2365	725	335	290	685
Sc	22.0	14.0	13.0	13.0	1.3
V	380	210	160	110	240
Cr	120.0	84.0	82.0	80.0	35.0
Mn	655	432	278	1220	64
Co	1.9	7.8	5.3	20.0	0.9
Ni	<10	50.0	20.0	80.0	10.0
Cu	75	45	35	45	20
Zn	110	130	55	85	10
Ga	23	17	22	24	<2
As	25	22	17	10	21
Se	2.3	0.9	<0.5	1.2	<0.5
Br	<0.5	1.5	<0.5	<0.5	0.7
Rb	40	5	92	5	10
Sr	164	141	118	110	26
Y	44	38	32	30	14
Zr	183	190	168	198	20
Nb	17	16	17	16	<2
Mo	INT	INT	INT	INT	INT
Ag	0.1	0.1	0.1	0.1	0.1
Sn	13	6	7	8	<5
Sb	6.3	5.4	4.1	2.6	4.0
Cs	1.6	0.8	6.4	<0.2	0.5
Ba	985	3211	777	445	72
La	39.1	42.7	39.6	41.9	6.1
Ce	81	89	85	91	7
Nd	34	39	38	41	6
Sm	5.60	6.40	6.00	7.00	1.80
Eu	1.08	1.21	1.04	1.29	0.56
Gd	4.9	6.7	4.2	5.6	2.2
Tb	1.0	0.9	0.8	0.9	0.3
Dy	5.6	4.8	5.0	5.3	1.7
Yb	2.27	3.04	2.62	2.95	0.87
Lu	0.40	0.46	0.39	0.42	0.14
Hf	4.8	5.2	4.0	5.2	0.3
Ta	1.2	1.5	1.2	1.2	<0.3
W	4	<1	4	2	<1
Ir	<1	<1	<1	<1	<1
Au	0.003	0.004	0.005	<0.002	0.007
Hg	<1	<1	<1	<1	<1
Pb	34	16	20	10	12
Bi	<5	<5	5	<5	<5
Th	14.00	16.00	15.00	15.00	1.20
U	7.40	8.40	6.00	6.00	5.90

Quartz breccias and associated fault gouges of type IV: (22) FM-8A1 (fault gouge); (23) FM-8A2; (24) FM-9A (fault gouge); (25) FM-9B; (26) FM-9C.

Table II -20 : Assay data for late breccias related with the reactivation of the NNE-SSW - NE-SW regional shears in França sector.

Breccias I

	(1)	(2)	(3)	(4)	(5)	(6)	(7)	(8)	(9)	(10)
Ce/Y	0.20	0.44	0.60	0.50	0.13	0.33	0.60	<0.25	<0.05	<0.07
La/Yb	6.00	8.00	12.50	9.54	0.64	1.30	0.44	4.00	1.11	2.85
La/Lu	30.00	40.00	83.33	70.00	4.29	8.33	7.00	26.66	7.00	20.00

Fault gouges II

	(17)	(16)	(15)
Ce/Y	1.88	0.69	1.67
La/Yb	12.38	8.91	10.14
La/Lu	79.25	45.56	66.67

Breccias and related fault gouges IV

	(23)	(22)
Ce/Y	2.34	1.84
La/Yb	14.04	14.11
La/Lu	92.82	97.75

	(24)	(25)	(26)
Ce/Y	2.66	3.03	0.50
La/Yb	15.11	14.20	7.01
La/Lu	101.54	99.76	43.57

	(28)	(27)
Ce/Y	1.40	2.44
La/Yb	6.95	9.20
La/Lu	47.73	64.07

	(30)	(29)
Ce/Y	3.77	2.23
La/Yb	19.81	13.79
La/Lu	121.16	77.63

<— iron oxides and hydroxides
<— clay minerals

Table II -21 : Ce/Y, La/Yb and La/Lu ratios of the analysed breccia matrices and fault gouges. Samples ordered as in Tables II- 17, 18, 20.

ANNEX

CHAPTER IV

Table IV - 1: ARSENOPYRITE CRYSTAL CHEMISTRY - FRANÇA SECTOR

ARSENOPYRITE Ia; N° analyses: 20

	S	Fe	As	Cu	Ag	Au	Pb	Zn	Cd	Sb
Minimum	20.76	32.97	41.0	0.01	0.00	0.00	0.00	0.00	0.00	0.00
Maximum	22.90	35.68	44.46	0.09	0.03	0.08	1.08	0.01	0.04	0.07
Std.dev.	0.48	0.62	0.72	0.02	0.008	0.001	0.24	0.002	0.01	0.02
Average	21.44	34.84	43.26	0.02	0.003	0.01	0.07	0.001	0.01	0.02
Median	21.34	35.06	43.36	0.02	0.00	0.00	0.00	0.00	0.00	0.01
Mode	21.51	34.12	43.51	0.02	0.00	0.00	0.00	0.00	0.00	0.00

ARSENOPYRITE Ib; N° analyses: 12

	S	Fe	As	Cu	Ag	Au	Pb	Zn	Cd	Sb
Minimum	22.51	33.07	41.89	0.00	0.00	0.00	0.09	0.00	0.00	0.00
Maximum	20.67	35.44	44.87	0.03	0.04	0.00	0.40	0.02	0.06	0.05
Std.dev.	0.52	0.67	0.79	0.01	0.01	0.00	0.09	0.007	0.02	0.02
Average	21.51	34.74	43.24	0.01	0.01	0.00	0.20	0.004	0.02	0.02
Median	21.63	34.93	43.00	0.01	0.00	0.00	0.17	0.00	0.00	0.02
Mode	21.47	35.03	43.79	0.01	0.00	0.00	0.17	0.00	0.00	0.00

ARSENOPYRITE II; N° analyses: 9

	S	Fe	As	Cu	Ag	Au	Pb	Zn	Cd	Sb
Minimum	21.51	34.82	41.12	0.00	0.00	0.00	0.00	0.00	0.00	0.00
Maximum	22.92	35.86	43.08	0.04	0.02	0.05	0.17	0.02	0.03	0.18
Std.dev.	0.46	0.37	0.71	0.01	0.01	0.02	0.07	0.01	0.01	0.04
Average	22.03	35.19	42.24	0.02	0.004	0.01	0.08	0.002	0.01	0.13
Median	21.87	35.18	42.42	0.02	0.00	0.00	0.10	0.00	0.00	0.13
Mode	21.73	35.29	42.15	0.02	0.00	0.00	0.10	0.00	0.00	0.14

ARSENOPYRITE IN MINERALIZED VEINS ALONG NW-SE SHEARS; N° analyses: 11

	S	Fe	As	Cu	Ag	Au	Pb	Zn	Cd	Sb
Minimum	20.40	34.03	42.49	0.00	0.00	0.00	0.00	0.00	0.00	0.00
Maximum	21.99	35.37	43.73	0.06	0.05	0.05	0.21	0.03	0.06	0.07
Std.dev.	0.14	0.44	0.41	0.02	0.02	0.01	0.08	0.001	0.02	0.02
Average	21.38	34.73	43.35	0.02	0.01	0.005	0.04	0.004	0.01	0.02
Median	21.39	34.76	43.54	0.02	0.00	0.00	0.00	0.00	0.00	0.03
Mode	21.37	34.46	43.38	0.02	0.00	0.00	0.00	0.00	0.00	0.00

ARSENOPYRITE IN QUARTZ BRECCIAS; N° analyses: 11

	S	Fe	As	Cu	Ag	Au	Pb	Zn	Cd	Sb
Minimum	21.97	34.21	41.01	0.00	0.00	0.00	0.00	0.00	0.00	0.00
Maximum	22.94	35.53	42.56	0.02	0.04	0.05	0.00	0.00	0.00	0.05
Std.dev.	0.39	0.34	0.46	0.001	0.01	0.02	0.00	0.00	0.00	0.01
Average	22.57	34.96	41.98	0.006	0.01	0.01	0.00	0.00	0.00	0.02
Median	22.78	34.97	42.06	0.00	0.01	0.01	0.00	0.00	0.00	0.02
Mode	21.99	34.97	42.06	0.00	0.00	0.00	0.00	0.00	0.00	0.02

	(1)	(2)	(3)	(4)	(5)
S	21.59	21.60	21.65	21.37	22.81
Fe	34.53	35.44	34.82	34.90	35.01
As	43.81	42.72	43.08	43.61	42.06
Cu	0.02	0.00	0.01	0.06	0.00
Ag	0.00	0.00	0.01	0.00	0.00
Au	0.00	0.00	0.00	0.00	0.00
Pb	0.00	0.17	0.10	0.00	0.00
Zn	0.00	0.01	0.00	0.00	0.00
Cd	0.00	0.03	0.00	0.00	0.00
Sb	0.00	0.02	0.12	0.03	0.03
Σ	99.95	99.99	99.78	99.98	99.91
Number of ions on a basis of 3 cations					
S	1.076	1.075	1.080	1.067	1.123
Fe	0.988	1.013	0.997	1.000	0.990
As	0.935	0.910	0.920	0.931	0.886
Cu	0.001	0.000	0.000	0.002	0.000
Ag	0.000	0.000	0.000	0.000	0.000
Au	0.000	0.000	0.000	0.000	0.000
Pb	0.000	0.001	0.001	0.000	0.000
Zn	0.000	0.000	0.000	0.000	0.000
Cd	0.000	0.000	0.000	0.000	0.000
Sb	0.000	0.000	0.002	0.000	0.000

Representative analyses of (1) Aspy Ia (FP-M), (2) Aspy Ib (F-23I), (3) Aspy II (F-23M), (4) Aspy in mineralized veins within regional shears (F-A), (5) Aspy relic in quartz breccia (F-11).

Table IV - 2:
ARSENOPYRITE CRYSTAL CHEMISTRY - MONTEMOR SECTOR

ARSENOPYRITE I; N° analyses: 5

	S	Fe	As	Cu	Ag	Au	Pb	Zn	Cd	Sb	Bi
Minimum	18.22	32.71	44.98	0.01	0.00	0.00	0.00	0.006	0.00	0.00	0.00
Maximum	19.39	33.31	47.26	0.04	0.04	0.40	0.006	0.03	0.01	0.00	0.00
Std.dev.	0.54	0.27	0.98	0.01	0.02	0.18	0.003	0.01	0.005	0.00	0.00
Average	18.63	33.07	46.40	0.02	0.01	0.11	0.002	0.02	0.004	0.00	0.00
Median	18.29	33.16	46.91	0.02	0.006	0.00	0.00	0.01	0.004	0.00	0.00
Mode	18.22	32.84	45.78	0.02	0.003	0.00	0.00	0.01	0.00	0.00	0.00

ARSENOPYRITE II; N° analyses: 16

	S	Fe	As	Cu	Ag	Au	Pb	Zn	Cd	Sb	Bi
Minimum	13.65	30.20	42.63	0.00	0.00	0.00	0.00	0.00	0.00	0.00	0.00
Maximum	21.78	34.79	53.36	0.04	0.07	0.124	0.35	0.02	0.02	0.01	0.00
Std.dev.	1.97	1.20	2.45	0.01	0.02	0.03	0.13	0.008	0.007	0.004	0.00
Average	19.01	33.06	46.03	0.008	0.02	0.01	0.06	0.005	0.003	0.001	0.00
Median	19.56	33.35	45.91	0.006	0.02	0.00	0.00	0.002	0.00	0.00	0.00
Mode	19.49	33.09	45.25	0.00	0.00	0.00	0.00	0.00	0.00	0.00	0.00

REPRESENTATIVE ANALYSES

	(1)	(2)
S	19.39	20.17
Fe	33.30	31.32
As	46.91	46.65
Cu	0.02	0.00
Ag	0.02	0.06
Au	0.40	0.00
Pb	0.00	0.33
Zn	0.02	0.00
Cd	0.00	0.00
Sb	0.00	0.00
Bi	0.00	0.00
Σ	100.06	98.53
N° of ions on the basis of 3 cations		
S	0.992	1.040
Fe	0.997	0.927
As	1.026	1.029
Cu	0.000	0.000
Ag	0.000	0.001
Au	0.003	0.000
Pb	0.000	0.003
Zn	0.001	0.000
Cd	0.000	0.000
Sb	0.000	0.000
Bi	0.000	0.000

(1) - Aspy I, (2) Aspy II

(sample MII8ab)

Table IV-3: REPRESENTATIVE ANALYSES OF ELECTRUM IN ORE SAMPLES OF THE FRANÇA SECTOR.

	(1)	(2)	(3)	(4)	(5)	(6)	(7)	(8)	(9)	(10)	(11)	(12)	(13)	(14)	(15)	(16)	(17)	(18)	(19)
S	0.47	0.18	0.15	0.15	0.23	0.29	0.23	0.06	0.13	0.12	0.12	0.20	0.15	0.19	0.08	0.11	0.10	0.82	0.80
Fe	0.79	0.04	0.18	0.02	0.15	0.28	0.04	0.04	0.00	0.00	0.03	0.08	0.06	0.18	0.09	0.10	0.09	0.05	0.05
As	0.24	0.00	0.00	0.00	0.00	0.00	0.00	0.00	0.00	0.00	0.00	0.00	0.00	0.00	0.00	0.00	0.00	0.01	0.00
Cu	0.01	0.03	0.03	0.01	0.09	0.02	0.06	0.01	0.02	0.02	0.02	0.02	0.06	0.00	0.00	0.00	0.00	0.09	0.05
Ag	32.21	19.49	19.34	75.82	74.17	76.63	78.50	64.72	60.56	61.56	61.02	76.86	79.08	75.96	61.89	76.21	75.64	83.05	83.20
Au	64.69	79.24	78.93	22.49	22.78	21.52	19.24	34.38	38.37	37.93	36.38	21.19	18.72	19.54	37.02	21.73	20.98	13.56	13.49
Bi	0.00	0.00	0.00	0.00	0.00	0.00	0.00	0.00	0.00	0.00	0.00	0.00	0.00	0.00	0.00	0.00	0.00	0.00	0.00
Pb	0.75	0.00	0.00	0.00	0.00	0.00	0.00	0.00	0.00	0.00	0.00	0.30	0.10	0.02	0.01	0.00	0.21	0.00	0.14
Zn	0.00	0.00	0.00	0.00	0.00	0.00	0.00	0.00	0.00	0.00	0.00	0.00	0.03	0.00	0.00	0.00	0.00	0.04	0.01
Cd	0.00	0.00	0.00	0.00	0.00	0.00	0.00	0.00	0.00	0.00	0.00	0.00	0.00	0.00	0.00	0.00	0.00	0.00	0.00
Sb	0.00	0.98	0.67	0.96	0.42	0.49	0.93	0.19	0.17	0.18	0.00	0.39	0.87	0.46	0.76	0.56	0.91	0.56	0.69
Σ	99.16	99.93	99.30	99.45	97.84	99.23	99.00	99.40	99.25	99.81	97.55	99.04	99.07	96.35	99.85	98.71	97.93	98.18	98.43

(1)-(14) - sample F-23A; (15)-(17) - sample F-18A1; (18)-(19) - sample F-23L1.

		Vapor Phase				Microthermometric data							Global composition					
Sample	Inclusion	CO2	CH4	N2	H2S	TmCO2	ThCO2	Mode	TmClat	Tm H2O	TH	Mode	H2O	CO2	CH4	N2	H2S	NaCl
COR 2A	1	51,6	45,1	2,9	0,43	-61,6			6,5	-3,3			95,6	1,8	1,6	1,00	0,01	0,8
	2	52,1	44,8	3,1	nd	-62,6			7,8	-2,3			95,7	2,0	1,8	0,01	0	0,4
	3	94,7	4,3	1,0	nd	-58,4			8,7	-2,4			95,6	3,9	0,2	0,10	0	0,2
	4	87,6	8,1	4,3	nd	-59,2			8	-6			92,0	5,4	0,6	0,20	0	1,9
	5	82,6	10,2	7,1	nd	-59,2			8,5	-6,8			88,7	7,7	0,9	0,70	0	2,0
	6	90,6	7,9	1,5	nd	-58,9			8,5	-4			94,1	4,5	0,4	0,10	0	1,0
66-1	3	85,8	11,8	2,4	nd	-59,1	5,1	V	7	-7,5	365	L	91,9	4,2	0,3	0,10	0	3,5
	4	85,5	12,4	2,1	nd	-59	15,2	L		-2,5	340	L	30,2	59,4	8,5	1,40	0	0,4
	5	88,9	9,0	2,1	nd	-58,5	6	V	8,1	-4	346	L	91,9	5,7	0,4	0,10	0	1,9
	7	88,0	11,9	nd	nd	-59,3	7,3	V		-7,3	370	L	89,0	7,0	0,7		0	3,3
66-4	1	81,8	18,2	nd	nd	-59,4	13,1	L		-4	342	L	78,7	16,5	3,1		0	1,7
	2	87,3	10,4	2,3	nd	-58,7	13,3	L		-3	350	L	27,8	62,7	7,4	1,70	0	0,4
67 - 0	1	90,3	6,3	3,4	nd	-57,7	26,5	L			291,8	V	29,3	63,3	4,4	2,35	0	0,8
	5	88,3	5,1	6,5	nd	-58,2	25	L			300*		18,3	71,8	4,1	5,28	0	0,5
	7	88,5	5,5	6,0	nd	-58	25,9	L			300*		28,7	62,6	3,9	4,16	0	0,8
	9	89,3	7,3	3,4	nd	-58	26	V	7		316,7	V	34,5	54,2	4,3	2,02	0	1,0
	10	92,1	5,3	2,6	nd	-57,9	22,2	L	7,3		352,5	V	76,0	20,4	1,1	0,52	0	2,0
	19	91,0	3,0	5,9	nd	-56,7	26,9	V			nv		23,9	68,7	2,3	4,45	0	0,6
	22	87,7	4,7	7,6	nd	-57,6	26,2	C	7,2		nv		55,3	38,1	2,0	3,16	0	1,5
	7	49,4	34,6	16,0	nd	-57,7	26,2	C			335,7	L	8,9	7,8	4,2	1,92	0	2,2
	10	93,2	1,6	5,3	nd	-57,7	26,2	C			nv		20,7	73,4	1,2	4,12	0	0,5
	11	92,0	4,1	3,9	nd	-57,7	26	C			327,8	V	35,2	58,8	2,6	2,45	0	0,9
	17	85,6	9,0	4,4	nd	-57,8	23,4	V	8,8		300*		69,2	25,3	2,5	1,20	0	1,8
70,85-1	9	94,0	3,8	2,2	nd	-58,1	27,4	V		-7			59,0	36,7	1,8	0,26	0	2,1
	3	90,9	4,1	5,0	nd	-58,3	26,7	V		-7			62,4	32,3	1,4	1,71	0	2,3
	2	83,7	5,8	10,5	nd	-58,2	27	V		-7			72,1	23,9	0,9	0,52	0	2,6
	10	94,4	4,9	0,7	nd	-58,4	26,8	L	8,7	-7			68,7	28,3	0,5	0,00	0	2,5
	7	98,2	1,8	nd	nd	-58,5	27,6	V	6,6	-7			68,3	24,8	1,6	2,91	0	2,5
147-0	23	93,7	4,6	1,6	nd	-57,6	10,4	L	8,5		292,5*		88,9	8,3	0,4	0,12	0	2,3
	23a	88,1	4,8	7,2	nd	-57,4	26,3	V	7,1		335,5*		92,5	4,7	0,1	0,21	0	2,4
	24	88,4	2,3	9,3	nd	-58,2	16,3	V	8,3		330,8*		92,3	5,0	0,1	0,30	0	2,4
147-1	15	84,0	9,1	6,9	nd	-58,2	19,1	V	6,1				89,9	6,9	0,5	0,38	0	2,4
	45	89,5	7,0	3,5	nd	-59,2	20,6	V					63,3	31,6	2,4	1,16	0	1,7
	59	89,4	6,3	4,3	nd	-57,9	24,1	C	6				91,1	6,0	0,3	0,18	0	2,4
	68	83,0	10,1	6,9	nd	-57,1	20,2	V	8,2				91,8	5,2	0,4	0,25	0	2,4
	100	79,9	16,8	3,1	0,27	-60,2	nv		9,1		295,8*		80,5	14,3	2,5	0,46	0,01	2,1
	107	83,3	14,3	2,5	nd	-58,1	18,6	V	6,9		373,5	C	88,3	10,3	1,2	0,20	0	
	111	85,5	10,7	3,9	nd	nv	18,7	V	5,3		328	L	91,6	5,4	0,4	0,14	0	2,4
	116	77,6	18,5	4,0	nd	-60	14,4	V	9,6		283,2*		83,4	11,7	2,2	0,47	0	2,2
	117	88,8	9,0	2,1	0,1	-59,3	19,5	V	8,3				67,7	27,2	2,6	0,62	0	1,8
	110	83,3	14,1	2,6	nd	nv	nv		9,3		327	L	91,3	6,1	1,0	0,20	0	1,4
	115a	85,4	12,2	2,4	nd	nv	nv		8,6		353*		94,7	3,9	0,6	0,10	0	0,7
	113	94,1	5,9	nd	nd	nv	nv		9,4		337,4	L	94,1	5,1	0,3		0	0,5
189-2	1	87,5	4,3	8,3	nd	-58,2	24,6	C			nv		21,8	67,9	3,3	6,36	0	0,6
	2	96,3	1,3	2,4	nd	-57,9	25,9	L			nv		17,1	79,4	1,1	1,93	0	0,5
	5a	72,3	22,8	3,8	1,14	-59,4	11,2	V	7,9		308,6	V	45,3	39,0	11,9	1,97	0,60	1,2
	10	96,6	0,0	3,4		-59,9	26,8	L			nv		17,1	79,7		2,75	0	0,5
	11	77,0	17,8	5,2	nd	-59,2	9,6	V	8,9		390,5	V	75,5	17,8	3,7	1,06	0	2,0
	8	100,0	nd	nd	nd	nv	nv		8,5		272,8	L	93,0	5,7			0	1,3
256-1	11	79,6	13,3	7,1	nd	-58,7	18,9	V	8,5	-5	381	V	57,8	32,7	5,2	2,78	0	1,5
	14	95,6	1,2	3,1	nd	-57,3	30,3	L	nv	-5	d		29,9	66,4	0,9	2,14	0	0,8
	17	92,6	0,0	7,4	nd	-57,3	-0,4	L	8,2	-5	nd		70,7	25,5	0,0	1,94	0	1,9
	3	83,6	12,7	3,6	nd	-58,5	21,4	V	8,1	-5	391	V	81,1	14,4	1,9	0,54	0	2,1
	10	87,7	12,3	0,0	nd	-58,1	23,2	V	6,9	-5	388,6	V	37,9	53,7	7,4	0,00	0	1,0
348,6-1	14	100,0	0,0	0,0	nd	-57,1	29,4	L	7,8	-5	d		30,2	69,1	0,0	0,00	0	0,8
	18	93,5	5,3	1,2	nd	-58	27	V	7,1	-5	346	V	52,9	42,8	2,4	0,51	0	1,4
	24	97,9	1,5	0,5	nd	-57,6	29,7	V	7,5	-5	360	V	34,1	63,8	1,0	0,35	0	0,9
	27	96,8	2,4	0,8	nd	-57,9	27,2	L	7,7	-5	333,5	L	48,6	48,6	1,2	0,37	0	1,3
	35	97,3	1,6	1,1	nd	-57,6	2,1	L	8,2	-5	d		87,6	9,9	0,1	0,09	0	2,3
365,7-1	1	96,8	0,9	2,3	nd	-57,7	30,3	L	nv	-5	nd		17,1	79,8	0,7	1,86	0	0,5
	13	98,1	0,8	1,1	nd	-57,3	30,2	C	nv	-5	nd		20,7	77,3	0,6	0,85	0	0,5
	25	65,2	31,9	2,9	nd	-60,2	nv	V	9,9	-3,5	382,7	L	92,9	4,1	2,0	0,20	0	0,8
	34	78,1	20,1	1,7	nd	-58,2	nv	V	8,7	-4	377,5	C	94,0	3,9	1,0	0,10	0	0,9
	8	98,6	0,0	1,4	nd	-57,2	30,3	L	6,7	-5	nd		30,2	68,1	0,0	0,99	0	0,8
14,55-1	19	73,5	23,1	3,4	nd	-59,2	nv		9,9	-3,5	350	V	93,7	4,3	1,3	0,20	0	0,5
	13	82,3	13,8	3,9	nd	-58,5	nv		9,1	-3,7	346	V	94,3	4,2	0,7	0,20	0	0,6
	22	79,2	20,8	0,0	nd	-60,3	nv		10,4	-3,4	347	V	93,9	4,7	1,2	0,00	0	0,2

Table IV - 4: Chemical composition of fluid inclusions from Corcoesto quartz veins obtained by Raman microprobe analysis and corresponding microthermometric data. Compositions are given in moles %. TmCO2 : melting temperature of CO2, Th CO2 : homogenization temperature of CO2, Tm cl : melting temperature of clathrates,. Tm H2O : melting temperature of H2O, TH : homogenization temperature L : Liquid, V: Vapour, C : Critic.

			Vapor Phase				Microthermometric data							Global composition					
Sample	Inclusion	Type	CO2	CH4	N2	H2S	Tm CO2	Tm H2O	Tm Clat	Th CO2	Mode	TH glob	Mode	H2O	CO2	CH4	N2	H2S	NaCl
GR6/1	1	L(c-m)-w	40,38	59,62	0	0	-65,2	-5	13			>510	L	92,87	2,84	1,86	0	0	2,44
	2	L(c-m)-w	54,36	45,64	0	0	-63	-5	9,6	-11,8	L	>510	L	83,92	9,08	4,8	0	0	2,2
	6	V(c-m)	55,92	40,64	3,44	0	-63,6	-5		-6,6	V			33,05	37,05	26,21	2,22	0	0,88
	8	L(c-m)	64,44	31,75	3,81	0	-61	-5		4	L			15,72	54,29	26,4	3,17	0	0,41
T5-104,05/2/4	1	L(c-m)-w	59,26	38,35	2,39	0	-62,5	-5,8	9,3	-5,7	L		L	75,77	14,24	7,25	0,45	0	2,29
	2	V(c-m)-w	53,95	41,4	4,2	0,45	-62,4	-5,8	10	-6,1	V		V	89,79	4,86	2,37	0,24	0,03	2,71
	3	Lc-w2	76,55	21,95	1,44	0,06	-59,6	-4,8	5,2	11,7	L	350,6	Lc	69,05	22,94	5,87	0,39	0,02	1,74
T5-104.05/2	1	Vc-w	80,4	11,56	8,04	0	-57,6	-4			V			63,64	28,5	3,84	2,67	0	1,35
Z3-5/1	5	L(c-m)-w	69,87	30,13	0	0	-60,7	-2	9,1	5,2	V	398	L	92,78	5,22	1	0	0	1
	9	Lc-w	86,81	6,05	7,09	0,05	-58,4	-3,5	7	19,1	L		L	85,44	11,65	0,61	0,71	0	1,59
	3	Lc	83,24	7,75	9,01	0	-59,2	-2		14	L			15,24	70,51	6,51	7,57	0	0,16
Z3-3	1	Lc-w2	95,44	0	4,56	0	-58,2	-6,6		20,7	L	389,6	Lc	55,44	40,77	0	1,89	0	1,89
Z3-1/2	1	L(c-m)-w	67,38	23,16	9,47	0	-61	-5	8,8	7,1	L	410	L	65,45	22,98	6,99	2,86	0	1,72
	5	L(c-m)-w	45,49	51,25	3,26	0	-62,9	-5	8,6	-7,8	V		L	90,94	4,4	2,14	0,14	0	2,38
	4	V(c-m)-w	61,47	33,91	4,62	0	-63,9	-5	9		V	372	V	79,93	11,88	5,36	0,73	0	2,1
Tom17/3	1	Lc-w	84,92	15,08	0	0	-59,1	-4,5	6	15,2	L			54,06	38,18	6,48	0	0	1,28
	4	Lc-w	86,99	13,01	0	0	-58,5	-3,7	7,6	18,8	L			53,95	39,37	5,63	0	0	1,06
	6	Lc-w	92,7	6,56	0,74	0	-58	-3,7	7,3	21,7	L			53,75	42	2,87	0,32	0	1,05
Tom17/2	1	L(c-m)-w	68,2	30,29	0,62	0,89	-61,7	-6	10,7	6	L	313,6	L	65,64	22,71	9,14	0,19	0,27	2,05
	2	L(c-m)-w	71,24	28,51	0	0,26	-60,5	-6	10,5	11	V	306	L	87,33	7,75	2,18	0	0,02	2,72
Z3-6/1/Z3	2	Lc-w	88,96	0,52	10,52	0	-56,9	-5,1	5,4	23,4	L	355	L	74,07	21,54	0,11	2,3	0	1,98
	16	Lc-w	85,71	3,68	10,61	0	-56,9	-3,7	6,8	26,6	V			92,33	5,36	0,13	0,37	0	1,81
Z3-6/1/Z2	38	Lc-w	93,39	6,61	0	0	-57,6	-1	8,8	17,4	L	285,5	L	88,6	10,35	0,57	0	0	0,48
	36	Lc-w	85,78	12,04	1,88	0,3	-58,4	-2	9,1	14,6	L			83,54	13,74	1,55	0,24	0,04	0,9
Z3-6/2	12	Lc-w	94,86	2,18	2,97	0	-57,1	-3,7	6,6	22	L	353	L	72	25,3	0,54	0,74	0	1,41
	4	Lc-w	86,14	12,73	1,13	0	-58,4	-2	9,1	16,8	L		L	81,42	15,62	1,91	0,17	0	0,87
	6	Lc-w2	89,99	8,2	1,81	0	-58	-2	8,8	19,6	L		Lc	81,78	15,85	1,22	0,27	0	0,88
Z3-6/1/Z1	1	Lc-w	95,8	2,02	2,15	0,03	-57,2	-4	7	22,8	L	314,4	L	83,31	14,38	0,26	0,28	0	1,76
	4	Lc-w	99,43	0,57	0	0	-57	-3,7	6,8	22,8	L	315,4	L	83,72	14,56	0,07	0	0	1,64
	5	Lc-w	100	0	0	0	-56,9	-4,4	6,4	22,4	L	328	L	83,02	15,06	0	0	0	1,93
	14	Lc-w	95,49	1,76	2,51	0,24	-57,4	-4	7	23,2	L			63,6	33,54	0,59	0,84	0,08	1,35
T9-190,30/1	1	L(c-m)-w2	64,8	25,58	9,43	0,19	-60,8	-3,7	11,4	3,7	L		Lc	55,79	28,6	10,55	3,89	0,08	1,09
T9-190,30/1a	1	Lc-w	98,35	0,22	1,42	0	-57,3	-3,7	7,3	28,8	L		L	84,84	13,31	0,03	0,16	0	1,66
	2	Lc-w2	98,22	0,2	1,58	0	-57,3	-4,4	6,4	25,7	L	276	Lc	38,85	59,19	0,12	0,94	0	0,9
	3	Lc-w	97,44	0,26	2,16	0,13	-57,3	-4,4	6,8	27,3	L		L	79,32	18,4	0,04	0,37	0,02	1,84
	5	Lc-w	95,92	0,53	2,86	0,69	-57,6	-3,7	7,5	27,2	L	312,5	L	85,09	12,78	0,06	0,32	0,08	1,67
	6	Lc-w	97,37	0,4	1,78	0,45	-57,5	-4	7	27,7	L	298,5	L	85,12	12,79	0,04	0,2	0,05	1,8

Table IV - 5: Chemical composition of fluid inclusions from Tomino area obtained by Raman microprobe analysis and corresponding microthermometric data. Compositions are given in moles %. TmCO2 : melting temperature of CO2, Th CO2 : homogenization temperature of CO2, Tm cl : melting temperature of clathrates, Tm H2O : melting temperature of H2O, TH : homogenization temperature L : Liquid, V: Vapour, C : Critic.

		Vapor Phase				Microthermometric data							Global composition					
Sample	Inclusion	CO2	CH4	N2	H2S	Tm CO2	Th CO2	Mode	Tm Clat	Tm H2O	TH	Mode	H2O	CO2	CH4	N2	H2S	NaCl
San Antonio																		
1a-2	1	66,55	32,24	0,79	0,42	-61,8	7,5	V	11,1	0,4	398,00	L	85,60	10,64	3,45	0,08	0,04	0,19
	2	70,95	27,83	1,22	nd	-62,0	11,4	V	12,0	-0,4	387,00	L	73,92	19,43	6,21	0,27	0	0,16
	3	79,25	20,75	0,00	nd	-60,5	7,7	V	5,1	-0,4	355,00	L	81,16	15,43	3,24	0	0	0,18
	4	95,24	4,76	0,00	nd	-60,3	8,5	C	6,6	-0,4	413,00	L	68,65	29,82	1,38	0	0	0,15
2a-3	1	92,65	4,74	2,61	nd	-57,5	8,9	L		-8,0	288,00	L	71,66	23,60	1,17	0,65	0	2,93
	3	88,32	7,52	3,87	0,28	-57,5	8,0	L		-8,0	310,00	L	71,14	23,09	1,84	0,95	0,07	2,90
3b-1	1	90,32	8,29	1,00	0,39	-58,8	11,0	L		-2,5	nv		25,74	66,83	6,07	0,73	0,29	0,34
	2	83,12	15,43	1,27	0,19	-59,1	11,6	L		-2,5	372,00	L	75,82	19,71	3,16	0,26	0,04	1,01
	3	87,93	10,51	1,22	0,34	-58,5	11,1	L		-2,5	nv		44,12	48,77	5,67	0,66	0,19	0,59
	4	83,12	15,18	1,17	0,53	-59,0	15,9	L	6,5	-2,5	398,00	L	77,86	18,01	2,78	0,21	0,10	1,04
Dacotim																		
Pen1	1a	60,12	35,23	4,03	0,63	-61,2	4,8	V	10,4	-5,5	347,7	L	82,29	10,24	4,51	0,52	0,08	2,36
	2a	67,47	28,63	3,90	nd	-60,8	nv		10,4	-8,9	313,9	L	89,87	7,71	1,66	0,23	0	0,54
	6a	81,06	15,54	3,40	nd	-60,1	10,7	L	10,6	-5,3	354,9	V	66,45	26,12	4,59	1	0	1,84
	15a	75,22	20,59	3,96	0,28	-61,0	nv		11,2	-5,0	341	L	86,96	10,54	1,94	0,37	0,03	0,16
	20a	71,32	23,63	5,04	nd	-60,1	nv		11,2	-5,0	337,7	L	87,4	9,84	2,14	0,46	0	0,16
	22a	77,79	15,84	6,37	nd	-61,4	nv		11,0	-5,1	335,2	L	87,5	10,41	1,36	0,55	0	0,16

Table IV - 6 : Chemical composition of fluid inclusions from Penedono area obtained by Raman microprobe analysis and corresponding microthermometric data. Compositions are given in moles %. TmCO2 : melting temperature of CO2, Th CO2 : homogenization temperature of CO2, Tm cl : melting temperature of clathrates, Tm H2O : melting temperature of H2O, TH : homogenization temperature L : Liquid, V: Vapour, C : Critic.

		Vapor Phase			Microthermometric data							Global compostion				
Sample	Inclusion	CO2	CH4	N2	Tm CO2	Tm H2O	Tm clat	Th CO2	Mode	TH	Mode	H20	C02	CH4	N2	NaCl
Pin 7-1	16a	85,87	4,22	9,91	nv	-5,4	7,9	nv		280	decrep.	94,75	4,57	0,06	0,14	0,47
	28a	93,01	1,70	5,28	-57,8			17,1	L			15,01	79,09	1,44	4,46	0
	29a	91,83	2,31	5,86	-57,4	-5,1	8,6	25,4	L	311,1	V	68,18	27,7	0,65	1,64	1,82
	40a	91,16	1,94	6,90	-57,4	-5,1	8,7	27,6	V	291,9	L	84,8	11,99	0,21	0,74	2,27
	43a	88,50	6,26	5,23	-58,4	-4,5	nv	19,7	L			16,25	73,84	5,19	4,34	0,39
	48a	90,68	4,69	4,63	-58,2	-5	8,7	22,4	C	318,2	V	74,33	21,69	1,02	1,01	1,95
	4b	92,91	3,54	3,55	-57,7	-5	9,1	23,3	V			84,73	12,27	0,39	0,39	2,22
	13b	80,14	12,54	7,32	-58,5	-4,8	8,1	19,5	V			69,54	23,42	3,34	1,95	1,75
	22b	91,31	5,24	3,45	-58,2	-4,5	nv	19,5	L			15,86	76,52	4,36	2,88	0,38
	40b	78,92	10,86	10,22	-57,2	-5	8	15,6	V			91,62	5,21	0,4	0,37	2,4
	45b	93,17	1,96	4,86	-56,8	-4,7	8,4	nv				93,13	6,31	0,07	0,17	0,32
	4d	96,35	3,65	0,00	nv	-5,1	5	nv				96,56	2,93	0,02	0	0,48
	9d	94,22	5,78	0,00	nv	-4,1	5,8	nv				95,97	3,63	0,07	0	0,33
	15d	73,91	14,70	11,40	nv	-3	6	nv				97,09	2,64	0,05	0,04	0,18
	18d	90,43	6,28	3,29	-58,4	-5,6	7,2	20,3	L			27,19	65,19	4,47	2,35	0,79
	19d	97,60	2,41	0,00	-57,4	-5,4	7,6	nv				95,46	4	0,03	0	0,51
Pin 8	10a	81,46	3,61	14,93	nv	-5	4,5	nv				96,71	2,67	0,02	0,09	0,51
	13a	89,65	2,00	8,34	-57,5	-5,2	4,5	nv				96,3	3,17	0,02	0,09	0,42
	8b	76,96	11,34	11,70	nv	-4,4	9,3	nv				94,33	4,82	0,22	0,22	0,41
	54b	82,22	8,37	9,42	-58,2	-4,4	7,5	19,3	L			47,23	42,79	4,18	4,71	1,1
	56b	83,79	6,95	9,26	-57,1	-4	7,5	18,6	C			34,48	54,47	4,43	54,47	0,73
	60b	81,27	10,06	8,68	-57	-5	8,7	nv				91,17	7,48	0,56	0,48	0,31
	75b	88,61	11,39	0,00	-58,5	-4,4	9,1	nv				86,95	11,75	1,17	0	0,13

Table IV - 7 : Chemical composition of fluid inclusions from Pino area obtained by Raman microprobe analysis and corresponding microthermometric data. Compositions are given in moles %. TmCO2 : melting temperature of CO2, Th CO2 : homogenization temperature of CO2, Tm cl : melting temperature of clathrates, Tm H2O : melting temperature of H2O, TH : homogenization temperature L : Liquid, V: Vapour, C : Critic.

Table IV-8A : França

Volatile composition of representative fluid inclusions.

Sample	Incl. nº	Type	CO2 (mole %)	CH4 (mole %)	N2 (mole %)	H2S (mole %)	Flw	TH (°C)	Observations
F-4A	1	.Lw-c	79.580	12.916	7.503	0.000	0.35	283.2	.QtzI
F-4A	2	?.Lw-c	77.760	20.102	1.804	0.335	0.35	273.4 (Td)	.QtzI
F-4A	4	.Lw-c	79.778	13.807	6.415	0.000	0.35	295.3	.QtzI, Sol.=carbonate
F-4A	5	.Lw-c	89.231	6.594	4.175	0.000	0.55	297.2	.QtzI
F-4A	12	?.Lw-c	84.988	11.429	3.582	0.000	0.65	260.2 (Td)	.QtzI
F-18A1	103	.Lw-c	93.395	5.505	1.100	0.000	0.70	320.7	.QtzI
F-4A	10	.Lw-c	89.773	5.753	4.474	0.000	0.55	289.9	.QtzI, trail N-S
F-4A	11	.Lw-c	90.544	7.290	2.166	0.000	0.60	310.3	.QtzI, trail N-S
F-4A	6	.Lw-c	94.347	5.653	0.000	0.000	0.45	302.4	.QtzI, trail N72E
F-18A1	96	.Lw-c	80.835	15.303	3.861	0.000	0.50	280.1	.QtzIIa
F-18A1	100	?.Lw-c	86.639	10.616	2.745	0.000	0.40	253.2 (Td)	.QtzIIa
F-23B	34	.Lw-c	84.038	12.660	3.302	0.000	0.40	273.2	.QtzIIb
F-23B	36	.Lw-c	82.622	13.310	4.067	0.000	0.45	270.4	.QtzIIb
F-23B	48	.Lw-(c)	93.496	5.914	0.598	0.000	0.65	173.2	.QtzIIb, trail N30W
F-23B	91	.Lw-(c)	78.351	17.484	4.165	0.000	0.50	147.8	.QtzIIb, trail N10E
F-23B	51	.Lw-c	87.889	10.917	1.195	0.000	0.65	210.2	.QtzIIb, trail N20W
F-21	72	.Lw-c	78.555	14.880	6.319	0.246	0.65	247.2	.Qtz (shear)
F-21	74	.Lw-c	84.042	6.484	9.475	0.000	0.70	244.9	.Qtz (shear)
F-21	81	?.Lw-c	77.618	3.120	19.262	0.000	0.40	150.1 (Td)	.Qtz (shear), trail N10W
F-21	85	?.Lw-(c)	87.334	6.304	5.938	0.424	0.55	130.5 (Td)	.Qtz (shear), trail N20E
FM-4	108	.Lw-(c)	25.945	26.468	47.588	0.000	0.60	179.9	.Qtz (shear), trail N35W
F-47	22	.Lw-n(m)	23.917	32.568	43.515	0.000	0.60	217.0	.QtzX
F-47	23	.Lw-m(c)	31.989	44.650	23.361	0.000	0.40	221.1	.QtzX, Sol.=graphite
F-47	95	.Lw-m(c)	31.123	49.945	18.932	0.000	0.50	220.9	.QtzX
F-47	30	.Lw-m(n)	0.000	61.484	38.516	0.000	0.55	199.8	.QtzY
F-47	29	.Lw-n(m)	0.000	32.446	67.554	0.000	0.75	201.7	.QtzY
F-47	18	.Lw-m(c)	41.361	34.061	24.568	0.000	0.55	152.6	.QtzX, trail E-W
F-47	19	.Lw-m(c)	44.028	31.886	24.085	0.000	0.65	152.9	.QtzX, trail E-W
F-47	21	?.Lw-m	0.000	100.000	0.000	0.000	0.75	140.1 (Td)	.QtZX, trail N10W

TableIV-8B : França

Bulk composition of representative fluid inclusions.

Sample	Incl. nº	X(H2O)	X(CO2)	X(CH4)	X(N2)	X(H2S)	wt%NaCl	d (g/cm.3)	Observations
F-4A	1	81.6	15.2	2.0	1.2	0.0	3.37	0.50	.QtzI
F-4A	2	77.3	18.2	4.0	0.4	0.07	4.94	0.55	.QtzI
F-4A	4	79.5	16.9	2.5	1.2	0.0	4.47	0.53	.QtzI, Sol.=carbonate
F-4A	5	91.3	8.0	0.4	0.3	0.0	6.29	0.66	.QtzI
F-4A	12	89.0	9.8	0.9	0.3	0.0	3.53	0.79	.QtzI
F-18A1	103	93.1	6.6	0.2	0.0	0.0	4.32	0.73	.QtzI
F-4A	10	83.8	14.8	0.8	0.6	0.0	3.05	0.75	.QtzI, trail N-S
F-4A	11	83.8	14.9	1.0	0.3	0.0	2.89	0.75	.QtzI, trail N-S
F-4A	6	85.5	13.8	0.7	0.0	0.0	3.53	0.61	.QtzI, trail N72E
F-18A1	96	84.3	13.2	2.0	0.5	0.0	5.70	0.74	.QtzIIa
F-18A1	100	84.0	14.2	1.4	0.4	0.0	4.94	0.62	.QtzIIa
F-23B	34	87.2	11.1	1.3	0.3	0.0	5.99	0.58	.QtzIIb
F-23B	36	87.4	10.8	1.4	0.4	0.0	7.72	0.72	.QtzIIb
F-23B	48	97.9	1.9	0.1	0.0	0.0	0.10	0.??	.QtzIIb, trail N30W
F-23B	91	98.1	1.5	0.3	0.1	0.0	0.60	0.61	.QtzIIb, trail N10E
F-23B	51	92.9	6.6	0.5	0.0	0.0	1.73	0.72	.QtzIIb, trail N20W
F-21	72	91.7	7.1	0.8	0.3	0.01	4.94	0.75	.Qtz (shear)
F-21	74	89.8	9.0	0.5	0.7	0.0	3.05	0.78	.Qtz (shear)
F-21	81	86.4	11.2	0.3	2.1	0.0	3.53	0.58	.Qtz (shear), trail N10W
F-21	85	99.6	0.2	0.1	0.1	traces	0.90	0.53	.Qtz (shear), trail N20E
FM-4	108	96.4	0.9	0.9	1.6	0.0	0.30	0.??	.Qtz (shear), trail N35W
F-47	22	89.6	2.5	3.4	4.5	0.0	0.30	0.67	.QtzX
F-47	23	92.7	2.3	3.2	1.7	0.0	0.70	0.47	.QtzX, Sol.=graphite
F-47	95	92.0	2.3	3.7	1.4	0.0	0.50	0.56	.QtzX
F-47	30	90.7	0.0	5.0	3.2	0.0	1.00	0.55	.QtzY
F-47	29	86.4	0.0	3.9	8.2	0.0	1.50	0.75	.QtzY
F-47	18	90.8	3.8	3.1	2.3	0.0	0.10	0.58	.QtzX, trail E-W
F-47	19	89.6	4.6	3.3	2.5	0.0	0.30	0.68	.QtzX, trail E-W
F-47	21	89.3	0.0	10.7	0.0	0.0	1.50	0.73	.QtZX, trail N10W

							MICROTHERMOMETRY							VOLATILE PHASE COMPOSITION				BULK COMPOSITION						
Sample	Quartz type	Incl. n°	Incl type	Occurr.	Rw	Rv	ThCH4	TmCO2	Tmi	Tmcl	Wt% NaCl	ThCO2	TH	CO2	CH4	N2	H2S	H2O	CO2	CH4	N2	H2S	NaCl	d
Segregation	Milky deformed	14/1	Vc-w	clust.	0,60	0,40		-59 9	-11 6	7,1	15,7	16 5 V	309 d	77,90	14,00	8,10		83,87	9,09	1,43	0,83		4,79	0,81
Quartz	(Q I)	2	Vc-w	clust.	0,70	0,30		-59 4	-10 8	7,8	14,8	17 0 V	330 L	84,90	10,30	4,80		89,00	5,49	0,51	0,23		4,77	0,85
	Hyaline	5	Vc-w	isolat.	0,75	0,25		-59 0	-9 6	6,1	13,6	15 0 V		78,90	11,10	9,60	0,40	89,86	4,87	0,49	0,42		4,33	0,89
	subheuedral	6	Lc-w	trails	0,20	0,80		-58 5		8,5		21 0 L		88,10	9,60	2,30		50,50	43,58	4,77	1,12		1,67	0,64
	(Q I A)	14	Vc-w	isolat.	0,75	0,25		-59 6	-5 5	8,5	8,5	17 0 V	283 L	77,90	9,60	12,50		90,19	5,98	0,54	0,70		2,59	0,88
	"	15	Vc-w	isolat.	0,70	0,30		-58 4	-9 0	4,2	12,9	-1 0 V	266 d	97,80	2,20	0,00		92,87	2,86	0,04			4,22	0,79
Qz veinlets in	Recryst polygonal	20/9	Vm-w-S	isolat.	0,70		-94 3 V		-1 7	10,3	2,9				90,70	8,70	0,50	95,39		3,39	0,32	0,02	0,87	0,74
black shales	(Q II)	10	Vm-w S	isolat.	0,80		-92 5 V		-1 7	12,9	2,9		297 L		89,30	10,00	0,70	96,90		1,97	0,22	0,02	0,89	0,83
Mineralized	Milky deformed	VE/2	Lc-w	clust.	0,50	0,50		-57 0		8,6		18 0 L	>330 V	98,40	1,60	0,00		79,08	20,52	0,40				0,88
Quartz	(Q III)	3	Lc-w	clust.	0,70	0,30		-58 2	-4 6	9,9	8,1	21 2 C	295 L	83,40	13,30	3,30		89,46	7,03	0,87	0,21		2,44	0,84
Veins	"	7	Vc-w	clust.	0,65	0,35		-58 8	-6 9	9,0	10,4	18 6 V	266 d	77,50	22,00	0,07	0,50	87,25	7,82	1,77	0,01	0,40	3,10	0,81
	"	14	Lc-w	trails	0,55	0,45		-57 2		6,4		24 8 L	287 d	93,00	5,70	1,30		84,03	14,79	0,97	0,22			0,81
	"	18	Lc-w	trails	0,50	0,50		-57 9		8,8		20 9 L	320 L	84,00	11,40	4,30	0,20	82,04	15,33	1,88	0,71	0,03		0,72
	"	VQ2-4/1	Vc-w	clust.	0,60	0,40		-58 8		8,8		17 7 V		78,20	17,14	4,67		87,81	10,27	1,55	0,41			0,73
	"	VQ1-9/1	Lc-w	clust.	0,50	0,50		-59 0				12 0 L		80,20	16,70	2,90	0,20	78,86	17,37	3,17	0,56	0,05		0,76
	"	VQ2-9/1	Lc-w	clust.	0,60	0,40		-57 5				15 8 L		80,30	15,70	3,90		85,08	12,55	1,89	0,47	0,01		0,78
	Hyaline	VC-5/2	Lc-w	clust.	0,60	0,40		-57 0		8,0		21 0 L		90,93	5,45	3,28	0,34	84,59	14,14	0,77	0,46	0,05		0,83
	(Q IV)	VC-5/3	Lc-w	clust.	0,60	0,40		-57 0		8,0		21 4 L		87,53	7,02	5,15	0,30	84,96	13,43	0,90	0,66	0,04		0,80
	"	VC-5/4	Lc-w	clust.	0,50	0,50		-57 0		8,0		21 0 L		89,43	7,12	3,14	0,32	84,37	14,14	0,99	0,44	0,05		0,83
	"	VC-17/1	Lc-w	clust.	0,60	0,40		-57 0		8,0		21 4 L		97,31	2,69	0,00		81,11	18,44	0,43				0,89
	"	VC-17/3	Lc-w	clust.	0,50	0,50		-57 0		8,0		21 0 L		98,21	1,79	0,00		75,01	24,58	0,40				0,86
	"	VC-17/4	Lc-w	clust.	0,50	0,50		-57 0				20 0 L		97,34	2,66	0,00		74,90	24,50	0,60				0,86
Silicified	Milky deformed	2	Lw - m - S	trails	0,56	0,20			-2 2	12,0	0,50		254 d	27,82	55,57	15,97	0,63	90,54	3,86	4,20		0,05	0,14	0,56
metasediments	(Q I TM)	7	Lw - m S	trails	0,40	0,20			-2 1	11,0	3,53			21,71	78,29			88,32	3,12	7,56			1,00	0,46
	"	19	Vc - w	trails	0,50	0,50		-62 3	-3 9	13,5		-21 2 V	314 L	79,77	20,23			84,48	11,54	2,23			1,74	0,66
	"	21	Vc - w	trails	0,50	0,50		-63 7	-3 8	14,3	6,14	-16 0 V	302 L	47,81	43,04	9,13		82,84	8,67	5,62			1,67	0,65
	"	23	Vc - w	trails	0,70	0,30		-65 7	-6 4	13,0	9,73		328 L	53,40	39,70	6,90		87,61	6,30	2,71			2,90	0,84
	"	28	Lw - m	trails	0,50	0,50			-2 2	13,5	3,69		309 L	30,30	69,70			88,24	4,42	6,29			1,04	0,58
	Recryst (Q II TM)	2II	Lw - m	isolat.	0,60	0,40			-3 0	12,0	4,94		351 L	28,07	70,42	0,70		92,48	2,63				1,48	0,66
	Microcrystalline	1III	Lw - m	isolat.	0,70	0,30			-1 7	13,8	2,89		357 L	4,77	88,50	5,30	1,40	94,78	0,54	3,34		0,06	0,87	0,74
	(Q III TM)	2III	Lw - m	isolat.	0,80	0,20			-1 8	13,5	3,05			21,85	63,60	14,55		94,60	2,30	1,77			0,92	0,84
	"	6III	Vm - w	isolat.	0,60	0,40	-93 0 V		-1 0	13,5	1,73		322 L		89,54	10,46		92,77		6,03			0,50	0,65
	"	7III	Vm - w	isolat.	0,75	0,25	-95 5 V		-2 0	7,5	3,37		310 L	21,04	73,80	3,88	1,27	96,93	1,01	0,96		0,02	1,04	0,78
	Hyaline (Q IV TM)	1IV	Lw - c	Isolat.	0,75	0,25			-3 8	8,0	6,14		284 L	89,58	7,10	3,30		94,48	3,47	0,10			1,90	0,80

Compositions are given in mole%. ThCH4: homogenization temperature of CH4. TmCO2: melting temperature of solid CO2. Tmi: melting temperature of ice. TmCl: melting temperature of clathrate. ThCO2: homogenization temperature of CO2. TH: global homogenization. L: liquid. V: vapour. C: critical d: decrepitation. All values in °C. Density in g/cm3.

Table IV - 9: Fluid inclusion data from VPA.

Deposit	Mica type	n	Si	R2+	Paragonite	Celadonite	IC
Penedono	Mica I	24	3,07-3,17	0,1 -0,2	4,86-11,4	10-20,3	0,91-0,99
			3,12 ±0,03	0,15±0,03	7,37±1,77	14,8±2,58	0,96 ± 0,02
	Mica II	28	3,07-3,025	0,1-0,39	1,86 - 7,67	10,1-37	0,8-1
			3,14±0,04	0,19 ± 0,06	4,23 ± 1,54	18,5 ±6,15	0,94±0,04
	Mica III	9	3,01-3,27	0,07-0,37	0,68-6,83	6,84-35,5	0,9-0,97
			3,16±0,09	0,21±0,11	3,09±1,87	20,8±10,9	0,94±0,02
	Mica IV	7	3,13-3,23	0,12-0,20	1,94 - 5,09	19,7-11,7	0,92-0,98
			3,18±0,05	0,17±0,03	3,08 ±1,02	16,7±2,77	0,94±0,02
	Mica V	31	3,1-3,18	0,16-0,24	1,35-7,62	10,4-34,9	0,9-1
			3,18±0,05	0,19±0,0,3	3,8±1,35	18,5±5,92	0,95±0,03
	Mica VI	7	3,19-3,28	0,16-0,24	0,8-2,73	15,8-23,6	0,91-0,98
			3,23±0,03	0,19±0,03	1,72±0,72	19,1±2,69	0,94±0,03
Dacotim	Mica I	9	3,07-3,16	0,11-0,16	4,86-8,14	11,3-16,2	0,91-0,99
			3,12±0,03	0,15±0,02	6,5±1,11	14,5±1,51	0,95±0,03
	Mica II .	13	3,09-3,19	0,14-0,16	2,57-5,64	11,6-23,2	0,8-0,98
			3,14±0,03	0,15±0,01	4,22±1	16,4±3,6	0,93±0,05
	Mica V	6	3,1-3,19	0,12-0,32	2,05-7,28	11,8-19,9	0,92-0,99
			3,13±0,03	0,19±0,07	4,47±1,82	18,6±6,88	0,96±0,03
Laboreira	Mica I	6	3,1-3,17	0,13-0,20	5,25-11,4	13,1-20,3	0,96-0,99
			3,13±0,03	0,16±0,03	8,35±2,45	16,3±3,37	0,98±0,01
	Mica II	6	3,1-3,19	0,14-0,22	2,56-5,73	14-21,6	0,94-0,97
			3,15±0,03	0,18±0,03	3,83±1,42	17,5±2,55	0,96±0,01
	Mica V	25	3,11-3,28	0,11-0,37	1,35-7,62	10,4-34,9	0,92-0,99
			3,19±0,05	0,19±0,06	3,64±1,2	18,5±5,82	0,93±0,03
Ferronha	Mica I	6	3,08-3,12	0,1-0,14	5,44-9,74	10-14,5	0,92-0,97
			3,12±0,02	0,13±0,01	7,84±1,57	12,8±1,44	0,95±0,02
	Mica II	6	3,08-3,25	0,16-0,39	1,82-6,2	15,8-37	0,92-1
			3,17±0,07	0,26±0,1	3,55±1,86	25,2±9,2	0,96±0,03
	Mica III	5	2,01-3,27	0,07-0,37	0,68-6,83	6,84-35,5	0,9-0,97
			3,2±0,11	0,25±0,15	2,64±2,41	24,5±14	0,95±0,03
	Mica VI	7	3,19-3,28	0,16-0,24	0,8-2,73	15,8-23,6	0,91-0,98
			3,23±0,03	0,19±0,03	1,72±0,72	19,1±2,69	0,94±0,03
Pino	Mica I	17	3,01-3,3	0,09-0,34	0,15-10,4	8,97-33,1	0,87-0,99
			0,12±0,08	0,16±0,08	6,21±3,65	15,4±7,21	0,93±0,03
	Mica II	11	3,06-3,42	0,13-0,49	0,42-7,95	12-49,5	0,79-0,97
			3,17±0,09	0,21±0,1	3,46±1,98	20,7±10	0,91±0,06
	Mica III	5	3,01-3,17	0,07-0,2	2,52-10	6,6-18,8	0,61-0,98
			3,08±0,06	0,12±0,05	5,82±3,25	11±4,74	0,85±0,14

Table IV - 10: Dioctahedral K-micas crystal chemistry. Penedono and Pino area
Ranges, mean and standards deviation for the studied parameters are given for each type of K - micas. Si, R^{2+} (Fe+Mg+Mn) and IC (interlayer charge) are given for half formula.Paragonite and celadonite are given in %.

Table IV - 11 :
DIOCTAHEDRAL K-MICAS CRYSTAL CHEMISTRY - FRANÇA SECTOR

	SiO2	TiO2	Al2O3	Cr2O3	FeO	MnO	MgO	CaO	Na2O	K2O
SERICITE E-I; N° analyses: 9										
Minimum	45.45	0.00	32.46	0.00	0.09	0.00	0.01	0.00	0.11	8.14
Maximum	47.82	0.13	36.74	0.03	1.66	0.04	0.[illegible]	0.06	0.33	10.32
Std.dev.	0.88	0.04	1.33	0.01	0.61	0.02	0.[illegible]	0.02	0.09	0.72
Average	46.42	0.02	35.26	0.01	0.92	0.01	0.27	0.03	0.21	9.31
Median	46.19	0.01	35.36	0.00	1.07	0.01	0.25	0.03	0.15	9.46
Mode	45.95	0.00	35.24	0.00	0.60	0.00	0.23	0.01	0.13	9.26
SERICITE E-II; N° analyses: 14										
	SiO2	TiO2	Al2O3	Cr2O3	FeO	MnO	MgO	CaO	Na2O	K2O
Minimum	46.73	0.08	29.83	0.00	1.81	0.00	0.55	0.00	0.02	6.57
Maximum	49.73	0.94	33.56	0.06	3.64	0.06	1.47	0.09	0.29	10.01
Std.dev.	0.86	0.29	1.08	0.02	0.49	0.02	0.25	0.03	0.08	0.91
Average	47.70	0.47	31.73	0.02	2.49	0.02	1.05	0.02	0.15	9.04
Median	47.65	0.50	31.82	0.02	2.47	0.02	1.07	0.01	0.23	9.12
Mode	47.22	0.08	31.76	0.00	2.27	0.00	1.07	0.01	0.12	8.80
SERICITE E-IIIa; N° analyses: 7										
	SiO2	TiO2	Al2O3	Cr2O3	FeO	MnO	MgO	CaO	Na2O	K2O
Minimum	42.97	0.00	30.09	0.00	2.56	0.00	0.68	0.00	0.05	9.12
Maximum	46.72	0.68	35.57	0.33	3.96	0.09	1.63	0.36	0.26	10.72
Std.dev.	1.26	0.31	2.37	0.12	0.54	0.03	0.35	0.12	0.08	0.70
Average	45.79	0.19	34.89	0.06	3.09	0.02	1.09	0.08	0.17	9.79
Median	46.13	0.01	34.02	0.03	3.01	0.01	1.08	0.04	0.16	9.66
Mode	46.11	0.01	31.08	0.03	2.66	0.00	0.89	0.02	0.12	9.12
SERICITE E-IIIb; N° analyses: 4										
	SiO2	TiO2	Al2O3	Cr2O3	FeO	MnO	MgO	CaO	Na2O	K2O
Minimum	47.27	0.18	28.95	0.00	1.76	0.02	0.63	0.03	0.08	8.09
Maximum	48.15	0.72	32.43	0.09	3.27	0.05	1.39	0.04	0.21	9.95
Std.dev.	0.37	0.26	1.51	0.04	0.67	0.01	0.33	0.006	0.06	0.90
Average	47.67	0.57	30.85	0.04	2.39	0.03	0.90	0.04	0.16	9.43
Median	47.66	0.69	31.02	0.04	2.26	0.03	0.79	0.04	0.17	9.85
Mode	47.27	0.69	28.95	0.00	1.76	0.03	0.63	0.04	0.08	8.09
SERICITE M-I; N° analyses: 9										
	SiO2	TiO2	Al2O3	Cr2O3	FeO	MnO	MgO	CaO	Na2O	K2O
Minimum	47.42	0.02	31.04	0.00	1.61	0.00	0.42	0.03	0.05	7.90
Maximum	49.92	0.29	34.89	0.19	1.98	0.06	1.18	0.25	0.25	9.76
Std.dev.	1.07	0.09	1.16	0.06	0.14	0.02	0.32	0.07	0.07	0.58
Average	48.74	0.17	33.04	0.04	1.86	0.02	0.79	0.10	0.11	8.89
Median	48.90	0.17	33.03	0.00	1.93	0.00	0.73	0.09	0.09	8.83
Mode	49.92	0.15	32.92	0.00	1.86	0.00	0.55	0.07	0.06	9.76
SERICITE M-II; N° analyses: 8										
	SiO2	TiO2	Al2O3	Cr2O3	FeO	MnO	MgO	CaO	Na2O	K2O
Minimum	46.97	0.00	31.10	0.00	2.02	0.00	0.55	0.02	0.06	8.09
Maximum	50.07	0.10	34.18	0.06	3.70	0.03	1.34	0.17	0.13	9.26
Std.dev.	0.91	0.03	0.90	0.02	0.55	0.01	0.30	0.05	0.02	0.42
Average	48.40	0.05	32.43	0.01	2.71	0.01	0.90	0.07	0.09	8.75
Median	48.50	0.04	32.33	0.00	2.69	0.01	0.81	0.05	0.09	8.77
Mode	47.95	0.03	32.01	0.00	2.40	0.01	0.75	0.03	0.10	8.50
SERICITE IN MINERALIZED VEINS ALONG NW-SE SHEARS; N° analyses: 10										
	SiO2	TiO2	Al2O3	Cr2O3	FeO	MnO	MgO	CaO	Na2O	K2O
Minimum	45.69	0.01	32.17	0.00	1.41	0.00	0.25	0.00	0.03	4.54
Maximum	48.80	0.60	35.71	0.07	3.38	0.04	1.22	0.04	0.31	10.02
Std.dev.	0.99	0.22	1.31	0.03	0.76	0.01	0.36	0.02	0.12	2.26
Average	46.91	0.24	33.76	0.02	2.18	0.02	0.71	0.02	0.14	7.40
Median	47.16	0.26	33.42	0.01	2.04	0.02	0.81	0.01	0.07	6.75
Mode	46.12	0.01	32.84	0.01	1.56	0.00	0.87	0.00	0.03	6.05
SERICITE IN QUARTZ BRECCIAS; N° analyses: 8										
	SiO2	TiO2	Al2O3	Cr2O3	FeO	MnO	MgO	CaO	Na2O	K2O
Minimum	47.32	0.08	29.45	0.00	1.87	0.00	0.21	0.05	0.03	8.76
Maximum	48.89	0.[illegible]21	33.01	0.06	3.06	0.05	1.94	0.26	0.20	10.06
Std.dev.	0.51	0.[illegible]04	1.20	0.02	0.45	0.02	0.57	0.0[illegible]	0.05	0.51
Average	47.85	0.12	31.87	0.01	2.67	0.02	0.60	0.12	0.09	9.43
Median	4[illegible]9	0.11	32.17	0.003	2.86	0.005	0.40	0.11	0.09	9.56
Mode	4[illegible]	0.10	31.38	0.00	2.75	0.00	0.32	0.11	0.09	8.94

Table IV -12:
DIOCTAHEDRAL K-MICAS CRYSTAL CHEMISTRY - FRANÇA SECTOR
REPRESENTATIVE ANALYSES

	(1)	(2)	(3)	(4)	(5)	(6)	(7)	(8)	(9)
SiO2	46.19	46.59	47.48	46.03	47.58	47.42	48.66	47.27	47.32
TiO2	0.02	0.00	0.39	0.01	0.69	0.29	0.03	0.34	0.09
Al2O3	34.95	34.50	31.79	35.57	30.42	33.19	32.01	33.19	31.70
Cr2O3	0.00	0.00	0.00	0.00	0.09	0.00	0.00	0.01	0.01
FeO	1.48	1.07	2.67	2.60	1.99	1.86	2.40	2.10	2.04
MnO	0.00	0.01	0.02	0.00	0.05	0.03	0.03	0.02	0.02
MgO	0.25	0.41	1.07	0.89	0.80	0.55	0.87	0.87	0.32
CaO	0.04	0.06	0.01	0.00	0.04	0.15	0.02	0.02	0.10
Na2O	0.33	0.32	0.23	0.16	0.16	0.20	0.07	0.07	0.07
K2O	10.01	8.40	8.80	9.12	9.87	9.76	8.56	6.20	8.89
Σ	93.25	91.36	92.96	94.38	91.70	93.48	92.65	90.09	90.56
	Number of ions on a basis of 22 oxygens								
S	6.252	6.350	6.498	6.159	6.563	6.402	6.574	6.465	6.533
Aliv	1.748	1.650	1.502	1.841	1.437	1.598	1.426	1.535	1.447
Σviv	8.000	8.000	8.000	8.000	8.000	8.000	8.000	8.000	8.000
Alvi	3.827	3.891	3.572	3.768	3.509	3.683	3.671	3.815	3.726
Ti	0.002	0.000	0.040	0.001	0.072	0.029	0.003	0.035	0.009
Cr	0.000	0.001	0.000	0.000	0.010	0.000	0.000	0.001	0.001
Fe	0.167	0.122	0.302	0.291	0.230	0.210	0.271	0.240	0.236
Mn	0.000	0.002	0.003	0.000	0.006	0.003	0.003	0.002	0.002
Mg	0.050	0.083	0.217	0.177	0.165	0.111	0.175	0.178	0.066
Σvi	4.046	4.098	4.133	4.237	3.991	4.037	4.125	4.272	4.041
Ca	0.005	0.009	0.002	0.000	0.006	0.022	0.002	0.003	0.015
Na	0.086	0.086	0.060	0.041	0.044	0.052	0.019	0.019	0.019
K	1.728	1.460	1.520	1.556	1.737	1.686	1.475	1.081	1.570
Σxii	1.819	1.555	1.582	1.597	1.787	1.760	1.496	1.103	1.604

Representative analyses of (1,2) Ser E-I (F-18A; F-23E), (3) Ser E-II (FP-A), (4) Ser E-IIIa (F-5), (5) Ser E-IIIb (F-5); (6) Ser M-I (F-18A1); (7) Ser M-II (FP-B); (8) Ser in regional shears (F-A), (9) Ser in quartz breccia (F-23L1).

Table IV - 13 :
SERICITE CRYSTAL CHEMISTRY - MONTEMOR SECTOR

SERICITE I; N° analyses: 26

	SiO2	TiO2	Al2O3	Cr2O3	FeO	MnO	MgO	CaO	Na2O	K2O
Minimum	44.19	0.02	27.00	0.00	0.41	0.00	0.48	0.00	0.01	6.53
Maximum	54.05	1.30	36.44	0.07	2.60	0.07	3.48	0.17	0.56	9.99
Std dev.	2.56	0.33	3.01	0.02	0.59	0.02	0.93	0.04	0.18	0.97
Average	47.08	0.52	33.05	0.02	0.93	0.01	1.45	0.03	0.24	8.74
Median	46.24	0.52	34.58	0.01	0.72	0.00	1.08	0.03	0.20	8.92
Mode	45.64	0.59	34.94	0.00	0.68	0.00	1.03	0.00	0.56	8.80

SERICITE II; N° analyses: 21

	SiO2	TiO2	Al2O3	Cr2O3	FeO	MnO	MgO	CaO	Na2O	K2O
Minimum	42.44	0.01	28.46	0.00	0.41	0.00	0.42	0.00	0.02	4.72
Maximum	52.59	1.50	37.32	0.06	9.65	0.05	5.18	0.24	0.86	10.41
Std dev.	2.29	0.37	2.29	0.02	2.04	0.02	1.14	0.07	0.25	1.51
Average	46.14	0.52	34.61	0.02	1.28	0.02	1.20	0.05	0.33	8.41
Median	45.79	0.42	35.10	0.01	0.73	0.01	0.64	0.03	0.27	8.83
Mode	46.09	0.65	35.08	0.00	0.76	0.00	0.44	0.00	0.27	8.69

SERICITE Mig; N° analyses: 10

	SiO2	TiO2	Al2O3	Cr2O3	FeO	MnO	MgO	CaO	Na2O	K2O
Minimum	42.98	0.00	30.30	0.00	0.52	0.00	0.09	0.01	0.12	7.5
Maximum	47.85	0.51	37.07	0.04	6.07	0.20	2.91	0.08	0.35	9.91
Std dev.	1.45	0.17	1.98	0.02	1.78	0.06	0.91	0.02	0.07	0.79
Average	45.99	0.18	33.31	0.01	2.28	0.06	1.43	0.04	0.23	8.96
Median	46.31	0.13	33.02	0.00	1.42	0.04	1.13	0.04	0.25	9.03
Mode	45.91	0.10	32.49	0.00	1.29	0.00	1.08	0.02	0.25	8.95

REPRESENTATIVE ANALYSES

	(1)	(2)	(3)
SiO_2	45.46	44.88	46.16
TiO_2	0.47	0.27	0.00
Al_2O_3	35.22	36.73	37.07
Cr_2O_3	0.02	0.00	0.00
FeO	0.82	0.78	0.52
MnO	0.01	0.02	0.03
MgO	0.68	0.47	0.09
CaO	0.03	0.03	0.04
Na_2O	0.44	0.86	0.26
K_2O	9.95	9.84	9.43
Σ^2	93.09	93.87	93.60
N° of ions on the basis of 11 oxygens			
Si	3.079	3.018	3.082
Al^{IV}	0.921	0.982	0.918
Σ^{IV}	4.000	4.000	4.000
Al^{VI}	1.890	1.928	1.998
Ti	0.024	0.014	0.000
Cr	0.001	0.000	0.000
Fe^{2+}	0.046	0.044	0.029
Mn	0.000	0.001	0.002
Mg	0.068	0.047	0.009
Σ^{VI}	2.030	2.34	2.039
Ca	0.002	0.002	0.003
Na	0.058	0.112	0.034
K	0.860	0.844	0.803

(1) - I (150 IV); (2) - II (150 IV); (3) - Mig (S5A II)

Table IV - 14:
CHLORITE CRYSTAL CHEMISTRY - FRANÇA SECTOR

CHLORITE E-I; N° analyses: 7										
	SiO2	TiO2	Al2O3	Cr2O3	FeO	MnO	MgO	CaO	Na2O	K2O
Minimum	24.09	0.05	21.15	0.00	25.99	0.12	12.65	0.00	0.00	0.02
Maximum	24.82	0.09	22.70	0.05	26.62	0.26	13.25	0.01	0.12	0.07
Std.dev.	0.23	0.01	0.64	0.02	0.24	0.04	0.22	0.005	0.04	0.02
Average	24.56	0.06	22.00	0.02	26.43	0.20	12.88	0.005	0.07	0.04
Median	24.58	0.06	21.96	0.02	26.52	0.21	12.78	0.01	0.07	0.04
Mode	24.57	0.06	21.99	0.04	26.47	0.21	12.88	0.01	0.06	0.03
CHLORITE E-II; N° analyses: 3										
	SiO2	TiO2	Al2O3	Cr2O3	FeO	MnO	MgO	CaO	Na2O	K2O
Minimum	23.28	0.04	19.82	0.00	31.50	0.06	6.07	0.00	0.02	0.00
Maximum	26.14	0.18	20.14	0.06	33.95	0.14	7.64	0.03	0.04	0.97
Std.dev.	1.54	0.07	0.17	0.03	1.26	0.04	0.86	0.02	0.01	0.56
Average	24.37	0.11	20.01	0.03	32.56	0.11	7.05	0.01	0.03	0.32
Median	23.70	0.11	20.07	0.04	32.24	0.13	7.45	0.00	0.03	0.00
Mode	23.28	0.04	19.82	0.00	31.50	0.06	6.07	0.00	0.02	0.00
CHLORITE E-III; N° analyses: 4										
	SiO2	TiO2	Al2O3	Cr2O3	FeO	MnO	MgO	CaO	Na2O	K2O
Minimum	23.18	0.02	17.21	0.00	32.79	0.13	5.10	0.00	0.04	0.00
Maximum	24.15	0.07	20.08	0.03	36.52	0.91	7.91	0.25	0.13	0.04
Std.dev.	0.43	0.02	1.32	0.01	1.98	0.37	1.33	0.12	0.04	0.02
Average	23.80	0.04	19.13	0.01	34.78	0.46	6.85	0.08	0.09	0.03
Median	23.93	0.04	19.62	0.005	34.91	0.39	7.20	0.03	0.10	0.03
Mode	23.18	0.02	17.21	0.00	32.79	0.13	5.10	0.00	0.04	0.03
CHLORITE M-I; N° analyses: 9										
	SiO2	TiO2	Al2O3	Cr2O3	FeO	MnO	MgO	CaO	Na2O	K2O
Minimum	23.70	0.00	18.81	0.00	31.96	0.17	6.22	0.00	0.00	0.01
Maximum	29.94	0.09	21.04	0.14	36.76	0.64	7.63	0.11	0.09	0.05
Std.dev.	1.92	0.03	0.63	0.05	1.68	0.18	0.43	0.03	0.03	0.01
Average	24.94	0.05	19.79	0.03	34.69	0.33	6.82	0.02	0.04	0.03
Median	24.44	0.05	19.71	0.02	35.10	0.28	6.77	0.02	0.03	0.03
Mode	24.29	0.03	19.54	0.00	34.41	0.18	6.48	0.00	0.06	0.03
CHLORITE M-II; N° analyses: 7										
	SiO2	TiO2	Al2O3	Cr2O3	FeO	MnO	MgO	CaO	Na2O	K2O
Minimum	22.64	0.04	19.01	0.00	31.69	0.03	7.30	0.01	0.00	0.02
Maximum	25.23	5.12	20.68	0.09	33.81	0.32	8.24	0.05	0.10	0.13
Std.dev.	0.85	1.90	0.58	0.03	0.78	0.09	0.39	0.02	0.03	0.04
Average	24.02	0.81	20.14	0.02	32.86	0.13	7.79	0.03	0.04	0.06
Median	23.87	0.10	20.43	0.00	33.17	0.10	7.86	0.04	0.04	0.04
Mode	23.72	0.09	20.11	0.00	32.36	0.10	7.51	0.05	0.04	0.04
CHLORITE M-III; N° analyses: 6										
	SiO2	TiO2	Al2O3	Cr2O3	FeO	MnO	MgO	CaO	Na2O	K2O
Minimum	23.47	0.01	18.34	0.00	32.34	0.1	5.23	0.00	0.00	0.00
Maximum	26.33	0.12	20.78	0.03	36.42	0.53	7.80	0.09	0.09	0.06
Std.dev.	1.07	0.05	0.84	0.01	1.35	0.16	0.94	0.03	0.03	0.02
Average	24.32	0.07	19.67	0.01	34.29	0.23	7.06	0.03	0.03	0.03
Median	24.02	0.09	19.59	0.01	34.19	0.19	7.23	0.03	0.03	0.04
Mode	23.58	0.02	19.44	0.01	33.68	0.11	7.14	0.00	0.01	0.02
CHLORITE IN MINERALIZED VEINS ALONG NW-SE SHEARS; N° analyses: 10										
	SiO2	TiO2	Al2O3	Cr2O3	FeO	MnO	MgO	CaO	Na2O	K2O
Minimum	23.12	0.02	17.59	0.00	22.50	0.08	4.56	0.00	0.00	0.00
Maximum	31.19	0.76	22.37	0.04	38.50	1.22	10.54	0.08	0.05	0.06
Std.dev.	2.34	0.25	1.71	0.01	4.51	0.45	2.04	0.03	0.02	0.02
Average	25.50	0.18	19.72	0.01	34.34	0.60	6.46	0.01	0.02	0.02
Median	25.21	0.09	20.47	0.01	35.82	0.72	5.59	0.00	0.03	0.02
Mode	24.76	0.09	18.08	0.00	33.85	0.19	4.67	0.00	0.04	0.00

Table IV - 15 :
CHLORITE CRYSTAL CHEMISTRY - FRANÇA SECTOR
REPRESENTATIVE ANALYSES

	(1)	(2)	(3)	(4)	(5)	(6)	(7)
SiO2	24.09	26.14	23.18	24.81	25.23	24.50	24.76
TiO2	0.06	0.11	0.05	0.09	0.11	0.12	0.09
Al2O3	21.96	20.07	19.92	19.71	20.49	19.44	20.51
Cr2O3	0.02	0.00	0.00	0.06	0.00	0.00	0.01
FeO	26.52	31.50	32.79	34.15	32.36	34.93	33.21
MnO	0.17	0.06	0.19	0.33	0.05	0.10	0.12
MgO	12.78	6.07	7.86	7.04	7.51	7.15	8.09
CaO	0.00	0.00	0.01	0.03	0.04	0.04	0.01
Na2O	0.07	0.02	0.13	0.06	0.00	0.04	0.02
K2O	0.03	0.97	0.03	0.03	0.09	0.05	0.00
Σ	85.70	84.95	84.16	86.30	85.88	86.41	86.82
	Number of ions on a basis of 14 oxygens						
S	2.623	2.951	2.679	2.799	2.820	2.774	2.754
Aliv	1.377	1.049	1.321	1.201	1.180	1.226	1.246
Σviv	4.000	4.000	4.000	4.000	4.000	4.000	4.000
Alvi	1.442	1.621	1.394	1.419	1.520	1.368	1.442
Ti	0.005	0.009	0.004	0.008	0.009	0.010	0.008
Cr	0.002	0.000	0.000	0.005	0.000	0.000	0.001
Fe	2.415	2.974	3.170	3.222	3.025	3.307	3.089
Mn	0.015	0.006	0.019	0.032	0.005	0.010	0.011
Mg	2.074	1.021	1.355	1.183	1.251	1.206	1.341
Σvi	5.952	5.632	5.941	5.868	5.809	5.900	5.891
Ca	0.000	0.001	0.002	0.004	0.005	0.011	0.001
Na	0.014	0.004	0.004	0.013	0.000	0.009	0.000
K	0.005	0.140	0.035	0.004	0.013	0.007	0.000

Representative analyses of (1) Chl E-I (FP-A), (2) Chl E-II (F-23E), (3) Chl E-III (F-23E), (4) Chl M-I (F-23H); (5) Chl M-II (FP-B); (6) CHl M-III (F-18A1); (7) - Chl in regional shears (F-A).

Deposit	Type	n	Si	Al	Fe	Mg	Aliv	AlVi	Fe %
Pendono	alt biot	4	2,83-2,94	2,89-2,75	2,39-3,31	0,64-1,37	1,06-1,17	1,37-1,76	0,64-0,84
			2,9±0,05	2,83±0,06	2,67-0,43	1,16±0,35	1,1±0,05	1,73±0,05	0,7±0,09
Pino	alt biot	7	2,85-3,2	2,51-2,73	2,66-2,99	0,87-1,53	0,8-1,15	1,43-1,79	0,65-0,76
			2,94±0,13	2,6±0,08	2,82±0,12	1,29±0,22	1,06±0,13	1,54±0,12	0,69±0,04
	neof	21	2,96-3,79	2,11-3,05	1,89-4,19	0,06-063	0,21-1,04	1,33-2,7	0,81-0,97
			3,49±0,22	2,66±0,29	2,71±0,64	0,21±0,16	0,51±0,22	2,15±0,4	0,93±0,05

Table IV - 16 : Chlorite crystal chemistry. Penedono and Pino area
Si, Al, Fe, Mg, Aliv and Alvi are given for half formula

Table IV - 17:
CHLORITE CRYSTAL CHEMISTRY - MONTEMOR SECTOR

	SiO2	TiO2	Al2O3	Cr2O3	FeO	MnO	MgO	CaO	Na2O	K2O
CHLORITE Ia; N° analyses: 10										
Minimum	26.41	0.03	16.34	0.00	12.97	0.02	6.23	0.10	0.10	0.11
Maximum	34.82	0.15	21.60	0.21	20.41	0.13	17.4	0.79	0.52	1.48
Std.dev.	2.73	0.04	1.81	0.06	2.53	0.03	3.70	0.19	0.13	0.42
Average	30.80	0.06	18.54	0.07	17.03	0.08	13.27	0.33	0.24	0.40
Median	31.44	0.05	18.52	0.06	16.97	0.09	14.18	0.28	0.20	0.23
Mode	30.93	0.05	17.34	0.00	16.62	0.10	12.92	0.26	0.20	0.14
CHLORITE Ib; N° analyses: 5										
	SiO2	TiO2	Al2O3	Cr2O3	FeO	MnO	MgO	CaO	Na2O	K2O
Minimum	25.15	0.33	17.03	0.01	17.31	0.13	12.72	0.01	0.01	0.22
Maximum	29.02	2.07	18.85	0.11	19.86	0.18	13.57	1.54	0.08	1.60
Std.dev.	1.37	0.74	0.73	0.04	0.97	0.02	0.35	0.64	0.03	0.50
Average	27.16	0.76	18.92	0.05	18.57	0.16	13.17	0.34	0.03	0.71
Median	27.27	0.47	18.51	0.03	18.38	0.16	13.28	0.03	0.02	0.56
Mode	27.13	0.34	17.95	0.01	18.18	0.16	12.89	0.02	0.02	0.48
CHLORITE Im; N° analyses: 10										
	SiO2	TiO2	Al2O3	Cr2O3	FeO	MnO	MgO	CaO	Na2O	K2O
Minimum	24.72	0.02	17.42	0.00	20.92	0.29	11.38	0.00	0.00	0.00
Maximum	29.35	4.95	21.52	0.01	26.07	0.52	13.76	4.86	0.10	1.74
Std.dev.	1.35	1.52	1.22	0.003	1.55	0.07	0.71	1.53	0.03	0.56
Average	26.97	0.65	19.49	0.001	25.12	0.41	13.20	0.52	0.03	0.34
Median	26.87	0.11	19.46	0.00	25.77	0.42	13.47	0.04	0.02	0.14
Mode	26.66	0.02	19.53	0.00	25.77	0.37	13.05	0.02	0.00	0.18

REPRESENTATIVE ANALYSES

	(1)	(2)	(3)	(4)	(5)	(6)
SiO_2	30.93	27.31	26.66	26.75	30.36	30.77
TiO_2	0.05	2.07	0.05	5.99	0.02	0.03
Al_2O_3	18.66	17.03	19.53	16.63	19.01	18.90
Cr_2O_3	0.06	0.01	0.00	0.06	0.11	0.00
FeO	17.04	18.38	25.85	14.83	15.53	20.31
MnO	0.06	0.15	0.37	0.06	0.09	0.09
MgO	16.92	13.28	13.76	14.75	17.49	10.68
CaO	0.27	1.54	0.00	0.33	0.22	0.25
Na_2O	0.38	0.08	0.01	0.13	0.10	0.22
K_2O	0.25	0.69	0.09	0.27	0.40	0.23
Σ^2	84.63	80.55	86.31	79.80	83.33	81.48
Number of ions on the basis of 14 oxygens						
Si	3.200	3.051	2.862	2.947	3.167	3.349
Al^{IV}	0.800	0.949	1.138	1.053	0.833	0.651
Σ^{IV}	4.000	4.000	4.000	4.000	4.000	4.000
Al^{VI}	1.475	1.293	1.333	1.106	1.504	1.774
Ti	0.004	0.174	0.004	0.496	0.001	0.003
Cr	0.005	0.001	0.000	0.006	0.009	0.000
Fe^{2+}	1.474	1.717	2.320	1.366	1.355	1.849
Mn	0.006	0.015	0.034	0.006	0.008	0.008
Mg	2.609	2.212	2.201	2.422	2.720	1.733
Σ^{VI}	5.572	5.412	5.892	5.402	5.597	5.368
Ca	0.030	0.184	0.001	0.040	0.025	0.029
Na	0.076	0.017	0.001	0.028	0.021	0.046
K	0.033	0.099	0.012	0.037	0.053	0.032

(1) - Ia (MI IB); (2) - Ib (150 XIV B); (3) - Im (S5AII i); (4),(5) - M (MII 5c); (6) - T (MII 9)

APPENDIX

Synthetic fluid inclusions - Experimental procedure (CREGU)

Synthetic fluid inclusions were prepared by hydrothermal synthesis in the CREGU experimental laboratory following the methodology of previous workers (Roedder and Kopp, 1975, Shelton and Orville, 1980, Sterner and Bodnar, 1984, Zhang and Frantz, 1987). Compositions of the standard solutions were the followings : (Ca + Mg) or (Na + K) = 0.5, 1, 2 and 4 molal and Mg/Ca or K/Na = 0.1, 0.5 and 1 for each (Ca + Mg) or (Na + K) concentration. Small prisms of synthetic quartz free of fluid inclusions were sawn (1.8 mm x 2 mm x 20 mm). They were fractured by heating, in an oven (350°C), and quenching into distilled cold water. Prisms were loaded into gold capsules (50 mm long) with silica gel and the standard solutions. The compositions of the solutions were checked by atomic absorption spectrophotometry. The experimental capsules were loaded into vessels and pressurized with water to 2500 ± 10 bars and heated at temperature of 650 ± 15°C. Temperature and pressure were monitored by a computer during the synthesis (8 days). At the end of the runs, the vessels were cooled to room temperature and the gold capsules were extracted. Microthermometric measurments were carried out on synthetic fluid inclusions and the composition of the extracted solutions from the capsules was analysed by atomic absorption. Quartz rods show growth zones with numerous synthetic fluid inclusions which contain liquid and vapour phases at room temperature.

Crush-Leach Procedure. (Leeds)

The details of the initial sample preparation and purification are identical to those of Bottrell et al (1988). Approximately 1g of the purified quartz is crushed in a specially cleaned pestle and mortar, crushed to a fine powder and transferred into Nalgene centrifuge tubes. If the sample is to be analysed for anions 10ml of double distilled water are added and for cations 10ml of 0.13N HNO_3/200ppm La is used. The mixture is centrifuged at 5000rpm for 10 minutes, decanted and filtered through 0.2mm nylon filters prior to analysis. All crushing and filtering of the solutions is carried out in laminar air flow cabinets. Cations are determined by inductively coupled mass spectrometry at the NERC facility, Royal Holloway. Anions are determined by ion chromatography (further details are given below). Na and K are determined on all solutions by flame emission spectromery.

Anion Analysis. (Leeds)

The separation of anions by the Dionex ion chromatograph is carried out using the Omnipac PAX-100 guard and analytical columns. The ions are eluted with a 3.9mM $NaHCO_3$/3.1mM Na_2CO_3/5% CH_3OH eluant and are detected by a high sensitivity conductivity detector. The normal combination of guard and analytical column is unsuitable for the detection of low levels of iodide as it is retained on the column for some 30 minutes which precludes its determination at the low levels required. It proved satisfactory to remove the analytical column and use the much smaller guard column to separate the iodide. This reduces the retention time of the ion and enhances the peak height making detection easier. The drawback is that the separation of the other ions is affected and this technique is only used to determine Cl and I. To obtain the complete anion analyses the leach solution must be run using both configurations and combined (using the Cl concentration from both runs).

Anion analyses of synthetic fluid inclusions						
Sample	**Concentration in Leach Solution (ppb)**				**Weight Ratio**	
		Cl	Br	I	Br/Cl	I/Cl
47	As Analysed	17007	274	148	0.0161	0.0087
	True Value	-	-	-	0.0163	0.0120
48	As Analysed	4701	31	5.2	0.0066	0.0011
	True Value	-	-	-	0.0071	0.0011
	Detection Limit	10	0.5	0.1	-	-

The cation procedure had previously been validated using synthetic standards and by analysing the same samples by different techniques. In order to validate the anion procedure synthetic standards with known Cl/Br/I ratios were prepared by M.C. Boiron at CREGU. The results in the following table show that within analytical uncertainty there is no difference between the ratios determined by ion chromatography and the true ratios.